33
12-3-79

H. 359

LBL-8648
UC-13

EARTH SCIENCES DIVISION

ANNUAL REPORT 1978

MASTER

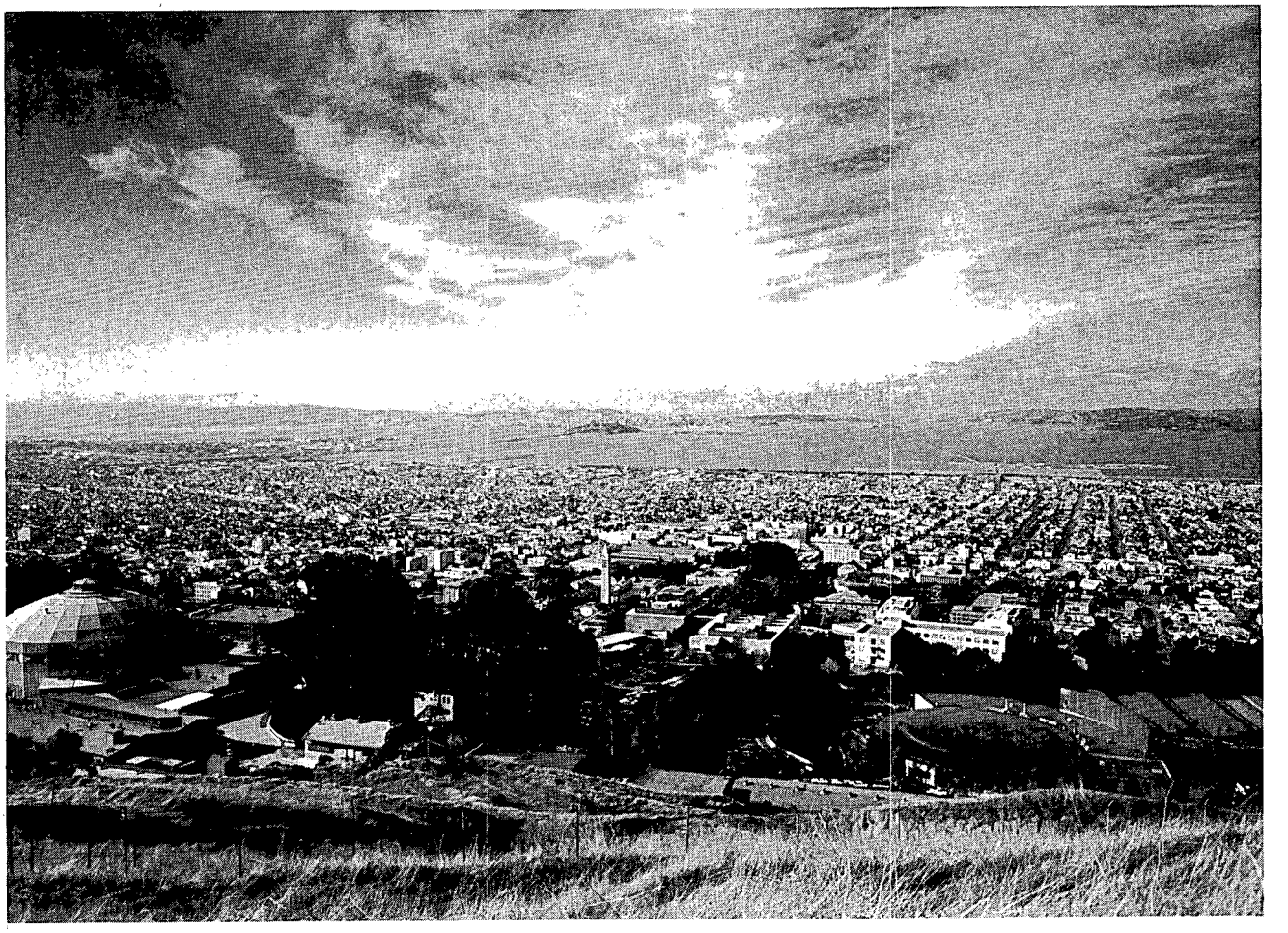

LAWRENCE BERKELEY LABORATORY
UNIVERSITY OF CALIFORNIA

Prepared for the U. S. Department of Energy under Contract W-7405-ENG-48

LBL-8648

DISTRIBUTION OF THIS DOCUMENT IS UNLIMITED

DISCLAIMER

This report was prepared as an account of work sponsored by an agency of the United States Government. Neither the United States Government nor any agency Thereof, nor any of their employees, makes any warranty, express or implied, or assumes any legal liability or responsibility for the accuracy, completeness, or usefulness of any information, apparatus, product, or process disclosed, or represents that its use would not infringe privately owned rights. Reference herein to any specific commercial product, process, or service by trade name, trademark, manufacturer, or otherwise does not necessarily constitute or imply its endorsement, recommendation, or favoring by the United States Government or any agency thereof. The views and opinions of authors expressed herein do not necessarily state or reflect those of the United States Government or any agency thereof.

DISCLAIMER

Portions of this document may be illegible in electronic image products. Images are produced from the best available original document.

LEGAL NOTICE

This report was prepared as an account of work sponsored by the United States Government. Neither the United States nor the United States Department of Energy, nor any of their employees, nor any of their contractors, subcontractors, or their employees, makes any warranty, express or implied, or assumes any legal liability or responsibility for the accuracy, completeness or usefulness of any information, apparatus, product or process disclosed, or represents that its use would not infringe privately owned rights.

Printed in the United States of America
Available from
National Technical Information Service
U.S. Department of Commerce
5285 Port Royal Road
Springfield, VA 22161
Price Code: A12

LBL-8648

EARTH SCIENCES DIVISION ANNUAL REPORT 1978

LAWRENCE BERKELEY LABORATORY
UNIVERSITY OF CALIFORNIA
BERKELEY, CALIFORNIA 94720

MASTER

DISCLAIMER

This book was prepared as an account of work sponsored by an agency of the United States Government. Neither the United States Government nor any agency thereof, nor any of their employees, makes any warranty, express or implied, or assumes any legal liability or responsibility for the accuracy, completeness, or usefulness of any information, apparatus, product, or process disclosed, or represents that its use would not infringe privately owned rights. Reference herein to any specific commercial product, process, or service by trade name, trademark, manufacturer, or otherwise, does not necessarily constitute or imply its endorsement, recommendation, or favoring by the United States Government or any agency thereof. The views and opinions of authors expressed herein do not necessarily state or reflect those of the United States Government or any agency thereof.

Prepared for the U. S. Department of Energy under Contract W-7405-ENG-48

DISTRIBUTION OF THIS DOCUMENT IS UNLIMITED

CONTENTS

Introduction 1

GEOTHERMAL ENERGY DEVELOPMENT

Geothermal Exploration Technology 4

ELECTRICAL AND ELECTROMAGNETIC COMPUTER MODELING TECHNIQUES 4
K. H. Lee, D. Pridmore, M. Hoversten, and H. F. Morrison

MINICOMPUTER FOR IN-FIELD PROCESSING OF MAGNETOTELLURIC DATA 7
R. H. Koch, W. M. Goubau, T. D. Gamble, R. F. Miracky, and J. Clarke

SUPERCONDUCTING THIN-FILM GRADIOMETER AND MAGNETOMETERS FOR GEOPHYSICAL APPLICATIONS 8
W. M. Goubau and J. Clarke

MAGNETOTELLURICS WITH SQUID MAGNETOMETERS 9
T. D. Gamble, W. M. Goubau, R. F. Miracky, and J. Clarke

CONTROLLED-SOURCE ELECTROMAGNETIC SYSTEM 12
H. F. Morrison, N. E. Goldstein, M. Hoversten, G. Oppliger, and C. Riveros

GEOTHERMAL SEISMIC FIELD SYSTEM DEVELOPMENT 15
T. V. McEvilly, E. L. Majer, J. Bartschi, and J. Heinson

KLAMATH BASIN GEOTHERMAL RESOURCE AND EXPLORATION TECHNIQUE EVALUATION 20
N. E. Goldstein, H. A. Wollenberg, and M. A. Stark

MT. HOOD GEOTHERMAL RESOURCE EVALUATION 23
N. E. Goldstein, H. A. Wollenberg, H. Bowman, and E. Mozley

EAST MESA SEISMIC STUDY 26
T. V. McEvilly, B. Schechter, and E. L. Majer

Geophysical Studies at Cerro Prieto 29

SEISMOLOGICAL STUDIES AT CERRO PRIETO 29
E. L. Majer and T. V. McEvilly

SELF-POTENTIAL STUDIES AT CERRO PRIETO 34
R. F. Corwin and H. F. Morrison

RESISTIVITY STUDIES AT CERRO PRIETO 37
M. J. Wilt and N. E. Goldstein

MAGNETOTELLURIC SURVEY AT CERRO PRIETO 41
T. D. Gamble, W. M. Goubau, N. E. Goldstein, and J. Clarke

PRECISION GRAVITY SURVEYS AT CERRO PRIETO 43
R. B. Grannell, D. W. Tarman, and N. E. Goldstein

Utilization and Conversion Technology 46

HEAT TRANSFER COEFFICIENTS FOR ISOBUTANE 47
B. W. Tleimat, A. D. K. Laird, H. Rie, and I. C. Hsu

FIELD TEST OF GEOTHERMAL/HYDROCARBON SHELL-AND-TUBE HEAT EXCHANGER 50
L. O. Beaulaurier

THERMODYNAMIC AND TRANSPORT PROPERTIES OF LIGHT HYDROCARBONS AND THEIR BINARY MIXTURES **52**
L. F. Silvester

DEVELOPMENTS IN DIRECT-CONTACT HEAT EXCHANGE **55**
R. L. Fulton

HEAT-EXCHANGER DESIGN OPTIMIZATION **57**
W. L. Pope

THERMODYNAMIC AND COST BENEFITS OF FLOATING COOLING FOR GEOTHERMAL BINARY-CYCLE POWER PLANTS **60**
H. S. Pines

GEOTHERMAL RESOURCES AND THE U. S. PULP AND PAPER INDUSTRY **66**
J. V. Davey and J. H. Howard

Reservoir Engineering 67

PRESSURE MEASUREMENTS USING A FLUID-FILLED CAPILLARY TUBE **68**
C. W. Miller

TWO-PHASE FLASHING FLOW IN GEOTHERMAL WELLS **70**
S. Juprasert

FLOW TO A WELL INTERCEPTING A VERTICAL FRACTURE: VALIDATION OF A NUMERICAL MODEL **72**
T. N. Narasimhan and W. A. Palen

EFFECT OF RADIALLY VARYING TRANSMISSIVITY ON THE TRANSIENT PRESSURE PHENOMENON **75**
L. D. Mlodinow and C. F. Tsang

MATHEMATICAL SIMULATION OF THERMAL BREAKTHROUGH UNDER INJECTION: COMPARISON OF TWO TECHNIQUES **77**
T. N. Narasimhan, S. Juprasert, and G. S. Bodvarsson

WELL TEST DATA ANALYSIS METHODS AT LBL **79**
S. M. Benson, C. B. Goranson, and R. C. Schroeder

SUMMARY OF WELL TESTS AND ANALYSES FOR THE EAST MESA GEOTHERMAL SITE **86**
S. M. Benson, C. B. Goranson, J. Haney, D. G. McEdwards, T. N. Narasimhan, and R. C. Schroeder

DEVELOPMENT OF THE SIMULATOR SHAFT78 FOR GEOTHERMAL RESERVOIR STUDIES **94**
K. Pruess, R. C. Schroeder, P. A. Witherspoon, and J. M. Zerzan

SITE-SPECIFIC GEOTHERMAL RESERVOIR ENGINEERING ACTIVITIES **97**
C. B. Goranson and R. C. Schroeder

MEXICAN-AMERICAN COOPERATIVE PROGRAM AT THE CERRO PRIETO GEOTHERMAL FIELD, BAJA CALIFORNIA, MEXICO **106**
M. J. Lippmann, P. A. Witherspoon, and H. A. Wollenberg

PRELIMINARY SIMULATION STUDIES RELATED TO THE CERRO PRIETO FIELD **111**
M. J. Lippmann, G. S. Bodvarsson, and P. A. Witherspoon

STUDY OF ALTERNATIVE REINJECTION SCHEMES FOR THE CERRO PRIETO GEOTHERMAL FIELD, BAJA CALIFORNIA, MEXICO **119**
C. F. Tsang, G. S. Bodvarsson, M. J. Lippmann, and J. Rivera R.

SUBSURFACE GEOLOGY OF THE EAST MESA GEOTHERMAL ANOMALY **124**
J. H. Howard, A. N. Graf, and P. C. van de Kamp

GEOTHERMAL SUBSIDENCE RESEARCH PROGRAM **128**
T. L. Simkin, J. E. Noble, and W. J. Schwarz

GEOTHERMAL RESERVOIR ENGINEERING MANAGEMENT PROGRAM **130**
J. H. Howard and W. J. Schwarz

Aquifer Thermal Energy Storage **135**

STUDY OF GROUNDWATER TEMPERATURE CHANGES DURING AQUIFER USES RELATED TO POWER PRODUCTION **135**
M. J. Lippmann, C. F. Tsang, and P. A. Witherspoon

MATHEMATICAL MODELING OF THERMAL ENERGY STORAGE IN AQUIFERS **139**
C. F. Tsang, T. Buscheck, D. Mangold, and M. J. Lippmann

GEOSCIENCES

A NOTE ON THE MEANING OF STORAGE COEFFICIENT **146**
T. N. Narasimhan and B. Y. Kanehiro

SIGNIFICANCE OF THE STORAGE PARAMETER IN SATURATED-UNSATURATED GROUNDWATER FLOW **148**
T. N. Narasimhan

USE OF AQUIFER RESPONSE TO EARTH TIDES AS A MEANS OF DETERMINING AQUIFER CHARACTERISTICS **151**
T. N. Narasimhan and B. Y. Kanehiro

PRELIMINARY ANALYSIS OF TIDAL DATA **153**
B. Y. Kanehiro, T. N. Narasimhan, and C. F. Tsang

BEHAVIOR OF ROCK-FLUID SYSTEMS AT ELEVATED PRESSURES AND TEMPERATURES **154**
W. H. Somerton, A. Ghaffari, R. Greenwald, V. Hoang, F. Martínez-Baez, H. J. Su, and L. Wong

THERMODYNAMICS OF HIGH-TEMPERATURE BRINES **158**
K. S. Pitzer, D. J. Bradley, P. Z. Rogers, and J. C. Peiper

SOLUBILITY OF ALBITE IN THE AQUEOUS PHASE AT ELEVATED TEMPERATURES **160**
J. M. Neil and J. A. Apps

THERMODYNAMIC PROPERTIES OF SILICATE MATERIALS **165**
I. S. E. Carmichael, M. S. Ghiorso, L. Moret, and S. A. Nelson

DEVELOPMENT OF A DATA BASE FOR AQUEOUS SOLUTIONS **168**
R. J. Otto, H. Ozbek, and S. L. Phillips

KINETICS OF PRECIPITATION OF AMORPHOUS SILICA FROM AQUEOUS SOLUTION **169**
O. Weres, A. Yee, and L. Tsao

ENHANCED OIL RECOVERY WITH MOBILITY AND REACTIVE TENSION AGENTS **173**
C. J. Radke and W. H. Somerton

URANIUM IN ALKALINE ROCKS **180**
B. Strisower, H. A. Wollenberg, M. Murphy, H. R. Bowman, S. Flexser, and I. S. E. Carmichael

GEODOSE PROJECT **185**
H. A. Wollenberg and B. Strisower

THERMAL EFFECTS IN OVERLYING SEDIMENTARY ROCK FROM IN-SITU COMBUSTION OF A COAL SEAM **187**
D. C. Mangold, H. A. Wollenberg, and C. F. Tsang

FOUR-CHANNEL SIMULTANEOUS COLLECTION SYTEM FOR HIGH-PRECISION MASS SPECTROMETRY **189**
M. C. Michel, D. F. Mosier, and W. R. Keyes

DETERMINATION OF THE PROPERTIES OF SOILS BY IN-SITU MEASUREMENTS **191**
W. C. B. Villet and J. K. Mitchell

STATISTICAL ANALYSIS OF THE CORRELATION OF EARTHQUAKES WITH RADON CONCENTRATION IN WATER FROM SHALLOW WELLS NEAR OROVILLE, CALIFORNIA **193**
B. Berlin

UNDERGROUND NUCLEAR WASTE MANAGEMENT

SWEDISH-AMERICAN COOPERATIVE PROGRAM ON RADIOACTIVE WASTE STORAGE IN MINED CAVERNS IN CRYSTALLINE ROCK **199**
P. A. Witherspoon, N. G. W. Cook, and J. E. Gale

REGIONAL THERMO-HYDROLOGICAL EFFECTS OF A RADIOACTIVE WASTE REPOSITORY IN HARD ROCK **210**
J. S. Y. Wang, C. F. Tsang, N. G. W. Cook, and P. A. Witherspoon

THE VERY DEEP HOLE CONCEPT: EVALUATION OF AN ALTERNATIVE FOR NUCLEAR WASTE DISPOSAL **214**
M. T. O'Brien, L. H. Cohen, T. N. Narasimhan, T. L. Simkin, H. A. Wollenberg, W. F. Brace, S. Green, and H. P. Pratt

GEOTECHNICAL ASSESSMENT AND INSTRUMENTATION NEEDS FOR NUCLEAR WASTE ISOLATION IN CRYSTALLINE AND ARGILLACEOUS ROCKS **215**
M. T. O'Brien

GEOHYDROLOGICAL STUDIES FOR NUCLEAR WASTE ISOLATION AT THE HANFORD RESERVATION **219**
J. A. Apps, T. Doe, B. Doty, S. Doty, R. Galbraith, A. Kearns, B. Kohrt, J. Long, A. Monroe, T. N. Narasimhan, P. Nelson, C. R. Wilson, and P. A. Witherspoon

NATURE AND DISTRIBUTION OF SECONDARY MINERALS IN THE BASALTS OF THE PASCO BASIN, WASHINGTON, AND THEIR RELATION TO THE DISPOSAL OF NUCLEAR WASTE **229**
L. V. Benson, C. L. Carnahan, J. A. Apps, D. J. Corrigan, C. J. Frisch, C. A. Mouton, and L. K. Teague

HANFORD NEAR-SURFACE TEST FACILITY HEATER EXPERIMENTS **232**
A. DuBois

WASTE ISOLATION SAFETY ASSESSMENT PROGRAM **241**
R. J. Silva, L. V. Benson, and J. A. Apps

APPENDIXES

APPENDIX A: PUBLICATIONS **247**

APPENDIX B: EARTH SCIENCES DIVISION STAFF **250**

INTRODUCTION

The evolution of the unifying theory of plate tectonics within the past two decades has provided an impetus for research in all aspects of the earth sciences. Post World War II industrial expansion and worldwide population growth have necessitated greater knowledge of the geologic processes connected with geothermal and mineral exploration, groundwater extraction, land use, urban planning, petroleum exploration, the nuclear fuel cycle, and construction of large structures underground and on the continental shelves. Exploration activities are probing the earth to depths where our experience is meager, our knowledge fragmentary, and where man's impact may cause changes that will have effects for ages to come.

LBL Earth Sciences Division activities are focused on the earth's crust and are dedicated to gaining knowledge of this important region. Making use of the close ties between LBL and researchers on the U.C. Berkeley campus, the Earth Sciences Division is conducting programs, primarily in geothermal and nuclear waste isolation research, to define the physical and chemical properties of rocks and rock-water systems, examine the thermodynamics of deep crustal regimes, design geophysical instrumentation and techniques for exploration and seismology, devise innovative well-testing techniques, and write computer codes to assess and evaluate deep hydrologic systems.

A multidisciplinary team of leading research scientists, with experience specifically related to the geologic regime at multikilometer depths, is working on projects ranging from fundamental studies on the physical and chemical properties of rock and the complex interactions that occur within anisotropic rock media, to very large applied research and development efforts to resolve specific problems in energy exploitation. All research activities capitalize on the unique laboratory-instrumentation-computer support available to LBL/UCB scientists. The creativity of Earth Sciences Division researchers is nurtured by knowledgeable technical support, excellent equipment, and the continual interplay between research and engineering applications.

The Earth Sciences Division will continue to emphasize laboratory and field experiments, instrumentation design and improvement, testing and analysis techniques, and modeling of geological systems. The goal is to improve man's knowledge of the crustal zone in order to assure its safe and efficient utilization. Because of the enormous size and complexity of this region, the coordinated efforts of geoscientists supported by comprehensive sampling, testing, and experimental activities are required to obtain this knowledge. The Earth Sciences Division projects are described in the papers which follow.

GEOTHERMAL ENERGY DEVELOPMENT

The Earth Sciences Division (ESD) program in Geothermal Energy Development began in 1973 in response to the national goal of developing alternate energy sources. This program initially consisted of: an exploration assessment of sites in northern Nevada for a proposed demonstration plant; development of a binary-fluid conversion process for high-temperature, low-salinity brines; and various geochemical and geophysical studies related to the chemistry of brines and the scaling and corrosion problems they cause. An additional support project, the National Information Resource (GRID), commenced to compile a computer data bank on topics related to geothermal energy.

Many of these programs continue, although not necessarily within the ESD (e.g. GRID), and many more have begun in the last few years. Within this section of the Annual Report we present current geothermal activities subdivided into five general project areas:

1. Geothermal Exploration Technology
2. Geophysical Studies at Cerro Prieto
3. Utilization and Conversion Technology
4. Reservoir Engineering
5. Underground Thermal Energy Storage

At present Exploration Technology projects are concerned with generic research, the goal of which is to develop new or improve existing geophysical exploration methods--mainly electric, electromagnetic, and seismic. Testing and verification of research results were done by LBL at various geothermal sites as part of site-specific resource assessments (e.g., Mt. Hood and Klamath Falls, Oregon) or as site-specific reservoir definition studies.

Among the latter, Geophysical Studies at Cerro Prieto represent an integrated geophysical program, part of the joint DOE-CFE agreement to study the reservoir. The geophysical work is to help define reservoir boundaries, to determine reservoir rock parameters and to commence seismic and subsidence monitoring of the field.

Utilization and Conversion Technology projects deal with (a) development of analytical tools and data needed to better understand how geothermal energy can be utilized economically, and (b) technical support on various DOE field and demonstration plant operations. Most of the conversion technology projects are focused on the binary-cycle process because this is likely to be the method chosen to exploit moderate-temperature resources. The direct-contact heat-exchange process is also being studied because of its potential importance to the economics of second-generation geothermal power plants.

Reservoir Engineering studies fall into three main categories. The first is developing and testing new well-test and numerical-modeling techniques for studying reservoir behavior under production conditions and determining resource size and reservoir longevity under various production/injection scenarios. Much of the LBL work is directed to the problem of two-phase flow in boreholes and within reservoir rocks. The second category is evaluating specific geothermal reservoirs (e.g., East Mesa, California, and Cerro Prieto, Mexico). The third category is management services for the U.S. Department of Energy, Division of Geothermal Energy (DOE/DGE). LBL manages both the Geothermal Reservoir Engineering Management Program (GREMP) and the Geothermal Subsidence Research Program (GSRMP).

Aquifer Thermal Energy Storage involves finding practical, low-cost methods for storing and retrieving hot water from underground geologic formations. Generically different from geothermal fluids, these hot waters are man-made--usually waters produced in conjunction with heat generating systems (solar or electric power plants). However, many of the techniques developed for modeling and studying natural geothermal systems can be applied to aquifer thermal storage.

Geothermal Exploration Technology

The geothermal exploration technology program at LBL began in 1973 in response to an AEC desire to install a 10-MW geothermal demonstration plant in northern Nevada, where numerous hot springs exist. Scientists at LBL and the University of California were requested to assist with site selection by performing geological, geochemical and geophysical investigations in selected promising areas. Although the goal for a demonstration plant was later dropped by ERDA, LBL was requested to continue with the research, changing the emphasis from site selection to exploration technique development and demonstration. As a result, conventional as well as less standard exploration techniques were tested. Available state-of-the-art equipment and techniques were used, but where these were either unavailable or inadequate for the task, new hardware and computer methods were developed by LBL. Among these were instruments and techniques for sampling and analyzing spring waters, up-down counters (signal averagers) and synchronous detectors for use in electrical-electromagnetic surveys, a modern seismic system, and various new computer techniques for data processing and interpretation. Although the northern Nevada work was concluded in fiscal year 1976 and numerous topical and site-specific reports have been issued since then, the geothermal exploration technology program continues.

The objectives of the program are:

1) to extend the state-of-the-art in geothermal exploration and reservoir delineation by developing new and improved exploration instruments, data processing/interpretation techniques, and exploration strategies; and

2) to apply the new technology by means of field surveys at geothermal areas, and to distribute the technology by means of well-documented case studies, demonstrations, and industry-coupled programs.

ELECTRICAL AND ELECTROMAGNETIC COMPUTER MODELING TECHNIQUES

K. H. Lee, D. Pridmore, M. Hoversten, and H. F. Morrison

INTRODUCTION

Since the beginning of the geothermal exploration technology project, computer modeling for electrical and electromagnetic (EM) geophysical methods has been an area of continuing interest and one in which considerable progress has been made. This work has been done by faculty, staff, and students in Engineering Geoscience, Department of Materials Science and Mineral Engineering, U.C. Berkeley, working through LBL.

The principal objective has been to optimize the use of electrical and electromagnetic techniques for geothermal exploration and reservoir delineation, transferring the knowledge gained to the geothermal industry through reports, journal articles, demonstrations, and consultations with industry representatives requesting advice and assisstance. The basic effort has been in developing new or improved numerical methods for interpreting electric/electromagnetic survey data. Geothermal areas are often geologically complex and this has prompted the need to extend computations into the realm of two- and three-dimensional models. Our ability to deal with these more realistic models has allowed us to improve our evaluation of various techniques, to interpret survey results in a more rigorous manner than previously possible, and to apply new techniques for which adequate interpretational procedures have not been available.

Results of these studies have been directly and immediately applicable to many LBL geothermal projects, notably the development of the controlled-source EM system (EM-60) and site-specific geothermal resource studies in northern Nevada; Cerro Prieto, Mexico; and Mt. Hood and Klamath Basin, Oregon.

Although we and others (University of Utah and USGS) working in this area have achieved considerable success, numerous problems remain, including that of developing simpler, more cost-effective algorithms for geologically complex areas. This problem was raised in a workshop on modeling electrical and electromagnetic methods organized by LBL and the University of Utah in May 1978 (Lawrence Berkeley Laboratory, 1978). Participants reported on recent progress, including problems encountered in applying various modeling techniques.

Conclusions on the state of modeling techniques are as follows: The classical techniques give satisfactory solutions to the scalar electromagnetic problems and one-, two-, and possibly three-dimensional resistivity problems. That is, the solutions are relatively well documented in the literature and the problems can be solved at reasonable expense on available computers. Solutions to vector EM problems, such as dipole sources over a two- and three-dimensional earth, require significant computational resources when approached by classical techniques. Research into hybrid techniques, use of different basis functions, and special methods for certain models is needed for this class of problem.

ACCOMPLISHMENTS IN 1978

TM-Mode Plane Wave Scattering

A numerical solution for two-dimensional TM-mode plane wave scattering has been obtained using an integral equation technique (Lee and Morrison, in preparation). In conjunction with the TE-mode solution (Hohmann, 1970), the TM-mode solution obtained completes the scattering analysis for arbitrary plane waves incident on simple two-dimensional inhomogeneities.

A remarkable advantage of the integral equation approach can be found in a magnetotelluric study. For simple inhomogeneities, such as a thin dyke or some other small conductors buried in a homogeneous half-space, it is shown that the computing cost with this method is much lower than that required for the finite element solution (Ryu, 1971). However, costs of the two methods become effectively the same for a model whose cross-sectional area is approximately 10 squared skin depths, which in finite element analysis is equivalent to 40 square cells of 0.5 x 0.5 skin depths.

MT Modeling

Intensive MT modeling has been carried out for the interpretation of the Grass Valley MT data collected in 1977. The program we used is TEM, a finite-element algorithm written by Ryu (1971) and later modified by Lee et al. (1978).

The program first computes the scalar electric fields or scalar magnetic fields, depending upon the mode (TE or TM) of the incident plane wave. The transverse components are then numerically calculated using Maxwell's equations, from which we calculate apparent resistivity.

A short compendium of apparent resistivity pseudosections over a series of two-dimensional models have been prepared and distributed (Lee et al., 1978). Interpretation of the Grass Valley MT data is based on this compendium and a report is in preparation (Morrison et al., in preparation).

EM Scattering

A solution has been developed for the EM scattering by an arbitrary two-dimensional distribution of subsurface conductivity due to an oscillating magnetic dipole located on or above the earth's surface. The problem is essentially three-dimensional, but since the half-space geometry is two-dimensional, the electromagnetic problem can be reduced to two dimensions by Fourier transformation. A finite-element technique is used on the discretized two-dimensional grid.

Until now, important two-dimensional geologic models approximating fault contacts and large tabular bodies (dykes, ore zones, etc.) have not been successfully treated for dipolar source fields. This is because existing three-dimensional modeling techniques, using either the finite difference or the finite element method, are extremely expensive to use. By reducing the model to a more tractable two-dimensional problem we will obtain needed solutions at lower cost.

A computer program, MDP2D (Lee, 1978), has been written and tested on a variety of simple models. The major restriction to this program is a common one for numerical techniques--the solution is somewhat questionable when high conductivity contrasts are involved in the model, i.e., $>10^3$. However, for the more realistic models where conductivity contrasts is $< 10^3$, the program generates reasonably good results.

Three-Dimensional Finite Element Modeling

Work continued on the evaluation of a finite-element program for the modeling of magnetotelluric phenomena in three dimensions. The finite-element scheme used electric fields as unknowns (Pridmore, 1978). It was found that the convergence of the iterative scheme used to solve the system of equations was extremely slow. In its present form the program is satisfactory only for calculating magnetic fields over three-dimensional bodies, since the derivatives of the unknowns converge significantly faster than the unknowns themselves. A direct solution would overcome this difficulty, but would cost significantly more.

A hybrid modeling scheme that uses both finite elements and Green's functions (integral equations) is being investigated. The method, which is similar to that reported by Scheen (1978), uses finite elements only in the region around the inhomogeneities. The secondary fields from the inhomogeneities at the edge of the finite element mesh are calculated using Green's functions. The technique can handle the same restricted class of models handled by the integral equation method; namely, models for which a Green's function can be calculated. The integral equation method yields a full matrix and the hybrid method gives a sparse matrix but requires many more evaluations of the Green's function. Initial computations suggest that the hybrid scheme will be more effective than the integral equation method for earth models where a large compact region is inhomogeneous. The algorithm is being written to facilitate modeling of an extremely important geological problem, that is, a good conductor beneath an irregular conducting overburden.

Frequency and Time Domain Prospecting Systems

In electromagnetic prospecting, measurements can be made in one of two ways. One is the frequency domain, where data are measured as a function of transmitter frequency. In this case measurements are made of the total field, composed of a primary field (due solely to the transmitter) and secondary fields (due to induced currents in the ground). The second possible

measurement domain is the time domain, where secondary fields, which are produced from eddy currents induced while the transmitter is on, are measured as they decay after the transmitter has been shut off.

The question of which measurement domain is best suited for detecting and resolving particular targets in the presence of geologic noise has been and continues to be a topic of much debate within geophysical circles. In order to address this question, we have developed a computer program to calculate the time-domain response of a layered earth to various commonly used primary wave forms. Using this program, together with our earlier programs that calculate the frequency domain response of a layered earth, we are investigating how changes in an earth model translate to change in frequency and time-domain response. Particular emphasis is on defining which changes can be detected with presently available field equipment.

In addition, the usefulness of both types of data in resolving a particular model, in the generalized least-squares sense, will be investigated using inversion techniques.

ACTIVITIES PLANNED FOR 1979

Numerous MT data have been collected and processed by our group in the past. These data will be interpreted with the help of the existing TEM program and the integral equation solution TEMINTG. We also expect to document these programs for the public in the immediate future.

Another important plan for 1979 is to analyze the ground EM (EM 60) data. This requires an extensive two-dimensional as well as three-dimensional EM modeling. Program MDP2D will be used for the two-dimensional analysis.

In addition to the planned interpretation of field data, there will be a substantial effort in the development of EM modeling programs. We are working on a hybrid EM modeling technique for the three-dimensional scattering problem. The grounded electric dipole source over a two-dimensional half-space will be implemented in the program MDP2D in order to increase the versatility of the program.

ACKNOWLEDGMENTS

During part of fiscal year 1978 we were fortunate to have the expertise and counsel of Drs. Keeva Vozoff and George Jiracek, on sabbatical leave from Macquarie University, Australia, and the University of New Mexico, respectively. Their interests are in electrical and electromagnetic methodologies and modeling.

REFERENCES CITED

Hohmann, G., 1970. Electromagnetic scattering by two-dimensional inhomogeneities in the earth. PhD thesis, Berkeley, University of California.

Hoversten, M., Dey, A., and Morrison, H. F., in preparation. A comparison of least square techniques for the inversion of dc resistivity data. Berkeley, Lawrence Berkeley Laboratory.

Lawrence Berkeley Laboratory, 1978. Proceedings, Workshop on modeling of electrical and electromagnetic methods, May 17-19, 1978, Berkeley, Lawrence Berkeley Laboratory, LBL-7053, 203 p.

Lee, K. H., 1978. Electromagnetic scattering by a two-dimensional inhomogeneity due to an oscillating magnetic dipole. PhD thesis, Berkeley, University of California, LBL-8275.

Lee, K. H., Labson, V., Wilt, M., and Goldstein, N., 1978. Catalogue of magnetotelluric apparent resistivity pseudosections over two-dimensional models. Berkeley, Lawrence Berkeley Laboratory, LBL-7057.

Lee, K. H., and Morrison, H. F., in preparation. TM-mode plane wave scattering by two-dimensional inhomogeneities. Berkeley, Lawrence Berkeley Laboratory.

Morrison, H. F., Lee, K. H., Oppliger, G., and Dey, A., in preparation. Magnetotelluric studies in Grass Valley, Nevada. Berkeley, Lawrence Berkeley Laboratory.

Pridmore, D. F., 1978. Three-dimensional modeling of electric and electromagnetic data using the finite element method. PhD thesis, Department of Geology and Geophysics, University of Utah.

Ryu, J., 1971. Low frequency electromagnetic scattering. PhD thesis, Berkeley, University of California.

Sheen, S. L., 1978. EMMMMA, a computer program for three-dimensional modeling of airborne electromagnetic surveys, in Proceedings, Workshop on modeling of electrical and electromagnetic methods, May 17-19, 1978. Berkeley, Lawrence Berkeley Laboratory,LBL-7053.

MINICOMPUTER FOR IN-FIELD PROCESSING OF MAGNETOTELLURIC DATA

R. H. Koch, W. M. Goubau, T. D. Gamble, R. F. Miracky, and J. Clark

INTRODUCTION

Magnetotelluric (MT) data consist of records of the natural, low-frequency time-varying magnetic [$\vec{H}(t)$] and electric [$\vec{E}(t)$] fields measured at the surface of the earth. From this information we hope to define the electrical properties of the subsurface through the impedance tensor $\underline{\underline{Z}}(\omega)$ which is defined as

$$\vec{E}(\omega) = \underline{\underline{Z}}(\omega)\ \vec{H}(\omega) \quad ,$$

where $\vec{E}(\omega)$ and $\vec{H}(\omega)$ are the Fourier components of $\vec{E}(t)$ and $\vec{H}(t)$ at the angular frequency, ω. The determination of $\underline{\underline{Z}}(\omega)$ from the raw data requires considerable data processing. In the past we acquired the raw data in analog form on FM magnetic tapes which then had to be returned to the laboratory for processing. Data tapes were first digitized and played back for visual editing so that obviously bad sections could be deleted. The acceptable data blocks were divided into time segments that were Fourier transformed, and the Fourier components averaged over many time segments. All of the average crosspowers and autopowers of the fields required for the determination of $\underline{\underline{Z}}(\omega)$ and the errors in $\underline{\underline{Z}}(\omega)$ were then computed. For our MT surveys we typically occupy six to eight stations, taking 6 hr of data per site. Thus, the subsequent data processing, particularly the digitizing and visual screening, become very time consuming and tedious.

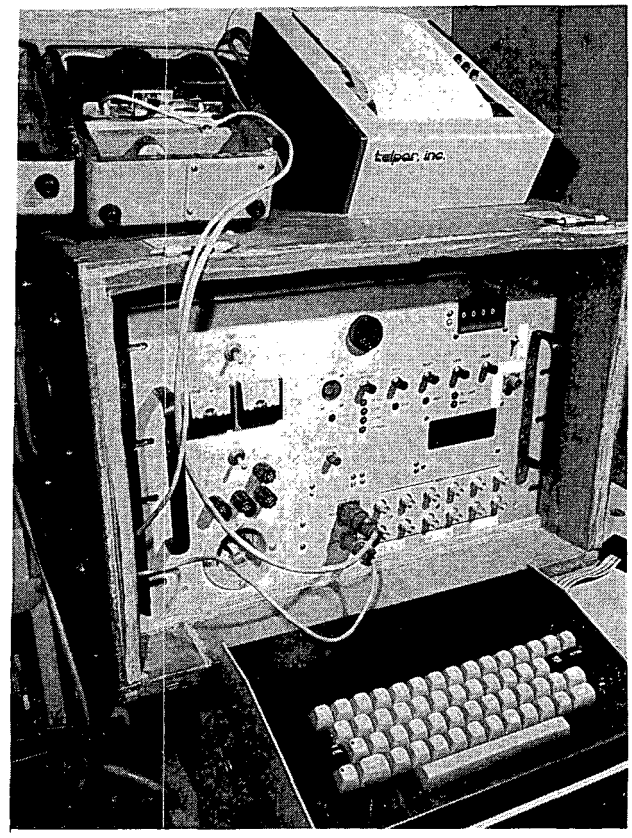

CBB 7811-14981

Figure 1. Mobile battery-powered digital data acquisition system showing the LSI-11 minicomputer with keyboard, cassette tape recorder, and thermal printer.

ACTIVITIES IN FISCAL YEAR 1978

We have designed and field-tested a battery-operated data acquisition system (Figure 1) for on-site processing of MT data. The system, which is the first of its kind, uses an LSI-11 minicomputer to digitize data, compute Fourier transforms, and compute average crosspowers and autopowers. The analog records are digitized in real time with a 12-bit analog-to-digital converter that has a selectable sampling period ranging from 4 ms to 6000 s. After 1024 samples of each field are taken, a fast Fourier transform is performed. All of the 15 possible crosspowers and six autopowers that can be formed from the horizontal components of $\vec{E}(\omega)$, $\vec{H}(\omega)$, and the reference magnetic field $R(\omega)$, are computed for each Fourier harmonic. The number of values of other crosspower and autopower is reduced from 1024 to 15 by band averaging the products contained within neighboring frequency windows of width $\Delta f \approx f_o/3$, where f_o is the center frequency of the band. The resultant numbers are stored in memory. The fields are then resampled and the processing repeated; the new cross- and autopowers are then averaged with the previous values. The operator can manually abort a data segment so that bad data resulting from equipment failure or excessive noise will not be averaged with the good data already in storage. At the end of a recording session, the average cross- and autopowers are dumped into a cassette tape that is returned to the laboratory for the final calculation of $\underline{\underline{Z}}(\omega)$, the statistical errors in $\underline{\underline{Z}}(\omega)$, and the functions of $\underline{\underline{Z}}(\omega)$ that are relevant to interpreting MT data.

We tested the data acquisition system over a two-week period during an MT survey near Milford, Utah. The system operated flawlessly throughout the survey.

PLANS FOR FISCAL YEAR 1979

In the future we hope to upgrade the system with additional input/output devices so that complete in-field processing will be possible. In this regard, we are preparing a program to normalize or correct all average powers for system sensitivities and variable gain settings. We will also adapt an existing program for in-field calculation of various parameters of the impedance tensor, for example, tensor rotation, skewness, and error bars.

ACKNOWLEDGMENTS

Work supported in part by the Division of Materials Sciences, Office of Basic Energy Sciences, U.S. Department of Energy, and in part by the Division of Geothermal Energy, U.S. Department of Energy.

SUPERCONDUCTING THIN-FILM GRADIOMETER AND MAGNETOMETERS FOR GEOPHYSICAL APPLICATIONS

W. M. Goubau and J. Clarke

INTRODUCTION

Superconducting thin-film magnetometers and gradiometers have applications in various geophysical techniques. Recently a number of commercial and research organizations have begun using SQUID magnetometers for magnetotelluric studies because of the higher sensitivity and somewhat easier portability of SQUIDs compared with induction coil magnetometers. A three-component SQUID magnetometer is also used as the detector in the controlled-source electromagnetic studies conducted at LBL with the EM-60 system.

A superconducting gradiometer incorporating a SQUID can be used to detect very small changes in the gradient of an external magnetic field. Such devices have applications in sorting out local magnetic signals with a high spatial gradient in the presence of a large, but more uniform, background magnetic field. These devices also have potential applications in applied geophysics and for studying the characteristics of local noise effects on natural signals from magnetospheric and ionospheric sources.

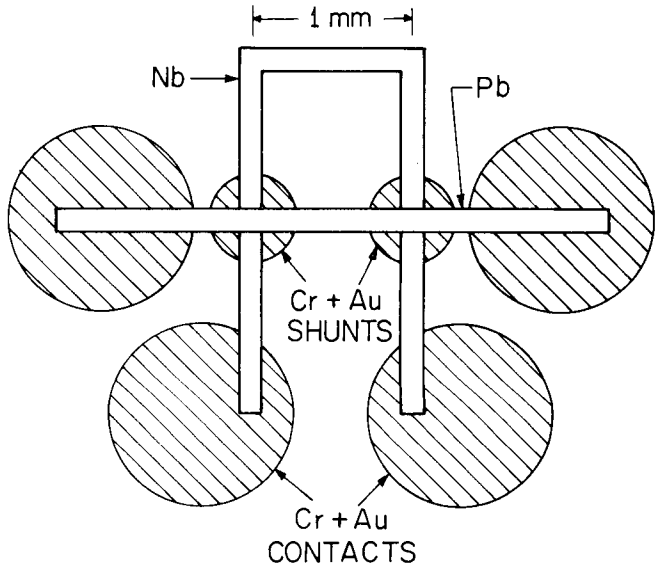

(XBL 7710-6155A)

Figure 1. Configuration of thin-film magnetometer.

ACTIVITIES IN FISCAL YEAR 1978

To have a better SQUID magnetometer for use with the EM-60 system, we decided that high sensitivity could be sacrificed to achieve a higher slewing rate, that is, the ability to track fields at higher frequencies. For this reason a planar, thin-film device similar to that shown in Figure 1 was built, tested, and incorporated into a complete magnetometer. This SQUID has a sensitivity of about 2×10^{-4} $\gamma/\sqrt{Hz}$* and a slewing rate of 2×10^{-4} G/sec at 1 kHz. It is a factor of 20 less sensitive than our cylindrical SQUIDs, but has a factor of 3 higher slewing rate. The device is easy to fabricate and three have been mounted in an orthogonal array within a cryostat to make a three-axis magnetometer.

Research continues on the use of thin-film dc SQUID galvanometers for measuring magnetic field gradients. Figures 2 and 3 show the configurations of SQUID and SQUID assembly that have been built and tested in the laboratory. The particular gradiometer shown in Figure 3 was used in two configurations. When the Pb

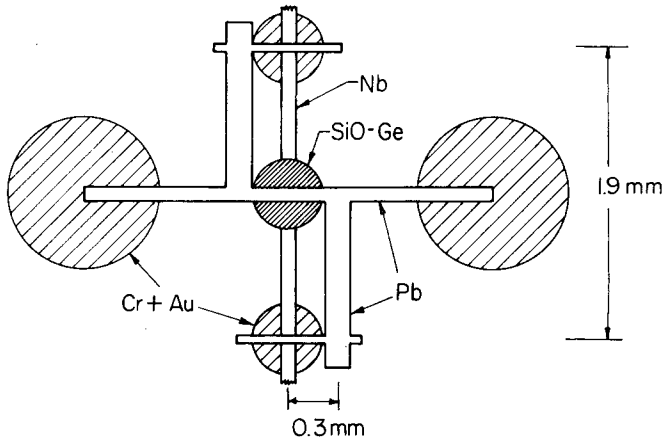

(XBL 7710-6155B)

Figure 2. Configuration of dc SQUID galvanometer.

strips were cut at points "A" the pick-up loops were in parallel, cut at points "B" they were in series. In either case, this gradiometer measured the off-diagonal gradient $\partial H_z/\partial x$. The gradient sensitivity was determined by measuring the response to a known flux imbalance

*1 gamma = 10^{-5} gauss = 1 nanotesla.

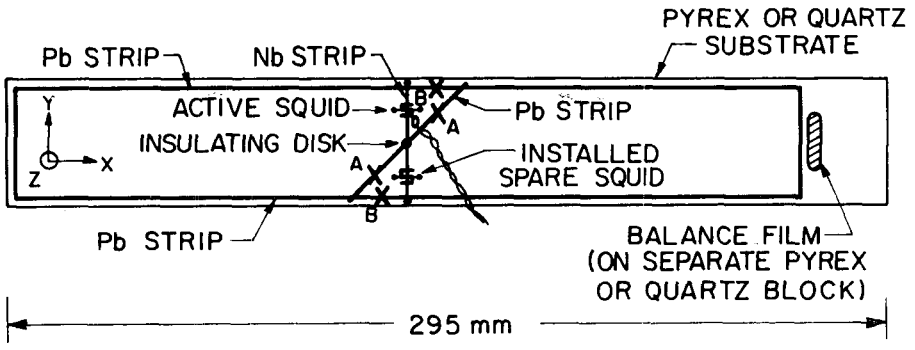

(XBL 7710-6145B)

Figure 3. Configuration of thin-film gradiometer.

between the pick-up loops. The sensitivities of the series and parallel-loop gradiometers were 3.7×10^{-4} $\gamma/m\sqrt{Hz}$ and 2.1×10^{-4} $\gamma/m\sqrt{Hz}$ respectively. These values were in good agreement with our theoretically predicted values.

PLANNED ACTIVITIES FOR FISCAL YEAR 1979

The lower sensitivity, higher slewing rate magnetometer will be tested in the field with the EM-60 system and direct comparisons of the two devices will be made.

Continued work is needed to design better gradiometers consisting entirely of thin films. In a future design, one would use photolithographic techniques to deposit films with a linewidth of about 5 μm and with a high degree of symmetry. Gradiometers made in this way should have an improved initial balance in the z-direction, and also in the x- and y-directions. We believe that in the present design the x- and y-balance are limited by the distortion of the magnetic field by the overlapping films in the SQUID, and a reduction in the volume of these films should correspondingly reduce the distortion. Furthermore, if the film widths were reduced by a factor of 30, the resolution of the SQUID, which is proportional to (film width)$^{1/2}$, should be improved by a factor of about 5. With the aid of photolithography, one could also make second derivative gradiometers, which would be particularly suitable for medical applications. Finally we note that this type of gradiometer may be particularly suitable for commercial production, since it involves only thin-film techniques that are well established in certain industries.

MAGNETOTELLURICS WITH SQUID MAGNETOMETERS

T. D. Gamble, W. M. Goubau, R. F. Miracky, and J. Clarke

INTRODUCTION

Magnetotellurics (MT) is a widely-used technique for subsurface mapping and has applications in fundamental geological, geothermal, oil and gas and mineral investigations (Vozoff, 1972). The goal of MT is to determine accurately the electromagnetic impedance tensor $\underline{\underline{Z}}(\omega)$ at the surface of the earth. $\underline{\underline{Z}}(\omega)$ relates the components of magnetic fields (H) resulting from disturbances in the ionosphere, and the components of the electric fields (E) induced at the surface of the earth through the relation $\vec{E}(\omega)=\underline{\underline{Z}}(\omega)\vec{H}(\omega)$. In the analysis of data $\vec{E}(\omega)$ and $\vec{H}(\omega)$ are treated as two-components column vectors and $\underline{\underline{Z}}(\omega)$ as a 2x2 matrix of complex terms. The matrix may be rotated analytically into a geographic orientation for which $|\underline{\underline{Z}}_{xx}|^2 + |\underline{\underline{Z}}_{yy}|^2$ is a minimum. The resulting off-diagonal terms, $\underline{\underline{Z}}_{xy}$ and $\underline{\underline{Z}}_{yx}$, are usually unequal and are assumed to describe the impedances in the principal electrical directions, which depend on local geology. From $\underline{\underline{Z}}_{xy}$ and $\underline{\underline{Z}}_{yx}$ it is customary to calculate apparent resistivity, $\rho_{ij} = 0.2T\,|\underline{\underline{Z}}_{ij}|^2$, ij = xy, yx. Here ρ is expressed in ohm·m, T is the period in seconds, and $\underline{\underline{Z}}$ is in (mV/km)γ, where $\gamma = 10^{-5}$ G.

One standard way to estimate $\underline{\underline{Z}}$ has been to express it in terms of cross- and autopower of the horizontal, orthogonal components of $\vec{E}$ and $\vec{H}$ (Madden and Nelson, 1964). For example, one could write

$$\underline{\underline{Z}}(\omega) = [EH]\,[HH]^{-1} \qquad (1)$$

where [AB] is the matrix of auto- and cross-spectral terms

$$[AB] = \begin{pmatrix} \overline{A_x B_y^*} & \overline{A_x B_x^*} \\ \overline{A_y B_x^*} & \overline{A_y B_y^*} \end{pmatrix} \qquad (2)$$

Unfortunately, such an expression for $\underline{\underline{Z}}$ contains positive definite noise contributions which do not average to zero regardless of how many data are acquired and analyzed, and can cause substantial bias errors in estimates of $\underline{\underline{Z}}$, especially at frequencies at which the magnetotelluric signals are small (Goubau, et al., 1978a).

ACCOMPLISHMENTS IN FISCAL YEAR 1978

Although various workers have recognized the problems and have proposed methods for eliminating bias errors, we have derived and tested a simple solution involving simultaneous measurements of the magnetic field at a remote site as a reference for the local signals (Gamble, et al., 1978a). We can then express the impedance tensor as $\underline{\underline{Z}}(\omega) = [ER][HR]^{-1}$, where $\vec{R} = (R_x, R_y)$ is the remote magnetic field. Provided there is no correlation between local signals and the noises in the remote signals, this estimate for $\underline{\underline{Z}}$, which we designate as $\underline{\underline{Z}}^R$, will be unbiased. Any crosspowers involving noise contributions will average to zero in the limit of an infinitely large data sample.

In the absence of bias errors, the accuracy of $\underline{\underline{Z}}^R$ is determined only by random errors. These can be minimized by averaging over many data sets. An estimate of these errors should be made, and confidence limits placed on all quantities derived from $\underline{\underline{Z}}^R$. In the past, no rigorous error analysis applicable to MT was available. We have found that such an error analysis is in fact possible for the remote reference method (Gamble, et al., 1978b).

The error $\underline{\underline{\Delta}}$ in $\underline{\underline{Z}}^R$ is given by

$$\underline{\underline{\Delta}} = [\eta R][HR]^{-1} \tag{3}$$

where η is the total noise contributed by $\vec{E}$ and $\vec{H}$, defined by

$$\vec{\eta} = \vec{E} - Z^R \vec{H} \quad . \tag{4}$$

The variance in the ij^{th} ($i = x,y$, $j = x,y$) element of $\underline{\underline{Z}}^R$ can be written as

$$<|\Delta_{ij}|^2> = \overline{|\eta_i|^2}\,\overline{|A_j|^2}/N|D|^2 \quad , \tag{5}$$

where $<\,>$ denotes an ensemble average,

$$\begin{aligned} A_x &= R_x \overline{H_y^* R_y} - R_y \overline{H_y^* R_x} \quad , \\ A_y &= R_y \overline{H_x^* R_x} - R_x \overline{H_x^* R_y} \quad , \\ D &= \overline{H_x R_x^*}\,\overline{H_y R_y^*} - \overline{H_x R_y^*}\,\overline{H_y R_x^*} \quad , \end{aligned} \tag{6}$$

and N is the number of terms in each average crosspower, The error $\underline{\underline{\Delta}}$ tends to zero as N increases. Thus, for a sufficiently large collection of data we can find the error in any function, ξ, of $\underline{\underline{Z}}^2$ by carrying out a Taylor expansion to first order in Δ_{ij} and Δ_{ij}^*. The variance in ξ can then be written simply as

$$\mathrm{Var}(\xi) = \sum_{k=1}^{4} G_{kk} <|\Delta_k|^2> + 2\mathrm{Re}\left[\sum_{k=1}^{3} \sum_{\ell=k+1}^{4} G_{k\ell} <\Delta_k \Delta_\ell>\right] . \tag{7}$$

where

$$G_{k\ell} = G_{\ell k}^* = \frac{d\xi}{dZ_k}\frac{d\xi^*}{dZ_\ell^*} + \frac{d\xi}{dZ_\ell^*}\frac{d\xi^*}{dZ_\ell} \quad , \tag{8}$$

and k and ℓ are labels for the xx, xy, yx, and yy components of $\underline{\underline{\Delta}}$. With the change in notation $\Delta_k (k = 1,2,3,4) \leftrightarrow \Delta_{ij} (i = x,y, j = x,y)$, $<\Delta_k \Delta^*>$ can be expressed in terms of known cross- and autopowers of the fields according to the expression

$$<\Delta_{ij}\Delta_{nm}^*> = \overline{\eta_i \eta_n^*}\,\overline{A_j A_m^*}/N|D|^2 \tag{9}$$

The confidence limits for ξ depend on the distribution of errors as well as on the variance. By the central limit theorem we know that the distribution will be normal for large N, independent of the distribution of noises in the fields. Thus, confidence limits are particularly easy to compute.

Our study of the statistics of the estimation of $\underline{\underline{Z}}^R$ has produced other equations that should be valuable in many other applications (Gamble, 1978). The signal power-spectral matrix of the ionospherically generated electric signals, $[E_s E_s]$, can be estimated by the quantity

$$\underline{\underline{Z}}^R[HE] = [ER][HR]^{-1}\,[HE] \quad . \tag{10}$$

Similar expressions hold for the magnetic and reference signal powers. Thus the ionospherically and locally generated signals can be separated and studied independently. Our ability to separate the contributions to the total signal permits us, for instance, to measure the noise power spectra of magnetometers in an unshielded environment.

During 1978 we have applied the remote reference technique to magnetotelluric surveys in Bear Valley, California; Grass Valley, Nevada; Cerro Prieto, Mexico; and Roosevelt Hot Springs, Utah. The area surveyed near Cerro Prieto is illustrated in Figure 1 (Gamble, et al., 1978c). Magnetotelluric measurements were taken at the locations numbered 1 through 7; the remote reference fields were measured at the position labeled R. Three-axis SQUID magnetometers were used to measure the magnetic field fluctuations, and the orthogonal electric fields were measured from the electric potential between pairs of buried copper-copper sulfate electrodes, 200 m apart. The data from the remote site were telemetered to the local site and all of the remote

and local signals were recorded simultaneously on tape. The tape was subsequently analyzed using the Lawrence Berkeley Laboratory CDC 7600 computer.

As an example of the results, the apparent resistivities, skewness, and strike angle as a function of period for station 6 are plotted with their probable errors in Figures 2 and 3. The skewness W, defined as $W = |(\underline{\underline{Z}}_{xx} + \underline{\underline{Z}}_{yy})/(\underline{\underline{Z}}_{xy} - \underline{\underline{Z}}_{yx})|$, is a measure of the complexity of the conductivity of the earth. If W is large, the structure at the site must be three-dimensional at those frequencies. The apparent strike angle is the angle by which $\underline{\underline{Z}}$ is rotated to minimize the quantity $|\underline{\underline{Z}}_{xx}|^2 + |\underline{\underline{Z}}_{yy}|^2$. We observe that the quantities plotted here are smooth functions of the period, and exhibit no observable bias errors in the region where the signal-to-noise ratios are smallest (around 10 sec period). The errors shown as the error bars for the 50% confidence level are generally very small. For example, in the apparent resistivities, 80% of the points shown have probably errors of less than 2.5%. The largest probable errors, up to 10% occur in ρ_{yx} at long periods for which the least quantity of data are available and where we normally expect problems in estimating the average power accurately. These data are typical of the high-quality results that have been obtained using the remote reference technique.

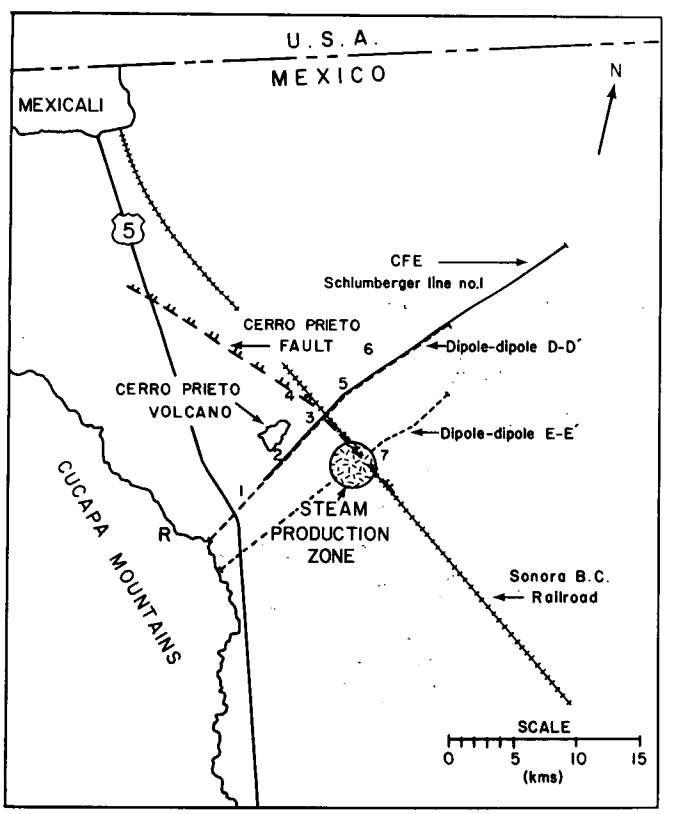

XBL 789-11107

Figure 1. Magnetotelluric sounding sites (1-7) near the Cerro Prieto geothermal field.

Beginning with the survey at Roosevelt Hot Springs, we are now able to perform in-field A-to-D conversion of all data sets and computation of all auto- and crosspower spectra by means of an LSI-11 computer mounted in the instrument rack.

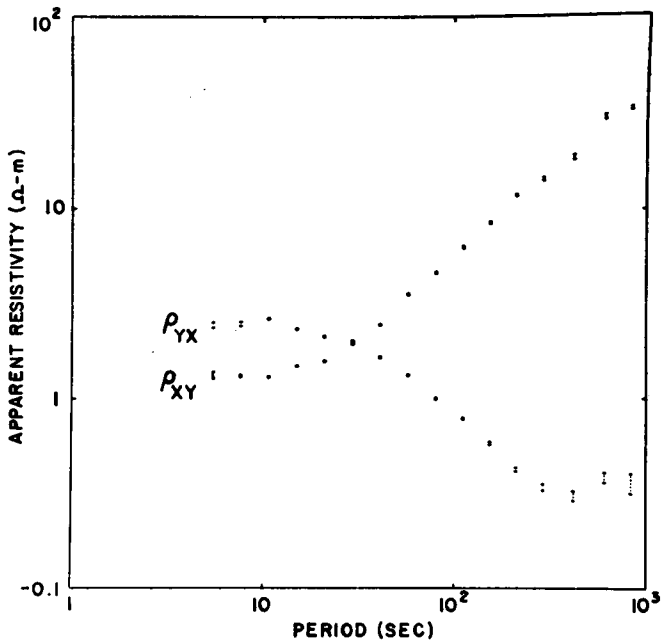

XBL 7810-5963

Fig. 2. Apparent resistivities in the coordinate system aligned with the apparent strike direction, location 6.

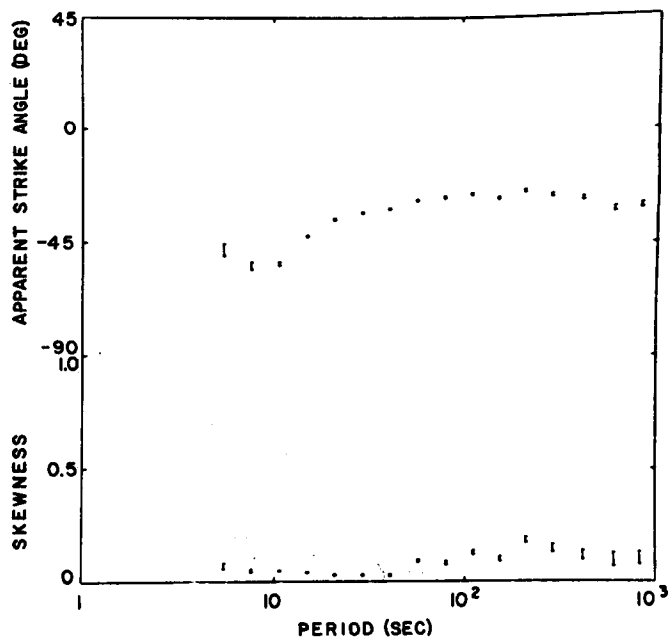

XBL7810-5957

Fig. 3. Apparent strike direction (relative to magnetic north) and skewness at location 6.

PLANS FOR FISCAL YEAR 1979

The data from Nevada and Utah are still in the process of analysis; however, considerable quantities of high-quality data were obtained at both sites. Both data sets will be completely analyzed and interpreted.

Our remote reference technique has now been tested at a sufficient number of sites, and we are confident enough in the technique to recommend it to commercial users of MT. We have found that the necessity of a second magnetometer and the need to telemeter data from the remote site to the local site has neither reduced the speed of field operations nor created new technical problems. The technique has been shown to yield unbiased estimates of the apparent resistivity of the ground, and of other quantities of interest in mapping out the true resistivity of the ground. Furthermore, our new error analysis enables one to obtain reliable estimates of the random errors in the data. We believe that, as a result, it will now be possible to considerably improve the accuracy of resistivity models of the ground based on MT data.

REFERENCES CITED

Gamble, T. D., 1978. Remote reference magnetotellurics with SQUIDs. Ph.D. thesis, Berkeley, University of California, Lawrence Berkeley Laboratory, LBL-8062.

Gamble, T. D., Goubau, W. M., and Clarke, J., 1978a. Magnetotellurics with a remote magnetic reference. Berkeley, Lawrence Berkeley Laboratory, LBL-7032.

_____, 1978b. Error analysis for remote reference magnetotellurics. Berkeley, Lawrence Berkeley Laboratory, LBL-7085.

Gamble, T. D., Goubau, W. M., Clarke, J., and Goldstein, N. E., 1978c. Referenced magnetotellurics at Cerro Prieto, in Proceedings of the first symposium on the Cerro Prieto geothermal field, Baja California, Mexico. Berkeley, Lawrence Berkeley Laboratory, LBL-7098.

Goubau, W. M., Gamble, T. D., and Clarke, J., 1978. Magnetotelluric data analysis: removal of bias. Geophysics, v. 43, pp. 1157-1166.

Madden, T., and Nelson, P., 1964. A defense of Cagniard's magnetotelluric method. Cambridge, Mass. Inst. Tech., Geophys. Lab., Office of Naval Res., Proj. NR-371-401.

Vozoff, K., 1972. The magnetotelluric method in the exploration of sedimentary basins. Geophysics, v. 37, pp. 98-141.

CONTROLLED-SOURCE ELECTROMAGNETIC SYSTEM

H. F. Morrison, N. E. Goldstein, M. Hoversten, G. Oppliger, and C. Riveros

INTRODUCTION

In 1976, during geothermal exploration investigations in northern Nevada, tests were made of a controlled-source, deep-probing, electromagnetic (EM) system pieced together mainly with components on hand. Despite the primitive nature of the equipment, data were obtained that yielded sounding results that compared well with the results form other electrical techniques (Jain and Morrison, 1976; Jain, 1978). Because a properly engineered system would fill a technological gap in electrical prospecting, we received DOE approval in 1977 to begin design and fabrication of a large-moment system. This system, designated the EM-60 because it operates from a 60-kW motor-generator, was completed and tested in 1978.

The system is shown schematically in Figure 1. It consists of two sections: (a) a transmitter section consisting of the power source, control electronics, timing and a transistorized switch capable of handling large current; and (b) a receiver section consisting of magnetic or a combination of magnetic and electric field detectors, signal conditioning amplifiers and anti-alias filters, and a multi channel programmable receiver (spectrum analyzer). Design goals called for a system that would be relatively inexpensive to duplicate, inexpensive and easy to operate in the field, and which would also provide useable information over a broad frequency range with transmitter-receiver separations of up to several km.

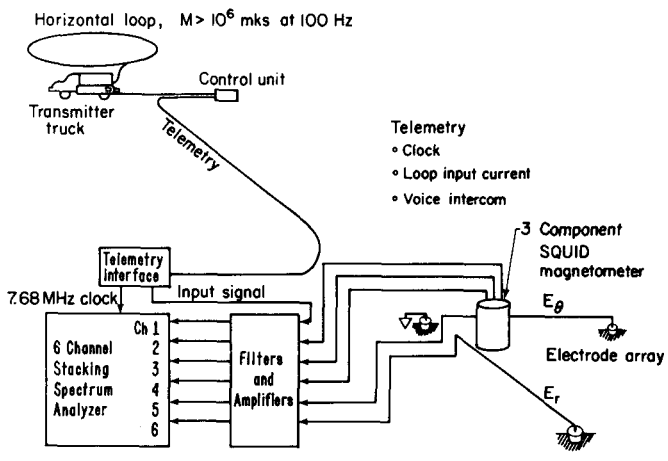

A low frequency electromagnetic prospecting system

XBL 786-2575

Figure 1. General layout of the EM-60 electromagnetic system.

Because the system does not require wires other than the transmitter loop, there would be no long wires to lay down and retrieve as there are in galvanic dc resistivity surveys. Because electrical contact to the ground is not needed, the system is suited to areas where high resistivity and high contact resistances are troublesome problems. Further, the system would also have some advantage over conventional magnetotellurics (MT) in frequency bands where MT signals are typically weak and reliable results are sometimes difficult to obtain.

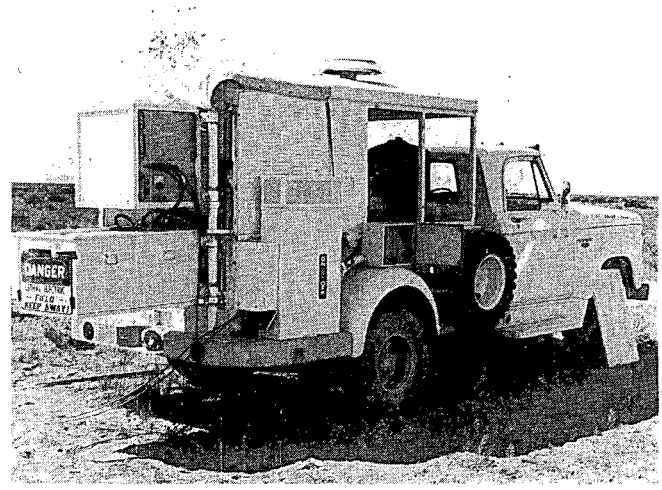

XBC 789-12515

Figure 2. The EM-60 transmitter in operation in Grass Valley, Nevada.

ACTIVITIES IN 1978

Transmitter Section

The transmitter section, designed by Carlos Riveros of the Field System Group at LBL, was completed and tested. It is powered by a Hercules gasoline engine linked to an aircraft 60-kW 400-Hz, 3ϕ alternator. These two components are mounted in the bed of a one-ton, four-wheel-drive truck. The output is full-wave rectified and capable of providing $\pm$150 V at up to 400 A to the horizontal coil. The square wave current pulses are created by means of a transistorized switch, which consists of two parallel arrays of from 6 to 60 transistors in interchangeable modules within the "crate." The crate is one box of two, the other containing the array driving electronics and timing, which pivot out of the truck during operation (Figure 2). The transmitter is operated by one man who controls the frequency of the primary magnetic field over the range of 10^{-3} to 10^{3} Hz by means of switches on a remote control box which contains a crystal-controlled oscillator and dividers (Morrison, et al., 1978).

The dipole moment is determined by the resistance and inductance of the loop. At low frequencies, below 50 Hz, inductive reactance is negligible and the dipole moment is governed by the load resistance. Four turns of #6 wire in a square or circular loop, 50 m in radius, will yield a dipole moment of about 3 x 10^{6} mks. At frequencies above about 100 Hz the inductance causes the moment to decrease and the current waveform to become quasisinusoidal. The current in the coil and the phase reference are obtained from a 0.01Ω, 0.1% shunt resistor in series with the coil. The reference voltage is transmitted to the receiver by a twisted pair of wires, where it is used for calibration and phase reference. The hard-wire links between transmitter and receiver through the twisted leads is a temporary feature of the system and will be eliminated.

Receiver Section

The key component in the receiver section is a six-channel programmable multifrequency phase-sensitive receiver (Figure 3). The receiver was designed by graduate student Gary Oppliger and built in the Engineering Geoscience Group, Department of Materials Science and Mineral Engineering, U. C. Berkeley. A three-component SQUID magnetometer served as the detector in field tests. Through the keypad on the receiver the operator is able to set the parameters controlling the signal processing, such as: (a) period of the current waveform; (b) maximum number of odd harmonics to be analyzed, up to 15; (c) number of cycles, N, to be stacked prior to Fourier decomposition in increments of 2^{N}; and (d) number of input channels of data to be processed.

The receiver operates as an independent unit in the sense that it does not depend on a control signal from the transmitter. The two operate asynchronously; each is driven by a separate crystal clock, having a frequency accuracy of only 10 ppm. Phase measurements relative to the transmitter current are made by processing the transmitter current waveform along with the magnetic field signals. This provides sufficiently accurate phase measurements so long as one limits the number of stacked waveforms to less than several thousand. Unlimited stacking can be obtained by locking transmitter and receiver clocks together through the external 7.68-MHz clock input on the receiver panel or by using more accurate internal clocks.

In operation the receiver provides the amplitude and phase, relative to the primary

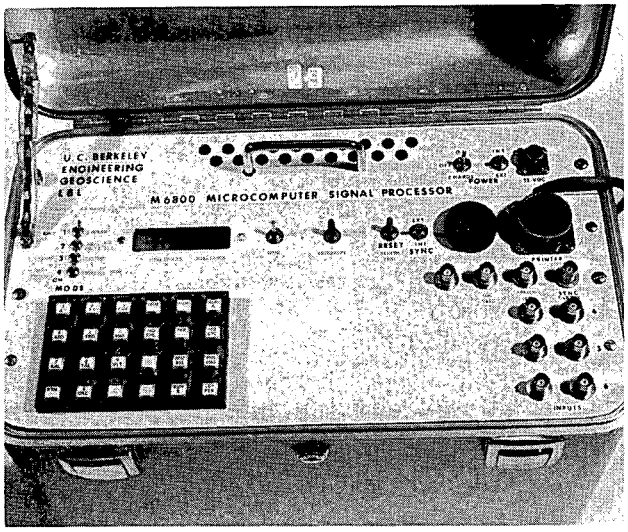

CBB 780-13519

Figure 3. The programmable microprocessor-controlled receiver for the EM-60.

field, of each component processed. These data are printed out by a battery-operated thermal printer for later analysis in the laboratory.

Data Analysis

Field tests were conducted in Grass Valley, Nevada, and Mt. Hood, Oregon, but only data from the former tests site have been fully analyzed. Analysis requires the joint inversion or the amplitude and phase spectra of the vertical magnetic (H_z) and radial magnetic (H_r) components. These values, plus the standard errors for each as determined from a statistical analysis of repeated measurements, are used to derive the best layered-earth model fitting all data sets simultaneously. Figures 4 and 5 are examples of survey results. The observed data points are shown as squares and circles, and the calculated spectra are shown as the solid and dashed lines for the best three-layer fit to the data. In this case the transmitter-receiver separation was 2 km and the data covered the range 0.02 to 200 Hz. Estimated resistivities (ρ_i) are in ohm-m and layer thicknesses (h_i) are in meters. In this area the second-layer thickness is difficult to resolve accurately because the layer is thick and conductive.

PLANNED ACTIVITIES FOR 1979

The EM-60 will be improved by substituting more accurate clocks in the transmitter and receiver sections so that the twisted lead between transmitter and receiver can be eliminated.

Displays and demonstrations of the EM-60 will be held at various sites to hasten commercialization. Among these sites will be geothermal "test areas" where good subsurface information is available. Industry will be invited to examine the EM-60 and witness the system in operation.

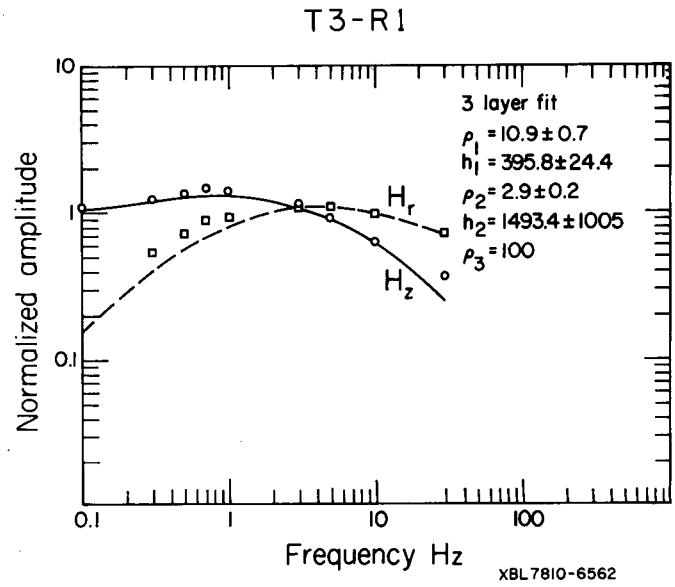

Figure 4. Observed and calculated amplitude spectra for a transmitter and receiver 2 km apart on line E-E', Grass Valley, Nevada.

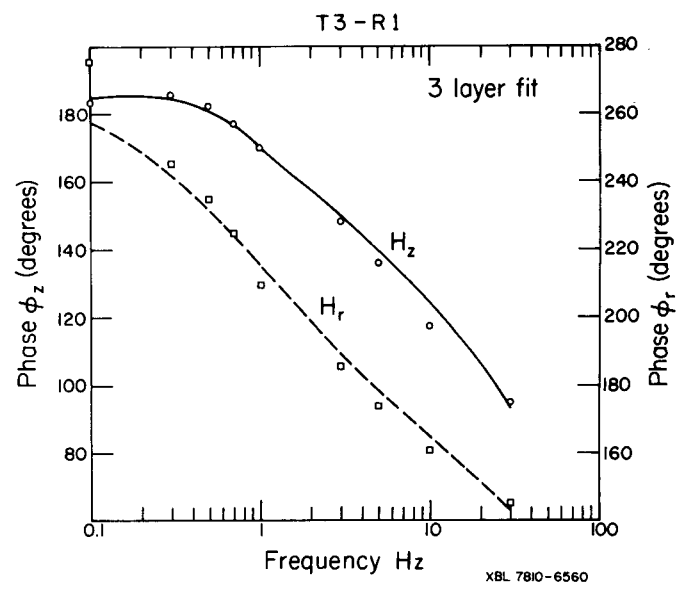

Figure 5. Observed and calculated phase spectra corresponding to Figure 4.

Further basic research needs to be done to improve data acquisition and interpretation. We plan to investigate techniques for obtaining reliable data at low frequencies where the induction effects from the earth are very small compared with the primary field and where they are small compared with the natural, geomagnetic "noise" whose amplitude follows, roughly, a 1/f dependency. We will investigate whether or not it is possible to recover data at the low-frequency end of the spectrum through the use of a noisecancelling reference magnetometer, combined possibly with measurements in the time-domain.

We are also planning to continue our efforts in data interpretation, which have not been carried beyond layered-earth models. Two-dimensional modeling is possible (Lee, 1978) and needs to be exercised in conjunction with the EM-60 results.

REFERENCES CITED

Jain, B., 1978. A low frequency electromagnetic prospecting system. D. Eng. thesis, Berkeley, University of California, LBL-7042.

Jain, B., and Morrison, H. F., 1976. Progress report, Inductive resistivity survey in Grass Valley, Nevada. Berkeley, University of California (internal report).

Lee, K. H., 1978. Electromagnetic scattering by a two-dimensional inhomogeneity due to an oscillatory magnetic dipole. Ph.D. thesis, Berkeley, University of California, LBL-8275.

Morrison, H. F., Goldstein, N. E., Hoversten, M., Oppliger, G., and Riveros, C., 1978. Description, field test and data analysis of a controlled-source EM system (EM-60). Berkeley, Lawrence Berkeley Laboratory, LBL-7088.

GEOTHERMAL SEISMIC FIELD SYSTEM DEVELOPMENT

T. V. McEvilly, E. L. Majer, J. Bartschi, and J. Heinson

INTRODUCTION

The role of seismological methods in geothermal reservoir definition has been under investigation for several years as a part of the LBL geothermal exploration technology study. A primary goal of the research was to evaluate the several seismic techniques in general use for geothermal exploration in the early 1970s. Unlike other geophysical disciplines, seismology provides a variety of methods that can be used in exploration. Chief among these were microearthquake and ground noise surveys.

A microearthquake survey involved the deployment of portable seismographs over a prospect area. Typically, 6 to 10 seismographs were spaced 5 to 10 km apart to detect and locate small earthquakes (magnitudes of 2 to -1, generally). Such earthquakes--a sign of active stress release through faulting--were considered indicative of potential fracture porosity at depth, and possibly of anomalous thermal stresses caused by the heat. The relation between anomalous seismicity and a geothermal reservoir was much discussed but not resolved because there were too few case histories during the early stages of geothermal exploration technique development.

The use of ground noise, or the ambient microseism level, in geothermal exploration involved mapping the amplitude and frequency variation of the ubiquitous background motion over the surface of the prospect, usually with a sampling density of one station per km. The physical basis for this technique rests on the possibility that the geothermal reservoir is a dynamic system radiating seismic energy generated by a hydrothermal or thermoelastic process. Anomalous amplitudes or frequencies would thus be detectable on the surface over the reservoir. At the onset of our study, there was also spirited controversy over the viability of this method. The few reports in the open literature gave differing viewpoints.

These two methods constituted the main thrust in what was termed "passive" seismic exploration; that is, they both involved measurements of naturally occurring seismic waves, either discrete local earthquakes or the microseismic background. A third passive approach involved recording waves from distant earthquakes or explosions above the suspected reservoir zone in a search for perturbations in amplitude or arrival time. These perturbations could then be related to local anomalies by the attenuation or velocity characteristics of the subsurface. Although we have recently shown that this approach has great potential, it was not in general use by the geothermal exploration community at the beginning of our study.

Another class of seismological methods are termed "active." In general use in petroleum exploration, engineering seismology, and crustal structure studies, these methods use controlled sources, such as precisely timed explosions, and specially placed arrays of sensors. The methods include the well-known reflection and refraction profiling techniques for subsurface structure determination. Despite their highly successful application in other studies, these methods were not felt to be demonstrably practical in geothermal reservoir delineation.

Uncertainty surrounding the use of seismology in geothermal exploration was based on a lack of case histories demonstrating success and

an absence of data on the physical properties of the reservoir, which would provide a model of the target. In addition, the high cost of seismic surveys, particularly active profiling, requires solid justification in a cost-benefit sense. In contrast to petroleum exploration, for example, there are no data on which to base an estimate of ultimate yield per dollar of exploratory effort.

Our research task thus became to evaluate seismological exploration methods for geothermal reservoir detection and delineation and to reduce and simplify field procedures so as to enhance cost-effectiveness. Technique evaluation has required the collection of high-quality data from a variety of geothermal environments. A radio-telemetered 12-station portable seismic system was fabricated. It featured battery-powered central recording on slow-speed FM magnetic tape. Detailed surveys have been conducted with this system in several geothermal regions: the northern Nevada high heat-flow region with classic basin-and-range tectonics (Beyer et al., 1976); The Geysers geothermal field in the northern California coast ranges (Majer and McEvilly, 1979); the Cerro Prieto, Mexico, geothermal field in the Imperial-Mexicali Valley (Majer et al., 1978); and the youthful volcanic caldera at Cerro la Primavera in central Mexico (Majer et al., 1978). In addition, data were processed and analyzed routinely from the U. S. Bureau of Reclamation seismic network surrounding the East Mesa geothermal field in the Imperial Valley (McEvilly and Schechter, 1977a, 1977b, 1978).

Results and analyses of these studies have been published in various forms such as Ph.D. theses (Liaw, 1977; Majer, 1978); LBL reports, UCID reports, and scientific journals (Liaw and McEvilly, 1977, 1979; Majer and McEvilly, 1979). Our general conclusions are that carefully designed field experiments have detected anomalies in microearthquake activity, seismic wave velocities, and seismic wave attenuation at one or more of the sites. At The Geysers field, anomalous velocity and attenuation appear to define the production zone. As conventionally obtained, ground noise data were found to be of little value, reflecting very shallow structure or surface hydrothermal activity.

However, an experiment for imaging on possible radiation from a deep source is being implemented by industry in at least one potential geothermal region, so the possibility of true reservoir noise should be tested soon. We have seen no indication that earthquakes associated with geothermal reservoirs possess unique characteristics. That is, we cannot define the "geothermal" earthquake. On the other hand, of the five structures surveyed, only the two producing fields exhibited seismicity clearly associated with a proven or suspected reservoir. There is some evidence that exploitation may affect seismicity, thus providing an indicator of field dynamics during production. At the same time the question of induced seismicity is introduced. At The Geysers, the earthquakes are quite shallow and appear to be associated with the field margins, with low seismicity in the main production zone. These features, however, can be detected only with a very dense station network with spacings of 1 km or less.

ACTIVITY IN FISCAL YEAR 1978

From the evidence and conclusions presented above, it was clear that several seismological methods could indeed provide valuable information in a geothermal exploration program. Of equal or greater importance, they offered potential for precise monitoring techniques on reservoirs under development. However, from our experience in collecting and processing the data, it was clear that there is a need for a less labor-intensive (and therefore more economical) data acquisition and processing system. Working with a triggered low-power digital recorder at The Geysers demonstrated the time-saving value of recording only events of interest (up to 100 per day can occur), and discarding the remaining background data. Another two orders of magnitude reduction in processing costs would result if the field system could automatically reduce the significant events from entire time series to arrival times and amplitudes of phases. Therefore, the seismologist could spend more time improving and developing new techniques rather than reducing data.

A system concept was developed, based on available components, which would transfer the maximum possible degree of data processing and reduction to the field. Furthermore, the system could be used in any of the several seismic field methods we found useful in previous reservoir delineation studies. System conceptualization began in June 1978 and the prototype system design was completed in the fall. Figures 1 and 2 illustrate the concept. Individual low-cost microprocessors at each detector handle data acquisition, event recognition, phase identification and timing, amplitude and polarity determination, and spectral calculations and parameterization. Operated as a microearthquake array, the system could have up to 128 channels, each microprocessor simultaneously scrutinizing its individual input data. Information contained in the detected events would be reduced to less than 10 diagnostic parameters, which are transferred to the master system microcomputer for analysis. All the standard results are thus available in the field so that the seismologist can optimize the survey parameters and scope. Our initial study indicated that it should be feasible to perform hypocentral locations, rupture parameter estimations, and a modest beam-forming search--all with sufficient speed to keep up with an earthquake sequence at a rate of one event every few minutes. Power consumption can be held to about 1 W per channel.

Encouraged by these exercises using device specifications, a two-channel prototype system was designed for a feasibility study using real hardware and software. The RCA 1802 CMOS processor, operating in 16-bit precision with hardware multiply, was selected. Parts were ordered,

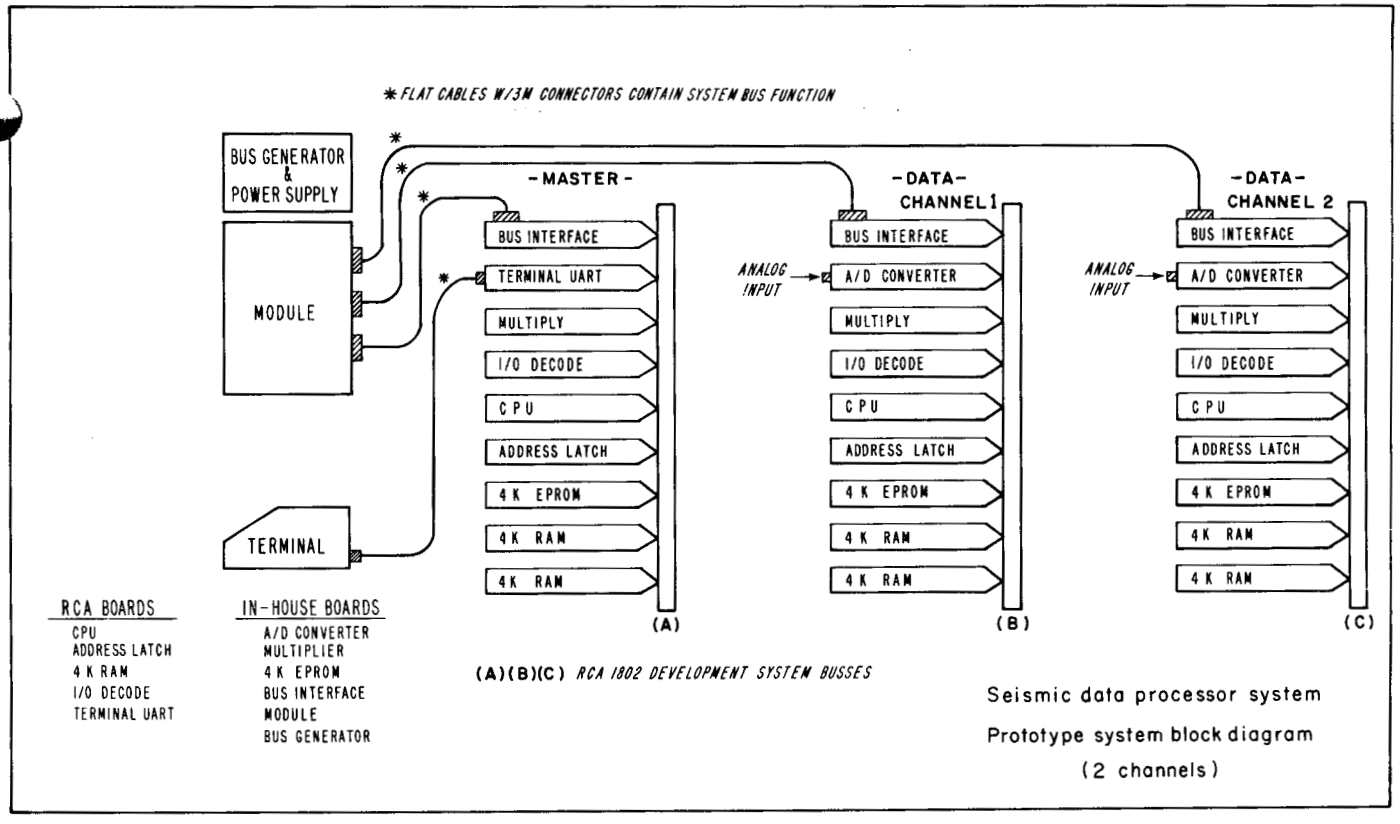

XBL 7812-14137

Figure 1. Block diagram, two-channel prototype seismic data acquisition/processing system, showing card structures for master and channel modules.

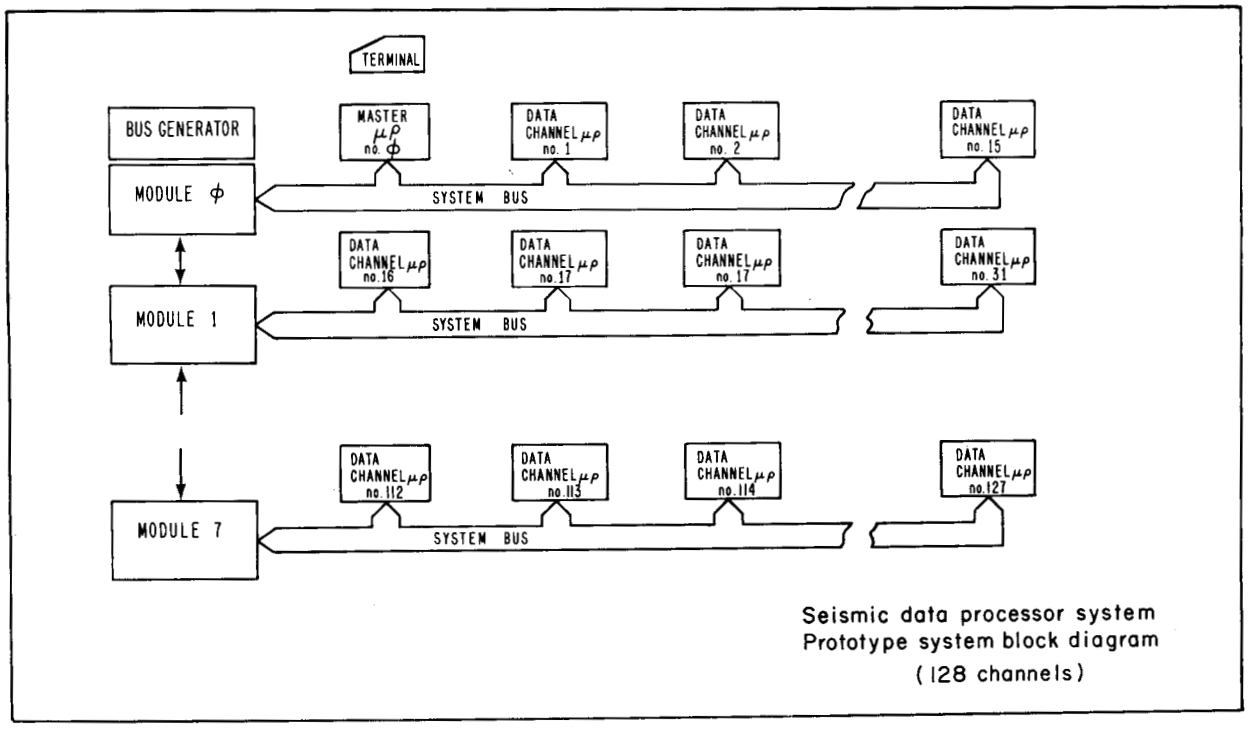

XBL 7812-14138

Figure 2. Generalized block diagram of 128-channel seismic field system, illustrating 16-channel modular architecture.

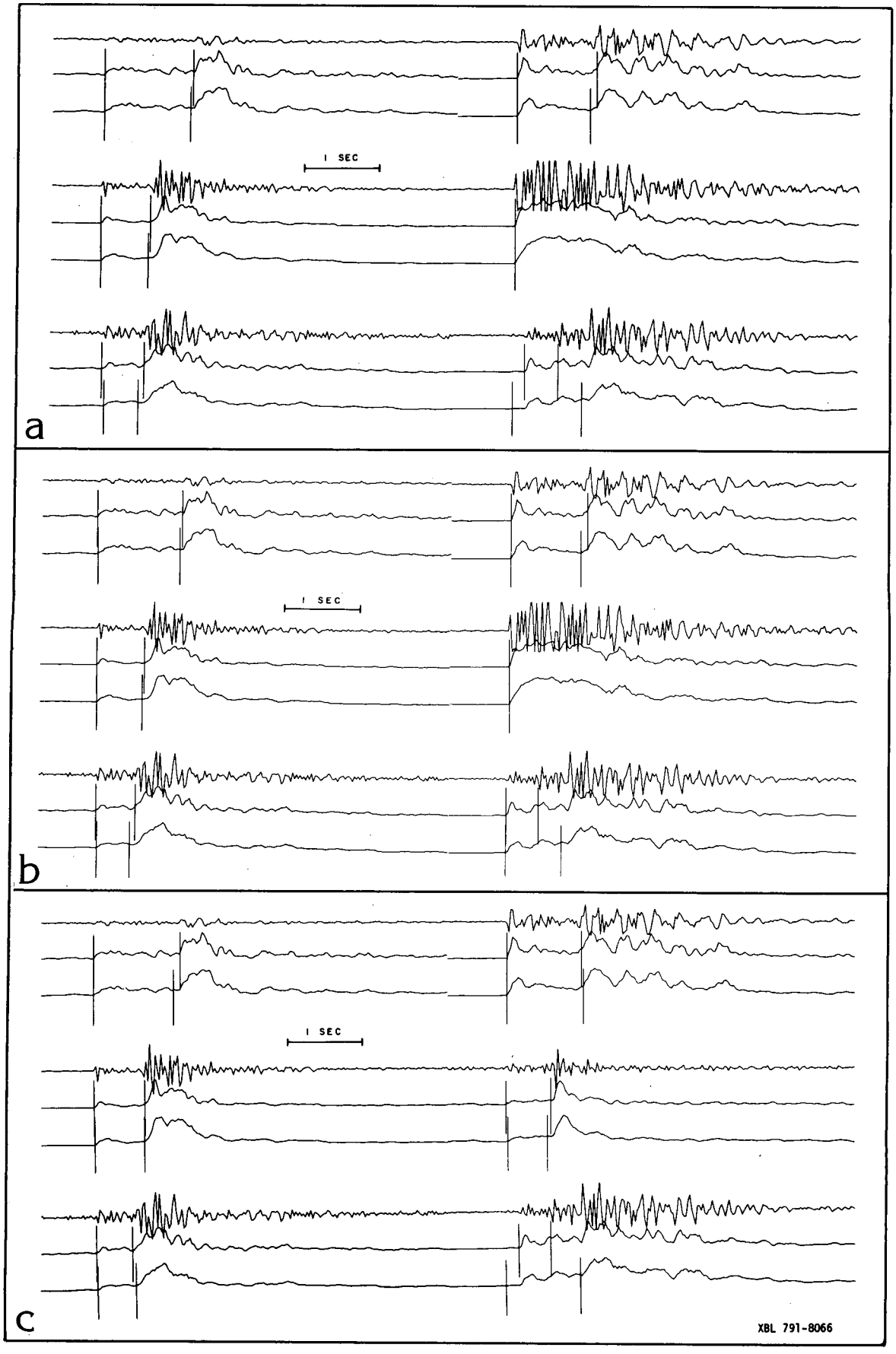

Figure 3. Example of detection/timing algorithm operation on six earthquakes exhibiting a range in quality of arrivals.

design of the prototype system was completed, and hardware fabrication was completed in September 1978.

PLANNED ACTIVITIES FOR FISCAL YEAR 1979

Software for channel and master processing will be developed on the two-channel prototype. Simultaneously, a 16-channel operational field system will be packaged for testing both with on-line network data at U.C. seismographic station, and with previously recorded analog tape data on hand from earlier geothermal field studies.

In the first quarter of the year, the detection, timing, and amplitude measuring algorithms will be defined and programming will begin on the 1802 channel devices. Our algorithm has been developed with simplicity in mind. Drawing on the results of Stewart (1977), Allen (1978), and Anderson (1978), and retaining the long-term to short-term average comparison (Ambuter and Solomon, 1974), a fast, effective detection and timing algorithm has been developed, which can operate in real time. Results of preliminary tests are shown in Figure 3, where event detection, phase (P and S) identification, and phase timing (the vertical bars) are reproduced for a set of average character microearthquakes. Top trace is original seismic signal, sampled at 200 sps. Middle and lower traces are the detection function with 16- and 32-point short-term averaging windows, respectively. Vertical lines show times picked for phases detected. The first phase is the P-wave arrival followed by the S-wave arrival. A 2048-point mean is removed from the time series initially. The P-wave detection threshold in all cases is three times the (2048-point) long-term average (LTA). the P-timing level is 1.25 LTA, 2.0 LTA, and 1.5 LTA in a, b, and c, respectively. P-timing in b and c is an extrapolation to LTA based on the slope of the detection function. The S-wave is detected using a level of two times PAVE, where PAVE is an average amplitude of 64 points following the P-wave detection. The S-wave is timed in several ways: by extrapolating back to LTA, to 2.0 PAVE, and to 1.0 PAVE, in a, b, and c, respectively. The parameters are selectable in the algorithms. Those results judged best for timing and detection are a for the P-wave and c for the S-wave.

During the second quarter, the basic channel device software will be implemented, the master device software will be tested, and the 16-channel system will be ordered. In the third quarter, the two-channel prototype will be exercising the entire basic software package, and fabrication of the 16-channel system will be under way.

During the last quarter, the 16-channel system will be exercised on real data. This will be the conclusive test. Final recommendations for system specifications will be made and the results disseminated to the exploration and seismic instrumentation industry. It is probable, however, that thorough testing of the system will be necessary in actual field use before general acceptance of the system. In fiscal year 1980, it would be valuable to make a 32- or 64-channel system available for field tests at various geothermal prospects. This would also provide much needed additional high-quality seismic data for case histories.

REFERENCES CITED

Allen, R. V., 1978. Automatic earthquake recognition and timing from single traces. Bull. Seism. Soc. Amer., v. 68, pp. 1521-1532.

Ambuter, B. P., and Solomon, S. C., 1974. An event-recording system for monitoring small earthquakes. Bull. Seism. Soc. Amer., v. 64, pp. 1181-1188.

Anderson, K. R., 1978. Automatic analysis of of microearthquake network data. Geoexploration, v. 16, pp. 159-175.

Beyer, H., Dey, A., Liaw, A., Majer, E., McEvilly, T. V., Morrison, H. F., and Wollenberg, H., 1976. Preliminary open file report, geological and geophysical studies in Grass Valley, Nevada. Berkeley, Lawrence Berkeley Laboratory, LBL-5262.

Liaw, A. L., 1977. Microseismics in geothermal exploration: studies in Grass Valley, Nevada. Ph.D. thesis, Berkeley, University of California, LBL-7002.

Liaw, A. L., and McEvilly, T. V., 1977. The role of ambient microseisms in geothermal exploration. Geoth. Res. Counc. Trans., v. 1, pp. 187-188.

_____, 1979. Microseisms in geothermal exploration: studies in Grass Valley, Nevada. Geophysics (in press).

Majer, E. L., 1978. Seismological investigations in geothermal regions. Ph.D. thesis, Berkeley, University of California, LBL-7054.

Majer, E. L., and McEvilly, T. V., 1979. Seismological investigations at The Geysers geothermal field. Geophysics (in press).

Majer, E. L., McEvilly, T. V., Albores, A., and Diaz C., S., 1978a. Seismological studies at Cerro Prieto, in First symposium on the Cerro Prieto geothermal field, Baja California, Mexico, September 20-22, 1978, Abstracts. Berkeley, Lawrence Berkeley Laboratory, LBL-7098 ABS, p. 23.

Majer, E. L., McEvilly, T. V., and Schechter, B., 1978b. Utility of seismological methods in the exploration, delineation and monitoring of geothermal reservoirs. EOS Trans. Amer. Geophys. Union, v. 12, p. 1200.

McEvilly, T. V., and Schechter, B., 1977a. East Mesa seismic study report no. 1. Berkeley, Lawrence Berkeley Laboratory, UCID-3908.

_____, 1977b. East Mesa seismic study report no. 2. Berkeley, Lawrence Berkeley Laboratory, UCID-4029.

_____, 1978. East Mesa seismic study report no. 3. Berkeley, Lawrence Berkeley Laboratory, UCID-4030.

Stewart, S. W., 1977. Real-time detection and location of local seismic events in central California. Bull. Seism. Soc. Amer., v. 67, pp. 433-452.

KLAMATH BASIN GEOTHERMAL RESOURCE AND EXPLORATION TECHNIQUE EVALUATION

N. E. Goldstein, H. A. Wollenberg, and M. A. Stark

INTRODUCTION

The Klamath Basin, located in south-central Oregon and northern California, has been a locus of geothermal exploration for several years. Three Known Geothermal Resource Areas (KGRAs) have been identified in the area; they are outlined in Figure 1. Hundreds of warm springs and wells, mostly in Klamath Falls KGRA, are used for space heating in and around the city of Klamath Falls. The waters range in temperature up to 113°C, and several companies and government agencies have searched for hotter water or steam suitable for electric power generation. Two unsuccessful deep holes have been drilled thus far in search of a high-temperature resource outside the immediate area of Klamath Falls, and the level of interest in the area has consequently declined over the last two or three years.

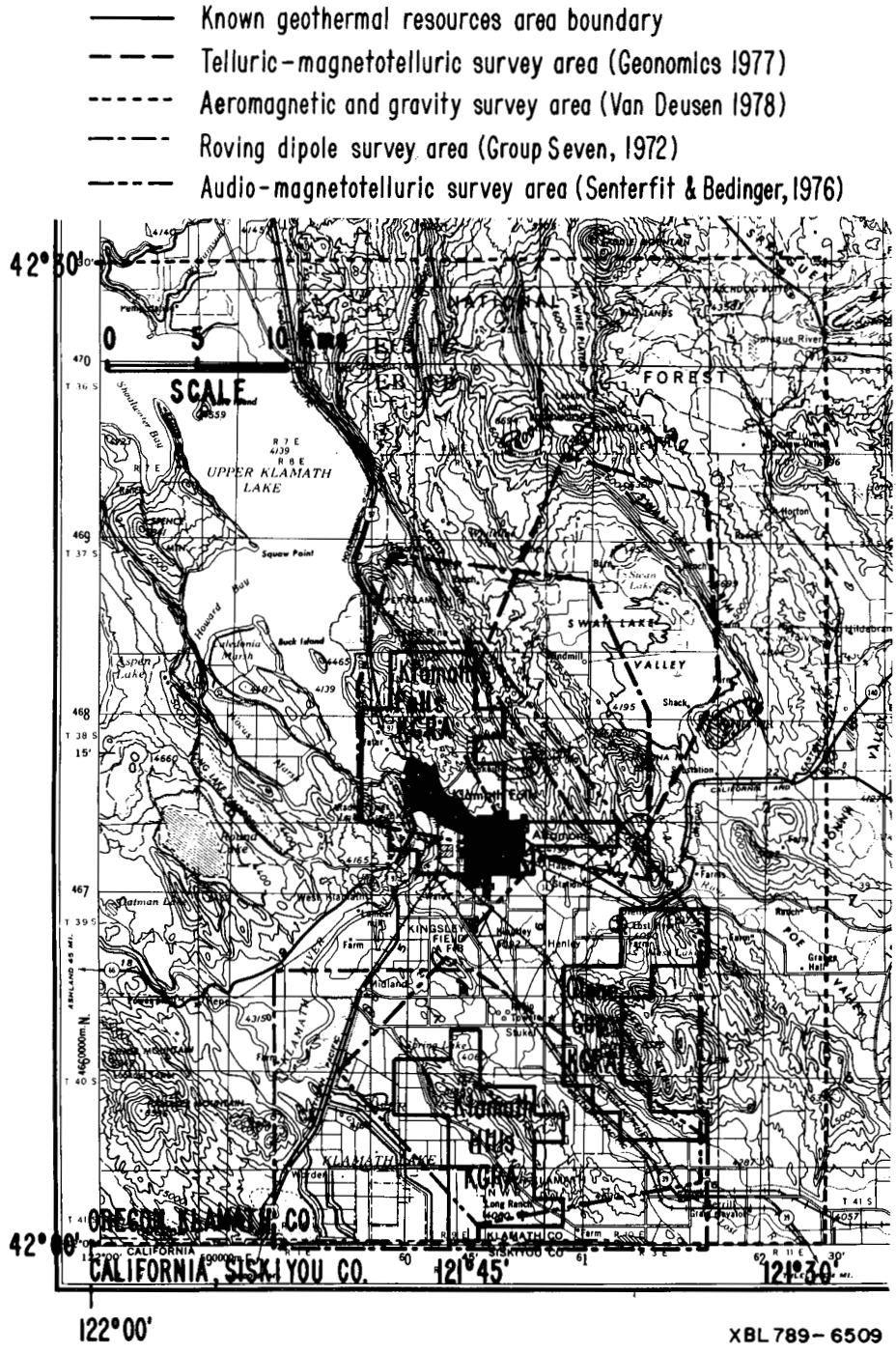

Figure 1. Index Map showing Klamath basin study areas.

In an attempt to restimulate exploration activity, LBL, working with the State of Oregon's Department of Geology and Mineral Industries (DOGAMI) and the U.S. Geological Survey (USGS), has attempted to collect, integrate and reinterpret all available exploration data from both public and private sources. Our primary goals were to develop a conceptual model for the hydrothermal system, to suggest targets for further exploration and to evaluate the exploration techniques used on a site-specific basis (Stark et al., 1979).

The Klamath graben is a dominating geological feature; it can be traced for 80 km from the Medicine Lake volcanic field in northern California to Crater Lake, Oregon, attaining a width of 15 km. The local geologic structure is characterized by numerous northwest-trending normal faults, with occasional northeast-trending cross-faults. Important rock units are late Tertiary and Quaternary volcanics and a late Tertiary lacustrine unit known as the Yonna formation.

ACCOMPLISHMENTS FOR 1978

We were able to gather, from the open literature and from companies working in the area, results of magnetotelluric (MT), audio-magnetotelluric (AMT), roving dipole resistivity, aeromagnetic, and gravity surveys. As shown in Figure 1, the survey blocks tend to cluster into two areas--the Swan Lake Valley area northeast of Klamath Falls and the Klamath Hills area, south of Klamath Falls.

For the Swan Lake Valley, we concentrated on reinterpreting the magnetotelluric data by means of two-dimensional modeling. Our models represent geoelectrical cross-sections beneath a profile line trending N. 47° E. across the northern portion of the Swan Lake Valley. The two-dimensional modeling technique is a significant improvement over conventional one-dimensional interpretation schemes for geologically complex areas such as the Klamath basin. However, it proved difficult to match the transverse electric (TE) and the transverse magnetic (TM) apparent resistivity modes with data calculated for two dimensional models. This problem, common in MT interpretation, is caused by the sensitivity of the method to lateral inhomogeneities and three-dimensional electric structure.

By trial and error, we obtained several models, each giving a reasonable fit to at least one of the modes. Moreover, these models are also consistent with interpretations of roving dipole, gravity and magnetic data in the area.

Two conductive zones, ranging in resistivity from 3 to 9 ohm-m, appear in the model (Figure 2). One is located beneath Meadow Lake Valley, about 1 km southwest of Swan Lake Valley. The other is located beneath the northwest margin of Swan Lake Valley. The depth extents of these zones are uncertain, but the proximity of the zones to major normal faults makes them possible targets for further exploration. A conductive layer lies beneath the Swan Lake Valley at a depth of 1 km, connecting the two zones.

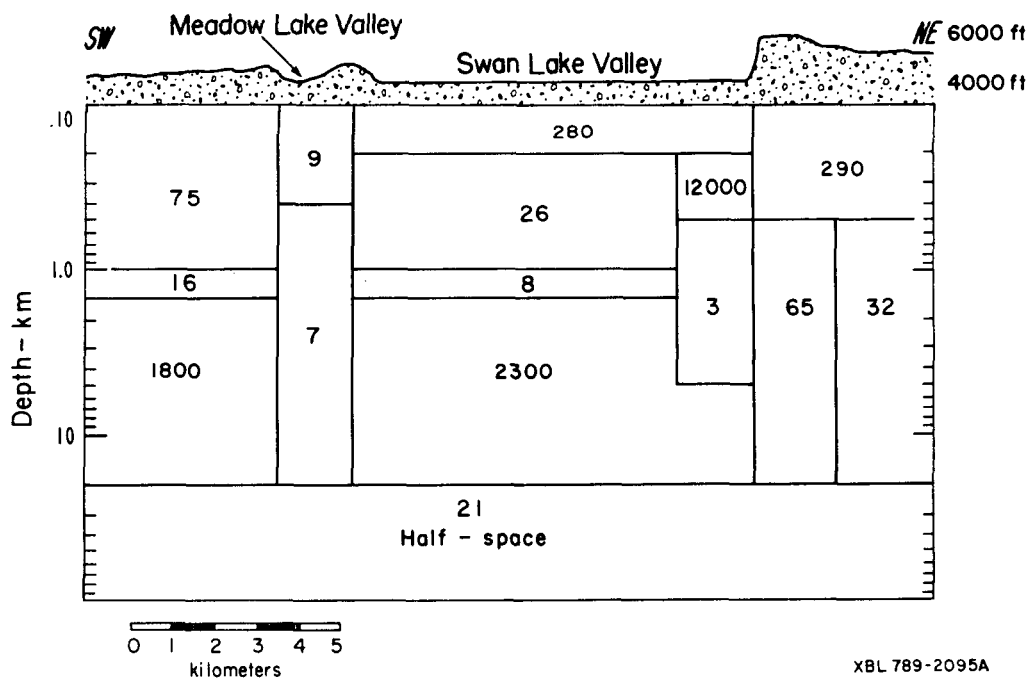

Figure 2. Resistivity model for Swan Lake Valley area with schematic typography (values in ohm-meters).

We have recommended an exploration strategy for the Swan Lake area consisting of resistivity soundings and gravity measurements, geochemical analyses of spring and well samples, and shallow thermal gradient drilling.

To the south, the Klamath Hills area has attracted interest because of two hot wells (>90°C) and a handful of warm wells located immediately southwest of the Hills. Figure 1 shows the areas covered by AMT, roving dipole, gravity and aeromagnetic data.

We reinterpreted some of the roving dipole data by means of two-dimensional resistivity modeling in the vicinity of the hot wells. Our final models indicate the presence of a conductive zone (4 ohm-m) around the hot wells, but it appears to be limited in both lateral and depth extent. The conductive zone probably represents valley sediments saturated with hot water that has ascended from depth along the fault zone bounding the Hills. We have suggested additional resistivity studies here to determine more accurately the extent of the conductor and to detect the source of the fluid at depth.

On the northeast side of the Klamath Hills, the AMT data suggest a linear northeast-trending conductive anomaly beneath the Hills and Olene Gap. We have interpreted this as a concealed cross-fault. The gravity and aeromagnetic data are consistent with this interpretation; the contours are aligned in a northeasterly trend, forming a saddle between the Klamath Hills and Stukel Mountain to the northeast. Thus it appears that the basement on the southeast side of the inferred fault has been upthrown, forming a raised northeast-trending ridge between Klamath Hills and Stukel Mountain.

The AMT anomaly is centered near the northwestern tip of Stukel Mountain, where several warm wells (up to 42°C) exist. The extremely low (<1 ohm-m) AMT apparent resistivities measured there are encouraging signs of geothermal activity. This area lies close to an intersection between several faults and the inferred concealed cross-fault. Fault intersections appear to be favorable locations for geothermal activity in this area. However, deeper electrical soundings are needed to determine the depth extent of this anomaly. We may be seeing the effect of leakage along fractured fault zones from a larger reservoir at depth, similar to the proposed mechanism near the hot wells.

In working with these data, we have had a chance to evaluate the geophysical methods on a site-specific basis. A brief assessment of each method follows.

1. Gravity and Magnetics. These methods seem suited for resolving structure, and are best used in conjunction with other techniques. They are useful for mapping faults and for helping to determine alluvium/sediment thickness in valleys.

2. Roving Dipole Resistivity. This can be a useful reconnaissance tool, but when used without other resistivity methods it is difficult to interpret in a meaningful, quantitative fashion. Computer modeling shows that the anomaly source may lie some distance from the anomaly.

3. AMT and MT. These methods offer more promise, but are more difficult to interpret properly than the other techniques discussed. A major advantage of MT is that it often allows crustal modeling to depths of tens of kilometers. However, owing to local surface inhomogeneities and three-dimensional deep structure, it is rarely possible to satisfy both TE and TM data sets by means of a two-dimensional model. Scalar AMT, as performed by the USGS, or scalar MT surveys are usually difficult to interpret in multidimensional geology. However, in the Lost River-Spring Lake valley, the scalar AMT data seem to reveal concealed structures.

In general, the study demonstrates the need for comparison and simultaneous interpretation of multiple data sets. In complex geology, individual geophysical data sets often cannot be interpreted clearly, and simultaneous interpretation of several types of data can lead to a clearer understanding of subsurface structure. The study also has demonstrated the importance of thorough interpretation of field data, particularly for the electrical prospecting methods. This requires computer modeling, which may involve a significant amount of time and money, but is necessary if the techniques are to be useful.

PLANS FOR 1979

In September, 1978, we received geophysical and geochemical data covering hundreds of square kilometers of land on the west and east shores of Upper Klamath Lake. The geophysical data include roving dipole, Schlumberger equatorial, dipole-dipole, and Schlumberger expander soundings and logs from an unsuccessful 2000-ft exploratory well. Preliminary work has begun with computer modeling of the electrical data. We plan to continue this type of analysis on all of our data, hoping to gain a clear understanding of the geothermal system in the entire area around Klamath Falls.

The extensive geochemical data will permit investigation of regional patterns of elements in shallow and deeper groundwaters.

REFERENCE

Stark, M. A., Goldstein, N. E., Wollenberg, H. A., Strisower, B., Hege, M. L., and Wilt, M., 1979. Geothermal exploration assessment and interpretation, Klamath Basin, Oregon--Swan Lake and Klamath Hills Areas. Berkeley, Lawrence Berkeley Laboratory, LBL-8186 (draft).

MT. HOOD GEOTHERMAL RESOURCE EVALUATION

N. E. Goldstein, H. A. Wollenberg, H. Bowman, and E. Mozley

INTRODUCTION

Mt. Hood is a young but dormant volcano located approximately 80 km east of Portland, Oregon (Figure 1). Beginning in 1977, a project began to evaluate the geothermal potential of the volcano. The DOE project is coordinated by the Oregon Department of Geology and Mineral Industries (DOGAMI) and supported in part by the U. S. Geological Survey and the U. S. Forest Service. This volcano was selected from others in the High Cascade Range because of its proximity to a major city, the abundance of federally controlled land on which to work, evidence of a heat source, and growing interest of private developers in the geothermal potential.

As part of the program to evaluate the resource, various exploration techniques were applied to determine their usefulness in this complex geological environment. LBL has the responsibility of coordinating surveys dealing with rock, gas, and water geochemistry and electrical resistivity.

ACTIVITIES IN FISCAL YEAR 1978

Geochemical Studies

Water, rock and gas samples were collected on or near Mt. Hood during fiscal year 1978, with the cooperation of DOGAMI and USGS. Periodic sampling of water from selected orifices at Swim Warm Springs (Figure 1) continued with a collection in February 1978. Results of analyses of major and trace elements indicated increased contents of magnesium and sulfur in winter samples, compared with samples collected the previous summer. It was expected that the winter sampling would yield higher contents of all elements, because surface runoff, diluting the hot water from depth, would be diminished. However, this was not substantiated because there were significant decreases, or only slight changes, in contents of some elements in the winter samples.

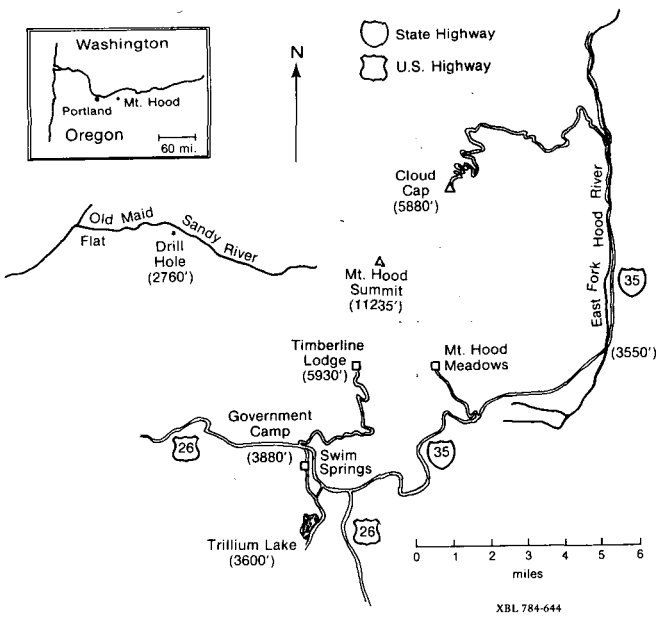

Figure 1. Simplified location map of the Mt. Hood area.

Sufficient data have been collected to provide some preliminary conclusions on the geochemical setting of Mt. Hood, which are given below. Descriptions of the sampling and results of analyses are detailed in LBL-7092 (Wollenberg, et al., 1979).

1. The warm water at Swim Springs on the south flank of Mt. Hood has a large component (~90%) of near-surface cold water. The flux of cold-water runoff nearly masks the surface indications of deeper-circulating hot water. The upper-slope orifices at Swim Warm Springs are the most diluted, those down slope are successively less diluted. The oxygen-hydrogen isotope data indicate that cold-spring waters have short pathways between their sources and the springs, although a component of the warm-spring water has its origin considerably higher on the mountain.

2. Chemical geothermometers indicate that temperature at depth of water entering the Swim Springs system is within the range 104-170°C. The silica mixing model gives a range of 190-240°C for unmixed hot water.

3. Water in the geothermal test hole in Old Maid Flat (see Figure 1), most likely from the Rhododendron formation, has a different chemical character than the water at Swim Warm Springs. The relatively low silica content of Old Maid Flat well water suggests that its temperature is due to the regional geothermal gradient and not to circulation within thermal anomalies associated with Mt. Hood.

4. Iridium, a platinum-group element, is present in identifiable abundance at one orifice at Swim Warm Springs, a cold spring, and in a small lake in the summit crater area. Iridium also occurs in altered andesite at one location on the western flank of Mt. Hood. The association of Ir with an andesitic volcano is surprising; it is generally considered to be associated with basic to ultrabasic igneous rock.

5. The similarity between major- and trace-element contents of Pliocene andesite and intermediate intrusive rocks of the Laurel Hill pluton on the west side of the mountain supports Wise's (1969) contention that the pluton represents the root zone of a center of andesite extrusion.

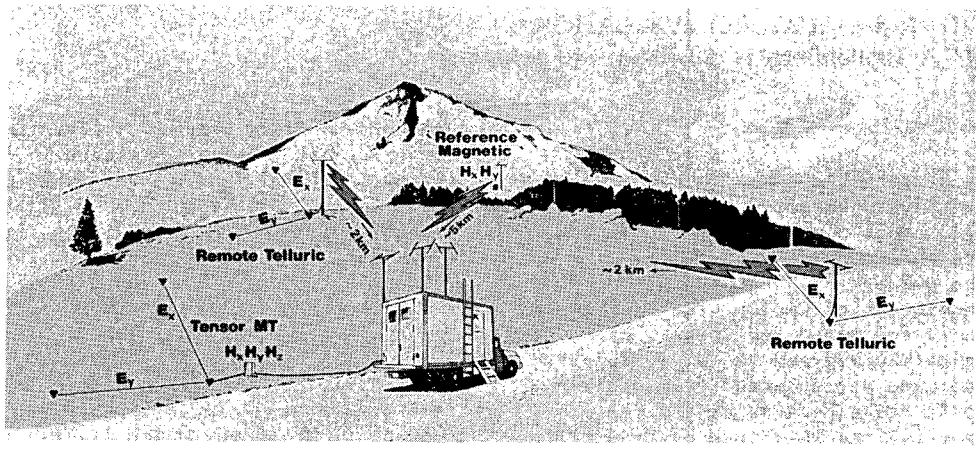

Figure 2. The array of sensors used for one set-up of the T-MT survey. Two such set-ups with the second tensor MT station over a previous remote telluric station constituted a station cluster.

CBB 770-12413

6. The basalt exposed in the Robin Hood quarry in the valley of the East Fork of the Hood River has major- and trace-element contents very similar to those of the Roza Flow of central Washington. This supports the supposition that the basalt on the east side of the valley is Columbia River basalt, and that the north-south valley marks the trace of a normal fault, upthrown side to the east.

Geophysical Studies

The telluric-magnetotelluric survey begun in fiscal year 1977 continued to early November 1978 when worsening weather conditions forced the contractor, Geonomics, Inc., to cease Phase II survey operations. During Phase II the survey aperture was opened; station density was decreased and stations were arranged in five clusters around the mountain to increase regional coverage. Each cluster was planned to consist of two complete telluric-magnetotelluric set-ups plus a reference magnetic station (Figure 2). A complete cluster yielded six data stations; two tensor MT stations plus four remote telluric stations. However, in some clusters it was convenient to put the reference magnetometer at a remote telluric site, thus obtaining another tensor MT station.

Geonomics performed the conventional data processing and we were to reprocess data using the reference magnetometer channels to obtain results in the troublesome parts of the spectrum (Gamble, 1978). Using the Geonomics results only, a preliminary interpretation report was issued in June 1978 (Goldstein and Mozley, 1978). The general conclusions reached are as follows:

1. The change in principal resistivity directions at stations around the volcano suggest that the volcano may be located at the intersection of a north-south and east-west structural trend. However, we see no evidence for the postulated north-south fault following the East Fork of the Hood River.

2. Although it was not possible to put a station close to the summit (the method is dependent on roads and easy access), encouraging results were obtained at Cloud Cap, a 12,000± y.B.P. eruptive center in the northeast side of the mountain. Conductive zones at depths of 600 to 1000 m and >2000 m were interpreted (Figure 3).

3. Anomalous low resistivities were also observed in the vicinity of the warm water emanations at the Still Creek campground (Swim Warm Springs). However, because of apparently complex local geology and incomplete data a full interpretation was not made.

4. Stations in the Old Maid Flat area, near the geothermal test well drilled by Northwest Natural Gas (Figure 1), show no suggestion of an encouraging low conductivity anomaly. Rather, resistivities increase with period, suggesting a decrease in porosity-permeability with increasing depth. This situation was

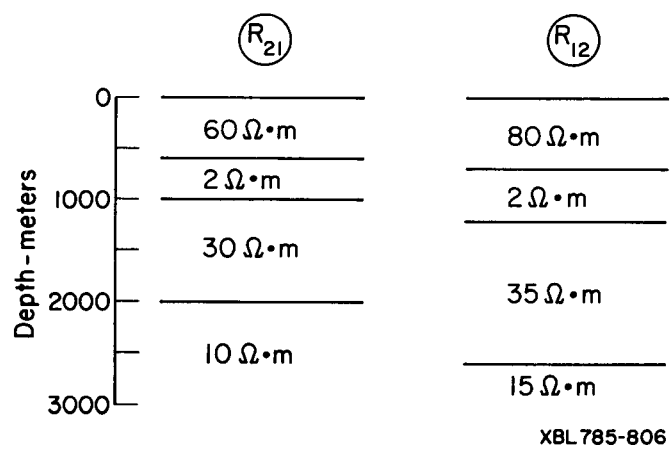

Figure 3. A one-dimensional interpretation of MT data at the Cloud Cap station. R_{12} and R_{21} are resistivities in the principal directions determined by rotation of the impedance tensor.

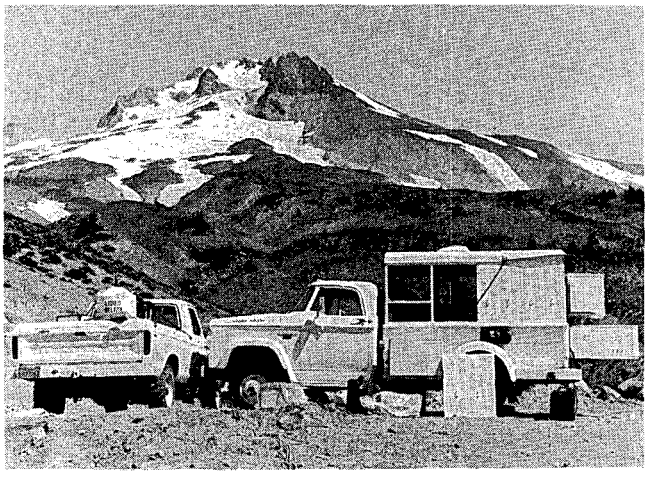

Figure 4. The EM-60 transmitter in operation near the Timberline Lodge, south flank of Mt. Hood, elevation 5900 ft. The most distant receiver station was at an elevation of 7000 ft, at the edge of the Palmer glacier seen directly above the truck on the left.

confirmed in 1978 when the hole was deepened from 2000 to >4000 ft.

To supplement the T-MT results, the controlled-source EM system (EM-60) developed at LBL was used at selected sites during August 1978. Transmitter sites were located near Timberline Lodge (Figure 4) for coverage on the south flank, at Summit Meadow for coverage at Swim Warm Springs, at Cloud Cap to confirm the MT anomaly there, and in Old Maid Flat for information at the deep drill hole. Two or three receiver sites were occupied relative to each transmitter except at Old Maid Flat where no data were taken. The data were returned to Berkeley for post-field processing and analysis, scheduled to begin early in fiscal year 1979.

ACTIVITIES PLANNED FOR FISCAL YEAR 1979

Geochemical Studies

Firmer conclusions on the usefulness of geochemistry in evaluating the geothermal resource potential of Mt. Hood await results of analyses presently under way. These include analyses of gas samples collected in October 1978 in the summit fumarolic area. In the 1977 sampling we were not able to collect sufficient water vapor to determine isotope ratios. The volume of water vapor collected in 1978 is sufficient for these analyses. This will afford comparison with the isotope ratios of cold- and warm-spring water.

Water analyses awaiting completion include a sample collected in October 1978 from the geothermal test hole drilled near Timberline Lodge and a set of samples collected at that time from the three orifices sampled periodically at Swim Springs. The deepened geothermal test hole in Old Maid Flat may permit us to obtain a fluid sample from a deeper aquifer (most likely within the Columbia River basalt) than the Rhododendron formation sampled in 1977.

Samples of altered and unaltered andesite from the fumarolic area in the summit crater were collected in October 1978. These are being analyzed for major and trace elements and will indicate if iridium and silver are present in the strongly altered ground, coinciding with the presence of these elements in the runoff water from the small lake.

We recommend that one or more geochemical test holes be drilled in the Swim Warm Springs area. They should be deep enough to obtain temperature measurements and fluid samples from below the zone of near-surface and shallow cold-water runoff, to permit major, trace-element, and isotope analyses of relatively unmixed hot water.

Geophysical Studies

In November 1978 the complete reference magnetic MT processing program, including the error analysis subroutine (Gamble, 1978), were checked and found to be fully operational. Edited data tapes will be reprocessed to the full extent possible; and comparisons will be made to sort out errors in the remote telluric station results due to noise (bias errors) or a nonuniform magnetic field between base and remote stations. Following this, the reprocessed data will be reinterpreted in terms of a subsurface resistivity model.

The data collected at Mt. Hood using the EM-60 system will be processed and interpreted and the results will be compared and correlated with the T-MT survey results. The EM-60 data will require additional corrections to account for the elevation differences between transmitter and receiver, and a tilted transmitter dipole vector due to sloping terrain. Interpretation of the EM-60 data will be done in terms of the layered inversion approach (Morrison, et al., 1978) and in terms of two-dimensional models (Lee, 1978).

A dc resistivity (dipole-dipole) survey will be performed in the Swim Springs area.

REFERENCES CITED

Gamble, T. D., 1978. Remote reference magnetotellurics with SQUIDs. Berkeley, Lawrence Berkeley Laboratory, LBL-8062.

Goldstein, N. E., and Mozley, E., 1978. A telluric-magnetotelluric survey at Mt. Hood, Oregon--a preliminary study. Berkeley, Lawrence Berkeley Laboratory, LBL-7050.

Lee, K. H., 1978. Electromagnetic scattering by a two-dimensional inhomogeneity due to an oscillating magnetic dipole. Berkeley, Lawrence Berkeley Laboratory, LBL-8275.

Morrison, H. F., Goldstein, N. E., Hoversten, G. M., Oppliger, G., and Riveros, C., 1978. Description, field test and data analysis of a controlled-source EM system (EM-60). Berkeley, Lawrence Berkeley Laboratory, LBL-7088.

Wise, W. S., 1969. Geology and petrology of the Mt. Hood area: a study of High Cascade volcanism. Geol. Soc. Am. Bull., v. 80, pp. 969-1006.

Wollenberg, H. A., Bowen, R. G., Bowman, H. R., and Strisower, B., 1979. Geochemical studies of rocks, water and gases at Mt. Hood, Oregon. Berkeley, Lawrence Berkeley Laboratory, LBL-7092 (in preparation).

EAST MESA SEISMIC STUDY

T. V. McEvilly, B. Schechter, and E. L. Majer

INTRODUCTION

Magnetic tape records collected by the U. S. Bureau of Reclamation (USBR) at their six-station seismic network around the East Mesa geothermal field were analyzed. The purposes of this study are: (a) to obtain further details of the faulting and associated stress fields as defined by local earthquakes; (b) to obtain baseline data on local seismicity before geothermal field exploitation; (c) to determine if the reservoir region causes anomalous elastic wave propagation characteristics and whether or not this information is useful for defining the reservoir; and (d) to provide USBR personnel and others with procedural guidelines for subsequent analysis of network data.

ACCOMPLISHMENTS IN 1978

Following the first report (McEvilly and Schechter, 1977a), which detailed the data analysis techniques, two subsequent reports (McEvilly and Schechter, 1977b and 1978) were issued. These reports summarize the results of observations and one (1978), gives a detailed review of past and present local seismicity.

Figure 1 shows the locations of the USBR seismograph stations. The open circles are epicenters of the larger events recorded: the primed numbers refer to epicenters located by means of the U. S. Geological Survey (USGS)-California Institute of Technology (CIT) network in the Imperial Valley. The magnitudes of these events ranged from M_L = 2.0 to 4.0. The USBR and USGS-CIT epicenters agree relatively well in computed distance, but have a discrepancy in azimuth. An azimuthal distortion may be caused either by local variations in seismic velocities within or near the USBR network or by refraction across a lateral discontinuity, possibly associated with the Brawley-Imperial fault system. Every locatable event was found to originate along the Brawley-Imperial fault. The location of the smallest events, magnitudes on the order of zero, are unresolved.

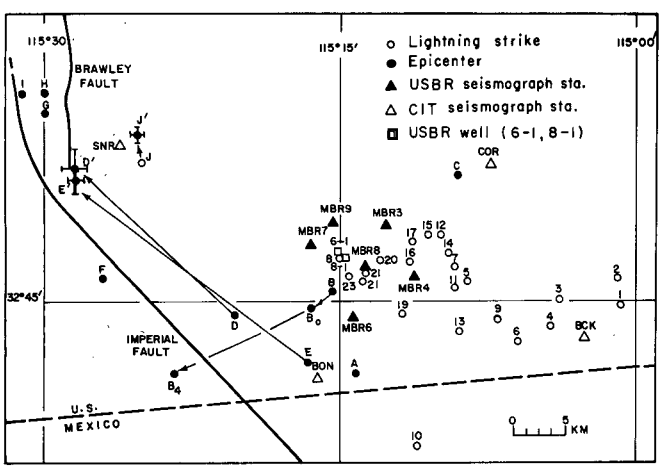

Figure 1. Regional map showing East Mesa network station, epicenters located, and USGS-CIT epicenters for larger events.

The primary finding to date in the East Mesa seismic study has been the complete lack of detectable local microearthquakes to an estimated detection threshold of at least M_L = 1.0. The detection of smaller shocks has been hampered by the high level of low-frequency surface noise in the field. These results are consistent with previous investigations in the Imperial Valley and the East Mesa area (Hill, 1975; Iyer, 1975), but inconsistent with other microearthquake studies at East Mesa in 1973 (Combs, 1974; Combs and Hadley, 1977).

Several possible explanations might account for the discrepancies:

First, the East Mesa fault was active in the period 1973-1975 but has been inactive during the present period of study (July 1977 to present). This does not seem likely, since local activity was assumed to be tectonically linked to the broader zone of seismicity associated with the Brawley-Imperial fault system, which has continued to be active throughout the period. According to this hypothesis, one would have expected to see local events during the recent Brawley swarms.

Second, the microearthquakes used to define the East Mesa fault in 1973 were actually located along the Brawley fault. Only vertical component instruments were then available to locate these events. McEvilly and Schechter (1977b) demonstrated the problems of accurately locating events using only P arrivals, especially those events located outside the array. A comparison of station deployment and the epicenter distribution shows the station distribution heavily weighted to the

east of the epicenters, a situation which could easily lead to mislocations. Relocation of these events farther to the west would also increase the computed focal depth to values more compatible with those reported by Johnson and Hadley (1976) for Brawley events. Only a reevaluation of the actual data can resolve this problem.

Third, "geothermal events" may not be seismic in origin. Illustrations of these events in Combs (1976) appear to be more consistent with air-coupled Rayleigh waves than with microearthquakes, featuring emergent low-frequency arrivals and similar waveforms which appear simultaneously on both vertical and horizontal records. The local velocity structure (very low velocities in the near-surface) constrains the ray paths (even for local events), to propagate almost vertically near the surface, clearly separating P- and S-waves as vertical and horizontal motions, respectively. The "geothermal event" waveforms (Combs, 1976, p. 34), if body waves, are not consistent with such characteristics.

In addition, the manner in which the S-wave arrival was determined is often ambiguous. Improper determination of S-P times, more than any other error, would heavily influence the determination of local seismicity.

The observation that local seismicity remained unaffected by withdrawal and injection of geothermal fluids could be interpreted as evidence that the observed seismicity is not of local origin. A reexamination of the data appears necessary to resolve these questions. Of specific interest should be the determination of the apparent velocities associated with the "geothermal events" and the temporal correlation of these events with the records of the USGS-CIT Imperial Valley array.

The small events detected at East Mesa during the present study may be analogous to the nanoearthquakes discussed by Combs (1974 and 1976), since they were observed at roughly the same location (MBR STA 9 lies close to Combs' MGA #3). However, S-P time of 1.5 sec assigned to these events by Combs, indicating a local origin, has not been observed (no S-wave arrivals are, in fact, seen for these events). Because these events appear only on MBR 9Z and 3Z, we may speculate that they are actually the smallest members of the Brawley earthquake swarms with origins northwest of East Mesa. One would also expect the signals to show up on STA 7Z; however, a map of seismic ground noise (Combs 1974, p. 33) shows high noise levels in the vicinity of MBR 7 relative to levels around MBR 3 and 9.

Regional seismic activity (events of magnitude 2.0 or less) is well-recorded at East Mesa and is distinguishable from local events by S-P time constraints (and less accurately by relative P-wave arrival times). The quality of the data makes it possible to locate accurately larger events, although local station corrections are not determined. Several seismic wave phases, in addition to the initial P- and S-wave arrivals, are commonly observed. Most of the regional events are associated with the active Brawley-Imperial fault system to the west and southwest. The closest events recorded, based on S-P time intervals, are located along this fault zone about 20 km west of the array. Other events recorded originated at distances exceeding 500 km and at all azimuths to the west. (A set of sources at varying distances and azimuths may provide data on subsurface properties within the network in the absence of local events.)

Other local disturbances not of earthquake origin have been detected and identified. These include meteorological disturbances, drilling activity, and weapons testing. Although these may have been previously identified as local seismic events, they are distinguishable because of waveforms, frequency content, and most important, by their slow (subseismic) apparent velocities.

The major Brawley swarms of October-November 1977 were well recorded at East Mesa. Again, no local microearthquakes were recorded during this period--a result contrary to the findings of a previous investigation in which local seismicity was reported to have peaked during swarm activity. Our results lead to the conclusion that there is no evidence that the local stress regime is associated with the Brawley-Imperial fault system.

The origin of small events remains unresolved, but they are believed to represent the smallest members of the Brawley fault swarm. Installation of a 4.5-Hz three-component geophone into a 300-ft borehole may aid in determining the source of these events and in detecting small "geothermal events" not presently observable because of the high level of surface noise in the seismic bandwidth. It is estimated that improvement of at least one order of magnitude in the threshold of detectability is required for serious study of the field seismicity.

Results of the study suggest that a reasonable and economical modification to the USBR network would provide a minimal capability of monitoring, at an improved threshold of detection, so that any seismicity within the field would be at a threshold magnitude of zero. To this end, a single three-component station should be considered with either downhole (100 m) geophones or a surface array of at least 36 geophones per channel, with a triggered digital event recorder. The downhole installation would be superior in sensitivity and probably less expensive. Such a station would provide long-term field seismicity data for induced seismicity studies.

PLANNED ACTIVITIES IN 1979

No seismic studies are planned at East Mesa. The USBR has relinquished control of the land to the Bureau of Land Management who will open the lease units to competitive geothermal leasing in 1979.

REFERENCES CITED

Combs, J., 1974. Microearthquake investigation of the Mesa geothermal anomaly, Imperial Valley, California. Final Report, USDI Bureau of Reclamation.

_____, 1976. Microearthquake studies before and during fluid withdrawal and reinjection test, East Mesa geothermal field, Imperial Valley, California. Final Report, USDI Bureau of Reclamation.

Combs, J. and Hadley, D., 1977. Microearthquake investigation of the Mesa geothermal anomaly, Imperial Valley, California. Geophysics, v. 42, p. 17.

Johnson, C. E., and Hadley, D. M., 1976. Tectonic implications of the Brawley earthquake swarm, Imperial Valley, California, January 1975. Bull. Seis. Soc. Am., v. 66, no. 4, p. 1133.

Hill, D. P., Mawinckel, P., and Peake, L. G., 1975. Earthquakes, active faults, and geothermal areas in the Imperial Valley, California. Science, v. 188, p. 1306.

Iyer, H. M., 1975. Short note, search for geothermal seismic noise in the East Mesa area, Imperial Valley, California. Geophys., v. 40, pp. 1066-1072.

McEvilly, T. V., and Schechter, B., 1977a. East Mesa seismic study, report no. 1. Berkeley, Lawrence Berkeley Laboratory, UCID-3908.

_____, 1977b. East Mesa seismic study, report no. 2. Berkeley, Lawrence Berkeley Laboratory, UCID-4029.

_____, 1978. East Mesa seismic study, report no. 3. Berkeley, Lawrence Berkeley Laboratory, UCID-4030.

Geophysical Studies at Cerro Prieto

The LBL geophysical field program was formulated to assist reservoir delineation and to provide baseline data against which future studies could be compared. Although standard geophysical exploration techniques were used, exploration was not the primary objective of the work. The techniques chosen were those used by LBL and U.C. Berkeley in earlier geothermal investigations, and which we had some reason to believe would provide useful information on the Cerro Prieto reservoir.

Dipole-dipole dc resistivity surveys, supplemented by magnetotellurics, were used to determine how well the reservoir or controlling geologic structures can be defined on the basis of resistivity. Permanent electrodes were emplaced so that future measurements can be made to detect resistivity changes that may occur due to changing reservoir conditions. Computer modeling was done to interpret observed data and to determine the accuracy needed to resolve changes in reservoir bulk resistivity. Because the electrical basement is difficult to resolve beneath the thick section of conductive sediments, magnetotelluric studies were conducted to provide supplementary deep structural information.

Self potential (SP), another type of electrical technique, was performed because it is relatively easy to conduct and has provided provocative and valuable results for other geothermal areas. The SP anomaly found at Cerro Prieto is a "text-book" example. Encouraged by the preliminary results, CFE has begun using self potential for geothermal exploration outside the known field.

Passive seismic surveys were conducted in two phases. First, a microearthquake study was conducted to establish the level and nature of seismicity within the area of the production zone and for comparison to regional values. Sometimes used in the exploration phase to map faults, microearthquake survey results may be applicable to detecting changes in reservoir conditions, for example, changes in temperature, pressure, fluid saturation and, most important, subsidence.

In the second phase of work, wave propagation studies were made. Propagation characteristics, such as V_p, V_s, Poisson's Ratio and amplitude attenuations, were determined within the reservoir area and compared to values outside the reservoir boundaries. These characteristics, which were derived from recorded regional earthquake signals, help to define the field boundaries.

Precision gravity surveys, performed at regular intervals in conjunction with first-order leveling, have been started at other geothermal reservoirs. Used also with electrical resistivity and seismic propagation surveys, precision gravity could be an exceptionally promising means for monitoring changes in reservoir conditions, for example, (a) densification due to changes in temperature-dependent water-rock chemical reactions, and (b) formation of a steam zone due to lowered pressure, or fluid withdrawal without compensating recharge.

SEISMOLOGICAL STUDIES AT CERRO PRIETO

E. L. Majer and T. V. McEvilly

ACCOMPLISHMENTS IN 1978

In a preliminary investigation of the seismicity and wave propagation characteristics of the Cerro Prieto geothermal field, 17 stations were occupied with vertical and horizontal seismographs from February 14 to March 11, 1978 (Figure 1). The objectives of this field experiment were to determine the level and nature of microearthquake activity in the field area and the velocity and attenuation of P- and S-waves in the production zone relative to regional values. Similar studies of the type described here were conducted at Leach Hot Springs, Grass Valley, Nevada (Majer, 1978) and at The Geysers geothermal field in northern California (Majer and McEvilly, 1979). The previous studies indicated significant velocity and attenuation characteristics associated with both The Geysers (vapor-dominated) and Leach Hot Springs (liquid-dominated) systems. The Geysers study also revealed high microearthquake activity (25-30 events/day) associated with the production regions.

Continued and possibly increased fluid withdrawal and Cerro Prieto may effect changes in pore pressures, temperature gradients, volume, and stress patterns, all of which have been shown to be related to seismicity. Changes in the present level or nature of seismicity may be an indication of expansion or alteration of the production zone properties and boundaries. By using detailed microearthquake locations it may also be possible to map the location and nature of faults striking NE-SW which have been hypothesized to exist in the production zone.

The stations for this study were spaced approximately one kilometer apart across the production region and extending outside the field for adequate reference values. Because the data were collected on a 12-channel system and 17

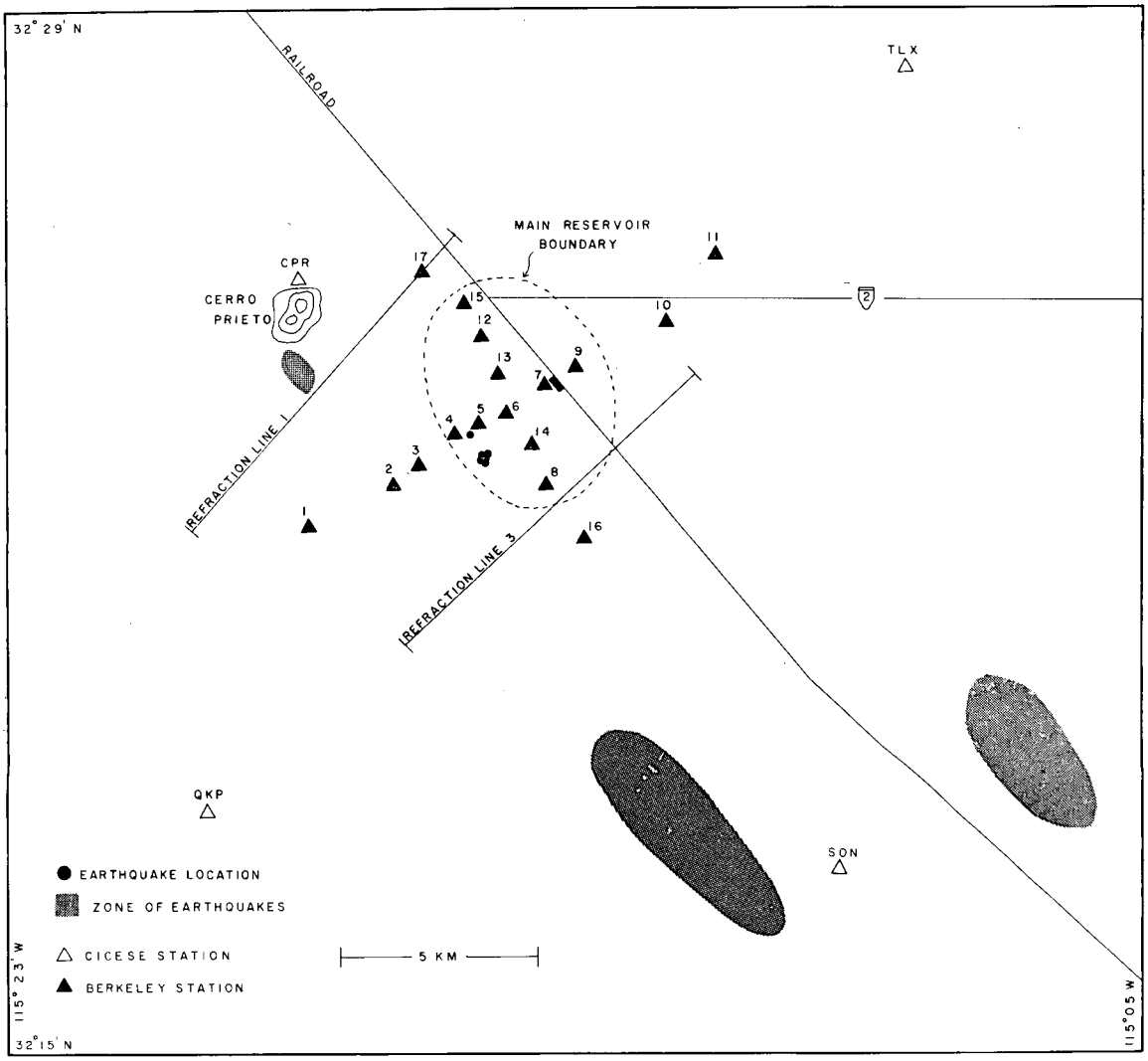

XBL 789-10723

Figure 1. Distribution of seismic stations, seismic refraction lines and microearthquake activity during the period February-March 1978, Cerro Prieto area.

stations were occupied, the study was conducted in several different phases at sites shown in Figure 1. Stations 1, 6, 8, 10, 11 and 12 served as reference stations for the entire period with vertical, then horizontal, components. The remaining stations were occupied with vertical, then horizontal, components for periods of 4 to 8 days. At each station the signal from a 4.5-Hz geophone was radio-telemetered to a central point and recorded with time- and tape-speed compensation data at 0.24, then 0.12 ips, on 14-channel FM tape recorders with 0-80 Hz and 0-40 Hz bandwidth, respectively. Additional arrival times and first motions were provided by CICESE who maintained short-period, smoked-paper recorders at stations CPR, TLX, QKP, and SON (see Figure 1).

In addition to the data provided by this study, refraction data obtained for CFE in 1962 by Geologos Consultores Asociadoes (GEOCA) (line 1 and line 3, Figure 1) were analyzed and interpreted along with the available gravity data. The combined interpretation was used to determine velocity structure and basement depths.

Microearthquake Data

During the recording period, 74 events with S-P times of less than 5 sec were observed at stations 1, 2 and 6 with a threshold of detection and location near $M_L \geq 1$ within the array area.

Of the events recorded on five or more stations, only six events were located near or within the production zone. These events occurred over a two-day period (February 18-19) and were part of a swarm of 20 events, 14 of which occurred within one hour with nearly identical S-P times. The events were located at depths between 2-3 km near stations 4 and 5 (Figure 1). The model used to locate the events was two layers over a half space with P- and S-wave velocities of (2.0, 0.8), (3.5, 2.0) and (5.5, 3.2) km/sec, and layer thickness of 1 and 2 km, respectively.

The other events detected occurred outside the array, allowing only approximate locations (shaded regions, Figure 1). Forty-eight events occurred southeast of the array in the region of a magnitude 4.7 shock which occurred one day after the completion of this study. Four events occurred just south of Cerro Prieto and 15 events originated to the northwest in the Laguna Salada region. Although accurate focal depths are not easily obtained for events outside of an array, the depths seemed to be in the 5-15 km range as contrasted to 2-3 km range for the events inside the production region.

Adequate azimuthal coverage for first motion studies was obtained for only the events occurring within the array, providing one fault-plane solution, consistent with right-lateral strikeslip motion on a NW-trending fault, similar to San Andreas fault movement. The fault plane could not be resolved unambiguously, however, between this motion or left-lateral slip on NE-trending faulting.

Considering the general tectonic nature of the Salton Trough and the complex faulting and structure within the production zone, it seems unusual that microearthquake activity should be so low. McEvilly and Schecter (1978) also report low microearthquake activity at the East Mesa geothermal field. Although low instrument magnifications were used on both surveys, it is doubtful that this can account for the apparent lack of activity. Using similar sensitivities at The Geysers field, we detected 25-30 events/day.

P- to S-wave velocity ratios (V_p/V_s) were estimated by using the Wadati diagram, where S-P time is plotted versus the P-wave arrival time at different stations for a single event, assuming the same V_p/V_s along all propagation paths. The slope of the line through the points is k-1, ($k = V_p/V_s$). Poisson's Ratio, σ, may then be calculated by the expression

$$\sigma = (k^2 - 2)/2(k^2 - 1)$$

The swarm of events near stations 4 and 5 provided adequate data to indicate a Poisson's Ratio of 0.4. This is an average Poisson's Ratio throughout the production zone for the upper 2-3 km. Studies at The Geysers (Majer and McEvilly, 1979) and Coso Hot Springs (Combs and Rotstein, 1975) indicated Poisson's Ratios between 0.15 and 0.20 for regions within the vapor-dominated zones. McEvilly and Schechter (1978) found Poisson's Ratio of 0.4 for the upper kilometer for sediments at the East Mesa geothermal field.

Because P-wave velocities are affected more by fluid content than S-wave velocity (Toksoz et al., 1976), the high Poisson's Ratio indicates fluid domination in the upper 2-3 km of the production zone. Somerton (1978) in a laboratory investigation of Cerro Prieto cores measured Poisson's Ratio near 0.1 for dry sandstone and 0.3 for water-saturated sandstone. These and similar laboratory studies indicate that if the reservoir changes from water domination to a two-phase fluid system, we can expect to observe a decrease in the Poisson's Ratio.

P-Wave Velocity and Attenuation Data

Because of noisy data, it was difficult to determine whether a velocity anomaly is associated with the production zone. The advances and delays in P- and S-wave arrivals may be due to faulting, varying sediment composition and thickness, or hydrothermal alteration.

To determine whether the production zone affects the amplitude and frequency of seismic waves, spectral studies were carried out using the P-wave of a regional event. The approach taken as used at The Geysers, California (Majer and McEvilly, 1979) and Leach Hot Springs, Nevada (Majer, 1978). The method is an adaptation of a technique developed by Teng (1968) for analysis of teleseismic data. The ratio of the spectrum of the P-wave at each station to an arbitrary reference station is used to obtain the differential attenuation. It is in assumed that Q is frequency-independent over the band used and that the paths to both stations are common except for the last fraction of the total path.

Stations 1, 2, 3 and 4, which are west of the production zone, exhibit slightly lower or near-normal attenuations over the 5-20 Hz range. Stations 10 and 11, which are east of the production zone, show slightly higher attenuation. Stations in the production zone exhibit significant attenuation (stations 5 and 8); however, station 6, which is the closest to the center of production, shows attenuation lower than normal. Due to high noise levels there is insufficient data at station 9 and only marginal data at station 11.

The higher attenuation noted at stations 5 and 8 may be associated with faulting, evidenced by the microearthquake activity in this region. The lack of attenuation closer to the center of the production zone (station 6) may be due to alteration by precipitation in this region. The increasing attenuation east of the field (stations 10 and 11) may only be due to increasing sediment thickness.

Refraction Data

In addition to the data obtained from the February 14-March 11 study, two lines of refraction data were analyzed to determine velocity structure and depth to basement. Unfortunately, none of the refraction lines crossed the present production zone; however, lines 1 and 3 (Figure 1) crossed near the edges of the field as presently defined by drilling.

The difference between the lines are the complexity of the travel time data and the high basement velocities (6 km/sec) along line 1 compared to those for line 3. The velocities of the layers obtained compare well with velocities for sediments in other parts of the Colorado Delta region (Kovach et al., 1962). The structure along the southern line appears much simpler than that of the northern line. There is evidence for a horst and garben structure along line 1. On line 3 there seems only to be down-faulting to the east. Although the two refraction lines

were only 6 km apart, it is obvious that the structure cannot be correlated from one line to the other.

To gain additional information we obtained two-dimensional model fits to gravity data along each line (Talwani et al., 1959). The gravity data were obtained from a CFE gravity map by Velasco and Martinez (1970). Care was taken to use only data points rather than the contoured gravity values. The starting gravity models were based on the refraction results. A density contrast of 0.3 g/cm^3 was assumed between bedrock and shallow sediments. Although a close fit could be obtained by using a fairly localized density contrast along line 1, it was necessary to distribute the density contrasts throughout the section on line 3. Other workers in the Salton Trough have cautioned against assuming that gravity strictly reflects depth to basement, for it may also be affected by differing sediment densities.

Figures 2,4 and 3,5 are interpretations of the gravity and refraction data along lines 1 and 3, respectively. The gravity high in the center of line 3 and the smoother gradient on the eastern limb of the high can be accounted for by an intermediate density layer coming close to the surface in the center of the line and continuing to the east at a greater depth (Figure 5). The refraction data shows an indication of higher velocity material near the surface in the center of the line. However, there is little evidence for extension to the east. A comparison of the two lines reveals greater apparent depth to basement to the south, line 3.

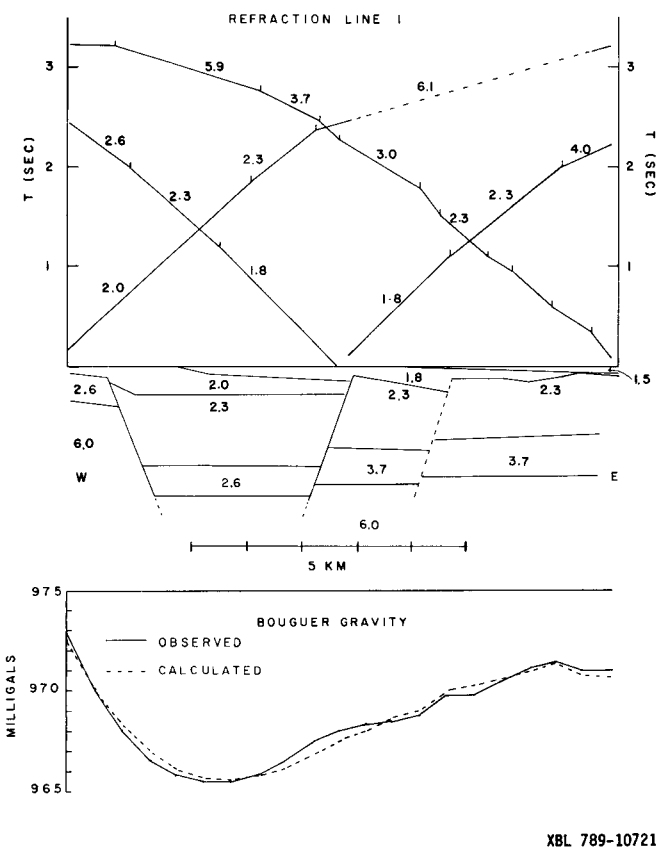

Figure 2. Interpretation of gravity and seismic refraction data along line 1, Cerro Prieto.

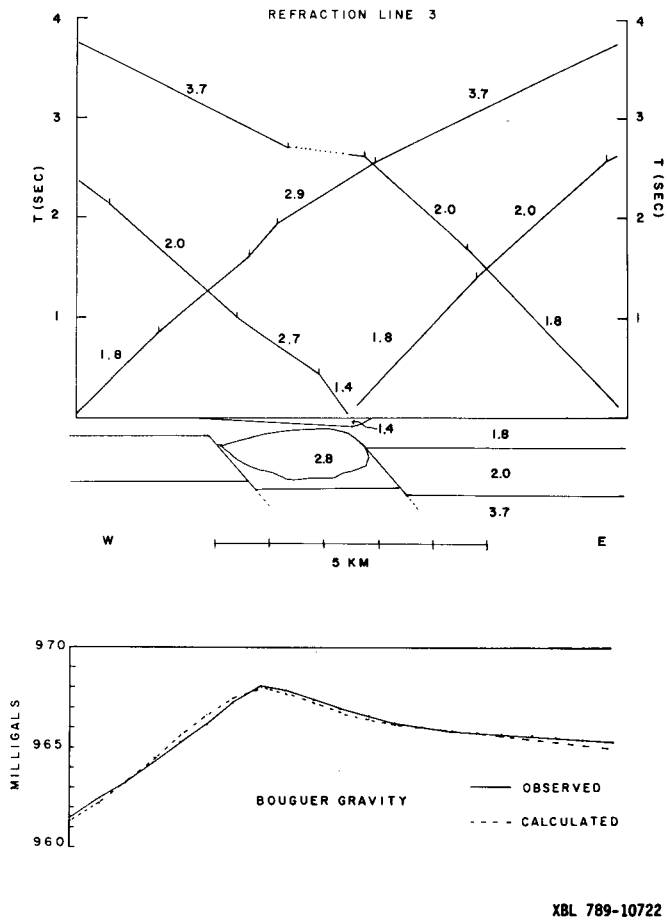

Figure 3. Interpretation of gravity and seismic refraction data along line 3, Cerro Prieto.

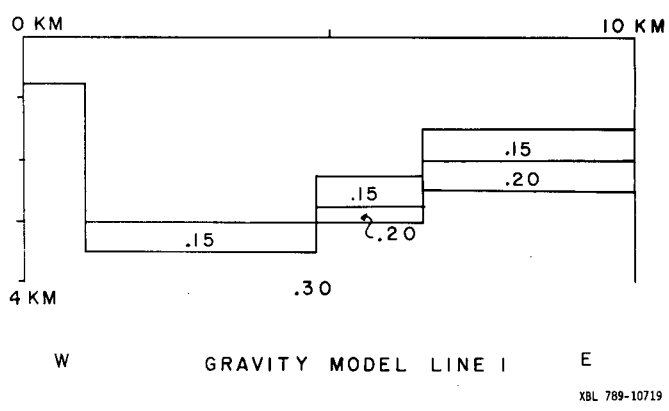

Figure 4. Two-dimensional gravity model along line 1. Values and density contrasts. Compare to Figure 2.

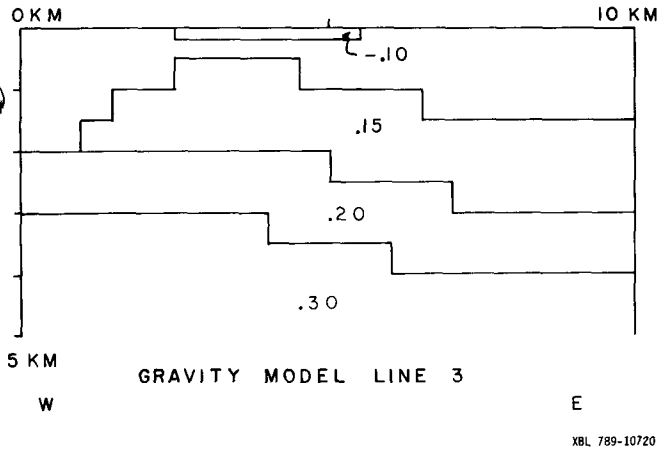

Figure 5. Two-dimensional gravity model along line 3. Values are density contrasts. Compare to Figure 3.

On the eastern edge of line 1, the northern line, the depth to basement was fixed at 2.5 km on the basis of drill cores obtained in Well #96, <1 km north of the line.

CONCLUSIONS AND WORK PLANNED FOR 1979

Seismological data indicate structural complexity associated with the Cerro Prieto geothermal field. Refraction data and microearthquakes suggest several major NW striking faults, possibly controlling the field boundaries. The refraction data also suggest high velocity sediments and shallow basement in the production zones. Compared to seismicity in surrounding areas, microearthquake activity is low in the production area. First motion studies indicate right-lateral strike-slip motion for events within the field on NW-SE trending faults. Further microearthquake data are necessary to reduce the ambiguity in earthquake source and occurrence properties for comparison to regional values.

High levels of man-made ground noise in the center of the production zone limit the amount of velocity and attenuation data that can be collected. The few data collected suggest P-wave velocity and attenuation anomalies associated with the production region. V_p/V_s values are high; further monitoring may reveal an eventual decrease, indicating a change to a two-phase reservoir. Microearthquake data may indicate steam zones if the events are related to large pressure or temperature gradients or to volume changes associated with fluid removal. There is sufficient seismic activity in the production zone to warrant continuous monitoring.

In future work, we will continuously monitor seismicity and V_p/V_s values within the production zone by means of a five-station array centered near station 5 (Figure 1). Each station will digitally record 12-bit data on a triggered cassette system from a three-component, 4.5-Hz geophone in a 100-m-deep well. The stations will be connected to a central station that will provide a periodic time fiducial and visual monitor of the activity. These data will provide the necessary information to infer the relation between fluid withdrawal/reinjection and future seismicity.

REFERENCES CITED

Combs, J., and Rotstein, Y., 1975. Microearthquake studies at the Coso geothermal area, China Lake, California, in Proceedings, second U. N. symposium on the development and use of geothermal resources, May 20-29, 1975, San Francisco. Washington, D. C., U. S. Government Printing Office, v. 2, p. 909.

Elders, W. A., Hoagland, J. R., and Olson, E. R., 1978. Hydrothermal mineralogy and isotopic geochemistry in the Cerro Prieto geothermal field, Mexico. Geothermal Resources Council Transaction, III, Practical Applications, v. 2, p. 177.

Kovach, R. L., Allen, C. R., and Press, F., 1962. Geophysical investigations in the Colorado delta region. J. Geophys. Res., v. 67, p. 2845.

Majer, E. L., 1978. Seismological investigations in geothermal regions. Ph.D. thesis, University of California, Berkeley, LBL-7054.

Majer, E. L., and McEvilly, T. V., 1979. Seismological investigations at The Geysers geothermal field. Geophysics, in press.

McEvilly, T. V., and Schechter, B., 1978. East Mesa seismic study, report no. 3. Berkeley, Lawrence Berkeley Laboratory, UCID-4030.

Somerton, W., 1978. Some physical properties of Cerro Prieto cores, in Proceedings of the first symposium on the Cerro Prieto geothermal field, Baja California, Mexico. Berkeley, Lawrence Berkeley Laboratory, LBL-7098.

Talwani, M., Worzel, J. L., and Landisman, M., 1959. Rapid computations for two-dimensional bodies with application to the Mendocino submarine fracture zone. J. Geophys. Res. v. 64, p. 49.

Teng, T., 1968. Attenuation of body waves and the Q structure of the mantle. J. Geophys. Res. v. 73, p. 2195.

Toksoz, M. N., Cheng, C. H., and Timur, A., 1976. Velocities of seismic waves in porous rocks. Geophysics v. 41, p. 621.

Velasco, H., and Martínez, B., 1970. Levantamiento gravimétrico de la zona geotérmica de Mexicali, Baja California. Consejo de Recursos Naturales No Renovables, Bol. 74, 20 p.

SELF-POTENTIAL STUDIES AT CERRO PRIETO

R. F. Corwin and H. F. Morrison

ACTIVITIES IN 1978

Self-potential anomalies are correlated with geothermal activity in many areas around the world (Corwin and Hoover, 1978). These anomalies often are associated with faults that are thought to serve as conduits for thermal fluids, or with areas of high heat flow or vigorous subsurface fluid flow. To see whether the self-potential method could prove helpful in delineating the zone of geothermal activity at the Cerro Prieto field, about 100 line km of data were taken in the vicinity of the presently operating geothermal wells and 75-MW power plant.

Field Procedure

The self-potential survey lines in the central part of the survey area and their relation to the present geothermal production zone are shown in Figure 1. Field procedures have been described

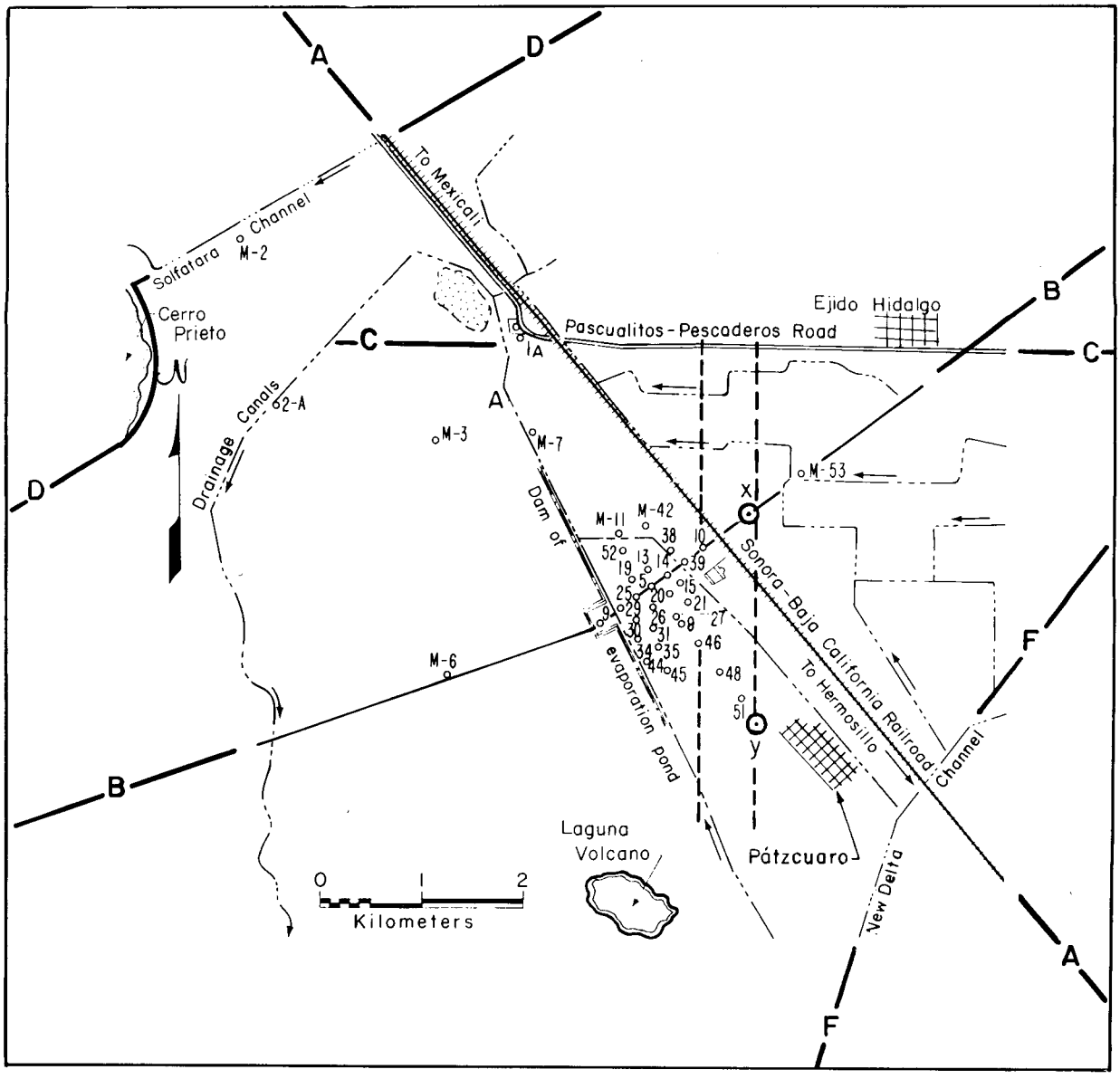

XBL 776-1179A

Figure 1. Self-potential survey lines in the central part of the Cerro Prieto geothermal field. A complete map of the survey lines is shown in Figure 3. The dashed lines indicate the location of the charged planes used to explain the source of the anomaly. Numbered circles are geothermal production wells.

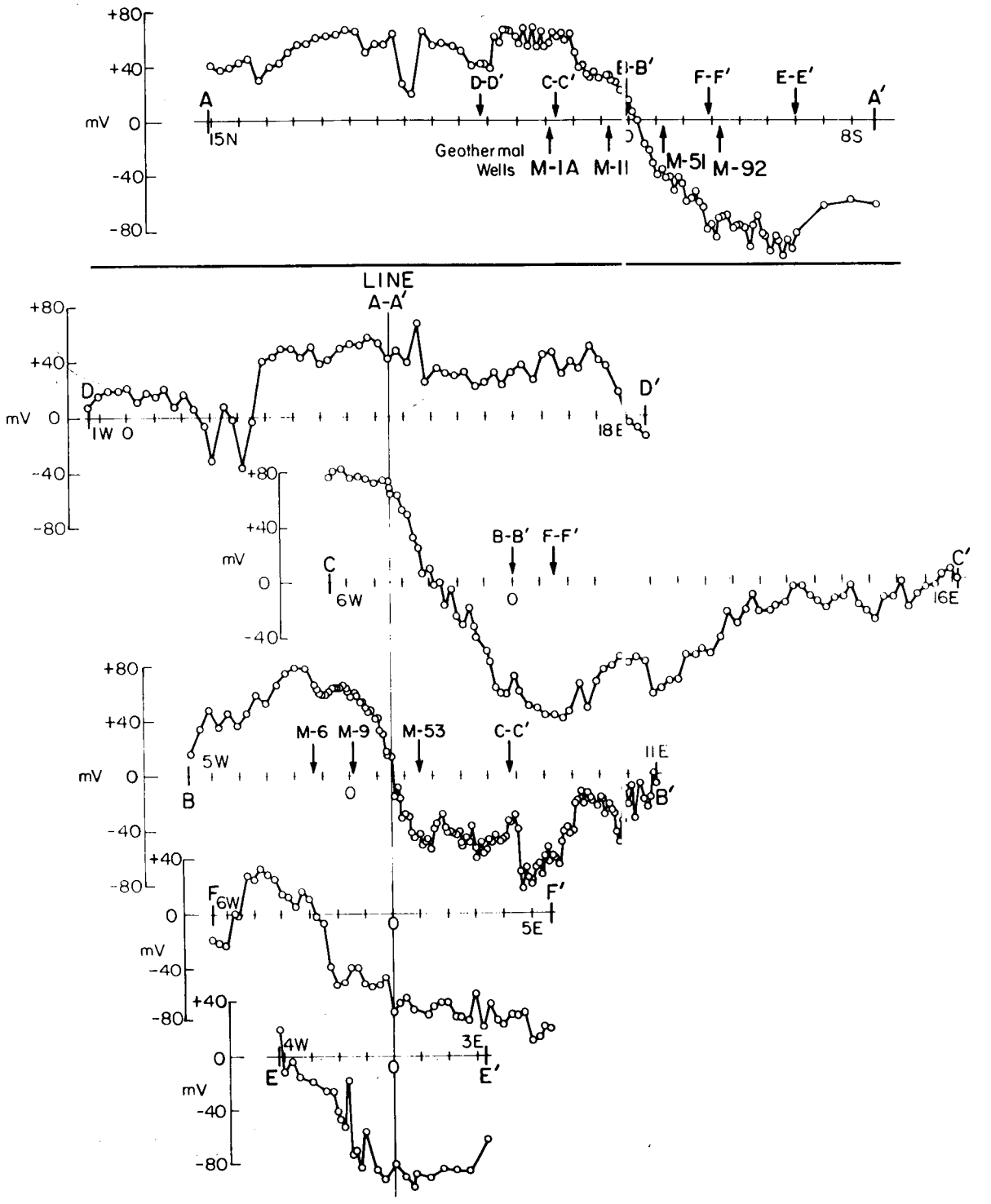

XBL 787-5327

Figure 2. Self-potential data profiles in the area of the Cerro Prieto geothermal field.

by Corwin et al. (1978). The survey data are shown in profile form in Figure 2 and contoured in Figure 3. The complete survey lines also are shown in Figure 3. Short-wavelength variations, less than 500-m wide, were ignored in the contouring.

A well-developed dipolar anomaly of about 160 mV peak-to-peak amplitude, positive to the west and negative to the east, is seen on line B-B' (Figure 2), which runs through the center of the present geothermal production zone.

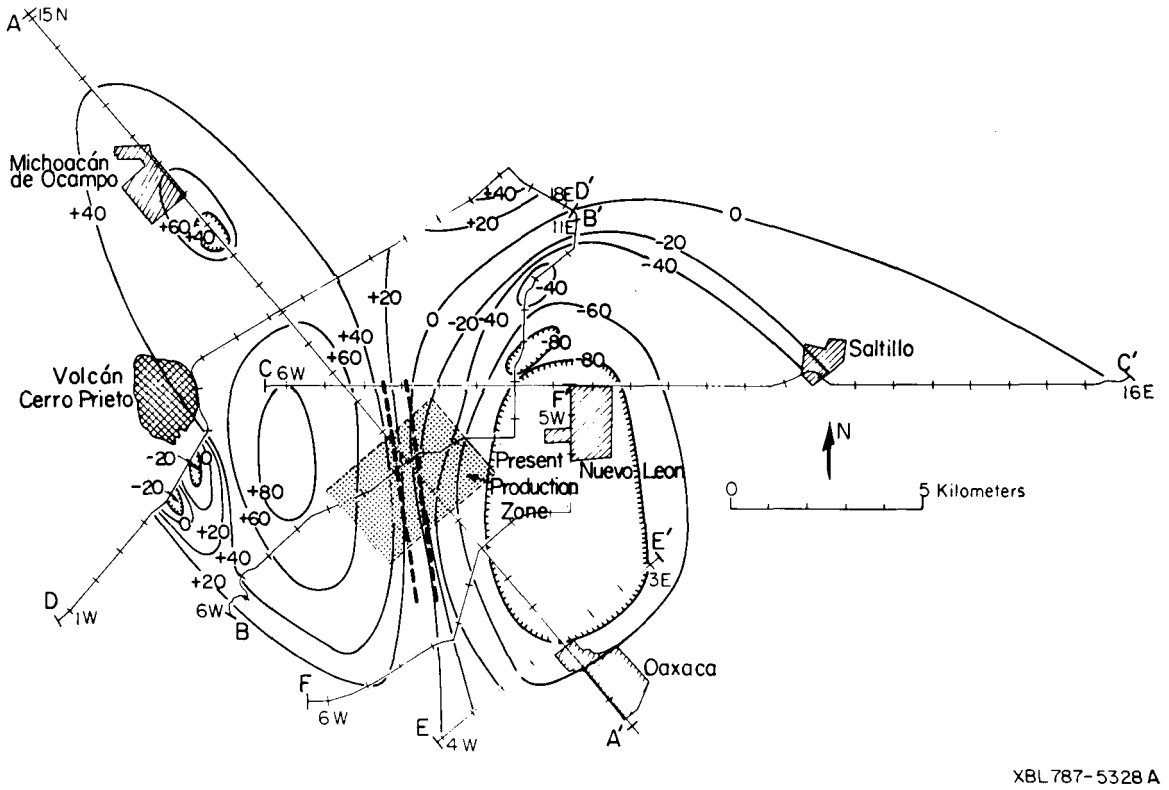

Figure 3. Self-potential contours, Cerro Prieto area. Contour interval is 20 mV.

The contours of Figure 3 shows that the axis of the dipolar anomaly (the 0-mV contour) passes through the approximate center of the present production zone, if the zone is considered to include the presently producing well M-53 (Figure 1). The axis of the anomaly trends about N.5° W., and to the east of the axis the anomaly appears to be somewhat elongated in both the north-south and east-west directions. The contours appear to be affected by a trend running parallel to and just south of the eastern portion of line D-D'. Aside from the major dipole anomaly, strong self-potential activity is seen on line D-D' just south of the Cerro Prieto volcano. Geophysical data indicate a major fault running through this area, but the self-potential coverage is insufficient to allow any conclusions to be drawn about the relation between this fault and the self-potential activity. Smaller but still significant anomalies are seen just to the northwest of Nuevo Leon and just to the southeast of Michoacan de Ocampo.

Analysis

As the self-potential anomaly shows no correlation either to surficial or cultural features or the thermally inactive Imperial fault zone, its cause is likely to be a deep-seated mechanism related to geothermal activity. The theory of how geothermal sources may generate surface self-potential anomalies was described by Nourbehecht (1963) and developed by Fitterman (1978) of the U. S. Geological Survey.

Briefly, the mechanism is based on the fact, established by laboratory measurements, that the flow of either fluid or heat through a rock creates a measurable voltage. The ratio of the developed voltage to the pressure gradient causing fluid flow is called the electrokinetic or streaming-potential coupling coefficient (CE). The ratio of the developed voltage to an applied temperature gradient causing heat flow is called the thermoelectric coupling coefficient (C_T).

The form of the Cerro Prieto anomaly resembles a potential distribution generated by flow parallel to a vertical plane separating regions of different coupling coefficients; the potential distribution developed over only a limited length and depth extent of the plane (Fitterman, 1978). Geologically, this would correspond to a vertical flow of fluid, heat, or both, in the vicinity of a vertical fault, fracture zone, or contact separating regions of differing coupling coefficients.

There appears to be geological and geophysical evidence for the existence of a major fault or fracture zone with location, strike direction, and depth extent similar to those postulated to explain the SP anomaly. This fault is thought to provide an important conduit for thermal fluids to ascend from the basement rocks into the reservoir formation (Noble et al., 1977). The sandstone and shale reservoir formation is capped by relatively impermeable clay to a depth of about 1 km and is underlain by a granite basement at a depth of about 3 to 4 km. This region, from

about 1 to 4 km depth, corresponds well to the source region postulated for the self-potential anomaly.

Our tentative conclusion, then, is that a difference in thermoelectric or electrokinetic coupling coefficients (or both) exists across the Patzcuaro fault or fracture zone, and that a vertical component of heat or fluid flow (or both) in the presence of this vertical discontinuity generates the observed self-potential anomaly. Thus, the Patzcuaro fault or fracture zone may represent an important structural feature of the Cerro Prieto geothermal field.

REFERENCES CITED

Corwin, R. F., and Hoover, D. B., 1978. The self-potential method in geothermal exploration. Berkeley, Lawrence Berkeley Laboratory, LBL-7075.

Corwin, R. F., Morrison, H. F., Diaz, S., and Rodríguez, J., 1978. Self-potential studies at the Cerro Prieto geothermal field, in First symposium on the Cerro Prieto geothermal field, September 20-22, 1978, abstracts. Berkeley, Lawrence Berkeley Laboratory, LBL-7098 ABS.

Fitterman, D. V., 1978. Private communication.

Noble, J. E., Mañon, A., Lippmann, M. J., and Witherspoon, P. A., 1977. A study of the structural control of fluid flow within the Cerro Prieto geothermal field, Baja California, Mexico. Preprint, 52nd annual meeting of the Soc. of Pet. Engrs., AIME.

Nourbehecht, B., 1963. Irreversible thermodynamic effects in inhomogeneous media and their application in certain geoelectric problems. Ph.D. thesis, Cambridge, Mass. Inst. Tech.

RESISTIVITY STUDIES AT CERRO PRIETO

M. J. Wilt and N. E. Goldstein

ACTIVITIES IN 1978

As part of a cooperative research venture between the U. S. Department of Energy (DOE) and the Comisión Federal de Electricidad de México (CFE), a series of dc resistivity investigations were performed at the Cerro Prieto geothermal field. The work has included Schlumberger and dipole-dipole field surveys, geoelectric computer modeling, and geological interpretation of results. The goals of this work are: (a) to determine whether the reservoir region or controlling geologic structure can be delineated by careful dc resistivity measurements; (b) to explore, with geoelectric modeling, the possibility of using the dipole-dipole resistivity technique for monitoring temporal changes in resistivity caused by changes in the reservoir; and (c) to perform the first set of replicate dipole-dipole measurements.

The dipole-dipole technique was chosen for temporal monitoring because it is inherently sensitive to lateral resistivity variations and because the relatively few permanent stations needed for remeasurement can be easily established.

Resistivity Surveys

During 1978, two long dipole-dipole lines were surveyed at Cerro Prieto by LBL resistivity crews each with dipole separations of 1 and 2 km (Figure 1). The northern line, D-D', is 18 km long and extends northeastward from the Cucapa Mountains into the Mexicali Valley, passing just south of the Cerro Prieto volcano. This line is roughly coincident with CFE Schlumberger-resistivity line 1, which was also used in interpretation; the two lines overlap for approximately 10 km. Line E-E' also begins at the Cucapa Mountains, is approximately 16 km long and trends subparallel with D-D'. It extends eastward into the Mexicali Valley passing through the central portion of the production zone.

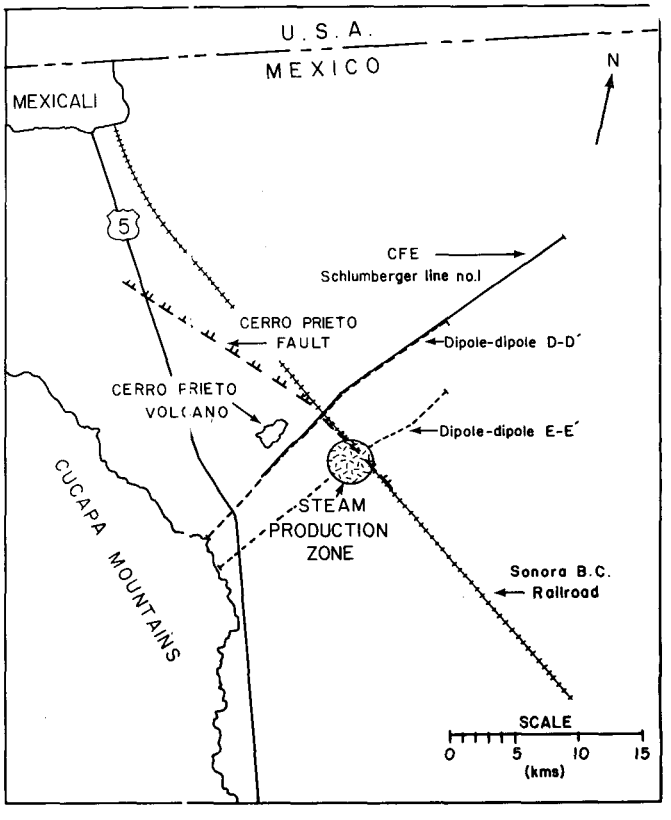

XBL 788-1632

Figure 1. Project location map, LBL resistivity project.

A finite-difference computer program capable of modeling resistivity variations in two dimensions was used for interpretation of Schlumberger and dipole-dipole data (Dey, 1976; Dey and Morrison, 1976). The program computes potentials at all nodal points within and on the surface of an arbitrary two-dimensional earth model. It is capable of calculating apparent resistivity for the Schlumberger, dipole-dipole, roving dipole, and several downhole arrays. A limitation to this program is the size of the network mesh. The 58 x 16 nodal size does not allow for detailed models of both shallow and deep structures simultaneously. For example, if a model of earth structure to 3 km is desired, then the minimum size body that may be incorporated with one mesh is 100 x 100 meters. This could exclude small surficial inhomogeneities in models, even though such features are evident in data sets.

Results

Some examples of field results of Schlumberger and dipole-dipole surveys are shown in the top portions of Figures 2, 3 and 4. All plotted values are apparent resistivity in ohm-m. Schlumberger apparent resistivities (Figure 3) are plotted, by convention, below the center of the array as a function of AB/2 (half the separation between the current electrodes). Dipole-dipole apparent resistivities (Figures 2 and 4) are plotted as a function of distance between current and potential electrode pairs in integer multiples of the electrode separation, or N spacing. The values appear at the intersection of 45° lines drawn from the centers of the current and potential dipoles.

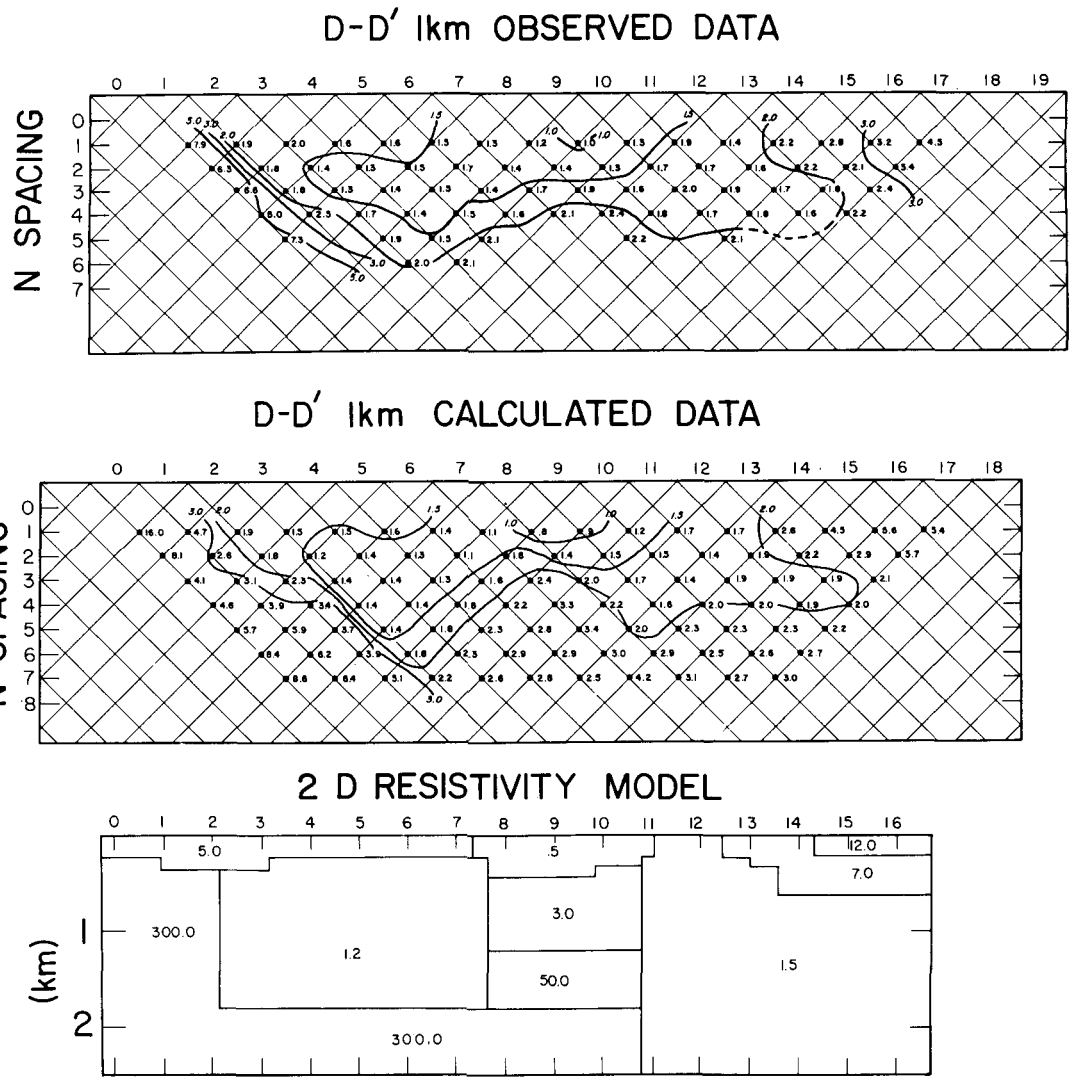

Figure 2. Dipole-dipole apparent resistivity pseudosection for 1-km dipoles along line D-D'; field data, model generated data, and two-dimensional resistivity model.

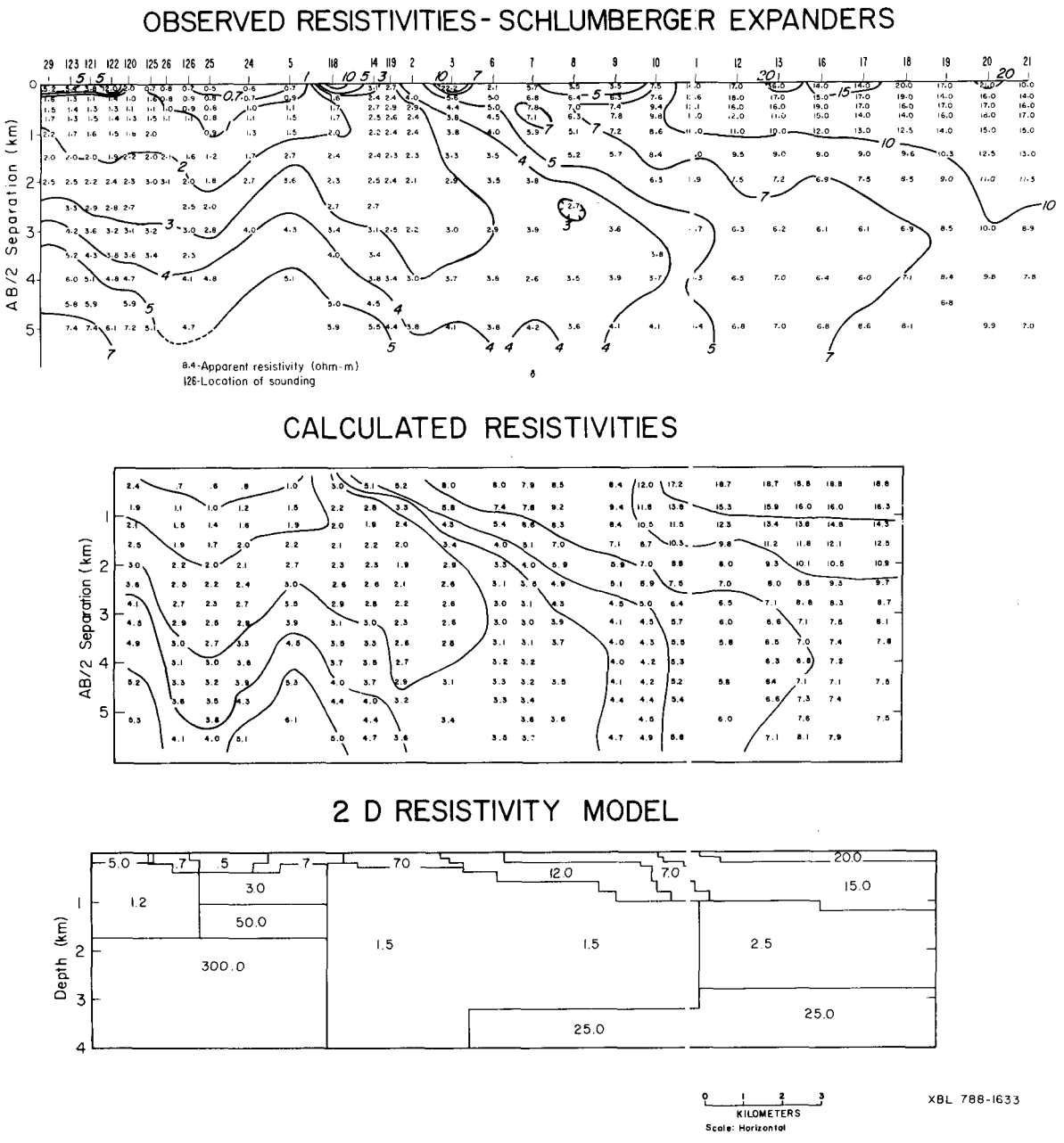

Figure 3. Schlumberger apparent resistivity pseudosection for data taken along line D-D'; field data, model generated data, and two-dimensional resistivity model.

Dipole-dipole models were first calculated for data taken with 1-km dipole lengths to obtain the near-surface features, then for 2-km dipoles to help resolve deeper boundaries. The model was considered acceptable only if it satisfied both data sets. Schlumberger data were modeled only for AB/2 spacing greater than 100 m because the grid network is insufficiently large to account for near-surface detail.

Discussion

Resistivity measurements show that the Cerro Prieto region has very low resistivities down to great depths. Surficial resistivities can be below 0.5 ohm-m, and the majority of electrical units defined have resistivities below 2 ohm-m. In such an environment, a low resistivity region expected for a geothermal reservoir in sediments may be totally masked. However, at Cerro Prieto we find evidence that the reservoir region may actually possess a higher resistivity than the overlying rocks. Resistivity measurements were found to be very useful in delineating structure and for deducing characteristics of rocks within and outside of the geothermal field. The following is a brief summary of the principal findings:

1. The production region at Cerro Prieto is characterized by high resistivity (4 ohm-m) relative to the surrounding region (1 to 2 ohm-m).

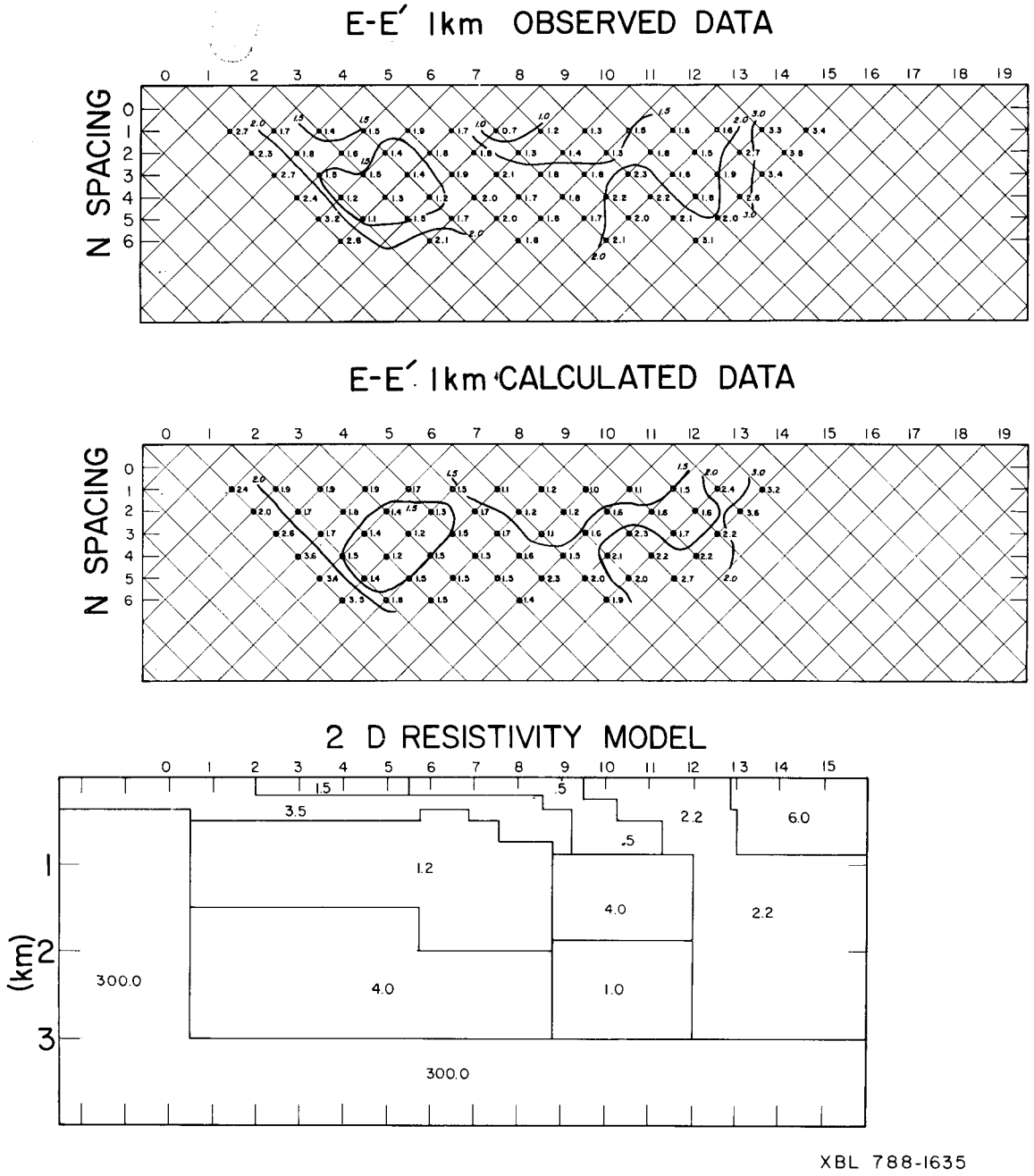

Figure 4. Dipole-dipole apparent resistivity pseudosection for 1-km dipoles along line E-E'; field data, model-generated data, and two-dimensional resistivity model.

2. Modeling studies suggest that significant increases with time of resistivity or thickness of the production zone are detectable with precision dipole-dipole measurements.

3. Several faults that may act as hydrologic barriers and are related to the production zone have been detected with dipole-dipole measurements.

4. Perturbation studies in the resistivity model over the reservoir region suggest that the northern nonproductive region adjacent to the volcano was more permeable in the past and resembled more closely the present production zone.

5. Modeling studies have shown that at Cerro Prieto, dc resistivity is not an effective tool for mapping basement surface or other deeply buried resistive horizons.

PLANS FOR FISCAL YEAR 1979

In 1979 we plan to remeasure the two established dipole-dipole lines, D-D' and E-E', extending each other 4 km to the east. In addition, a new dipole-dipole line trending northwest and connecting D-D' and E-E' will be established. The purpose of this new line is for detecting any anisotropy in the rocks and for tying the other dipole-dipole lines together for purposes

of three-dimensional resistivity modeling. All resistivity measurements will be performed with new receiver instrumentation. This new device will allow for resistivity measurements to be reproducible to within 2%, which is within the accuracy required for dipole-dipole monitoring of temporal resistivity changes.

E-field ratio telluric studies will be performed at the same time, using the same electrodes and receiver instrumentation as in the dipole-dipole study. The purpose of this study is to determine the effectiveness of the method in a highly conductive environment. This study will also test the applicability of telluric phase measurements, which are now done easily with the new general-purpose microprocessor-controlled receiver.

We will exercise for the first time a three-dimensional resistivity modeling program to investigate the effects of three-dimensional structure on results derived from two-dimensional models. The study will be based on new and existing dipole-dipole data obtained by LBL and on Schlumberger resistivity data obtained by CFE. In addition, a more complete analysis of possible resistivity perturbations caused by reservoir depletion and mineral deposition will be performed, and resistivity well logs will be correlated to surface resistivity measurements.

REFERENCES CITED

Dey, A., 1976. Resistivity modeling for arbitrary shaped two-dimensional structures. Part II, User's guide to the FORTRAN algorithm RESIS2D. Berkeley, Lawrence Berkeley Laboratory, LBL-5283, 56 p.

Dey, A., and Morrison, H. F., 1976. Resistivity modeling for arbitrary two-dimensional structures. Part I, Theoretical formulation. Berkeley, Lawrence Berkeley Laboratory, LBL-5233, 18 p.

_____, 1977. Resistivity modeling for arbitrarily shaped three-dimensional structures. Berkeley, Lawrence Berkeley Laboratory, LBL-7010.

Noble, J. E., Mañon, A., Lippmann, M. J., and Witherspoon, P. A., 1977. A study of the structural control of fluid flow within the Cerro Prieto geothermal field, Baja California, Mexico. Preprint, 52nd Annual Meeting of the Society of Petroleum Engineers, AIME.

Razo M., A., and Arellano G., F., 1978. Prospección eléctrica de la porsion norte del Valle de Mexicali y campo geotermico de Cerro Prieto, Baja California. Informe por Comisión Federal de Electricidad.

MAGNETOTELLURIC SURVEY AT CERRO PRIETO

T. D. Gamble, W. M. Goubau, N. E. Goldstein, and J. Clarke

ACCOMPLISHMENTS IN 1978

Magnetotelluric (MT) soundings were made at seven sites at Cerro Prieto to obtain deep resistivity information. Surveys were performed using the remote magnetic reference technique, which has recently been shown to provide more accurate results than conventional MT in areas of interfering noise or when the natural field strength is weak (Gamble 1978; Gamble et al., 1978).

The seven sites and the reference site, R, on the edge of the Cucapa mountains are shown in Figure 1. Two components of the reference signals were telemetered to the local sounding site by FM radio. Three-component SQUID magnetometers were used for magnetic field measurements, and 200-m dipoles in an L-shaped array were used for the electric field measurements. The dc telluric voltages were filtered out by means of a 0.001-Hz high-pass single-pole filter. All channels had matching 60-Hz notch filters. The seven channels of data were recorded on a Honeywell FM analog tape recorded at 1-7/8 ips. Up to 6 hours of data were recorded at each station. Data were later digitized in Berkeley using a Varian minicomputer. Subsequent digital processing and analysis were conducted on the LBL CDC-7600 system.

The data were collected in two overlapping frequency bands but only the lower band, covering the period range of 8 to 840 sec, has been completely analyzed. Analysis and interpretation have been directed mainly to the results from stations 1 through 6, which lie along a line nearly coincident with a line of dipole-dipole and Schlumberger dc resistivity measurements. The MT results have been interpreted for comparison with the dc resistivity interpretations (Razo et al., 1978; Wilt et al., 1978).

In contrast to dc resistivity measurements, MT provides a great volume of information at each station, only a fraction of which we are capable of using in quantitative interpretations. For each frequency component, MT yields at least six independent complex values but only the real parts of two are commonly used in interpretations. These are the apparent resistivities rotated into the two principal horizontal resistivity directions (Figure 2). In this case, ρ_{xy} is the apparent resistivity in the parallel-to-strike direction (associated with the TE mode of propagation) and ρ_{yx} is in the perpendicular-to-strike direction (associated with the TM mode of propagation). The vertical bars indicate the probable errors (50% confidence limits), which become very small for the good data obtained. Unless the surface layer is anisotropic, ρ_{yx}

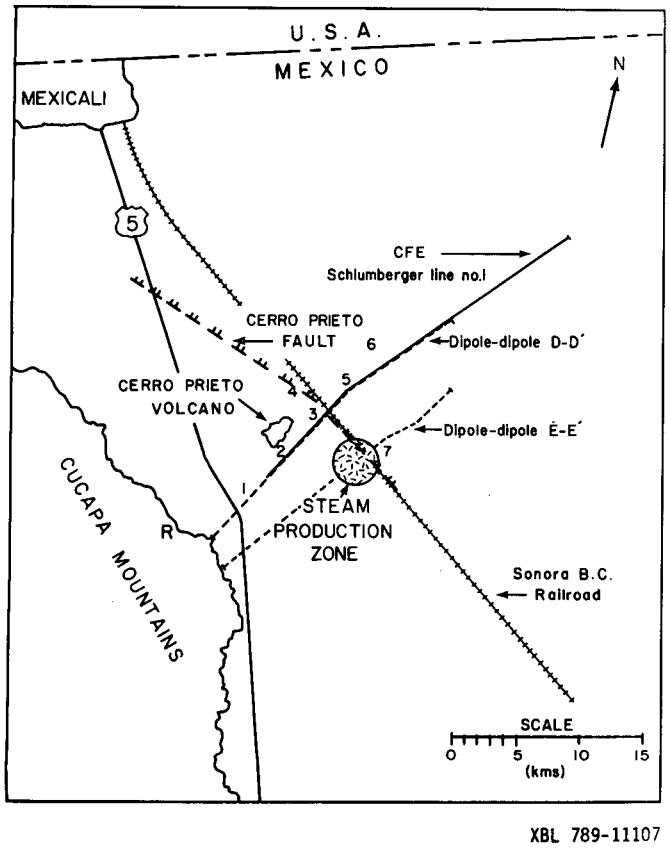

Figure 1. Magnetotelluric sounding sites 1 through 7 and remote magnetometer site R at Cerro Prieto.

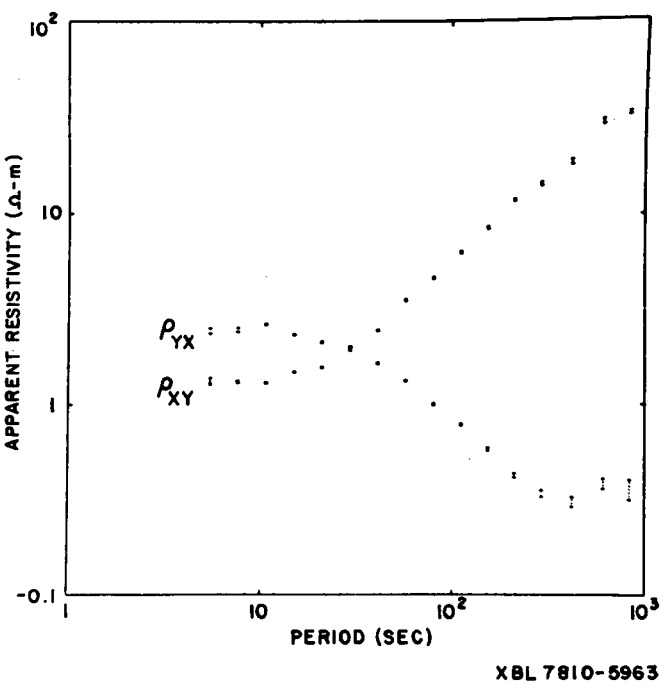

Figure 2. Rotated apparent resistivities and their probable errors for Station 6.

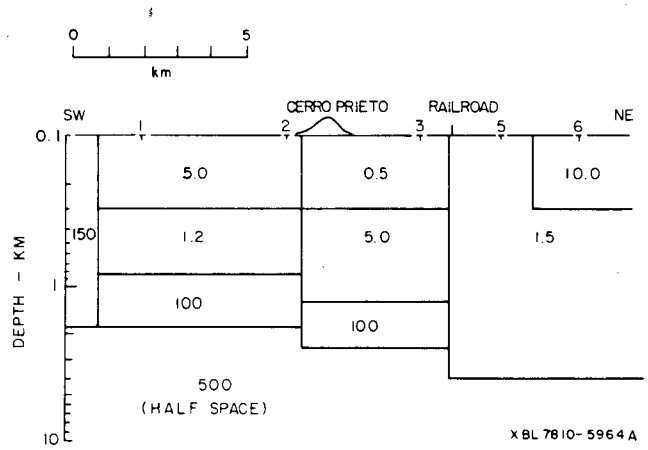

Figure 3. Two-dimensional model of the resistivity structure derived from the ρ_{xy} data set.

and ρ_{xy} coverage at shorter period (higher frequency), but their divergence at longer periods is evidence of a multidimensional geological structure.

Because the general results indicate a two-dimensional geometry, the MT results were fitted to two-dimensional models. Starting with the model derived from dc resistivity, we obtained the model (Figure 3) that fits the ρ_{xy} (TE mode) data. The calculated resistivities for this model (Figure 4) may be compared with the observed resistivities (Figure 5).

A preliminary interpretation of the MT results shows that the model derived from the ρ_{xy} data set agrees, in general, with the model fitting the dc resistivity data along the same line. Clear evidence for both the Cucapa fault, west of Station 1, and the Cerro Prieto fault, between Stations 3 and 5, can be seen in the MT interpretation.

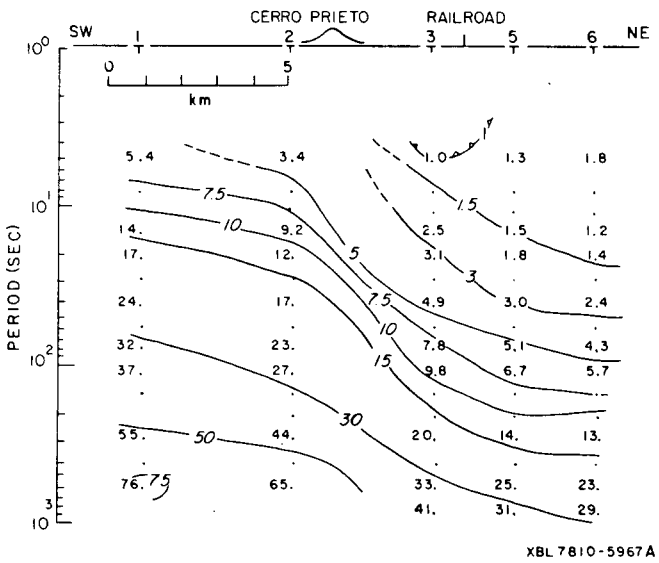

Figure 4. Pseudosection of apparent resistivities ρ_{xy} calculated from the model in Figure 3.

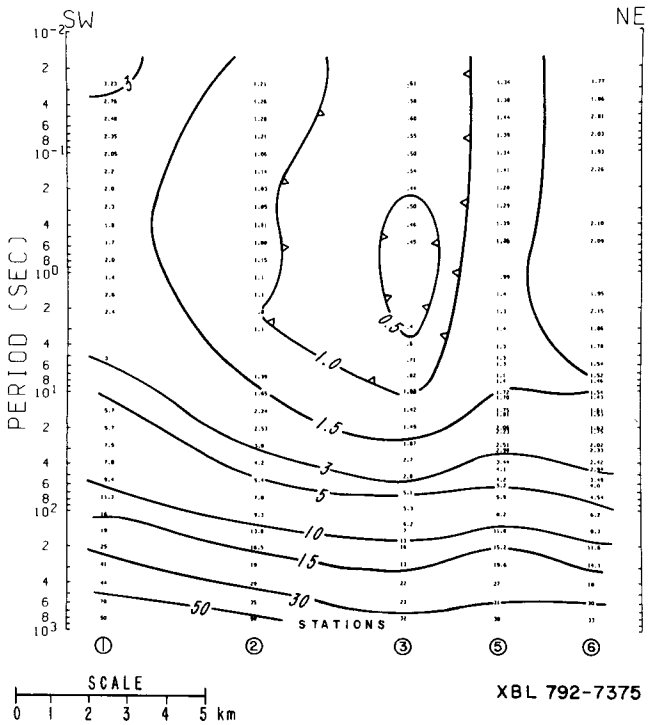

Figure 5. Pseudosection of observed apparent resistivities ρ_{xy} at Stations 1, 2, 3, 5, and 6.

PLANS FOR FISCAL YEAR 1979

The higher frequency band of data collected at each of the seven sites will be processed. This will provide complete coverage over the period range of 0.02 to 900 sec.

An additional group of MT stations will be occupied at selected sites over the producing part of the reservoir, including the Patzcuaro fault zone, locus of the large SP anomaly (Corwin et al., 1978). Further modeling of the results will be done and correlated with other subsurface resistivity data.

REFERENCES

Corwin, R. F., Morrison, H. F., Diaz, C. S., and Rodriguez, B. J., 1978. Self-potential studies at the Cerro Prieto geothermal field, in First symposium on the Cerro Prieto geothermal field, Baja California, Mexico. Berkeley, Lawrence Berkeley Laboratory, LBL-7098 ABS.

Gamble, T. D., 1978. Remote references magnetotellurics with SQUIDs. Ph.D. thesis, Berkeley, University of California, LBL-8062.

Gamble, T. D., Goubau, W. M., and Clark, J., 1978. Magnetotellurics with a remote magnetic reference. Berkeley, Lawrence Berkeley Laboratory, LBL-7032.

Razo M., A., Arellano G., F., Fonseca L., H., 1978. CFE resistivity studies at Cerro Prieto, in First symposium on the Cerro Prieto geothermal field, Baja California, Mexico, Abstracts. Berkeley, Lawrence Berkeley Laboratory, LBL-7098 ABS.

Wilt, M., Goldstein, N., and Razo M., A., 1978. LBL Resistivity studies at the Cerro Prieto geothermal field, in First symposium on the Cerro Prieto geothermal field, Baja California, Mexico, Abstracts. Berkeley, Lawrence Berkeley Laboratory, LBL-7098 ABS.

PRECISION GRAVITY SURVEYS AT CERRO PRIETO

R. B. Grannell, D. W. Tarman,† and N. E. Goldstein*

ACTIVITIES IN 1978

Fifty-five gravity stations and five alternates were established over an area of approximately 500 km^2 centered on the geothermal field (Figure 1). All stations are permanent, and consist of concrete pads large enough to accommodate a gravity-meter base plate. Two control stations were placed on bedrock which might be presumed stable with respect to production-induced subsidences: (a) Station 1 on granite in the Cucapa Mountains some 15 km west of the geothermal plant, and (b) Station 20 on the flanks of the Cerro Prieto volcano less than 10 km northwest of the power plant. The five alternate stations were established either to augment the bedrock stations or to provide more reliable valley stations where the initial stations were found to be unsuitable for long-term studies.

During the year all of the stations were leveled by CFE engineers and tied into the established first- and second-order level networks around the field. Complete sets of gravity readings were made at most of the stations (Grannell et al., 1978). To maximize the precision of the gravity values, each station was occupied an average of four times, twice each with two La Coste and Romberg G model gravity meters. During each occupation, a minimum of four readings was obtained, two each by two operators. The meter set-ups were changed before each reading so that errors due to leveling or orientation could be distributed. The occupations were also distributed in time to minimize the differential effects of tares caused by vehicular noise on roads, instrument drift, external temperature changes and wind conditions.

Three base stations were used for reference, and 24 hours of tidal monitoring were conducted to obtain more accurate constants for the tidal-drift correction.

*California State University, Long Beach.
†California Polytechnic Institute, Pomona.

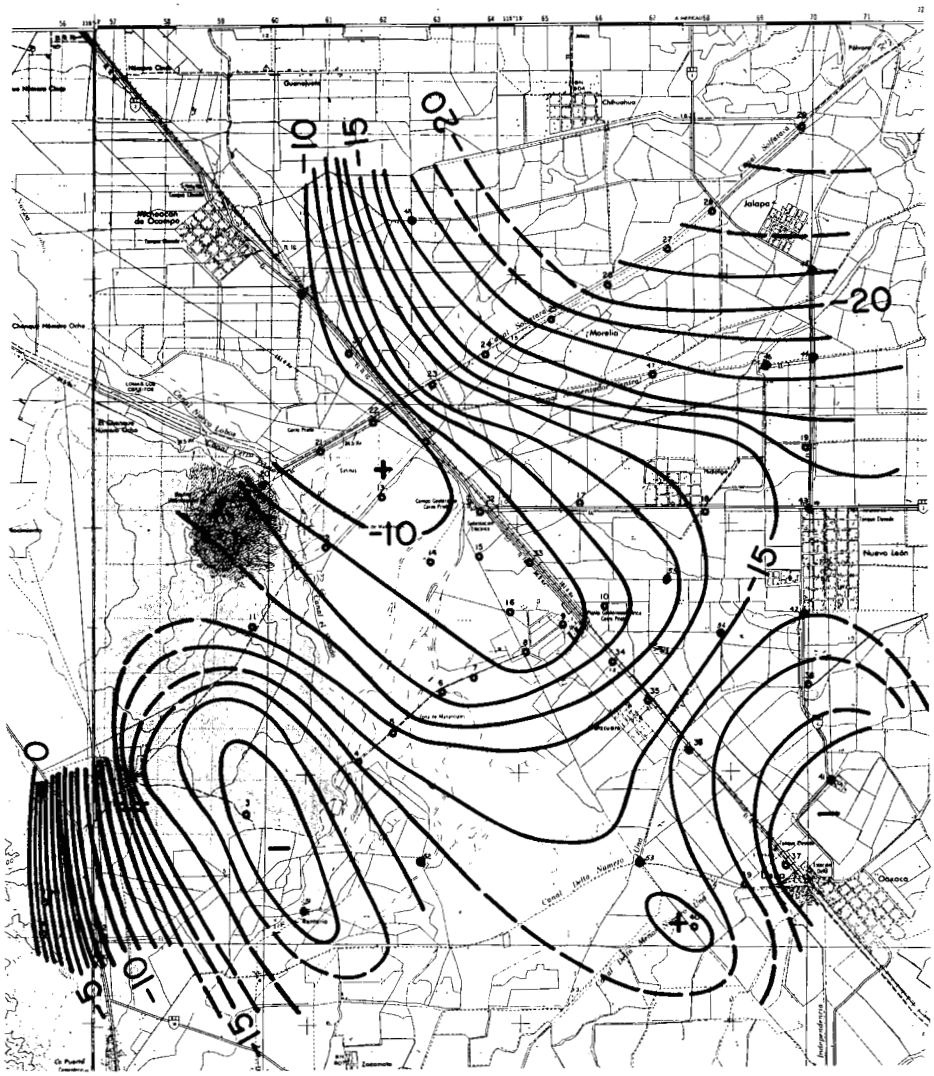

XBL 791-162

Figure 1. Bouguer anomaly map of the Cerro Prieto geothermal field and its vicinity. Contour interval is 1 mgal, permanent gravity stations are shown as the numbered dots.

Because some sizeable long-term drift in the meters occurred, it was not possible to compare directly the gravity values for a particular station at greatly differing times. However, station data obtained in each gravity loop were subtracted from the value of internal base station 23, yielding an array of gravity differences which were comparable. The desired final observed gravity value for each station was obtained (a) by calculating the mean gravity difference with respect to station 23 and (b) by converting those values to a mean gravity difference with respect to station 1 in the Cucapa Mountains. Figure 1 shows the contoured gravity data reduced to the Bouguer anomaly. Station 1 was arbitrarily assigned a gravity of 0.0 mgal and all Bouguer values are referred to this zero base.

The standard deviations of half the station values were smaller than 15 μgal, indicating that a fairly high degree of replicability was achieved in spite of some unfavorable field conditions such as high ambient temperatures (>105°F) during part of the survey period, rough roads, and wind.

Although the gravity data obtained can be interpreted in terms of a subsurface mass distribution, it is too soon to know whether changes in gravity are occurring within the region of the geothermal field. Data collection of the first data set spanned a time of four months, during which most stations showed either little variation or gave reasonably small erratic changes. At a few stations we noticed a different and more interesting behavior. Station 33 exhibited a large step function increase of 0.28 mgal during four occupations spanning one month. Also, the gravity between base station 23 on the valley floor and base station 1 in the Cucapa Mountains increased 0.05 mgal in four months, suggesting

relative subsidence of 25 cm in the valley relative to the Sierra Cucapa.

PLANNED ACTIVITIES FOR 1979

The second cycle of complete gravity measurements and leveling will be made during the winter of 1978-1979 so that initial estimates of short-term temporal changes can be made. We hope to collect data over a shorter interval of time and during a cooler time of the year to avoid the instrumental problems encountered when ambient temperature exceeds 105°F.

Additional tidal monitoring will be done for greater accuracy of the correction factors.

REFERENCE

Grannell, R. B., Tarman, D. W., Clover, R., Goldstein, N. E., Chase, D. S., Eppink, J., and Leggevie, R., 1978. Precision gravity studies at Cerro Prieto, in First symposium on the Cerro Prieto geothermal field, Baja California, Mexico, Abstracts. Berkeley, Lawrence Berkeley Laboratory, LBL-7098 ABS.

Utilization and Conversion Technology

The development of geothermal energy requires accurate economic and technological assessments of developmental projects. Yet the information required to make these assessments is not always available. The LBL program of utilization and conversion technology attempts to provide this information; it is an extension of present technologies into areas that were not of interest previously.

The program is divided into two parts: technology development and utilization projects. In technology development, we are providing analytical tools and data required to fully understand the processes by which geothermal energy can be economically utilized. These tools and data, plus other laboratory resources, are then applied to a number of DOE-sponsored projects that serve as paths to the geothermal industry.

Because the binary-cycle process is expected to be the method chosen to exploit most moderate-temperature hydrothermal resources for electrical energy, most of our conversion technology development projects are focused on this binary process. The Binary Fluid Experiment is providing laboratory-quality data on heat-transfer film coefficients of the various candidate hydrocarbon working fluids, while the DOE/EPRI heat-exchanger test will provide a verification of these data under field conditions. A study of fluid properties is under way that seeks to provide the best available thermodynamic and transport data on brines and working fluids. Direct-contact heat exchange is being investigated since it is expected to improve the economics of second generation geothermal power plants.

The development of a shell-and-tube heat-exchanger design code has led to a new method of determining the optimum design fouling factor and overall heat-transfer coefficient, taking into account capital, operating, and cleaning costs.

In addition to studying the benefits of operating binary cycle power plants in the floating cooling mode, program GEOTHM was used to study the relationship between optimum thermodynamic and optimum energy-cost power plant designs. This work, which will be reported in 1979, will compare energy costs from binary cycle and flashed steam power plants, including production and injection pumping costs, for a range of resource temperatures.

Utilization projects in 1978 included continued work on DOE's Niland Geothermal Loop Experimental Facility (GLEF) and Geothermal Demonstration Power Plant. LBL also provided continued technical review and evaluation assistance to DOE's San Francisco Operations office for their direct-use activities.

Work for GLEF consisted primarily of data reduction and retrieval, and began in 1977. By mid-1978, the GLEF experimental plan had been changed, eliminating the need for computerized data reduction, and LBL's involvement in the project was cut back.

Members of the LBL staff acted as technical advisors to the DOE Geothermal Demonstration Plant Source Evaluation Board. Demonstration plant proposals were reviewed and evaluated in light of the Program Opportunity Notice criteria. A report on each proposal was prepared and presented to DOE.

The direct-heat utilization project at LBL continued its technical support of DOE's direct-use program, and expanded into additional reservoir engineering and commercialization support. The major effort in fiscal year 1978 was the technical support to DOE/SAN. Reviews, evaluations, and written comments were submitted to DOE/SAN on contracts resulting from earlier Program Research and Development Announcements. Three contracts for engineering and economic studies of nonelectric applications of geothermal energy were monitored. They were for the retrofit of a raw sugar-cane processing plant and for district space heating. An LBL staff member served on the Technical Advisory Committee that evaluated proposals from a direct-use Program Opportunity Notice. Approximately 15 proposals were recommended for negotiation, and it is expected that four to five of the resulting contracts will be assigned to LBL for monitoring. LBL also contributed to the planning of a DOE direct-use commercialization program, including presentation of an invited paper at a Massachusetts Institute of Technology workshop on geothermal energy in the pulp and paper industry. Reservoir engineers from LBL began planning fiscal year 1979 activities in support of district-heating projects in Klamath Falls, Oregon, Susanville, California, and Mammoth Hot Springs, California.

The LBL geothermal utilization and conversion technology activities will continue into fiscal year 1979 with continued technical assistance on the geothermal demonstration power plant and direct-use program, the construction of the 500-kW direct-contact pilot plant, completion of the DOE/EPRI heat-exchanger field test, further development and application of GEOTHM, and additional data gathering at the Binary Fluid Experiment.

HEAT TRANSFER COEFFICIENTS FOR ISOBUTANE

B. W. Tleimat, A. D. K. Laird, H. Rie, and I. C. Hsu

Assessments of potential of geothermal energy resources have pointed to hot brines as a viable source of large amounts of geothermal power in the next two or three decades. Recent power-plant feasibility studies and exploratory drilling confirm this opinion and show that low-salinity, intermediate temperature (150 to 230°C) brines are the most plentiful.

To take full advantage of this source of energy, the binary cycle has been proposed, particularly with brines in the lower part of the temperature range, with brines at higher salinities, or with brines that have noncondensable noxious gases. In this system, geothermal brine is used to heat another or secondary fluid used as the working fluid of a turbogenerator power cycle much as in an ordinary steam power plant. Depending on the temperature range and other conditions, the secondary fluid may consist of water, ammonia, refrigerants, isobutane and other light hydrocarbons, other fluids, or appropriate mixtures of fluids. Although isobutane has received the most attention for use in the intermediate temperature range, mixtures of isobutane and propane, Freons 22 and 113, and ammonia are being considered.

In specifying heat-transfer equipment for a process, the designer is usually armed with well-tested information on the performance of similar equipment under similar or identical conditions. In an unusual application, such as specifying heat-transfer equipment in a geothermal binary-cycle plant using isobutane as the working fluid, the engineer is forced to search the literature for design information. In the absence of data specifically applicable to the design at hand, designers usually refer to the heat-transfer coefficient prediction method embodied in the correlation equations of Dittus and Boelter, of Colburn, and of Sieder and Tate found in standard works. These general correlations are based on fluid transport properties and give the mean, or most probable value of a large amount of reliable experimental data. Unfortunately, because of the large influence sometimes exerted on heat transfer by minor and frequently unrecognized variations in conditions, a designer can only be sure that the performance of an individual heat exchanger will be within ±35% of the mean. Consequently, to assure fulfillment of a performance guarantee on a design embodying a minor innovation, the designer would select a heat-transfer coefficient value at the lower limit, that is, 35% less than the mean.

The correlation equations for the prediction of the heat transfer coefficients need accurate and reliable data on the transport properties of the fluid at the operating conditions. Lack of data at these conditions makes the designer's task difficult at best. This lack of data is especially true for designs where the working fluid is in the supercritical region. This is important because computer studies (LBL's GEOTHM, for example) indicate that heating of the secondary fluid in the supercritical region will be the most efficient. Consequently, the most effective and reliable method for specifying the equipment is to determine the value of the heat-transfer coefficient experimentally and at the proposed operating conditions.

The Binary Fluid Experiment, or BFE (Tleimat and Laird, 1978), was designed to provide experimental data to determine heat-transfer coefficients of the various working fluids. It will establish, under clean conditions, baseline data on film coefficients for several light hydrocarbons starting with isobutane, mixtures of light hydrocarbons such as isobutane and propane, refrigerants, and ammonia. Data will be gathered from the BFE for the ranges of heating and condensing temperatures and pressures contemplated in geothermal binary-cycle power plants.

The BFE is located at the University of California's Richmond Field Station. Figure 1 is a photograph of part of the apparatus and Figure 2 is a schematic flow diagram of the apparatus showing the major components.

The tubes in the heater and condenser were made from one piece of type-316 stainless steel, machined on the inside and on the outside to 0.756-in. I.D. and 1.189-in. O.D. and fitted with a total of 15 type-K thermocouples at five stations. Figure 3 shows the location of three thermocouples at one station and Figure 4 shows a photograph of a portion of the tube with three thermocouples at one of the stations.

Shakedown data were obtained at the end of fiscal year 1977 and the instrmented tubes were installed at the end of December 1977. Data were obtained on the heating and condensation of isobu-

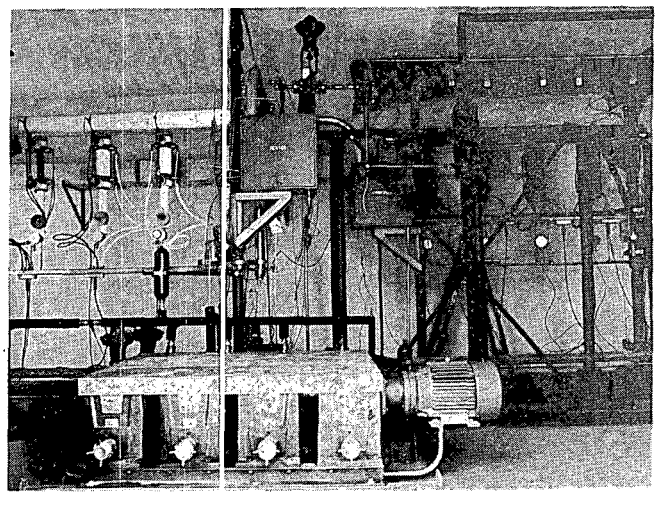

Figure 1. Binary Fluid Experiment showing high-pressure pump in the foreground; isobutane heater and its special condensate flowmeters in the upper left; isobutane throttling valve in the middle; surface desuperheater, isobutane condenser and its special condensate flow meters in the upper right.

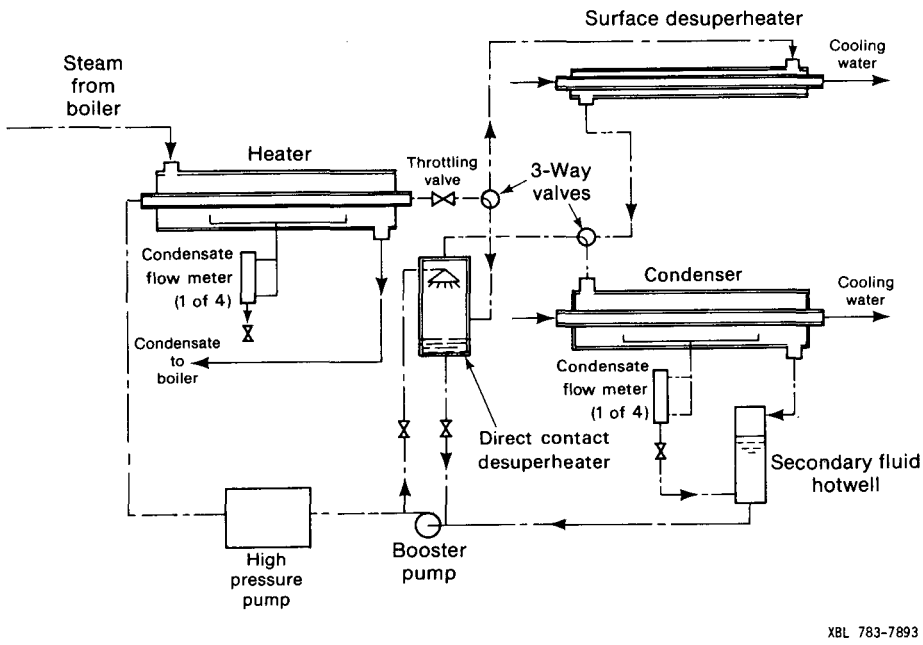

Figure 2. Schematic flow diagram of the Binary Fluid Experiment.

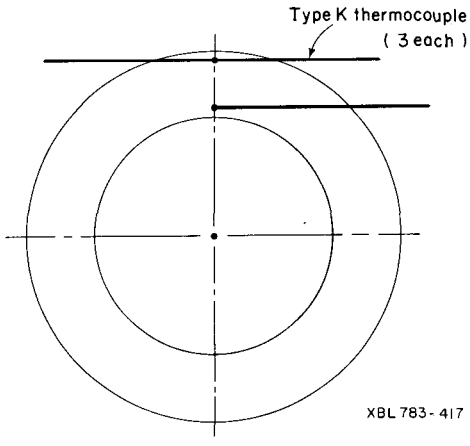

Figure 3. Tube cross section showing location of thermocouples.

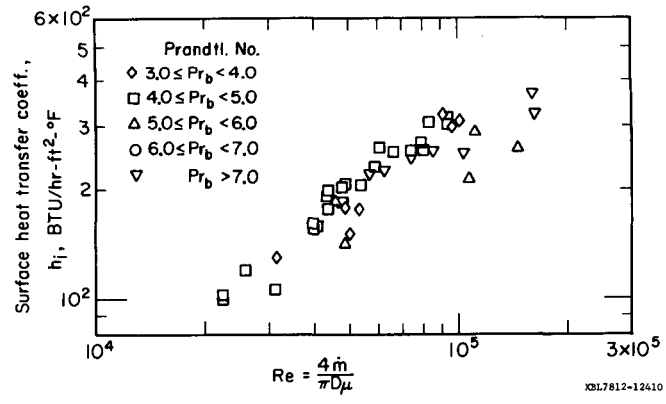

Figure 5. Film coefficient for heating isobutane at 600 psia inside a tube as a function of Reynolds number.

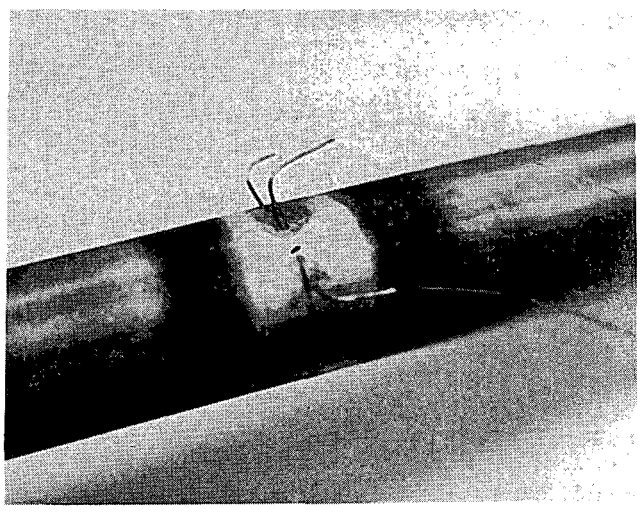

Figure 4. Instrumented tube with three imbedded thermocouples at one of the five stations.

tane during the first six months of 1978. Figure 5 shows a plot of the inside film coefficient for heating the isobutane at 600 psia as a function of Reynolds number, where: $\dot{m}$ is the weight flow rate of isobutane inside the tube; μ is the viscosity of the isobutane at the bulk fluid temperature, as measured by the traveling probe; and D is the inside diameter of the tube. Figure 6 shows a dimensionless plot of these data as a function of the Reynolds number where k and C_p represent the thermal conductivity and specific heat of isobutane calculated at the bulk fluid temperature. The solid line in Figure 6 shows the Dittus-Boelter correlation with values of transport properties taken from Hanley (1976) while other properties were taken from thermodynamic tables (ASHRAE, 1969). The dashed line represents the best fit for the data using the least-squares method.

Figure 7 shows a plot of the outside heat-transfer film coefficient, h_o, for the condensation of isobutane on the outside of the instrumented

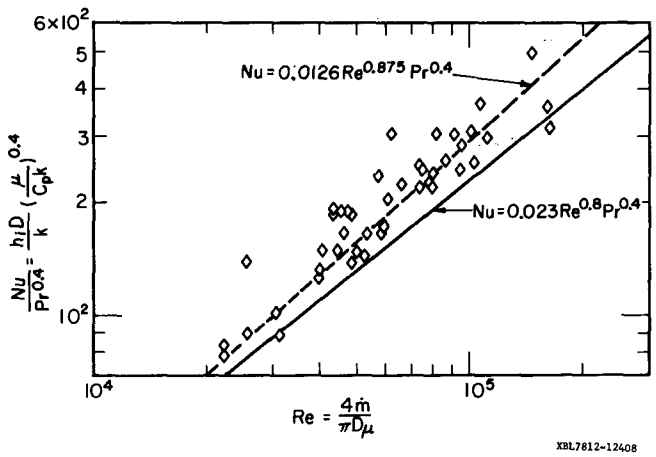

Figure 6. Dimensionless plot of data on heating isobutane inside a tube at 600 psia. Solid line represents Dittus-Boelter correlation. Dashed line represents best-fit line using least-squares method.

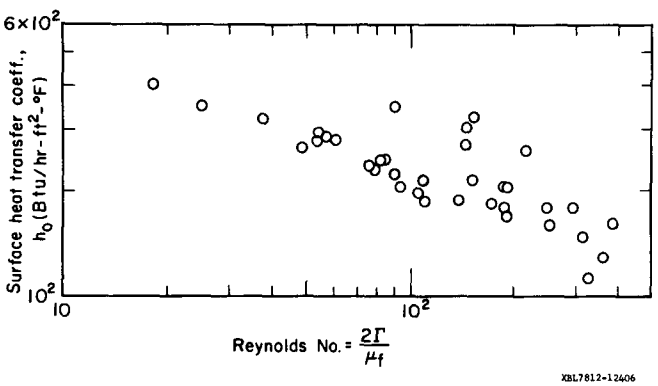

Figure 7. Film coefficient for isobutane condensing on the outside of tube as a function of Reynolds number.

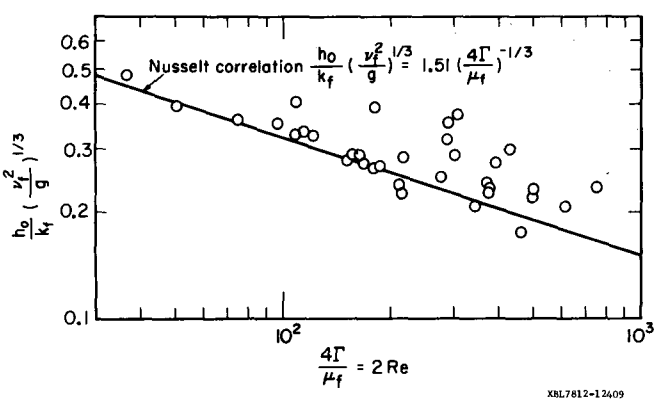

Figure 8. Dimensionless plot of data on condensation of isobutane on the outside of tube. Solid line shows Nusselt correlation.

tube as a function of Re, the condensate Reynolds number, where Γ represents the condensate rate per unit length of tube, and μ_f represents the condensate viscosity. Figure 8 shows a dimensionless plot of these data as a function of $4\Gamma/\mu_f$, twice the Reynolds number, where k_f and ν_f represent the thermal conductivity and kinematic viscosity of the isobutane condensate, with all properties calculated at the vapor temperature; and g is the acceleration of gravity. The solid line shows the Nusselt correlation for isobutane (McAdams, 1954) with transport and thermodynamic properties taken from Hanley (1976) and ASHRAE (1969).

The data used in the calculation of the results shown on Figures 5 and 6 were obtained with the instrumented tube oriented such that the imbedded thermocouples at stations 1, 3, and 5 were located at the top of the tube in a vertical plane, and in a horizontal plane at stations 2 and 4. There was evidence of some secondary junctions in some of the imbedded thermocouples. These secondary junctions produced erratic thermocouple readings at two stations in the vertical plane. Therefore, the temperatures at stations 2 and 4 were used to calculate the average film coefficient for the 4-ft-long section between stations 2 and 4. The rate of heat input to the isobutane was calculated from the steam condensate rate on the outside of the tube, collected in the specially designed meters, between stations 2 and 4.

During these runs, the isobutane turbine flow meter was located between the booster pump and high-pressure pump. However the flow meter readings were not used because of fluctuations caused by cyclic variation of suction pressure at the inlet to the high-pressure pump. Consequently, for all of these runs, the mass flow rate of the isobutane inside the heater was calculated from a heat balance on the tube between stations 2 and 4. Therefore, since no direct measurement of isobutane flow rate was available, the results presented in Figure 5 and 8 are considered to be preliminary.

In June 1978, the system was shut down for modification. The instrumented tubes were taken out and only some of the faulty imbedded thermocouples were replaced. The two tubes were reinstalled with the imbedded thermocouples located radially at 45 degrees above a horizontal plane passing through the axis of the tube. The isobutane flow meter was also relocated downstream of the high-pressure pump, and in-situ calibration system for this flow meter was installed.

After these modifications, runs were made and data were obtained on heating the isobutane at 600 psia to check the original results. These data are being analyzed and initial results indicate that although they give essentially the same results as the previous data, there is much less scatter and higher heat coefficients than those predicted by the Dittus-Boelter correlation. These new data for heating the isobutane at 600 psia can be correlated empirically by the equation

$$Nu = 0.022\ Re^{0.82}\ Pr^{0.4}$$

with maximum deviation of ±10%.

PLANS FOR FISCAL YEAR 1979

The data on heating the isobutane at 600 psia have been obtained and are under evaluation. Data on the heating of isobutane at 800, 500, and 400 psia are planned for the balance of 1978. After evaluation of the above data, runs on mixtures of isobutane and isopentane will be planned and made.

REFERENCES CITED

American Society of Heating, Refrigrating and Air-Conditioning Engineers, 1969. ASHRAE thermodynamic properties of refrigerants. New York, ASHRAE.

Hanley, H. J. M., 1976. Prediction of the viscosity and thermal conductivity coefficients of mixtures. Cryogenics, v. 16, pp. 643-652.

McAdams, W. H., 1954. Heat transmission. New York, McGraw-Hill, p. 338.

Tleimat, B. W., and Laird, A. D. K., 1978. Investigation of heat transfer coefficients of binary cycle working fluids, in Earth Sciences Division annual report 1977. Berkeley, Lawrence Berkeley Laboratory, LBL-7028, pp. 109-112.

FIELD TEST OF GEOTHERMAL/HYDROCARBON SHELL-AND-TUBE HEAT EXCHANGERS

L. O. Beaulaurier

INTRODUCTION

A field test of shell-and-tube heat exchangers is to be performed cooperatively by the Electric Power Research Institute (EPRI) and the U.S. Department of Energy (DOE) using geothermal brine from Magma Power Co. wells at East Mesa, California. Heat-transfer coefficients will be determined first with isobutane, and later with a mixture of isobutane and isopentane, as the working fluid in a simulated power cycle.

The objectives of the project are as follows:

Verify the performance of shell-and-tube heat exchangers in geothermal service.

Verify heat-exchanger performance while heating either selected pure light hydrocarbons or selected mixtures of light hydrocarbons in the vicinity of their respective critical pressure and temperature.

Determine overall heat-transfer coefficients, and tube-side and shell-side film coefficients, that might be used for design of commercial-size geothermal power plants using similar geothermal brines and the same light hydrocarbon working fluids.

Determine the effects of heat-enchanger cleaning techniques on subsequent heat-exchanger performance.

Determine the overall transfer coefficients and condensing film coefficients that might be used for design of condensers for commercial-size geothermal power plants using the same light hydrocarbon working-fluids.

Investigate the above under representative field operating conditions with pumped production wells.

1978 ACTIVITIES

Lawrence Berkeley Laboratory has been assigned management responsibility for DOE's portion of this project. The mechanism for cooperation between LBL and EPRI on this project is the Project Group, consisting of one representative from EPRI and one from LBL. A project manager, reporting to the Project Group, provides the day-to-day contact with the Contractor, including technical direction, schedule control, and invoice review and approval. Because this is a cooperative project and not jointly funded, the two sponsoring organizations have each assumed certain responsibilities. LBL is responsible for the system design, procurement of the equipment, and analysis of the data. EPRI is responsible for construction and operation of the test apparatus, and distribution of the final report.

The major emphasis in this project will be on the primary brine/hydrocarbon heat exchangers. This heat exchanger train consists of six exchangers, both sides of which are in series, with the brine in the tubes and the hydrocarbon in the shell. Table 1 lists the main features of the primary heat exchangers.

The heat exchanger test apparatus consists of three fluid loops: brine, hydrocarbon, and cooling water (see Figure 1). The three

Table 1. Primary heat exchanger details.

No. of tubes per exchanger:	62
No. of passes:	1 shell side, 1 tube side
Tube length:	24 ft
Tube size:	3/4 in O.D., 16 B.W.G.
Tube material:	carbon steel (SA-214)
Tube pitch:	15/16 in., triangular array
Shell I.D.:	8-3/4 in.
Baffle spacing:	12 in.
Area per exchanger:	292 ft^2
Number of exchangers:	6

Table 2. Condenser details.

No. of tubes:	332
No. of passes:	1 shell side, 2 tube side
Tube length:	24 ft
Tube size:	3/4 in. O.D., 14 B.W.G.
Tube material:	carbon steel (SA-214)
Tube pitch:	15/16 in., triangular array
Shell I.D.:	22 in.
Baffles:	none

loops are interconnected through the primary brine/hydrocarbon heat exchanger train and the desuperheater-condenser-subcooler train. The heat load is rejected to the atmosphere through a wet cooling tower. The high-pressure (heater) portion of the hydrocarbon loop is separated from the low-pressure (condenser) portion by a pressure-reducing valve in lieu of a turbine.

The working fluids will be heated at supercritical pressure (600 psia), and the test is designed to gain insight into the behavior and heat transfer characteristics of the working fluids near the critical point.

Heat-transfer coefficients determined from the test will be compared with values predicted by standard correlations and by various models such as the LBL SIZEHX computer code. The test results will also be compared with predictions made using film coefficients determined in LBL's Binary Fluid Experiment.

In order to reduce the head required from the hydrocarbon feed pump, the working fluid will be condensed at 245 psia (197°F) during primary heat-exchanger tests. The subcooler will reduce the liquid hydrocarbon temperature to 120°F entering the primary heat exchangers.

To determine condensing coefficients, the condensing pressure will be reduced in steps from 245 psia to at least two other lesser values. At each condensing pressure setting, readings will be taken over a range of hydrocarbon flow rates. Thus, condensing coefficients can be obtained from various condensing pressures as a function of condensate loading on the tubes. Table 2 lists the main features of the condenser.

Initially, a series of tests with pure isobutane will be run. These will be followed by a series of tests using a mixture of 80% isobutane and 20% isopentane on a mole fraction basis. Several runs, separated by tube-side cleaning, will be made to investigate the effect of tube cleaning on heat-exchanger performance.

The test operation is scheduled to begin by April 1, 1979. Four months of testing have been planned. All primary heat exchangers, desuperheater, condenser, subcooler, cooling tower, circulating pumps, and metering instruments have been procured and are on hand. Colley Engineers and Constructors of Gardena, California, have completed the design. They will procure the balance of the materials, and construct and operate the test facility.

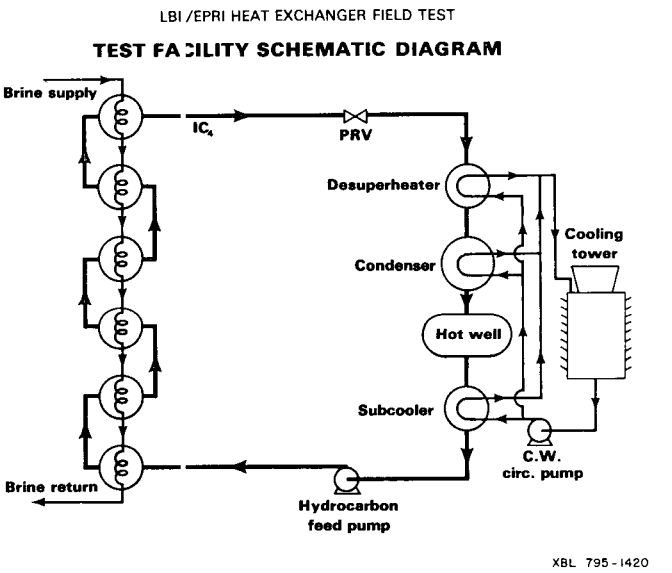

Figure 1. Schematic flow diagram of the heat exchanger test loop.

THERMODYNAMIC AND TRANSPORT PROPERTIES OF LIGHT HYDROCARBONS AND THEIR BINARY MIXTURES

L. F. Silvester

INTRODUCTION

A knowledge of fluid properties is essential for any design work associated with a geothermal-based Rankine-cycle binary process. For example, in designing the heat transfer equipment, the turbo-expander, or the configuration of the binary process, the designer needs to know: (1) the thermo-physical behavior of the working fluids (e.g., PH, PV, and TS diagrams); (2) the transport properties of the working fluid (e.g., viscosity and thermal conductivity); (3) the errors associated with a given property; (4) those regions of PVT space where data are lacking; (5) if data are lacking, whether correlating expressions exist that can predict the fluid properties; and (6) how the fluid properties are formulated.

Fluid properties for pure hydrocarbons are avaliable either in tabular form or more commonly, as algorithms (e.g., equations of state). The correlating equations are generally within 1 to 5% of experimental values for areas away from the critical-point region. Experimental data on binary mixtures are less readily available, and consequently most design calculations are

Table 1. Fluids marked are available for calculation of indicated properties in either the GEOTHM thermodynamic process simulation code or the binary mixture properties code.

	GEOTHM code		Binary mixtures	
Fluid	Thermodynamic properties	Transport properties	Thermodynamic properties	Transport properties
Water	x	x		
NaCl brine	x	x		
Methane			x	x
Ethane			x	x
Propane	x	x	x	x
Normal-butane, isobutane	x	x	x	x
Normal-pentane, isopentane	x	x	x	x
Normal-hexane			x	
Normal-heptane			x	
Normal-octane			x	
Ethylene			x	
Propylene			x	
Carbon dioxide	x		x	
Hydrogen sulfide			x	
Nitrogen	x	x	x	x
Air (ideal gas)	x			
Air-water mixtures (ideal gas)	x			

based on predicted properties, usually computed from some form of the Bendict-Webb-Rubin (BWR) equation of state. Predicting the liquid-vapor coexistence curve for a binary mixture in the vicinity of its critical point and locating the critical point are the greatest areas of uncertainty in calculating fluid properties for binary mixtures.

1978 ACTIVITIES

Interest in the fluid properties of light hydrocarbon systems by the Cycles Study Group comes from the fact that fluid properties touch almost every aspect of development work for geothermal power plants using a binary process.

Consequently, during fiscal year 1978, the Cycle Studies Group engaged in various activities related to fluid properties. Most noteworthy was work on the computer code GEOTHM, development of a binary-mixture computer code, initial development of a heat-exchanger data-analysis computer code, and start of a fluid-properties study related to the LBL heat-exchanger programs.

Expansion of the fluid-properties repertoire used in the thermodynamic simulation computer code GEOTHM continued in fiscal year 1978. The present in-house version of GEOTHM can access the fluids shown in Table 1.

Because a binary mixture of light hydrocarbons has been proposed as the secondary working fluid for a geothermal Rankine-cycle binary process (EPRI, 1976), stand-alone computer codes were developed for computing the thermodynamic and transport properties for the proposed binary mixtures. The binary mixture code will be incorporated into GEOTHM as the code's process models are modified to handle mixtures.

The binary mixture code consists of two separate computer programs, one for thermodynamic properties and one for transport properties. The thermodynamic code uses a modified BWR equation of state (Starling, 1975) with the mixing rules of Bishnoi and Robinsion (1972). The code can compute thermodynamic properties for the liquid-vapor coexistance curve, and the liquid and vapor subcritical and supercritical regions for any binary mixture made from the fluids marked in Table 1.

The transport code is from Hanley (1976) and can compute transport properties (e.g., viscosity and thermal conductivity) for binary mixtures made from the fluids indicated in Table 1.

The remainder of the fiscal year 1978 work on fluid properties centered on starting a study aimed at detailing the uncertainties associated with the fluid properties of those light hydrocarbon binary mixtures proposed for various geothermal power-plant processes. The work involves not only identifying the problem areas, but also assessing the implications of these problem areas, particularly regarding the LBL heat-exhanger programs.

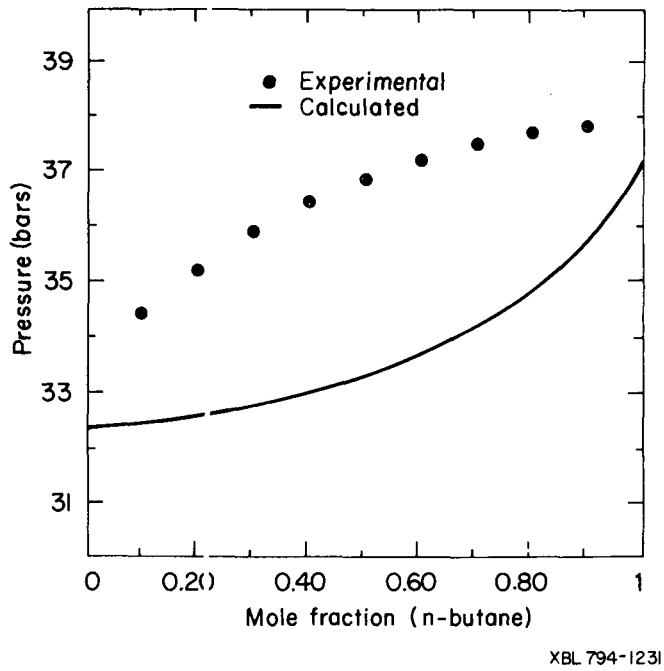

Figure 1. Comparison of experimental and calculated critical pressures for normal-butane/normal-pentane mixtures as a function of the mole fraction of normal-butane.

A recently reported turbine design study by Smourin and Kennelly (1978) points up the serious implications of uncertainty about the region bounding the critical point of a binary mixture. The Smourin and Kennelly report recommends for an 80/20 mole % isobutane/isopentane secondary working-fluid mixture, turbine inlet conditions of 500 psia at 295°F.

The fluid properties used in the design study come from a modified BWR equation. The BWR equations yield critical point parameters of 496.5 psia and 287.7°F. Based upon the reported conditions, the turbine inlet state point is supercritical. Yet, experimental evidence suggests a different story (Hicks and Young, 1975).

Figures 1 and 2 display the calculated and experimental values of the critical pressure and temperature respectively for binary mixtures of normal-butane/normal-pentane as a function of the mole fraction of normal-butane. The discrepancy is obvious. For the 80/20 mixture, the error is 40.6 psia in pressure and 7.2°F in temperature. The experimental and calculated data for other light hydrocarbon binary mixtures reveal the same negative departure for the BWR equation. Unfortunately no literature data were found for the isobutane/isopentane system. However, since the isomer forms part of a homologous series, the errors associated with the normal-butane/normal-pentane mixtures will be approximately correct for the isomer mixtures. Finally, since the BWR equations predict a critical point lower than the experimental point, the BWR equations are incapable of determining the liquid-vapor coexistence curve between the

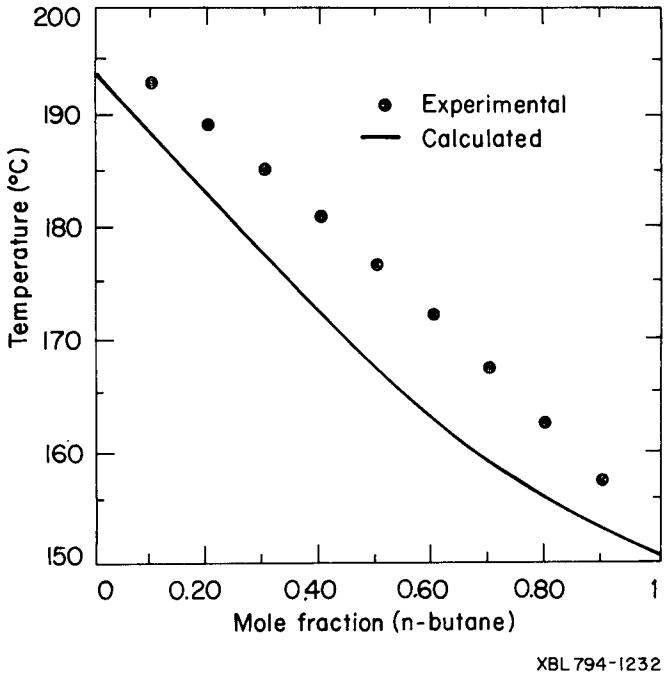

Figure 2. Comparison of experimental and calculated critical temperatures for normal-butane/normal-pentane mixtures as a function of the mole fraction of normal-butane.

calculated critical point and the experimental critical point because the equations predict supercritical behavior over this region. Consequently, the area of uncertainty for an 80/20 isobutane/isopentane mixture could extend from 496 to 537 psia in pressure by 282 to 290°F in temperature.

The uncertainty in fluid properties leaves the door open for several unsatisfactory conditions. The turbine inlet state might lie inside the two-phase region, although this appears unlikely because of the retrograde nature of the liquid-vapor coexistence curve and the margin of superheat provided by the design state point. Secondly, the heat-transfer process will probably be subcritical rather than supercritical, meaning liquid carryover into the turbine is a distinct possibility. The overall result of fluid properties uncertainties translates into degraded plant efficiency relative to the design conditions.

The problem area of fluid properties, as exemplified by the Smourin and Kennelly study, have a direct bearing on three LBL heat-exchanger programs: The Direct Contact Pilot Plant, the Binary Fluid Experiment (BFE), and the Heat Exchanger Field Test (HEFT). Although different in design, the heat-exchanger programs are highly complementary in their goals. Each program is designed to test heat exchanger performance for various hydrocarbon secondary working fluids near the fluid's critical point. Although the three programs cannot directly measure fluid properties, the performance of these systems is a direct indication of the benefits and liabilities of a given working fluid operating under conditions proposed for a geothermal binary power plant. The performance tests will indicate areas for more detailed research and identify the problems of operating with light hydrocarbon working fluids. Also, the tests will provide performance data against which the importance of fluid property uncertainties can be translated into actual performance.

A computer routine for analyzing a shell-and-tube heat exchanger using water on both the shell and tube sides was developed in fiscal year 1978. The routine will be made part of a code to be developed during fiscal year 1979 for the BFE and HEFT programs.

PLANNED ACTIVITIES FOR FISCAL YEAR 1979

To extract heat-exchanger performance parameters from the tests scheduled for each of the LBL heat-exchanger programs requires accurate and reliable fluid properties data at the test conditions and accurate data analysis routines. Consequently, during fiscal year 1979, heat-exchanger data-analysis computer codes tailored to each heat-exchanger program will be developed.

The data analysis codes will compute fluid properties based on the best available correlations. The computed fluid properties will in turn be used to compute dimensionless groups (e.g., Reynolds, Prandtl, and Nusselt numbers, etc.) used for constructing and verifying heat-exchanger design correlations, and for deducing film coefficients, overall heat-transfer coefficients, fouling factors, and so on. These stand-alone codes will be made available for general use.

The last area of fluid properties work scheduled to begin in fiscal year 1979 will be studies designed to provide direct information, both experimental and theoretical, on transport and thermodynamic properties of light hydrocarbons and their binary mixtures, particularly around the critical point and in the dilute gas region.

REFERENCES CITED

Bishnoi, P., and Robinson, D. B., 1972. New mixing rules for the BWR parameters to predict mixture properties. Con. Jour. Chem. Engin., v. 50, p. 101.

Hanley, J. M., 1976. Prediction of the viscosity and thermal conductivity coefficients of mixtures. Cryogenics, pp. 643-652.

Hicks, C. P., and Young, C. L., 1975. The gas-liquid critical properties of binary mixtures. Chem. Rev., v. 75, p. 119.

Holt/Procon, 1976. Geothermal demonstration plant feasibility study. Pasadena, The Ben Holt Company and Procon Inc., study for EPRI.

Smourin, N. A., and Kennelly, J. R., 1978. Expander turbines for the conversion of hydrothermal resources to electrical energy. Trans. ASME Winter Mtng., 1978.

Starling, K. E., 1975. Fluid thermodynamic properties for light petroleum systems. Houston, Gulf Publishing Co.

DEVELOPMENTS IN DIRECT-CONTACT HEAT EXCHANGE

R. L. Fulton

INTRODUCTION

The U.S. Department of Energy's Division of Geothermal Energy has undertaken a program to delineate and demonstrate the economic advantages of the direct-contact heat-exchange process in geothermal power generation. Following a proof-of-concept phase, the program elements measure subsystem performance and demonstrate overall system performance. These will be followed by development of economically optimum process designs and an estimate of the cost of electrical energy produced by such optimized plants.

1978 ACTIVITIES

LBL was involved in both the subsystem and overall system program elements during 1978. LBL subcontractors, Barber-Nichols Engineering and DSS Engineers, continued field testing a turbine/direct-contact heat exchanger (turbine/DCHX) loop reported in the 1977 Annual Report (Fulton, 1978). Modifications were made to the 10-kW turbine/DCHX loop to reduce the amount of liquid brine carried to the turbine, to measure the salinity of the water in the condensate, and to improve the turbine efficiency. A knockout drum was installed between the direct-contact heat exchanger and the turbine inlet. This reduced the amount of liquid brine carried into the turbine, thus significantly reducing the turbine scaling problems observed in the initial tests. The results of both the initial tests and the second set are reported by Barber-Nichols Engineering (1978a).

Under subcontract to LBL, DSS Engineers continued to investigate the performance of the direct-contact heat exchanger and of a method of recovering working fluid from the exit brine stream (Urbanek, 1978).

Pilot Plant

Late in 1977, LBL began a project to design and operate a 500-kW direct-contact pilot plant in a series of baseline performance tests at the East Mesa, California, Geothermal Component Test Facility. The first step was to subcontract with Barber-Nichols Engineering for a design definition study. The design definition study final report contains the study ground rules, results, and a description and layout of the pilot plant and its major components (Barber-Nichols Engineering, 1978b).

The selected pilot plant configuration brings the incoming brine through a sand trap and CO_2 separating vessel, boosts the pressure of the brine for injection into a spray-column-configured DCHX and returns the brine to the facility pond for reinjection after passing it through a working-fluid recovery system. The isobutane (IC_4) working fluid is taken from the hot well, pumped to high pressure, and injected into the bottom of the DCHX. As the IC_4 droplets flow to the top of the DCHX through the descending brine, the IC_4 is heated, boiled, and taken off the top of the DCHX as a vapor. The vapor passes through a single-stage radial inflow turbine and on to the condenser, where it is condensed and returned to the hot well. The high-speed turbine is coupled through a gearbox to a 60-cycle, 480-V, three-phase generator. The output from the generator is used to power the pumps and other pilot-plant support equipment, and the excess, the pilot plant's net output, is passed to a load bank for dissipation as heat.

The plant was designed in modular form so that it can be moved from the East Mesa site to a site at Raft River, Idaho, for further testing. Design requirements and specifications were developed for all the major components, the electrical power subsystem, the pilot-plant control subsystem, and the instrumentation and data-recording subsystems. A preliminary interface specification and a baseline test plan outline were also completed for the pilot plant during the design-definition study.

A thorough study of thermodynamic cycles for this direct-contact geothermal pilot plant was made. The intent of the cycle studies was to define a baseline system that would provide the highest utilization efficiency conistent with proven concepts and previous experience. The limitations of proven concepts and previous experience were the primary constraints on the DCHX approach. Testing experience on DCHX fluids limited the cycle study to three possible fluids: isobutane, isopentane, and normal pentane. To assure that no aspect of cycle evaluation would be overlooked and to resolve the divergent opinions about the best cycle, four other independent sources were asked to evaluate various cycles to a prescribed set of baseline conditions and ground rules. The results of these studies were presented and discussed, and the baseline cycle selected in a meeting with the five evaluators and with DOE representatives as moderators. The cycle selected will have an efficiency of 8.9% with a 94°F condenser and will produce 5.48 Wh/lb of 340°F brine flow.

Partial results of the study are shown in Figure 1. The curves show a distinct superiority in terms of brine utilization for the IC_4 with the 340°F East Mesa brine. Because the system is also to be used at Raft River, Idaho, studies were run using Raft River conditions of 290°F brine and a 94°F condenser with the same system configuration and component efficiencies. With the lower brine temperature, the performance advantage of IC_4 over the pentanes

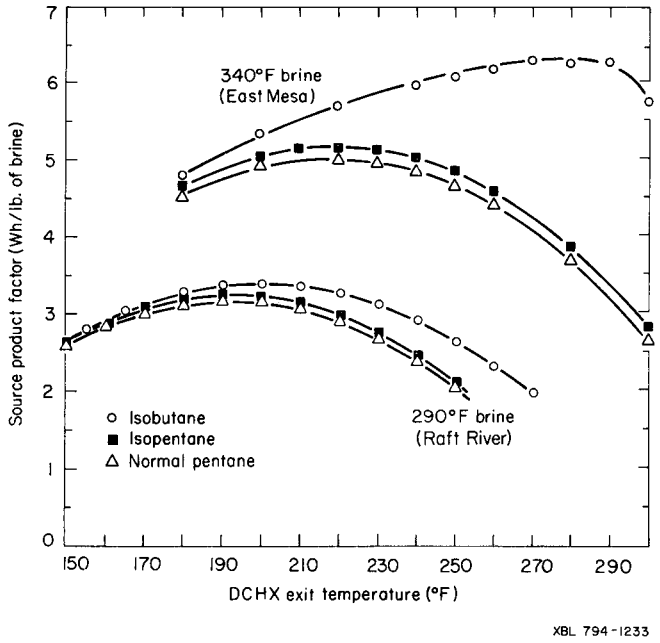

Figure 1. Source production factor as a function of DCHX exit temperature for East Mesa, California, and Raft River, Idaho, brines.

is minimal. For both sites, an optimized peak efficiency point is apparent for pentane. The IC_4 optimizes at a reasonable temperature and pressure for the Raft River conditions, but for the East Mesa conditions with hotter brine the optimum occurs near the critical point. Near-critical or supercritical operating points for the IC_4 were not explored because of practical limitations in trying to work at these higher pressure levels with off-the-shelf hardware.

The obvious superiority of IC_4, particularly at the higher well temperatures found at East Mesa, indicates that it should be the selected working fluid. The pentane system appears to be simpler and less expensive than an IC_4 system. The pentane cycles run at lower DCHX pressures, which eliminates the need for the brine boost pump and the hydraulic pressure recovery turbine. The delivered pressure from the well is sufficient for achieving the optimum pentane cycle temperature. Additionally, the power required for the feed pump is much less for the pentane than for the IC_4 system. The resulting pentane systems thus can be designed for a lower gross power level and the required pressure vessels can be designed and built with lighter-gauge materials. Since initial investment costs have a strong effect on the price of geothermal energy, a cost differential for the two pilot plant systems was evaluated to try to establish whether the increased complexity of the IC_4 system outweighed the improved utilization efficiency. The cost comparison of the IC_4 and pentane systems was surprising in view of the compexity of the IC_4 system and its higher operating pressure levels. The anticipated savings in the pentane systems over the IC_4 system were offset by the increased costs of the larger-diameter pentane DCHX and turbine. For the pilot plant, the costs of the IC_4 and the pentane systems were approximately equal. With equivalent plant costs one would automatically select the IC_4 system with its higher utilization factor. All parties participating in the study agreed that the baseline power plant should be based on the isobutane cycle.

The comparison between pentane and isobutane systems was based on selected East Mesa operating temperatures of 240°F for the pentanes and 250°F for the isobutane. The pentane temperature was selected slightly past the optimum point because of improved cycle efficiency and potentially lower condenser costs with a small reduction in utilization efficiency. The isobutane peak cycle temperature of 250°F was selected to limit the amount of power required by the pumps and thus the gross power level and the pressure levels in the system. The IC_4 temperature appears to be below its optimum point for utilization, but as the higher temperatures and required pressures are approached, the size of the IC_4 system also grows rapidly to produce the parasitic power required by the pumps in the system. At the higher operating pressure levels these components will introduce more system problems and become more critical in terms of efficiencies.

After completion and review of the design-definition study, a subcontract was awarded to Barber-Nichols Engineering for the design, fabrication, installation, and baseline testing of the 500-kW pilot plant.

Supporting Studies

In parallel with the detailed design work going on at Barber-Nichols Engineering, in-house effort at LBL was focused on the effect of noncondensable gases on the predicted performance of the 500-kW pilot plant. Noncondensable gases entering the pilot plant in the brine supply affects three major plant subsystems: the turbine, the condenser, and the hydrocarbon recovery system.

Noncondensables, if not removed from the brine before they enter the DCHX, will be stripped from the brine by the vaporizing IC_4 and carried through the turbine to the condenser. In passing through the turbine, noncondensables form a portion of the total turbine mass flow, but do not contribute a corresponding enthalpy drop, thereby reducing the overall turbine efficiency. Noncondensables entering the condenser also add their partial pressure to the working-fluid condensing pressure, reducing the available pressure ratio across the turbine.

In an unvented condenser, the total pressure builds up to an equilibrium value that depends on the rate at which noncondensables entering the condenser can be removed by dissolving in the condensed working fluid. This buildup of gases in the condenser interferes with heat transfer and requires a much larger unit. Venting the condenser to eliminate this problem requires working-fluid recovery from the condenser vent gas.

Recovery of dissolved working fluid from spent geothermal brine can be done by flashing the brine at subatmospheric pressures and then condensing the resulting vapors. The presence of noncondensables seriously impairs the condensation process and makes this method of working fluid recovery uneconomical.

A modification of the original 500-kW pilot-plant design has been studied that includes a three-stage flash evaporator upstream of the DCHX. The brine would be flashed down a total of 5°F and calculations show that 96% of the available CO_2 would be vented. The multistage flash evaporator would then recondense the flashed steam while heating and vaporizing approximately 3% of the total IC_4 mass flow. This arrangement allows efficient use of the brine thermal energy while removing the noncondensable gases.

The 500-kW pilot plant will incorporate a single-stage flash for noncondensable removal, with recovery of the vapor stream heat in a separate IC_4 heat exchanger. It was judged that this arrangement will be more adaptable to the planned wide range of pilot-plant operating conditions. The multistage flash evaporator concept, however, appears to hold good promise for commercial-size plants.

PLANNED 1979 ACTIVITIES

The 500-kW pilot plant will be installed at East Mesa and a set of baseline performance tests will be run. A subcontract to evaluate the economics of commercial-size DCHX power plants will be let and the work will begin.

REFERENCES CITED

Barber-Nichols Engineering, 1978a. Final report, direct-contact heat exchanger 10-kW power loop test. Berkeley, Lawrence Berkeley Laboratory, LBL-7036.

____, 1978b. Design definition of a 500-kW direct-contact geothermal pilot plant. Berkeley, Lawrence Berkeley Laboratory, UCID-8009.

Urbanek, M. W., 1978. Development of direct-contact heat exchangers for geothermal brines. Berkeley, Lawrence Berkeley Laboratory, LBL-8558.

Fulton, R. L., 1978. Test of a geothermal power cycle incorporating a direct-contact heat exchanger, in Earth Sciences Division annual report 1977. Berkeley, Lawrence Berkeley Laboratory, LBL-7028, pp. 112-114.

HEAT-EXCHANGER DESIGN OPTIMIZATION

W. L. Pope

ABSTRACT

A new general surface heat-exchanger design relationship is presented which uniquely couples the optimum design fouling resistance and the optimum design overall heat transfer coefficient with the ratio of cleaning cost to capital plus operating costs at the optimum design condition. ~~Details are given by Pope et al. (1978).~~

INTRODUCTION

Heat exchangers are a necessary component of all energy conversion processes. Industrial shell-and-tube heat-exchanger design is an extremely complex part of overall process economic design. With the recent escalation of fuel costs relative to equipment capital costs, and the large fraction of heat-exchange cost in low-temperature Rankine-cycle processes such as geothermal, the economic evaluation of heat-exchange subsystems becomes a critical part of overall process economics.

The fouling resistance of surface heat exchange is an additive and sometimes controlling series thermal resistance which reduces overall heat transfer efficiency. Excess surface area is normally incorporated into the heat exchanger design so that the required thermal performance is maintained as fouling builds up, with time, to the design fouling resistance, R_D. At the design condition the exchanger (and/or plant) is usually shut down or bypassed for mechanical or chemical cleaning of the fouled surface. Insufficient excess area (fouling allowance) can lead to inadequate thermal performance. Conversely, too large a design fouling allowance can lead to costly overdesign.

The proper amount of excess exchanger area can be determined from an economic balance between the cost of exchanger cleaning (including process downtime) and the cost of excess heat transfer area

An optimum design fouling resistance, $(R_D)_{OPT}$, or optimum design cleaning frequency, $(N_D)_{OPT}$, can be determined for any given heat exchanger subsystem if the fouling rate, a, the cleaning cost, X_{CL}, the cost of process downtime, $X_{CL,DT}$, the capital cost, X_A, and pumping power costs, X_{Po} and X_{Pi}, are quantified.

We derived an expression (Pope et al., 1978) for the optimum cleaning frequency for process exchangers for which the fouling rate, a, is a linear function of time (Lombard, 1975). For the simple case of fixed or specified terminal temperatures (i.e., utility fluid cost, X_{UF},

immaterial) the resulting expression was:

$$(N_D)^2_{OPT} = \frac{a\, U_c C_A \cdot FCR \left[1 + \frac{(X_{Pi} + X_{Po})}{X_A}\right]}{(1 + b\, U_c)\,(C_{CL} + C_{DT})} \qquad (1)$$

where U_c is the overall heat transfer coefficient under clean start-up conditions; C_A is the installed capital cost per unit outside surface area; FCR is the fixed charge rate; C_{CL} is the cleaning cost per cleanout per unit inside surface area; C_{DT} is the cost of process downtime (chargeable to the exchanger) per cleanout per unit inside areas; b is the residual (constant) fouling resistance after cleaning; and X_{Pi} and X_{Po} are the costs of tube-side and shell-side pumping power, respectively.

Equation (1) is similar but not identical to that obtained by Muller (1954) and recently reported by Neill (1976). The difficulty of using equation (1) for design stems from the fact that $(N_D)_{OPT}$ is a function of U_c, X_{Po}, X_{Pi}, and X_A. U_c in turn is a function of the tube-side and shell-side velocities or pressure drops and thus, X_{Pi} and X_{Po}. Consequently equation (1) could be "satisfied" by many combinations of the foregoing variables.

The development of equation (1) was continued (Pope et al., 1978) in search of that unique combination of all the foregoing physical and economic variables for which the total annual cost of the heat exchanger subsystem is a minimum.

After defining a design cleaning effectiveness, ε_{CL}, by:

$$\varepsilon_{CL} = (R_D - b)/R_D = 1 - b/R_D \qquad (2)$$

and assuming that simultaneous optimum values of X_A, X_{Pi}, and X_{Po} could ultimately be determined, the following final dimensionless expression for cleaning cost, X_{CL}, was obtained (Pope et al., 1978).

$$[X_{CL}/(X_A + X_{Pi} + X_{PO} + X_{CL})]_{OPT} = \varepsilon_{CL}(U_D R_D)_{OPT} = (aU_D/N_D)_{OPT} \qquad (3)$$

From equation (3) we can see that at the optimum design condition, the product of the overall heat transfer coefficient, $(U_D)_{OPT}$, and the optimum design fouling resistance, $(R_D)_{OPT}$, is uniquely determined for an optimum set of cleaning cost, capital cost, and process energy costs.

In physical/economic terms, equation (3) simply states that at the optimum design condition, the ratio of cleaning cost to total cost (excluding the utility fluid cost, X_{UF}) is equal to the ratio of the optimum design fouling resistance to the total exchanger (series) resistance.

Equation (3) is a necessary condition for an optimum surface heat-exchanger design.

Although equation (3) is a useful check of any so-called optimum heat exchanger, to apply (3) in design requires a heat-exchanger simulator with multiparameter optimization capabilities. These capabilities exist in the LBL-developed shell-and-tube heat-exchanger design program, SIZEHX (Green et al., 1977; Pope et al., 1978).

VERIFICATION OF EQUATION (3)

After developing the foregoing optimum cleaning frequency/cost relationship, a sample problem was chosen. This problem illustrates that in the general case of total exchanger cost minimization, where all four terminal temperatures are not kown (utility fluid cost, X_{UF}, material), equation (3) is satisfied. We selected as a suitably complex, general example of current interest--the supercritical isobutane/H_2O primary heater (from Holt and Ghormley, 1976). This example is interesting for several reasons:

1. The shell-side fluid (isobutane) thermodynamic and transport properties vary markedly due to operating proximity to the critical point.

2. The tube-side fouling rate, though linear, is a complex function of the brine (H_2O) temperature (Holt and Ghormley, 1976).

3. The shell-side fluid is generally controlling, but tube-side fouling dominates at the cold brine-exit end.

After selecting reasonable shell-side matrix proportions assuming single segmental baffles, and carefully normalizing all fixed process state points and costs to those given by Holt and Ghormley (1976), the SIZEHX/GEOTHM code was used in the Design Optimization Mode to optimize the exchanger of Holt and Ghormley with equation (4) as the objective function.

$$X_{TOT} = X_A + X_{Pi} + X_{Po} + X_{UF} + X_{CL} \qquad (4)$$

Figure 1 is a sensitivity plot illustrating that equation (3) is indeed satisfied in the general case when equation (4) is a minimum. The numerical example chosen assumed a complex step-function fouling-factor distribution (Holt and Ghormley, 1976) and the SIZEHX optimization included the pinch point temperature difference and the tube-side and shell-side pressure drops as optimizable parameters. The powerful multiparameter optimization capabilities of the SIZEHX/GEOTHM code were used to generate an optimum set of X_A, X_{Pi}, X_{Po}, X_{CL}, and X_{UF} and therefore to verify equation (3); whereas for tractability, in the derivation it was necessary to assume that X_A, X_{Pi}, and X_{Po} were optimum values. This new technique obviously has other applications.

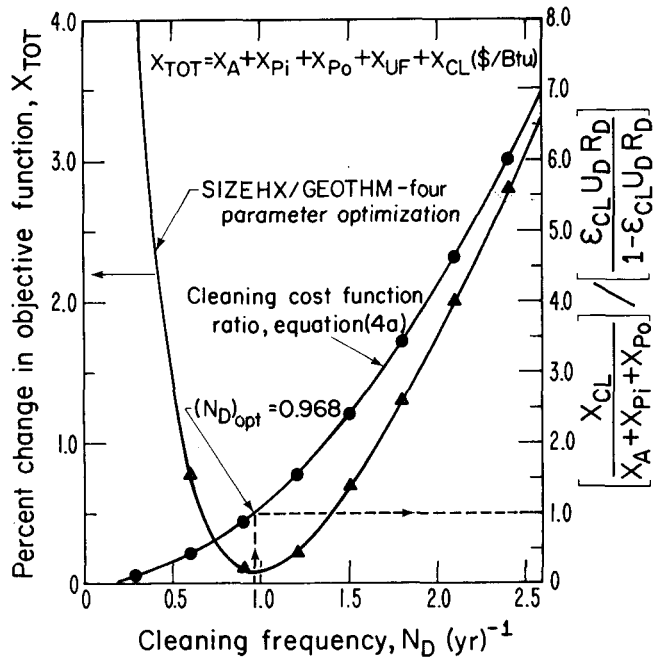

Figure 1. Comparison of exchanger optimum cleaning frequency determined by SIZEHX and given by equation (3).

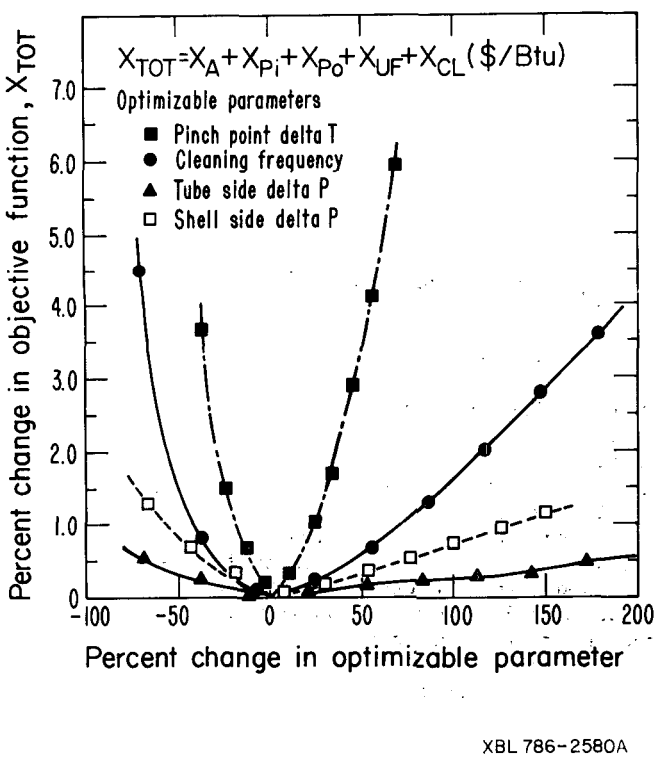

Figure 2. Sensitivity plot illustrating relative importance of pinch point temperature difference and cleaning frequency compared with pressure drop for the primary heater of a geothermal binary cycle power plant.

Figure 2 is another sensitivity plot that shows the relative importance of accurately specifying the optimum pinch point temperature difference and cleaning frequency (design fouling factor) for this geothermal exchanger compared with the optimum tube-side and shell-side pressure drops. Several other computer-generated plots are contained in LBL-7067 (Pope et al., 1978), which illustrate the general economic design space for this geothermal heat-exchanger example.

CONCLUSIONS

A general functional relationship was presented for linear fouling that describes, in simple economic terms, a unique linear coupling between the overall design heat-transfer coefficient and the design fouling factor (or fouling rate, cleaning frequency) at the optimum condition. This relationship is a necessary condition for an optimum surface heat-exchanger design. The state-of-the-art multiparameter optimization capabilities of the SIZEHX/GEOTHM code were used to verify the derived results.

Incorrect pinch point temperature difference and/or design fouling factor specifications can lead to costly exchanger overdesign or inadequate performance.

SIZEHX has significant potential for application in new low-temperature energy-conversion systems (i.e., OTEC cycles) where heat-exchanger cost is a dominant characteristic. With modifications to the basic heat-balance equation for phase change, shell-and-tube boilers and surface condensers could also be cost optimized. This modification is under development.

REFERENCES CITED

Green, M. A., Healey, R. N., Pines, H. S., Pope, W. L., Silvester, L. F., and Williams, J. D., 1977. GEOTHM, part 1, a user manual for GEOTHM, computer design and simulation of geothermal energy cycles. Berkeley, Lawrence Berkeley Laboratory, Pub. 202.

Holt, B., and Ghormley, E. L., 1976. Energy conversion and economics for geothermal power generation at Heber, California, Valles Caldera, New Mexico, and Raft River, Idaho--case studies. Pasadena, Holt/Procon ER-301, Project 580, Topical Report 2.

Lombard, G. L., 1975. Test and evaluation of a geothermal heat exchanger at Heber, California. San Diego, San Diego Gas and Electric Co., EPRI 376.

Mueller, A. C., 1954. Thermal design of shell and tube heat exchangers for liquid-to-liquid heat transfer. Lafayette, Purdue Univ., Engin. Exp. Sta., Res. Bull. no. 121.

Neill, D. T., 1976. Geothermal shell and tube heat exchanger augmentation. Idaho Falls, Idaho Nat. Engin. Lab., TREE-1023.

Pope, W. L., Pines, H. S. Fulton, R. L., and Doyle, P. A, 1978. Heat exchanger design--Why guess a design fouling factor when it can be optimized? Berkeley, Lawrence Berkeley Laboratory, LBL-7067.

THERMODYNAMIC AND COST BENEFITS OF FLOATING COOLING FOR GEOTHERMAL BINARY-CYCLE POWER PLANTS

H. S. Pines

INTRODUCTION

The vast majority of geothermal reserves in the United States are in liquid-dominated reservoirs with corresponding wellhead temperatures less than 180-200°C. Recent economic studies indicate that these medium- to low-temperature resources are best suited to organic fluid binary-cycle power plants for the production of electrical energy (Holt and Ghormley, 1976; Bloomster and Knutsen, 1975).

A method of operating a binary-cycle power plant, known as the "floating cooling" or "floating power" concept, promises to significantly enhance net power output and reduce energy costs associated with these plants (Ezzat Khalifa, 1978; Shaffer, 1977). In recognition of a highly favorable site-specific investigation of floating cooling performed by EG&G Idaho (Schaffer, 1977) the 5-MWe binary-cycle thermal loop under construction at Raft River, Idaho, which is a 150°C hydrothermal resource, has been designed to operate in this mode. Stimulated by these preliminary investigations, it would be highly desirable to assess the impact of floating cooling when applied to power plants operating upon various other candidate hydrothermal resources.

OBJECTIVES

The LBL geothermal cycle studies group has undertaken the task of quantifying the thermodynamic and cost benefits of the floating cooling concept for a variety of hydrothermal resource temperatures and climatological regimes. The initial phase of these investigations, performed in fiscal year 1978, used the LBL thermodynamic process computer code GEOTHM in a series of computer-modeling case studies of commercial-size geothermal isobutane binary-cycle power plants located at Heber, California. The Heber site was selected as the baseline case because: (a) it is a typical moderate-temperature (180°C) low-salinity hydrothermal resource; (b) it is being considered as the site for the world's first large-scale geothermal binary-cycle power plant; (c) a substantial body of well-documented A&E design and cost information already exists for this resource (Holt and Ghormley, 1976) and; (d) the climate of the region appears to be especially amenable to floating cooling operation.

The baseline studies performed by the LBL cycle studies group in fiscal year 1978 (Pines et al., 1978a,b) substantiate the economic attractiveness of the floating cooling concept suggested by previous thermodynamic analyses (Khalifa, 1978; Shaffer, 1977). They provide strong motivation for the continuing study of the benefits of floating cooling for a broad class of hydrothermal resource and climatic conditions. The experience acquired from these initial site-specific investigations will facilitate the performance of the more comprehensive Phase 2 investigations planned for fiscal year 1979.

BACKGROUND

Floating Cooling--A Definition

The floating cooling concept refers to the off-design operation of an atmospheric-cooled geothermal power plant rejecting heat to a forced-draft wet or dry cooling tower. The cooling system always operates at full capacity in response to a naturally varying wet- or dry-bulb sink temperture. The turbine back pressure (i.e., the condensing temperature) is periodically adjusted to generate the maximum available net power provided by the variable sink temperature. The net power output of the plant will vary or float with the daily and seasonal atmospheric temperature fluctuations. A fixed cooling cycle, on the other hand, operates at a constant condensing temperature and delivers constant net power during the time of the year that the design wet- or dry-bulb temperature is not exceeded.

Thermodynamic Considerations

The practical thermodynamic advantages of floating cooling for medium temperature geothermal energy systems are threefold. First, floating cooling can significantly increase the net power production of plants located in regions where the climate exhibits large daily and seasonal wet- and dry-bulb temperature variations. Second, the percentage increase in net power is greater at lower resource temperatures. Floating cooling operation is therefore more effective for plants operating at lower resource temperatures. Floating cooling systems will also counteract the adverse influence on plant performance due to a declining resource temperature over time. Third, the percentage increase in net power is greater for geothermal plants designed to operate at higher condensing temperatures, e.g., dry cooling systems. Floating cooling will counteract the adverse influence on plant performance inherent in the design of dry cooling systems operating at higher condensing temperatures than wet cooling systems.

The fortuitous thermodynamic match among moderate- to low-temperature hydrothermal resources, organic fluid binary cycles, and the floating cooling operation of these cycles is amplified by another favorable factor. These organic fluids have higher vapor pressures and lower

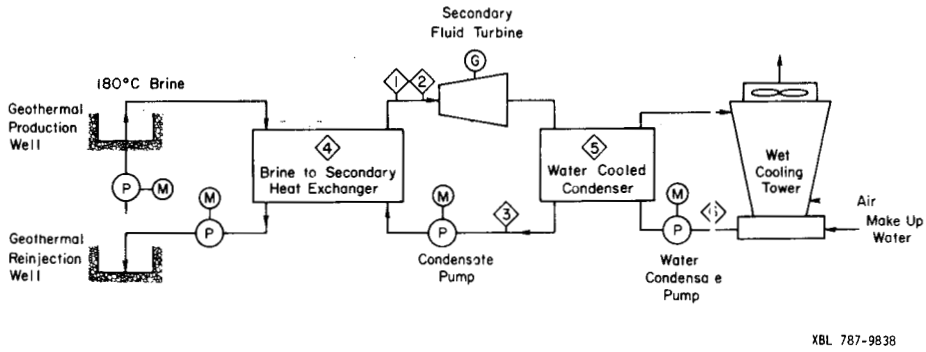

Figure 1. A typical evaporative (wet) cooled binary geothermal power cycle with 180°C inlet brine.

specific volumes than steam at similar condensing temperatures. This allows turbines to be constructed that can operate over the entire range of back-pressures associated with variations in sink temperature with only minor degradation from their peak design efficiency ratings (Pines et al., 1978). The design and cost of turbines that will operate in the floating cooling mode is not radically different from those built to operate at fixed exhaust pressures. A steam turbine operated over the range of condenser back-pressure required by floating operation would suffer a major off-design efficiency degradation. A steam power cycle is therefore not compatible with the floating cooling operating mode.

ACCOMPLISHMENTS IN FISCAL YEAR 1978

The primary accomplishments during fiscal year 1978 are illustrated by a series of computer-modeling case studies, which demonstrate the thermodynamic and cost benefits derived from the floating cooling operation of comercial-size isobutane binary-cycle power plants located at Heber, California. The resource and sink characteristics of the Heber site are typical of a number of medium temperature hydrothermal resources in California's Imperial Valley.

Floating cooling is particularly suited to exploiting the source and sink conditions characteristic of the Heber site for the following reasons: (a) The local desert climate exhibits high maximum annual wet- and dry-bulb temperatures over relatively few degree days and large daily and seasonal wet and dry bulb temperature variations. (b) The temperature of this resource

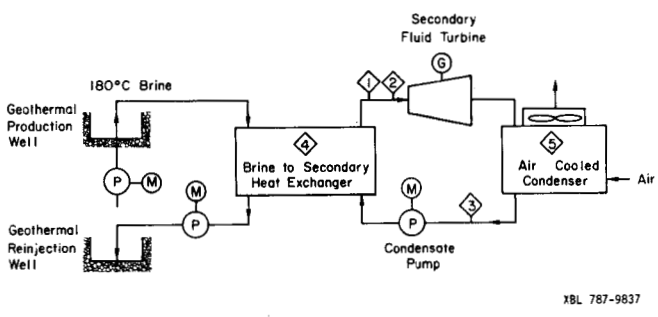

Figure 2. A typical dry air cooled binary geothermal power cycle with 180°C inlet brine.

(180°C) is best matched with an organic-fluid binary-cycle power plant (Holt and Ghormley, 1976). (c) A suitable cooling water make-up supply cannot be guaranteed over the life of the plant according to preliminary design studies (Holt and Ghormley, 1976). (d) The large additional capital and operating expenses incurred with a dry cooling system are offset by operating the plant in the floating cooling mode. (e) As the reservoir is developed to a full generating capacity of about 200 MWe, the resource temperature is predicted to decline about 30°F over 25 years, making the floating cooling binary cycle even more appropriate.

Computer Modeling Scenario Using GEOTHM

The computer model used in this study is the LBL-developed thermodynamic process computer code GEOTHM. The first step is to design two minimum-energy-cost, 50-MWe net baseload power plants. The first plant, shown in Figure 1, incorporates a water-cooled condenser coupled to a forced-draft wet cooling tower. The second plant, shown in Figure 2, is identical to the first except that a forced-draft air-cooled isobutane condenser has replaced the evaporative heat-rejection system. These are fixed-capacity 1% wet- and dry-bulb temperature designs, i.e., the plant will deliver 50 MWe constant net power during the summer months (June through September) that the design wet- and dry-bulb temperatures are not exceeded. The methodology used to design these plants is described in two reports (Pines et al., 1978a,b).

The two minimum-energy-cost designs depicted in the T-Q plot of Figure 3 are a striking contrast in many respects. The higher condensing temperature imposed by the dry cooling heat rejection system reduces the energy available in the turbine expansion process. Therefore, there is a large increase in all fluid mass flows, which when coupled with the large parasitic fan power requirement, results in a much greater total heat load upon the cycle. The much larger mean temperature difference across the air-cooled condenser is an attempt by the optimizer to minimize the area of this relatively expensive finned-tube heat exchanger. Note that the brine reinjection temperature is higher for the dry cooled plant. The fixed capacity air-cooled plant is much less efficient and

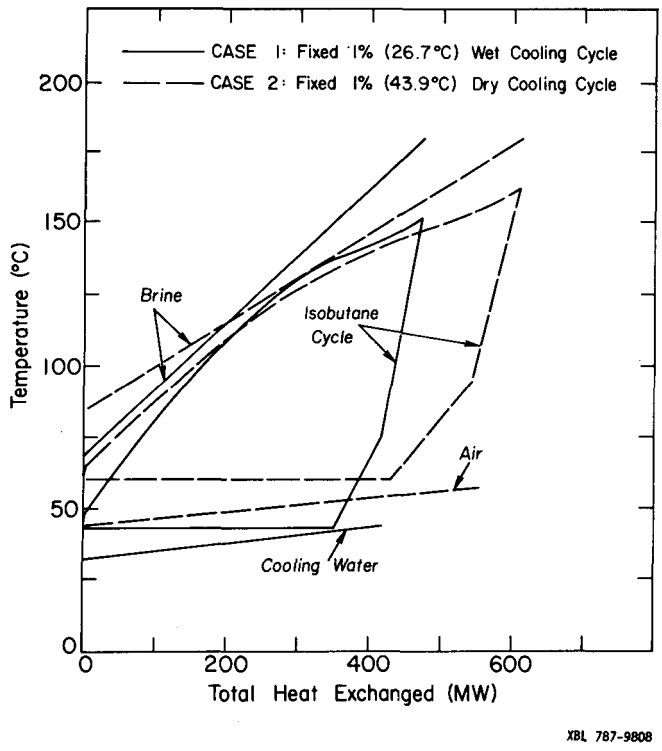

Figure 3. A temperature heat flow plot comparing an evaporative (wet) cooled cycle with a dry cooled cycle at the 1% design condition.

therefore a much larger-sized plant than its evaporatively cooled counterpart. A fixed-capacity air-cooled plant is nearly 50% more expensive (see Table 1) from a capital and busbar cost standpoint than a fixed-capacity evaporatively cooled plant.

Once the plants have been designed (equipment sizes, costs, and fluid mass flows established at the GEOTHM minimum-energy-cost designs for fixed-capacity operation), the off-design optimization routines can be invoked to operate the plants in the floating cooling mode during daily and seasonal temperature variations. In addition to fixing the brine flow rate, the GEOTHM floating cooling model assumes that the following conditions will remain constant throughout the year: turbine inlet temperature, turbine inlet pressure, heat exchanger area, condenser area, cooling tower packing area (wet system only), and cooling water or air flow rate. Coupling these constraints with the system state variables listed in Figures 1 and 2 mathematically dictates a unique solution for the turbine back pressure at any given wet- or dry-bulb temperature (Pines et al., 1978b). In order to maximize the off-design production of floating power throughout the year, the turbines for each of the plants have been designed to operate at their peak efficiency for a turbine back pressure corresponding to the annual mean wet- or dry-bulb temperature, respectively. The floating cooling plants will generate more than 50 MWe net power throughout the year. Assuming that these are baseloaded plants, that is, that all floating power can be sold at the same rate, the cost of energy for the floating cooling plants will be computed to include the revenues derived from the surplus energy sales. The cost of energy for both the floating and fixed operating modes are then compared.

Output for Heber Power Plants

The monthly mean net power generated by a floating cooling power plant for the 180°C Heber resource is computed using published monthly mean climatic data (Imperial Irrigation District, 1977). Figure 4 is a plot of the monthly mean floating net power output for both the wet- and dry-cooled plants. Note that the mean net power production during all months exceeds the 50-MWe fixed-capacity rating since the mean monthly wet- or dry-bulb temperatures are always less than the 1% design temperatures. Average annual floating capacities are obtained by integrating the area beneath each curve. Figure 4 shows that operation as a floating cooling plant can increase the output of a 50-MWe fixed-capacity plant to an average annual net power of 60.5 MWe for wet cooling or 81.3 MWe for dry cooling. This is a 21% and a 63% increase respectively, provided that the generator, electrical auxiliary, and switching gear equipment are designed to accommodate the largest anticipated floating power output (85 MWe electricity gross, wet; 129 MWe gross, dry). The average cycle efficiency is also improved from 11% to 12% for the wet cooling plant and from 8.6% to 11.8% for the dry cooling plant.

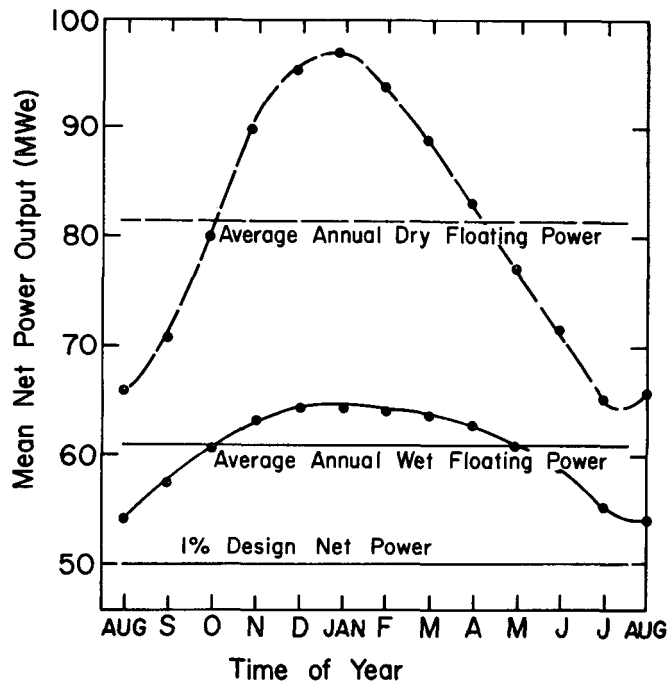

Figure 4. Floating net power as a function of the month of the year for floating evaporative and dry cooled plants which generate 50 MWe at the 1% design condition.

Table 1. Power plant parameters for fixed and floating wet- and dry-cooled binary plants at Heber, California.

	Fixed-capacity plants		Floating-cooling plants	
Process design parameters	Wet	Dry	Wet	Dry
Avg. net power (MWe)	50.0	50.0	60.5	81.3
Avg. gross power (MWe)	70.9	82.8	82.4	114.1
Avg. cycle efficiency (%)	11.0	8.6	12.0	11.8
Brine flow rate (kg/sec)	950	1427	992	1492
Avg. plant yield (kWh/tonne of brine)	14.6	9.7	16.9	15.1
Heat rejection system power requirement (MWe)	4.3	9.4	4.3	9.5
Annual brine cost (x $1000)	6.8	10.2	7.1	10.6
Plant capital cost (x $1000)	30.8	43.7	32.0	46.6
Plant capital cost per kW of average net power ($)	616	874	529	573
Busbar energy cost* (mills/kWh)	37.8	52.4	32.6	35.2

*85% plant availability is assumed.

Cost Benefits of Floating Cooling

The results of these power plant case studies for the optimized fixed and floating, wet and dry designs are summarized in Table 1. Modification of the fixed capacity plants to operate in the floating cooling mode requires only a minor increase in plant capital investment. Nevertheless, revenues derived from the sale of surplus floating power substantially reduce the cost of energy produced compared with the same plant operated at fixed capacity. This energy cost reduction is particularly dramatic in the case of the dry-cooling plant. Whereas energy produced by the fixed-capacity dry-cooling plant costs 43% more than for its (fixed-capacity) wet-cooling counterpart, the energy cost of the dry floating plant exceeds that of the wet floating plant by only 8%. Clearly, the incremental thermodynamic advantages of the dry-floating cycle over the wet-floating cycle translates into significant cost benefits. The cost of energy for the dry floating plant is less than that for the fixed-capacity evaporatively cooled system.

Table 1 indicates the seemingly attractive prospect of producing energy from a dry floating cooling plant at costs competitive with wet cooling systems. This pleasantly surprising result must be examined with the following qualifications.

First, the dry-cooled plant, which produces 50 MWe at the 1% design condition and 81.3 MWe average annual floating power, requires about 50% more plant capital investment expenditures than a comparable 50-MWe fixed-capacity evaporatively cooled plant.

Second, the net power output of a floating cooling plant fluctuates significantly with daily and seasonal atmospheric temperature variations. Maximum daily power production occurs during late evening and early morning hours. Maximum seasonal power production occurs during the winter months (see Figure 4). These times are usually considered off-peak demand periods by utilities.

Third, this report assumes that all energy produced by a floating cooling power plant can be sold at the same rate, that is, the utility can integrate all floating power produced by this baseload plant into the grid. This assumption may be subject to adjustment to reflect a utility's attitudes toward the seasonal and daily power production schedule. However, this may be a reasonable assumption in view of the rather minor fluctuations in power output for a 50-MWe geothermal plant, which must be compensated for by adjustments in the operation of the larger fossil plants in the grid.

The cost of brine is charged on a dollars

per pound basis for a floating plant operating at a constant year-round brine flow requirement, even though the brine reinjection temperature fluctuates with the sink temperature variation. The validity of this brine cost assumption for floating plant operations must await actual contractual negotiations between field producer and utility.

Cost Comparison Study

A cost comparison study for fixed-capacity plants versus floating power plants is more meaningful if both the fixed and the floating plants are designed for the same average annual net power capacity. Figure 5 is a plot of the busbar energy cost and plant capital cost for four fixed-capacity evaporatively cooled plants and for four corresponding dry floating cooling plants, which generate the same average annual net power as the fixed plants (Pines, et al., 1978b). Comparison of the cost curves in Figure 5 shows that a dry floating cooling plant can deliver the same amount of average annual power as a fixed-capacity wet cooling plant for a slightly lower capital cost and at a lower energy cost. These results suggest that electrical power in the Imperial Valley can be competitively generated from geothermal resources without the need to impact upon the precious fresh water supplies so badly needed for agricultural and consumer needs.

Declining Resource Temperature Scenario

In order to illustrate the increasing benefits of floating cooling at lower resource temperatures, a declining resource temperature modeling scenario for the development of the Heber resource has been devised (Pines et al., 1978a). Four fixed-capacity 1% 50-MWe evaporatively cooled plants and their corresponding floating wet cooling plants were designed to operate over their 25 year lifetimes at average resources temperatures of 180°C, 175°C, 170°C, and 165°C, respectively. As predicted for the floating cooling plants, the average annual floating net power output will increase for plants designed to operate at lower resource temperatures.

The busbar cost of energy for each plant operating in both the fixed and floating modes is plotted in Figure 6. As the cost of energy increases with decreasing resource temperature, floating cooling is seen to mitigate this cost increase by as much as 14%. The increasing thermodynamic benefits of floating cooling, as the resource temperature declines, translates into greater percentage energy cost reductions. Figure 6 also shows that floating cooling can generate power from a 167°C resource for the same cost of energy (for a slightly greater capital investment) as a fixed-capacity plant operating from a 180°C resource. From an equivalent-cost-of-energy standpoint, floating cooling

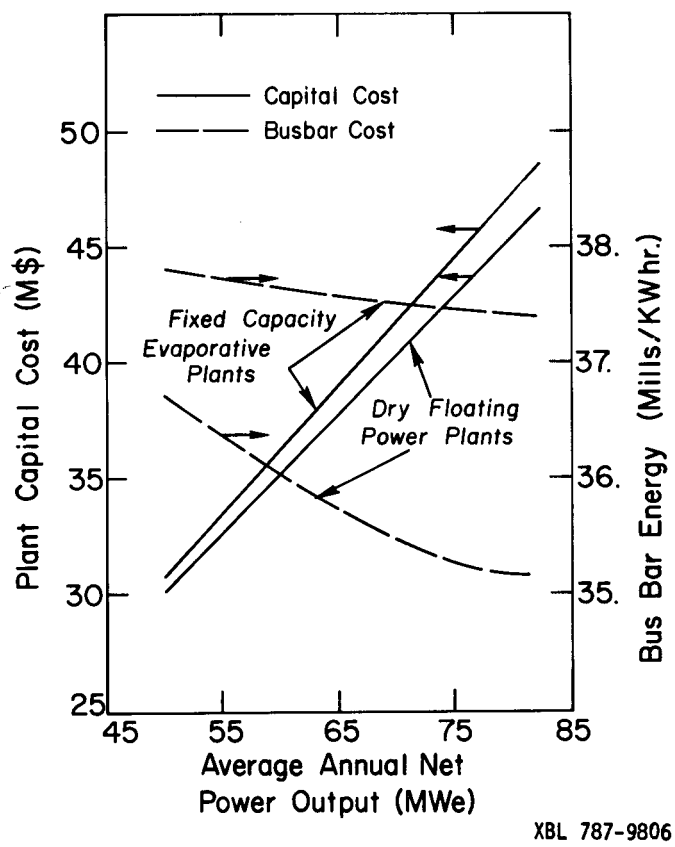

Figure 5. Plant capital cost and busbar energy cost as a function of average annual net power output from fixed wet cooled plants and floating dry cooled plants.

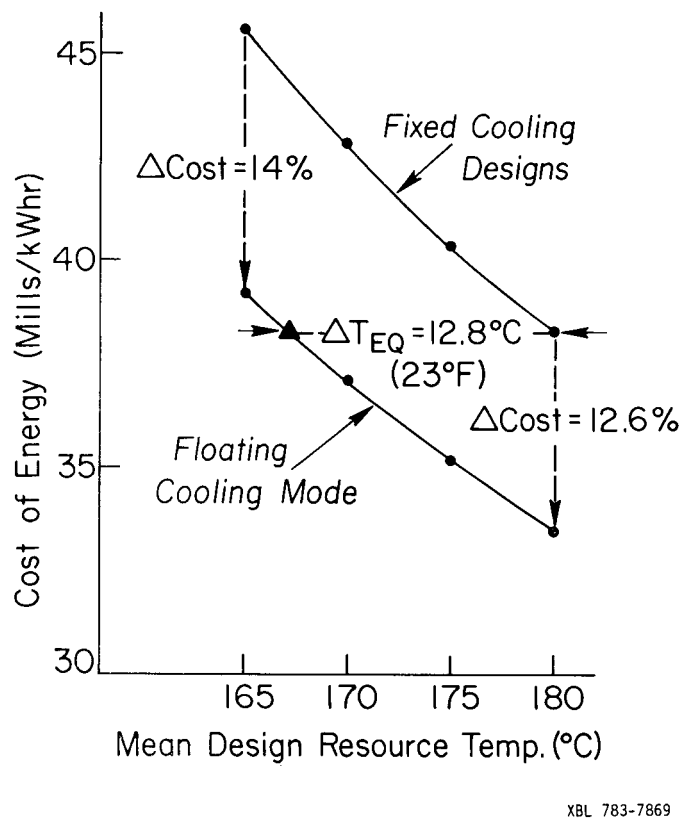

Figure 6. Busbar cost of energy for 50-MWe (1%) plants operating in both fixed and floating modes for different mean design resource temperatures.

has the effect of increasing the Heber resource temperature by 12.8°C (23°F). This temperature-cost equivalence suggests that floating cooling may allow geothermal binary cycles to: (a) maintain their general economic attractiveness because of lower resource temperatures than was previously believed; and (b) compete more effectively with flashed-steam cycles at higher resource temperatures.

PLANNED ACTIVITIES FOR FISCAL YEAR 1978

The fiscal year 1978 Heber case studies have demonstrated a variety of thermodynamic and cost benefits of significant magnitude, which result from the operation of geothermal binary-cycle power plants in the floating cooling mode. These extremely positive findings suggest a number of phase 2 follow-on studies for the fiscal year 1979 research agenda.

1. A series of case studies that quantify the potential thermodynamic and economic benefits of floating cooling plant operation for a broad class of hydrothermal resource and climatic conditions.

2. Site-specific case studies of the thermodynamic and economic benefits of floating cooling for proposed plants of particular interest to DOE or DOE contractors.

3. Exploratory studies of the benefits of floating cooling when appied to the operation of various types of Rankine-cycle process designs such as: direct-contact process plants; hybrid flash-steam/Rankine-process bottoming systems; and Rankine-process bottoming of nongeothermal topping systems, for example, fossil fuel cogeneration.

4. A survey of prevailing utility attitudes and constraints with respect to the accommodation of variable-power geothermal plants into the overall structure of the grid.

5. A critical examination of the role that floating dry cooling geothermal plants can play in providing electrical energy to California's Imperial Valley without threatening the scarce fresh water resources of this region.

6. A comparative study that quantifies how operation of a fixed-capacity binary plant in the floating mode allows binary plants to be cost competitive with flash-steam cycles at higher resource temperatures.

REFERENCES CITED

Bloomster, C. H., and Knutsen, C. A., 1975. The economics of geothermal electricity generation from hydrothermal resources. Richland, Battelle Pacific Northwest Lab., BNWL-1989.

Holt, B., and Ghormley, E. L., 1976. Geothermal energy conversion and economics--case studies. Palo Alto, Electric Power Research Institute, EPRI-301.

Imperial Irrigation District, 1977. Imperial Valley annual weather summary 1977--monthly high, low and mean temperatures and rainfall, 1914-1977. Records of Watermaster, Imperial Irrigation District.

Khalifa, E. H., 1978. Effect of seasonal variations of ambient temperature on the performance of low temperature power cycles. Providence, Brown Univ., Div. Engin., Report, COO/4051-10.

Shaffer, C. J., 1977. Floating power optimization studies for the cooling system of a geothermal power plant. Idaho Falls, EG&G Idaho, Inc., Idaho Nat. Engin. Lab., TREE-1164.

Pines, H. S., Pope, W. L., Green, M. A., Doyle, P. A., and Fulton, R. L., 1978a. The thermodynamic and cost benefits of a floating cooling geothermal binary cycle power plant at Heber, California. Berkeley, Lawrence Berkeley Laboratory, LBL-7040.

Pines, H. S., Green, M. A., Pope, W. L., and Doyle, P. A., 1978b. Floating dry cooling, a competitive alternative to evaporative cooling in a binary cycle geothermal power plant. Berkeley, Lawrence Berkeley Laboratory, LBL-7087.

GEOTHERMAL RESOURCES AND THE U.S. PULP AND PAPER INDUSTRY

J. V. Davey and J. H. Howard

INTRODUCTION

In partial support of the direct-use commercialization program for DOE/SAN, we presented an invited paper at the Workshop on Industrial Process Applications for Geothermal Energy Resources held at Massachusetts Institute of Technology in October 1978 (Davey and Howard, 1979). The purpose of the presentation was to describe possible use of geothermal resources to satisfy some of the needs for energy in the pulp and paper industry.

ACTIVITIES IN FISCAL YEAR 1978

The MIT paper reviewed the following major points:

1. The U.S. pulp and paper industry is a major energy user; it ranks fifth as an energy consumer and used about 2 x 10^{15} Btu's in 1977.

2. Although this industry has improved its energy/product ratio and its substitution of cheaper fuels for more costly purchased electricity, oil, and natural gas, it faces a serious problem in the future in costs for and availability of energy.

3. Several process plans of pulp and paper operations using geothermal resources as a source of energy have been conceived by DSS Engineers, Inc. (1975). These plans are specific to the high-pressure, methane-rich "geopressure" geothermal resource of the Gulf Coast, for both retrofitted and new operations.

4. Plans based on the use of geothermal resources are presented as technically feasible and economically appealing. (Rates of return on the cost of special equipment to use the geothermal resource and on the cost of wells are greater than 15%.)

5. In many areas in the United States, geothermal resources and existing pulp and paper operations are located near each other. The potential for use of geothermal resources clearly exists.

6. A major problem facing the pulp and paper industry is overcoming concerns over risks associated with definition and exploitation of a geothermal anomaly.

Industry response to the presentation appeared to be one of guarded interest, as evidenced by questions following the presentation and several follow-up phone calls.

ACTIVITIES PLANNED FOR FISCAL YEAR 1979

Although there is promising potential for the use of geothermal resources to satisfy some of the needs of the pulp and paper industry, no special program to further define this potential is planned at LBL in fiscal year 1979. LBL does plan to continue to support the review of proposals (one of which in the past included a pulp and paper mill) and to conduct reservoir analyses in areas that coincidentally include pulp and paper operations.

REFERENCES CITED

Davey, J. V., and Howard, J. H., 1979. Geothermal resources and the pulp and paper industry. Presented at the Workshop on Industrial Applications for Geothermal Energy Resources: the Case of the Paper and Pulp Manufacturing, Cambridge, Massachusetts Institute of Technology, October 10, 1978.

DSS Engineers, Inc., 1975. Geothermal resource utilization, paper and cane sugar industries. Livermore, Lawrence Livermore Laboratory, UCRL-13633.

Reservoir Engineering

The following series of papers illustrates the activities of the Geothermal Reservoir Engineering Group in fiscal 1978. These activities can be placed into three groups: research, investigations of specific geothermal reservoirs, and management services for the U.S. Department of Energy, Division of Geothermal Energy (DOE/DGE). These three groups are, in fact, the topic areas that describe the responsibilities covered by the LBL program: to conduct research, to provide expert advice on specific reservoirs where DOE/DGE has a special interest, and to manage certain programs on DGE's behalf.

RESEARCH

Seven articles explaining the results of research related to geothermal reservoir engineering are included. Two articles describe fluid flow in geothermal wells: Miller on single-phase transient flow, and Juprasert on steady-state two-phase flow. Two papers address problems of modeling reservoirs with special features of permeability distribution. Narasimhan and Palen investigate use of the code TERZAGI to model flow to a well intercepted by a vertical fracture. The paper concludes that TERZAGI has the flexibility to model finite conductivity fractures. Mlodinow and Tsang consider the effect of radially varying transmissivity on transient pressure phenomena. Comparison of the codes METERNIQ and TRUMP for forecasting thermal breakthrough caused by injection is presented by Narasimhan, Juprasert, and Bodvarsson. The article illustrates the "tradeoffs" one might anticipate and have to resolve in selecting a fast-running, fairly easy-to-use code (METERNIQ) with certain simplifying assumptions compared with a slower-running code having a more sophisticated description of heat and mass transport phenomena.

A very comprehensive contribution concerning well-test data-analysis methods at Lawrence Berkeley Laboratory is presented by Benson, Goranson, and Schroeder. Through the last several years, LBL has developed, perfected, and applied several well-test-analysis computer codes. Among these programs are codes for certain special purposes such as: graphically plotting pressure data and flow-rate data on the same diagram; generating meshes for use in transport codes; and carrying out analyses of well-test data in order to evaluate transmissivity and storativity of the reservoir. Also included in the article is an overview of computer programs which, although intended primarily as forecasting devices, can also be used to analyze well-test data under the proper circumstances. The reader's attention is drawn to Table 1, 2, and 3 where a short description of each of these codes is given. The complexity of well-test-data collection, processing, storage, and the degree of sophistication in treating these data at LBL is shown in Figure 1. Likewise, the complexity of interference-test data analysis is shown in Figure 4. Graphical output of special importance in reports involving the data are illustrated in Figures 2, 3, and 5.

Over all, one of LBL's principal objectives has been to develop a superior well-test-data collection, processing, storage, and analysis capability. The fact that such an outstanding capability has been established is succinctly illustrated in the article by Benson et al.

Since its inception, the Earth Sciences Division of Lawrence Berkeley Laboratory has been concerned with the development of mass, energy, and reactants transport codes. The article by Pruess et al. is a synopsis of the status of the code SHAFT78. SHAFT78 has veen verified with a number of problems and can satisfactorily simulate transport of mass and energy, particularly as they apply to understanding geothermal reservoirs. The code is applicable to real problems to the extent that appropriate initial and boundary conditions can be assigned. In addition, the code has been used in an imaginative way to understand previously unappreciated phenomena in geothermal reservoirs. A key insight into the limitations of currently popular techniques of reserve estimates for vapor-dominated geothermal reservoirs has been revealed through use of this code. As illustrated by Pruess et al., SHAFT78 has led to an appreciation of the importance of saturation--namely, the fraction of steam to the total of liquid and steam in the pores of a geothermal reservoir. In the past, it had been thought that pressure decline in a vapor-dominated geothermal reservoir was logarithmic as a function of time. Insight through the use of SHAFT78 has shown that the fraction of pore space filled with liquid is vitally important in determining the time during which vapor pressure declines logarithmically. When the pore water itself is depleted and transformed completely to steam, precipitous pressure decline occurs, as illustrated in Figure 7 of the article. Accordingly, the reserve (or cumulative Production) must be integrated beneath a function different from a simple logarithmic function. LBL considers SHAFT78 an extremely powerful analytical forecasting tool for use in the geothermal community.

INVESTIGATIONS OF SPECIFIC GEOTHERMAL RESERVOIRS

The section on investigations of specific geothermal reservoirs includes six papers. LBL has worked cooperatively during fiscal 1978 to understand the geothermal resources at particular sites in the United States and elsewhere in the world. Activities are reviewed in the article by Goranson and Schroeder (see Table 1). Three articles are concerned with the geothermal reservoir at Cerro Prieto, Mexico. The United States and Mexico have a cooperative program to study this geothermal resource, which should serve as a valuable conceptual model for developing similar resources in the Salton Trough in California. Lippmann, Bodvarsson, and Witherspoon illustrate in their article the importance of leakage from a shallow, untapped portion of the geothermal reservoir into a deeper producing zone. They indicate that, although temperature changes because of the leakage may not be significant, changes in chemistry of fluid may become important and may call for changes in the energy conversion

plan. They emphasize the importance of understanding the permeability of those horizons that separate the producing from the nonproducing zones.

In their article, Tsang et al. emphasize the significance of choice of wells at Cerro Prieto to be used for reinjection. Depending on this choice, breakthrough times can occur after different durations of reinjection. Likewise, choice of wells affects the efficiency of recovery of heat in areas between injection and production wells. Proper reservoir management calls for an appreciation of the flow patterns of reinjected fluid, and of thermal breakthrough times from injection to production wells.

In fiscal 1978, Lawrence Berkeley Laboratory expended substantial effort in understanding the East Mesa geothermal resource. The geology of this resource is described in the article by Howard, Graf, and Van de Kamp. Well testing at East Mesa is described by Benson et al. in the article on well-test data analysis methods. This article illustrates LBL's ability to gather data that lead to the important conclusions summarized in the tables. In addition to the desire to establish a strong analytical capability, LBL has had as one of its objectives the establishment of an outstanding field operations group. The capability of this group is well illustrated by the work at East Mesa.

MANAGEMENT SERVICES FOR DOE/DGE

During fiscal 1978, LBL continued to play a role in the management of contract research for the U.S. Department of Energy, Division of Geothermal Energy. LBL accepted this assignment from the Department of Energy and agreed to the following: to develop a plan for support of research; to have the plan reviewed by a third-party groups of experts; to follow through with the administrative tasks of announcing, reviewing, awarding, and procuring contracts; and to monitor progress of the work. To date, a total of 18 contracts have been managed under the Geothermal Reservoir Engineering Management Program (GREMP), and a total of 8 contracts have been supervised under the Geothermal Subsidence Research Management Program. Reviews of the highlights of these two programs (GREMP and Subsidence) are given in articles by Howard and Schwarz and by Simkin, Noble, and Schwarz. Subcontracted work is consistent with the mission of the Division of Geothermal Energy, and is compatible with in-house programs being done at LBL. The dollar value of contracts handled by LBL is of the same order of magnitude as the in-house budget at LBL. The Management Services Program has been a major part of the Geothermal Reservoir Engineering Group activities in fiscal 1978.

PRESSURE MEASUREMENTS USING A FLUID-FILLED CAPILLARY TUBE

C. W. Miller

INTRODUCTION

Well testing is an important step in assessing reservoir properties and accurate pressure measurements are essential. Due to the harsh environment of the geothermal well, most existing downhole pressure-measurement devices cannot be used. For single-phase flow in the wellbore, downhole pressure changes can be calculated from wellhead data by modeling the transient flow. For two-phase flow in the wellbore, the flow modeling is not yet accurate enough to do this. One method of continuously monitoring downhole pressure is to use another fluid, which does not flash at these temperatures and pressures, to sense the pressure changes. This method uses a fluid-filled capillary tube, attached to a pressure transducer at the surface and to a larger chamber downhole (Ashby, 1977). The tubing must be small in diameter so it is flexible enough to be handled and lowered into the well. The interface between the brine and the fluid is maintained in the larger chamber instead of in the small tubing to minimize the change in its position for any pressure variations. However, care must be taken in using the data obtained with this device. The pressure signal from downhole is delayed and distorted because of the viscosity and compressibility of the fluid. Any temperature changes increase the distortion. Because this seems to be the best tool at present for high-temperature and long-flow tests, a complete assessment of the tool was made (Miller and Haney, 1978). Some of the modeling techniques developed can also be used to simulate the wellbore flow directly.

ACTIVITIES FOR 1978

The pressure signal through the fluid-filled capillary tube is effected by choice of fluid, size of tubing including length and diameter, temperature changes with time, and the average temperature and pressure in the tube. To do a complete assessment of the tool, it was necessary to obtain a solution to the transient equations of mass and momentum for the appropriate boundary conditions. The temperature changes in the tube were assumed to be controlled by changes in the well itself, because the tubing diameter was so small in comparison to the well diameter. Because temperature effects can be important, we must know the temperature-profile changes with time if very early-time data are to be used.

Two fluids were investigated, 10-cs silicone oil and nitrogen. Because the oil is not very compressible, most changes downhole will result in small changes in density and can be considered a small disturbance. A very simple diffusion-like equation was found to accurately predict the pressure signal, P, at wellhead for a given downhole change when oil was the transmitting fluid:

$$\frac{\partial P}{\partial t} = \frac{R^2}{8\mu C_t}\frac{\partial^2 P}{\partial x^2} + \frac{\beta}{C_t}\frac{\partial T}{\partial t}$$

where R is the capillary tube radius, μ is the absolute viscosity of the fluid, C_t and β are the isothermal compressibility and volumetric expansivity, respectively, and T is temperature. The first term is the diffusion of the pressure; the second is the pressure pulse generated by any temperature changes in time. Frictional effects dominate so the diffusion-like equation results. This equation was compared with experimental data when oil was used as the fluid and was found to predict the pressure signals accurately (Miller and Haney, 1978).

The same simple equation was not adequate to assess the use of nitrogen as the fluid sensing system, because of the larger compressibility of the gas. A numerical model was necessary to solve the general case of one-dimensional, compressible, transient, single-phase flow. By including the energy equation, the program was also extended to solve the flow in the well itself when the brine was not flashing. The density is related to pressure and temperature with an equation of state. One important aspect of the numerical model is that any compressibility effects are handled in an implicit manner because of the severe time restrictions imposed otherwise. Again, the solution with nitrogen as the fluid was compared with experimental data for several cases and was found to give excellent agreement (Miller and Haney, 1978).

Using the appropriate models, a complete assessment of the pressure instrument was done. Figure 1 illustrates the effect of the tubing measurement system on the downhole pressure signal for the isothermal case. Curve (a) is the postulated downhole signal. Curves (b), (c), and (d) show the response which would be measured at wellhead with the different fluids. The calculations were done for a tubing, 8,000 ft in length and with an I.D. of 0.054 in. Curves (b) and (d) show the signal with 10-cs silicone oil for 356°F and 70°F, respectively. The difference in signal is because of the large effect of temperature on the viscosity. There is at least an order of magnitude drop in the viscosity for this temperature increase. Curve (c) is the response with nitrogen in the tube. The nitrogen-filled tube is effected more significantly by the average pressure in the tube because the compressibility is proportional to the inverse of the pressure.

The comparison done above was for the isothermal case. However, when the flow rate is changed in the well, there will be a change in the temperature of the brine at any point. Even if the change were very small (about 3°F for a doubling of the flow rate), significant changes in the generated signal were found. The largest changes were found to be with the oil. Figure 2 shows the comparison between the isothermal case and the case where an average temperature change of 2.7°F takes place in about 10 minutes. The signal has been distorted and delayed significantly longer.

The effect of the tubing diameter on the signal was also considered. Figure 3 shows a comparison of three possible tubes. The comparison shown here is for a nitrogen-filled tube with a slight temperature change. The small tubing of 0.026 in. distorts the signal excessively.

Some brief conclusions on the best use of the instrument are: (a) the small tubing of 0.026 in. I.D. should not be used; (b) at low temperatuers but high pressures, nitrogen would be the better fluid; (c) when significant temperature changes result, nitrogen would be better; but (d) for high temperatures and lower pressures (say 500 to 1000 psia) oil might be best.

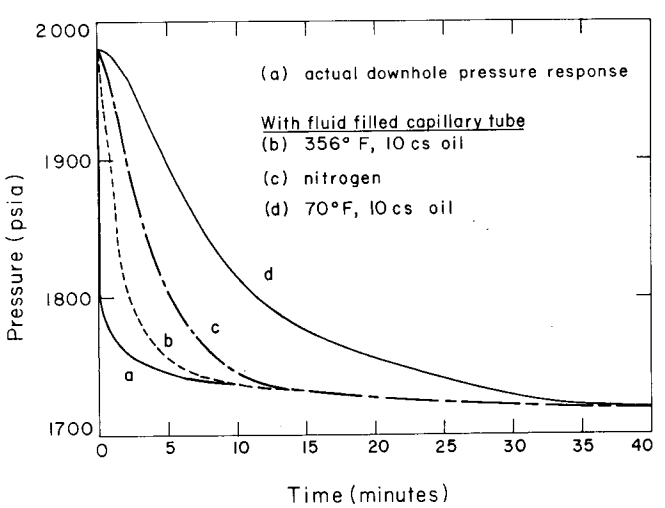

Figure 1. Pressure signal measured by fluid-filled capillary tube comparing oil and nitrogen as the fluid. The downhole signal is also given.

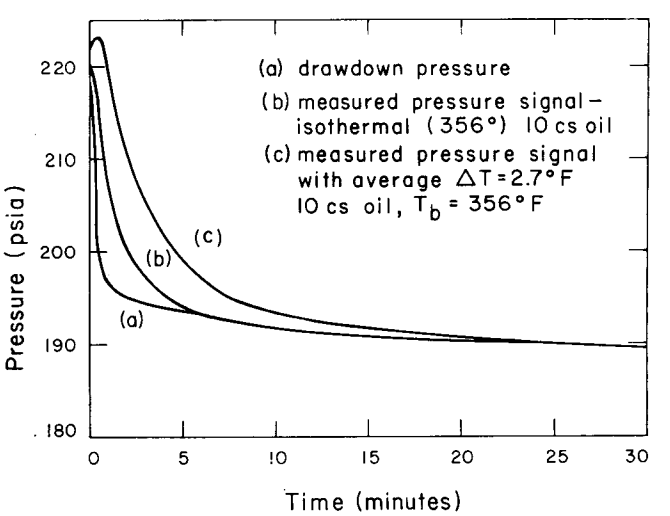

Figure 2. Pressure signal measured by fluid-filled capillary tube comparing isothermal and nonisothermal response with oil as the fluid.

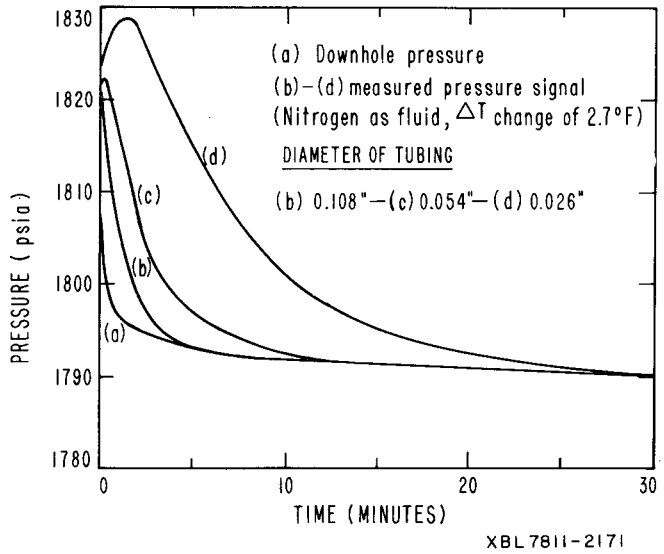

Figure 3. Pressure signal measured by fluid-filled capillary tube comparing the effect of different diameter tubes. Nitrogen is used as the fluid.

PLANS FOR FISCAL YEAR 1979

To obtain downhole pressures from the wellhead, the inverse problem must be solved. At present, one can guess the downhole signals, calculate the pressure response for that signal, and compare it with the measured signal. However, this is tedious and it is desirable to find a more direct method. This is not particularly simple because small changes at wellhead produce large changes downhole. The problem being worked on at present is to obtain a more direct method to the inverse problem, at least for the small disturbance case.

Another planned activity is to expand the program that solves the transient single-phase flow so that transient two-phase flow can be modeled. Steady-state approximations to the two-phase flow in the well exist. However, when the brine flashes, wellbore storage effects can become quite important. Also, frictional effects are time and history dependent. LBL has reservoir simulators and models to predict the performance of a geothermal power plant. To provide a complete model of the system as a whole, a model of transient, compressible, one-dimensional two-phase flow is desired.

REFERENCES CITED

Ashby, T. J., 1977. Continuous bottom-hole pressures are measured by non-electric system, in Proceedings, First Invitational Well-Testing Symposium, Berkeley, California, October 1977. Berkeley, Lawrence Berkeley Laboratory, LBL-7027, pp. 44-45.

Miller, C.W., and Haney, J., 1978. Response of pressure changes in fluid-filled capillary tube, in Proceedings, Second Invitational Well-Testing Symposium, Berkeley, California, October 1978. Berkeley, Lawrence Berkeley Laboratory, LBL-8359.

TWO-PHASE FLASHING FLOW IN GEOTHERMAL WELLS

S. Juprasert

INTRODUCTION

A knowledge of the pressure, temperature, enthalpy, and steam quality of the geothermal effluent is indispensable in assessing the practical value of a geothermal resource. To design a geothermal power plant, one needs a 20- or 30-year forecast of these properties for the geothermal effluent at the wellhead. Reservoir simulation or analytical techniques can be used to forecast these properties at the well bottom or at the depth at which fluid enters the wellbore from the reservoir. A wellbore flow simulator has been developed that can calculate wellhead properties of the effluent from the forecast of those properties at the well bottom. Properties of the geothermal effluent are measured at the wellhead during flow tests. The simulator can be used to calculate the properties of the geothermal fluid downhole. Such calculations are often necessary to understand the basic characteristics of the reservoir, to interpret well tests, to determine well completions; and to make other decisions, such as the optimum depth of setting downhole pumps.

As compressed hot water enters the wellbore from the reservoir, it flows up the wellbore with continuous drop in pressure and temperature. If the pressure drop is sufficiently large for flashing, a two-phase (steam-water) mixture will form and continue to flow up the wellbore, with changing pressure, temperature, enthalpy, and steam qualtiy. The situation is similar if the water has flashed inside the reservoir and enters the wellbore as a two-phase mixture.

The model uses two-component, two-phase pressure drop correlations that have been used for two-phase flow in oil and gas wells, that is, Duns and Ros (1963), Orkiszewski (1967), Beggs and Brill (1973), and Hagedorn and Brown (1965) correlations. These correlations were applied to the one-component, two-phase geothermal system, taking into account the possible existence of several flow regimes along the pipe for a given set of operating conditions: single-phase liquid flow, bubble flow, slug (plug) flow, transition flow, and finally annular-mist flow. Application also required the calculation of heat transfer and phase transfer (vapor-liquid) in the wellbore.

ACTIVITIES IN FISCAL YEAR 1978

A simulation of the flow conditions in well 6-1 at East Mesa, Imperial Valley, California,

was performed in an attempt to duplicate the tests conducted in January 1973 by the U.S. Bureau of Reclamation (Howard et al., 1979). During the test, the well flowed at a constant rate of 250 gpm. The calculations were made from bottom-hole to the wellhead in the direction of the flow.

By giving the temperature, pressure, and flow rate of the water (or steam-water mixture) at the bottom of the well; the diameter, length, and friction factor of the wellbore; and the static temperature profile along the wellbore, the program calculates the pressure, temperature, enthalpy and steam quality of the steam-water mixture (or water, if no flashing takes place) at the wellhead, or at any specified depth in the wellbore. Conversely, given the fluid condition at the wellhead, the program can calculate the fluid condition downhole. Thus, the program provides a continuous profile of the flowing pressure, temperature, enthalpy and stream quality in the wellbore.

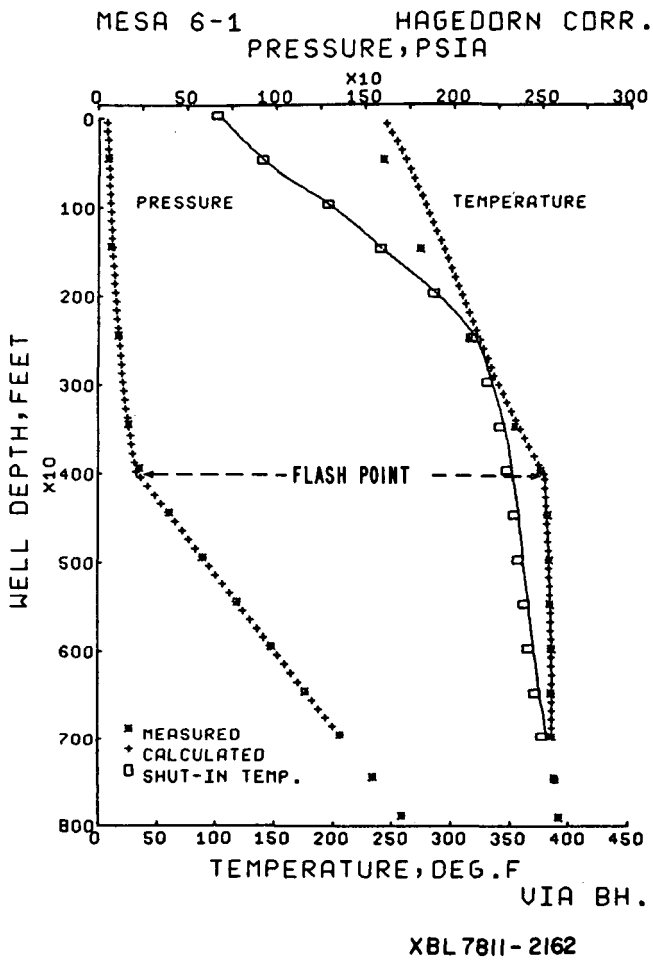

Figure 1. Comparison of measured and calculated pressure and temperature profiles of well 6-1, East Mesa, California.

Beginning with single-phase water at the 7000-ft depth, the model predicts flashing at about 4000 ft, which reasonably matches the actual observation. As steam formed after flashing, the model showed progressive change in the two-phase flow regime from bubble to slug and finally to transition flow. All of the four correlations were used in the simulation. It was found that the Hagedorn and Brown correlation yielded the best agreement between the observed and calculated profiles of flowing pressure and temperature, as shown in Figure 1.

FUTURE DEVELOPMENT

During fiscal 1979, we will modify the program to incorporate noncondensible gas evolution and handle variable casing dimensions.

REFERENCES CITED

Beggs, H. D., and Brill, J. P., 1973. A study of two-phase flow in inclined pipes. Trans. AIME, v. 255, pp. 607-617.

Duns, H., Jr., and Ros, N. C. J., 1963. Vertical flow of gas and liquid mixtures in wells. Proc. Sixth World Petrol Cong., Frankfurt, v. II, pp. 451-455.

Hagedorn, A. R., and Brown, K. E., 1965. Experimental study of pressure gradients occurring during continuous two-phase flow in small-diameter vertical conduits. Trans. AIME. v. 234, pp. 475-484.

Howard, J., Apps. J.A., Benson, S., Goldstein, N. E., Graf, A. N., Haney, J., Jackson, D., Majer, E., McEdwards, D., McEvilly, T. V., Narasimhan, T. N., Schechter, B., Schroeder, R., Taylor, R., van de Kamp, P., and Wolery, T., 1979. Geothermal resource and reservoir investigations of U.S. Bureau of Reclamation leaseholds at East Mesa, Imperial Valley, California. Berkeley, Lawrence Berkeley Laboratory, LBL-7094.

Orkiszewski, J., 1967. Predicting two-phase pressure drops in vertical pipe. Trans. AIME, v. 240, pp. 829-838.

FLOW TO A WELL INTERCEPTING A VERTICAL FRACTURE: VALIDATION OF A NUMERICAL MODEL

T. N. Narasimhan and W. A. Palen

INTRODUCTION

Hydraulic fracturing is often used in petroleum reservoirs to stimulate production. Depending on the in-situ reservoir stresses, hydraulic fractures may have a horizontal or vertical orientation and may extend from a few to several tens of meters from the production well. In such wells, the early-time pressure response due to fluid production will be dominated by flow through the fracture. It is of considerable practical interest in well-test analysis to evaluate the role of fractures in the production-well response. Analyses of pressure response of wells intercepting fractures have been carried out by previous workers using analytical and quasinumerical methods. A comprehensive review of these studies can be found in Raghavan (1977). However, to be able to study a sufficiently large class of problems involving wells intercepting fractures, it is preferable to have a numerical model with few or no analytic assumptions. The suite of computer programs currently used by the Reservoir Engineering Group of the Earth Sciences Division for analyzing fluid-flow problems constitute a set of fully numerical tools that is valuable for analyzing flow to wells intercepting fractures. The applicability of one of these computer programs, TERZAGI, was investigated during fiscal 1978 to analyze fluid flow to a well intercepting a single vertical fracture. The program is very capable of studying the class of problems under consideration, including effects of wellbore storage and wellbore damage. TERZAGI is based on an integral finite difference scheme (Narasimhan and Witherspoon, 1976) and can handle fluid flow in arbitrarily heterogeneous or anisotropic flow regions with complex geometry, time-dependent material properties, or boundary conditions and sources. This report briefly summarizes the validation of TERZAGI with reference to flow to wells intercepting fractures.

THE PROBLEM

Consider a well fully penetrating an infinite, horizontal reservoir with thickness, h, absolute permeability, k, and storage coefficient, $\phi c_t H$ (Figure 1). The reservoir has a vertical fracture with width, w_f, also fully penetrating the aquifer, and with fracture length, $2x_f$. The well is assumed to be at the center of the fracture and has a wellbore radius, r_w, and produces at a constant volumetric rate, q. The fracture has a permeability, k_f, and storage coefficient $(\phi c_t h)_f$. The reservoir is at an initial pressure of p_o throughout. The problem is to predict the pressure drawdown ($\Delta p = p - p_o$) in the wellbore caused by the fluid production as a function of time.

The aforesaid problem can be described within the time range of interest (Cinco-Ley et al., 1978) using the following four dimensionless quantities:

Dimensionless time, $t_D = kt/\phi c_t \mu x_f^2$

Dimensionless wellbore pressure,

$$P_{WD} = 2\pi kh\Delta P/q\mu$$

Dimensionless fracture conductivity,

$$C_r = w_f k_f / kx_f$$

Dimensionless wellbore capacity,

$$\bar{C} = C/2\pi\phi c_t h x_f^2$$

The pressure response of an infinitesimal-radius well intercepting a vertical fracture of finite conductivity has been studied by Cinco-Ley et al. (1978). In their study they used a quasinumerical approach in which the region beyond the fracture was modeled by the finite difference method and the flow in the fracture itself was modeled by an analytical approach. At the fracture interface, the two solutions were appropriately coupled.

NUMERICAL SIMULATION

The same problem was solved in a fully general numerical fashion using program TERZAGI. The mesh used was of a variable grid, variable symmetry nature, as shown in Figure 2. The mesh was designed to model radial flow close to the wellbore and at the edge of the fracture. Various

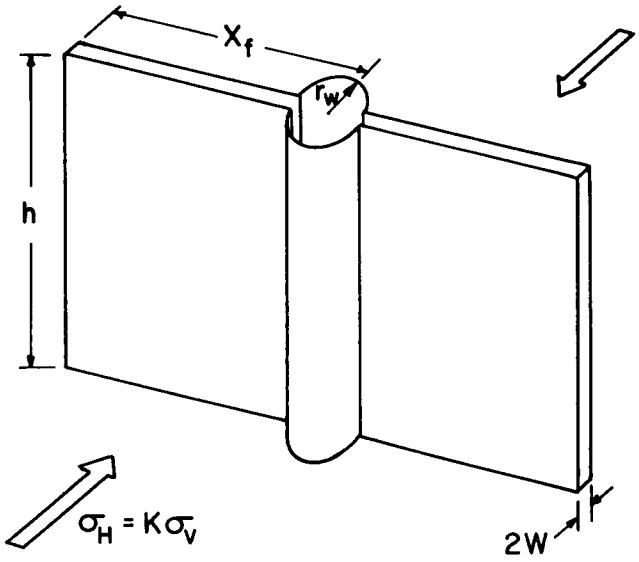

XBL 792-5743

Figure 1. Description of the problem.

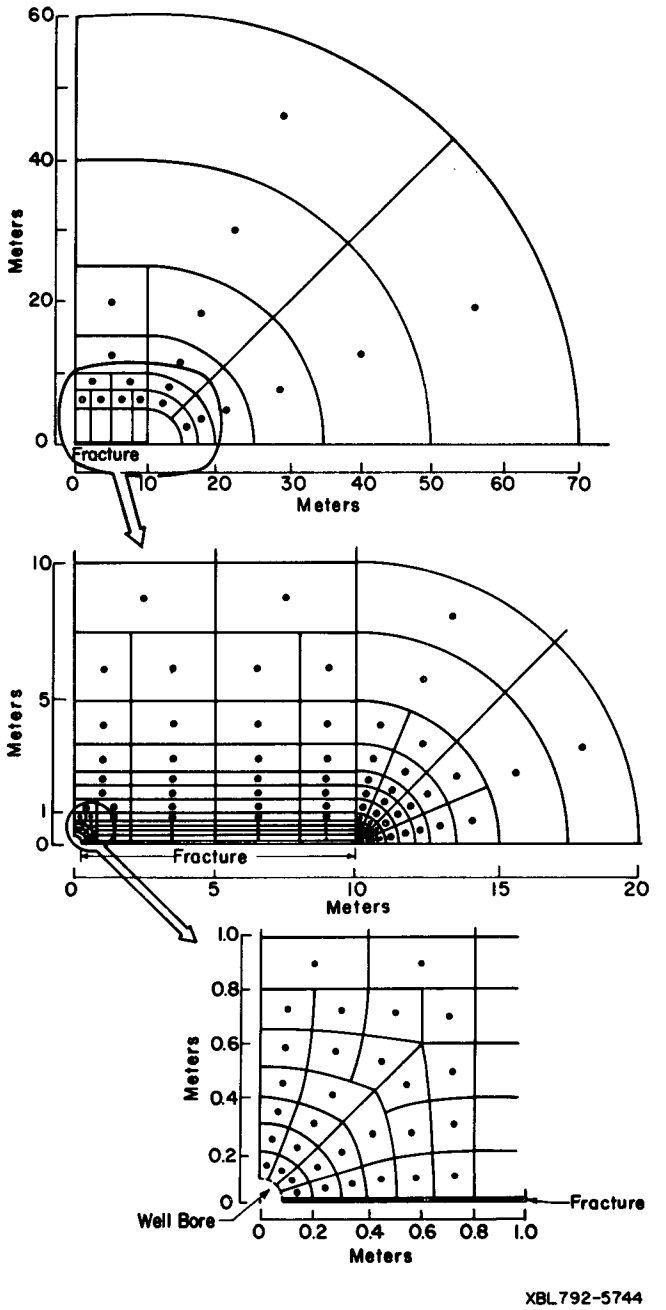

Figure 2. Mesh used in the simulation.

simulation runs were carried out in order to study the effect of fracture conductivity variation, and the effect of wellbore storage on pressure response in the well. The results are discussed below.

Effect of Fracture Conductivity Variation

These simulations were carried out with a well of small diameter (r_w = 0.005 m) and assuming that the fluid level changes in the wellbore. In other words, wellbore storage is caused by liquid level changes. The number of fracture elements used in the simulation varied from two elements at high conductivity (C_r = 100) to eight elements at low conductivity (C_r = 0.2).

The results of the simulations are shown in Figure 3 and are compared with the quasianalytic solution of Cinco-Ley et al. (1978). Note the very good agreement between the solutions up to t_D = 30. The observed departures beyond t_D = 30 are due to the impermeable boundary effects introduced by the finite mesh. Also, the small departures observed for $t_D = 10^{-2}$ in the case

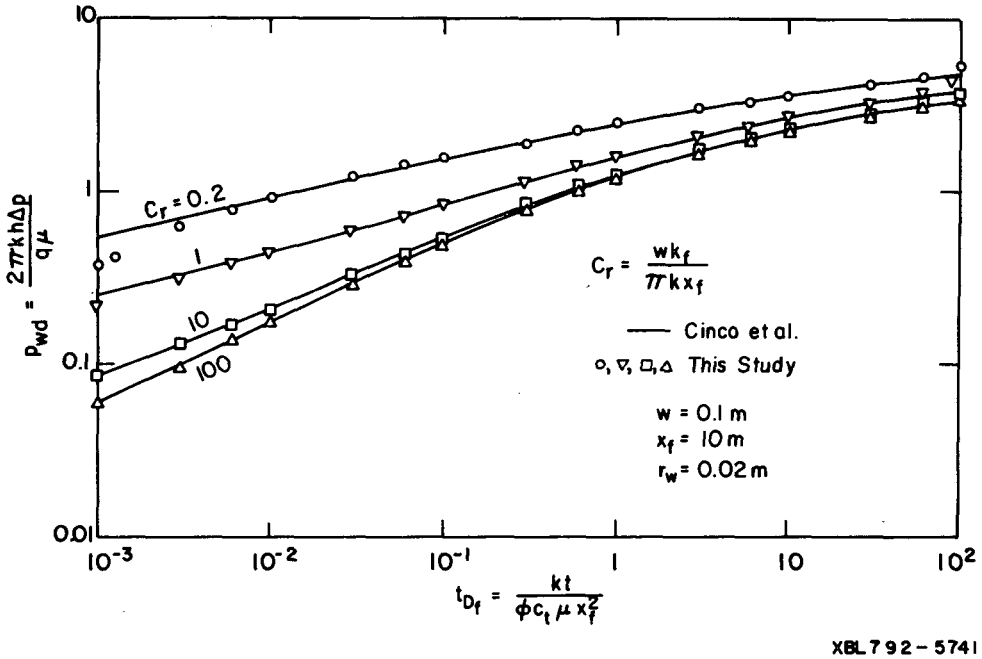

Figure 3. Plot of t_D versus P_D for various values of C_r.

of C_r = 0.2 and 1 are due to the effects of the small wellbore storage of the 0.005-m well ($\bar{C}$ = 1.25m x 10^{-3}).

Effect of Wellbore Storage

The ability of TERZAGI to handle wellbore storage effects was studied for the near-infinite conductivity case (C_r = 100) with $\bar{C}$ varying from 1.25 x 10^{-3} to 5 x 10^{-1}. These results are presented in Figure 4. Note that when $\bar{C}$ is large the early-time data show a pronounced

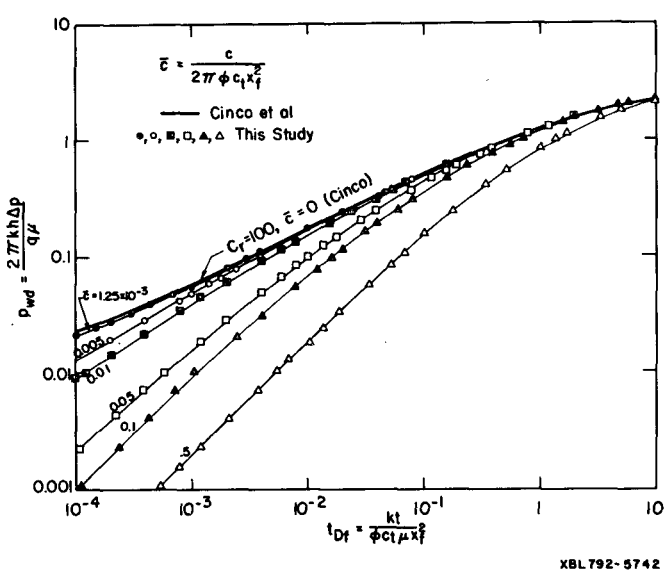

Figure 4. Effect of $\bar{C}$, the wellbore storage constant, on P_D.x for the case C_r = 100.

unit slope. With time, the wellbore storage effect is dissipated and the system behaves as though there is no wellbore storage. Note also that when $\bar{C}$ = 0.5, wellbore storage effects persist until $t_D \approx 10$. That is, all the early-time details characteristic of the fracture are masked until t_D = 10.

CONCLUSION AND FURTHER WORK

This study has shown that TERZAGI constitutes a flexible, powerful numerical tool for analyzing fluid flow in systems with finite conductivity fractures in conjunction with wellbore storage. Future work will include investigations of partially penetrating fractures, deformable fractures, fractures that grow with time, and heat-and-mass transfer in fractures.

REFERENCES CITED

Cinco-Ley, H., Samaniego, F., and Domínguez, A., 1978. Transient pressure behavior for a well with a finite-conductivity vertical fracture. Soc. Petrol. Engin. Jour., v. 18, no. 4.

Narasimhan, T.N., and Witherspoon, P.A., 1976. An integrated finite difference method for analyzing fluid flow in porous media. Water Resources Res., v. 12, no. 1, pp. 57-64.

Raghavan, R., 1977. Pressure behavior of wells intercepting fractures, in Proceedings, First Invitational Well-Testing Symposium, Berkeley, California, October 1977. Berkeley, Lawrence Berkeley Laboratory, LBL-7027, pp. 117-160.

EFFECT OF RADIALLY VARYING TRANSMISSIVITY ON THE TRANSIENT PRESSURE PHENOMENON

L. D. Mlodinow and C. F. Tsang

INTRODUCTION

During reinjection of cooled geothermal fluid into a reservoir, chemical precipitation and other processes may occur that change the permeability of the aquifer. In general, the permeability becomes a function both of time and space. This will, of course, affect the injection well. Some attempts have been made to predict the pressure response analytically. The present paper describes our calculations, which yield analytic expressions, in terms of a single integral for a wide class of physically reasonable permeability functions.

ACCOMPLISHMENTS DURING FISCAL YEAR 1978

Governing Equation and Its Solution

Consider an aquifer consisting of a horizontal slab of thickness, h, penetrated normally by a line source supplying a flow, Q. The acquifer medium is taken to be isotropic. In our simplified model we neglect gravity, consider the system to be isothermal, and consider only a single fluid phase. If we assume that $\beta_o \underset{\sim}{\nabla} p \cdot \underset{\sim}{\nabla} p \ll (1/K) \underset{\sim}{\nabla} \cdot K \underset{\sim}{\nabla} p$, then the governing equation is given by

$$\beta_o \mu\phi \frac{\partial p}{\partial t} = \underset{\sim}{\nabla} \cdot K \underset{\sim}{\nabla} p \qquad (1)$$

where $\beta_o \equiv$ compressibility, $\mu \equiv$ viscosity, $\phi \equiv$ porosity, $K \equiv$ permeabiity, and $p \equiv$ pressure.

Given a permeability function of space and time, equation (1) yields the pressure distribution that results. Equation (1) has been solved for a large class of physically reasonable permeability functions to be determined below.

Let r_o be the distance from the line source to the fluid front. Since the volume of fluid pumped into the aquifer equals the porosity times the volume of aquifer occupied, we see that the fluid front propagates to

$$r_o(t) = Ct^{1/2}$$

where C is a constant. Thus, if r is the distance from any point in the aquifer to the source, then points with $r^2/t < C^2$ will have permeability K_∞, and points with $r^2/t > C^2$ will have permeability K_o. Points with the same value for the ratio r^2/t will have the same permeability. We shall solve equation (1) first for permeabilities of the form

$$K(\underset{\sim}{r},t) = K_o \, \beta \, (r^2/t) \qquad (2)$$

where r is the cylindrical radial coordinate, and β is an arbitrary function.

For the radial symmetry problem we may apply the Boltzmann transformation to the governing equation, that is, the change of variables

$$\begin{matrix} r \\ t \end{matrix} \rightarrow \begin{matrix} z \equiv r^2/t \\ w \equiv t \end{matrix} .$$

The boundary conditions are:

$$p(r,o) = p_o$$
$$p(\infty,t) = p_o$$

$$\lim_{r \to o} 2\pi rhK(\underset{\sim}{r},t)(\partial p/\partial r) = -Q$$

$$\lim_{t \to \infty} 2\pi rhK(\underset{\sim}{r},t)\, \partial p/\partial r = -Q$$

where Q is the flow rate and h is the aquifer thickness. After some manipulation, the solution for p(r,t) can be shown to be

$$p(r,t) = p_o + \frac{\mu Q}{4\pi hK_o} e^{(1/4)I(0)} \int_{r_D}^{\infty} \frac{e^{-(1/4)I(z')}}{z'\beta(z')} dz'$$

where

$$I(z') \equiv \int^{z'} \frac{dz'}{\beta(z)} \quad \text{and} \quad r_D = \frac{\beta_o \mu\phi}{K_o} \frac{r^2}{t}$$

Finally, we obtain the solutions for a more general class of permeability functions from those solutions already obtained. The method depends on a property of the differential equation

$$\frac{\partial f}{\partial t} = K(r,t) \frac{\partial^2 f}{\partial_r 2} + \left[\frac{K}{r} + \frac{\partial K}{\partial r}\right] \frac{\partial f}{\partial r} \qquad (4)$$

and does not depend on the specific form of K other than its being a function of r and t only. For example, the same method could be used to generate new solutions if (4) is initially solved for other forms of K.

To get the new solutions, assume that (4) has been solved for f with a given K. Then consider the transformed function

$$f_\alpha(r,t) \equiv f\left[r, \int_o^t \alpha(t')\, dt'\right]$$

where α is an arbitrary positive function. Therefore f_α does not satisfy (4) since

$$\frac{\partial f}{\partial t} = \alpha(t) \frac{\partial f}{\partial t} .$$

Rather, f_α satisfies

$$\frac{\partial f_\alpha}{\partial t} = K_\alpha(r,t)\,\frac{\partial^2 f_\alpha}{\partial r^2} + \left[\frac{K_\alpha}{r} + \frac{\partial K_\alpha}{\partial r}\right]\frac{\partial f}{\partial r}$$

where

$$K_\alpha(r,t) \equiv \alpha(t)\,K\left[r, \int_0^t \alpha(t')dt'\right] .$$

Furthermore, the boundary conditions on f_α and f are the same. Hence, if p is the pressure response due to K, then to find the pressure at the point (r,t) when the permeability is K_α, we just evaluate p at the point (r,τ) where

$$\tau = \int_0^t \alpha(t')dt' \quad .$$

Numerical Results

We have calculated the pressure distributions resulting from the following permeability functions:

$$K_o = K_o$$

$$K_1 = K_o\left[1 - \frac{\rho}{z+\varepsilon}\right]$$

$$\rho = 10^{-7},\ \varepsilon = 4\rho/3$$

$$K_2 = K_o\left[1 - \frac{\rho}{z+\varepsilon} + \frac{1}{3}\,\frac{\rho^2}{(z+\varepsilon)^2}\right]$$

$$\rho = 10^{-6},\ \varepsilon = 2\rho/3$$

$$K_3 = K_o\ \exp\left[-\rho/(z+\varepsilon)\right] ,$$

$$\rho = 10^{-6},\ \varepsilon = 4\rho/3 .$$

The constant permeability, K_o, leads to the Theis solution. As an illustration, Figures 1 and 2 show the graphs of K_1 and K_2 and the corresponding calculated pressure distributions.

Summary

We have obtained an analytical solution for the pressure response in a reservoir with permeability of the form $K = K(r^2/t)$.

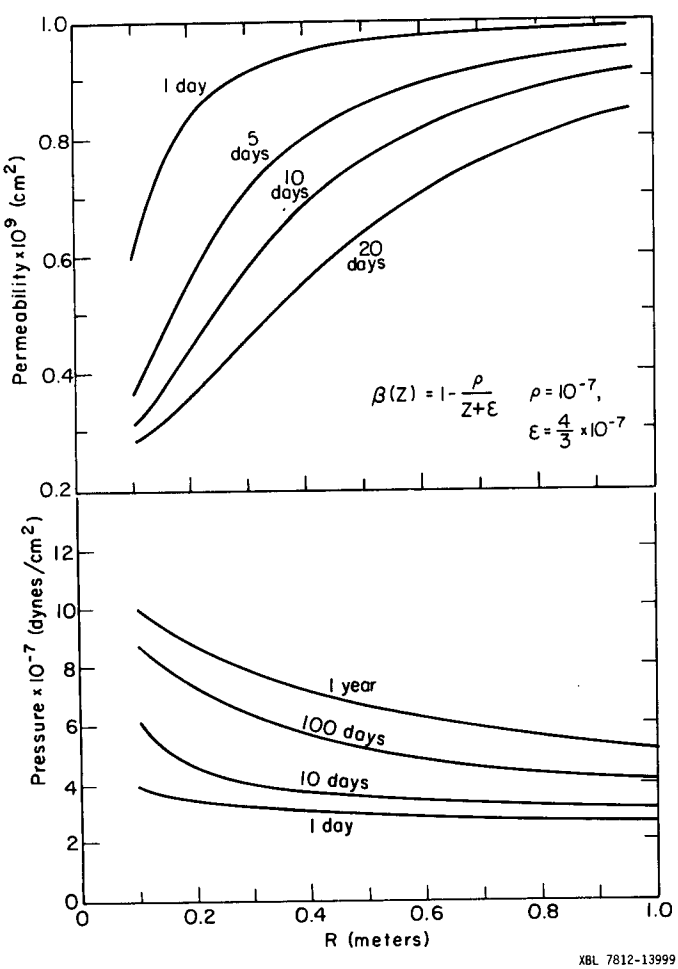

Figure 1. Graph of K_1 and corresponding calculated pressure distributions.

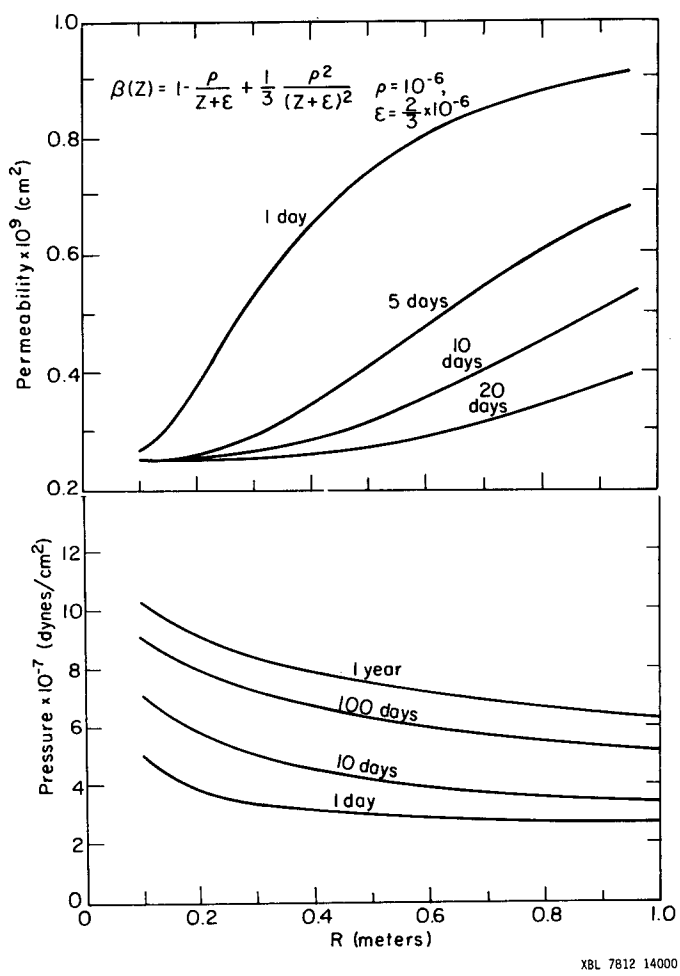

Figure 2. Graph of K_2 and corresponding calculated pressure distributions.

Several function forms for $K(r^2/t)$ have been studied and the resulting pressure distributions calculated.

A general method was developed for generating the pressure response, $\bar{p}$, for a permeability

$$\bar{K}(r,t) = \alpha(t)K\left[r, \int_0^t \alpha(t')dt\right]$$

once the solution $p(r,t)$ has been obtained (analytically or numerically) for a permeability function $K(r,t)$. The solution for $\bar{K}(r,t)$ is

$$\bar{p}(r,t) = p\left[r, \int_0^t \alpha(t')dt\right] .$$

The only restriction on α is that it be positive.

PLANS FOR FISCAL YEAR 1979

The project was completed during fiscal year 1978.

MATHEMATICAL SIMULATION OF THERMAL BREAKTHROUGH UNDER INJECTION: COMPARISON OF TWO TECHNIQUES

T. N. Narasimhan, S. Juprasert, and G. S. Bodvarsson

INTRODUCTION

The injection of waters having distinctly different temperatures from the reservoir into which they are emplaced is being actively investigated by many workers. Such a procedure can help in either sweeping heat out of the country rock in geothermal energy extraction or storing thermal energy in aquifers. The economics of the injection process are very much related to the dynamics of the interface between hot and cold fluids within the reservoir. For this reason, mathematical techniques have been developed in the literature to compute the position of the hot-cold interface in space and time. Over all, the location and nature of the interface are functions of such diverse parameters as reservoir geometry, well spacings, flow rate, porosity, and permeability of the host rock, and the thermal properties of both host rock and water. Because the problem is very complex, simplifying assumptions are usually made in developing mathematical tools, depending on the quality of input data available and the accuracy of the required solutions.

In this report, we consider two mathematical models. One is based on relatively more restrictive assumptions than the other and is capable of solving a certain class of large problems (e.g., many production and injections wells) with little effort. The other more general model can handle a wide class of physically complex problems but is rather inconvenient for solving certain large problems. Both models are very valuable in reservoir simulation. In this report we will solve the same problem with both tools in order to validate them and compare the solutions.

THE MODELS

The models chosen are: METERNIQ, a program developed by Gringarten and Sauty (1975); and TRUMP, a program developed by Edwards (1969). Both models consider the general problem of convective and conductive heat transport in a system with a steady groundwater flow field. METERNIQ deals specifically with well fields involving any number of production and injection wells piercing an areally infinite, homogeneous aquifer, with known regional groundwater flow pattern and with conductive heat transfer across the upper and lower boundaries of the aquifer. TRUMP, on the other hand, can handle more general, heterogeneous, three-dimensional systems with arbitrary initial and boundary conditions. Concerning the physics of the transport phenomenon, a primary difference between the two models is the manner in which heat transfer due to conduction is handled within the reservoir. Thus, in METERNIQ, heat transport due to conduction is neglected within the reservoir. In other words, the thermal front advances as a "piston" and heat transport is solely due to convection. In contrast, TRUMP gives due consideration to conductive heat transport within the reservoir.

THE PROBLEM

To compare the solutions obtained with the two models, consider the problem of an infinite five-spot array of production and injection wells (inset, Figure 1). Hot water is produced from the reservoir at a temperature of 182°C at the rate of 1,000 gpm per well, while cold water is injected into the reservoir at a temperature of 75°C at a rate of 1,000 gpm per well. The reservoir rock has a porosity of 10%, thickness of 500 ft, density of 2.65 gm/cm^3, specific heat of 0.2 cal/gm°C, and thermal conductivity of 4.5 cal/cm-sec°C. The hot water is assumed to have a density of 0.92 gm/cm^3, specific heat of 0.83 cal/gm°C and negligible thermal conductivity. The distance between a production well and the nearest injection well is 2120 ft. The problem is to predict the temperature of the produced water in the production well as a function of time.

The problem was solved with METERNIQ with a finite array of 30 production and injection wells. For practical purposes the peripheral effects of the finite array can be neglected in the center

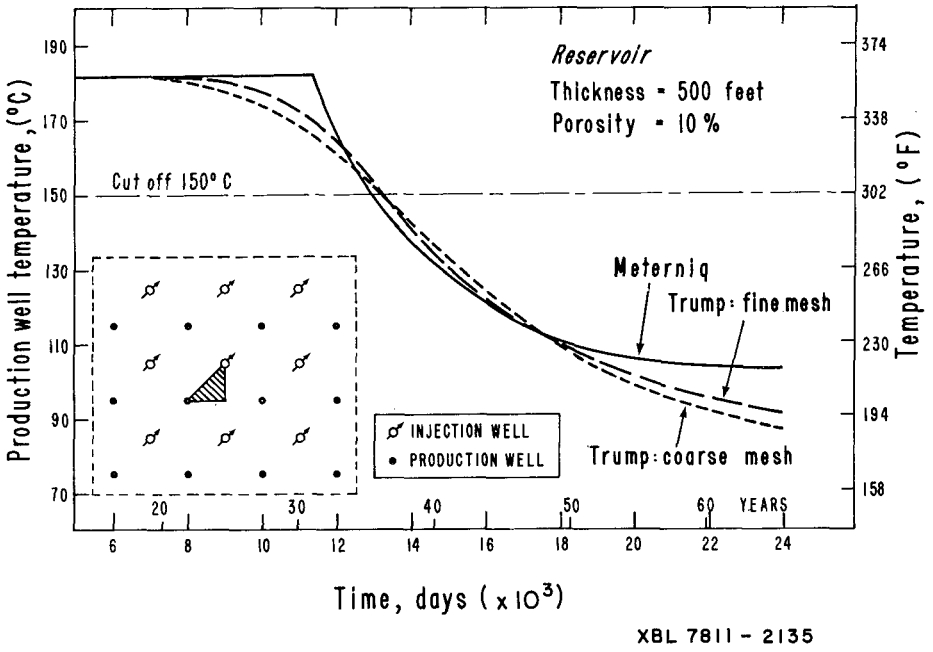

Figure 1. Five-spot production-injection pattern, temperature profile at production well. Inset: five-spot scheme; hatching shows the flow region numerically modeled.

of the finite array. The basis of the METERNIQ algorithm is first to set up a finite number of stream lines (40 were chosen) emanating from each well. Heat is then transported by convective "piston" displacement in each stream line, and finally waters from the different stream tubes are mixed in the production well to determine the weighted average temperature of the discharged water.

Because of symmetry considerations, only the triangular region shown by hatching in Figure 1 need be modeled with the TRUMP scheme. Two meshes were used: a coarse mesh having 120 volume elements (Figure 2), and a fine mesh having 260 elements. In both cases, a 1-ft-diam. well was assumed. Before implementing the heat transport simulation, the fluid flow problem was first solved to obtain the mass flux rates between neighboring volume elements in Figure 2. These mass flux rates were then used as input parameters for the heat transport problem.

THE RESULTS

The results obtained with METERNIQ and TRUMP are graphically summarized in Figure 1. Three important facts are shown in this figure. First, both the coarse-mesh and the fine-mesh solutions of TRUMP agree very closely, suggesting that the TRUMP solution is not subject to undue mesh errors. Second, due to the absence of heat conduction within the aquifer and the lack of mixing, the METERNIQ solution indicates a later arrival of the thermal front at the production well, and a sudden decrease in production well temperature subsequent to the breakthrough. On the other hand, the presence of conduction in the TRUMP solution causes a somewhat earlier arrival of the thermal front at the production well and a more gradual decline in production well temperature. Third, if we consider a "cutoff" temperature of 150°C, all three solutions give about the same result.

CONCLUSION

The results presented above clearly show that, subject to minor differences attributable to model assumptions, both METERNIQ and TRUMP yield substantially the same results and validate each other. Both models will continue to be used in 1979 for appropriate problems dealing with production-injection scenarios in geothermal and thermal storage simulations.

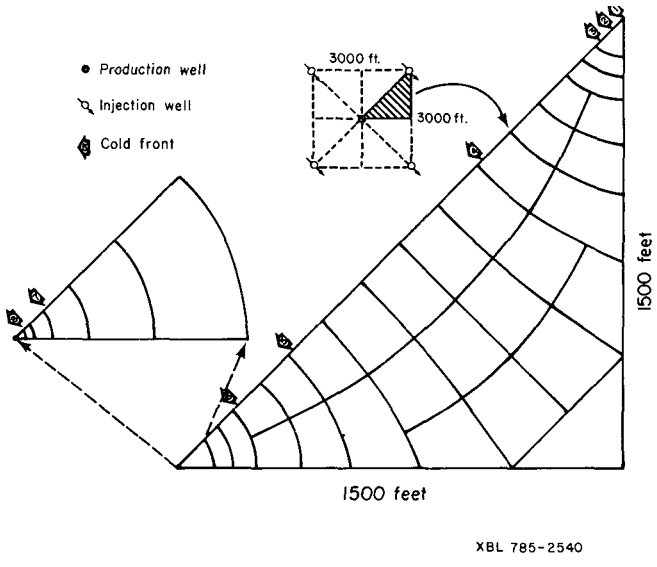

Figure 2. Mesh used in numerical modeling.

REFERENCES CITED

Edwards, A. L., 1969. TRUMP: A computer program for transient and steady-state temperature distributions in multidimensional systems. Livermore, Lawrence Livermore Laboratory, UCRL-14574, Rev. I.

Gringarten, A. C., and Sauty, J. P., 1975. A theoretical study of heat extraction from aquifers with uniform regional flow. Jour. Geophys. Res., v. 80, no. 35, pp. 4956-4962.

WELL TEST DATA ANALYSIS METHODS AT LBL

S. M. Benson, C. B. Goranson, and R. C. Schroeder

INTRODUCTION

In fiscal year 1978, LBL participated in and conducted well tests in several locations (see Goranson and Schroeder, 1978). The pressure response data from these sites were analyzed for reservoir transmissivity (kh/μ), storativity (φch), leakage, wellbore damage, and geometry. Pressure, temperature, and chemistry data were obtained in flowing and observation wells. To expedite the manipulation, processing, and storage of the large amounts of well test data, all the data are entered into a large computer. A series of computer programs has been written to read, process, and store this data.

Production tests are designed to obtain as much information as possible about the condition of the well and the reservoir in the vicinity of the producing well. Interference tests are conducted to obtain information about average reservoir characteristics such as transmissivity, storativity, recharge, barriers, and inhomogeneities. Although the fundamental theory used for analyzing both types of tests is usually the same, the methods used are different because a different type of information is obtained from each test.

Production tests are analyzed using standard transient-pressure, isothermal oil-field, and groundwater-hydrology methods. They are well-documented techniques and will not be discussed here (see Ferris et al., 1962; Erlougher, 1978). The well tests are designed to minimize the error introduced into the calculation using these techniques. In high-temperature geothermal wells, this is accomplished by changing the flow rate in a series of small step-rate changes. A flow rate change is not initiated until the pressure response caused by the previous rate change has reached its approximate steady-state value and the transient thermal changes have become insignificant.

Interference tests conducted with multiple flowing wells require computer-assisted analysis. LBL has developed several computer programs for interference-test-pressure data analysis. These programs fall into two basic categories. The first includes programs that use the analytic solution to a fully penetrating line source in an isothermal, isotropic, homogeneous, areally infinite porous media of constant thickness (Theis, 1935). LBL has developed a least-squares computer matching program, ANALYZE, which analyzes pressure data at an observation well that is effected by the production of multiple wells, each with a variable flow rate. Using the method of images, the program can locate the distance to an image well, indicating either a constant potential or barrier boundary (Tsang et al., 1977).

The second category includes programs that employ the integrated finite-difference method of numerical modeling to simulate the pressure response at an observation well (Narasimhan et al., 1976; Lippmann et al., 1977; Pruess et al., 1979). The advantage of this technique is that it allows for the incorporation of partially penetrating observation and production wells. In addition, the effect of reservoir inhomogeneities such as multilayer systems, shale lenses, and partial barriers, as well as nonisothermal reservoir effects, may be included in the analysis. The program SHAFT78 is a two-phase three-dimensional nonisotropic computer code that is currently being applied to several difficult well-test problems.

DATA COLLECTION, PROCESSING, AND STORAGE

Some well tests are conducted for a duration of several weeks with simultaneous observation of both production (injection) and observation wells. During long-term tests of this type, wellhead pressures in observation wells are automatically recorded at 5-min. intervals on magnetic cassette tapes by a data logger. Downhole pressure data in the producing wells are recorded at 1-sec intervals when the flow rate is changed, and at longer intervals when the pressure is changing slowly. To expedite the manipulation and storage of this large quantity of data, a series of computer programs has been developed to read, sort, process, display, and store the data. Figure 1 is a schematic of the well-test data collection, processing, storage, and retrieval system at LBL.

In general, after pressure data are entered into the main computer system, only minimal preprocessing is required for analysis. Occasionally, a spurious pressure point caused by a faulty electrical signal is present. These points are removed from the data by a computer program,

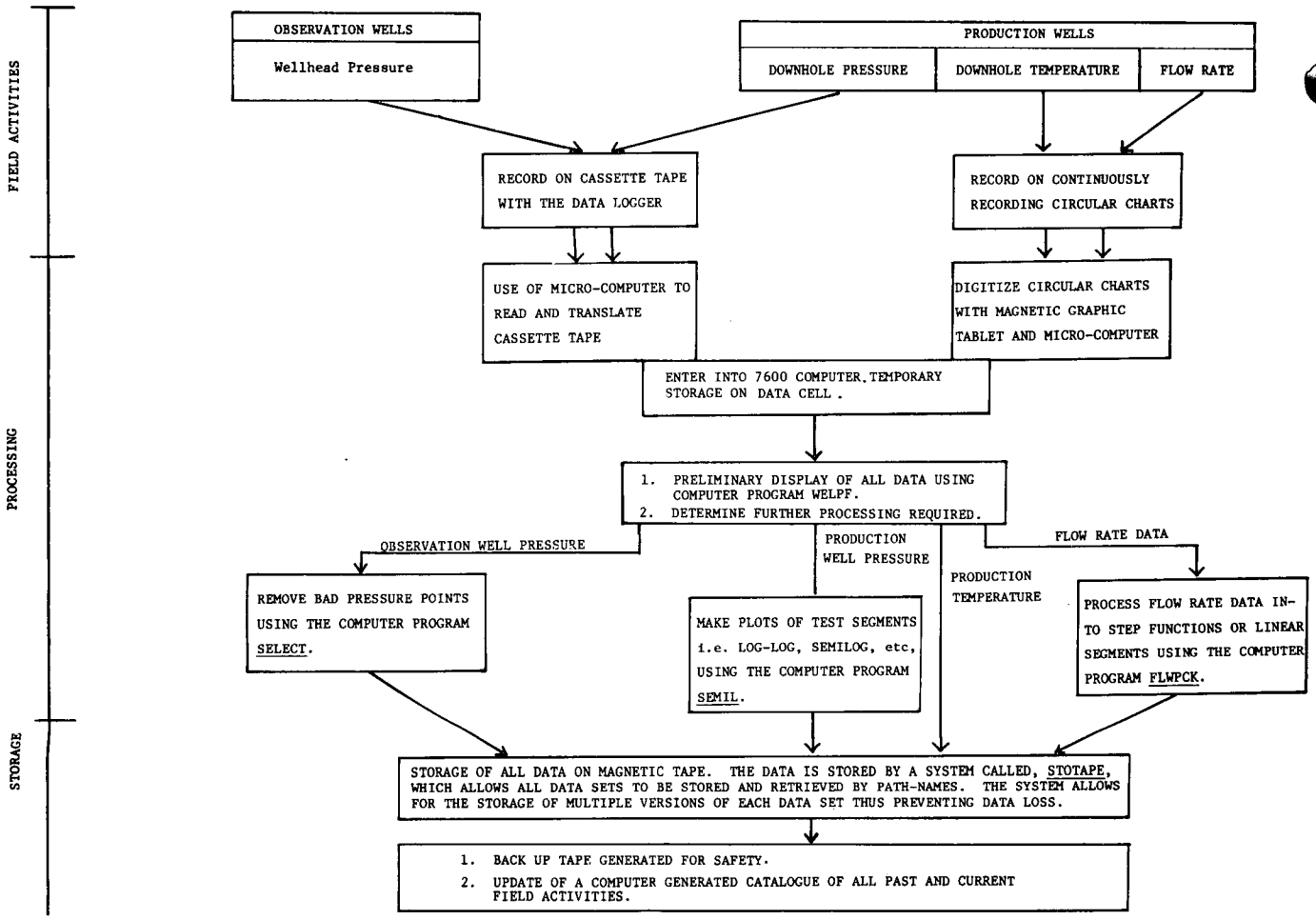

Figure 1. Schematic of well-test data collection and processing.

SELECT, or by hand if they are very few. When the pressure response at an observation well is small, the effects of earth tides on the reservoir pressure are apparent. These are usually diurnal fluctuations with a maximum amplitude of about 0.2 psi. For the purpose of well-test data analysis, these are smoothed to remove the tidal (noise) effects.

Flow rate data from individual production wells are usually recorded continuously on a circular chart recorder. These data are then digitized using a magnetic graphic tablet digitizer with an accompanying microcomputer program. The microcomputer temporarily stores the digitized flow-rate data before it is transferred to the main computer.

The majority of well-test data processing for eventual analysis depends on the graphic display of both pressure and flow-rate data. The computer program WELPF is used for a simultaneous display of both types of data. The program is a device-independent plotting package that allows for data display on a pen-and-paper plotting device, microfiche, 35-mm film, or an interactive graphics terminal. To run the program the user needs only to specify the path name to the specific set of data to be plotted. The remaining information needed by the program is stored with the individual data sets on magnetic tape. If the default values specified on the magnetic tape are not those desired, the user has the option of resetting the scale, type of display, or format of both the printed input and output, and displaying any desired segment of the data.

PRODUCTION TESTS

For hot geothermal wells, production-test design usually consists of a series of small step-rate changes of the flow rate (50 to 100 gpm). A flow-rate change is not initiated until the pressure response, caused by the previous flow-rate change, is small or negligible during the time to be considered for analysis (see Figure 2). In this manner we are able to minimize the error introduced into the analysis using conventional production test analysis techniques. In isothermal or near-isothermal aquifers and wells, there is less restriction in the choice of rates and rate changes, since the transient thermal effects are negligible. The computer program

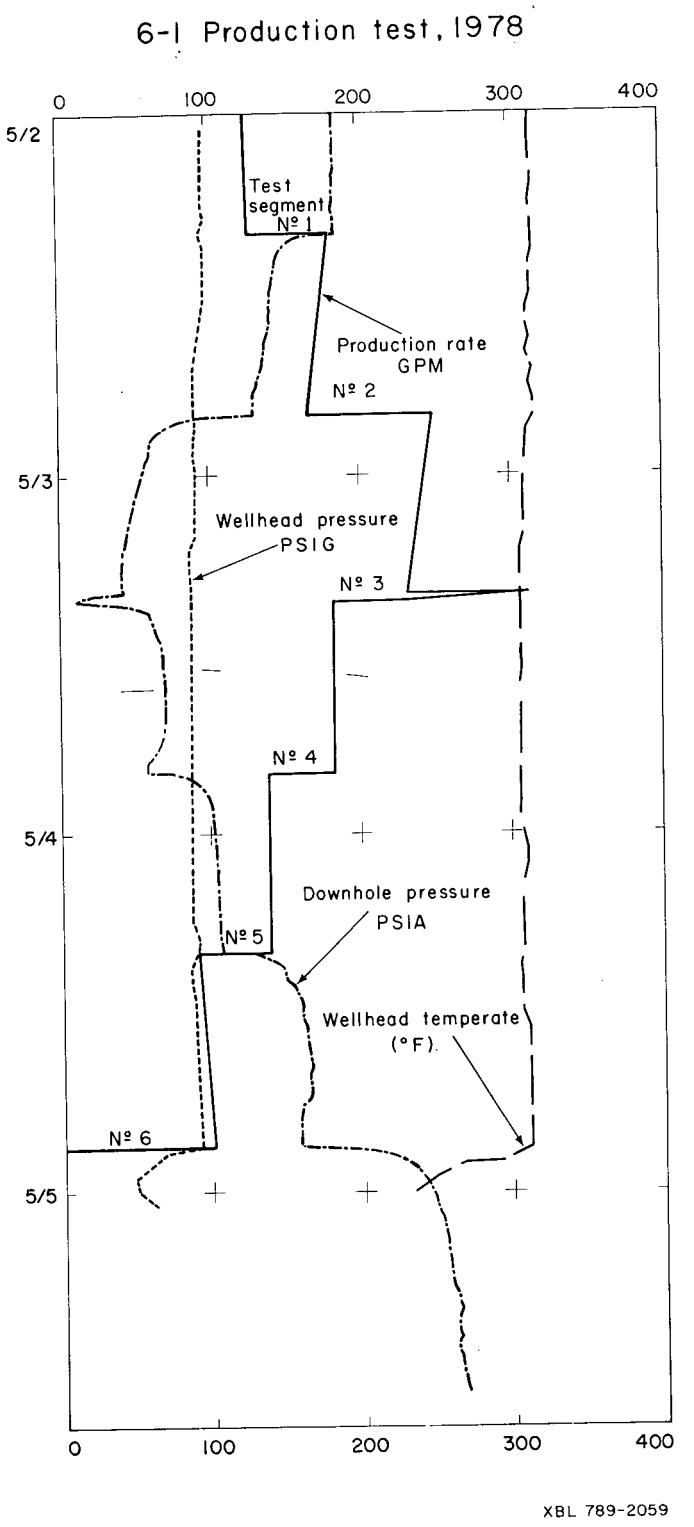

Figure 2. A typical production test with observed downhole pressures, flow rates, and wellhead temperature and pressures.

SEMIL is used to prepare production-test data for conventional analysis techniques. It makes semilog, log-log, pressure vs. log $[(t + \Delta t)/\Delta t]$ plots, and for two-rate tests, plots [P vs. log $(t + \Delta t/\Delta t) + Q_1/Q_2 \log \Delta t$] of selected segments of the pressure data on a pen-and-paper plotter (see Figure 3).

The degree of confidence one has in any analysis depends strongly on the quality of data available. The high temperatures and salinity of some geothermal brines made collecting accurate downhole pressure and flow-rate data difficult. A system for obtaining downhole pressure data in flowing wells, which uses a fluid- or gas-filled capillary tube and chamber to transmit the downhole pressure behavior to a wellhead pressure transducer, has the advantage of allowing downhole pressure measurements over an indefinite period with a high degree of resolution. Unfortunately, there is a significant time lag associated with the tubing when sensing a large and rapid pressure change, which obscures the actual early-time downhole pressure response. Thus, information that can only be obtained from analysis of early-time data (0 to 20 minutes) is lost. To remedy this situation, a program is being developed by C. W. Miller (Miller et al., 1978) that--given the tubing length and diameter; fluid properties, and flowing temperatures--will back out the real downhole pressure response.

INTERFERENCE TESTS

Interference tests are typically conducted with multiple production wells, and often have a variable flow-rate history. Observation wells, subject to interference effects from tests such as these, require computer-assisted analysis. The ideal interference test would be one in which all of the observation wells had a well-defined static initial pressure before production, and a pressure response that was clearly caused only by the flowing wells in the test. In addition, all the wells would be completed and perforated in the same interval in the reservoir. Needless to say, these conditions are rarely satisfied. For this reason, LBL has developed several computer programs for analyzing well-test data.

Figure 4 is a schematic of the interference-test data analysis procedure. Well-test data analysis is rarely as simple as finding a set of reservoir parameters that will model the observed pressure response. Before analysis can begin, one must first decide what type of analysis is applicable. Even if the assumptions about the reservoir and the well used in the computer program ANALYZE are not applicable, the program is still applied to obtain preliminary analysis of the data. If the match or the analysis is unsatisfactory, numerical methods may be applied in order to incorporate some of the complicating factors (such as leakage and partial penetration) into the analysis.

There are times when a satisfactory analysis of the data, for any number of reasons, cannot be obtained. In these cases, using either numerical or analytical methods, we can only hope to get rough estimates of the reservoir transmissivity and characteristics. Ideally, this information

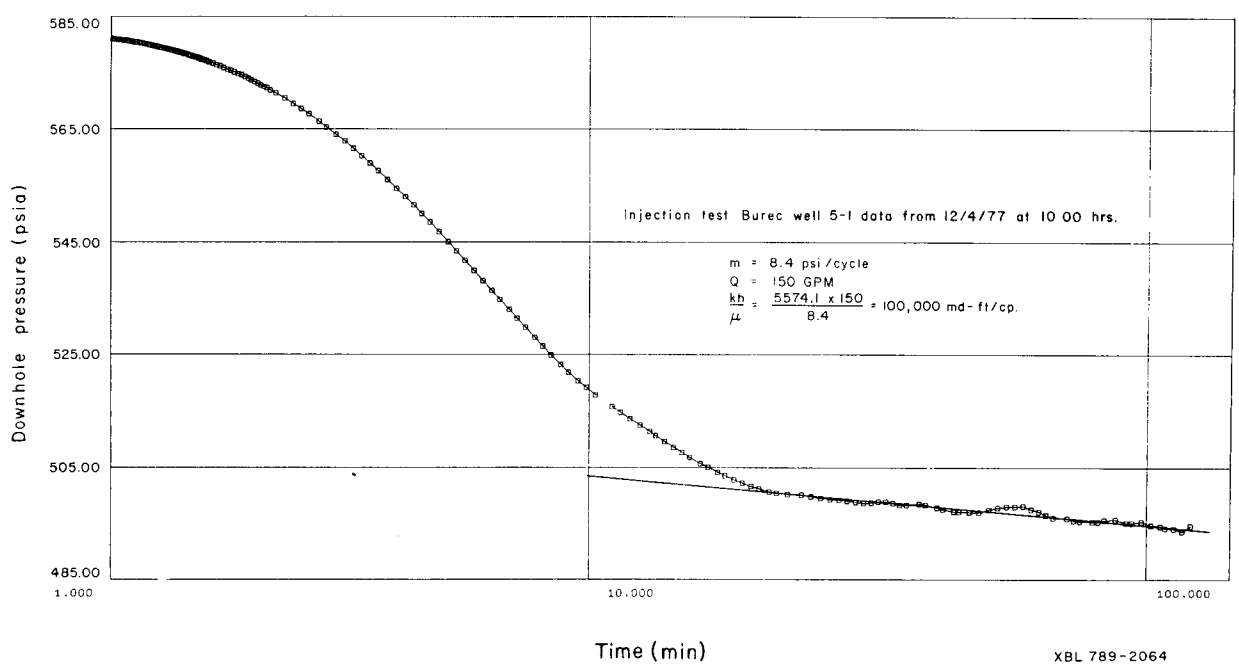

Figure 3. Example of a semilog plot generated by the computer program SEMIL.

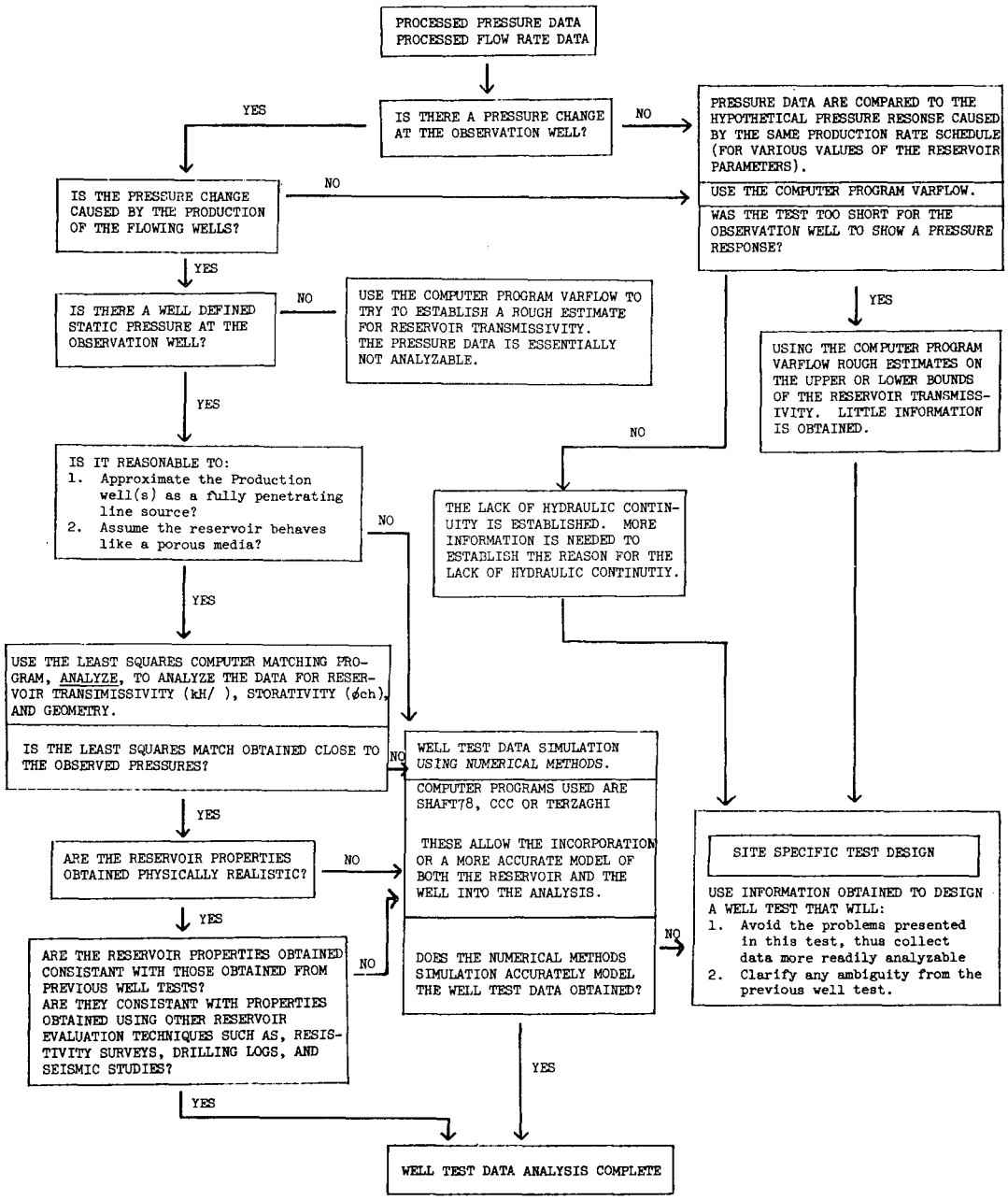

Figure 4. Schematic of interference-test data analysis.

should be used to design a site-specific well test to clarify the data already obtained, and to get new data that will be more readily analyzable.

COMPUTER PROGRAMS FOR WELL-TEST DATA ANALYSIS

LBL computer programs used for well-test data analysis can be divided into three groups. The first are those that use the analytic solution for a fully penetrating line source or sink in an isothermal, isotropic, homogeneous, areally infinite porous media of constant thickness. Using superposition, a variable-rate formulation, and the method of images, pressure calculations can be made for multiple production wells, rigorously variable flow rates, and a pressure response affected by the presence of a vertical reservoir boundary. These programs are presented in Table 1. Future development of these programs include incorporating the analytic solutions for partially penetrating production wells, aquifers with leaky caprocks, and multilayered systems (Jacob, 1946; Hantush, 1959; Neuman and Witherspoon, 1969; Javendel and Witherspoon, 1967; Neuman, 1974). See Figure 5.

The second group are those programs that use numerical methods for reservoir simulation. They are all formulated using the integrated

Table 1. Analytic computer programs used for well-test data analysis at LBL.

Computer program	Type of calculation	Special features* MOW	MPW	VFR	Other
VARFLOW	Pressure		x	x	Input can be in any set of inconsistent units. The program converts all of the data into standard units for all calculations. The output can be in any specified units. The program can rigorously handle variable flow rates. They do not need to be step functions. The input is compatible with the least-squares computer matching program.
WELF	Pressure	x	x	x	Can handle up to 200 production wells, each with a variable flow rate.
MAXDRAW	Pressure				Excellent two- and three-dimensional graphic output (see Figure 5).
ANALYZE	(kH/μ), φch, distance to an image well	x	x	x	Least-squares matching subroutine is used to match observed pressure data. The program can rigorously handle variable flow rates. They do not need to be step functions. See the section on computer programs for a more complete discussion of this program.

*MOW = Multiple Observation Wells, MPW = Multiple Production Wells, VFR = Variable Flow Rates.

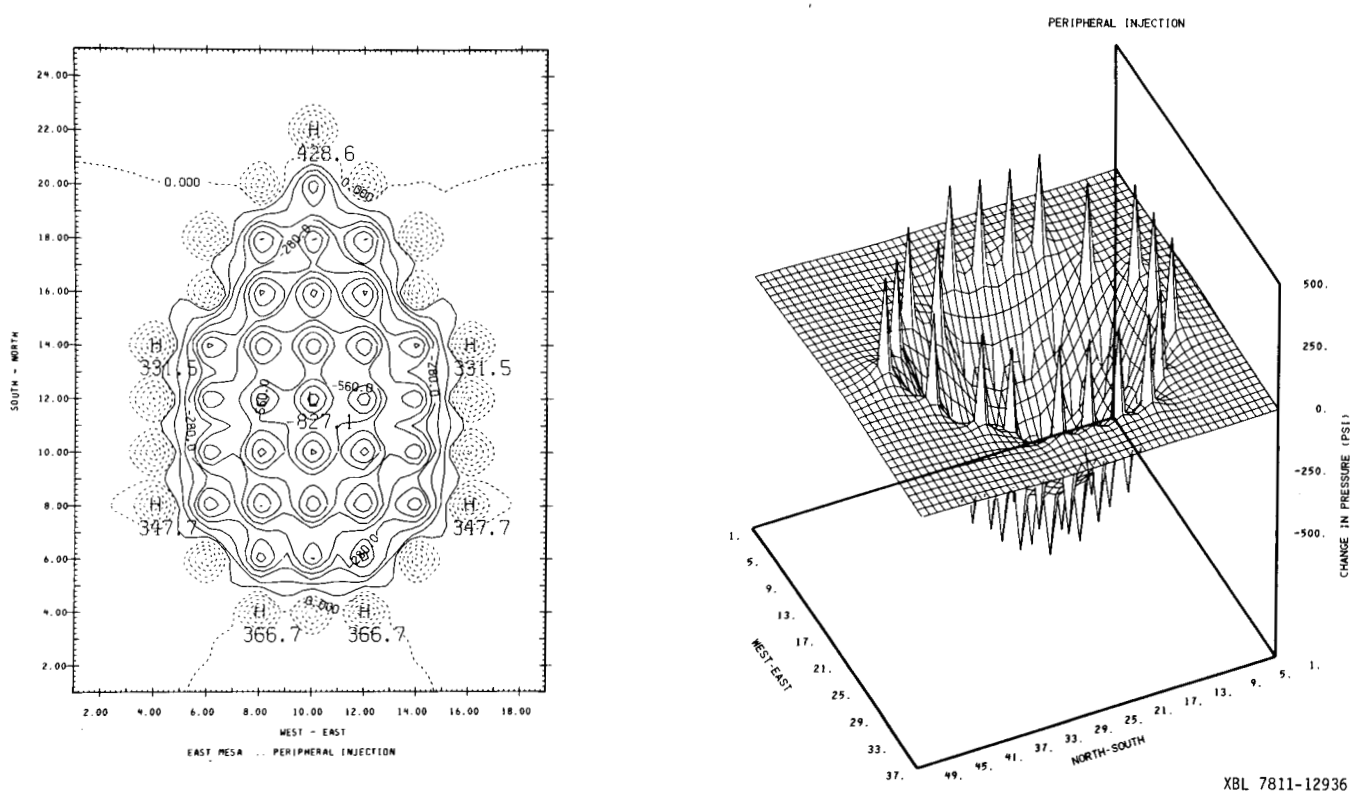

Figure 5. A contour plot and three-dimensional plot of a 30-well peripheral injection configuration generated by MAXDRAW.

Table 2. Numerical methods computer programs used for well-test data analysis.

Computer program	Type of calculation	Characteristics
TERZAGI	Pressure Subsidence	Isothermal Three dimensional Integrated finite difference formulation Single phase
CCC	Pressure Temperature Compaction	Nonisothermal Three dimensional Single phase Can be used for calculation of thermal breakthrough times Integrated finite difference formulation
SHAFT78	Pressure Vapor saturation Phase Temperature	Nonisothermal Nonisotropic media (i.e., directional permeability) Multiphase, steam-water Three dimensional

finite difference technique. Future development of these, for the purpose of well-test data analysis, include increased flexibility and specificity of the input and output. These programs are presented in Table 2.

The third group of programs, although not directly used for well-test data analysis, are programs that support and facilitate well-test data analysis at LBL. These are presented in Table 3.

Table 3. Supplementary programs used for well-test data analysis.

Program name	Purpose	Special features
WELPF	Computer-generated plots	Plots both pressure data and flow-rate data on the same plot Plots data with alphanumeric labels on the time axis, i.e. dates Handles variable input formats automatically Self-scaling program for aesthetic and practical purposes Device-independent output (microfiche, 35-mm film, paper, interactive graphic terminal)
SEMIL	Computer-generated analysis plots	Self-scaling log-log, semi-log, P vs. log $[(t + \Delta t)/\Delta t]$ and variable-rate plots. Device-independent output (microfiche, 35-mm film, paper, interactive graphics terminal)
SELECT	Remove extraneous pressure points	
FLWPCK	Process flow-rate data for analysis	Prepare flow-rate data for use in the program analysis Processes flow-rate data into step functions and linear segments
OGRE	Mesh-generating computer program	Facilitates the construction of geologically realistic meshes Given the x, y, and z coordinates of discrete element locations, the program constructs a grid for integrated finite-difference type computer programs.

CONCLUSION

Reservoir evaluation from well-test data analysis requires careful consideration of the assumptions inherent in the different well-test data analysis techniques. Using numerical methods we are able to include data obtained from other aquifer evaluation techniques such as well logging, temperature surveys, and resistivity surveys, in the analysis of well-test data. Although numerical modeling allows the incorporation of additional detailed information into the analysis of the transient well-test data, uniqueness of the solution is not guaranteed. However, analytical solution matching is also subject to nonuniqueness, particularly when complications are included, since each complication introduces an additional parameter that adds a dimension in the least-squares fitting space.

REFERENCES CITED

Erlougher, R., Jr., 1977. Advances in well test analysis. Dallas, Soc. Petrol. Engin. AIME. Monograph Series, v. 5.

Ferris, J. G., Knowles, D. B., Brown, R. H., and Stallman, R. W., 1962. Theory of aquifer tests. USGS water-supply paper 1536-E.

Goranson, C. B., and Schroeder, R., 1979. Site-specific geothermal reservoir engineering activities. This report.

Hantush, M. S., 1959. Nonsteady flow to flowing wells in leaky aquifers. Jour. Geophys. Res. v. 64, no 8.

Jacob, C. E., 1946. Radial flow in a leaky aquifer artesian aquifer. Trans. Amer. Geophys. Union., v. 27, no. II.

Javendel, I., and Witherspoon, P. A., 1967. Use of thermal model to investigate the theory of transient flow to a partially penetrating well. Water Resources Res., v. 3, no. 2,

Lippmann, M. J., Tsang, C. F., and Witherspoon, P. A., 1977. Analysis of the response of geothermal reservoirs under injection and production procedures. Dallas, Soc. Petrol. Engin. AIME, SPE-6537.

Miller, C., and Haney, J., 1978. Pressure transient response of a fluid in a capillary tube, in Proc. Second Invitational Well Testing Symposium, Berkeley, California, October 1978. Berkeley, Lawrence Berkeley Laboratory, LBL-8883.

Narasimhan, T. N., and Witherspoon, P. A., 1976. An integrated finite difference method for analyzing fluid flow in porous media. Water Resources Res., v. 12, no. 1.

Neuman, S. P., 1974. Effect of partial penetration on flow in unconfined aquifers considering delayed gravity response. Water Resources Res., v. 10, no. 2.

Neuman, S. P., and Witherspoon, P. A., 1969. Theory of flow in a confined two aquifer system. Water Resources Res., v. 5, no. 4.

Pruess, K., Schroeder, R., Witherspoon, P. A., and Zerzan, J., 1979. SHAFT78, a two-phase multidimensional computer program for geothermal reservoir simulation. Berkeley, Lawrence Berkeley Laboratory, LBL-8264A.

Theis, C. V., 1935. The relation between lowering of the piezometric surface and the rate and duration of discharge of a well using groundwater storage. Am. Geophys. Union, Trans., pt. 2.

Tsang, C. F., McEdwards, D. G., Narasimhan, T. N., and Witherspoon, P. A., 1977. Variable flow well test analysis. Dallas, Soc. Petrol. Engin. AIME, SPE-6547.

SUMMARY OF WELL TESTS AND ANALYSES FOR THE EAST MESA GEOTHERMAL SITE*

S. M. Benson, C. B. Goranson, J. Haney, D. G. McEdwards, T. N. Narasimhan, and R. C. Schroeder

INTRODUCTION

Since 1976, LBL has conducted numerous well tests at the East Mesa KGRA, Imperial Valley, California (Figure 1). These include production, injection, and interference tests using all the available wells in the northern, central and southern portions of the reservoir. From analyses of interference test data, it has been possible to locate hydraulic barriers, infer reservoir recharge, prove continuity between the northern and southern ends of the field, and provide global estimates of reservoir parameters, transmissivity, and storativity (Figure 2). Analysis of production test data has also provided information about the condition of individual wells and local estimates of transmissivity.

*Adapted from Howard et al. (1979).

ACTIVITIES IN FISCAL YEAR 1978

Well Tests at East Mesa

Well testing activities before 1976 consisted of measuring stabilized wellhead and downhole pressures for various flow rates of wells 6-1, 6-2, 5-1, and 8-1 (Mathias, 1976) and of conducting transient pressure tests of relatively short duration (~10 hours) on wells 6-1, 5-1, 8-1, and 31-1. In addition, well 6-1 was flowed for several

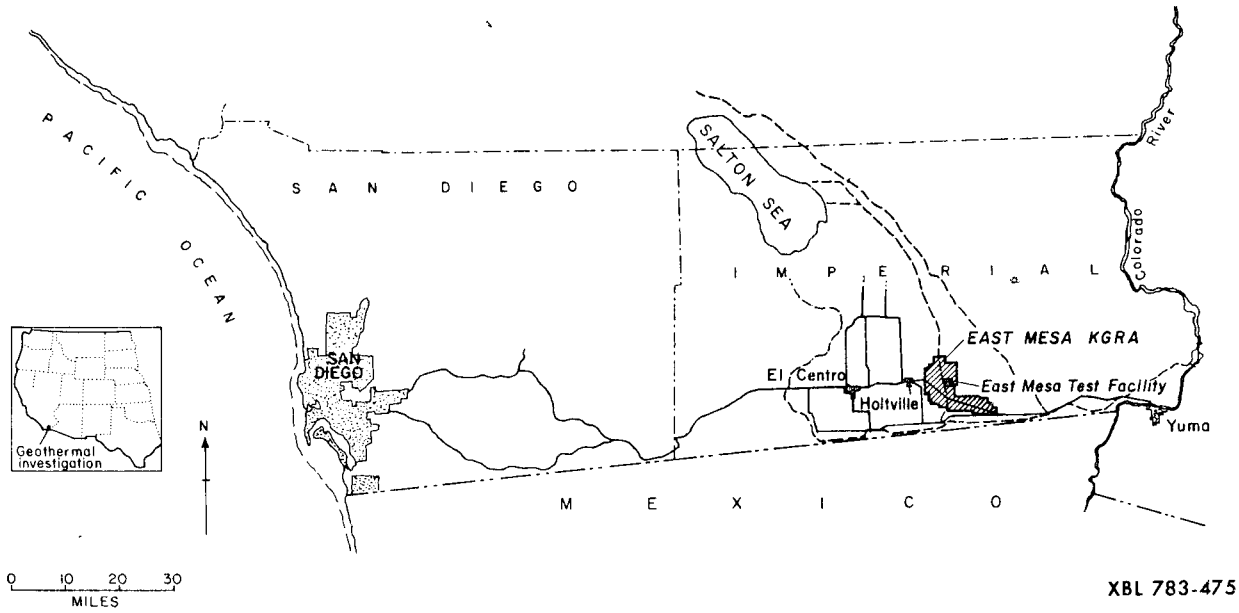

Figure 1. East Mesa geothermal resource, location map.

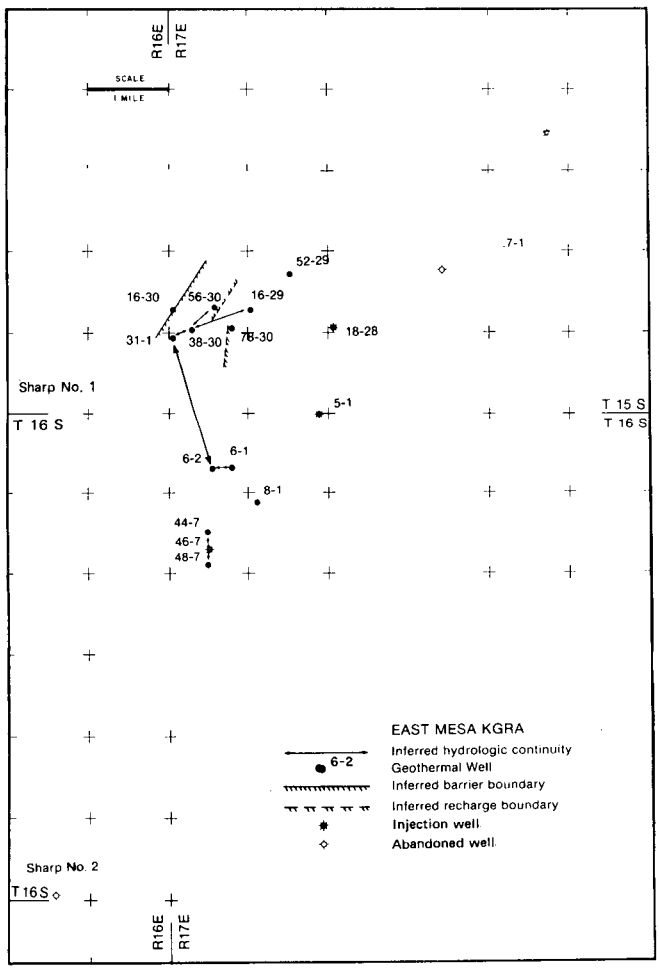

Figure 2. East Mesa KGRA well field.

months under compressed liquid conditions in a desalting test run during which the wellhead pressure was monitored. Injection and production tests, both using a downhole pressure gauge, were run on well 5-1, in which the injectivity and productivity indices were measured as functions of time (Mathias, 1976). Productivity indices for wells 6-1, 6-2, 5-1, and 8-1 having a single flow rate (unrestricted flow) were calculated from the available data and are presented in Table 1. The well 6-1 desalting test data and the 5-1 injectivity index data provide additional estimates of transmissivity for these two wells. These estimates are included in a summary of the pre-1976 transient pressure test results, shown in Table 2. The test results shown in Tables 1 and 2 are compared with the latest production test results given below.

From February 13, 1976, to September 29, 1977, several interference and production tests were conducted by LBL in the U.S. Department of the Interior, Bureau of Reclamation (USBR), Republic Geothermal Co., and Magma Power Co. portions of the East Mesa field (Narasimhan et al., 1977a, b, 1978; Witherspoon et al., 1978). Several contractual well tests for USBR were begun on December 1, 1977, and completed on May 4, 1978. Table 3 presents the chronology of these well tests.

Contractual Well Tests for USBR

According to recent contractual obligations with USBR, LBL agreed to perform well tests in order to: (a) determine productivity indices for wells 6-1, 6-2, 8-1, and 31-1 at various flow rates; (b) perform a long-term interference test by flowing 8-1 and recording pressure changes at appropriate observation wells; and (c) determine

Table 1. Productivity indices for full flow (after Mathias, 1974).

Well	$P_{shut-in}$ (bars)	$P_{flowing}$ (bars)	P (bars)	Q (kg/min)	Q/ΔP kg/min / bar	Q/ΔP gpm / psi	Q/ΔP m^3/sec/Pa
6-1	219	159	60	1600	26.7	0.590	5.40×10^{-9}
6-2	169	134	35	1134	32.4	0.715	6.54×10^{-9}
5-1	169	156	13	800	61.5	11.35	1.23×10^{-8}
8-1	168	157	11	1394	126.	22.79	2.55×10^{-8}

the injectivity index of well 5-1 at various injection rates and evaluate its current condition.

Production tests were carried out on wells 6-1, 6-2, and 8-1 and an injection test was performed on well 5-1. Because no satisfactory method was found to dispose of the produced fluid, well 31-1 was not available for testing. An interference test using well 8-1 as the flowing well and 48-7 and 6-1 as observation wells was also completed.

USBR Production Tests

Flow rate measurements. Production rates of wells 6-1, 6-2, and 8-1 were measured using an atmospheric flash tank and a weir box equipped with a v-notch weir plate and a clock-driven water level recorder. The liquid flow was measured and the total flow was calculated by assuming a steam quality of 11% for unflashed brine. This value was measured previously using temperature and pressure data of unflashed brine.

Table 2. Transmissivity values from pre-1976 pressure transient tests (after Narasimhan et al., 1977a).

Well	Date	Test type	Duration (hours)	Transmissivity md-ft/cp (m3/sec/Pa)
31-1	7/21/75	Drawdown Recovery	5.5 4.7	123,000 (3.70×10^{-8})
31-1	7/30/75	Recovery	10.0	166,000 (5.00×10^{-8})
5-1	1/08/75	Drawdown	10.0	32,000 (9.6×10^{-9})
5-1	2/28/75	Injection	10.0	37,000 (1.1×10^{-8})
8-1	4/21/75	Drawdown Recovery	5.7 5.0	75,000 (2.3×10^{-8})
6-1	12/28/72	Recovery (before perforation)	16 days	1,600 (4.8×10^{-10})
6-1	1/24/73	Recovery (before perforation)	2.5	1,600 (4.8×10^{-10})
6-1	9/17/74	Desalting run drawdown (after perforation)	3 mos.	70,000 (2.1×10^{-8})

Table 3. Summary of all tests by LBL at East Mesa KGRA.*

Date of Test	Well 38-30	Well 56-30	Well 31-1	Well 16-29	Well 78-30	Well 18-28	Well 16-30	Well 6-1	Well 6-2	Well 5-1	Well 8-1	Well 44-7	Well 46-7	Well 48-7
2/13/76 to 2/24/76								WF	OBS		OBS			
4/01/76 to 4/16/76	OBS		WF											
1/28/77 to 2/20/77			OBS					OBS	WFO		OBS	OBS		
2/20/77 to 4/13/77	OBS		OBS						WF	WF		OBS		
7/14/77 to 7/28/77	WFO	OBS	OBS	OBS		INJO								
7/26/77 to 8/30/77		OBS	OBS	WFO		INJO	OBS							
8/26/77 to 10/5/77	WF	OBS	OBS		OBS	INJO	OBS							
9/29/77												WF	OBS	OBS
12/1/77 to 12/6/77										INJO				
12/15/77 to 12/20/77											WFO			
1/06/77 to 1/27/77								OBS			WF			OBS
1/27/78 to 3/09/78								OBS			WF†	WF	INJ	OBS
4/17/78 to 4/21/78								OBS	WFO					
5/01/78 to 5/04/78								WF						

*SYMBOLS: WF = well flowing; WFO = well flowing, pressure recorded (production test); INJ = water injected; INJO = water injected, pressure recorded (injection test); OBS = pressure recorded, interference test.

†Well 8-1 was shut in 2/9/78.

Pressure measurements. Changes in downhole pressure were measured using a small-diameter steel capillary tube (0.54 in. I.D., 0.94 in. O.D.) filled with silicon oil or nitrogen gas. The tube was placed in the well at an appropriate depth and a sensitive pressure transducer, accurate to 0.01 psi, was attached to it at the wellhead. Pressures were continuously monitored, but readings were recorded at intervals of 1 sec to 1 hr, depending on the rate of pressure change.

Production test design. All production tests consisted of a series of step changes in the flow rate. Consideration of transient temperature effects on the downhole pressure monitoring system strongly influenced production test design and data analysis. All production test wells were first flowed at a rate that would provide a quasi-steady-state temperature profile in the well. Subsequent small rate changes and pressure readings provided transient pressure data relatively free of temperature effects and therefore amenable to analysis. The average duration of the flow periods was about 18 hrs, and the average rate change is about 60 gpm.

Analysis techniques. Transient pressure data of selected test segments were analyzed for transmissivity (kh/μ) and storativity (ϕchr_e^2) using conventional isothermal oil-field techniques (Mathews and Russel, 1967; Earlougher, 1977; and Lippmann et al., 1978). The quantity ϕchr_e^2 is the storativity ϕch multiplied by the square of the effective well radius, r_e. The effective well radius is related to the skin effect value by $r_e = r_w e^{-s}$ where r_w is the nominal well radius, and s is the skin effect value. Because production test analyses directly yield the lumped parameter ϕchr_e^2, to estimate skin values it is necessary to know ϕchr_w^2. Unfortunately, ϕchr_w^2 for each well is not known with sufficient accuracy to permit calculation and comparison of skin-effect values. However, productivity indices (P.I.) corresponding to equal periods of production can be calculated from the kh/μ and ϕchr_e^2 estimates and used for comparison of damage and/or reservoir permeability among wells.

Productivity indices (P.I.) corresponding to 18 hr of flow were calculated analytically rather than using measured stabilized pressures and flow rates because the latter calculation is redundant and constitutes less complete information when transient pressure data are available. Furthermore, for the instrument system used in these tests, stabilized pressure values do not reflect downhole conditions at late times because pressure changes at the top of the capillary tube caused by transient temperature effects along the length of the capillary tube, while small, partially obscure the reservoir response. These temperature effects, however, do not appreciably affect the transient pressure data. P.I. values increase with increasing permeability and/or the quality of well completion. The P.I. value therefore combines the influence of the skin effect and reservoir permeability.

Production test results. The final kh/μ, ϕchr_e^2 and P.I. values found for each well are given in Table 4. These results are average values obtained from several test segments of each well test. The accuracy of kh/μ is governed by the accuracy of the flow-rate measurements and the quality of the pressure data. In general, the accuracy of the pressure data and its interpretation far exceeds that of the flow-rate measurements. Therefore, kh/μ values are believed to be correct to within the accuracy of the flow-rate values, which is on the order of 10%. Because values of ϕchr_e^2 are calculated using kh/μ values, their accuracy is also within 10%.

Discussion of production test results. The pressure data for wells 8-1 and 6-1 are typical of a single production zone reservoir, and the test results from each test segment of each well test are generally consistent. However, well test data for wells 5-1 and 6-2 display atypical behavior.

Table 4. Summary of production test results.

Well	Transmissivity md-ft/cp (m^3/sec/Pa)	Storativity ft^3/psi (m^3/Pa)	Productivity or Injectivity* gpm/psi (m^3/sec/Pa)
5-1	43,000 (1.3×10^{-8})	7.14×10^{-8} (2.93×10^{-13})	0.79 (I.I.) (7.23×10^{-9})
8-1	60,000 (1.8×10^{-8})	0.028 (1.15×10^{-7})	2.47 (2.26×10^{-8})
6-2	73,000 (2.2×10^{-8})	0.105 (4.31×10^{-7})	3.39 (3.10×10^{-8})
6-1	14,000 (4.2×10^{-9})	0.101 (4.15×10^{-7})	0.83 (7.59×10^{-9})

*At 18 hours.

The injection test data from well 5-1 shows evidence of a vertical fracture. Three independent lines of evidence support this conclusion: First, spinner survey showed all flow exiting the well in a 400-ft (122-m) section at the top of the perforated interval. Second, the 5-1 injection log, December 26, 1976 (USBR, 1977), shows a rapid decrease in wellhead pressure from 1200 to 400 psi (8.3×10^7 to 2.8×10^7 Pa) concurrent with a constant injection rate of 100 gpm (6.3×10^{-3} m^3/sec). A wellhead pressure of 1200 psi is sufficient to cause a vertical fracture at the depth of the perforations. Third, the increase of the measured injectivity index (I.I.) with an increased rate of injection suggests a dilation process in the well that is indicative of a fracture. The value of 43,000 md-ft/cp (1.3×10^{-8} m^3/sec/Pa) is representative of a fractured interval, and the value of 7.14×10^{-8} ft^3/psi (2.93×10^{-13} m^3/Pa) is associated with a large positive skin effect probably caused by plugging of the fracture surface during injection.

Pressure data for well 6-2 suggest that two distinct production zones of widely different kh/μ are present. The more permeable zone exists in the upper 500 ft of perforation, and the less permeable zone is located deeper in the well. Well log permeability data are consistent with the existence of two production zones in 6-2 and their relative locations as stated above. The value of 73,000 md-ft/cp (2.2×10^{-8} m^3/sec/Pa) given for 6-2 is characteristic of both production zones acting together. Because the productivity index is calculated from the analysis of early-time pressure behavior, it is valid only for those times when both zones act together. However, the influence of the less permeable zone becomes dominant at later times when the two zones do not act together as a single reservoir. For this reason a P.I. value of 3.8 gpm/psi (3.5×10^{-8} m^3/sec/Pa) represents an optimistic upper bound value that is applicable only to early-time behavior.

From a comparison of the latest test results (Table 4) and the pre-1976 test results (Tables 1 and 2), we draw the following conclusions.

1. Well 8-1 has not changed its character significantly since 1975. Both its transmissivity and P.I. values agree closely between the tests.

2. Well 6-1 has been damaged. The transmissivity has decreased five-fold from 70,000 md-ft/cp (2.1×10^{-8} m^3/sec/Pa) measured from the desalting test (after perforation) to 14,000 md-ft/cp (4.2×10^{-9} m^3/sec/Pa) given by the LBL well test. This decrease may be due to plugging or scaling caused by chemical incompatibility of produced fluids.

3. Well 5-1 has an increased transmissivity value due to the presence of a vertical fracture. The injectivity index has decreased, however, due to plugging of the well by some chemical precipitate mechanism.

East Mesa Interference Tests

Since early 1976, LBL has completed numerous interference tests at the East Mesa KGRA (Table 3). Test designs ideally included a stabilized shut-in pressure at all observation wells, a production-well flow rate large enough to create significant drawdowns at all observation wells, and a test of sufficient duration to indicate reservoir inhomogeneities at each of the observation wells. Analysis of the well test data was carried out by means of a least-squares pressure-matching computer program developed at LBL (McEdwards and Tsang, 1977). This program is capable of analyzing data dependent on more than one production well, each with a variable flow rate. The program computes an analytical solution to the well test data using properly adjusted values of kh/μ, ϕch, and image well distances, where the distance between an image and an observation well (image well distance) may be used to locate either barrier or recharge boundaries. In the program, the production wells are modeled as line sources and the reservoir is considered to be isotropic, laterally infinite, and of constant thickness.

A summary of the chronology, details and results of all interference tests conducted by LBL at the East Mesa KGRA is presented in Table 5. Two production tests and one injection test were conducted in conjunction with the interference test at the northern end of the field. Table 6 lists the details of these tests.

Discussion of interference test results. Interference tests conducted in the northern and central portions of the field yield transmissivity estimates ranging from 105,000 to 175,000 md-ft/cp (3.2×10^{-8} to 5.3×10^{-8} m^3/sec/Pa) and storativity estimates ranging from 2×10^{-3} to 6.4×10^{-3} ft/psi (8.8×10^{-8} to 2.8×10^{-7} m/Pa). Transmissivity estimates obtained for the northern portion of the field are consistently larger than those obtained for the central portion. This reduction of transmissivity may be associated with higher grades of metamorphism in the hotter central portion of the field.

Hydrologic boundaries and continuity between wells. The presence of several hydrologic boundaries has been inferred from the numerous interference tests. A barrier (no-flow) boundary with a northeasterly trend is believed to exist between well 16-30 and the remainder of the field. Another barrier, possibly discontinuous, is inferred to exist between wells 56-30 and 16-29. A partial barrier positioned between wells 38-30 and 78-30 has been inferred.

Hydrologic continuity between USBR wells 6-1, 6-2, and 31-1 was established when wells 6-1 and 6-2 were produced and 31-1 was observed. Interpretation of the test results suggests the existence of a recharge boundary in the area. Due to the small drawdown, low flow rate, and large distance between the observation well and the production wells, this interpretation must be viewed cautiously. The absence of pressure response at 8-1 while 6-2 was being produced, together with its lack of response during a

Table 5. Interference tests and results at East Mesa.

Producing well	Date	Flow rate	Observation well	Transmissivity md-ft/cp (m^3/sec/Pa)	Storativity ft/psi (m/Pa)	Image well	Comments
Test 1 6-2	2/13/76 to 2/24/76	90 gpm	6-1	62,000 (1.9×10^{-8})	5.7×10^{-3} (2.5×10^{-7})	leaky	Vertical offset between producing well and observation well makes analysis uncertain
Test 2 31-1	4/01/76 to 4/12/76	130 gpm	38-30	136,000 (4.09×10^{-8})	2.1×10^{-3} (9.3×10^{-8})	barrier	
Test 3 6-2	2/10/77 to 2/20/77	60 gpm	6-1	111,000	6.0×10^{-3}		Uncertain initial pressure when production commenced
			8-1	(3.34×10^{-8})	(2.6×10^{-7})		No observable drawdown indicative of hydraulic barrier
Test 4 6-1, 6-2	2/20/77 to 4/13/77	Combined rate ~ 110 gpm	31-1 38-30 44-7	147,000 (4.41×10^{-8})	2.0×10^{-3} (8.8×10^{-8})	10,000 ft (3,000 m) leaky	Total drawdown 0.2 psi No observable drawdown Uncertain initial pressure when production commence
Test 5 38-30	7/14/77 to 7/18/77	Variable (step) 500 gpm, 750 gpm 900 gpm, 750 gpm 500 gpm, 250 gpm	56-30	146,000 (4.40×10^{-8})	6.0×10^{-4} (2.6×10^{-8})	4,630 ft (1,410 m)	
			31-1	194,000 (5.85×10^{-8})	2.0×10^{-3} (8.8×10^{-8})	barrier 2,600 ft	
			16-29	117,000 (3.51×10^{-8})	4.0×10^{-3} (1.8×10^{-7})	barrier	
Test 6 16-29	7/26/77 to 7/30/77	Highly variable 200-700 gpm	56-30 31-1 16-30				No drawdown observed‡ No drawdown observed‡ No drawdown observed‡
Test 7 38-30	8/24/77 to 10/5/77	~ 400 gpm	56-30	131,000 (3.94×10^{-8})	6.4×10^{-4} (2.8×10^{-8})	3,470 f (1,060 m) barrier	
			31-1	176,000 (5.30×10^{-8})	2.4×10^{-3} (1.1×10^{-7})	2,450 ft (750 m) barrier	
			16-30 78-30				No observable drawdown Nontypical behavior, partial barrier inferred
Test 8 44-7	9/29/77		48-7 46-7	uncertain			Small drawdown observed No effect seen, shallow injection well (not conclusive)
Test 9 8-1,6-2		Variable rate 8-1 ~ 200 gpm 6-7 ~ 50 gpm	48-7 6-1				No observable drawdown No observable drawdown
Test 10 8-1, 6-2 44-7	1/27/78 to 3/09/78	Highly variable 8-1 ~ 200 gpm 6-2 ~ 50 gpm 44-7, 0-750 gpm	6-1* 48-7†	140,000 (4.2×10^{-8}) 250,000 (7.5×10^{-8})	2.0×10^{-3} (8.8×10^{-8}) 3.0×10^{-3} (1.3×10^{-7})		

*No communication between wells 44-7 or 8-1 and 6-1

†Effect of 6-2 production and 46-7 injection not certain. Concurrent production of well 44-7 obscures the effect, if any of 8-1 production on the drawdown in well 48-7.

‡Interpretation remains ambiguous due to an unknown quantity of cold water influx into well 16-29 during production.

Table 6. Production tests in the northern portion of East Mesa KGRA done by LBL.

Well	Description of test	Instrumentation	Transmissivity md-ft/cp (m^3/sec/Pa)	Comments
38-30	Four days Variable rate Artesian flow 500 gpm, 750 gpm, 900 gpm 750 gpm, 500 gmp, 250 gpm	Tubing to 6100 ft. (nitrogen gas filled) Sperry Sun pressure monitor	133,000 (4.01×10^{-8})	P.I. is 5 gpm/psi.
16-29	Four days Variable rate Artesian flow 200-700 gpm	Tubing to 6100 ft. (nirtogen filled) Sperry Sun pressure monitor	178,000 (5.35×10^{-8})	Only build-up data available Cold water influx into well from top 150 m.
18-28	Injection Test 7/1/77 to 9/22/77	Hewlett Packard downhole pressure	76,000 (2.3×10^{-8})	Wellhead temperatures range from 150° to 200°F.

previous test, indicates a lack of hydrologic continuity between 8-1 and 6-2.

In the southern portion of the field, hydrologic continuity between 8-1 and 48-7 is uncertain. If communication does exist, it is of a limited nature. Well 8-1 (and later 44-7 and 8-1) was produced while 48-7 was monitored for pressure changes. Interpretation of test results yield transmissivity estimates which are anomalously large. However, the interpretation of pressure changes in 48-7 are complicated by the unknown effects of concurrent fluid injection into well 46-7, a shallow (3,000-ft, 900-m) well located a 1/4 mile away from 48-7, and by the unknown fluid conductive properties of a geophysically inferred fault that intersects well 44-7.

Well 6-1 showed a total drawdown of 2.5 psi for the duration of the test. In addition to this anomalously low drawdown, well 6-1 did not show any build-up after wells 8-1 and 44-7 ceased production. The analysis of this result is complicated by the fact that well 6-2 was producing about 50 gpm during the entire time. Although analysis is complicated by the different perforation intervals of wells 6-1 and 6-2, late-time pressure data can be approximated by assuming a transmissivity of 140,000 md-ft/cp and a storativity of 2×10^{-3} ft/psi. Indications are that wells 8-1 and 44-7 do not communicate with well 6-1.

REFERENCES CITED

Earlougher, R. C., 1977. Advances in well test analysis. Monograph, Dallas, Soc. Petrol. Engin. AIME, v. 5.

Howard, J., Apps, J. A., Benson, S., Goldstein, N. E., Graf, A. N., Haney, J., Jackson, D., Majer, E., McEdwards, D., McEvilly, T. V., Narasimhan, T. M., Schechter, B., Schroeder, R., Taylor, R., van de Kamp, P., and Wolery, T., 1979. Geothermal resource and reservoir investigations of U.S. Bureau of Reclamation leaseholds at East Mesa, Imperial Valley, California. Berkeley, Lawrence Berkeley Laboratory, LBL-7094.

Lippmann, M. J., Bodvarsson, G. S., and Witherspoon, P. A., 1979. Preliminary simulation studies of the Cerro Prieto reservoir, in Proceedings, First Symposium on the Cerro Prieto Geothermal Field, Baja California, Mexico, September 20-22, 1978. Berkeley, Lawrence Berkeley Laboratory, LBL-7098.

Mathias, K. E., 1976. The Mesa geothermal field --a preliminary evaluation of five geothermal walls, in Proceedings, Second UN Symposium on the Development and Use of Geothermal Resources, San Francisco, May 1975. Washington, D.C., U.S. Government Printing Office, v. 3, pp. 1741-1747.

Matthews, C. S., and Russel, D. G., 1967. Pressure build-up and flow tests in wells. Monograph, Dallas, Soc. Petrol. Engin. AIME, v. 1.

McEdwards, D. G., and Tsang, C. F., 1977. Variable rate multiple well testing analysis, in Proceedings, Invitational Well Testing Symposium, October 1977. Berkeley, Lawrence Berkeley Laboratory, LBL-7027, pp. 92-99.

Narasimhan, T. N., McEdwards, D. G., and Witherspoon, P. A., 1977a. Results of reservoir evaluation test, 1976, East Mesa geothermal field in California. Berkeley, Lawrence Berkeley Laboratory, LBL-6369.

Narasimhan, T. N., Schroeder, R. C., Goranson, C. B., McEdwards, D. G., Campbell, D. A., and Barkman, J. H., 1977b. Recent results from tests on the Republic geothermal wells, East Mesa, California. Berkeley, Lawrence Berkeley Laboratory, LBL-7017.

Narasimhan, T. N., Schroeder, R. C., Goranson, C. B., and Benson, S. M., 1979. Results of reservoir engineering tests, 1977, East Mesa, California. Berkeley, Lawrence Berkeley Laboratory, LBL-7191.

U.S. Bureau of Reclamation, 1977. Geothermal resource investigations, East Mesa test site, Imperial Valley, California, status report. U.S. Department of the Interior, Bureau of Reclamation.

Witherspoon, P. A., Narasimhan, T. N., and McEdwards, D. G., 1978. Results of interference tests from two geothermal reservoirs. Jour. Petrol. Tech., v. 30, pp. 10-16.

DEVELOPMENT OF THE SIMULATOR SHAFT78 FOR GEOTHERMAL RESERVOIR STUDIES

K. Pruess, R. C. Schroeder, P. A. Witherspoon, and J. M. Zerzan

INTRODUCTION

SHAFT is an acronym for simultaneous heat and fluid transport. It is the name given to a package of computer programs for simulating geothermal reservoirs, that is, for computing two-phase flow in porous media.

Initial work by Lasseter in 1974 and 1975 led to the development of a basic concept for SHAFT, outlining a physical and mathematical model for two-phase flow in porous media (Lasseter et al., 1976). The implementation of the concept in existing computer programs was incomplete. The main obstacle was in the handling of the equation of state. Other unresolved problems existed in the definition of two-phase flow terms, and in the coupling between mass and energy flow.

Despite these difficulties we believed that the basic concepts of SHAFT were sound and warranted full implementation and testing. This has been achieved, and a first satisfactory version of the program, called SHAFT78, has been constructed. SHAFT78 has been used for computing a variety of one-and two-phase flow problems, and the accuracy of the calculations has been verified by comparing them with results published in the literature (Pruess et al., 1978a, 1979). SHAFT78 is currently applied for simulating the performance of three-dimensional regular- and irregular-shaped geothermal reservoirs before and during exploitation.

The present report focuses on those aspects that required particular attention in developing a working computer program. After briefly reviewing the basic concepts, we shall outline the treatment of fluid properties (equation of state of water) and the solution procedure for the coupled energy- and mass-transport equations. We also give some results of calculations and indicate areas of future improvement of SHAFT78.

A more in-depth presentation of SHAFT78 and its associated pre- and postprocessor programs is available in a number of reports (Pruess et al., 1978a, b, 1979). Interested users can obtain a manual that includes sample problems and detailed instructions for applying SHAFT78 to two-phase porous flow problems (Pruess et al., 1978b).

THE BASIC CONCEPTS

Of the various assumptions made in SHAFT78 in defining a general physical model of geothermal reservoirs, perhaps the most fundamental is that the rock matrix can be treated as a porous medium. This ignores special effects due to fractures, which are known to exist in many geothermal reservoirs. Other simplifications of the physical system to be modeled include: (a) neglect of noncondensible gases, and (b) neglect of dissolved chemicals in the reservoir fluid. Thus, geothermal reservoirs are modeled as systems of porous rock, with the pore space being filled with pure water in liquid or vapor form. The macroscopic physical processes in these systems include: (a) transport of mass via fluid flow; (b) transport of energy via fluid convection, fluid boiling and condensation, and fluid and rock heat conduction; and (c) transport of momentum via fluid flow.

Momentum transport is approximated with Darcy's law, and energy transport is simplified by assuming that liquid, vapor, and rock matrix are in local thermodynamic equilibrium, that is, at the same temperature and pressure at all times.

With the above-stated assumptions and approximations, the flow of (two-phase) fluid and heat in a porous medium can be described in terms of balance equations for mass and energy.

What distinguishes SHAFT78 from other two-phase simulators discussed in the literature is the way in which these equations are treated and solved. The basic differential equations are formulated in terms of specific (internal) energy and density of the fluid, which allows the same two variables to be used even if phase transitions occur. This formulation is also the most elegant one mathematically, and offers advantages for obtaining overall heat-and-mass balances. Space discretization is achieved with the integrated finite-difference method (IFD). This method is as easily applied to irregular geometries of actual reservoirs as it is to idealized regular geometries, and no distinction needs to be made between one-dimensional and multidimensional systems. At the same time, the relative simplicity of the finite-difference method is retained in the theory and algorithms.

Time is discretized as a first-order forward finite difference. For each time step, energy and density changes are computed semi-implicitly using an iteration method derived from Evans et al. (1954). Because the rate of relative energy change is often considerably smaller than that of relative density change, SHAFT78 solves the energy equation first for a longer time step, and then takes a few (typically 2 to 4) density steps to cover the same time interval as computed in the energy step. Time steps are chosen automatically during program execution in a way that ensures that relative and absolute changes in important variables do not exceed certain values, to be specified by the user. No iteration is performed for the coupling between energy and density equations, and time steps have to be chosen small enough to make this coupling negligible. Other approximations made in the current version of SHAFT78 include (a) neglect of dependence of rock properties upon temperature and pressure, and (b) neglect of capillary pressure differences between liquid and vapor phases.

In each time step a number of material parameters, notably temperature and pressure, have to be computed as a function of specific (internal) energy and density of the fluid. Because anaytical approximations for this purpose are not available, an interpolation scheme is employed. Temperature, pressure, and other required parameters are tabulated over a rectangular grid of energy and density values, and linear (bivariate) interpolation is performed to compute parameters between grid points.

EQUATION OF STATE

The tabular equation of state for SHAFT78 is obtained by inverting steam tables, which give specific internal energy (u) and density (ρ) of water as a function of temperature (T), pressure (p), and vapor saturation (S). The inversion is performed in two steps:

$$\begin{Bmatrix} u(T,p,S) \\ \rho(T,p,S) \end{Bmatrix} \xrightarrow{(1)} \begin{Bmatrix} u(p,\rho) \\ T(p,\rho) \end{Bmatrix} \quad (2) \quad \begin{Bmatrix} T(u,\rho) \\ p(u,\rho) \end{Bmatrix}$$
$$S(p,\rho) \qquad\qquad S(u,\rho)$$

A preprocessor program called PROPER computes an equation of state in a form suitable for the program CYCN, which then performs the actual simulation.

Special provisions were made in PROPER and CYCN to ensure that interpolation is never made across the saturation line, at which all parameters change slope. PROPER also contains a provision for automatically selecting basis points (u_n, ρ_m) in the liquid region (subcooled water), which is very much compressed in a (u, ρ)-diagram due to the minimal compressibility of liquid water.

We found that input data for liquid water had to be extremely accurate. Relative errors in densities had to be less than 10^{-6} in order to get acceptable accuracy for pressures. A program called WATER was written, which computes u(T,p,S) and ρ(T,p,S) in a form suitable for input to PROPER, using the analytical steam table equation as given by the International Formulation Committee (1967). Liquid water, superheated steam, and two-phase mixtures over a temperature range of 5 to 400°C and a pressure range of 10^{-2} to 220 bars can be covered with a single fluid table with good accuracy. Typical accuracies are ±0.1% for temperature, ±0.01% for vapor saturation, and ±0.2% for pressure. An exception is pressure for liquid subcooled water, which is accurate to ±0.5 bars typically. Increased accuracy can be obtained by more closely spacing the basis points in the tabulation.

COUPLED EQUATIONS FOR MASS AND ENERGY TRANSPORT

The actual simulation of a porous flow problem is performed with a program called CYCN. An overview of the solution procedure is given in Figure 1. We first solve the energy equation for a time step Δt_u. Then the density equation is solved for a time step $\Delta t_\rho \leq \Delta t_u$. After the density step, a correction for the rock/fluid equilibration is performed. If this correction cannot be done with a preset accuracy, the density step is repeated with half the time step. After an accepted density step, the program either proceeds to the next density step (if the total time, $\Sigma\Delta t_\rho$, of all density steps is less than the energy time step, Δt_u), or begins another energy step (if $\Sigma\Delta t_\rho = \Delta t_u$).

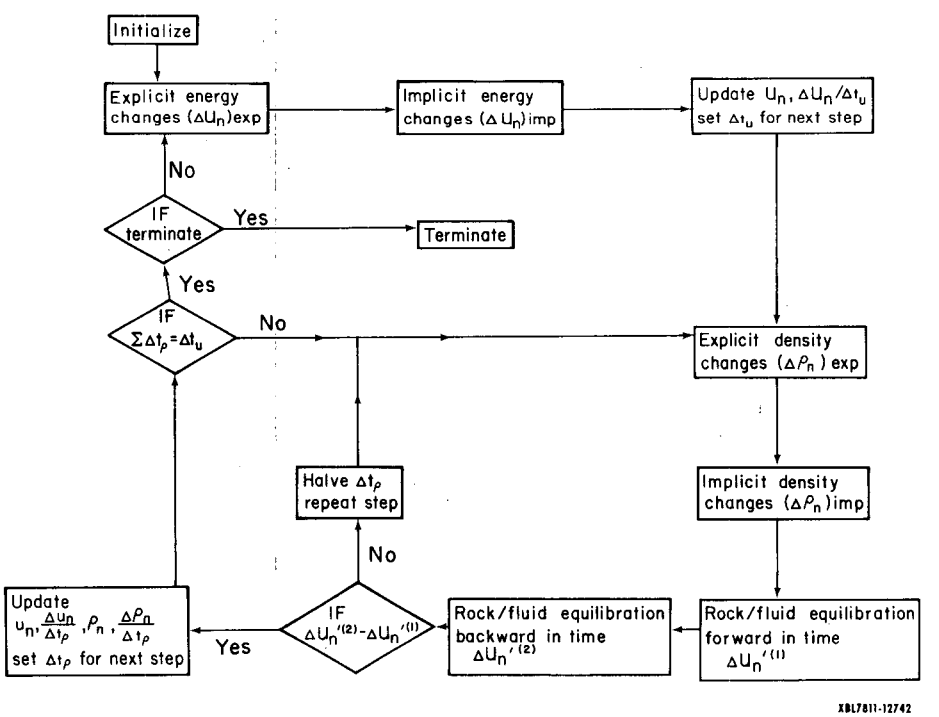

Figure 1. Solution procedure of the program CYCN.

CYCN retains much of the solution procedure that was initially devised for SHAFT. In developing CYCN, a careful review was made of the governing energy and mass transport equations, and their conversion into integrated finite-difference form. A consistent method was devised for computing interface (aerial) quantities from volume averages. The most significant novelty in CYCN is execution of an explicit equilibration between rock and fluid temperatures after each density step. This equilibration was shown to ensure energy conservation and overall accuracy of the calculation. It also provides for high accuracy when computing phase transitions.

Other new features in CYCN include provisions for inputting initial conditions in terms of the more physical quantities T,p,S rather than in terms of (u,ρ). Source terms have been made more flexible to allow for alternative ways to model wells. Various weighting procedures have been devised to optimize computations which involve propagation of sharp phase fronts.

SOME RESULTS OF CALCULATIONS

We have made careful checks of the accuracy of the various components of SHAFT78, as well as of the program package as a whole. A rather severe test of SHAFT78 is afforded by a radial production problem, which was previously investigated by Garg (1978). The problem, which is specified in Garg's paper, involves withdrawal from a reservoir initially filled with a subcooled water. As production proceeds, water begins to boil and several elements cross the saturation line. Figure 2 shows that the SHAFT78 calculation agrees well with the results obtained by Garg. Calculations for other one- and two-phase problems, which verify the accuracy of SHAFT78, are discussed by Pruess et al. (1978a, 1979).

SHAFT78 has been applied to study the pressure drawdown in two-phase reservoirs as they are depleted during production. An investigation of systems with different initial conditions and different parameter values revealed that two-phase reservoirs are capable of a great variety of pressure responses upon production.

Although pressure usually declines as production proceeds, we found that this trend sometimes can be reversed due to effects of propagating flash fronts and residual immobile water saturations. Combining SHAFT78 calculations with results from an analytical model, we were able to show that pressure decline curves do not allow conclusions about the amount of fluid in place. In particular, we showed that the standard technique of estimating reserves by extrapolating a plot of p/Z vs. cumulative production, which is frequently employed in the literature, is not applicable to two-phase geothermal reservoirs. Figure 3 gives pressure drawdowns for three two-phase reservoirs as investigated recently by Brigham and Morrow (1977) with porosity equal to 5%, 10% and 20%, and all other parameters being identical. Thus, the initial masses of fluid in place differ by a factor of 2 between reservoirs, whereas initial pressure drawdowns are virtually indistinguishable. We established that pressure-decline curves can be used, however, to estimate the total amount of heat residing in the rock matrix.

Apart from idealized model studies, SHAFT78 has also been applied to simulate natural geothermal reservoirs in three dimensions. A study of production and recharge in the Krafla, Iceland, geothermal field is reported by Jonsson (1978). Work was begun to develop a history match for production and injection in the highly irregular-shaped field of Serrazzano, Italy (Weres, 1977).

PRESENT STATUS AND FUTURE WORK

The simulator SHAFT78 has been verified to accurately compute the phenomena of flow of steam and water in porous media, boiling and condensation, and heat exchange between rock and fluid. Extensive application has shown SHAFT78 to be a useful tool for studying the performance of idealized or natural multidimen-

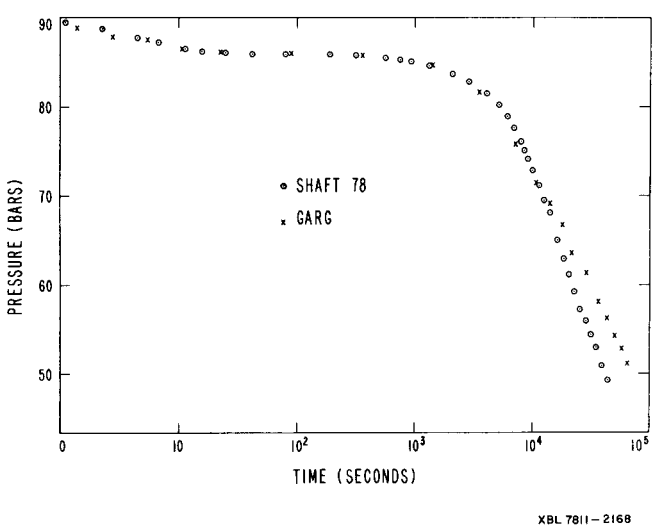

Figure 2. Pressure drawdown in a liquid reservoir with propagating flash front.

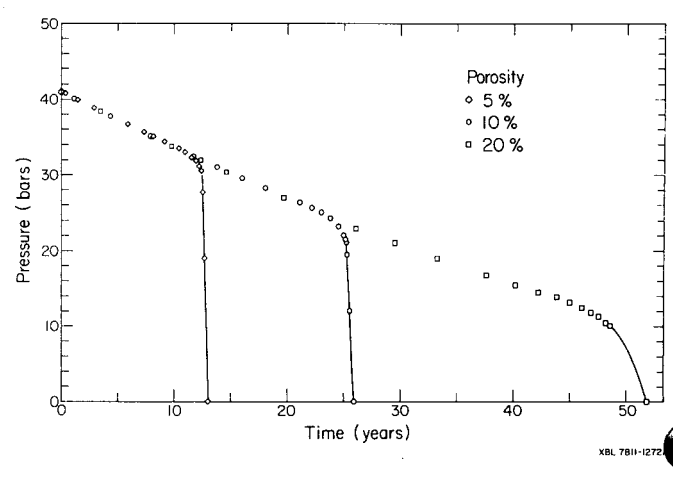

Figure 3. Pressure drawdown in two-phase reservoirs with different porosity.

sional geothermal reservoirs. Various pre- and postprocessor programs and plotting routines have been developed, which aid in carrying out reservoir studies.

The applications have also revealed areas in which the original concepts devised for SHAFT should be modified to improve accuracy and efficiency of the calculations, and to increase the flexibility of SHAFT78. The most important modification to be implemented in the future for increased calculational efficiency is an iterative technique for solving the coupled equations for mass-and-energy transport. The present noniterative treatment imposes severe limitations on permissible size of time steps. Typically some 300 time steps are required to accurately traverse the entire two-phase region from subcooled water to superheated steam (or vice versa).

Because of the strength and nonlinearity of the coupling between mass and energy flow, the concept of solving the energy equation for a larger time step than the density equation should be abandoned. When solving both equations iteratively for the same time step, it will be advantageous to solve first the density equation and then the energy equation. This is preferable because density changes affect the way in which volumetric energy changes are partitioned between rock and fluid.

It is desirable to improve the treatment of sources in SHAFT78. Analytical approximations should be devised for modeling the boundary conditions near wells without introducing many small volume elements.

While the indicated improvements are under development, it will be possible to continue application of the existing program SHAFT78 to geothermal reservoir studies.

ACKNOWLEDGMENT

We thank V. Jonsson for his help in developing the WATER program.

REFERENCES CITED

Brigham, W. E., and Morrow, W. B., 1977. p/Z behavior for geothermal steam reservoirs. Soc. Pet. Eng. Jour. (December 1977) pp. 407-412.

Evans, G. W., Brousseau, R. J., and Keirstead, R., 1954. Instability considerations for various difference equations derived from the diffusion equation. Livermore, Lawrence Livermore Laboratory, UCRL-4476.

Garg, S. K., 1978. Pressure transient analysis for two-phase (liquid water/steam) geothermal reservoirs. Soc. Pet. Eng. of AIME, SPE-7479.

International Formulation Committee, 1967. The 1967 IFC formulation for industrial use, a formulation of the thermodynamic properties of ordinary water substance. Dusseldorf, Verein Deutscher Ingenieure.

Jonsson, V., 1978. Simulation of the Krafla geothermal field. Berkeley, Lawrence Berkeley Laboratory, LBL-7076.

Lasseter, T. J., Witherspoon, P. A., and Lippman, M. J., 1976. Multiphase multidimensional simulation of geothermal reservoirs, in Proceedings, Second United Nations Symposium on the Development and Use of Geothermal Resources, San Francisco, May 1975. Washington, D. C., U.S. Government Printing Office (Lawrence Berkeley Laboratory), v. 3, pp. 1715-1723.

Pruess, K., Schroeder, R. C., and Zerzan, J. M., 1978a. Studies of flow problems with the simulator SHAFT78. Paper presented at the Fourth Stanford Workshop on Geothermal Reservoir Engineering, Stanford, Calif. (13-15 December 1978).

Pruess, K., Schroeder, R. C., Witherspoon, P. A., and Zerzan, J. M. 1978b. SHAFT78, a two-phase multidimensional computer program for geothermal reservoir simulation. Berkeley, Lawrence Berkeley Laboratory, LBL-8264A.

____, 1979. Description of the three-dimensnal two-phase simulator SHAFT78 for use in geothermal reservoir studies. Soc. Pet. Eng. of AIME, SPE-7699 and Berkeley, Lawrence Berkeley Laboratory, LBL-8802.

Weres, O., 1977. A model of the Serrazzano zone, in Proceedings, Third Stanford Workshop on Geothermal Reservoir Engineering, Stanford, Stanford Univ., pp. 214-219.

SITE-SPECIFIC GEOTHERMAL RESERVOIR ENGINEERING ACTIVITIES

C. B. Goranson and R. C. Schroeder

INTRODUCTION

LBL personnel have been engaged in geothermal reservoir engineering since 1975, when T. N. Narasimhan and P. A. Witherspoon tested and analyzed well RRGE-1 at Raft River, Idaho (1977). Since 1975 the LBL field capabilities have been expanded and improved. Our studies have included cooperative projects with several private companies, city governments, and federal agencies. Our purpose has been to develop new and improved techniques, tools, and analysis methods for use in assessing and modeling hydrothermal systems. The important tasks in carrying out these activities are to: collect site-specific data, develop field techniques, measurement tools, and analysis methods, and model site-specific aquifers. This report covers only the first of these activities

and only work performed in fiscal year 1978. A review of our analysis and data processing activities is given in a separate paper by Benson et al. (1979).

The site-specific studies include data from many sources, in addition to LBL field measurements. These data include geological, geophysical, hydrological, and geochemical information about each site. The well testing requires well completion data, well logs, and wellbore geophysical interpretations in order to carry out detailed analyses of the well test data. In general, the purposes of the well testing are to determine hydrological parameters, identify aquifer limits (barriers), identify aquifer recharge (if it exists), determine well damage (if it exists), determine thermal characteristics, and obtain representative reservoir fluid samples.

All of this information is used when a resource assessment is initiated and subsequent modeling is carried out. Clearly, the amount of information available for site-specific resource evaluation determines the degree of confidence in estimating reserves and resource lifetime for proposed exploitation strategies.

Table 1 and Figure 1 show the specific geothermal sites where LBL personnel have played a role in reservoir engineering measurements, evaluation, or planning during fiscal year 1978.

Table 1. Locations of site-specific reservoir engineering activities during fiscal year 1978.*

Site	Activity
Desert Hot Springs	Well test analysis
Casa Diablo	Well test planning
Coso Hot Springs	Measurements, workover, and resource evaluation
Susanville	Measurements, well siting, and resource evaluation
East Mesa	Measurements workover, and resource evaluation
Klamath Falls, Oregon	Measurements, planning, and resource evaluation
Cerro Prieto, Mexico	Measurements and resource evaluation

*Minor activities included Valles Caldera, New Mexico; Salton Sea geothermal field and Heber, California; and Raft River, Idaho.

REVIEW OF SITE-SPECIFIC ACTIVITIES

Desert Hot Springs KGRA

LBL reviewed data from a well test carried out in June 1977 by B. F. Russell, California State University at Fullerton (Goranson et al., 1978a). The test incorporated three wells in the Desert Hot Springs KGRA near Palm Springs, California. One well was produced at 110 gpm for 4.5 hours. Water level changes were measured in the production well and in two observation wells at distances of 102 and 212 ft from the flowing well. Maximum produced wellhead fluid temperature was 148°F.

The data were analyzed assuming that there is a partial penetration effect which yields a total reservoir height of 1,000 ft. Transmissivity values between 1.7 and 3.7 x 10^6 md-ft/cp were calculated from the production and observation well data.

However, our confidence in the calculated transmissivity values is small. Analysis of data from well tests is directly dependent on geological and lithological information available for the reservoir. In this case, little is known about the aquifer that was tested.

Lithologic and geophysical well logs were not available. Furthermore, the areal geology was not well defined. Our main conclusions were that the test was not long enough to estimate the total amount of heat available, maximum producible temperature, geologic extent of the resource, or maximum production capabilities. This anomaly appears promising as a candicate for direct utilization applications. However, a modest investment in well testing, geological studies, and their evaluation is necessary to provide estimates for the resource extent and its hydrothermal characteristics.

Casa Diablo Site

LBL reservoir engineers visited the Diablo Hot Springs, California, geothermal area in the Mono-Long Valley KGRA, in June 1977. We reviewed the site for possible well test activities to delineate reservoir boundaries and maximum long-term production rates. The studies would be used in a direct heat utilization program for the city of Mammoth Lakes. This reservoir has a maximum temperature of approximately 360°F at about 400 ft depth. The first well was drilled by Magma Power Co. in 1957. Preliminary short-term flow tests reported flows between 300,000 to 500,000 lb/hr. These rates and temperatures should be more than sufficient to supply space heating demands for the city of Mammoth Lakes. However, these short term tests do not indicate reservoir extent or total capacity of the reservoir.

LBL has no plans in the immediate future for extensive well testing. However, the heat load demands for the city of Mammoth Lakes have been illustrated by Sims and Racine (1977), and rela-

tively high-temperature water is available from this relatively shallow aquifer. Therefore, drilling costs would be minimal and pipelines would be of reasonable length. These considerations make Diablo Hot Springs an interesting site for geothermal production. However, chemical precipitation during production or injection may be a problem (based on samples taken by Magma Power Co.).

The reservoir boundaries and reservoir capacity for long-term production have not been determined, but the area shows promise. Additional testing and fluid sampling is required for initial resource evaluation.

Coso Hot Springs

An exploratory well, Coso Geothermal Exploratory Hole Number 1 (CGEH#1), was completed at the China Lake Naval Weapons Center on December 2, 1977, to a total depth of 4,845 ft from ground level (CER Corp., 1978; Goranson et al., 1978b). The subsurface geology consists of a fractured granitic complex overlain with rhyolitic debris and intruded by rhyolitic dikes (Galbraith, 1978). LBL presonnel monitored the downhole thermal equilibrium of the well. The first LBL temperature survey was performed on December 8, 1977. In all, eight temperature surveys were performed. Three downhole fluid samples were taken and one downhole pressure survey was made.

During drilling numerous fractures were encountered. These fractures are observable in Figure 2 as large mud losses along the length of the wellbore. Moreover, as seen in the temperature surveys, these fractures are also evident in the abnormally cooled portions along the well where mud entered the formation, thereby cooling it down (at 2,100, 2,700 and 3,500 ft). The well had come to a thermal equilibrium by June 1978, as seen in Figure 3. The maximum temperature measured was 385°F at 2,000 ft, and bottom-hole temperature was 350°F.

On September 6, 1978, the well was stimulated with nitrogen using a 1-in.-diam. tubing placed downhole. After 12 hours of nitrogen flow, the well was dry with approximately 200 ft of fill at bottom hole. At this time the well stimulation operation was ended.

On November 2-6, 1978, well start-up and workover procedures commenced. The cleanout procedure consisted of pumping a nitrogen-foam and water mixture into the wellbore. The foam has the ability to entrain particles and float them to the surface. The foam cleanout operation was successful and a large amount of material was brought to the surface. However, a blockage was encountered, which prevented touching TD. The well again was dry after nitrogen stimulation. The water level buildup in the well was measured and indicated an inflow rate of approximately 4 gpm.

Our conclusion is that there is not an appreciable amount of fluid in the formation from 3,500 to 4,845 ft. The small amount of fluid

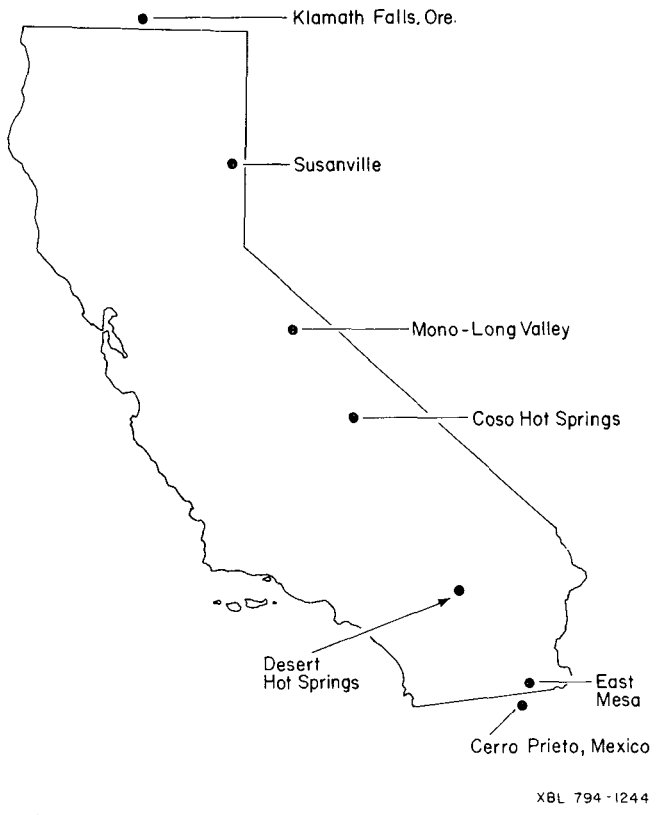

Figure 1. Map showing locations of LBL reservoir engineering activities for fiscal year 1978.

seems to originate outside the casing at about 3,500 ft (CGEH#1 is cased to 3,500 ft). The zones of large mud losses in the cased portion mentioned above are the probable origin of the geothermal fluid in the well. The zone at 1,900 ft had an influx of about 60 gpm while drilling with air, and hydrothermally altered rock was encountered. This zone also has the highest recorded temperature of 385°F.

The well has proved to be useful in preliminary resource evaluation. To verify preliminary resource models there is a need for further drilling in nearby areas to determine fracture orientations and resource characteristics in the Coso Hot Springs KGRA.

Susanville Geothermal Anomaly

Personnel from the U.S. Department of the Interior, Bureau of Reclamation (USBR), are performing an extensive resource identification program in the Susanville-Honey Lake KGRA in northern California (USBR, 1976a, b; Figure 1). During the summer of 1978, USBR drilling crews concentrated on the City of Susanville area, since the geothermal resource there is expected to be capable of meeting heat load demands within the city limits. Thermal waters are being used at this time to heat the city swimming pool. Other private users include a greenhouse, a lumber company, and a church. The maximum downhole temperature measured to date is 150°F at a depth of 350 ft (see Figure 4).

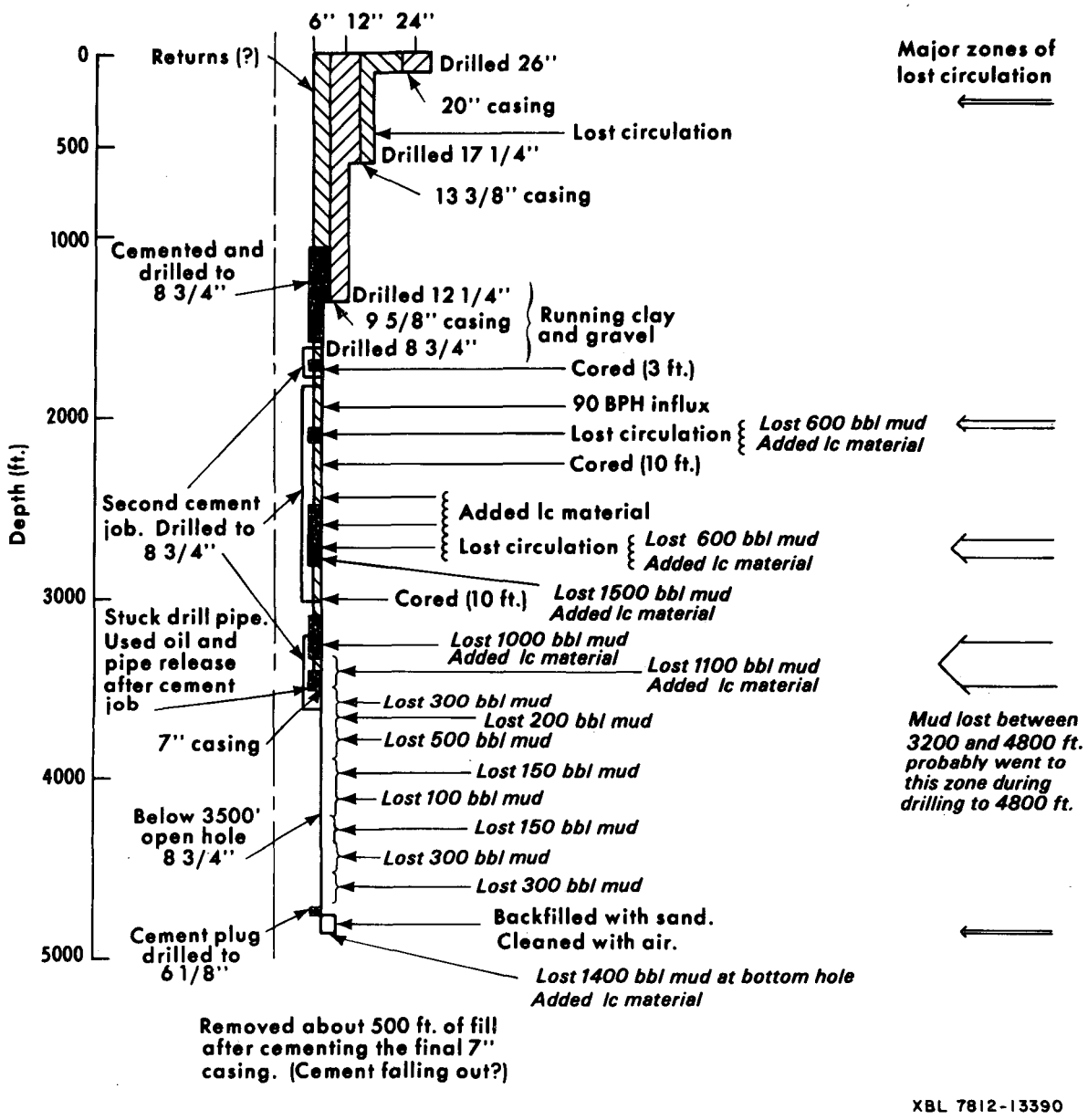

Figure 2. Summary of drillers log for CGEH-1, Coso Hot Springs, California.

There are 10 wells in the west side of Susanville that were incorporated in a well test beginning November 27, 1978. Numerous drill logs and geophysical well logs have been obtained from USBR. The approximate depth of the maximum temperature is known from well logs. However, the hydrothermal mechanism that maintains this resource is not known at this time. The interference test is early fiscal year 1979 should outline the resource boundaries and yield information on the long-term production characteristics of the resource. The test will also yield information related to further well drilling activities in the area. After analysis of the well test data, we will collaborate with USBR to choose an optimum site for the first production well to supply fluid for Susanville buildings. A productivity test is scheduled after the production well has been completed and developed. Injection and future production strategies will be studied using reservoir simulation computer programs.

Klamath Falls, Oregon, Geothermal Anomaly

Klamath Falls, Oregon, has been designated as a Known Geothermal Resource Area (Sammel and Peterson, 1976). The city is one of the earliest large-scale users of geothermal energy in the continental United States. There are approximately 350 hot-water wells in the area used for space heating in about 450 structures. Downhole water well temperatures range from 30°C to 105°C (see Figure 5). Large quantities of data have been published by the Oregon Institute of Technology

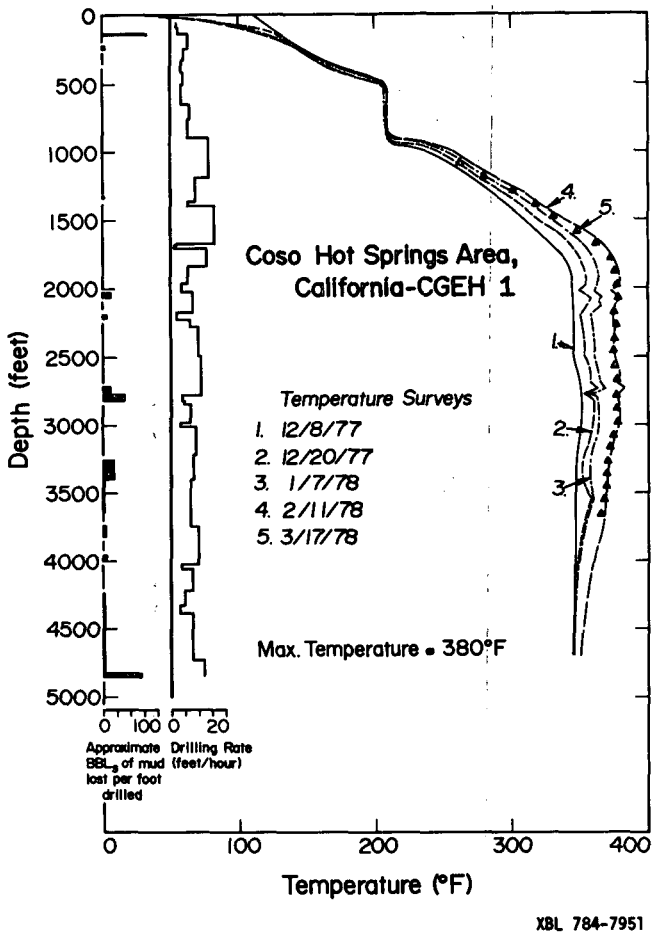

Figure 3. Temperature versus depth for CGEH-1 at selected time intervals, Coso Hot Springs, California.

Geo-Heat Utilization Center on the properties and characteristics of the Klamath Falls resource (Lund et al., 1978).

LBL has analyzed data from two well tests in the area performed by Oregon Institute of Technology. One test was performed in July 1976, another test was carried out in July 1978, with LBL participation. In the first test, the Museum well was flowed (located near the downtown area), and 23 nearby wells were monitored for water level changes (at distances ranging from 129 to 1,425 ft from the pumped well). The Museum well has been considered for supplying makeup water during large heat load demands. No drawdowns were measured in the museum well and the maximum produced temperature was 84°C. Subsurface geology in the area is rather complex with alternating lacustrine and volcanic materials as the main geologic structures. This geologic complexity hampers data analysis because the tests were too brief to uniquely define partial penetration, confined or unconfined aquifer behavior, leaky aquifer behavior, and other reservoir characteristics. Calculated values of effective transmissivity range from 6 x 10^6 md-ft/cp at the observation well (130 ft from the production well) to 35 x 10^6 md-ft/cp at a distance of 1,000 ft. The differences in the transmissivity values indicate a partial penetration effect. However, there were not enough data available to obtain unique interpretations. Flow rate changes were made at the production well before semi-steady-state behavior had been reached and hampered analytical analysis techniques.

The second well testing activity incorporated a well located on Old Fort Road about 1 mile from the center of town. This well is in an area where maximum downhole temperatures of 105°C exist, and may be penetrating a fault zone. The well was

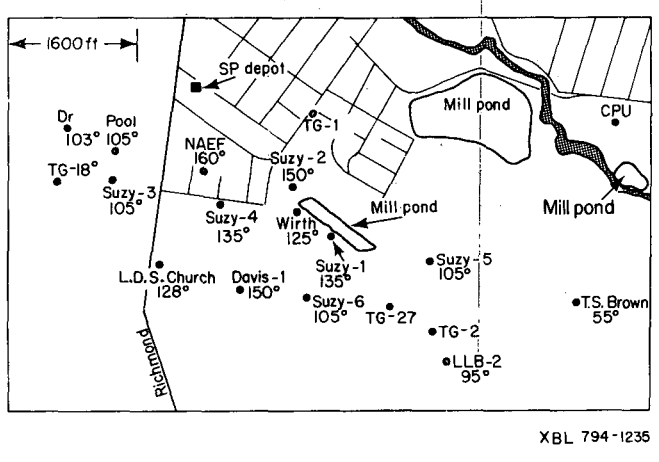

Figure 4. Geothermal well temperatures, Susanville, California.

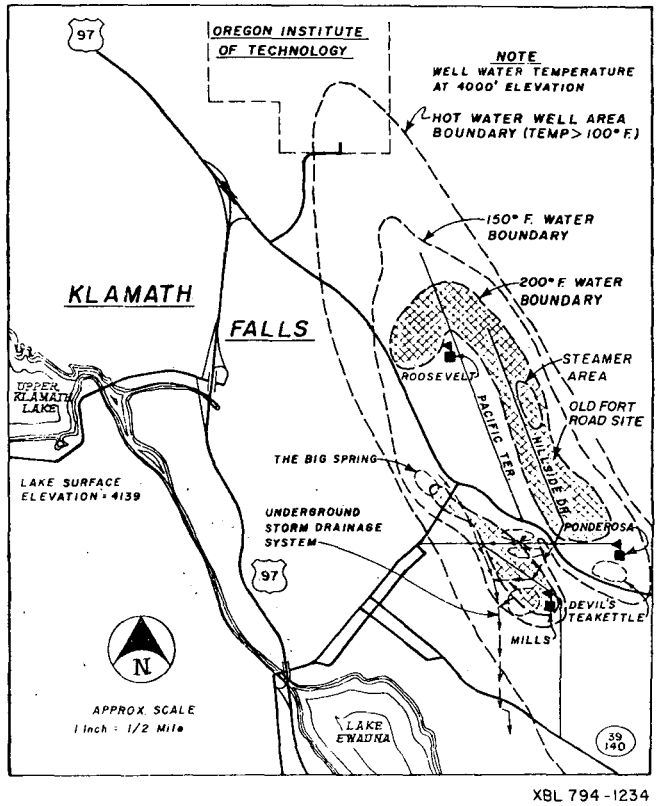

Figure 5. Well water temperatures at 4000-ft elevation, Klamath Falls, Oregon.

produced for two days at 250 gpm, shut in for two days, then flowed for two days for production, with injection in a well 600 ft from the production well. The production well is 800 ft deep, the injection well was 200 ft deep. Due to flow measurement problems and production well collapse, the flow time was limited to 24 hours (during the injection portion of the test). The 17 monitored observation wells had shallow completions (200-350 ft) while the production well was completed to 800 ft. The geology in the area of Old Fort Road is similar to that mentioned above for Klamath Falls. Drawdowns in the observation wells were quite small (15 cm) and the formation parameters have not been uniquely defined. However, a preliminary analysis indicates transmissivity values of the same order of magnitude as in the Museum well test. Although production well data were obtained, the data show complications that have not yet been identified (such as partial penetration, leaky aquifer, fracture, and so on). The test was not long enough to classify the reservoir from a hydrological standpoint. However, communication between producing and observation wells has been proved. Additional testing to determine the characteristics of the aquifer system is needed to confirm preliminary resource models of the area.

LBL reservoir engineers plan to carry out production tests, and possibly a long-term interference test, in the area of Old Fort Road during fiscal year 1979. These tests should hydrologically identify this resource. Oregon Institute of Technology personnel, working with the Geo-Heat Utilization Center, plan to drill two wells in the area of Old Fort Road during fiscal year 1979. LBL plans to assist them in drilling and geophysical well logging to identify the lithology of the area. Continuous water-level monitoring in a few chosen wells will be important in the long-term resource evaluation at Klamath Falls.

Cerro Prieto Geothermal Field, Mexico

The Cerro Prieto geothermal field is located in the Mexicali Valley in the southern extension of the Salton Trough, as shown in Figure 6. The field has 18 wells supplying steam to generate 75 MWe. Well depths in the field vary from 1200 to 2200 m. Numerous hot-water springs and fumaroles have existed in the area in the past, and some still exist today.

For testing purposes we have divided the field into four areas; west, south, east, and north, as shown in Figure 7. The western area encompasses the main producing field and well M-6. Data were available from a float-type water-level meter installed by the Mexican

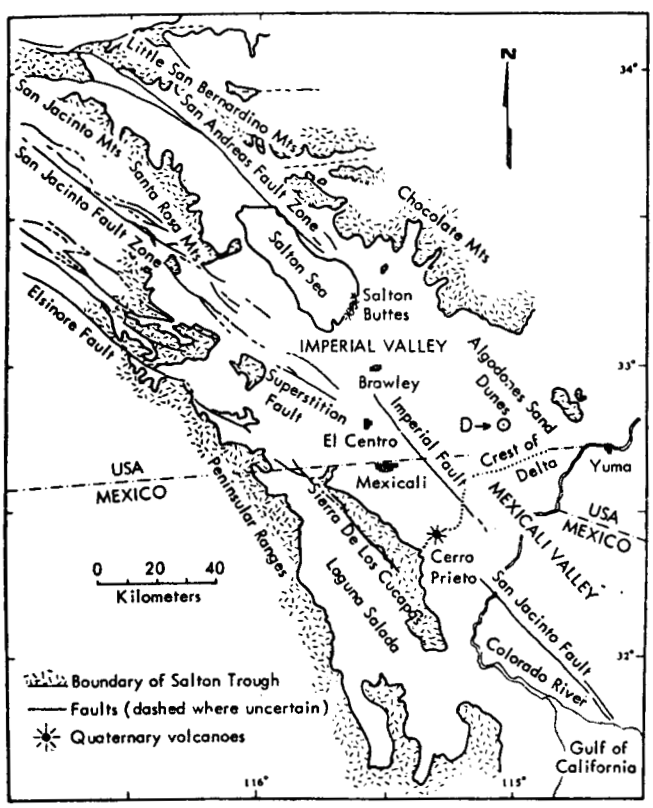

XBL 764-1182

Figure 6. Salton Trough showing Imperial and Mexicali Valley (from Palmer et al., 1975).

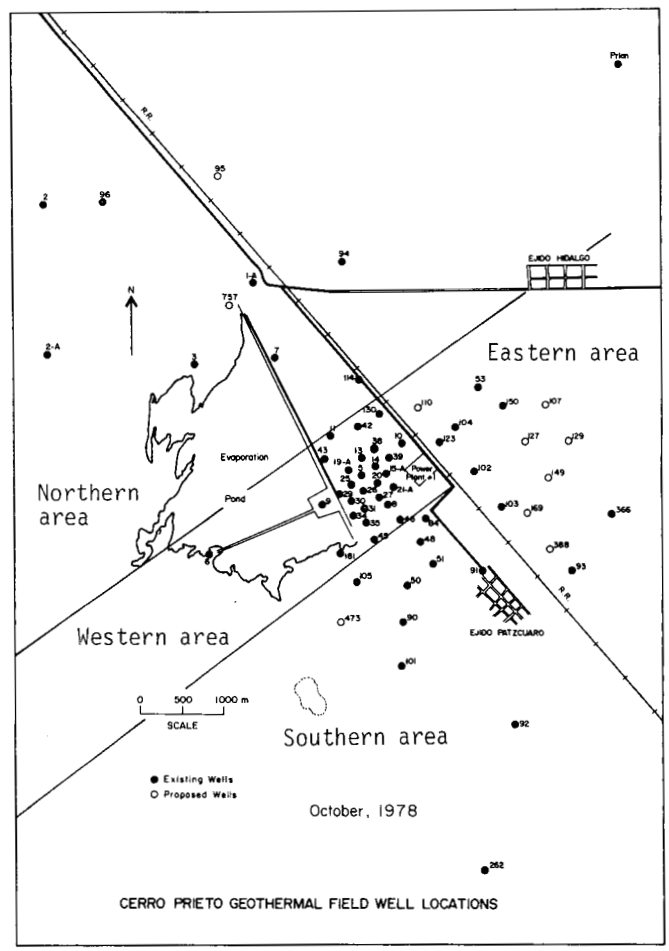

XBL 7811-12804

Figure 7. Cerro Prieto geothermal field showing LBL reservoir engineering subdivisions.

Department of Water Resources headquartered in Mexicali. The analysis of these data is difficult due to differences in the geologic regimes between M-6 and the main producing field (fanglomerates versus marine deltaic environment). This is indicated in lithologic and geophyical well logs. The geological differences of well M-6 are also indicated in the low downhole temperatures relative to the main field (≃105°C). Another difficulty in the analysis arises from the elevation differences of the open intervals in well M-6 and in wells in the field. The open interval in M-6 is 500 to 700 m. Open intervals in the producing field in most cases are between 1,100 to 1,500 m. Because the temperature in M-6 is 150°C and the temperature in the main field is over 300°C, the viscosity of the fluids is vastly different. Due to these difficulties, calculated transmissivity values using M-6 data indicate higher-than-actual permeability. Calculated transmissivity values are on the order of 4.7 x 10^6 md-ft/cp (1.4 x 10^{-6} m^3/Pa·sec).

From January 25 to March 15, 1978, LBL carried out an interference test in the southern portion of the field. Four wells were developed by the Comisión Federal de Electricidad (CFE) with maximum flow rates of 600,000 lb/hr. Production temperatures varied from 290 to 300°C. Development intervals were staggered with flow periods ranging from 4 to 10 days (see Figure 8). Well M-101 was chosen as the observation well while wells M-90, M-91, M-50, M-51 were produced. Again the analysis is made difficult due to sub-geological characteristics. The reservoir has recently been modeled (on the basis of well-log interpretations) in to three units--unconsolidated sediments, consolidated sediments, and basement rock. The consolidated unit has been divided essentially into four layers: layer 1, layer 2, reservoir A, and reservoir B. Reservoirs A and B are separated by a shale layer varying in thickness between 30 and 100 m. The observation well penetrates partially into reservoir A. Production wells penetrate partially into reservoirs A and B.

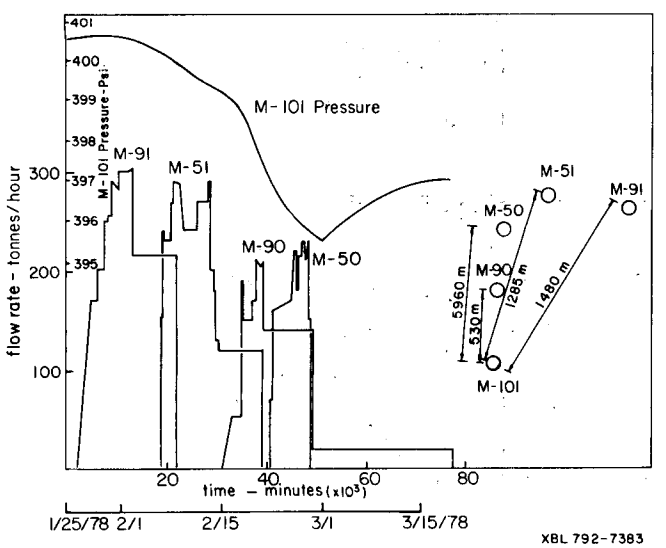

Figure 8. Measured pressures in well M-101, Cerro Prieto, with flow rates of four nearby wells superimposed.

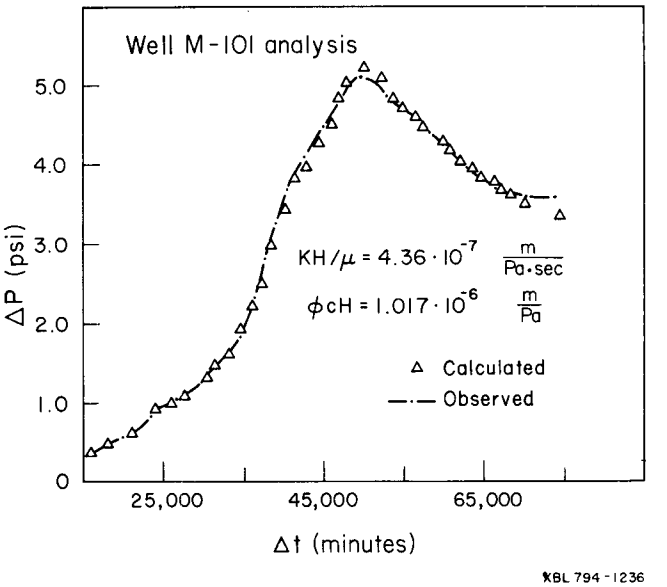

Figure 9. Calculated and observed pressure response of well M-101, Cerro Prieto.

Downhole temperatures are approximately the same through this portion of the field. The data were analyzed using an isothermal line-source, isotropic, homogeneous, infinite-aquifer, nonlinear, least-squares fitting routine to match the observation well data. Figure 8 illustrates measured pressure response with flows superimposed. Figure 9 shows calculated pressures versus observed pressures. The calculated transmissivity is 1.5 x 10^6 md-ft/cp (4.36 x 10^{-7} m^3/Pa·sec). A storativity value of 2.3 x 10^{-2} ft/psi (1.017 x 10^{-6} m/Pa) was also calculated. The calculated and observed pressure response fits rather well. However, due to he aforementioned subsurface geological characteristics, we feel our estimates are higher than they should be.

Another interference test was carried out in the eastern portion of the field. Well M-53 was developed during May 1978. The well was then put on line to supply steam to the power plant. M-104 was chosen as an observation well near M-53. Well M-10 was also observed during this time. Observation in these wells began about May 1 and concluded on July 17, 1978. Figures 10 and 11 show measured pressures in these wells. The initial pressure drop at M-10 was due to faulty equipment. This problem was fixed within a few days after the instrument was installed downhole. However, as noted in the figures, pressures began to increase immediately. Well M-10 is near the main producing field, and the measured pressure response should have been one of slow decline due to the nearby long-term production. M-104 was in an area of the field where no production had taken place within a few months before setting the instrument in the well. On May 5, 1978, an earthquake occurred

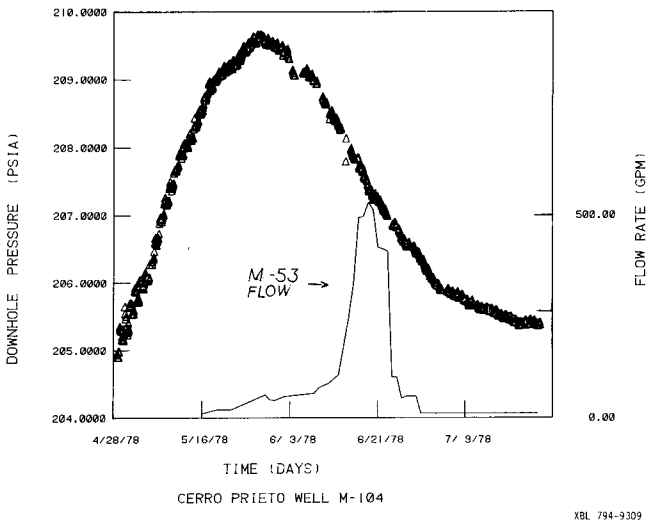

Figure 10. Cerro Prieto well M-104 pressure versus time with M-53 flow rates superimposed.

with an epicenter approximately 20 km south of Cerro Prieto, magnitude 5.1 (Richter).

Pressures continued to rise after the earthquake, then began falling. On May 16, 1978, well M-53 began production. Note in Figure 11 that a change in the slope of the pressure buildup occurred about two days later. (Equipment was checked during these periods and found to be functioning correctly.) The data obtained are not readily analyzable due to the unknown pressure buildup associated with the earthquake before flowing well M-53. However, using the transmissivity and storativity values obtained in the M-101 interference test, the pressure drop at the end of the observation period in M-104 should have been about 4 or 5 psi. The order of magnitude of the permeability, therefore, is similar to that in the southern portion of the

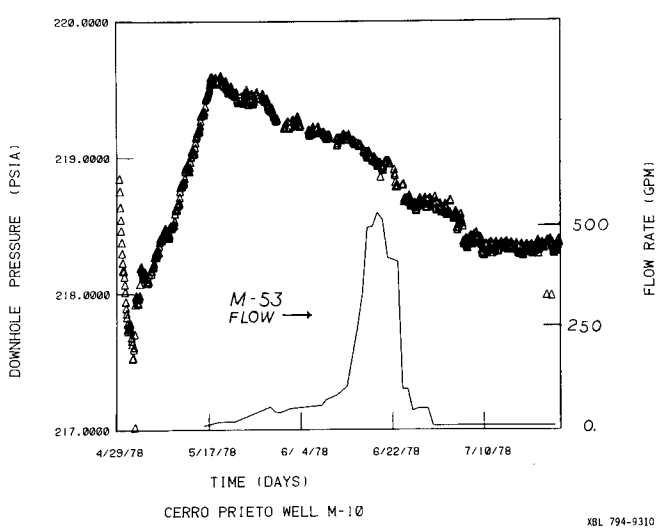

Figure 11. Cerro Prieto well M-10 pressure versus time with M-53 rates superimposed.

field. The subsurface geologic conditions are relatively the same in the eastern and southern portions of the field. However, another interference test should be carried out to determine if this indeed is the case.

In addition to the interference tests described above, there have been several productivity tests and two-rate flow tests performed during the development of the wells. Data have been examined for three two-rate tests. Wells M-51, M-90, and M-91 were varied in rate during their development. This was when M-101 was also monitored. The wells are all penetrating different aquifers, or combinations of aquifers. The presence of multiple aquifers, shale layers, or a combination of these is evident in the data, and makes unambiguous determination of the reservoir characteristics difficult. The use of reservoir simulation might allow a more acceptable model for the system to be developed.

The subsurface geological characteristics of the Cerro Prieto field are being clarified as new data become available from CFE's extensive drilling program. We have introduced our instrumentation and some computer programs to CFE personnel for interference and production well testing and for data analysis. CFE has begun an interference and production test in the southern and eastern portions of the field. Recent flowing pressure and temperature profiles in some of the wellbores may indicate two-phase flow in the well and possibly in the reservoir near the wellbore. One new well drilled in the eastern portion of the field exhibits bottomhole temperatures approaching 360°C.

Our plans in fiscal year 1979 include: downhole reservoir fluid sampling; two-phase wellbore numerical modeling; numerical reservoir modeling to match subsurface geological and fluid characteristics; and analysis of new interference and production well data.

All the information obtained to date, and new information becoming available, will give us an understanding of the Cerro Prieto geothermal field and will help to define similar geothermal fields in the United States.

East Mesa KGRA, California

East Mesa is at the eastern edge of the Salton Trough in the Imperial Valley of southern California. In fiscal year 1978, an agreement was negotiated with the U.S. Department of the Interior, Bureau of Reclamation, for well testing at the East Mesa site. The agreement included a review of all past well testing and analysis. In addition, productivity tests for wells 6-1, 6-2, 8-1, and 31-1 were agreed upon. Well 31-1 has no surface piping from the wellhead, and environmental restrictions prevented surface disposal. Hence, 31-1 was not tested, but the remaining tests were completed. A long-term interference test was also completed using well 8-1 as the flowing well while monitoring nearby wells (see Narasimhan et al., 1977a, b; Howard et al., 1979).

Table 2. Locations of site-specific reservoir engineering ativities during fiscal year 1979.*

Site	Activity
Susanville, California	Measurements, well siting and resource evaluation
Klamath Falls, Oregon	Measurements, resource evaluation
Valles Caldera, New Mexico	Resource evaluation
Cerro Prieto, Mexico	Measurements, resource evaluation
Others†	Measurements, resource evaluation

*Minor activities are expected to continue at Niland, East Mesa, and Heber, California, and Raft River, Idaho.
†This is still vague, since final committments at several geothermal sites have not yet been finalized.

The review of previous well testing at East Mesa provided estimates for the well productivity. Benson et al. (1979) summarize all the data for the USBR, Magma Power Co., and Republic Geothermal, Inc., wells from which the test data are available.

PLANS FOR FISCAL YEAR 1979

During fiscal year 1979, LBL reservoir engineering activities will be concentrated at the geothermal sites indicated in Table 2.

The first field test of fiscal year 1979 is under way at Susanville, were two flowing wells and eight observation wells are being used to delineate aquifer continuity and material parameters. Computer modeling is under way to evaluate the resource. At Cerro Prieto the measurement program for fiscal year 1979 is being negotiated to determine whether one long-term production test can be used to identify the inhomogeneities that have been identified from well logs and cores. Computer modeling using SHAFT78 (Pruess et al., 1978) have been started to evaluate previous measurements and to estimate the future two-phase behavior of the aquifers. All other activities are in the preparatory phase at this time.

REFERENCES

Benson, S., Goranson, C., and Schroeder, R., 1979. Well test data analysis methods at LBL. This report.

Benson, S., Goranson, C., Haney, J., McEdwards, D., Narasimhan, T. N., and Schroeder, R., 1979. A summary of well tests and analyses for the East Mesa geothermal site. This report.

CER Corporation, 1978. COSO geothermal exploratory hole no. 1, CGEH no. 1, Completion report. Las Vegas, U.S. Department of Energy, Nevada Operations Office, NV/0655-04.

Galbraith, R., 1978. Geological and geophysical analysis of Coso geothermal exploratory hole no. 1. (CGEH#1), Coso Hot Springs KGRA, California. Salt Lake City, University of Utah Research Inst., IDO/78-1701.b.4.2.

Goranson, C., and Schroeder, R., 1978. Static downhole characteristics of well CGEH-1 at Coso Hot Springs, California. Berkeley, Lawrence Berkeley Laboratory, LBL-7059.

——, 1979. Recent activities at the Cerro Prieto field, in Proceedings, First Symposium on the Cerro Prieto Geothermal Field, Baja California, Mexico, September 20-22, 1978. Berkeley, Lawrence Berkeley Laboratory, LBL-7098.

Goranson, C., McEdwards, D., and Schroeder, R., 1978a. Review of Desert Hot Springs well test. Berkeley, Lawrence Berkeley Laboratory, UCID-4028.

Goranson, C., Schroeder, R., and Haney, J., 1978b. Evaluation of Coso geothermal exporatory hole no. 1 (CGEH-1), Coso Hot Springs KGRA, China Lake, California, in Summaries, Fourth Workshop on Geothermal Reservoir Engineering. Stanford, Stanford University.

Howard, J., Apps, J. A., Benson, S., Goldstein, N. E., Graf, A. N., Haney, J., Jackson, D., Majer, E., McEdwards, D., McEvilly, T. V., Narasimhan, T. N., Schechter, B., Schroeder, R., Taylor, R., Van de Kamp, P., and Wolery, T., 1979. Geothermal resource and reservoir investigations of U.S. Bureau of Reclamation leaseholds at East Mesa, Imperial Valley, California. Berkeley, Lawrence Berkeley Laboratory, LBL-7094.

Lund, J., Lienau, P., Culver, G., and Svanevik, L., 1978. Geothermal hydrology and geochemistry of Klamath Falls, Oregon, urban area. Klamath Falls, Oregon Inst. Tech., Geo-Heat Utilization Center.

Narasimhan, T. N., Schroeder, R., Goranson, C., and Benson, S., 1977a. Results of reservoir engineering tests, 1977, East Mesa, California. Dallas, Soc. Pet. Eng. AIME, SPE-7482.

Narasimhan, T. N., Schroeder, R., Goranson, C., Campbell, D., and Barkman, J., 1977b. Recent results from tests on the Republic geothermal field, East Mesa, California. Berkeley, Lawrence Berkeley Laboratory, LBL-7017.

Narasimhan, T. N., and Witherspoon, P. A., 1977. Reservoir evaluation tests of RRGE-1 and RRGE-2, Raft River geothermal project, Idaho. Berkeley, Lawrence Berkeley Laboratory, LBL-5958.

Palmer, T. D., Howard, J. H., and Lande, D. P., 1975. Geothermal development of the Salton Trough, California and Mexico. Livermore, Lawrence Livermore Laboratory, UCRL-51775, 45 p.

Pruess, K., Schroeder, R., Zerzan, J., and Witherspoon, P., 1978. SHAFT78, a three-dimensional two phase computer program for geothermal reservoir simulation. Berkeley, Lawrence Berkeley Laboratory, LBL-8264 (Abstract).

Sammel, E. A., and Peterson, K. L. 1976. Hydrologic reconnaisance of the geothermal area

near Klamath Falls, Oregon, with a section on preliminary interpretation of geophysical data. Menlo Park, USGS open-file report WRI 76-127.

Sims, A., and Racine, W., 1977. Geothermal space/water heating for City of Mammoth Lakes. Sacramento, Energy Res. Cons. Devel. Comm., (contract no. 500-038 with Ben Holt Co.).

U.S. Bureau of Reclamation, 1976a. Water quality analysis, inferred geothermal temperatures and reservoir evaluation test. Sacramento, U.S. Dept. Interior, Bureau of Reclamation, Mid-Pacific Region.

____, 1976b. Susanville geothermal investigations, California, Supplemental Technical Data, Special Report. Sacramento, U.S. Dept. Interior, Bureau of Reclamation, Mid-Pacific Region.

MEXICAN-AMERICAN COOPERATIVE PROGRAM AT THE CERRO PRIETO GEOTHERMAL FIELD, BAJA CALIFORNIA, MEXICO

M. J. Lippmann, P. A. Witherspoon, and H. A. Wollenberg

INTRODUCTION

Mexico's Cerro Prieto geothermal field is the only liquid-dominated geothermal system presently generating electric power in North America. About 35 km south of Mexicali in Baja California, it is situated in the Sea of Cortez-Salton Trough and named after the nearby Cerro Prieto ("black hill") volcano (Figures 1 and 2).

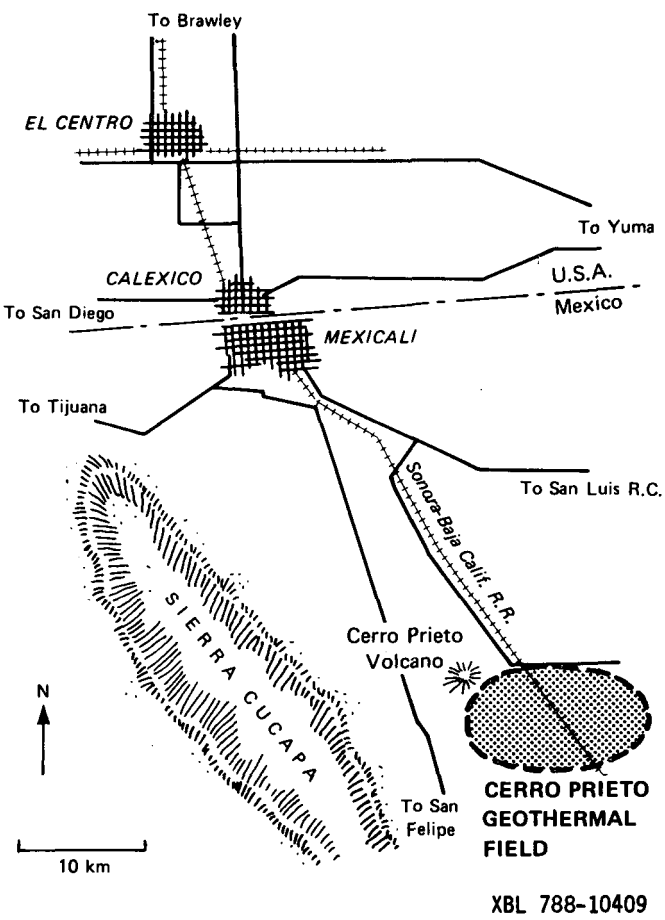

Figure 1. Location map of the Cerro Prieto geothermal field.

Production of electric power commenced in 1973. The Comisión Federal de Electricidad of Mexico (CFE), which manages and operates the field, plans to expand the power output from its current 75 MW to 150 MW by early 1979. In 1982, a 30-MW lower-pressure turbine will be installed to extract additional energy from the pressurized hot water presently not being used. The total generating capacity of the field is expected to reach 400 MW by 1985. This goal will be attained through an intensive drilling program, started in 1976, to provide steam for the power plants. The location of the wells within the Cerro Prieto field, as of October 1978, is given in Figure 3.

Geothermal studies are now being performed as part of a cooperative project, which was established and operated through an agreement signed on July 21, 1977, between CFE and the U.S. Department of Energy (DOE). Lawrence Berkeley Laboratory (LBL) coordinates U.S. technical activities carried out under this project. The Coordinadora Ejecutiva de Cerro Prieto of CFE is organizing all Mexican participation.

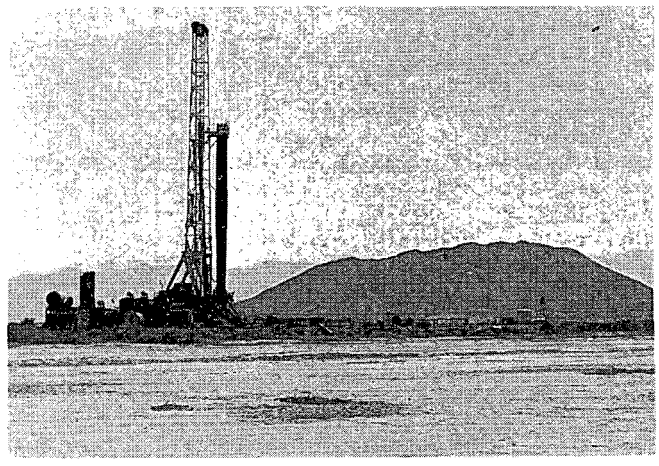

Figure 2. One of the drilling rigs in operation. Cerro Prieto volcano and the Sierra Cucapa in the background.

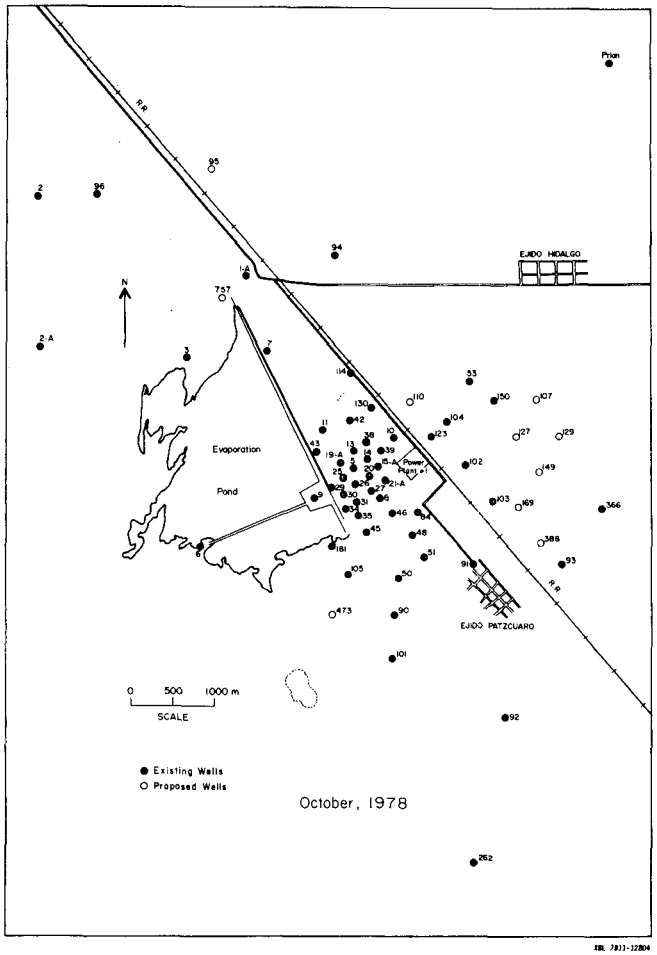

Figure 3. Cerro Prieto geothermal field well locations.

The principal scientific, technical, and governmental organizations cooperating in the Cerro Prieto project are listed below.

Mexico

Comisión Federal de Electricidad (CFE)
Instituto de Investigaciones Eléctricas (IIE)
Dirección General de Estudios del Territorio Nacional (DETENAL)
Centro de Investigación Científica y Educación Superior de Ensenada (CICESE)
Consejo Nacional de Ciencia y Tecnología (CONACYT)

United States

Department of Energy (DOE)
Lawrence Berkeley Laboratory (LBL)
U.S. Geological Survey (USGS)
University of California, Riverside (UCR)

The Cerro Prieto project incorporates studies of the geologic, hydrogeologic, geochemical, and geophysical settings of the geothermal field, as well as investigations of its structural, reservoir engineering, and subsidence characteristics.

The primary objective of the program is to develop an understanding of the geologic setting and hydrothermal circulation of the Cerro Prieto geothermal system. Through the scientific analysis of surface and subsurface geophysical and geochemical measurements, scientists and technicians will develop a thorough understanding of the nature and magnitude of the energy source and will determine the impact of exploiting a geothermal system of this type and size.

Cerro Prieto is considered an ideal system for studying the long-term response of a liquid-dominated geothermal field in continuous production. Much of the information obtained here will be applicable to the development of geothermal

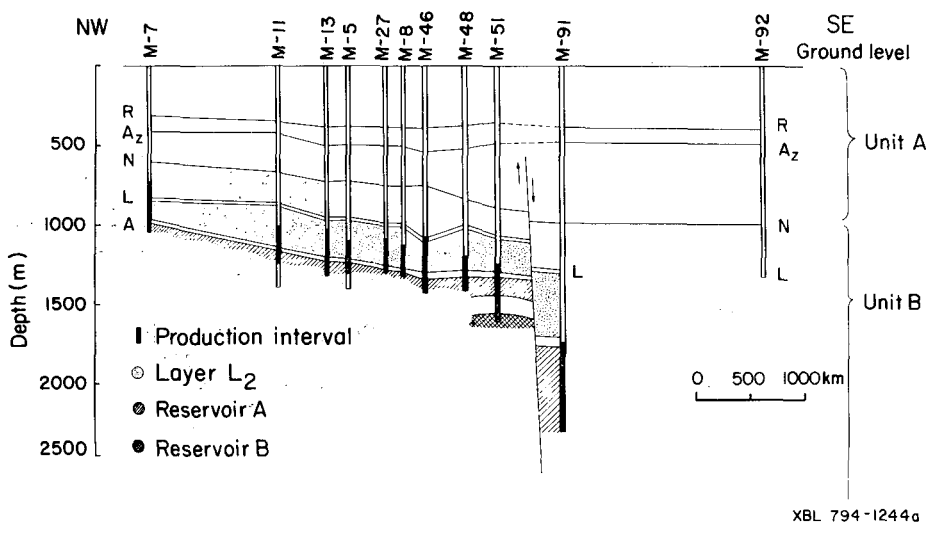

Figure 4. Northwest-southeast section across the Cerro Prieto field (modified from Abril and Noble, 1979).

resources in similar geologic settings such as the Mexicali Valley, Mexico, and the Imperial Valley, California. This information could be useful for geothermal development in other parts of the world.

FISCAL YEAR 1978 ACTIVITIES

Although the Cerro Prieto cooperative program started in fiscal year 1977, the activities carried out that year by the U.S. organizations consisted mainly of collecting and analyzing fluid samples and drill-cuttings, and interpreting data provided by the Mexican groups. The program began in earnest early in fiscal year 1978. Due to the extreme summer heat in the Mexicali Valley, most of the field activities were conducted from January to May 1978. The rest of the year was spent interpreting the collected information and preparing for the next season's field activities.

Most of the results obtained since the beginning of this international project were presented at the First Symposium on the Cerro Prieto Geothermal Field held in San Diego, September 20-22, 1978 (Lawrence Berkeley Laboratory, 1979). The geophysical, reservoir engineering, and reinjection work done at Cerro Prieto is discussed in detail elsewhere in this volume.

Geology

The information collected from the older and more recently drilled wells was used to develop a number of geologic cross sections of the Cerro Prieto area (Figure 4). CFE and LBL based their lithologic correlations mainly on the analysis of geophysical well logs. A number of these logs were digitized and computer programs were used to complement standard well-log correlation techniques. A study was begun to evaluate effects of wellbore cooling and complex mineralogies on geophysical well log responses (Lawrence Berkeley Laboratory, 1979).

Detailed petrologic and mineralogic studies of drill cuttings and cores were carried out by UCR. In the Cerro Prieto field, a number of regularly distributed metamorphic mineral zones could be recognized (Elders et al., 1977). These progressive changes in mineralogy seem to exhibit a systematic relationship with reservoir temperatures (Figure 5).

Information on this field was collected as needed and incorporated into the open-file data bank assembled at LBL (Lippmann et al., 1977).

Geophysics

Various electrical, gravity, and passive seismic surveys were completed by LBL and CFE during this year. The purpose of these ongoing studies was to determine the geologic structure and dimensions of the geothermal system and to establish a network to monitor changes in the reservoir properties and seismicity resulting from fluid extraction.

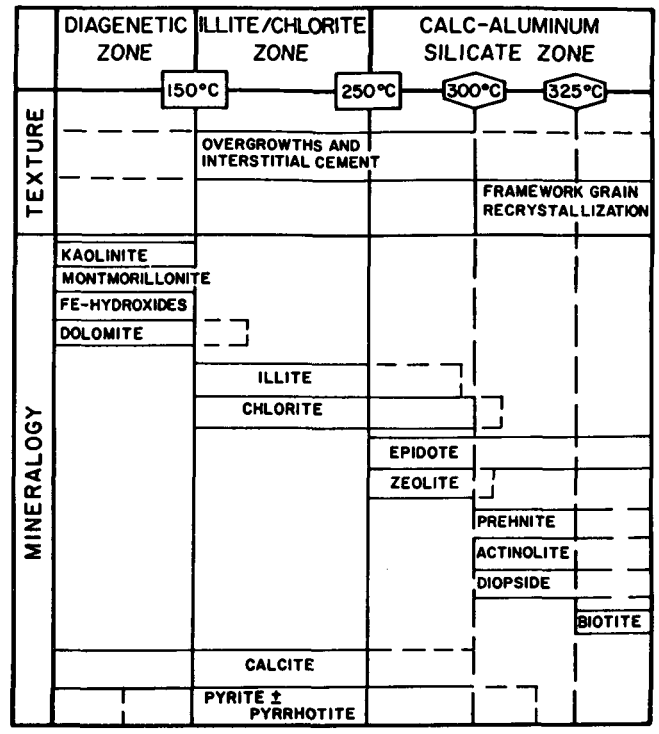

XBL 7812-14097

Figure 5. Temperature ranges of key minerals at Cerro Prieto (from Hoagland and Elders, 1978).

Reservoir Engineering

In fiscal year 1978 two long-term well-interference and build-up tests were carried out by LBL at Cerro Prieto, and CFE completed a number of two-rate flow tests. Preliminary simulation studies of reservoir behavior were also made. At the University of California, Berkeley, physical properties of core samples were measured at elevated pressures and temperatures.

Geochemistry

A great wealth of fluid chemical data has been collected at Cerro Prieto since the beginning of the field's development. During fiscal year 1978, analysis of this information continued, while new fluid and rock samples were gathered and analyzed.

CFE, USGS, UCR, LBL, and the Scripps Institution of Oceanography participated in the geochemical activities. The results are reported in various papers and reports (Lawrence Berkeley Laboaratory, 1979; Elders et al., 1977; Mañon et al., 1977; Truesdell and Mañon, 1979). These studies furnished information for preliminary geochemical model of the field. The most significant conclusions are as follows:

1. The geothermal waters at Cerro Prieto probably originate from Colorado River water rather than from local precipitation (Figure 6).

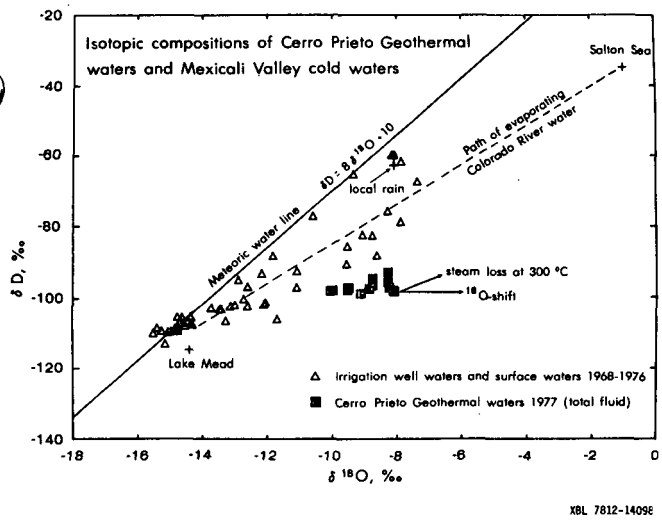

Figure 6. Isotopic compositions of Cerro Prieto geothermal waters and Mexicali Valley cold waters. Delta values are the hydrogen and oxygen isotope ratios, compared to standard mean ocean water (from Truesdell et al., 1979).

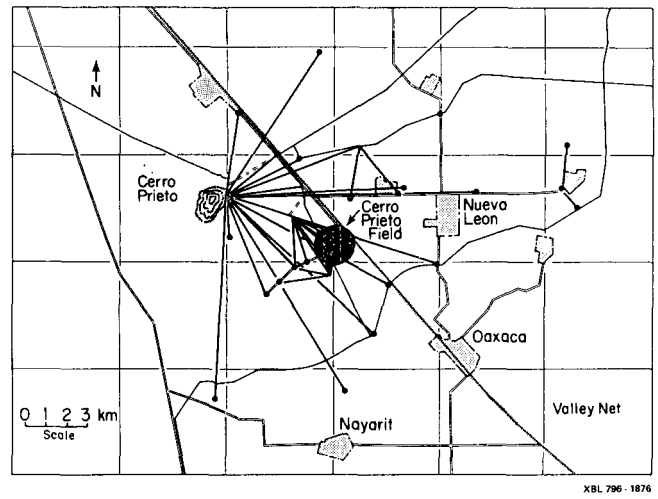

Figure 7. Local network of precise horizontal-control, Cerro Prieto geothermal field (map provided by U.S. Geological Survey).

2. Lowering of pressure apparently has caused boiling to occur in parts of the producing reservoir and has caused brine of lower chloride content to recharge the exploited aquifer.

3. Oxygen-isotope ratios of calcite combined with the mineralogy of cutting samples are used to predict the temperatures of fluid at depth while drilling.

4. Based on tritium analyses, the age of the Cerro Prieto fluids exceeds 50 years.

5. Most carbon dioxide in the Cerro Prieto reservoir appears to originate from metamorphism of detrital grains of marine carbonate minerals, altered during diagenesis of the sediments by mixture with organic-derived carbon.

6. Nitrogen and argon in the separated steam are probably of atmospheric origin; however, a small component of these elements may be derived from decomposition of organic matter.

7. The gaseous hydrocarbons in the separated steam probably originated from thermal metamorphism of the organic matter contained in the sediments.

8. Gases derived from the mantle become diluted at Cerro Prieto with crustal helium and dissolved air as they move toward the surface. The gases either reequilibrate at lower temperatures or are mixed with organic methane near the surface.

Subsidence

A first-order leveling control and two precise horizontal control networks were established and surveyed by DETENAL and USGS, respectively, in the Mexicali Valley (Figure 7). These nets tied the Cerro Prieto geothermal area to networks north of the Mexico-U.S. border. The results of this year's activities, including the stations' descriptions and measured distance and elevation data, are given in a number of papers and reports (Lawrence Berkeley Laboratory, 1979; USGS, 1978; Lofgren and Massey, 1979; and García G., 1978).

The geodetic information collected this year will constitute the baseline data for this area. Periodic monitoring surveys will allow the detection of regional as well as local horizontal and vertical ground surface deformations. The first resurveys of the nets are scheduled for early 1979.

Reinjection

The artificial recharge of the geothermal reservoir is an important consideration. In this respect preliminary studies were initiated of the feasibiltiy of reinjecting some of the brine produced. Numerical models simulated several possible well reinjection patterns and analyzed the thermal response of the geothermal reservoir.

Conferences

To discuss results and plan future activities, periodic topical meetings were held between U.S. and Mexican researchers. The First Symposium on the Cerro Prieto Geothermal Field was held in San Diego on September 20-22, 1978, followed by a field trip to the geothermal site. About 400 people from industry, universities, and national laboratories participated (Lawrence Berkeley Laboratory, 1979).

PLANNED ACTIVITIES FOR FISCAL YEAR 1979

LBL will continue coordinating the U.S. activities to be carried out at Cerro Prieto under the CFE/DOE agreement.

A three-dimensional geological model of the field will be developed, based on available information. Additional geophysical well logs provided by CFE will be digitized and analyzed. The effect of wellbore conditions and mineralogy on well-log interpretation will continue. Paleomagnetic studies will be carried out to establish the age of the Cerro Prieto volcano. Petrologic and mineralogic analysis of cores and cuttings will continue. The open-file data bank will be expanded as new information becomes available.

The precision gravity and dipole-dipole networks established in fiscal year 1978 will be resurveyed to determine changes related to geothermal fluid production. The resistivity and magnetotelluric nets will be expanded to cover a larger part of the geothermal system. Five downhole seismic stations will be installed in and around the present main production area. Passive seismic monitoring using temporary stations will also continue.

Additional long-term well tests will be performed to obtain more information on the hydraulic characteristics of the reservoir. The program of laboratory measurement of core properties will be expanded. Continued refinement of the geologic model will permit a more thorough simulation of the system's behavior.

Collection and analysis of fluid and rock samples will continue and the preliminary geochemical model of the geothermal system will be refined.

The regional and local horizontal networks will be resurveyed to monitor crustal deformations related to tectonic and man-made activities.

Experiments on silica precipitation from Cerro Prieto brines will be initiated. Numerical simulation of different reinjection schemes will continue. A group of U.S. and Mexican experts will analyze alternatives for a future full-scale reinjection experiment at Cerro Prieto, which might begin early in fiscal year 1980.

Periodic technical meetings of the project's participants will continue. The Second Symposium on the Cerro Prieto Geothermal Field will be held in Mexicali in October 1979 (fiscal year 1980).

REFERENCES CITED

Abril G., A., and Noble, J. E., 1979. Geophysical well log correlations along various cross sections of the Cerro Prieto geothermal field. in Proceedings, First Symposium on the Cerro Prieto Geothermal Field, Baja California, Mexico, September 20-22, 1978, San Diego. Berkeley, Lawrence Berkeley Laboratory, LBL-7098.

Craig, H., 1961. Standard for reporting concentrations of deuterium and oxygen-18 in natural waters. Science, v. 133, p. 1833.

Elders, W. A., Olson, E. R., Hoagland, J. R., Barker, C. E., Johnson, P. D., and Collier, P., 1977. A comprehensive study of samples from geothermal reservoirs: petrology and light stable isotope geochemistry of wells M-48, M-84, M-90, M-91, M-92 and Prian no. 1 in the Cerro Prieto geothermal field, Baja California, Mexico. University of California, Riverside, UCR/IGPP-77/37, 153 p.

Garcia G., J. R., 1978. Proyecto Cerro Prieto. Estudios de Nivelación de Primer Orden. DETENAL, internal report.

Hoagland, J. R., and Elders, W. A., 1978. Hydrothermal mineralogy and isotopic geochemistry in the Cerro Prieto geothermal field, Mexico; I, hydrothermal mineral zonation. Geoth. Res. Council, Trans., v. 2, pp. 283-286.

Lawrence Berkeley Laboratory, 1979. Proceedings of the first symposium on the Cerro Prieto geothermal field, Baja California, Mexico, September 20-22, 1978, San Diego, California. Berkeley, Lawrence Berkeley Laboratory, LBL-7098.

Lippmann, M. J., Domínguez, A., B., Wollenberg, H. A., and Witherspoon, P. A., 1977. Open-file data on the Cerro Prieto geothermal field. Berkeley, Lawrence Berkeley Laboratory, LBL-6321, 10 p.

Lofgren, B. E., and Massey, B. L., 1979. Monitoring crustal strain, Cerro Prieto geothermal field, Baja California, Mexico. U.S. Geological Survey, Open-file Report 79-204.

Mañon M., A., Mazor, E., Jiménez, M., Sanchez, A., Fausto, J., and Zenizo, C., 1977. Extensive geochemical studies in the geothermal field of Cerro Prieto, Mexico. Berkeley, Lawrence Berkeley Laboratory, LBL-7019, 113 p.

Truesdell, A.H., and Mañon M., A., 1979. Geochemical indications of boiling in the aquifer of the Cerro Prieto geothermal field, in Proceedings Primera Reunión de Intercambio Técnico sobre Geotermia, San Felipe, B.C. México, November 1977 (in press).

Truesdell, A. H., Rye, R. O., Pearson, F. J., Jr., Olson, E. R., Nehring, N. L., Huebner, M. A., and Coplen, T. B., 1979. Preliminary isotopic studies of fluids from the Cerro Prieto geothermal field, in Proceedings, First Symposium on the Cerro Prieto Geothermal Field, Baja California, Mexico, September 20-22, 1978, San Diego. Berkeley, Lawrence Berkeley Laboratory, LBL-7098.

U.S. Geological Survey, 1978. Subtask 6.B, Regional Trilateration, Open File Report, U.S. Geological Survey, Topographic Division, Mexicali Valley Geothermal Project, 25 p.

PRELIMINARY SIMULATION STUDIES RELATED TO THE CERRO PRIETO FIELD

M. J. Lippmann, G. S. Bodvarsson, and P. A. Witherspoon

INTRODUCTION

This year as part of the reservoir engineering activities carried out under the agreement between the Comisión Federal de Electricidad of Mexico (CFE) and the U.S. Department of Energy (DOE) to study the Cerro Prieto geothermal field, LBL began numerical modeling studies directed toward simulating the behavior of this geothermal system.

The Cerro Prieto geothermal field has been under large-scale production since 1973. At the present time, about 2,700 tonnes/hr of fluids (brine and steam) are extracted to generate 75 MW of electric power. No reinjection of cooled brines is being done. The vast amount of fluids produced over the last five years has changed some of the characteristics of the geothermal system. For example, there are geochemical evidences of boiling in the main reservoir (Truesdell and Mañon, 1979), and of recharge by cooler brines percolating down from shallower layers in response to the drawdown in the producing aquifer (Truesdell et al., 1979).

A number of questions are presently being asked as the development of the Cerro Prieto geothermal resource continues. How much pressure drawdown (and temperature reduction) should be expected as new wells and power plants are put on line? What will be the effects of brine reinjection? Where should the reinjection be done (at what points and depths) to optimize the mass and thermal recharge of the producing reservoir? What will be the rate and amount of ground surface deformation, if any, resulting from fluid extraction? What is the minimal recommended distance between wells? These are just some of the questions that could be answered with the help of simulation studies, provided an accurate geologic model of the geothermal system is available.

Based on the information presented at this symposium, three-dimensional models of the geologic structure and layering will be developed. During 1979 these models, in conjunction with computer codes available at Lawrence Berkeley Laboratory (LBL), will be used to simulate the behavior of the geothermal field in an attempt to answer some of the questions posed above.

ACTIVITIES IN FISCAL YEAR 1978

Some of the preliminary numerical simulation studies relevant to the Cerro Prieto field are discussed below. One study examines the effect of using standard (isothermal) well testing data analysis in geothermal (nonisothermal) systems. The second group of results, using a simplified model of the field, illustrates the effect of recharge from the upper and lower aquifers on the temperature of the producing geothermal reservoir.

PUMPING TEST SIMULATION

A number of well tests have been and will be carried out at Cerro Prieto to determine the hydraulic characteristics of the producing reservoir and of some geologic boundaries (Schroeder et al., 1979). The standard techniques used to analyze the collected data are in most cases based on isothermal models. The following cases are intended to illustrate the errors that may occur when data from nonisothermal systems are studied using isothermal methods.

Pumping tests in two different radially symmetric systems were simulated using the computer code CCC developed at LBL (Lippmann, et al., 1977). The only difference between the two cases was that in the first ("large system") the outer impermeable adiabatic boundary was placed 6,000 m from the center, and in the second ("bounded system") it was at 170 m. The initial temperature profile, the different layers and their properties are given in Figure 1 and Table 1. The upper and lower constant temperature boundaries were

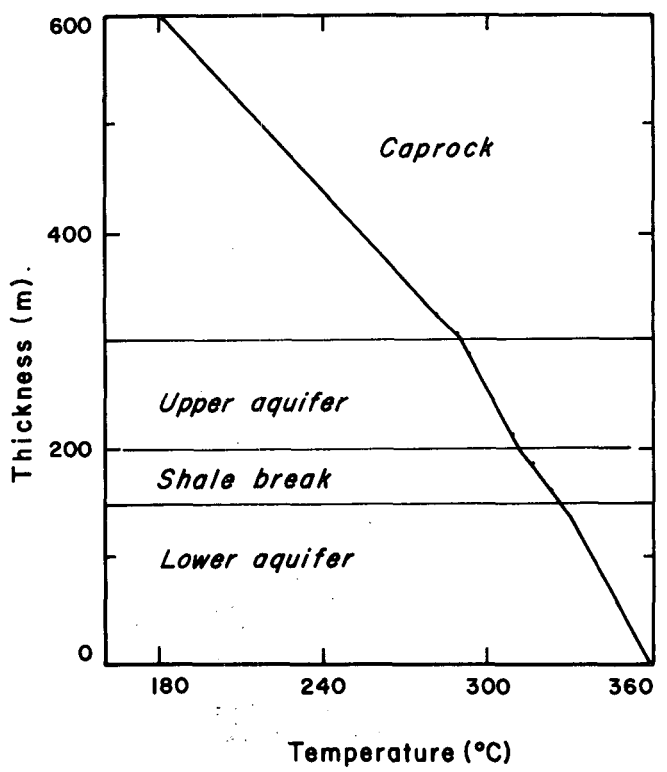

Figure 1. Pumping test simulation. Cross section of the model used and initial temperature profile.

Table 1. Material properties used for pumping test simulations.

Property	Lower aquifer	Shale break	Upper aquifer	Caprock
Intrinsic permeability (md)	80	0.5	50	0.005
Porosity	0.22	0.40	0.20	0.40
Specific storage (m^{-1})	10-4	1.6 x 10-3	10-4	1.6 x 10-3
Thermal conductivity (cal/sec·cm°C)	10 x 10-3	7.5 x 10-3	10 x 10-3	6.0 x 10-3
Heat capacity (cal/g°C)	0.250	0.230	0.250	0.230

assumed to be closed to fluid flow. A fully penetrating well was placed into the lower aquifer at the center of the system producing at a constant rate of 100 tonnes/hr. The resulting pressure response was observed in the lower and upper aquifer at a node located at a distance of 12.76 m from the axis.

The effect of temperature on pressure drawdown was analyzed by comparing the results from a nonisothermal system with those from an isothermal one whose temperature and fluid properties corresponded to the average values of the lower (pumped) aquifer of the nonisothermal system. In the nonisothermal case, the initial heat flow rate across the system was 22×10^{-6} cal·cm^{-2}·sec^{-1}, and the fluid density and viscosity were temperature dependent. In the isothermal case the temperature was 343.6°C; the fluid density 641.6 kg·m^{-3}; and the viscosity 7.59×10^{-2} cp.

Large System

The results obtained from the numerical simulations are given in Figure 2 and Tables 2 and 3.

In the lower (pumped) aquifer, at the node located at a radial distance of 12.76 m from the axis, the pressure changes in the isothermal and nonisothermal cases are almost identical. Especially at earlier times, the drawdowns computed are somewhat larger than those of Hantush's (1960) solution for $\beta = 5 \times 10^{-3}$. The parameters used in the numerical model give a value of $\beta \cong 6.7 \times 10^{-3}$ which would further reduce the drawdown. This difference can be attributed to the assumptions used in the analytical solution, which are not strictly true in the numerical model. Hantush's β-solution, which is valid for small values of time (in our case t < 1115 days), assumes that the flow is horizontal in the (lower) aquifer and vertical in the shale break.

In the upper (unpumped) aquifer at early times there are some minor differences between the pressure drawdown determined in the nonisothermal and isothermal cases. However, this difference, in percentage, diminishes with time (Table 3). Reasonable agreement was obtained between the computed drawdowns in the upper aquifer and those corresponding to the analytical solution of Neuman and Witherspoon (1969). Because of the number of dimensionless parameters to be matched and the difficulty in reading accurately the graphs available for Neuman and Witherspoon's solution, only a few values were compared.

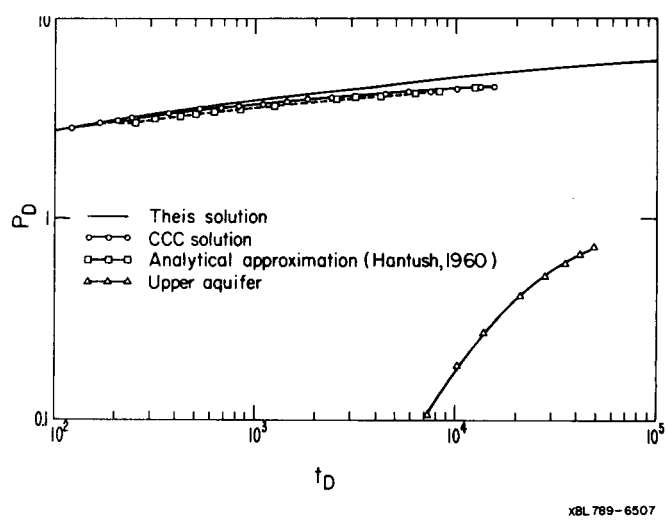

Figure 2. Pumping test simulation of the large system; plot of P_D vs t_D.

Table 2. Pumping test simulation--larger system; pressure drawdown in the lower aquifer.

	ΔP (Pascals)			Dimensionless			
				Numerical		Analytical	
	Numerical		Analytical	Isothermal (343.6°C)			
Time (days)	Isothermal (343.6°C)	Nonisothermal	Isothermal (343.6°C)	t_D	P_D	t_D	P_D
10	0.1418×10^6	0.1422×10^6	0.1380×10^6	352	3.26	352	3.17
30	0.1599×10^6	0.1604×10^6	0.1576×10^6	1055	3.67	1055	3.62
100	0.1750×10^6	0.1756×10^6	0.1749×10^6	3518	4.02	3518	4.02
406	0.1919×10^6	0.1927×10^6	0.1915×10^6	14270	4.41	14270	4.40

Bounded System

The drawdown in the lower aquifer was observed at the same point as in the larger system. The outer radial boundary, which is closed to any flow, is 170 m from the axis of the system. That is, the ratio between the radial distance from the axis to the boundary (r_e = 170 m) and the observation point (r = 12.76 m) is equal to 13.32. The pressure drawdowns obtained are shown on Figure 3 and Table 4. The numerical results are compared with the analytical results presented by Witherspoon et al. (1967, Appendix L).

Small differences are observed between the pressure changes computed for the isothermal and nonisothermal systems. Note that as time increases the relative differences also increase. At early times, the numerical results fall between the analytical results corresponding to r_e/r equal to 10 and 15. At later times as leakage becomes important, the numerically calculated drawdowns are smaller than the analytical ones. In the analytical solution no leakage into the pumped aquifer is assumed.

Table 3. Pumping tests simulation--larger system; pressure drawdown (in pascals) in the upper aquifer.

Time (days)	Isothermal (343.6°C)	Nonisothermal
10	2.93×10^1	2.74×10^1
30	6.32×10^2	5.99×10^2
100	1.21×10^4	1.16×10^4
204	4.75×10^4	4.62×10^4
406	1.20×10^5	1.19×10^5

Remarks

The results of the described numerical simulations indicate that isothermal data analysis of pumping tests performed in nonisothermal system are warranted under the following conditions.

1. The fluid properties used in the analysis should correspond to the average values of the producing aquifer.

2. The mass flow should be essentially horizontal (isothermal) in the pumped aquifer, toward the producing well.

In the simulations presented, both conditions have been met in the lower (pumped) aquifer. This was true at most times in the larger system and at earlier times in the bounded system. As the amount of leakage increases in response to the larger pressure drops in the producing reservoir, the flow in the lower aquifer tends to have a vertical component. This results in changes in

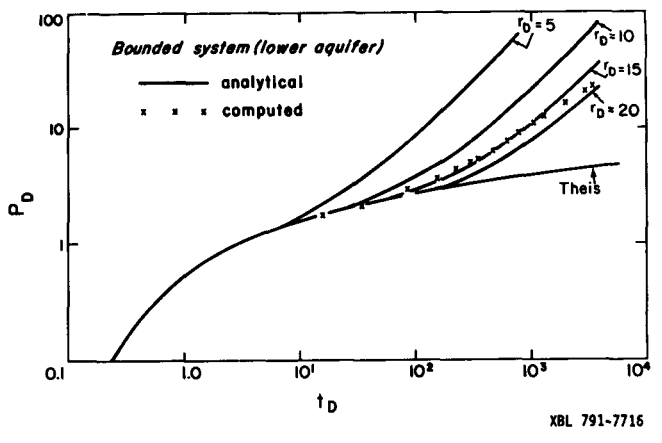

Figure 3. Pumping test simulation of the bounded system; plot of P_D vs t_D for the lower aquifer.

Table 4. Pumping test simulation of the bounded system; pressure drawdown (in pascals) in the lower aquifer.

	Numerical		Analytical	
Time (days)	Isothermal (343.6°C)	Nonisothermal	Isothermal (343.6°C) $r_D = 10$	$r_D = 15$
10	0.2376×10^6	0.2384×10^6	0.3725×10^6	0.2207×10^6
30	0.4832×10^6	0.4872×10^6	0.9385×10^6	0.4722×10^6
100	0.9991×10^6	0.1007×10^7	0.3134×10^7	0.1415×10^7

the reservoir temperature and in the viscosity and density of its fluids, and is reflected in the increasing, but small differences in the computed pressure changes in the isothermal and nonisothermal systems (Table 4).

In the upper (unpumped) reservoir and the shale break, between both aquifers, the water movement has a vertical component resulting in nonisothermal flow. The small differences observed in Table 3 are the result of changes in temperature-dependent fluid properties in these layers and differences with those of the pumped aquifer, which in the isothermal case are used throughout the system. In other words, if the flow field created in response to production tends to move waters across zones of different temperatures, a nonisothermal analysis of the well-test data would be more adequate. The degree of error introduced by an isothermal analysis will depend on the variations in fluid temperature and properties, especially viscosity.

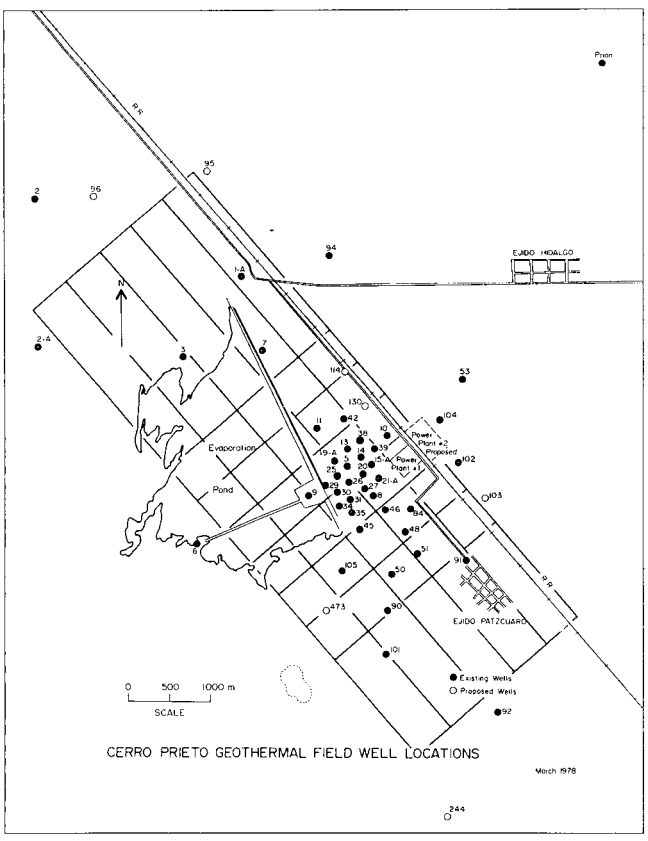

XBL 793-8725

Figure 4. Plan view of the mesh used in the three-aquifer system simulation and its relation to the Cerro Prieto field.

THREE-AQUIFER SYSTEM

The purpose of the second group of simulations is to study the temperature variations in a liquid-dominated geothermal reservoir under production when there is leakage through less permeable layers above and below. The waters recharging the reservoir will have not only different temperatures but also different chemical characteristics. The chemical changes will not be studied here. However, the following relation should be kept in mind. The ratio of the volume of aquifer, where the original water has been replaced and possibly chemically changed (V_H), to the volume where the temperature has been altered (V_T) is equal to,

$$\frac{V_H}{V_T} = \frac{(1-\phi)\rho_R c_R + \phi\rho_F c_F}{\phi \quad \rho_F c_F}$$

where ϕ is porosity, ρ is density, c specific heat capacity, and the subindices R and F refer to the rock and fluid, respectively.

Case 1

In this numerical study a simplified model of the Cerro Prieto reservoir was used. A plan view of the three-dimensional mesh used is given in Figure 4, which also shows its relation to the present field. Figure 5 presents a cross-section of the model, and the initial temperature profile across it. On top of the "upper shale break" and below the "lower shale break" two constant pressure and temperature aquifers are assumed to exist. The lateral boundaries of the system are assumed to be impermeable and adiabatic. Table 5 lists the properties used for the different layers.

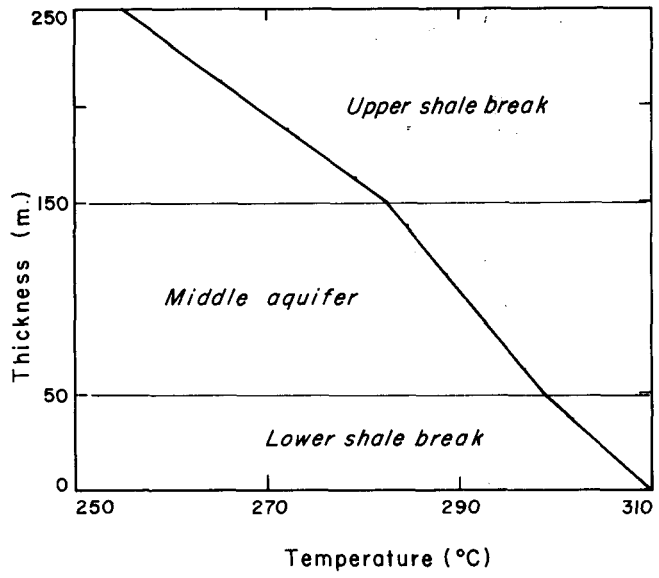

XBL 789-2078

Figure 5. Cross section of model and initial temperature distribution used in the three-aquifer system simulations.

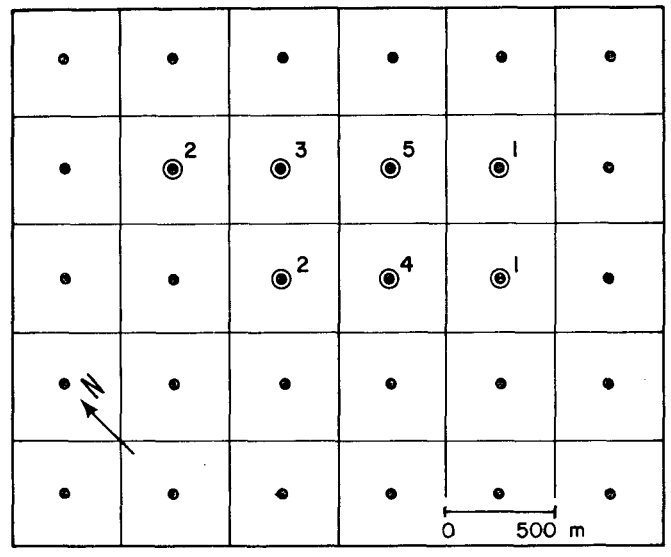

XBL 791-7316

Figure 6. Distribution of wells within the central (square) mesh used in the three-aquifer system simulations. The values indicate the number of wells in the different nodes.

It is assumed that the total fluid production rate from the middle reservoir is 2400 tonnes/hr, divided uniformly among 18 totally penetrating wells. The distribution of the wells within the mesh are given in Figure 6. Figures 4 and 6 should be used to orient, within the field, the results shown in figures that follow. Figure 7 shows the temperature change at the top and bottom of the middle reservoir after five years of continuous production. There is a decrease of temperature at the top and an increase at the bottom, as colder waters leak into the aquifer from above and warmer ones from below. The greater temperature changes at the top are a result of higher permeabilities in the upper shale break.

Table 6 lists the mass of water coming into the system from the upper and lower reservoir and its percentage of total production. In the first year most of the fluid produced (82%) comes from the middle aquifer and both shale breaks. As time goes on, the leakage from the upper and lower aquifers increases; it reaches 93.4% of the total fluid produced between the third and fifth year. The change in the average temperature of the middle aquifer (1.75×10^9 m^3) over the five-year period is only -0.31°C.

Table 5. Material properties used in the three-aquifer system.

Property	Lower aquifer	Lower shale break	Middle aquifer	Upper shale break	Upper aquifer
Intrinsic permeability (md)	80	0.5	50	2.5	50
Porosity	0.22	0.40	0.20	0.40	0.20
Specific storage (m^{-1})	10^{-4}	1.6×10^{-3}	10^{-4}	1.6×10^{-3}	10^{-4}
Thermal conductivity (cal/sec·cm°C)	10×10^{-3}	7.5×10^{-3}	10×10^{-3}	6.0×10^{-3}	10×10^{-3}
Heat capacity (cal/g°C)	0.250	0.230	0.250	0.230	0.250

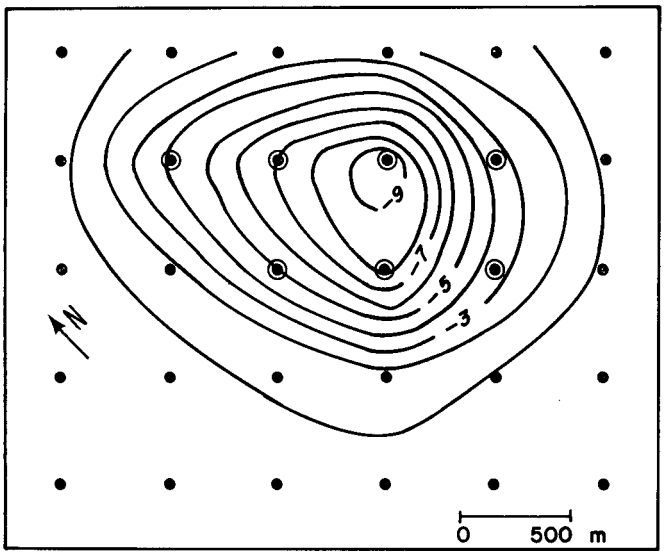

XBL 791-7313

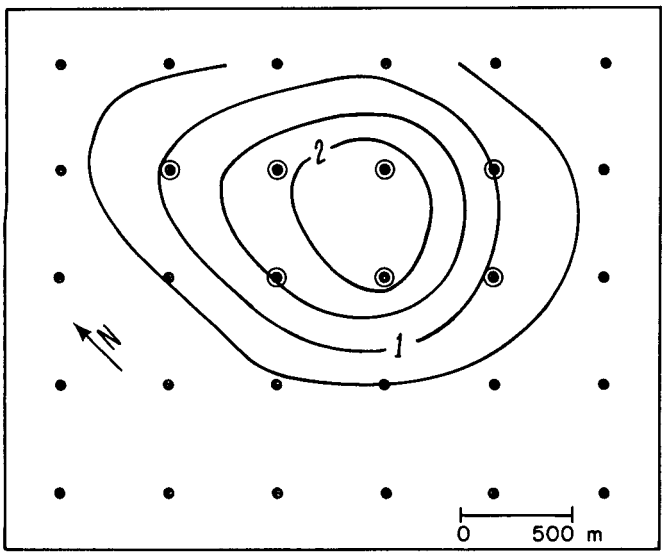

XBL 791-7314

Figure 7. Three-aquifer system (Case 1). Change in temperature (°C) after five years of continuous production (A) at the top and (B) at the bottom of the middle aquifer.

However, under these assumed conditions, the changes in chemical characteristics of the produced fluids should be appreciable.

Comparison with Case 1

In order to evaluate the effects of the different hydraulic properties of the shale breaks on the temperature (and possibly chemistry) changes in the producing reservoir, a number of cases were studied and compared with the changes observed in Case 1.

In reviewing these results, the thought occurred to us that the porosity of the shale breaks (40%) was too high. A case was studied in which the porosity of these shales was reduced to 5%, all other parameters kept unchanged. The differences in temperature changes in the middle aquifer with respect to those of Case 1 were less than 1%. This can be explained because the heat capacity of the shale layers ($c_s\rho_s$), which is assumed to be equal to a weighted average of the fluid rock capacities [that is, $c_s\rho_s = (1 - \phi)\ c_R\rho_R + \phi c_F\rho_F$] is only slightly changed with porosity. Using the average values for the shale and water under the simulated conditions (that is, $c_R = 230\ \mathrm{kcal \cdot kg^{-1} \cdot {}^oC^{-1}}$; $\rho_R = 2600\ \mathrm{kg \cdot m^{-3}}$; $c_F = 750\ \mathrm{kcal \cdot kg^{-1} \cdot {}^oC^{-1}}$; and $\rho_F = 757\ \mathrm{kg \cdot m^{-3}}$), $c_s\rho_s \simeq (598 - 30\phi)\ \mathrm{kcal \cdot m^{-3} \cdot {}^oC^{-1}}$. Reducing the shales porosity from 40 to 5% increased their heat capacity by only 1.8%, thus only slightly affecting the temperature change of the waters moving from the upper and lower aquifers toward the producing reservoir.

Three other cases listed on Table 7 were considered. The change in average temperature of the pumped aquifer and the mass of water leaking into the system from the upper and lower aquifers, after one year of production, are given in Table 8. The corresponding changes in temperature in the upper and lower part of the middle aquifer, for Cases 1, 2, and 3 are given on Figure 8. For Case 4, the changes are minor; at all points they are below 0.1°C.

In reviewing Table 8 and Figure 7, it is evident that it is quite important to determine as well as possible the properties of the less permeable layers above and below the producing aquifer. For example, a decrease in specific storage of the shales (Case 3) increases the amount of water leaking into the system, composed by the middle aquifer and the shale breaks. A decrease in permeability in one or both shales reduces and alters the recharge pattern into the system (Cases 2 and 4).

Table 6. Three-aquifer system simulation (Case 1).

Period (yr)	Total production (kg)	Mass (kg) flowing into system from: Upper reservoir	Lower reservoir
0 - 1	2.100×10^{10}	2.775×10^{9} (13.2%)	1.016×10^{9} (4.8%)
1 - 3	4.203×10^{10}	2.095×10^{10} (49.8%)	8.532×10^{9} (20.3%)
3 - 5	4.203×10^{10}	2.754×10^{10} (65.5%)	1.172×10^{10} (27.9%)

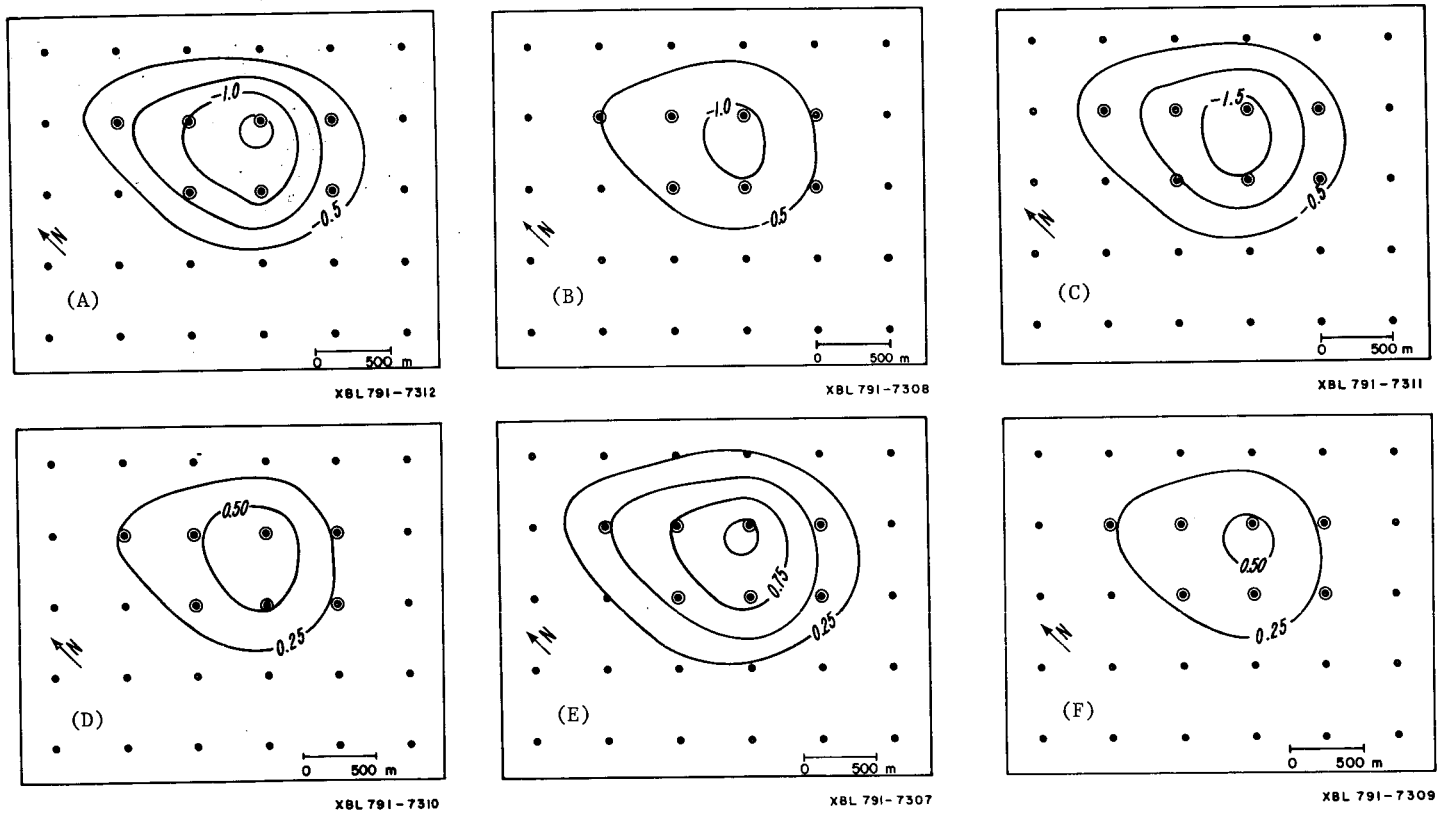

Figure 8. Three-aquifer system. Change in temperature (°C) in the upper (A,B,C) and lower (D,E,F) part of the middle aquifer after one year of production. Case 1 (A and D), Case 2 (B and E), and Case 3 (C and F).

Table 7. Hydraulic properties of the shale breaks in the three-aquifer system (all other properties unchanged).

Case	Property	Upper shale break	Lower shale break
1	Intrinsic permeability (md)	2.5	0.5
	Specific storage (m^{-1})	1.6×10^{-3}	1.6×10^{-3}
	Porosity	0.4	0.4
2	Intrinsic permeability (md)	0.5	0.5
	Specific storage (m^{-1})	1.6×10^{-3}	1.6×10^{-3}
	Porosity	0.4	0.4
3	Intrinsic permeability (md)	2.5	0.5
	Specific storage (m^{-1})	1.6×10^{-5}	1.6×10^{-5}
	Porosity	0.05	0.05
4	Intrinsic permeability (md)	2.5×10^{-2}	5.0×10^{-3}
	Specific storage (m^{-1})	1.6×10^{-5}	1.6×10^{-5}
	Porosity	0.05	0.05

Remarks

In the examples just described, it has been shown that appreciable variations are possible in the amount of recharge and the temperatures observed in a producing reservoir, depending on the leaky aquifer conditions that are present. As mentioned before, the difference in leakage patterns will also affect the chemical characteristics in the producing reservoir as the amount of waters from various sources changes.

At Cerro Prieto, geochemical evidences of leakage from above into the producing reservoir have been described (Truesdell, et al., 1979). The amount of leakage and its evolution in time are presently not known and could be studied using computer models simulating mass, heat and chemical transport throughout the geothermal system. For this purpose, several parameters would be needed, among them the hydraulic properties of the leaky layers which control the cross flow between different aquifers. Laboratory studies of cores and well test data analysis, as described by Witherspoon and Neuman (1972), will be needed. Planning of future well-testing activities at Cerro Prieto should include wells opened in the less permeable layers.

PLANNED ACTIVITIES FOR FISCAL YEAR 1979

Preliminary models of the geology of the Cerro Prieto field are being developed. In 1979, numerical simulations of the reservoir behavior will be made based on these models. The first efforts in predicting the response of the system to the increasing development of the field will be restricted to mass and heat calculations in the present main area of production. Later, ground deformations and chemical transport calculations may be added and the simulations extended to cover the entire Cerro Prieto geothermal anomaly.

REFERENCES CITED

Hantush, M. S., 1960. Modification of the theory of leaky aquifers. J. Geophys. Res., v. 65, pp. 3713-3725.

Lippmann, M. J., Tsang, C. F., and Witherspoon, P. A., 1977. Analysis of the response of geothermal reservoirs under injection and production procedures. 47th Annual Calif. Reg. Mtg. Soc. Petrol. Engr. AIME, Bakersfield, CA, April 13-15, 1977 (SPE 6537, LBL-6328).

Table 8. Three-aquifer system simulation (after one year of production).

Case	Change in average temperature of middle aquifer (°C)	Mass (kg) flowing into systems from Upper reservoir	Lower reservoir
1	-5.5×10^{-2}	2.78×10^{9}	1.02×10^{9}
2	-8.0×10^{-4}	6.24×10^{7}	1.65×10^{9}
3	-5.3×10^{-2}	1.13×10^{10}	4.86×10^{9}
4	-5.2×10^{-3}	2.09×10^{8}	7.36×10^{7}

Neuman, S. P., and Witherspoon, P. A., 1969. Transient flow of ground water to wells in multiple-aquifer systems. Berkeley, Dept. Civil Engr., Inst. Transp. Traffic Engr., Univ. California, Publ. 69-1, 182 p.

Schroeder, R. C., Goranson, C. B., Benson, S. M., and Lippmann, M. J., 1979. Well interference tests at the Cerro Prieto geothermal field, Baja California, Mexico, in Proceedings, First Symposium on the Cerro Prieto Geothermal Field, Baja California, Mexico, September 20-22, 1978, San Diego. Berkeley, Lawrence Berkeley Laboratory, LBL-7098.

Truesdell, A. H., and Mañon M., A., 1979. Geochemical indications of boiling in the aquifer of the Cerro Prieto geothermal field. Proc. Primera Reunión Intercambio Técnico sobre Geotermia, San Felipe, Baja California, November 1977 (in press).

Truesdell, A. H., Mañon M., A., Jiménez, M., Sánchez, A., and Fausto, J., 1979. Geochemical evidence of drawdown in the Cerro Prieto geothermal field, Baja California, Mexico, in Proceedings, First Symposium on the Cerro Prieto Geothermal Field, Baja California, Mexico, September 20-22, 1978, San Diego. Berkeley, Lawrence Berkeley Laboratory, LBL-7098.

Witherspoon, P. A., Javandel, I., Neuman, S. P., and Freeze, R. A., 1967. Interpretation of aquifer gas storage conditions from water pumping tests. New York, Amer. Gas Assoc., 273 p.

Witherspoon, P. A., and Neuman, S. P., 1972. Hydrodynamics of fluid injection, in Cook, T. D., ed., Underground waste management and environmental implications. Amer. Assoc. Petrol. Geol., Mem. 18, pp. 258-272.

STUDY OF ALTERNATIVE REINJECTION SCHEMES FOR THE CERRO PRIETO GEOTHERMAL FIELD, BAJA CALIFORNIA, MEXICO*

C. F. Tsang, G. S. Bodvarsson, M. J. Lippmann, and J. Rivera R. †

INTRODUCTION

It has become generally accepted that reinjection will be necessary for optimizing the exploitation of a geothermal field. Not only does this provide a way to solve the problem of disposal of cooled geothermal brine, it also serves the purpose of maintaining reservoir pressure, thus reducing possible subsidence effects, and sustaining production flow rates. In addition, reinjection enhances thermal energy extraction from the reservoir rocks.

However, reinjection creates a zone of relatively cold water aorund each injection well that will grow with time and eventually reach the production wells. When the cold water arrives ("breaks through") at the producing wells, the efficiency of the operation may be drastically reduced. It is therefore important to design the system of injection wells to prevent cold water breakthrough before a specified time. For a given production field, it is essential that both the location and flow rates of the injection wells be optimized.

In this project, possible reinjection patterns for the Cerro Prieto geothermal field, Baja California, Mexico, were studied. Recent water-level data in the production area have indicated a decline in the reservoir pressures (Bermejo et al., 1979) and the subsequent inflow of lower temperature water into the production region (Truesdell et al., 1979). Reinjection would aid in stabilizing the reservoir pressure and minimizing the inflow of the colder water.

ACTIVITIES IN FISCAL YEAR 1978

The different reinjection schemes were studied using a two-dimensional steady-state model based on work of Gringarten and Sauty (1975).

This model, which assumes constant fluid property parameters, is capable of simulating a system of many production and injection wells in a horizontal aquifer system. In such a system, steady-state fluid flow is expected within a relatively short time. Then the fluid velocity may be written down explicitly as a sum of contributions from each well. Natural regional flow in the reservoir can also be included very simply. Along each flow line thus constructed, the temperature is evaluated by considering heat transfer with bedrock and caprock, and by assuming instantaneous local thermal equilibrium between fluid and rock matrix. It is true that more sophisticated numerical models are available; but due to their complexity, nearly all of these are limited to the study of a small number of wells, or wells arranged in a highly symmetrical pattern. The simpler model adopted for the present work has the great advantage of being able to handle a system of many production and injection wells located throughout the field.

At Cerro Prieto, about 16 production wells are directing steam to the power plant and the

*This paper is extracted from Tsang et al., 1978a.

†Comisión Federal de Electricidad, México, D. F., México.

separated brine is disposed to a large evaporation pond. This study explores the effect of reinjecting part of the produced water into the reservoir. At the present time a total of about 2,750 m^3/hr of brine-steam mixture is being produced.

In our calculations, we assume that 50% of the produced fluids (1,375 m^3/hr), will be reinjected into three or four wells. The thickness of the actual aquifer varies from place to place. We do not have enough data to obtain a typical average thickness. However, we assume a reasonable value of 250 m. The breakthrough time at the production wells (the time it takes for cold water to reach the production wells) is simply proportional to this thickness. Further field tests are now being performed at Cerro Prieto to establish the characteristics of this geothermal system. As more data come in and as the geological model of the field is improved, a more detailed analysis will be made.

Figure 1 shows the positions of all the wells used in the study. A well label beginning with M represents a currently existing well. A well label beginning with X represents a hypothetical reinjection well yet to be drilled and tested for injection. Only three or four of the wells are used for injection in any particular case. Thus not all the wells indicated are used at the same time. The production wells indicated in the figure are those currently used to supply steam to the Cerro Prieto power plant. They are located toward the northeast, next to the railroad. Note that wells M-11 and M-42 are somewhat separated from the rest of the producing wells and are relatively closer to wells M-3 and M-7. This will have certain implications if M-3 and M-7 are used for reinjection, as is shown below.

All together, 13 alternative reinjection schemes have been studied. Eight of these

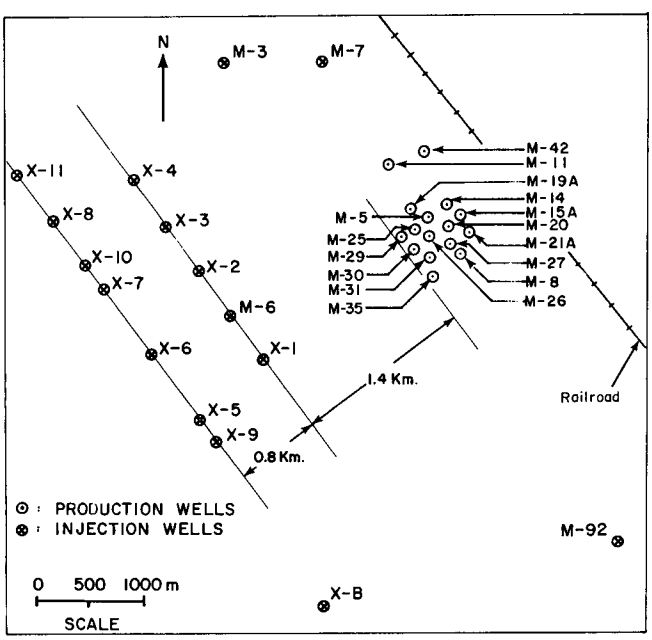

XBL 783-482

Figure 1. Relative locations of the production and injection wells used.

assume that we basically use the presently available wells outside the production region for reinjection. The other five cases assume a line of four injection wells southwest of the production area. The parameters assumed in these calculations are listed in Table 1, and the results are summarized in Table 2. The first and second breakthrough times shown in Table 2 are the earliest times required for cold water to break through at any two production wells, the numbers of which are indicated in brackets. A brief description of these runs follows.

Run #1. Water is injected into the existing wells, M-3, M-6, M-7, and M-92, at the rate of 343.75 m^3/hr at each one. On the other hand, the 16 production wells, operating at the same rate, produce a total of 2,750 m^3/hr. The results indicate that the first breakthrough of cold water will occur at well M-11 after about 32 years, due to cold water from well M-7. Note that the second breakthrough does not occur until 18 years later. Thus, if M-11 is discarded as an active production well after approximately 32 years, production from the other wells remains undisturbed for an additional 18 years. During these 18 years, M-11 will serve as a screening well (Tsang et al., 1978b).

Run #2. In this run the injection rates in wells M-7 and M-6 are smaller than in run #1, but the total injection rate of 1,375 m^3/hr is maintained. As expected, this variation improves the breakthrough times from wells M-7 and M-6, but only by five and two years, respectively.

Run #3 (Figure 2). In the first two runs, injection well M-7 was determined to be the critical well with respect to breakthrough times. Therefore, M-7 is omitted in this run and the total injection rate is maintained by doubling the injection rate at M-92. The results obtained show considerable improvement, as breakthrough occurs at well M-29 after 56 years.

Run #4 (Figure 3). For this run, a fourth injection well, X-B, is added to the three employed in run #3. The injection rates are unequally distributed, and the total injection

Table 1. Constants used.

Rock thermal conductivity	=	0.006 cal/cm/sec/°C
Intial reservoir temperature	=	300°C
Injected water temperature	=	100°C
Aquifer thickness	=	250 m
Aquifer porosity	=	19%
Rock volumetric heat capacity	=	0.5 $cal/cm^3/°C$
Density of brine	=	$1 g/cm^2$

Table 2. Summary of reinjection studies for the Cerro Prieto geothermal field.

Run	Inj. wells	Inj. rate (m^3/hr) each	Inj. rate (m^3/hr) total	No. prod. wells	Prod. rate (m^3/hr) each	Prod. rate (m^3/hr) total	Breakthrough time (years) 1st (well)	Breakthrough time (years) 2nd (well)	Comments
1	M-3	343.75	1375	16	171.88	2750	82 (M-19A)	107 (M-5)	
	M-6	343.75					60 (M-30)	61 (M-29)	
	M-7	343.75					32 (M-11)	50 (M-5)	
	M-92	343.75					169 (M-25)	170 (M-8)	
2	M-3	343.75	1375	16	171.88	2750	79 (M-11)	84 (M-19A)	
	M-6	250.00					62 (M-29)	64 (M-25)	
	M-7	187.50					37 (M-11)	56 (M-5)	
	M-92	593.75					140 (M-8)	140 (M-27)	
3	M-3	343.75	1375	16	171.88	2750	73 (M-11)	92 (M-19A)	
	M-6	343.75					56 (M-29)	60 (M-25)	
	M-92	687.50					131 (M-8)	133 (M-27)	
4	M-3	250.00	1375	16	171.88	2750	80 (M-11)	101 (M-19A)	X-B, a new
	M-6	187.50					62 (M-29)	69 (M-25)	injection well
	X-B	375.00					143 (M-31)	146 (M-35)	introduced.
	M-92	562.50					137 (M-8)	138 (M-27)	
5	M-3	343.75	1375	16	171.88	2750	74 (M-11)	89 (M-19A)	
	X-B	468.75					134 (M-31)	143 (M-35)	
	M-92	562.50					133 (M-8)	136 (M-27)	
6	M-3	250.00	1375	16	171.88	2750	80 (M-11)	97 (M-19A)	
	X-B	562.50					126 (M-31)	132 (M-35)	
	M-92	562.50					131 (M-8)	136 (M-27)	
7	M-3	343.75	1375	14	196.43	2750	85 (M-19A)	89 (M-25)	M-11, M-42
	M-6	343.75					56 (M-30)	61 (M-26)	not used for
	M-7	343.75					47 (M-19A)	48 (M-5)	production.
	M-92	343.75					163 (M-8)	164 (M-27)	
8	M-3	343.75	1375	15	183.33	2750	86 (M-19A)	102 (M-25)	M-11 not used
	X-B	468.75					132 (M-31)	137 (M-35)	for production.
	M-92	562.50					131 (M-27)	134 (M-27)	
9	X-1	343.75	1375	16	171.88	2750	45 (M-30)	47 (M-25)	New injection
	M-6	343.75					45 (M-29)	51 (M-26)	wells introduced
	X-2	343.75					55 (M-25)	56 (M-29)	X-1, X-2, X-3
	X-3	343.75					81 (M-19A)	>200 (---)	
10	X-1	187.50	1375	16	171.88	2750	53 (M-30)	56 (M-26)	
	M-6	187.50					50 (M-30)	54 (M-26)	
	X-2	437.50					49 (M-29)	53 (M-25)	
	X-3	562.50					68 (M-19A)	78 (M-20)	
11	M-6	187.50	1375	16	171.88	2750	54 (M-30)	87 (M-26)	New injection
	X-2	187.50					54 (M-29)	60 (M-25)	well introduced,
	X-3	437.50					63 (M-25)	64 (M-29)	X-4
	X-4	562.50					87 (M-19A)	97 (M-11)	
12	X-5	343.75	1375	16	171.88	2750	90 (M-30)	95 (M-31)	New injection
	X-6	343.75					88 (M-29)	90 (M-25)	wells introduced
	X-7	343.75					110 (M-25)	112 (M-20)	X-5, X-6, X-7,
	X-8	343.75					168 (M-19A)	>200 (---)	X-8.
13	X-9	343.75	1375	16	171.88	2750	93 (M-30)	95 (M-31)	New injection
	X-6	343.75					91 (M-29)	93 (M-25)	wells introduced,
	X-10	343.75					125 (M-25)	144 (M-20)	X-9, X-10, X-11.
	X-11	343.75					>200 (---)	>200 (---)	

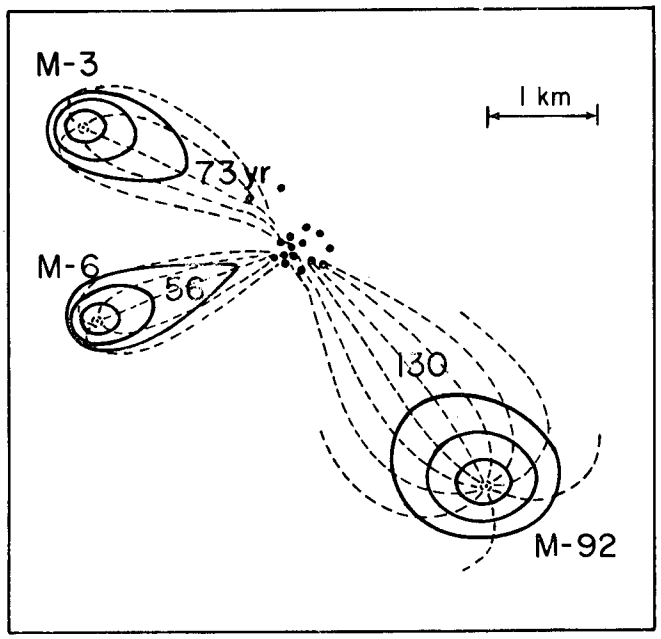

XBL 783-485

Figure 2. Brine flow characteristics for run #3. The dotted lines are the streamlines and the solid lines are the thermal fronts after 5, 20, and 50 years of injection. The numbers indicate the first breakthrough time (years).

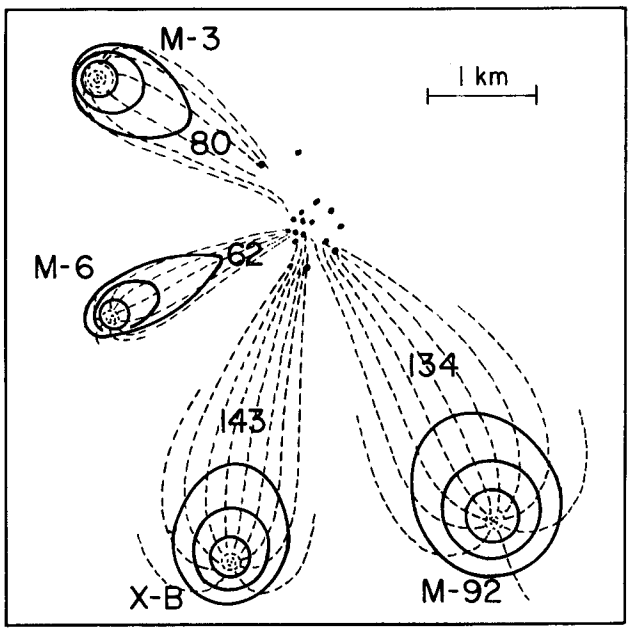

XBL 783-486

Figure 3. Brine flow characteristics for run #4.

rate is unchanged. Again, the first breakthrough occurs at M-29 as brine injected at M-6 arrives 62 years after injection began. Secondary breakthrough of brine from well M-6 arrives seven years later at M-25.

Run #5. In this run, well M-6 is not used, and the brine is injected into M-3, X-B, and M-92 at rates of 343.75, 468.75, and 562.50 m^3/hr, respectively. The first breakthrough occurs at well M-11 after a 74-year period of injection, and the second occurs 15 years later at M-19A. Both breakthroughs are due to the injection at well M-3.

Run #6. For this run, the same injection-production scheme as in the previous run is used. The only difference is the decrease of the injection rate at M-3. In this case, the breakthrough occurs at M-11, 80 years after injection begins, thus indicating some improvement in the breakthrough times.

Run #7. In this run, only 14 production wells are employed. Wells M-11 and M-42 are considerably closer to injection well M-7 than are the other 14 (see Figure 1) and have been omitted in this run to avoid early breakthrough times. However, the total production rate of 2,750 m^3/hr remains unchanged. In all other aspects this run is identical to run #1. In a comparison between runs 1 and 7, the earliest breakthrough time is increased from 32 to 47 years.

Run #8. This run is identical to run #5, except that M-11 is omitted as a production well. Comparison with run #5 shows a 12-year improvement in the first breakthrough time, resulting in 86 years of undisturbed production.

Run #9. This case is the first of a series of runs in which injection is made along a line of wells southwest of the present production area. In this run, wells X-1, M-6, X-2, and X-3 are injected at equal rates. The 16 production wells operate at a total rate of 2,750 m^3/hr. Breakthrough occurs after 45 years of injection, as brine from wells X-1 and M-6 arrives at wells M-29 and M-30.

Run #10. The well pattern used in the previous run is repeated here. The injection rates at X-1 and M-6 are decreased, but increased at X-2 and X-3. However, the total injection rate is maintained. In this run there is minor improvement (five years) in the breakthrough time.

Run #11. For this run, a new injection well, X-4, is introduced (see Figure 1), and injection well X-1 is dropped. Otherwise, run #11 is identical to run #10. The breakthrough occurs after 54 years, so only minor improvement is found in the breakthrough time (by four years).

Run #12 (Figure 4). In this run the use of injection wells X-5, X-6, X-7, and X-8 is considered. These are positioned farther from the production area than those of the last runs. The breakthrough times are consequently longer, with the shortest breakthrough occurring 90 years after injection began.

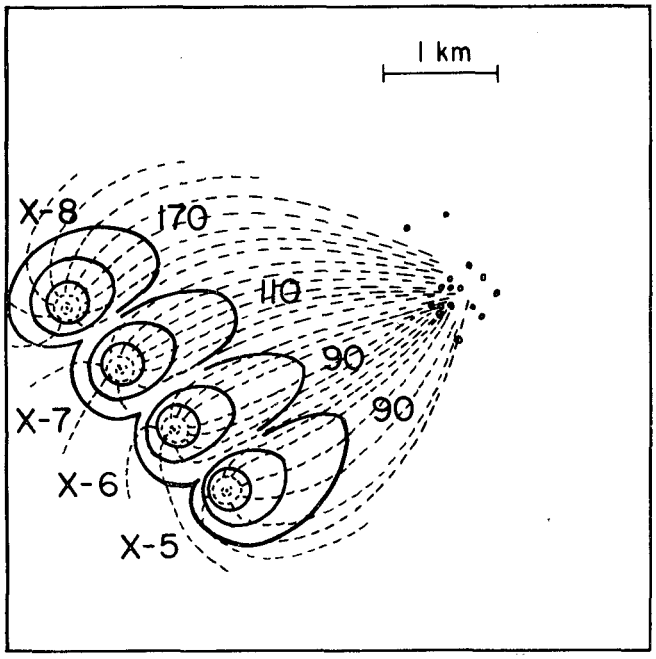

XBL 783-494

Figure 4. Brine flow characteristics for run #12.

Run #13. For this run, the conditions are the same as those of run #12, but different spacings are used between the injection wells. The results indicate minimal change in breakthrough times when compared with run #12.

In summary, these preliminary studies suggest that reinjection of cold brines into the Cerro Prieto reservoir can be safely accomplished without a premature reduction in the temperature of the produced fluids. If the presently available wells (M-3, M-6, M-7, and M-92) are used for injection, the productive life of the field will be strongly dependent upon well M-7. The use of M-7 would probably limit undisturbed production to approximately 30 years; whereas, replacing M-7 by an injection well further away from the production area would lengthen the productive life of the field to over 50 years.

The results from the runs involving brine injection into wells placed along a straight line southwest of the production area (including well M-6) indicate that breakthrough of cold water should not occur for at least 50 years. When the injection line is moved farther away from the production area, the productive life of the geothermal field is significantly increased. In general, cold water breakthrough time is strongly dependent on the distance of the production wells from the closest injection well. On the other hand, varying the relative flow rates among the injection wells does not change the breakthrough times by more than a few years. As colder water is injected into the reservoir, it is heated by the rock matrix through which it passes. Thus the hydrodynamic front, corresponding to the mass of injected water, precedes the thermal front across which the change of water temperature occurs. (The lag of the temperature front behind the injected fluid front depends on well distribution and reservoir properties.) Since the molecules of injected brine follow the hydrodynamic front, if one tags the injected fluid with a tracer, the approach of the cold front may then be predicted by periodic chemical analysis of the produced waters. This would provide time for remedial actions if necessary.

PLANS FOR FISCAL YEAR 1979

During the next fiscal year, these reinjection studies will be continued. As better understanding of the Cerro Prieto field is obtained, the reinjection patterns will be modified and new schemes studied. The simplified model of Gringarten and Sauty enables rough estimates of the thermal breakthrough times to be expected. More sophisticated numerical models will then be used in examining some of more favorable reinjection patterns. Primary emphasis will be on the following:

1. Injectability of the reinjection wells, i.e., whether they are able to accept a given flow rate

2. The effect of the different viscosity and density of hot and cold water as thermal breakthough at the production wells

Furthermore, an injection field test is in the planning stage for late fiscal 1979 or early 1980. Numerical analysis will be made to aid in the planning and to predict the expected behavior to be tested against the field test data.

REFERENCES CITED

Bermejo M., F. J., Cortez A., C., and Aragon A., A., 1979. Physical and thermodynamic changes observed in the Cerro Prieto geothermal field, in Proceedings, First Symposium on the Cerro Prieto Geothermal Field, Baja California, Mexico, September 20-22, 1978. Berkeley, Lawrence Berkeley Laboratory, LBL-7098.

Gringarten, A. C., and Sauty, J. P., 1975. A theoretical study of heat extraction from aquifers with uniform regional flow. Jour. Geophys. Res., v. 80, no. 35, pp. 4956-4962.

Truesdell, A. H., and Mañon M., A., 1979. Geochemical evidence of drawdown in the Cerro Prieto, Mexico, geothermal field, in Proceedings, First Symposium on the Cerro Prieto Geothermal Field, Baja California, Mexico, September 20-22, 1978. Berkeley, Lawrence Berkeley Laboratory, LBL-7098.

Tsang, C. F., Bodvarsson, G., Lippmann, M. J., and Rivera R., J., 1978a. A study of alternative reinjection schemes for the Cerro Prieto geothermal field, Baja California, Mexico, in Geothermal energy: a novelty becomes a resource. Trans. Geoth. Res. Council Annual Mtng. 25-27 July 1978, v. 2, sec. 2, pp. 659-662.

Tsang, C. F., Witherspoon, P. A., and Gringarten, A. S., 1978b. The physical basis for screening geothermal production wells from the effects of reinjection. Berkeley, Lawrence Berkeley Laboratory, LBL-5914.

SUBSURFACE GEOLOGY OF THE EAST MESA GEOTHERMAL ANOMALY

J. H. Howard, A. N. Graf, and P. C. van de Kamp

INTRODUCTION

During fiscal year 1978, the Earth Sciences Division at Lawrence Berkeley Laboratory completed two major works in which the subsurface geology of the East Mesa geothermal resource was reviewed (Howard et al., 1978, 1979). Principal developments included a synthesis of all subsurface geologic data of interest to exploitation of this resource and substantiation of the concept of a prototype geothermal resource having a "degenerate" core. These efforts also showed that seismic reflection profiling may define, for geothermal resources in sedimentary rock, a significant change with depth in physical rock properties, namely, to quite low porosities (less than 10%) and to permeabilities controlled by fracturing rather than by intergranular flow paths.

FISCAL YEAR 1978 ACTIVITIES

As part of ongoing responsibilities to the Division of Geothermal Energy of the U.S. Department of Energy, and to the Bureau of Reclamation of the U.S. Department of the Interior in fiscal year 1978, LBL developed a synthesis of all data available on the distribution of temperature,

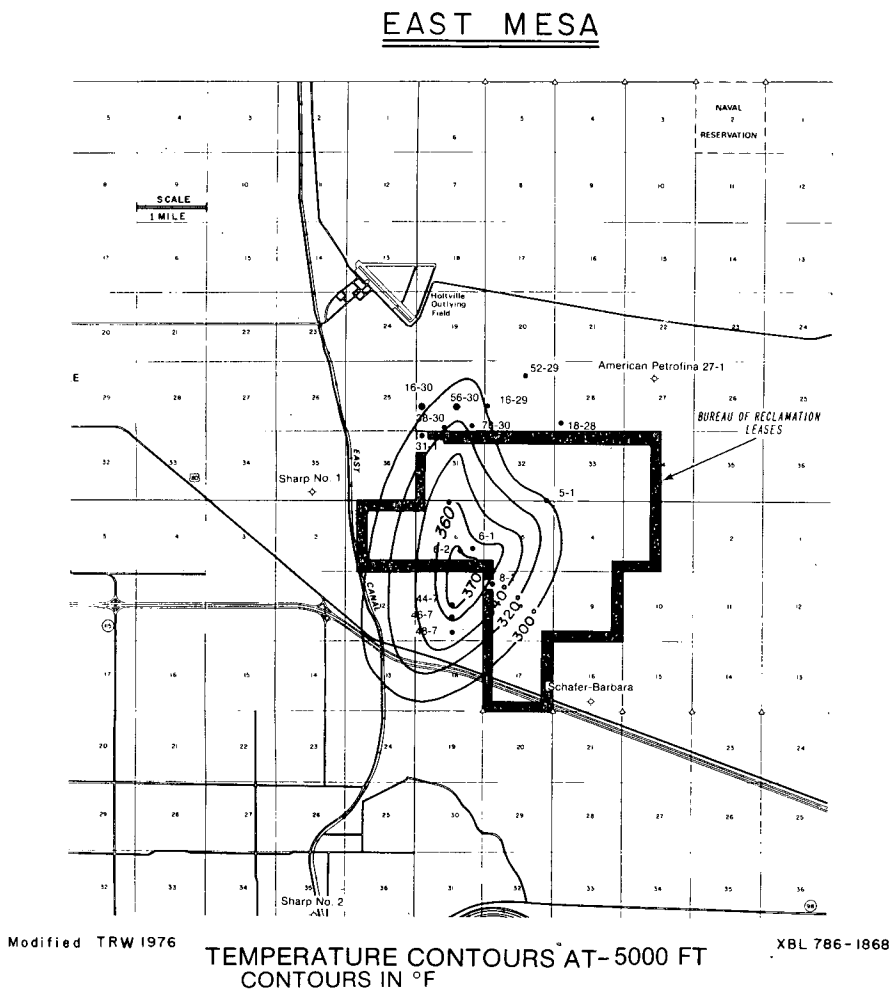

Figure 1. Distribution of temperature at 4,000 ft, East Mesa reservoir, California.

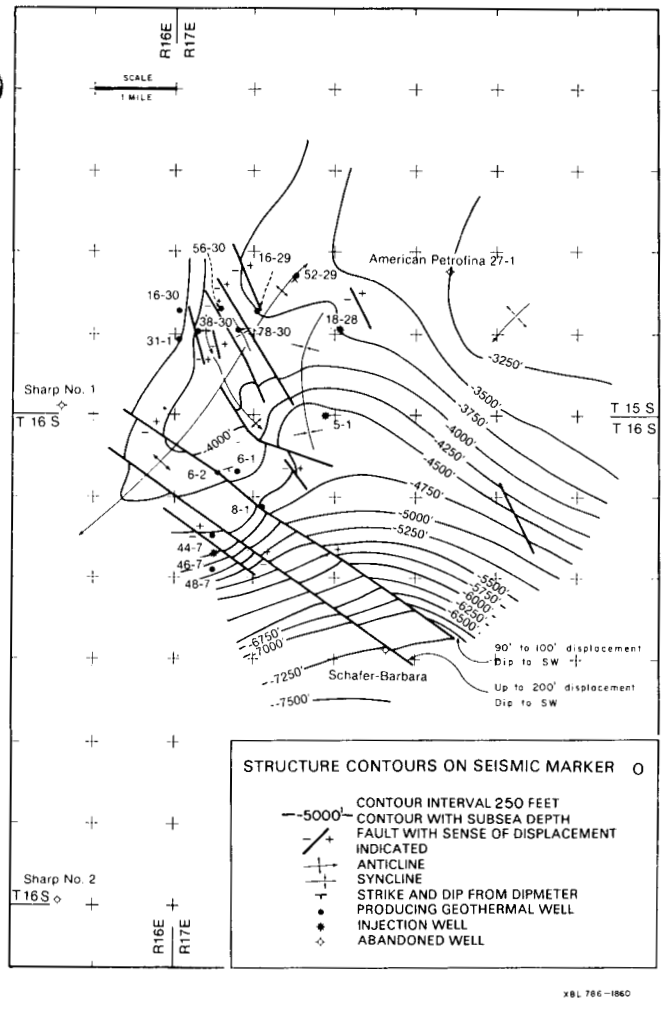

Figure 2. Structure contour map on the "orange" horizon, East Mesa reservoir, Califoria.

pressure, porosity, and permeability within the field. Figure 1 is an example of the distribution of temperature. Figure 2 is an example of the geologic structure of the field.

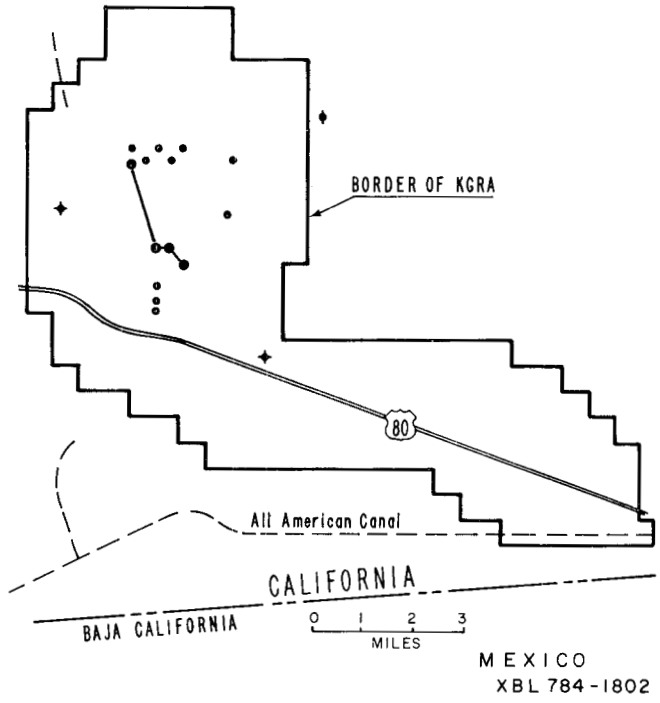

Figure 3. Map showing location of cross section.

Information on the distribution of temperature and porosity enables us to calculate the amount of energy in the geothermal fluid in situ. Such calculations were done for the U.S. Bureau of Reclamation (USBR) site at East Mesa and are summarized in Table 1. Approximately 1.7 x 10^{15} Btu of energy in fluids above 300°F are present in the reservoir to a depth of 7,500 ft. Assuming that all of this fluid can be produced, and that 2.5% of this energy can be converted to electrical energy, the in-situ energy is equivalent to 1,421 MW-years of electrical energy.

Smith (1978) suggested that the East Mesa reservoir is typical of a class of geothermal resources in which the central part has the highest heat flow, highest density, and highest

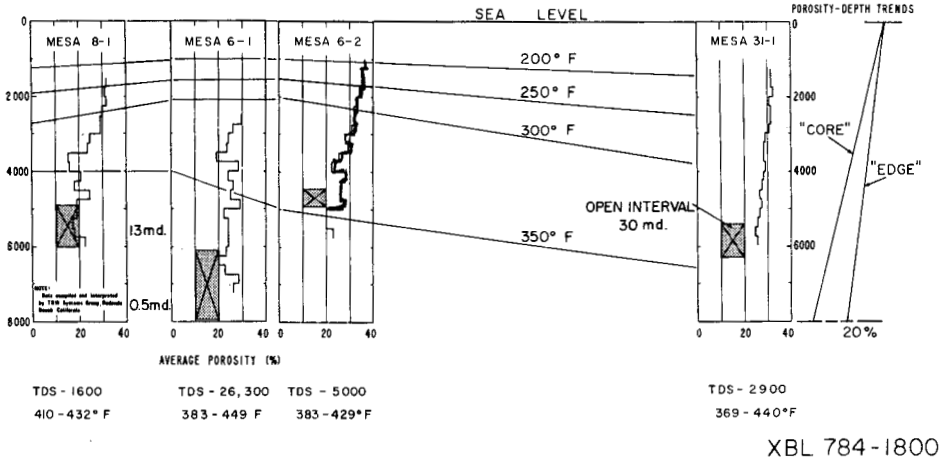

Figure 4. Cross-section, north-south, through the zone of highest heat flow, East Mesa reservoir, California. Note that at a depth of, for instance, 5,000 ft, the highest temperatures, lowest porosities, and lowest permeabilities occur near Mesa 8-1 and 6-1 wells, namely at the core of the reservoir.

Table 1. USBR leases 1, 2, and 4 at East Mesa, California. Estimate of Btu in fluid above 300°F to a depth of 7,500 ft.

Interval	385°F	375°F	365°F	355°F	350°F	345°F	330°F	310°F	Total Volume of Fluid (ft.^{3})	Total Pounds of Fluid	Total BTUs in Fluid
2,500' - 3,500'											
Average Sand Thickness: 824'											
Average Porosity: 0.205											
Volume of Fluid (ft.^{3})				3.58×10^{8}		1.33×10^{9}	5.20×10^{9}	6.86×10^{9}	1.37×10^{10}		
Pounds of Fluid[1]				2.03×10^{10}		7.55×10^{10}	2.95×10^{11}	3.90×10^{11}		7.81×10^{11}	
BTUs of Fluid[2]				6.02×10^{12}		2.16×10^{13}	8.00×10^{13}	9.80×10^{13}			2.06×10^{14}
3,500' - 4,500'											
Average Sand Thickness: 753'											
Average Porosity: 0.167											
Volume of Fluid (ft.^{3})			5.58×10^{8}		3.06×10^{9}		4.41×10^{9}	5.31×10^{9}	1.33×10^{10}		
Pounds of Fluid[1]			3.17×10^{10}		1.74×10^{11}		2.50×10^{11}	3.02×10^{11}		7.56×10^{11}	
BTUs of Fluid[2]			9.72×10^{12}		5.07×10^{13}		6.78×10^{13}	7.59×10^{13}			2.04×10^{14}
4,500' - 5,500'											
Average Sand Thickness: 845'											
Average Porosity: 0.175											
Volume of Fluid (ft.^{3})		4.81×10^{8}	2.01×10^{9}		4.63×10^{9}		6.70×10^{9}	6.72×10^{9}	2.05×10^{10}		
Pounds of Fluid[1]		2.73×10^{10}	1.14×10^{11}		2.63×10^{11}		3.80×10^{11}	3.82×10^{11}		1.17×10^{12}	
BTUs of Fluid[2]		8.64×10^{12}	3.49×10^{13}		7.67×10^{13}		1.03×10^{14}	9.60×10^{13}			3.19×10^{14}
5,500' - 6,500'											
Average Sand Thickness: 924'											
Average Porosity: 0.173											
Volume of Fluid (ft.^{3})		2.21×10^{9}	3.55×10^{9}		7.00×10^{9}		8.44×10^{9}	8.84×10^{9}	3.00×10^{10}		
Pounds of Fluid[1]		1.25×10^{11}	2.02×10^{11}		3.97×10^{11}		4.79×10^{11}	5.02×10^{11}		1.71×10^{12}	
BTUs of Fluid[2]		3.96×10^{13}	6.19×10^{13}		1.16×10^{14}		1.30×10^{14}	1.26×10^{14}			4.74×10^{14}
6,500' - 7,500'											
Average Sand Thickness: 637'											
Average Porosity: 0.175											
Volume of Fluid (ft.^{3})	1.65×10^{9}	2.45×10^{9}	4.59×10^{9}		5.61×10^{9}		6.95×10^{9}	7.55×10^{9}	2.88×10^{10}		
Pounds of Fluid[1]	9.37×10^{10}	1.39×10^{11}	2.61×10^{11}		3.19×10^{11}		3.95×10^{11}	4.29×10^{11}		1.64×10^{12}	
BTUs of Fluid[2]	3.06×10^{13}	4.40×10^{13}	8.00×10^{13}		9.30×10^{13}		1.07×10^{14}	1.08×10^{14}			4.63×10^{14}
									1.06×10^{11}		
										6.06×10^{12}	
											1.67×10^{15}

[1]Average fluid density: ~0.91 gm/ml.
[2]Mean specific heat: ~1.005 BTUs/lb°F

XBL 7810-11895

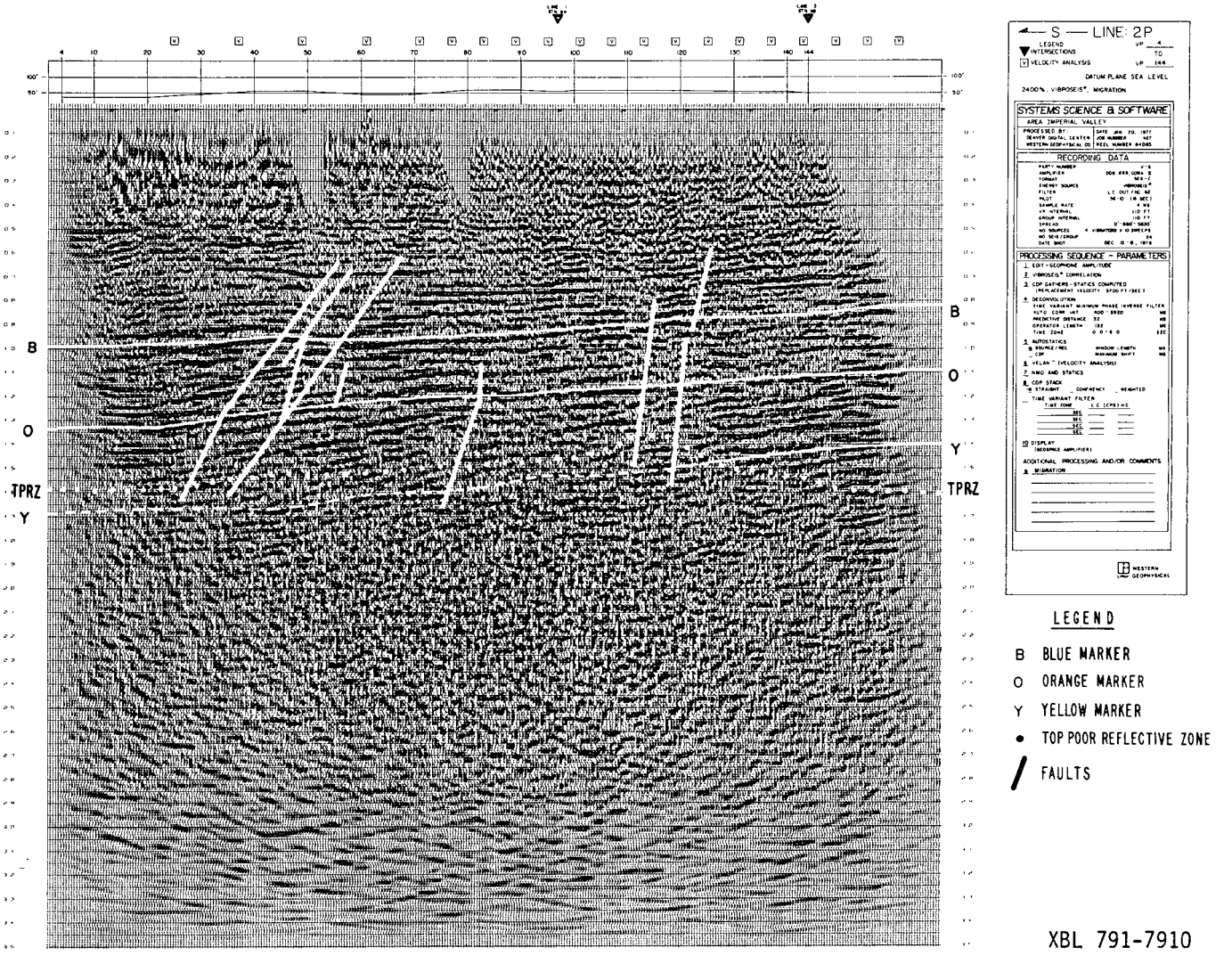

Figure 5. Seismic profile northeast-southwest through the East Mesa reservoir. Note the deterioration of reflections with depth and the location of TPRZ (top of the poorly reflecting zone).

temperature on a horizontal plane at a given depth. LBL's review of data supports this hypothesis (Figures 3 and 4). Those factors which lead to occurrence of a geothermal resource (high temperatures at modest depths) may also, with time, lead to adverse effects such as loss of primary porosity and permeability.

Study of seismic reflection profiles across the field show that reflection becomes "fuzzy" and less well-defined with depth (Figure 5). A surface referred to as the top of the poorly reflecting zone (TPRZ) has been mapped throughout the field. Based on the observation that porosities decrease with depth in the stratigraphic section (Figure 3), we hypothesize that this surface corresponds in a general way to quite low porosities and loss of intergranular permeability. (Permeability below TPRZ must be fracture controlled if present.) Although electrical methods, gravity, and heat flow are usually considered the principal geophysical tools for definition of a geothermal resource, seismic reflection profiling may prove to be of appreciable importance in determining the apparent loss of significant intergranular porosity and permeability in geothermal resources in sedimentary sequences.

PLANNED ACTIVITIES FOR FISCAL YEAR 1979

Activities at East Mesa for fiscal year 1979 have been suspended until an arrangement for monitoring the reservoir and simulating reservoir performance can be worked out with the field operators. LBL has proposed to conduct more realistic simulation of field performance than has been done to date. In part, the delay is due to the availability of open acreage set for lease in the middle of the fiscal year.

REFERENCES CITED

Howard, J. H., Campbell, D. A., Hinrichs, T. C., Mathias, K. E., and Narasimhan, T. N., 1978. Geothermal resource investigations and development plans at East Mesa, California.

Berkeley, Lawrence Berkeley Laboratory, LBL-9026.
Howard, J. H., Apps, J. A., Benson, S., Goldstein, N. E., Graf, A. N., et al., 1979. Geothermal resource and reservoir investigations of U.S. Bureau of Reclamation leaseholds at East Mesa, Imperial Valley, California. Berkeley, Lawrence Berkeley Laboratory, LBL-7094.
Smith, J. L., 1978. Republic Geothermal Inc., personal communication.

GEOTHERMAL SUBSIDENCE RESEARCH PROGRAM

T. L. Simkin, J. E. Noble, and W. J. Schwarz

INTRODUCTION

A major consequence of development of a geothermal reservoir may be subsidence due to withdrawal of voluminous amounts of fluids. Unexpected and uncontrolled subsidence can have detrimental social, environmental, and economic effects. In order to understand geothermal subsidence, its causes and effects, Lawrence Berkeley Laboratory initiated the Geothermal Subsidence Research Program (GSRP) in 1976.

The goals of the GSRP are to develop methods for assessing naturally occurring subsidence, inferring a geothermal reservoir's compaction potential, and minimizing potential subsidence effects during exploitation of a geothermal reservoir. Attainment of these goals is expected to provide the tools needed to measure subsidence and to predict the subsidence potential of a reservoir. The program is expected to provide guidance with which regulatory agencies may take appropriate action to minimize the impact of subsidence.

In fiscal year 1978, research was conducted or begun in the following three areas.

Subsidence characterization. Subsidence characterization is concerned with studying examples of subsidence and its effects. Research was conducted to document cases of known subsidence in geographic areas having geological and physical environments representative of geothermal areas. Where data were available (for Wairakei, New Zealand, and the Geysers, California), case histories have been written. Associated studies have also been conducted on the economic and environmental impact of subsidence. These latter studies indicated that a lack of data prevented the assessment of the direct impact of subsidence.

Subsidence measurement. Researchers have developed guidelines for surface monitoring surveys to establish background deformation rates and monitor possible deformation induced by geothermal development. Researchers have also assessed the state-of-art of wellbore extensometers to measure changes in vertical distances between points in a wellbore. Several suggestions for improved instrumentation that have resulted from this research will make substantial contributions toward creating direct measurement instrumentation for use in geothermal wells.

Subsidence prediction. The ability to predict subsidence is dependent upon an understanding of the response of geologic materials and systems to natural and man-made stress fields. To gain this understanding, the Geothermal Subsidence Research Program began studies of the response of reservoir material to various stress fields and changes in those fields.

Other research was started in 1978 to assess various subsidence models, review their relative anaytical merits, and, if necessary, make recommendations for new models. A related project will develop methods for physical modeling using a centrifuge. Predictions of subsidence made by numerical modeling can thus be evaluated by comparison with a centrifuge model.

Out of these efforts may evolve a better understanding of how geological materials and systems respond to dynamic stress fields, enabling earth scientists to predict subsidence over a given reservoir more accurately.

1978 ACCOMPLISHMENTS

Case Histories

Most documented subsidence has been due to extraction of hydrocarbons or groundwater. Useful analogies may be drawn for the production of geothermal fluids. In some cases, deep extraction of fluids has produced little or no subsidence. A case history of the geologic and physical environments, the stress history, and the response or lack of response at land surface, has proved useful in making comparisons to similar potential geothermal systems.

Four case histories were completed by Systems Control, Inc., in the following areas: Wairakei, New Zealand; Chocolate Bajou, Texas; The Geysers, California; and Raft River, Idaho. The four subsidence sites were selected on the basis of: (a) physical relevance to high-priority U.S. geothermal sites in terms of withdrawn geofluid type, reservoir depth, geology and rock charcteristics, and overburden characteristics; and (b) data completeness, quality and availability. These case histories can serve as models for developers and regulators in assessing the subsidence potential for their area of interest.

Environmental and Economic Effects

A contract with EDAW/Earth Sciences Associates resulted in assessment of data available from areas where subsidence has occurred. A detailed appraisal was made of areas with the most comprehensive data base. Areas studied included desert basins in central and southern Arizona; Baldwin Hills, Inglewood, San Joaquin Valley, Santa Clara Valley, and Wilmington Beach, California; Las Vegas Valley, Nevada; Galveston, Texas; Mexico City, Mexico; and Wairakei, New Zealand. The quantity and quality of data collected for the areas studied were disappointing: no comprehensive studies of the effects of subsidence were found for any of these areas, most cost data were based on estimates rather than actual expenditure records, and there was a general lack of public awareness of subsidence except in areas where other hazards, such as flooding, are aggravated.

Although there is a serious lack of reliable data on the direct effects of subsidence in the areas studied, it does appear possible to predict quantitatively, many types of subsidence effects using conventional engineering techniques to supplement the limited subsidence data.

Surface Monitoring--Guidelines Manual

The fundamental objective of a monitoring program is to quantify the magnitude and direction of surface movements that may occur in a geothermal reservoir area before, during, and after the removal of geothermal fluids. A geothermal development program must include monitoring of horizontal and vertical displacements at the surface and at depth before and during production. It should be possible to differentiate between induced subsidence, caused by geothermal operations for instance, and naturally occurring subsidence.

Thus, guidelines need to be developed to obtain data directly related only to geothermal fluid production. These guidelines should consider the geologic structure, stratigraphy, and seismicity of the area, as well as the existing and proposed groundwater, gas, and oil developments. The guidelines should also consider, if available, any known ground deformation characteristic of the region and any natural deformations of nearby fluid-producing fields.

Woodward-Clyde Consultants has produced a manual that reviews various surface-monitoring methods and compares their installation, utilization, and accuracy. Utilization of these methods should enable planners and regulators to determine the natural rate of subsidence. In addition, such a manual can be used to ascertain induced subsidence during development and production of a geothermal field.

Instrument Study

Another Woodward-Clyde Consultants study reviewed instruments available for monitoring wellbore displacements, both vertical and horizontal. Techniques and materials for improving existing or developing new instruments were evaluated. Elements of sensor and signal technology with potential for high-temperature monitoring of vertical wellbore changes were identified.

Woodward-Clyde has recommended hostile-environment testing for the following four components: (a) induction coil with slip-collar well casings; (b) reed switches with magnet emplaced in slip collars; and (c) electromagnetic oscillators with magnets emplaced to either slip collars or directly into the formation.

ACTIVITIES FOR FISCAL YEAR 1979

Program Review and Revision

In October 1978 a workshop was convened to review the results of completed research, assess the adequacy of the program plan, and make suggestions on revision of the original Geothermal Subsidence Research Program planning document (Lawrence Berkeley Laboratory, 1977). The workshop provided to LBL management a timely review of the entire GSRP effort. A revised planning document will be issued in the second quarter of fiscal year 1979.

Research Activities

Three contracts started in fiscal year 1978 will be continued in fiscal year 1979.

1. An assessment by Golder Associates (Seattle, Washington) of existing mathematical subsidence and deformation models

2. High-temperature and high-pressure compressibility studies by Terra Tek, Inc. (Salt Lake City, Utah) of cores from geothermal reservoirs

3. Centrifuge compaction studies by Colorado School of Mines (Golden, Colorado) of reservoir materials

In addition, the following research projects will begin.

1. The Chocolate Bayou Case Study will be expanded to make it more comprehensive. An expanded study could also be useful as a model for researchers at the Brazoria geopressure field locatd south of the Chocolate Bayou field.

2. The four suggestions for improved wellbore extensometers made by Woodward-Clyde Consultants will be component-tested.

3. Additional review of radioactive bullet logging will be made to assess the applicability of this technique to monitoring subsurface compaction.

4. Indirect measurement methods will be evaluated. Gravity, resistivity, and microseismic methods show promise as inexpensive,

areal survey techniques. Research will be conducted to evaluate the ability of these methods to detect changes in the physical properties of a geothermal reservoir, and to relate these changes to reservoir compaction and subsidence.

5. Existing subsidence theory and its applicability to geothermal reservoirs will be assessed. Most subsidence theories were developed to describe the compaction of oil and gas reservoirs or of relatively shallow unconsolidated aquifers. The applicability of these theories or deep, thermodynamically complex geothermal systems needs to be examined.

6. Related to the assessment of existing subsidence theory is an assessment of rock creep and inelasticity at high temperature and high pressure. The effects of this phenomena are little understood and limit the accuracy of predicting subsidence. Research will be conducted to study its contribution to compaction and subsidence.

REFERENCES CITED

Grimsrud, G. P., Turner, B. L., and Frame, P. A., 1979. Areas of ground subsidence due to geofluid withdrawal. Berkeley, Lawrence Berkeley Laboratory, LBL-8618.

Lawrence Berkeley Laboratory, 1977. Geothermal subsidence research program plan. Berkeley, Lawrence Berkeley Laboratory, LBL-5983.

Simkin, T. L., and Noble, J. E., 1978. Geothermal subsidence research program project summaries. Berkeley, Lawrence Berkeley Laboratory, UCID-8035.

Van Til, C. J., 1979. Guidelines manual for surface monitoring of geothermal areas. Berkeley, Lawrence Berkeley Laboratory, LBL-8617.

GEOTHERMAL RESERVOIR ENGINEERING MANAGEMENT PROGRAM

J. H. Howard and W. J. Schwarz

INTRODUCTION

Fiscal year 1978 was the second year of LBL's responsibility for the Geothermal Reservoir Engineering Management Program (GREMP) on behalf of the U.S. Department of Energy, Division of Geothermal Energy. The history of this program through fiscal year 1977 is explained in LBL's Earth Sciences Division Annual Report for 1977 (Schwarz and Howard, 1978a,b).

ACTIVITIES IN FISCAL YEAR 1978

Administrative Highlights

All projects started under the NSF-RANN program were continued. These include work done at Standford University; Princeton University; Systems, Science and Software; University of California at Riverside; and the University of Colorado. All of these programs were further extended into fiscal year 1979 with the exception of the University of Colorado program, which was concluded.

Several new projects were started. These projects are outlined in Table 1.

The Division of Geothermal Energy (DGE) reemphasized its concern that all projects under the GREMP program clearly and directly relate to DGE's "power-on-line" mission. The Review Task Force, originally constituted to overview the GREMP program, was dissolved, and plans were made to assemble a new task force. LBL was urged to solicit industry to assure that there is federal support of research for all reservoir engineering related technical impediments to "power-on-line." LBL was asked to revise and update the original GREMP planning document (Lawrence Berkeley Laboratory, 1977).

With the exceptions noted below, all project areas of the original GREMP plan have been addressed as have all known serious technical reservoir-related impediments to geothermal resource development (such as formation damage during drilling). Important projects that have not yet received their full measure of support are: work on mass flow measurement techniques; use of tracers; and decline curve analysis, particularly enthalpy decline curve analyses. In keeping with the recommendation of the Review Task Force, nothing has been done on economics and on exploitation strategies.

A GREMP publication series was started. Henceforth, all reports prepared under GREMP contracts will be published or reprinted as part of this series. Systems, Science, and Software's summary of the Wairakei field (Pritchett et al., 1979) and Terra Tek's bibliographic review (Randall and Harrison, 1979) will be the first two publications of this series.

The program began issuing a "News from GREMP." The first was issued August 1, 1978; the second, November 3, 1978. The purpose of the newsletter is to summarize the highlights of progress in research and to direct readers to new, complete reports on the research. (The newsletter is available by request.)

Technical and scientific progress accomplished during the year can be divided into five work areas. These work areas and the contracts within them are shown in Table 1. Brief descriptions of these contracts and their achievements are discussed below.

Table 1. GREMP major program areas and contracts.

Program areas	Contractor and work performed
Status of Geothermal Reservoir Engineering	Terra Tek.* Review of the literature in geothermal reservoir exploitation engineering.
Measurements of Interest to Exploitation Engineers	Measurement Analysis Corporation.* Review of the status of instrumentation to make measurements of interest to reservoir engineers, e.g., temperature, mass flow rate, and so on U.C. Riverside. Use of mineral species as an indicator of reservoir temperatures; use of stable isotopes to determine temperatures and total fluid flux throughout the reservoir Battelle Memorial Institute/Pacific Northwest Laboratory.* measurement of wellhead enthalpies on a real-time basis Terra Tek.* Measurement of noncondensable gases, particularly carbon dioxide, in the flow stream on a real-time basis Stanford University. Techniques for measuring saturation and relative permeability and for use of natural tracers (radon) in reservoir studies; rock to fluid heat transfer; thermal stress cracking
Analytical Tools	Terra Tek.* Analysis of near-bore formation damage as a consequence of mud-type, and drilling and completion practices Republic Geothermal Incorporated.* Analysis of calcium carbonate precipitation in the near-bore area due to inappropriate pressure drawdowns there Stanford University. Development of parallelepiped models for use in well testing to obtain lumped reservoir properties; decline curve analysis; incorporation of high noncondensable gas content into analytical mathematical models Intercomp.* Development of analytical techniques for interpretation of wellhead temperature, pressure, and mass flow-rate data when the reservoir is in part in two-phase flow.
Forecasting Reservoir Performance	Princeton University. Codes for the simulation of mass and energy transport in fractured reservoirs University of Colorado. Analytical model for mass and energy transport in a half space characterized by a vertical conduit (i.e., fault)
Synthesis of Data and Applications of Forecasting and Analytical Tools	Systems, Science, and Software. Synthesis of data for the Wairakei geothermal field. Stanford University. Synthesis and analysis of data from the Travale-Radicondoli and the Bagnore fields. Systems, Science, and Software. Analysis of production history of the Wairakei field. University of Colorado. Application of analytical model to the East Mesa field. U.C. Riverside. Synthesis of subsurface geology based on lithology logging at the Cerro Prieto field.

*New contract in fiscal year 1978.

Geothermal Reservoir Engineering

Terra Tek. The objective of this contract has been to develop an annotated bibliography, narrative review, and thesaurus of geothermal reservoir engineering in a broad sense. Literature in English, Russian, Italian, and Japanese has been searched using computer search services, abstracts, and index services. Topics include: analytical modeling; numerical modeling; physical modeling; formation evaluation including well testing and case studies, but not well logging; exploitation strategies including production-disposal strategies, stimulation, and well spacing; and interpretation of production trends including isotope analysis, heat and mass flux histories, and tracer injection techniques. There has been a need to gather together and synthesize the literature pertaining to reservoir engineering in order to understand more clearly where this technology now stands and plan more

effectively for support of research in the future. The contract has been completed as of December 1, 1978. A report (the second in the GREMP series) has been prepared, which includes thesaurus, annotated bibliographic entries, and short narrative review.

Exploitation Studies

Measurement Analysis Corporation. This project evaluates measurement needs and methods for reservoir parameters including permeability, flow rate, particulate count, conductivity, density, void fraction, quality, pH, and others. There is a need to determine what measurements are sought by the geothermal resource exploitation community and to evaluate the current accuracy of those measurements. To date the contractor has reported high interest in detection and measurement of fractures and in a nonfouling temperature probe. Mass-flow measurement and enthalpy measurement at the wellhead appear to be of lesser interest.

U.C. Riverside. An objective of the program at U.C. Riverside is to map mineral assemblages and other indices of temperatures in order to determine the maximum temperatures to which the strata in a geothermal reservoir have been subjected. Although supported originally as a topic of basic research, this task has appreciable practical value as a guide to decisions regarding progress of drilling toward zones sufficiently hot to be interesting economically. U.C. Riverside has reported its results in many publications, among the most recent being publication of three papers in the proceedings of the Hilo Geothermal Resources Council meeting in July 1978 (Hoagland and Elders, 1978; Olson and Elders, 1978; Elders et al., 1978).

Battelle Memorial Institute/Pacific Northwest Laboratories. The objective of this study is to evaluate calorimetry systems that will permit economical, reliable and accurate measurement of enthalpy values at the geothermal wellhead. The saleable product from a geothermal well is the energy contained in the wellhead fluid. The energy content per mass unit passing from the well should therefore be known. Furthermore, for power-plant design, it is important that enthalpy of the wellhead product be known as a function of time. The project began November 1, 1978, and Phase 1 is to conclude on March 30, 1979.

Terra Tek. The objective of this project is to develop a simple and convenient instrument to measure noncondensable gases on a real-time basis in geothermal discharges. Information on the noncondensable content in the flow stream is needed in order to estimate the power potential of a well and reservoir and to design power stations. A draft final report on the instrument design has been written. Construction of the instrument should begin following design approval. Laboratory and field testing are scheduled for completion by September 1979.

Stanford University. Among the many objectives of this program is a study of the petrophysics of rock and high-salinity fluid systems including: techniques for measuring liquid content in brine/steam systems using a capacitance probe; effect of salinity on surface tension and related phenomena; and effect of temperature on permeability and relative permeability. Other projects being done at Stanford include: evaluation of the utility of radon in understanding geothermal reservoir behavior and response during production; study of heat flux from collections of rock fragments of vaious shapes and sizes to geothermal fluids; and evaluation of thermal stress cracking in rocks of known geometry. All of these projects are necessary in order to understand the fundamental behavior of mass and energy distribution and transport in geothermal reservoirs. Stanford has issued annual reports and topical reports on their findings.

Analytical Tools

Terra Tek. The objective of this project is to evaluate the consequences of drilling and completion practices and mud type on the development of a "baked" skin around the wellbore. It has been proposed that several geothermal wells are not producing because of formation damage in the near-bore area as a consequence of standard drilling and completion practices applied to very-high-temperature environments. To date, Terra Tek has acquired some core material, and has begun evaluation of operating practices and choices for mud, and conceptualization of a laboratory program to simulate formation damage in order to understand the factors controlling it.

Republic Geothermal Incorporated. This program will empirically evaluate the consequence of pressure drop in the near-bore area on the precipitation of carbonate minerals from calcium-carbonate, carbon-dioxide-rich geothermal fluids. Such fluids are to be flushed through core by a pressure differential. Carbonate precipitation is well known as a fouling agent in geothermal wells and is suspected to be a cause of impaired permeability around wellbores.

Stanford University. Among the many activities under way at Stanford University is a project to develop analytical mathematical models for response of wells drilled into a parallelepiped. Models of this kind can be suitably and quickly changed in order to approximate the geometry of all or part of a reservoir.

There is an advantage to reservoir analysts in having a suite of rapidly solvable analytical mathematical solutions. Review of pressure signatures for well tests, with respect to various choices of these models, can lead to a new perspective on the intrinsic parameters and possible geometries of a reservoir. Stanford has used these models to analyze data from certain Italian fields. Decline-curve analyses and treatment of noncondensables in analytical mathematical models have also been addressed in the program.

Intercomp. The objectives of this project are to develop an understanding of well testing where there is two-phase flow in the reservoir and to explain how analyses based on single-phase reservoir need to be modified to account for the presence of two phases. The consequences of a two phase reservoir need to be understood when estimating reservoir parameters. The contract started at the beginning of the fiscal year.

Forecasting Reservoir Performance

Princeton University. There are multiple objectives to this project, the general one being to improve the methodology for geothermal reservoir simulation. Particular objectives include: (a) development of a nonisothermal three-dimensional, two-phase code for heat transport in fractured geothermal reservoirs and (b) solution (using finite-element techniques) of transient partial differential equations that are of special importance to such a code. There has been a great deal of interest in a capability to simulate and forecast geothermal reservoir performance, particularly for fractured reservoirs. Princeton has made significant progress in the formulation of the theoretical basis for the code and has developed certain important codes and subroutines particularly those useful in solving nonlinear coupled partial differential equations.

University of Colorado. The objective of this project has been to develop a semianalytical model for naturally occurring mass and energy transport in a half space in which the system is charged at some depth within an imbedded vertical conduit (i.e. fault). The model has been applied to the East Mesa, California, field. There has been and continues to be interest in understanding prototype models of geothermal reservoirs. The project has developed one such model. The project ended with publication of a final report (Kassoy and Goyal, 1979).

Systems, Science and Software. The objective of this project was to compile all possible reservoir-related data on the Wairakei, New Zealand, field. Interest in case histories for purposes of sharing experience and for use in history matching with simulators has always been evident in the development of geothermal resources. This project has been completed, and a comprehensive report and executive summary report have been issued (Pritchett et al., 1979).

Stanford University. Among the objectives of the Stanford program are activities to synthesize certain data from Larderello, Italy. Stanford investigators have constructed, for example, pressure maps of the fields and graphs of reservoir static pressures vs masses produced for different times in the development of the field. Many people interested in vapor-dominated reservoirs have also expressed interest in learning from the experiences in the Italian geothermal fields. The project has issued quarterly reports as well as specific reports at the Italian/Larderello-1977 and Stanford-1976 and 1977 workshops (Kruger and Ramey, 1977).

Systems, Science and Software. The objective of this project, which is a continuation of earlier work on data compilation at Wairakei, is to construct a geologic model of the field and to match production and subsidence history in the field from 1953 to 1976. Systems, Science, and Software will also forecast future production from the field under different assumptions for the imposed production rates. Because of its exceptional data base, Wairakei offers an unusual opportunity for reservoir simulation. This project was initiated in September 1978 and will conclude in May 1979.

University of Colorado. The University of Colorado has applied an analytical model (described above) to the East Mesa reservoir in order to gain insight into the natural phenomena that may have led to the occurrence of the geothermal resource there. This project has been completed.

University of California, Riverside. An objective of the U.C. Riverside program is to develop an advanced model of the subsurface geology in the Cerro Prieto, Mexico, geothermal field. In particular the project addresses the distribution of temperature, porosity, and temperature-related mineral assemblages. This project is a significant part of the cooperative Mexican-U.S. project to elucidate the Cerro Prieto geothermal resource. U.C. Riverside continues to issue reports on a regular basis.

Progress in Fiscal Year 1978

Technical progress on the program in fiscal year 1978 has been very satisfactory. The following accomplishments are worthy of special note:

1. A comprehensive bibliographic review of the literature pertaining to geothermal reservoir exploitation has been completed (Randall and Harrison, 1978).

2. A quantitative model of a prototype geothermal resource has been developed, namely one dominated by a vertical fault (Goyal, 1978).

3. The entire production history of Wairakei, an important liquid-dominated geothermal reservoir, has been completed (Pritchett et al., 1978).

4. The program has increased our awareness of the importance of lithology logging as a practical tool during drilling of geothermal wells (Hoagland and Elders, 1978; Olson and Elders, 1978; Elders et al., 1978).

5. For the third time, program staff attended the annual Stanford Geothermal Workshop (Kruger and Ramey, 1977). This workshop has become the outstanding public forum for exchange of ideas and information in geothermal reservoir engineering.

ACTIVITES PLANNED FOR FISCAL YEAR 1979

Activities planned in fiscal year 1979 include the continuation of all contracts in force and the inception of those contracts and categories of work shown in Table 2. As noted above, nearly all categories of the original GREMP now have been addressed.

REFERENCES CITED

Elders, W. A., Hoagland, J. R., and Olson, E. R., 1978. Hydrothermal mineralogy and isotope geochemistry in the Cerro Prieto geothermal field, Mexico--practical applications. Proceedings, Geothermal Resource Council, Hilo, Hawaii, UCR/IGPP Contribution No. 78/10, 4 p.

Goyal, K. P., 1978. Heat and mass transfer in a saturated porous medium with application to geothermal reservoirs. Ph.D. thesis, Boulder, Mechanical Engineering Department, University of Colorado, 294 p.

Hoagland, J. R., and Elders, W. A., 1978. Hydrothermal mineralogy and isotope geochemistry in the Cerro Prieto geothermal field, Mexico: III, practical applications. Proceedings, Geothermal Resources Concil, Hilo, Hawaii, UCR/IGPP Contribution No. 78/8, 4 p.

Kassoy, D. R., and Goyal, K. P., 1979. Modeling heat and mass transfer at the Mesa geothermal anomaly, Imperial Valley, California. Berkeley, Lawrence Berkeley Laboratory, LBL-8784, GREMP-3.

Kruger, P., and Ramey, H. J., Jr., eds., 1977. Proceedings, third workshop, geothermal reservoir engineering, Stanford University. Stanford, SGP-TR-25, 218 p.

Olson, E. R., and Elders, W. A., 1978. Hydrothermal mineralogy and isotope geochemistry in the Cerro Prieto geothermal field, Mexico: II, isotopic geochemistry. Proceedings, Geothermal Resources Council, Hilo, Hawaii, UCR/IGPP Contribution No. 78/9, 4 p.

Lawrence Berkeley Laboratory, Earth Sciences Division, 1977. Geothermal reservoir engineering management program (GREMP) Plan. Berkeley, Lawrence Berkeley Laboratory, LBL-7000, 136 p.

Table 2. Planned GREMP projects for fiscal year 1979.

		FY 1979				FY 1980			
GREMP category	Subject	1	2	3	4	1	2	3	4
Well Testing	Decline curve analysis	+	o				Δ		
	Two-phase mass flow				o		Δ		
Geochemical-technical	Tracers to follow flow								
	Trace element studies	o						Δ	
Properties of Materials	Permeability/porosity from cuttings				o			Δ	
Numerical Modeling				+	o				Δ
Site-Specific Studies				+	o				Δ
Fundamental Studies				+	o				Δ
Analytical Modeling					+				
Surface Geophysics									
Physical Modeling					+				
Economics				+	o				Δ
Exploitation Strategy				+	o				Δ

Legend

o Proposed start of project/task.
+ CBD announcement or existing qualified contractors list.
Δ Anticipated report, project milestone, or termination.

Pritchett, J. W., Rice, L. F., and Garg, S. K., 1979. Reservoir engineering data: Wairakei geothermal field, New Zealand. La Jolla, Systems, Science, and Software, SS-R-78-3597-11, v. 1 and v. 2, 490 p.

Randall, G., and Harrison, R., 1978. Annotated research bibliography for geothermal reservoir engineering. Salt Lake City, Terra Tek.

Schwarz, W. J., and Howard, J. H., 1978a. NSF RANN legacies, in Earth Sciences Division annual report 1977. Berkeley, Lawrence Berkeley Laboratory, LBL-7028, pp. 84-88.

_____, 1978b. Geothermal reservoir engineering management program plan, in Earth Sciences Division annual report 1977. Berkeley, Lawrence Berkeley Laboratory, LBL-7028, pp. 88-89.

Aquifer Thermal Energy Storage

The need for practical, low-cost methods of storing large amounts of thermal energy became apparent with the development of solar energy and the implementation of total-energy systems, which make use of waste heat from industrial processes and power production. The basic function of a storage system is to bridge the gap between periods of energy availability and those of power demand.

Aquifers provide one of the most promising solutions for long-term seasonal storage. Found at depths ranging from a few meters to several kilometers, aquifers are porous formations that contain and conduct water. Confined aquifers are bounded above and below by impermeable layers and are saturated by water under pressure. They are physically well suited for thermal energy storage because of their low heat conductivities, large volumetric capacities, and their ability to contain water under high pressure. For many years confined aquifers have been used for disposing liquid wastes and for storing fresh water, oil products, and natural gas.

Since the early 1970s, there has been a strong worldwide interest in thermal storage in aquifers. Major field experiments in hot-water storage have been conducted in the United States (Auburn University, Alabama), France, Switzerland, and Germany. Field experiments in chilled water storage have been conducted in the United States (Texas A & M University), China, and Japan. Lawrence Berkeley Laboratory first became involved in aquifer storage in 1976 when numerical modeling and generic studies of the concept were initiated. In May 1978, LBL was host to the first international workshop on thermal energy storage. In response to requests from workshop participants, LBL is now publishing a quarterly newsletter to keep researchers informed of work in progress. The high level of interest being expressed in aquifer thermal energy storge is expected to lead to a substantial increase in the number of research activities in coming years.

STUDY OF GROUNDWATER TEMPERATURE CHANGES DURING AQUIFER USES RELATED TO POWER PRODUCTION

M. J. Lippmann, C. F. Tsang, and P. A. Witherspoon

INTRODUCTION

Thermoelectric (fuel-burning) power plants are the largest users of water in the U.S. and their needs are expected to increase significantly in the future (Giusti and Meyer, 1977). About 99% of the total water intake of these plants is used for condensing spent steam from the generators (Table 1). In many cases, to avoid thermal pollution of surface water bodies, or to save water where it is expensive or scarce, cooling towers or ponds are employed. This allows the water to be used repeatedly in the condensers, but large volumes of water are lost to the atmosphere. In 1975 the amount of water consumed by U.S. fuel-burning power plants was 94 m^3/sec (Table 1). As the reuse of water becomes more prevalent, the water consumed by these plants will increase (Murray and Reeves, 1977).

The cooling waters carry with them large amounts of sensible heat, which might be used in district heating or in agricultural and industrial applications. The aquifer storage project, which is reported elsewhere in this volume, is studying the concept of storing some of the heated cooling waters in underground geologic formations for later uses. Since this idea involves injecting these waters into the aquifer with minimal contact with the atmosphere, only small volumes of water will be allowed to evaporate (i.e. consumed) and most of the thermal energy contained in the cooling water will be conserved.

The purpose of the present study, which grew out of the aquifer storage project, is to analyze the concept of using groundwater for cooling thermoelectric power plants and reinjecting the heated water into the same, or another, confined aquifer for storage purposes. In this way, water consumption will be reduced and some thermal energy will be conserved. Also, an alternative to a surface water supply will have been found. In localized areas the development of groundwater has advantages over surface water sources. It offers a more steady supply, a relatively constant

Table 1. U.S. water use for generation of thermoelectric power for 1975.

Water source	Condenser and reactor cooling (m^3/sec)	Other thermoelectric uses (m^3/sec)
Surface water		
Fresh	5700	88
Saline	2800	2
Groundwater		
Fresh	48	13
Public supplies	9	2
TOTAL	8557	105

	Water consumed
Fresh	83
Saline	11
TOTAL	94

Source: Modified from Murray and Reeves (1977, Table 9).

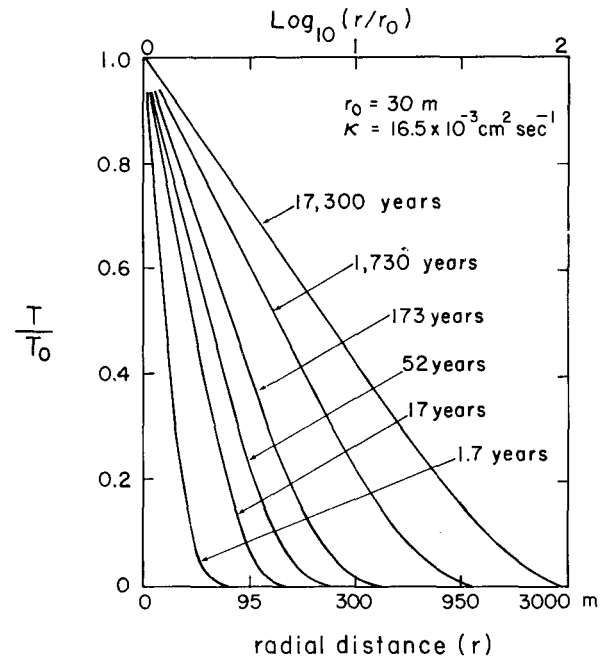

XBL 784-1803

Figure 1. Temperature in the region bounded internally by a cylinder $r = r_o$ with zero initial temperature and constant surface temperature T_o (modified from Carslaw and Jaeger, 1959, Fig. 41).

temperature and quality, and a broader area for site selection (Smith, 1978). In 1975 only a small percentage of water used in thermoelectric power plants came from groundwater sources (Table 1), but this is expected to increase (Smith, 1978).

FISCAL YEAR 1978 ACTIVITIES

The first studies in this project, which started this year, were aimed at computing the temperature variations in a confined aquifer when one well supplies cold water to a plant cooling system, and a second well is used to reinject this water into the same aquifer once the water has been heated.

Classical heat conduction studies (e.g., Carslaw and Jaeger, 1959) have shown that conduction is relatively slow in typical geologic formations. Figure 1 shows the transient temperature profile radially away from an infinitely long, 30-m radius (r_o) cylinder kept at a constant temperature (T_o), embedded in a medium whose thermal diffusivity (κ) is equal to 16.5 x 10^{-3} $cm^2 \cdot sec^{-1}$ and initial temperature is equal to zero. The figure shows that no temperature changes are felt 500 m away from the cylinder even after 100 years.

These results indicate that geologic materials with thermal properties similar to that of the example shown in Figure 1 are good thermal insulators. This makes it feasible to store waters of different temperature underground.

The previous analysis only considered conduction. If convection is incorporated, the heat transport through the materials is much faster. Tsang et al. (1977) have established that in the case of doublet systems (one injection well and one production well) placed in an aquifer with no natural regional groundwater flow, the breakthrough time (t_B) at the production well is given by equation (1). (Breakthrough time is the time it takes the injected hot water to reach the production well.)

$$t_B = \frac{1}{3}\left\{\frac{\pi H D^2}{Q}\right\}\frac{(1-\phi)\,\rho_R c_R + \phi\rho_W c_W}{\rho_W c_W} \qquad (1)$$

where H = aquifer thickness [L]
D = distance between wells [L]
Q = volumetric flow rate [L^3/T]
ϕ = porosity
ρ = density [M/L^3]
c = specific heat [L^2/t^2T]
R = rock, and
W = water.

Because the effect of the regional groundwater flow on the breakthrough time is uncertain, several cases were studied using a computer model developed by Gringarten and Sauty (1975). This code computes heat transport in porous media, assuming a steady-state mass flow field.

Different distances (D) between wells and regional groundwater regimes were considered. The parameters used in these studies and the

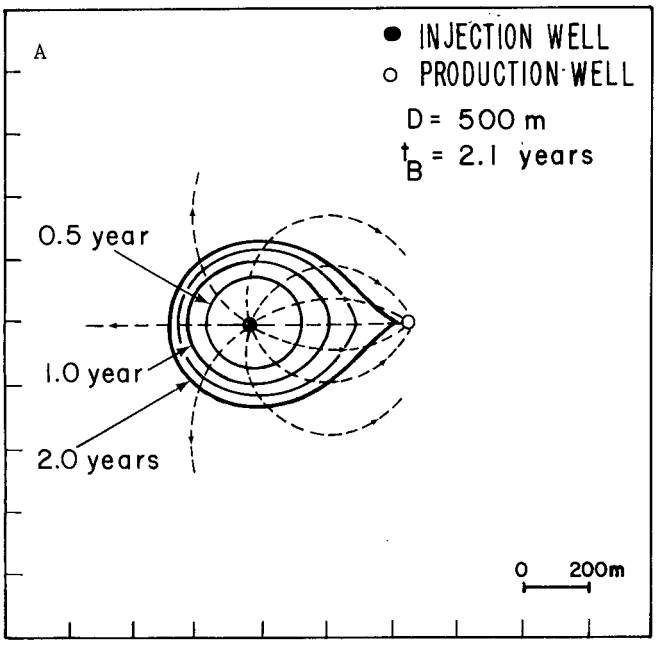

XBL 784-1805

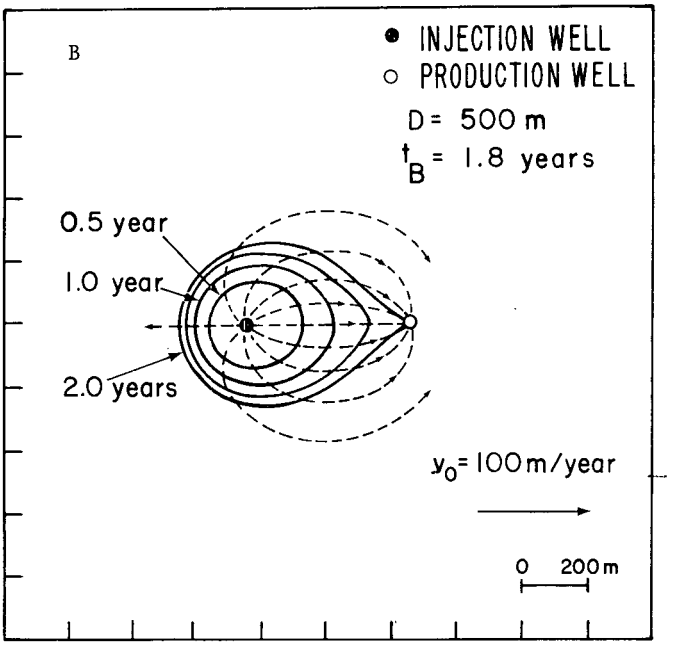

XBL 784-1807

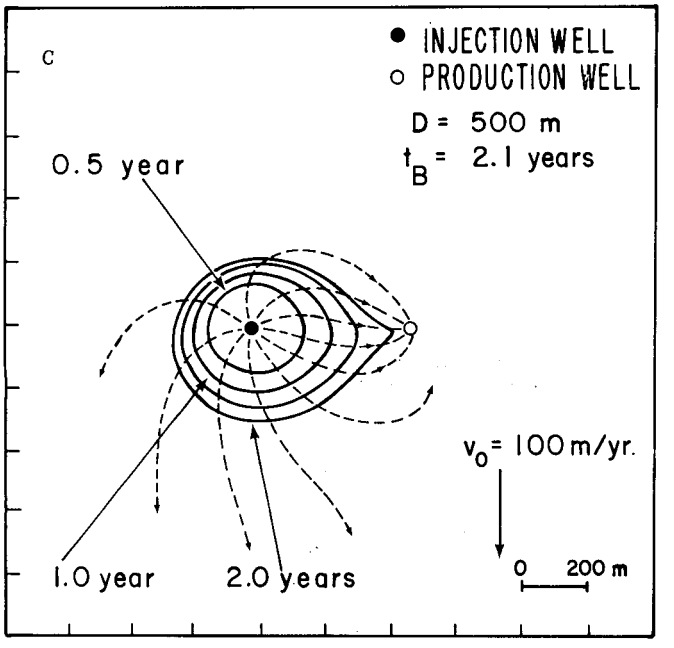

XBL 784-1811

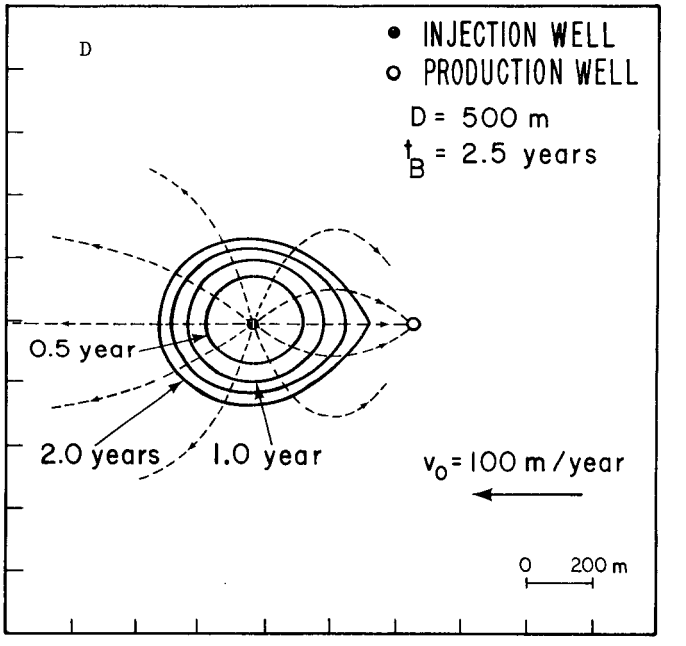

XBL 784-1804

Figure 2. Doublet well system (D = 500 m) under different regional groundwater conditions. Solid lines are hot temperature fronts and dotted lines are streamlines.

results obtained are given in Tables 2 and 3, respectively. The direction of the regional groundwater flow is given by the angle α measured counterclockwise between the vector connecting the injection and production wells, and the groundwater flow vector. Figures 2 and 3 illustrate the results. The solid lines indicate the position of the thermal front at different times; the dashed lines the flow lines between the wells.

Conclusions

The preliminary results of this study indicate that the use of groundwater for cooling in power plants, and the subsequent underground storage of the heated water could be an interesting proposition. The resulting reduction in water consumption (evaporation) and the possible energy conservation (if the stored hot water is later used) might make this economically feasible, especially in arid regions.

This study also indicates that the "thermal pollution" resulting from the injection of hot water into aquifers is reasonably localized around the injection wells. When the operation of the well system is finally stopped, the plume of hot water will drift in the direction of the natural groundwater flow. As the hot water drifts, it will give up heat to the granular skeleton of the aquifer, and become cooler.

Table 2. Doublet system, parameters used.

Flow rate (Q)	= 0.116 m^3/sec
Aquifer thickness (H)	= 50 m
Porosity (ϕ)	= 0.20
Volumetric heat capacity of water ($\rho_W c_W$)	= 1.0 cal/°C·cm^3
Volumetric heat capacity of rock ($\rho_R c_R$)	= 0.5 cal/°C·cm^3

Table 3. Results of doublet system.

Distance between wells (m)	Regional groundwater velocity (m/yr)	α (degrees)	Breakthrough time (years)
500	0	-	2.1
500	100	270	2.1
500	100	0	1.8
500	100	180	2.5
750	0	-	4.6
1000	0	-	8.2
1000	10	270	8.2
1000	100	270	8.9

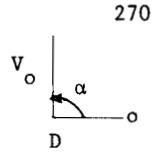

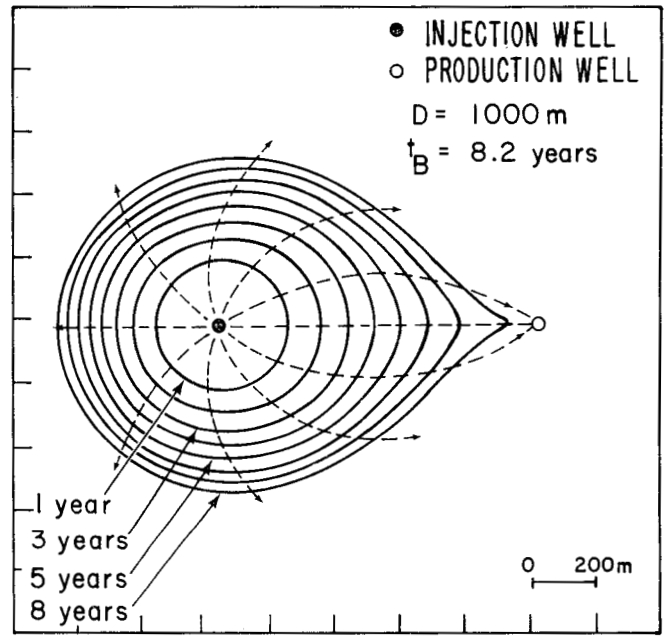

XBL 784-1806

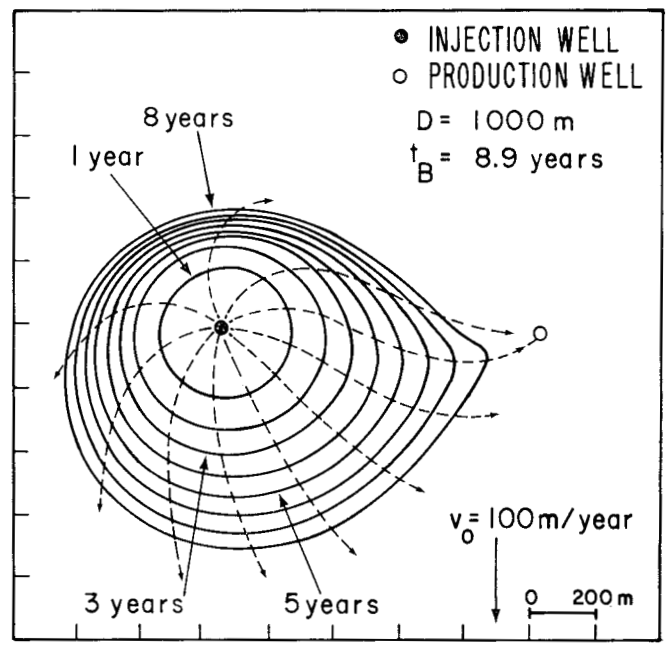

XBL 784-1808

Figure 3. Doublet well system (D = 1000 m) under different regional groundwater conditions. Solid lines are hot temperature fronts and dotted lines are streamlines.

When the wells are in operation, the regional flow will not affect the breakthrough times appreciably unless: (a) the direction of flow is from the injection well toward the production well ($\alpha = 0$) or in the opposite direction ($\alpha = 180^{o}$); or (b) the magnitude of flow (v_o) is greater than 10 m/yr. A careful design of the well pattern including the use of screening wells (Tsang and Witherspoon, 1975) will significantly reduce the effects of the regional groundwater flow. If necessary, the magnitude (and direction) of the natural flow could be changed locally by the use of screening wells, but in very few confined aquifers velocity of the regional flow will be much greater than 10 m/yr.

Using the parameters given in Table 2 it was shown that it will take between two and eight years before the temperature of the water extracted at the production well begins to increase. These time periods might be short compared with the design life of a typical power station (about 30 years), but increasing the distance between the wells or extracting some of the stored hot water will dramatically increase the breakthrough times.

FUTURE PLANS

The effect of temperature-dependent fluid properties on the breakthrough times will be studied. For this purpose, program CCC, developed at LBL (Lippmann et al., 1977) will be utilized. This would result in a better estimate of the environmental impact of storing hot water in an aquifer.

Chemical effects due to incompatibilities of injected and native groundwaters and rock-fluid interactions might be included in the computation. Economic feasibility studies of the concept of using groundwater for cooling purposes might also be initiated.

REFERENCES CITED

Carslaw, H. S., and Jaeger, J. C., 1959. Conduction of heat in solids, 2nd ed. Oxford, Clarendon Press, 510 p.

Giusti, E. V., and Meyer, E. L., 1977. Water consumption by nuclear power plants and some hydrological implications. Geological Survey Circ. 745, 14 p.

Gringarten, A. C., and Sauty, J. P., 1975. A theoretical study of heat extraction from aquifers with uniform regional flow. Jour. Geophys. Res., v. 80, no. 35, pp. 4956-4962.

Lippmann, M. J., Tsang, C. F., and Witherspoon, P. A., 1977. Analysis of the response of geothermal reservoirs under injection and production procedures. 47th Annual Calif. Reg. Mtg. Soc. Petrol. Eng. AIME, Bakersfield, California, April 13-15, 1977. Soc. Pet. Eng. SPE-6537.

Murray, R. C., and Reeves, E. B., 1977. Estimated use of water in the United States in 1975. Geological Survey Circ. 765, 39 p.

Smith, E. M., 1978. Ground-water use for nuclear plants. Ground Water, v. 16, no. 5, pp. 352-354.

Tsang, C. F., Lippmann, M. J., and Witherspoon, P. A., 1977. Production and reinjection in geothermal reservoirs. Geoth. Res. Coun. Trans., v. 1, pp. 301-303.

Tsang, C. F., and Witherspoon, P. A., 1975. An investigation of screening geothermal production wells from effects of reinjection, in Kruger, P., and Ramey, J. J., Jr., eds., Geothermal reservoir engineering. Stanford, Stanford Geothermal Program Rpt. SGP-TR-12, pp. 62-64.

MATHEMATICAL MODELING OF THERMAL ENERGY STORAGE IN AQUIFERS

C. F. Tsang, T. Buscheck, D. C. Mangold, and M. J. Lippmann

INTRODUCTION

The development of practical low-cost methods for storing large volumes of thermal energy is of fundamental utilization of solar energy and implementation of total-energy systems. The concept of hot-water storage wells was suggested by Rabbimov et al. (1971), Meyer and Todd (1973), and others. The basic concept is to store the large volumes of hot water that have been produced in conjunction with electric power plants, solar energy collectors and other heat-generating systems and use it in periods of heat demand. This would not only recover normally wasted energy, but would also greatly reduce thermal pollution around power systems. In addition, success of this type of energy storage would facilitate the implementation of large-scale total-energy systems in which utilities would produce and market both electricity and useful heat.

The objective of the present study is to use numerical models and other methods to (a) study and understand the hydrodynamic and thermal behavior of an aquifer under a variety of possible situations when used for hot or chilled water storage; (b) estimate the efficiency of storage and retrieval; and (c) model field experiments.

ACCOMPLISHMENTS DURING FISCAL YEAR 1978

The current project makes use of a numerical model developed at Lawrence Berkeley Laboratory to investigate hot and chilled water storage. The model, called CCC for conduction, convection, and compaction, is based on the integrated finite difference method. CCC computes heat and mass flow in three-dimensional, water-saturated, porous systems while simulating the vertical deformation of the system using the one-dimensional consolida-

tion theory of Terzaghi. Thus, the following physical effects are included in the calculations: (a) effects of temperature on fluid heat capacity, viscosity and density; (b) heat convection and conduction in the aquifer; (c) effects of regional groundwater flow; (d) spatial variations in aquifer properties; and (e) gravitational effects. The numerical model has been validated for examples having analytical or semianalytical solutions (e.g., Theis, 1935; Avdonin, 1964; Gringarten and Sauty, 1975).

Cases Studied

Annual cycle--seasonal storage. In this case, hot water is stored in the aquifer for 90 days in summer and is produced from the aquifer for 90 days during spring or fall. For successive cycles, the recovery temperature increases as the aquifer is heated, making it a more efficient hot-water storage system. The energy recovered was greater than 80% after only a few injection-production cycles.

Different cycle periods. In addition to annual cycle storage, we also looked at the semiannual cycle, that is: storage in fall, production in winter for space heating; and storage in spring, production in summer for air conditioning. Very similar results were obtained. The percentage of energy recovered for successive cycles is shown in Figure 1.

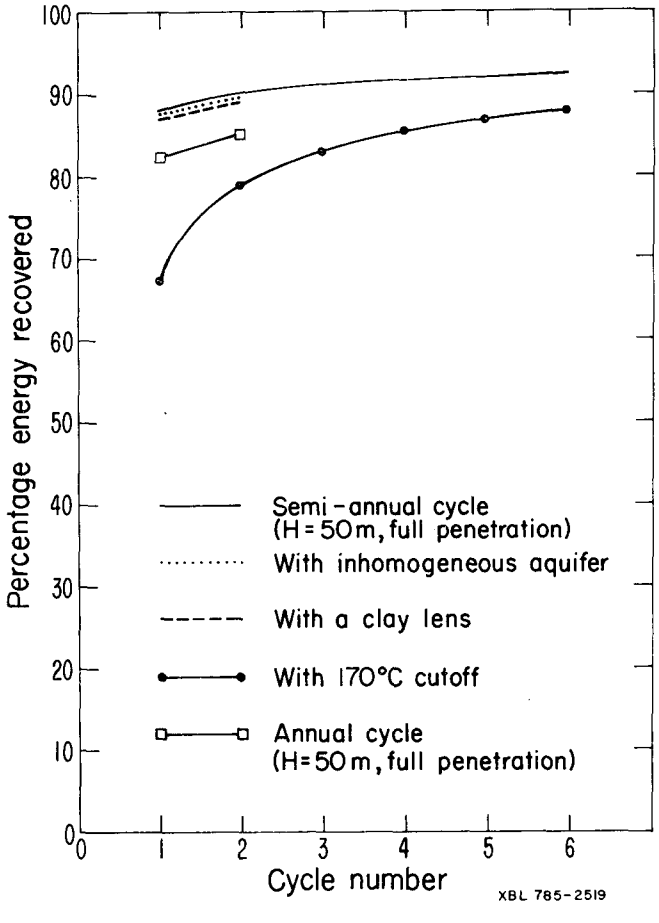

Figure 1. Percentage of energy recovered for different cycles.

Well partially penetrating the aquifer. Calculations were also performed assuming the well to be open only for the upper half of the aquifer. Although the buoyancy effect of low-density hot water was clearly demonstrated, the percentage of energy recovered for successive cycles was only slightly affected.

Storage of water of different temperatures. We have looked at storage of water at 120, 220, and 320°C. We found that, as far as the hydrodynamic and thermal behavior of the aquifer is concerned, the results appear to scale as (T_s - T_o), where T_s is the temperature of water stored and T_o is the original aquifer temperature.

Effect of a clay lens in the aquifer. In this case the aquifer is divided into two parts by a clay lens with a radius of 20 m. If the well is open only below the lens, the result of hot-water injection and production is as shown in Figure 2, which displays the temperature contours after 90 days of injection and 90 days of subsequent production. The effect of the clay lens on these temperature contours is clearly demonstrated. However, it is found that the percentage of energy recovered is not much affected (Figure 1).

Inhomogeneity of the aquifer. If the aquifer is composed of two layers, one more permeable than the other, then the flow and the temperature contours will be changed. An example in which one region is twice as permeable as the other is shown in Figure 3. The water tends to flow into the

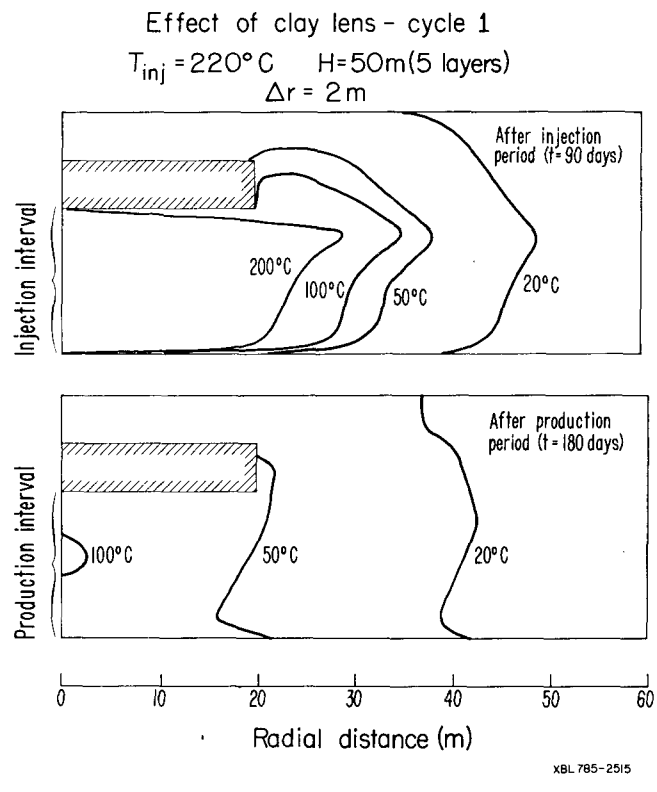

Figure 2. Effect of a clay lens (Cycle 1); 90-day production and injection periods.

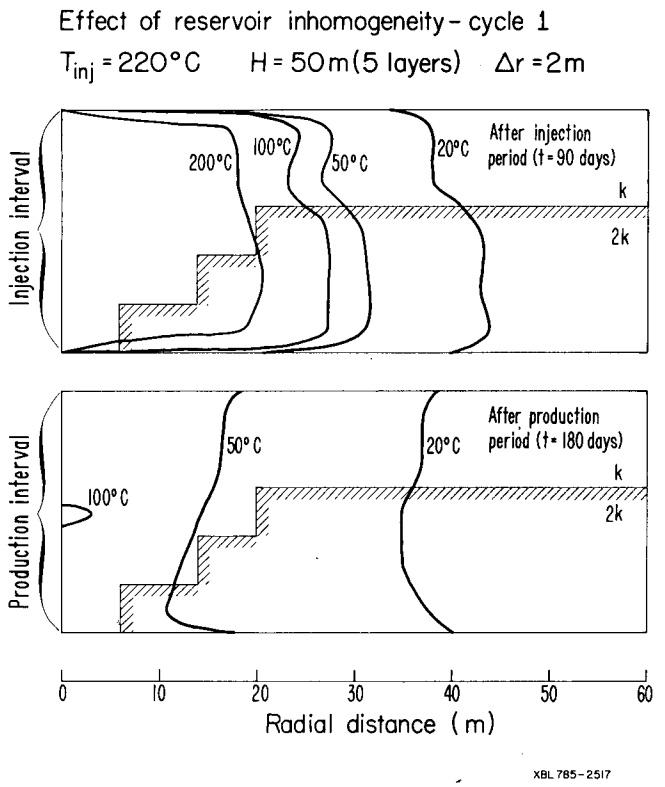

Figure 3. Effect of reservoir inhomogeneity (Cycle 1); 90-day production and injection periods.

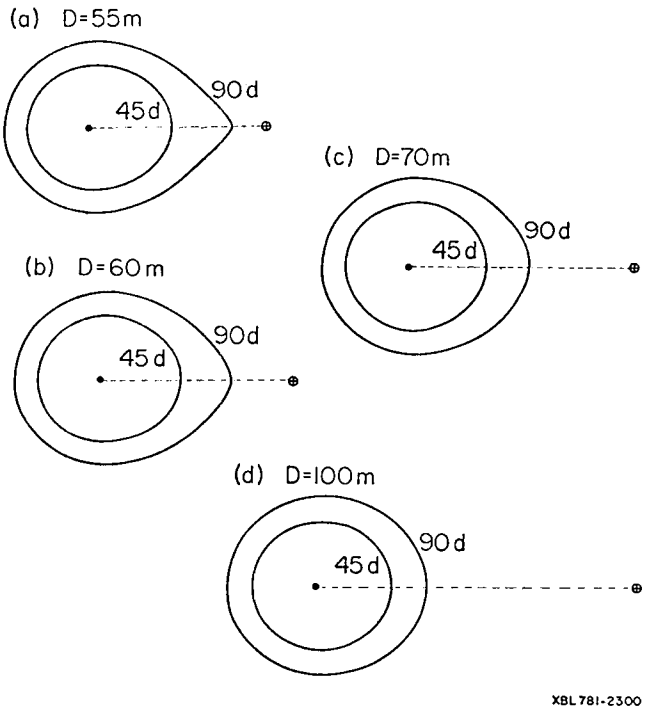

Figure 4. Effect of separation distance between storage and supplying wells at 45 and 90 days.

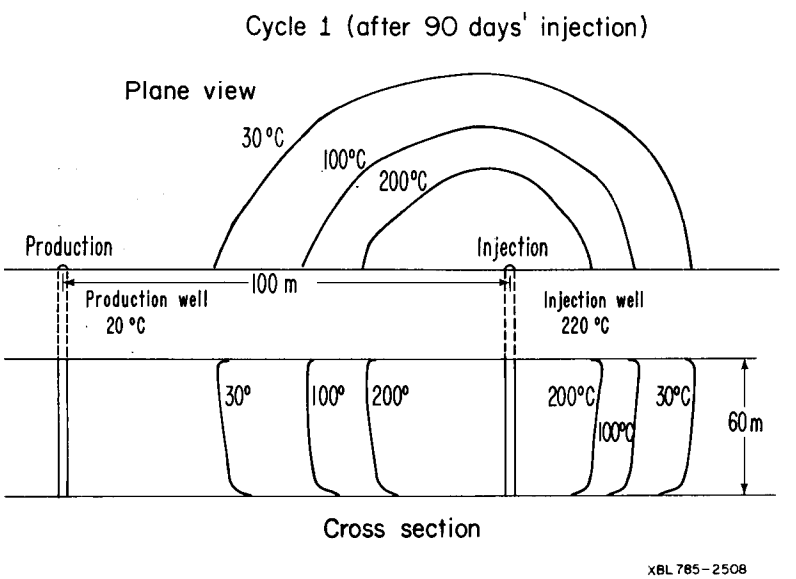

Figure 5. Isotherms for a two-well system after 90 days of injection. Plane and cross section views.

higher permeable region as would be expected. However, it is again found that the percentage of annual recovery is not much affected (Figure 1).

Chilled water storage. In addition to hot-water storage, we have studied the concept of storage of winter-chilled water to be used in summer for air conditioning. If we assume storage of 4°C water for 90 days in winter and production for 90 days in summer, then the production temperature after a few cycles is expected to be below 10°C for the entire production period.

Two-well system. In this case, we studied a system of two wells, where one well supplies the water that is heated and injected into the other well. In studies described above, the thermal front moves radially from the single well. However, in this case, because of the presence of the second well, the thermal front will be distorted. In Figure 4, the thermal fronts are shown as a function of the separation between the storage well and the supplying well. As indicated, if the two wells are a reasonable distance apart, single-well results are applicable. To study this case in more detail, we have performed three-dimensional numerical modeling of the two-well system. A fine mesh is used near the storage well to ensure an adequate description of the temperature changes in that region. Results of the calculations are shown in Figure 5. Here, the effect of the supplying well and the gravitational buoyancy effect are clearly indicated.

Possibility of consolidation or uplift. To demonstrate the capability of the model to calculate the consolidation or uplift effect, we have performed calculations based on two sets of arbitrarily chosen parameters. Results indicate that consolidation and uplift are strongly parameter-dependent (i.e., site-specific).

Natural regional flow. The effect of natural regional flow has been studied using both a two-dimensional steady-state fluid-flow model and a three-dimensional model. Results indicate that a natural flow rate on the order of 1 m/yr will not adversely affect storage capabilities. Appreciable effects are found if the flow is unusually large (~100 m/yr).

Other Work

In addition to these modeling studies, we have also performed the following work during fiscal year 1978.

Workshop on thermal energy storage in aquifers. LBL organized and hosted the Workshop on Thermal Energy Storage in Aquifers held May 10-12, 1978. The purpose of the workshop was to provide an exchange of ideas and technical information. More specifically, the workshop reviewed the potential of thermal energy storage in aquifers; addressed possible technical, environmental, and institutional problems; and examined storage projects currently under way. There were 76 participants including 6 foreign speakers who discussed aquifer storage projects in their countries. Proceedings from the workshop are published (Lawrence Berkeley Laboratory, 1978).

Aquifer thermal energy storage newsletter. At the request of DOE, Oak Ridge National Laboratory, and foreign participants at the Aquifer Workshop, LBL has accepted the responsibility of publishing a quarterly Aquifer Thermal Energy Storage Newsletter. The purpose of the newsletter is to keep workers in this field informed of major results and the current status of aquifer storage projects throughout the world. The first issue, consisting of brief descriptions of storage projects discussed at the Aquifer Workshop, was distributed to 116 persons including 33 foreign recipients in 10 countries.

Well test analysis of Auburn University field data. Data are being collected from field experiments conducted at Auburn University. Older data have been stored on the LBL computer and well-test analysis of the field data has been initiated to verify aquifer parameters and geometry. By using a variable-flow well-test analysis method we hope to determine the properties of the aquifer and its nearby barriers. Once aquifer parameters have been determined, a computer simulation will be made of the aquifer when used for hot-water storage.

PLANS FOR FISCAL YEAR 1979

A simulation study will be made of the Auburn University field experiments to understand the hydrodynamics and heat-flow processes in these experiments and to calibrate and validate our numerical model. The results and experiences of this study will be useful to other planned demonstration projects.

LBL will continue to be responsible for publication of the Aquifer Thermal Energy Storage Newsletter. Articles will be solicited from researchers throughout the world.

Depending on the time available under the present level of funding, modeling of typical situations in thermal energy storage will be made. These modeling studies will include a calculation of daily cycle storage. A program will be written to include the effect of heat loss along the wellbore as water is injected into or produced from the aquifer. If the percentage of heat recovery is high, this case will have particular application for solar power systems.

REFERENCES CITED

Avdonin, N., 1964. Some formulas for calculating the temperature field of a stratum subjected to thermal injection. Izv. Vyssh. Uchebn. Zaved. Neft. Gaz, v. 7, no. 3., pp. 37-41.

Gringarten, A. C., and Sauty, J. P., 1975. A theoretical study of heat extraction from aquifers with uniform regional flow. Jour. Geophys. Res., v. 80, no. 35, pp. 4956-4962.

Lawrence Berkeley Laboratory, 1978. Thermal energy storage in aquifers workshop, proceedings, May 10-12, 1978, Berkeley. Berkeley, Lawrence Berkeley Laboratory, LBL-8431.

Lippmann, M. J., Tsang, C. F., and Witherspoon, P.A., 1977. Analysis of the response of geothermal reservoirs under injection and production procedures. Soc. Petrol. Eng. 47th California Meeting, Bakersfield, California, April 13-15, 1977. Dallas, Soc. Petrol. Eng., SPE-6537.

Meyer, C. F., and Todd, D. K., 1973. Conserving energy with heat storage wells. Envir. Sci. Tech., v. 7, no. 6, pp. 512-515.

Rabbimov, R. T., Umarov, G. Y., and Zakhidov, R. A., 1971. Storage of solar energy in a sandy-gravel ground. Geliotekhnika, v. 7, no. 5, pp. 57-64.

Theis, C. V., 1935. The relation between the lowering of piezometric surface and the rate and duration of discharge using ground-water storage. Trans. Am. Geophys. Union, v. 2, pp. 519-524.

Tsang, C. F., Lippmann, M. J., Goranson, C. B., and Witherspoon, P. A., 1976. Numerical modeling of cyclic storage of hot water in aquifers. Berkeley, Lawrence Berkeley Laboratory, LBL-5929.

GEOSCIENCES

The summary papers which follow describe fundamental studies addressing a variety of earth science problems in support of the U.S. Department of Energy's missions. They have applications in such diverse areas as geothermal energy, oil recovery, in-situ coal gasification, uranium resource evaluation and recovery, and earthquake prediction.

Funding for studies described by approximately half of the papers comes from the U.S. Department of Energy Office of Basic Energy Sciences (OBES). The U.S. Department of Energy's Division of Fossil Fuel Extraction (DFFE) and Division of Geothermal Energy (DGE), Bendix Field Engineering Corp., E. G. & G., Inc., and Lawrence Berkeley Laboratory's Director's Development Fund provide support for the remainder. Most of the studies are conducted under ongoing projects. For descriptions of earlier work, the reader is referred to the 1977 Annual Report of the Earth Sciences Division (LBL-7028) and the 1976 and 1975 Annual Reports of the Energy and Environment Division of Lawrence Berkeley Laboratory (LBL-5982 and 5299, respectively).

In the following paragraphs, a brief discussion of the papers is given in order that the reader may appreciate the diversity of the work being accomplished and find his way to the subjects that interest him most.

The most promising geothermal energy resources are found in so-called "liquid dominated" reservoirs, where the energy is produced through the recovery and use of underground hot water. Two major problems associated with this process are (a) the uncertainty of the properties and behavior of the fluid recovered, and (b) the productive capacity and duration of the supply of hot water from the reservoir. In papers by Otto et al., Pitzer et al., and Weres et al., various aspects of geothermal fluids are discussed including, respectively, the compositional characteristics, thermodynamic properties, and tendency of the fluid to precipitate amorphous silica. All of these aspects have an important bearing on the choice of design for and configuration of a geothermal plant, whether for power generation or for heating alone. Questions relating to subsurface factors controlling the chemical composition of geothermal fluids are considered in an ongoing study of rock-water interactions. In the paper by Neil and Apps, the solubility of albite, an importnt rock-forming mineral in the aqueous phase at geothermal reservoir temperatures, is discussed.

Geothermal reservoir problems are investigated in a series of four fundamental papers by Narasimhan and his coworkers, Kanehiro and Tsang. These papers are primarily concerned with the aquifer response to earth tides and the meaning of an important reservoir parameter, the storage coefficient. The physical properties of reservoir rocks when saturated with brine are considered by Somerton et al. in the paper on rock-fluid systems.

Mention should also be made of a potential source of geothermal energy: molten magmas. The thermodynamic and transport properties of synthetic melts representative of natural magmas and the properties of the solid phases that crystallize from melts are being studied by Carmichael et al.

Two papers concern the exploitation of fossil fuels. One by Radke and Somerton covers the subject of increasing oil recovery through the use of reactive tension agents. The other, by Mangold et al., makes predictions of the thermal effects on the surface after in-situ combustion of shallow coal seams.

Uranium resources are evaluated in a paper by Strisower et al. Specifically addressed are disseminated low-grade deposits found associated with peralkaline intrusive rocks in the United States. Another paper by Wollenberg and Strisower on the Geodose Project summarizes the results of a literature search for data on uranium, thorium, and potassium contents of major rock types. This was done in order to characterize rock types by their natural gamma-ray exposure rates.

A paper by Villet and Mitchell, with broad implications in several energy fields, covers the subject of determining the properties of soils and soft rocks by in-situ measurements. Reliable information on these geotechnical parameters is required for the design of structure foundations, stable slopes, and underground excavations, including those required for energy storage.

The ability to correlate earthquakes with the radon content of well waters was investigated by Berlin. His conclusions with regard to data collected from two wells near Oroville, California, are summarized in his paper.

Finally, the results of efforts to increase the precision of measurements of the ratios of the heavy isotopes, using a 5-ft-radius mass spectrometer are presented by Michel. This work has important implications in the precise age determination of geological materials, and in the interpretation of the early history of the earth.

A NOTE ON THE MEANING OF STORAGE COEFFICIENT

T. N. Narasimhan and B. Y. Kanehiro

INTRODUCTION

The term storage coefficient (S) and the synonymous terms coefficient of storage and storativity, have been used extensively in the groundwater literature. It has been defined (Ferris et al., 1962) as "the volume of water which an aquifer releases from or takes into storage per unit surface area of aquifer per unit change in the component of head normal to the surface." Historically, this somewhat restricted definition appears to have been introduced to satisfy the need for a coefficient occurring in the differential equation describing nonsteady groundwater flow.

ACTIVITIES IN FISCAL YEAR 1978

The definition and applicability of the storage coefficient was examined by the authors. The impetus for this came from our observation of the response of aquifers to earth tides. The result of this study was some clarification of the assumptions made in defining storage coefficients and a useful comparison of different storage coefficients employed by various fields involved in the study of porous media. A brief summary of the results is presented below.

Although the aforementioned definition of storage coefficient is convenient and adequate for applications related to well testing, it is not adequate for the consideration of all nonsteady flow in arbitrary, heterogeneous, three-dimensional systems. A more concisely defined and more general coefficient is specific storage (S_s) also referred to as specific storativity. It can be defined directly in terms of the compressibility of the skeleton of the aquifer and the compressibility of water.

In examining the nature of the coefficients used to describe change in storage, the applicability of and expressions for the various coefficients used by different fields were considered. The specific storage coefficient is strictly applicable only to situations where the total stress on the porous medium is constant. This corresponds to a drainage problem where there is addition or removal of fluid from the system, as in the case of pumping tests. The seemingly different expressions for the coefficients used to describe change in storage arise from different choices of normalizing volumes.

The mass of fluid stored in a given volume of a porous medium may be expressed as (Narasimhan and Witherspoon, 1977):

$$M_f = V_v \rho_f S_f \qquad (1)$$

where

M_f = the mass of fluid,

V_v = the volume of the voids,

ρ_f = the density of the fluid, and

S_f = the saturation of the fluid.

It is known empirically that V_v, ρ_f, and S_f are all functions of the average fluid pressure in a given volume of the porous medium. Hence, it is possible to define a fluid mass capacity, M_c^*, which expresses the rate of change of mass of fluid with respect to the change in average fluid pressure within the volume.

$$M_c^* = \frac{dM_f}{dp_f}$$

$$= V_v S_f \frac{d\rho_f}{dp_f} + \rho_f S_f \frac{dV_v}{dp_f} + V_v \rho_f \frac{dS_f}{dp_f} \qquad (2)$$

The first term on the right-hand side of equation (2) represents the change in volume of the pore fluid. The second term represents the deformation of the skeleton of the porous medium, and the third term represents the desaturation of the medium.

At least in the fields of hydrology and petroleum engineering, the medium is generally assumed to be completely saturated. The expression for fluid mass capacity then simplifies to

$$M_c^* = V_v \frac{d\rho_f}{dp_f} + \rho_f \frac{dV_v}{dp_f} . \qquad (3)$$

The first term is evaluated by assuming a slightly compressible fluid of compressibility c_w. The fluid mass capacity may then be written as

$$M_c^* = \rho V_v c_w + \rho_f \frac{dV_v}{dp_f} . \qquad (4)$$

The second term is generally evaluated by assuming that the total stress on the porous medium is constant. Because the effective stress (σ') of the skeleton is generally related to the fluid pressure (p_f) and total stress (σ) as $\sigma' = \sigma - p_f$ for a saturated system, the magnitude of the change in fluid pressure is equal to the magnitude of change in effective stress. This makes it possible to write the fluid mass capacity as

$$M_c^* = \rho_f V_v c_w - \frac{dV_v}{d\sigma'} .$$

Note, however, that the expression now refers directly only to situations where fluid is either being removed from or added to the system.

This formulation of fluid mass capacity is related to an arbitrary volume element. For convenience it is generally necessary to have a volume normalized coefficient. Actually two normalization volumes are necessary. First, the second term of the expression for M_c^* must be normalized so that it can be expressed in terms of some compressibility related to the skeleton of the porous medium. Then the entire expression for the fluid mass capacity is volume-normalized to give a specific fluid mass capacity. To conform with the more common practice of using specific fluid volume capacity with respect to hydraulic head, fluid pressure is converted to hydraulic head assuming constant fluid density.

It is in choosing various normalizing volumes that much of the confusion between the different coefficients arises. In general, there are three choices available. These are (a) the bulk volume, V_b; (b) the solid volume, V_s; and (c) the pore volume, V_v.

The results of choosing various combinations of normalizing volumes may be summarized as the following four cases (Narasimhan and Kanehiro, 1978).

1. Bulk volume, V_b, used in both cases,

$$S_s = \rho_f g\,[nc_w + m_v]$$

2. Solid volume, V_s, used in both cases,

$$S_s = \rho_f g\,[ec_w + a_v]$$

3. Pore volume, V_p, used for deformation, and V_b used for volume over which specific storage is defined,

$$S_s = \rho_f gn\,[c_w + c_p], \text{ and}$$

$$nc_t = n\,[c_w + c_p]$$

4. V_s used for deformation and V_b used for volume over which specific storage is defined

$$S_s = \rho_f g\,[nc_w + (1-n)\,a_v]$$

Here, m_v is the volumetric coefficient of compressibility defined as

$$m_v = -\frac{1}{\Delta\sigma'}\frac{\Delta V_v}{V_b}$$

where a_v is the coefficient of compressibility defined as

$$a_v = -\frac{1}{\Delta\sigma'}\frac{\Delta V_v}{V_s},$$

and c_p is the pore volume compressibility defined as

$$c_p = -\frac{1}{\Delta\sigma'}\frac{\Delta V_v}{V_v}.$$

Finally, in view of the definition of the storage coefficient (S) specific storage is simply the storage coefficient normalized with respect to the thickness of the aquifer. That is,

$$S = S_s b$$

where b is the thickness of the aquifer. Also, because nc_t is change in storage with respect to fluid pressure,

$$S_s = \rho_f gnc_t,$$

and the commonly used petroleum engineering term, ϕch ($= nc_t b$ in the present notation) can be written as:

$$\phi ch = nc_t b = \frac{S_s}{\rho_f g} b = \frac{S}{\rho_f g}.$$

REFERENCES CITED

Ferris, J. G., Knowles, D. B., Brown, R. H., and Stallman, R. W., 1962. Theory of aquifer tests. Geological Survey Water Supply Paper 1536-E.

Narasimhan, T. N., and Kanehiro, B. Y., 1978. A note on the meaning of storage coefficient. Berkeley, Lawrence Berkeley Laboratory, LBL-8295.

Narasimhan, T. N., and Witherspoon, P. A., 1977. Numerical model for saturated-unsaturated flow in deformable porous media: Part I, Theory. Water Resources Res., v. 13, no. 3, pp. 657-666.

SIGNIFICANCE OF THE STORAGE PARAMETER IN SATURATED-UNSATURATED GROUNDWATER FLOW

T. N. Narasimhan

INTRODUCTION

The primary phenomenon that distinguishes transient from steady groundwater flow is change in storage. The quantity of water stored in a groundwater system may change due to expansion of water (usually very small), change in void volume of the skeleton, or change in water saturation. These independent phenomena often occur simultaneously. In particular, change in storage in fully saturated media is usually dominated by soil deformation, while the phenomenon of desaturation usually dominates change in storage in the unsaturated zone. The customary assumption that the skeleton is rigid in a desaturating soil is realistic only under those conditions when saturation is relatively low. The assumption is particularly unrealistic in the transition regime between saturated and unsaturated flow. The importance of soil deformation in this transition regime cannot be overlooked. In fact, soil deformation at high saturations provides the key bond between saturated and unsaturated regimes of transient groundwater flow (Narasimhan and Witherspoon, 1977; Narasimhan and Holzer, 1978; Narasimhan, 1978).

STORAGE AND CHANGE IN STORAGE

The quantity of water stored in a small elemental volume of a soil is given by:

$$M_w = \rho_w V_v S \tag{1}$$

where M_w is mass of water, ρ_w is water density, V_v is void volume, and S is saturation. It is known empirically that ρ_w, V_v, and S are functions of the fluid pressure head ψ. Therefore, the quantity can be defined as fluid mass capacity, M_c, which is the derivative $dM_w/d\psi$. M_c represents the quantity of water released from the volume element as the average pressure head is dropped by unity. If, for convenience, the compressibility of water is neglected, then M_c can be obtained, using the chain rule of differentiation:

$$M_c = \rho_w \left[S \frac{dV_v}{d\psi} + V_v \frac{dS}{d\psi} \right]. \tag{2}$$

The term $dV_v/d\psi$ on the right-hand side of equation (2) denotes void volume change as a function of ψ. However, soil deformation is properly a function of the effective skeletal stress (σ') rather than pore pressure ($\rho_w g \psi$). Therefore an explicit constitutive law between ψ and σ' is required. From the soil mechanics literature, this relation is assumed to be

$$\sigma' = \sigma - \chi \rho_w g \psi \tag{3}$$

where σ is the total external stress, $\chi \leqslant 1$ in partially saturated soils and $\chi = 1$ in fully saturated soils, and g is acceleration due to gravity. In most groundwater problems, σ can be treated as constant and hence,

$$\frac{d\sigma'}{d\psi} = -\left[\chi + \psi \frac{d\chi}{d\psi} \right] \rho_w g = -\chi^* \rho_w g . \tag{4}$$

In view of equation (4), equation (2) can be written as

$$M_c = \rho_w \left[-S\chi^* \rho_w g \frac{dV_v}{d\psi} + V_v \frac{dS}{d\psi} \right] . \tag{5}$$

If we stipulate that the volume element has constant volume of solids and normalize equation (5) with reference to the solid volume (V_s) of the elemental volume, then

$$M_c = V_s \rho_w \left[S\chi^* \rho_w g a_v + e \frac{dS}{d\psi} \right] \tag{6}$$

where a_v is the coefficient of compressibility defined by $a_v = -de/d\sigma'$.

In dealing with unsaturated soils, it is customary to treat the soil skeleton as rigid (that is, $a_v = 0$), and attribute M_c in equation (6) entirely to the desaturation phenomenon. Conceptually, however, it is more rational to consider that in unsaturated soils, χ^* is extremely small, rather than stating that $a_v = 0$. If we recall that for a fully saturated soil, $\chi^* = 1$, then it is obvious that χ^* has to decrease from 1 when the soil is saturated to nearly zero or when saturation is significantly small. This implies that when the soil has high saturations, $\chi^* > 0$, and hence there will always be some deformation accompanying desaturation as pore pressure changes. This perspective is extremely important in unifying saturated-unsaturated flows. To understand this, suppose for a moment that the soil is rigid whenever pore pressure is less than atmospheric. As progressive suction is applied to a saturated soil, the soil will not begin to desaturate unless suction exceeds a critical air-entry value, K_A. In the pressure range, $\psi_A < \psi_A < 0$, it is obvious that $dS/d\psi = 0$. If in this range A_v is also assumed to be zero (rigid soil), then $M_c = 0$ in equation (6) means that the soil has no capacity to release water from storage and it cannot participate in transient flow. Of course this anomaly would not exist if $\chi^* > 0$ when $\psi_A < \psi < 0$, and the soil skeleton has nonzero a_v corresponding to its existing stress level.

An Example

The fact that χ^* may not be zero except in extremely dry soils implies that soil deformation may occur simultaneously with desaturation in unsaturated soils. Although normally one considers deformation only in fully saturated soils (e.g.,

land subsidence), there is some evidence to suggest that deformation of partially saturated soils may be responsible for field problems of considerable interest. One such problem is that of large earth fissures observed in areas of heavy groundwater withdrawal and large water-level declines in the arid tracts of Arizona and elsewhere (Davis, 1978). To investigate whether or not sufficient effective stresses could be mobilized in the zone of partial saturation, to cause contractions leading to earth fissuring, numerical simulations were carried out on a hypothetical soil column as described below.

Consider an 85-m-tall column of soil, barely saturated at the initial timme, with a hydraulic potential of 85 m of water everywhere in the flow region (Figure 1). For $t > 0$, water is allowed to drain at the bottom at a constant rate of 2.746×10^{-5} m^3/sec. With the onset of drainage, desaturation is initiated at the top of the column. The purpose of simulation is to investigate if significant volume deformations can accompany desaturation.

Two hypothetical soils with different soil moisture characteristics were considered but with essentially the same X-vs-saturation relationships (Figure 2). Both soils were assumed to have the same nonlinear deformation coefficient, $C_c = 0.1$, and to have absolute permeability, k, given by

$$k = \left(\frac{4.628}{4.628+|\psi|^{1.645}}\right)(5.67 \times 10^{-14}\ m^2)$$

The effective stress to pore-pressure relationship for the two soils is given in Figure 2.

The column was subjected to a drainage simulation equal to 10 years, with simultaneous compaction. The profiles of variation of some of the important parameters for Soil 2 at the end of 10 years are given in Figure 3.

The computed deformations in the unsaturated zone are summarized in Table 1.

As can be seen from the table, for both soils deformation in the unsaturated regime is over 25% of the total volume strain. This leads to the inference that, under certain conditions of heavy groundwater withdrawal from unconfined aquifers, one could expect significant column strains to accompany the desaturation process. Such strains may, if conditions are favorable, cause contractions leading to earth fissures.

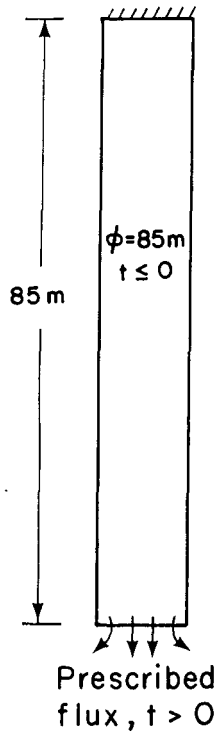

XBL785-936

Figure 1. Earth fissure problem: initial and boundary conditions.

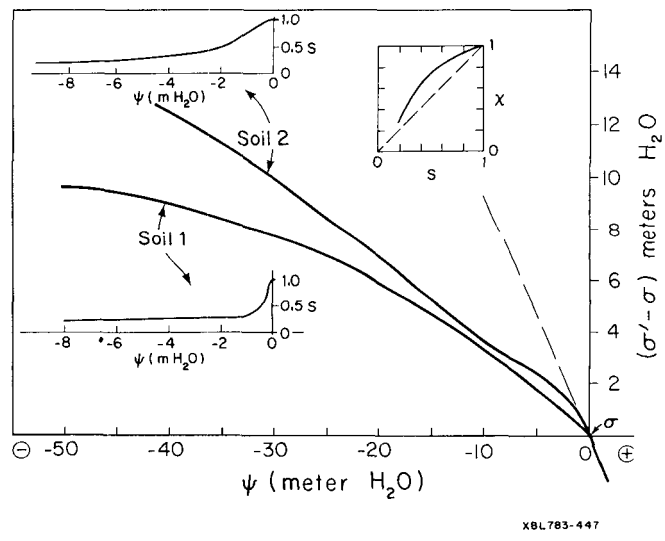

Figure 2. Earth fissure problem: variations of effective stress with ψ for two hypothetical soils.

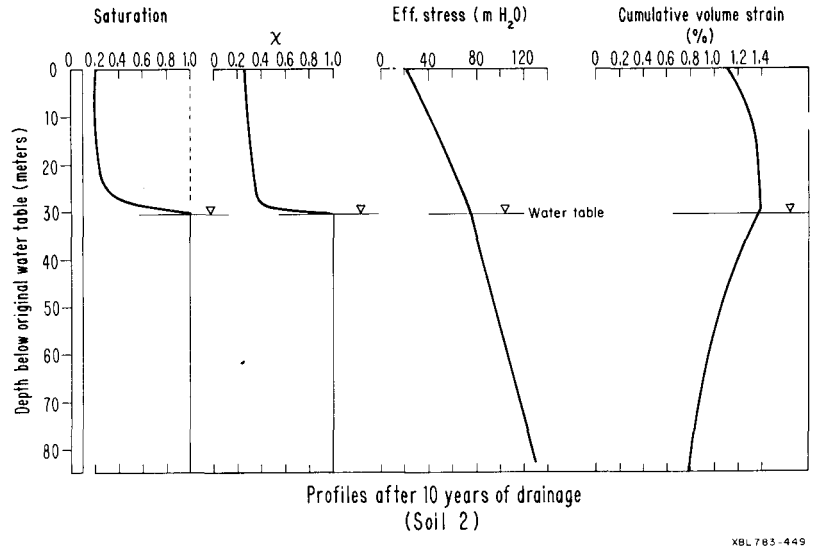

Figure 3. Earth fissure problem: profiles of S, χ, σ', and volume strain after t = 10 years.

Table 1. Computed deformations in the unsaturated zone.

	Soil assumed rigid in unsaturated zone (%)	χ = χ(S)	
		Soil 1 (%)	Soil 2 (%)
Total volume strain above water table after 10 yr	0.95	1.31	1.24
Volume strain in the saturated regime	0.95	0.96	0.91
Volume strain in the unsaturated regime	0	0.35	0.33

REFERENCES CITED

Davis, S. N., 1978. Origins of earth fissures. Geol. Soc. Am., Abstracts with Programs, v. 10, no. 3, p. 102.

Narasimhan, T. N., 1978. The significance of the storage parameter in saturated-unsaturated groundwater flow. Berkeley, Lawrence Berkeley Laboratory, LBL-7041.

Narasimhan, T. N., and Holzer, T. H., 1978. Possibility of soil deformation in the partially saturated zone due to pore pressure changes. Geol. Soc. Am., Abstracts with Programs, v. 10, no. 3, p. 188.

Narasimhan, T. N., and Witherspoon, P. A., 1977. The significance of the storage parameter in saturated-unsaturated groundwater flow. Invited Paper, Symposium on Unified Studies of American Geophysics Union, Annual Meeting, Washington, D.C.

USE OF AQUIFER RESPONSE TO EARTH TIDES AS A MEANS OF DETERMINING AQUIFER CHARACTERISTICS

T. N. Narasimhan and B. Y. Kanehiro

INTRODUCTION

The use or observation of periodic fluctuations of water levels in wells resulting from aquifer response to tidal phenomena is not new. The earth is within the gravitational fields of the sun and the moon, and as such is subject to tidal forces. Because the motions of these celestial bodies are very nearly periodic, the strains in the earth related to tidal forces also exhibit periodic variations in time. Because these tidal strains arise from forces that are gravitational in nature, they must exist in all parts of the planet. In general, however, tidal forces only cause readily observable responses in the hydrosphere in the form of ocean tides. While tides do exist in the atmosphere and lithosphere, they are of very small magnitude. For these reasons, a substantial body of knowledge exists on the use of aquifer response to ocean tides under various circumstances, but comparatively little is known about the response to atmospheric (barometric) or lithospheric (earth) tides. In the former case, the barometric tide is generally lost in the daily variations in barometric pressure that are not related to tidal forces. In the latter case, the inability to make accurate measurements in deep wells of small changes in pore-fluid pressure has thwarted attempts to quantify the response of aquifers to earth tides.

With the advent of the present generation of extremely sensitive pressure transducers using quartz crystal sensors, good measurements of small pressure fluctuations have become possible. Further, these measurements can be made in artesian (flowing) wells that have been shut in where there is reason to believe that larger responses to earth tides occur.

ACTIVITIES IN FISCAL YEAR 1978

In fiscal year 1978, the authors studied some aspects of the practical utility of the response of aquifers to earth tides for the determination of aquifer characteristics. The result of this study was a preliminary means for estimating the specific storage of an aquifer. A summary of the derivation of this method is presented below.

The determination of aquifer characteristics based on response to earth tides requires that the fluctuation at a well be related to the tides by a theory incorporating coefficients describing the desired aquifer characteristics. The intrinsic complexities of the tide, accentuated by the presence of spurious fluctuations, generally necessitates the decomposition of the well signal into sine-wave components before any theory can be applied. Finite Fourier analysis is used to determine the amplitudes of five tidal components of the signal at the well together with the tide itself (Kanehiro et al., 1978).

In the analysis presented here, the aquifer is considered to be a closed system with a small shut-in well that does not affect the system. The well merely provides a means of observing the change in the fluid pressure of the system. Fluid is not being added to or withdrawn from the system, so the problem is an undrained one. This implies that the pressure response of the aquifer is related to the compressive properties of the skeleton and the fluid, and the relative proportions of each. In groundwater hydrology it is common to combine these properties into a coefficient called specific storage, S_s. Specific storage is defined as the volume of fluid removed from or taken into storage per unit volume per unit change in hydraulic head. Defined as such, specific storage is basically related to a drained problem. If specific storage is to be determined from the pressure response of aquifers to earth tides, a definition directly relating specific storge to the compressibilities of the skeleton and fluid will have to be employed. Specific storage may be written as

$$S_s = \rho_f g(nc_w + m_v)$$

where

ρ_f = density of the fluid,

g = acceleration due to gravity,

n = porosity,

c_w = compressibility of the fluid, and

m_v = compressibility of the skeleton.

In this definition, ρ_f, g, and c_w are reasonably well known, leaving n and m_v to be determined. The purpose of this study was to estimate m_v, and hence S_s.

The earth tide can be expressed as a potential, which in turn can be used to determine a dilatation by adopting an earth model. Knowing this dilatation and the pressure response as measured at the well, it is not possible to determine both the porosity and the compressibility of the skeleton. It is, however, relatively easy to estimate the porosity of an aquifer within about 5%. This leaves only the skeleton compressibility, or change in volume of voids with respect to the bulk volume per change in effective stress. That is

$$m_v = \frac{dV_v}{V_b} \frac{1}{d\sigma'} \quad ;$$

where

V_v = volume of the voids,

V_b = bulk volume, and

σ' = effective stress.

With appropriate substitution this may be written as

$$m_v = nc_w \frac{dp_f}{d\sigma' - dp_f}$$

where everything is known (or assumed) except the total stress, and with the assumption that for undrained response, change in void volume equals change in water volume.

The change in the total stress on the aquifer is due to the change in weight of the overburden and the deformation of the earth. The change in weight of the overburden results from the change in gravity. This effect can be shown to be comparatively small even for relatively deep aquifers, and hence can be neglected. The estimation of the deformation of the earth requires some knowledge or assumption about the nature of the earth.

In spherical coordinates, dilatation is defined as

$$\Delta = \varepsilon_{rr} + \varepsilon_{\theta\theta} + \varepsilon_{\phi\phi}$$

where ε refers to strain. Near a free surface

$$\sigma_{rr} = 0 = \lambda\Delta + 2\mu\, \varepsilon_{rr}$$

where μ is rigidity or shear modulus and λ is Lamé's constant.

Further, it can be shown that:

$$\varepsilon_{\theta\theta} + \varepsilon_{\phi\phi} = \left\{\frac{2\bar{h} - 6\bar{\ell}}{a}\right\}\left\{\frac{W_2}{g}\right\} ,$$

where

$\bar{h}$ = Love number,

$\bar{\ell}$ = Love number,

a = radius of the earth,

W_2 = potential, and

g = acceleration due to gravity.

Dilatation may therefore be written as

$$\Delta = \left\{\frac{1}{1 + \frac{\lambda}{2\mu}}\right\} \left\{\frac{2\bar{h} - 6\bar{\ell}}{a}\right\} \left\{\frac{W_2}{g}\right\} .$$

The situation is now analogous to having a confined sample in a lab where the change in fluid pressure and the dilatation resulting from an unknown change in confining pressure are known. Because the problem is undrained, the change in fluid pressure is not equal to the change in effective stress. The change in total stress is therefore needed to evaluate the compressibility of the skeleton.

This would seem to imply that the bulk modulus, K, will have to be known or estimated. The bulk modulus, however, can be related to μ and λ as

$$K = \lambda + (2/3)\mu.$$

Because λ and μ already appear in the equation for dilatation, the change in total octahedral stress can be written as

$$d\sigma_{oct} = (\lambda + \frac{2}{3}\mu) \left\{\frac{1}{1 + \frac{\lambda}{2\mu}}\right\} \left\{\frac{2\bar{h} - 6\bar{\ell}}{a}\right\} \left\{\frac{dW_2}{g}\right\}$$

without introducing any new coefficients. Before accepting this expression, however, some consideration should be given to the applicability of the previous equation for dilatation. The change in potential can be calculated for any point on the earth from astronomical considerations. The values for $\bar{h}$, $\bar{\ell}$, μ, and λ, however, are estimated for a very large region of the earth at best. The expression for dilatation, therefore, really represents a given region of the earth. The question then becomes one of using the values of λ and μ, already inherent in the expression for dilatation, to get the implied change in octahedral stress or estimate a bulk modulus that may be more representative of the region near the aquifer. At least, conceptually, the dilatation may be thought of as the result of measuring a large region of the earth with strain meters. This would seem to indicate that although the dilatation represents a regional value, it might be more reasonable to use an estimate for some local value of K to calculate the change in total stress.

In practice, using the earth model and coefficients of Takeuchi (1950), $K = 1 \times 10^{11}$ Pa. The expected bulk modulus of a deep aquifer would be on the order of 1×10^{10} Pa to 1×10^{11} Pa. This is extrapolated from measured values for various rocks. Of course, the absolute lower limit is 2×10^{9} Pa, the bulk modulus of water.

Preliminary calculations using a range of values for bulk modulus were made for wells at Raft River, Idaho, and East Mesa, California. Although there are data problems associated with both areas which are further complicated by ocean loading problems at East Mesa, reasonably good results were obtained.

PLANNED ACTIVITIES FOR FISCAL YEAR 1979

Final calculations and comparison with a numerical model is planned for the first quarter of the next fiscal year.

REFERENCES CITED

Kanehiro, B. Y., Narasimhan, T. N., and Tsang, C. F., 1978. Preliminary analysis of tidal data. This report.

Takeuchi, H., 1950. On the earth tide of the compressible earth of variable density and elasticity. Trans. Am. Geophys. Union, v. 31, pp. 651-689.

PRELIMINARY ANALYSIS OF TIDAL DATA

B. Y. Kanehiro, T. N. Narasimhan, and C. F. Tsang

INTRODUCTION

The earth is theoretically within the gravitational fields of all other celestial bodies and as such is subject to tidal forces. The sun and the moon, because of their respective size and proximity, account for virtually all the tidal forces experienced by the earth. The ocean tides of the hydrosphere provide, by far, the most dramatic evidence of the tidal forces at work. The same tidal forces also act on the atmosphere and the lithosphere generating atmospheric and solid earth tides, respectively. These tides, however, are of small magnitude and are relatively difficult to measure accurately.

The time dependency of the tides results from the relative movements of the earth, sun, and moon and as such is very nearly periodic. Unfortunately, this periodicity is complicated and has superposed on it substantial amounts of nonperiodic noise. Although the solid earth tide and the reservoir response to this tide do not suffer from problems like those associated with the period of free oscillations of the ocean basins, it is still desirable to do some preliminary analysis.

From a practical point of view it is sufficient to determine the amplitudes and phase relations for the five or six largest components of the tide; at least in theory, this should remove much of the nonperiodic noise.

ACTIVITIES IN FISCAL YEAR 1978

Two methods for analyzing tidal signals were tried. The first is the widely used finite Fourier analysis. This approach is based on the fact that the finite Fourier series for an odd number of points (2N + 1) may be written as:

$$F(x) = \frac{A_o}{2} + \sum_{k=1}^{N} \left[A_k \cos\left(\frac{2\pi k}{L} x\right) + B_k \sin\left(\frac{2\pi k}{L} x\right) \right],$$

where F(x) is a function that is defined over the set of points $\{x_p\}$, and A_o, A_k, and B_k are coefficients such that:

$$A_k = \frac{1}{N} \sum_{p=o}^{2N} F(x_p) \cos\left(\frac{\pi}{L} k x_p\right)$$

and

$$B_k = \frac{1}{N} \sum_{p=o}^{2N} F(x_p) \sin\left(\frac{\pi}{L} k x_p\right)$$

with k being the harmonic number and L being the length of the interval considered (Hamming, 1973).

To avoid the problem of having coefficients that are not invariant under translation, the series may be written as:

$$F(x) = \frac{C_o}{2} + \sum_{k=1}^{N} c_k \cos\left(\frac{2\pi k}{L} x\right) + \phi_k$$

where

$$C_k = (A_k^2 + B_k^2)^{1/2}$$

and

$$\phi_k = \arctan \frac{B_k}{A_k} .$$

The algorithm actually used to calculate the series is based on a Fourier transform scheme rediscovered by Cooley and Tukey (1965). This calculational scheme is significantly faster than the more direct calculational scheme of the coefficients based on the equations above.

The second method of tidal decomposition is one specifically designed for earth-tide analysis by Lecolazet (1956). This method is not as direct or conceptually simple as the finite Fourier analysis. It is basically a filtering scheme where specially designed band-pass filters are employed. The method allows for the examination of a larger number of tidal components and a greater degree of accuracy.

As an offshoot of the above, attempts were made to remove tidal noise from data to be used for well-test analysis. Both least-square filtering schemes and schemes based on the analysis above were tried with very limited success.

FISCAL YEAR 1979

The simple finite Fourier analysis presented above has proved to be adequate for the present needs of examining aquifer response to earth tides.

The removal of tidal noise without seriously degrading the desired signal is not a simple problem. Attempts to improve methods of dealing with this noise will continue.

REFERENCES CITED

Cooley, J. W., and Tukey, J. W., 1965. Algorithm for the machine calculation of complex Fourier series. Mathematics of Computation, v. 19, no. 90, pp. 297-301.

Hamming, R. W., 1973. Numerical methods for scientists and engineers. New York, McGraw-Hill.

Lecolazet, R., 1956. Application à l'analyse des observations de la marée gravimétrique de la méthode de H. et Y. Labrouste dite par combinaisons linéaires d'ordonnées. Annales de Geophysique, v. 12, no. 1, pp.59-71.

BEHAVIOR OF ROCK-FLUID SYSTEMS AT ELEVATED PRESSURES AND TEMPERATURES

W. H. Somerton, A. Ghaffari, R. Greenwald, V. Hoang, L. F. Martínez-Baez, H. J. Su, and L. Wong

INTRODUCTION

The objective of this project is to develop methods and apparatus to measure rock-fluid properties at temperature, pressure, and fluid saturation conditions that may be encountered in deep high-temperature oil and gas reservoirs, geothermal reservoirs, and reservoirs in which high temperatures are used in the extraction process. These properties include porosity, permeability, electrical resistivity factor, thermal properties including thermal expansion, pore and bulk compressibilities, compressional and shear velocities, and the dynamic elastic properties that may be derived from these properties.

Methods of measuring most of the above properties have been developed as reported in an earlier work (Somerton, 1977). These methods permit measurement of only two properties at the most in a single apparatus, and the measurements are limited to temperatures of 200°C and 1 kbar stress. Correlation of the results of measurements of properties in different apparatuses, using different test specimens and with the possibility of different stress histories, is very difficult. A second objective of the present work, therefore, is to develop an apparatus in which all or most of the desired properties may be measured at the same time under identical test conditions. Basic design of this apparatus has been presented earlier (Somerton, 1977).

Measurement of physical properties and behavior of rock-fluid systems at elevated temperatures and pressures is difficult and very time consuming. A third objective of the present work is to develop models and correlations that will make it possible to predict properties and behavior from more easily measured characteristics of the rock-fluid system. The greatest progress has been made in the case of thermal properties. Having estimates of such characteristics as mineral composition, porosity, and grain size, models have been developed for predicting thermal conductivity under any fluid saturation condition at a base pressure and temperature. Other correlations have been developed to permit prediction of thermal behavior at other pressure and temperature conditions. Well-log data may also be useful in this regard. An investigation is currently in progress for predicting relative thermal conductivity by analysis of temperature gradients in wellbores.

Some applications of data obtained in this and related projects are also currently under investigation. One application is the role of the so-called heat-pipe effect observed in earlier work (Somerton, 1975), in high-temperature fluid flow systems in which phase changes may occur. Under certain conditions of temperature and pore fluid pressure, some shallow formations could behave as heat thiefs from geothermal and steam injection wells.

RESEARCH ACTIVITIES IN FISCAL YEAR 1978

Much of the research accomplished during fiscal year 1978 is presented in reports prepared by the six coauthors (Ghaffari, 1978; Martínez-Baez, 1979; Hoang, 1978; Su, 1978; Wong, 1978; Greenwald, 1978). These activities will be reviewed briefly here. Following this, progress on the multirock properties apparatus will be reviewed.

Thermal Properties and Behavior

Ghaffari (1978) has developed his three-dimensional model of heat conduction in porous media to obtain excellent agreement between predicted and experimental thermal conductivities, particularly for unconsolidated media. The agreement for a number of materials is shown in Figure 1. Figure 2 is a working graph based on model results. From Figure 2, we can predict the effective thermal conductivity. The agreement of model results for consolidated media is not as favorable as for unconsolidated sands. Some additional flattening of the cubic packing of

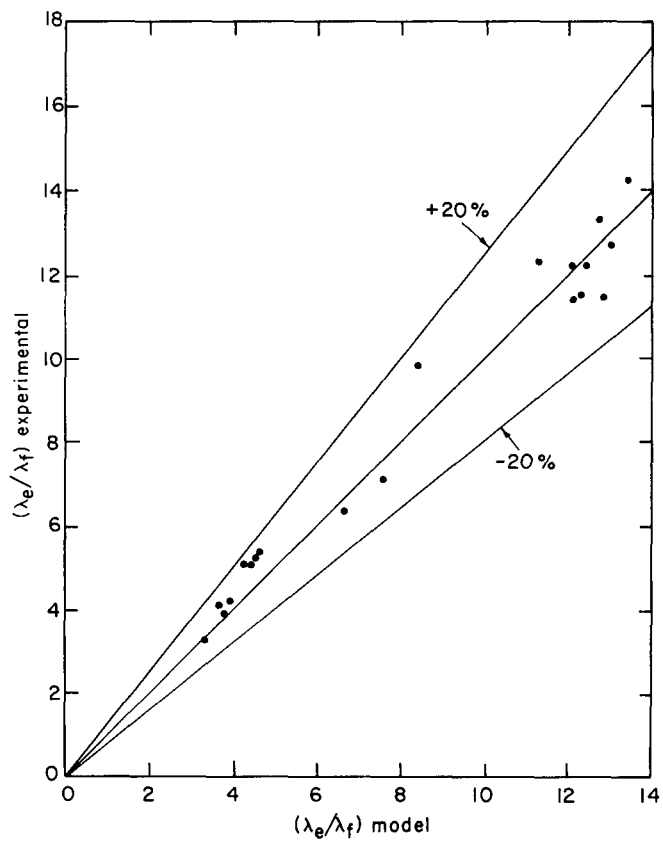

Figure 1. Agreement between experimental conductivities and conductivities predicted from the model.

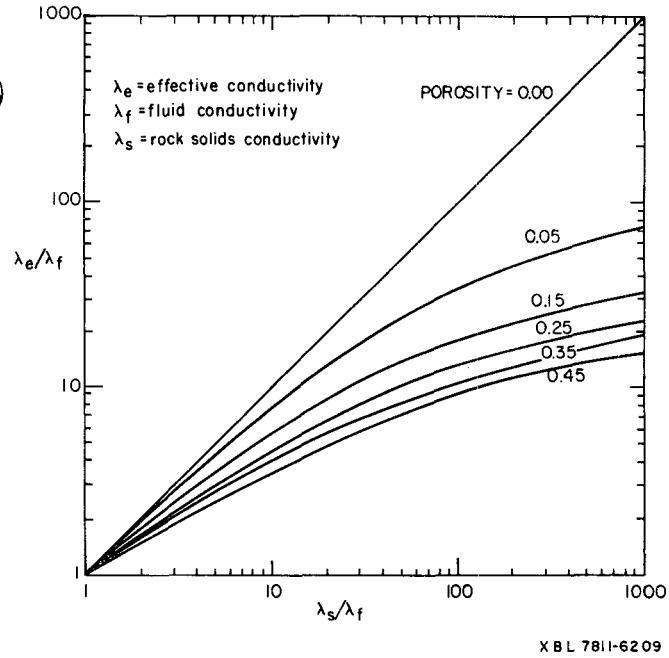

Figure 2. Graph for predicting effective thermal conductivities based on model results.

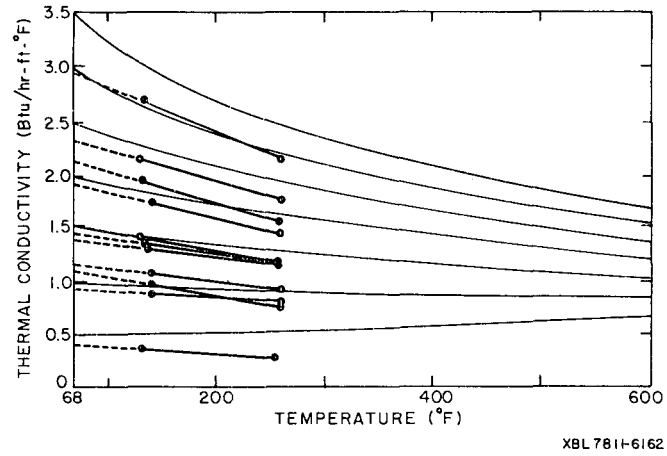

Figure 3. Thermal conductivity temperature behavior of Cerro Prieto cores.

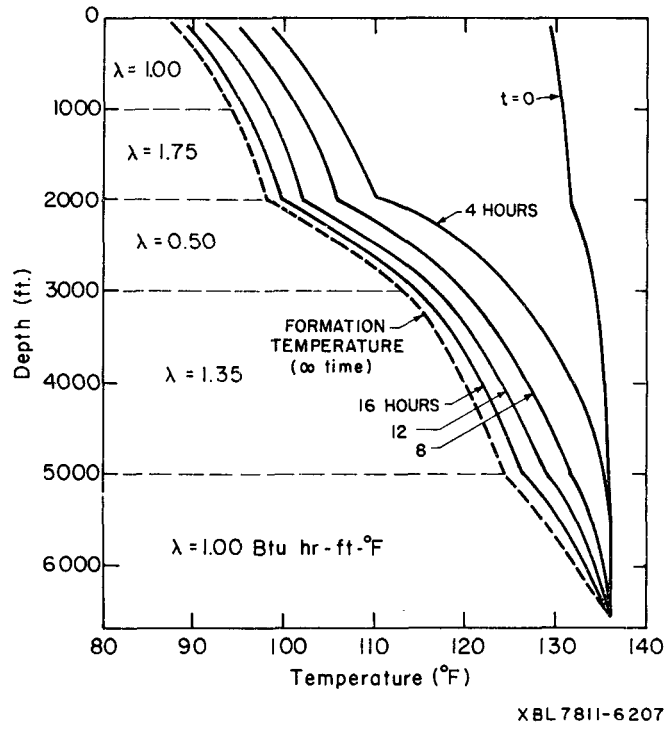

Figure 4. Calculated temperatures in wells for various shut-in times with variable thermal conductivities.

spheres used in the model in the horizontal planes of contact will be applied. The degree of flattening will be related to the formation resistivity factor. In addition, a grain-size parameter will be incorporated into the model to express the effects of contact resistance.

Martínez-Baez (1979) has used methods developed in earlier work (Anand et al., 1973) to obtain correlations of the thermal behavior of Cerro Prieto core samples. By use of regression analysis, he correlated experimental measurements with physical properties of the rock-fluid system. The best fit to the experimental data was found when the following properties were included in the correlations: porosity, median grain size, grain size distribution (δ_{90}/δ_{10}), and conductivities of the saturating fluid and the rock solids. The multiple regression coefficient was 0.924, which means that the correlation may be used with considerable confidence for similar rocks from this area having properties within the range of the samples tested. The change of conductivity with temperature for the cores tested showed quite consistent results but were at some variance with previous correlations. Figure 3 shows that some modification of the correlation would be needed in order to predict the thermal conductivity-temperature behavior of these Cerro Prieto cores with accuracy.

Hoang (1978) has studied temperature gradients in wells as a means of predicting in-situ thermal conductivities. Assuming the earth's heat flux through the formations surrounding a well to be constant in magnitude and direction, calculations have been made to show the effects of differences in thermal conductivities of formations on the temperature gradients in a well. Calculations were based on initial conditions in the well being at a state of quasi-equilibrium for fluid flowing at a constant prescribed rate from the lowest (highest-temperature) formation. The well was then shut in and temperatures were calculated for various times, as shown in Figure 4. It is apparent that the variation in temperature gradients after as little as 4 hours shut-in time will clearly reflect the variation in thermal conductivities of surrounding formations. These results are now being tested against actual wellbore measurements where thermal conductivity data on cores from the well are available. Hoang is also developing the modified needle-probe technique for measuring themal properties in the multiproperty apparatus.

Su (1978) is continuing work on the heat-pipe effect and is evaluating its importance in fluid flow in porous media at temperatures high enough that phase changes may occur. In the thermal conductivity test cell (about 3.28-cm long), the apparent thermal conductivity may be several times the true conductivity for two-phase systems. Some of the parameters that determine the magnitude of the heat-pipe effect are known. Su has developed an experimental apparatus (Figure 5) that should help to evaluate the magnitude of the mixing zone and its nature and properties in a flowing system. If the effect is important, it will be incorporated into a three-dimensional finite-difference model being developed by Su for study of fluid flow where phase changes occur.

In addition to the above thermal work, the several investigators have an ongoing program of measuring thermal properties of an increasing number and range of rock types. These results are being used to test the various correlations and models and to add to our catalog of thermal data.

Fluid Flow and Storage Capacity

Work is progressing on the measurement of fluid flow and storage capacity of rocks at elevated pressures and temperatures. This work is partly funded by a grant from industry.

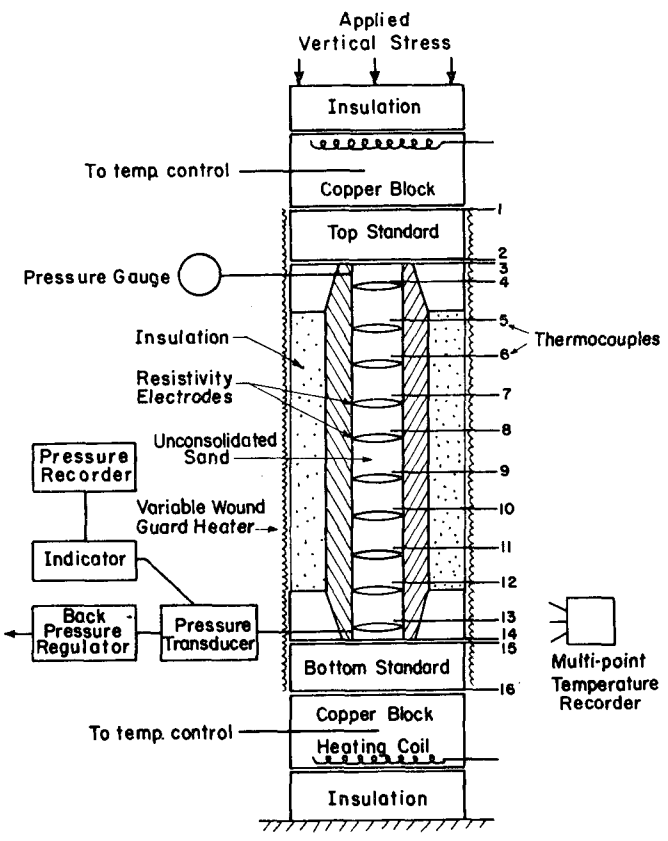

Figure 5. Experimental apparatus for evaluating the magnitude of the heat-pipe effect in flowing systems.

Wong (1978) has measured the permeability of a number of sandstones and has shown that permeability decreases sharply with increase in temperature. Figure 6 shows an example of this effect for a Cerro Prieto sandstone. Three possible causes of this effect are being investigated. The first of these is the effect of thermal expansion in closing pore necks to fluid flow. This is being investigated using a network model of porous media in which tube diameters are decreased by thermal expansion of the matrix. However, this is not believed to be a very important effect since porous media not containing clay, quartz, or water as the flowing fluid do not show any significant reduction in permeability with increased temperature. Second, the dissolution of quartz with subsequent plugging by the redeposition of silica in pore necks has been proposed as a cause of permeability reduction. Since much of the permeability is recovered upon cooling, the latter factor cannot be considered of major importance. Analysis of silica in the effluent water has not disclosed any conclusive evidence. The third possible cause is that of clay swelling and migration. For this to be a cause of permeability reduction, clay swelling and migration would have to be greatly increased at elevated temperatures. A current study of clay swelling pressures at elevated temperatures may shed some light on this matter.

An apparatus for measuring pore and bulk compressibilities at elevated temperatures has been designed by Greenwald (1978), constructed in LBL shops, and is now being tested. The bulk-compressibility part of the apparatus makes use of three deflection sensor cartridges (DSC) transducers, which are able to measure deflections up to 0.015 in. and operate at temperatures as high as 480°C. The pore volume compressibility portion of the apparatus makes use of a high-pressure Jergesen sight gauge. This latter component is somewhat limiting and will be replaced in the multi-properties apparatus by a gas-pressure balanced displacement cylinder (displacement being measured by a linear potentiometer). Problems with leaks in the system have hindered the calibration of the apparatus and its application to measurements

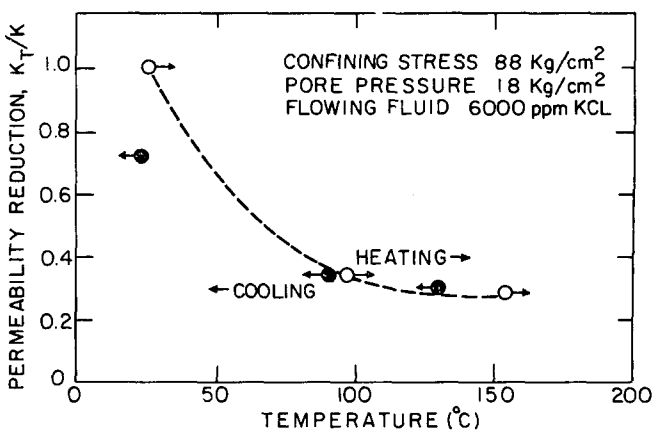

Figure 6. Effect of temperature on the permeability of a Cerro Prieto sandstone.

on actual cores. However, progress has been made on the development of a model that will attempt to duplicate the volume changes in a two-component rock system (solid framework subjected to confining stress, and softer inner pore lining subjected to pore pressure). This two-component model may also be important in analysis of the fluid-flow capacity at elevated temperatures. It should finally be noted that bulk and pore thermal expansions may also be measured with the experimental apparatus described above.

Electrical Resistivity Factor

Wong (1978) has designed a new control system for measuring the electrical resistivity factor at elevated temperature. This sytem has been constructed in the electronic shop of the U.C. Berkeley Mechanical Engineering Department. This new control system makes it possible to impose a constant alternating current at various levels across a radial electrode system. The current is imposed only long enough to obtain a constant voltage across the system and at specified intervals. The frequency of the current may be varied over a wide range, making it possible to evaluate any frequency-dependent effects. Some preliminary tests have been made using the new control system. Good contact of the center electrode with the rock test specimen was found to be very important in order to obtain useful results.

Sonic Velocities

During this period, Palen (1978) completed his thesis dealing with the measurement of P- and S-wave velocities in fluid-saturated rocks at high temperatures and pressures. His most significant results were the substantial effects of temperature in reducing both compressional and shear-wave velocities. From these data, he calculated elastic moduli with the expected results that bulk and Young's moduli decreased with temperature. Poisson's ratio also decreased with temperature. An important finding in this work was the nearly twofold difference in Poisson's ratio between dry and liquid-saturated cores, as may be seen for Cerro Prieto sandstone shown in Figure 7. These results confirm earlier observations made by Al-Khafaji (1975).

Dr. Michael S. King, University of Saskatchewan at Saskatoon, spent several weeks at LBL during spring 1978, helping to improve the design of our sonic measuring equipment. He dealt in particular with special design problems associated with the multiproperties measuring apparatus. We now feel confident that we will be able to measure P- and S-wave velocities with good precision, and measure other properties concurrently.

Multiproperties Testing Apparatus

Considerable progress has been made on the new rock-properties test facility. Having received the assurance of industry participation in funding of the facility, a design engineer was

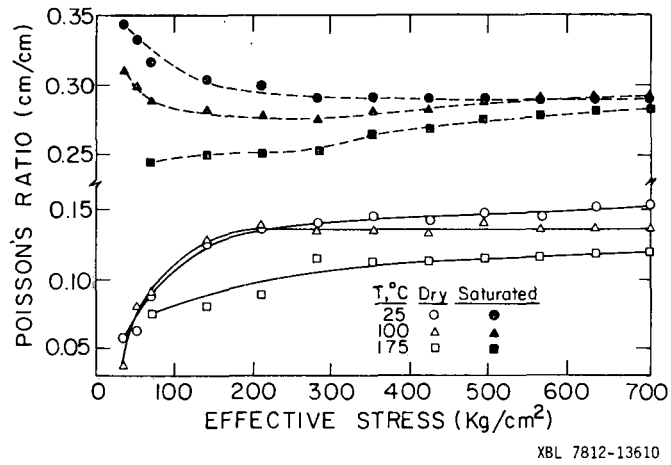

Figure 7. Effect of temperature, stress, and fluid saturation on Poisson's ratio for Cerro Prieto sandstone.

retained to complete the final design and to supervise the construction and installation of the apparatus. The pressure vessel will soon go out for bids and the pressuring system has been obtained on loan from Lawrence Livermore Laboratory. Preparations for space, power, and peripheral equipment and facilities are well under way. Mockups of the various control and measuring components are being made for testing in our present pressure vessels. The target date for running the first test with this new apparatus is July 1, 1979.

PLANNED RESEARCH PROGRAM, FISCAL YEAR 1979

Research on all fronts as described above will be continued in fiscal year 1979, with particular emphasis on the multiproperties measuring apparatus. Two new projects will be started. The first of these will be a cooperative project with Greenwald's research, in which pore and bulk thermal expansions will be measured during the heating period of the pore and bulk compressibility runs. These tests will be run at constant confining stress and pore-fluid pressure. The second new project will be an attempt to correlate sonic velocities with thermal conductivities. Such a correlation may make it possible to deduce in-situ thermal properties from sonic velocity log data.

In the area of thermal properties, completion of the thermal conductivity model is planned by the end of fiscal year 1979. We expect enough progress on the one-dimensional heat-pipe experiment and the three-dimensional finite-difference model for fluid flow with phase changes to begin construction of a laboratory model to confirm these effects. In the wellbore temperature-gradient studies, the effects of convective heat transfer in the wellbore and in the surrounding formations will be studied. Thermal conductivity measurements with the steady-state comparator apparatus will be continued as core and drill-cutting samples become available.

In the fluid flow and reservoir storage capacity studies, we plan to measure permeabilities and compressibilities on wellbore core samples at reservor conditions. The data obtained from these tests will be used to test the theoretical models now being developed.

The multiproperties measuring apparatus will be in the final testing and calibration stage by the end of fiscal year 1979. The target date for installing the apparatus is July 1, 1979. Before this date, each of the measuring components will have been tested in the present pressure vessels.

REFERENCES CITED

Al-Khafaji, A. H., 1975. The effect of temperature on shear wave propagation in dry and liquid saturated rocks. M.S. thesis, Berkeley, University of California.

Anand, J., Somerton, W. H., and Gomaa, E., 1973. Predicting thermal conductivity of formations from other known properties. Soc. Pet. Eng. Jour., v. 13, no. 5, p. 267.

Gaffari, A., 1978. Thermal conductivity of porous systems. Berkeley, University of California, Pet. Eng. Lab., progress report.

Greenwald, R., 1978. Design of apparatus for measuring compressibilities of reservoir type rocks at elevated temperatures. Berkeley, University of California, Pet. Eng. Lab., research progress report.

Hoang, V. T., 1978. Estimation of in-situ thermal conductivities from temperature gradient measurements. Berkeley, University of California, Pet. Eng. Lab., research project report.

Martínez-Baez, L. F., 1979. Thermal conductivities of core samples from the Cerro Prieto geothermal field and an improved prediction method, in Proceedings, First Symposium on the Cerro Prieto Geothermal Field, Baja California, Mexico, September 20-22, 1978, San Diego. Berkeley, Lawrence Berkeley Laboratory, LBL-7098.

Palen, W. A., 1978. The effect of temperature, pressure, and saturation on sonic velocities and dynamic elastic moduli of reservoir sandstones. M.S. thesis, Berkeley, University of California.

Somerton, W. H., 1975. Thermal properties of partially liquid-saturated rocks at elevated temperatures and pressures. Berkeley, University of California, final report of API research project 155.

____, 1977. Apparatus for measurements of properties and behavior of rock-fluid systems at high temperatures and pressures. Berkeley, University of California, Pet. Eng. Lab., report.

Su, H. J., 1978. Heat transfer in porous media with fluid phase changes. Berkeley, University of California, Pet. Eng. Lab., research proposal.

Wong, L., 1978. The effect of temperature on absolute permeability and formation factor. Berkeley, University of California, Pet. Eng. Lab., research project report.

THERMODYNAMICS OF HIGH-TEMPERATURE BRINES

K. S. Pitzer, D. J. Bradley, P. Z. Rogers, and J. C. Peiper

INTRODUCTION

An understanding of brines is essential to the exploitation of many geothermal resources. Consequently, a study of the solution thermodynamics of brine systems, both simple and complex, weak and strong, covering a wide temperature and pressure range, and combining both modeling and experimental work, began in 1975.

The initial work involved analysis of existing thermodynamic data on simple electrolyte systems using equations developed by Pitzer and coworkers (Pitzer, 1973; Pitzer and Mayorga, 1973, 1974; Pitzer and Kim, 1974). The goal of the modeling was to provide a compact set of equations capable of reproducing, at various temperatures and pressures, the existing data within experimental error up to practical concentrations (~6M) in terms of parameters having physical significance.

The program to measure heat capacities arose because of inadequate literature data on electrolyte systems. The primary goal of the experimental program is to supply data on simple and complex electrolyte systems at high temperatures and pressures, both along and away from the liquid-vapor saturation curve. In addition to the direct use of these data, they will provide a base for checking and refining various models.

Though the modeling and experimental work relate directly to electrolyte systems common to geothermal brines, the results are applicable to such areas as biological fluids, battery electrolytes in aqueous and nonaqueous solvents, plating baths, waste effluents, materials corrosion from electrolyte systems, and marine chemistry.

PROGRAM IN FISCAL YEAR 1978

During the period of this report, modeling calculations were undertaken for several areas of interest.

Of most general interest is an expression for the Debye-Hückel parameters for aqueous electrolytes over the full range of temperature and pressure. This requires equations for both the volumetric and dielectric properties of water. In connection with this program, Silvester and

Pitzer (1977) proposed an equation, for the dielectric constant for water, which was quite satisfactory along the saturation curve. But the pressure derivatives of this equation failed to fit the data as well as desired; hence we sought an improved form of equation. The result is an equation that is valid from 0 to 350°C, and saturation pressure to 2,000 bars below 100°C and 5,000 bars above 100°C. The equation has the following form:

$$D = D_{1000} + C \log\left[\frac{B + P}{B + 1{,}000}\right] \qquad (1)$$

where

$$D_{1000} = U_1 \exp\,[U_2T + U_3T^2\,], \qquad (2)$$

$$C = U_4 + U_5/(U_6 + T), \text{ and} \qquad (3)$$

$$B = U_7 + U_8/T + U_9T. \qquad (4)$$

The temperature, T, and the pressure, P, have units of Kelvin and bars, respectively. The uncertainty in the fit is approximately 0.1% below 70°C and better than 1% at higher temperatures. The values of U_1 to U_9 are as follows:

U_1	= 3.4279E2	U_6	= -1.8289E2
U_2	= -5.0866E-3	U_7	= -8.0325E3
U_3	= 9.4690E-7	U_8	= 4.2142E6
U_4	= -2.0525	U_9	= 2.1417
U_5	= 3.1159E3		

With the volumetric equation of Keenan et al. (1969) and this expression for the dielectric properties of water, the Debye-Hückel parameters for activity and osmotic coefficients, enthalpy, heat capacity, apparent molal volume, compressibility, and expansivity were calculated over the range from 0° to 350°C, and saturation pressure to 1,000 bars. Values of the various parameters have been compared with those believed to be reliable from the literature and found to agree to within 1% over the range of 10° to 50°C, and to within 5% from 0° to 70°C. A direct check of the parameters at temperatures above 70°C is not possible; however, indications are that the error is less than 10% at temperatures below 300°C. At temperatures above 300°C and pressures near the saturation pressure, the error probably increases to as much as 25%. Tables of values of the slopes have been prepared and will be published soon, as a part of a complete report of this work (Bradley and Pitzer, 1979).

The thermodynamic properties of very high-valance electrolytes were considered and a paper published (Pitzer and Silvester, 1978). By combination of both enthalpy and Gibbs energy data with theoretical guidance, previously confused results have been given a satisfactory interpretation.

Partially in preparation for the treatment of our own experimental results, the literature data for both volumetric and thermal properties of NaCl and KCl solutions were modeled for the full range of temperature and pressure. Although reasonably satisfactory representations were obtained, the limitations of accuracy and range of data were also most apparent. If our own measurements can be added soon, that will be done before publishing on these topics. However, interim equations are available if desired.

Our experimental instruments are described below. Each is now in operation and beginning to yield useful data.

Calorimeter

The flow calorimeter follows the basic design of Picker et al. (1971). Water flows through stainless steel tubing past a wire resistance heater, and the temperature rise of the water is measured using a platinum resistance thermometer. Solution is displaced at the same rate through a second unit of identical construction. Either the difference in the two temperature rises, or the change in heating power needed to balance the temperature rises, can be measured to yield the heat capacity difference between water and solution. Because platinum resistance thermometers are used as the temperature sensors, the absolute temperature rise can also be determined, giving an accurate measurement of the power loss of the heaters. Heat capacity measurements accurate to 0.1% or better can be obtained.

The calorimeter is encased in an evacuated copper block, which can be heated to over 300°C by a fluidized bath. A fluid pump designed for use in high-pressure liquid chromatography provides constant flow rates at pressures up to 10,000 psi. Thus, heat capacity measurements as a function of both pressure and temperature can be taken over these ranges.

Densimeter

A mercury displacement densimeter of the type described by Ellis (1966) has been constructed. The only major design change from Ellis's is that the volume of displaced mercury is measured with a cathetometer and a precision-bore glass capillary, rather than by weighing.

The densimeter is designed for use at temperatures up to 300°C and pressures to 600 bars. The sample reservoir has been constructed of a corrosion-resistant nickel-based alloy, which should be suitable for investigating the densities of very corrosive salts like $MgCl_2$.

The accuracy of the measurements depends on the accuracy of the volumetric data for water, which is used to calculate the volume of the sample chamber. The data on water over the temperature and pressure range to be investigated is accurate to approximately 100 ppm. The equipment is designed to give a precision of approximately 15 ppm at 200°C, and 30 ppm at 300°C.

PLANS FOR FISCAL YEAR 1979

First priority will be given to experimental heat capacity and density measurements for the primary brine components, NaCl, $MgCl_2$, Na_2SO_4, and KCl. The results for NaCl and KCl will be added to the data bases from the literature to complete the already well-advanced modeling programs for these substances. Similar modeling work will follow for $MgCl_2$ and Na_2SO_4. Thereafter we will examine mixed electrolytes and other special topics such as carbonate solutions.

REFERENCES CITED

Bradley, D. J., and Pitzer, K. S., 1979. Thermo dynamics of electrolytes, XII, dielectric properties of water and Debye-Hückel parameters to 350° and 1 kbar. Jour. Phys. Chem., v. 83, p. 1599.

Ellis, A. J., 1966. Partial molal volumes of alkali chorides in aqueous solutions to 200°C. Jour. Chem. Soc. A, p. 1579.

Keenan, J. H., Keyes, F. G., Hill, P. G., and Moore, J. G., 1969. Steam tables. New York, John Wiley.

Picker, P., Leduc, P., Philip, P., and Desnoyer, J., 1971. Heat capacity of solutions by flow microcalorimetry. Jour. Chem. Thermo., v. 3, p. 631.

Pitzer, K. S., 1973. Thermodynamics of electrolytes: I, theoretical basis and general equations. Jour. Phys. Chem., v. 77, p. 268.

Pitzer, K. S., and Kim, J. J., 1974. Thermodynamics of electrolytes. Jour. Amer. Chem. Soc., v. 96, p. 5701.

Pitzer, K. S., and Mayorga, G., 1973. Thermodynamics of electrolytes: II, activities and osmotic coefficients for strong electrolytes with one or both ions univalent. Jour. Phys. Chem., v. 77, p. 2300.

____, 1974. Thermodynamics of electrolytes, III, activities and osmotic coefficients for 2-2 electrolytes. Jour. Soln. Chem., v. 3, p. 539.

Pitzer, K. S., and Silvester, L. F., 1978. Thermodynamics of electrolytes: XI, properties of 3-2, 4-2, and other high-valence types. Jour. Phys. Chem., v. 82, p. 1239.

Silvester, L. F., and Pitzer, K. S., 1977. Thermodynamics of electrolytes, VIII, high-temperature properties, including enthalpy and heat capacity, with application to sodium chloride. Phys. Chem., v. 81, p. 1822.

SOLUBILITY OF ALBITE IN THE AQUEOUS PHASE AT ELEVATED TEMPERATURES

J. M. Neil and J. A. Apps

INTRODUCTION

Albite, $NaAlSi_3O_8$, is a common rock-forming mineral belonging to a group of minerals called the feldspars. It crystallizes in a variety of rock types, including such diverse types as saline lake beds, limestones, altered tuffs and basalts, and many igneous and metamorphic rocks. These different rock types are formed over a wide range of temperatures and pressures. Albite is, therefore, of interest not only because of its common occurrence, but also because of the diverse range of environments in which it forms.

The purpose of this study is to find out how albite affects the groundwater composition over a range of temperatures from 25° to 400°C and from pressures from 1 to 500 bars. This temperature-pressure range encompasses the conditions likely to be found in all exploitable geothermal resources, waste isolation sites, hot-water storage aquifers, oil reservoirs, and uranium resources. The study is designed to investigate not only the equilibrium relations between the albite and the groundwater, but also the rates of equilibration expected under differing conditions of pH and salinity.

The most stable albite structure at low temperatures consists of a framework of ordered silica and aluminum atoms each surrounded by a tetrahedron of oxygen atoms. Interstices of the tetrahedral framework contain sodium atoms. However, most naturally occurring albites are subject both to disordering of the silicon and aluminum atoms and substitution of potassium and calcium for sodium. Charge is conserved in the latter substitution by additional aluminum in place of silicon.

For a precise evaluation of the kinetics of solution and equilibrium relations, the albite must be well characterized so that the effect of solid solutions and ordering can be determined. For this reason, care was taken to analyze and measure the crystallographic properties of several albites before beginning the experimental program (Apps and Neil, 1978). A metamorphic albite from the Franciscan formation at Cazadero in northern California was finally selected on the basis of its purity and degree of ordering. The following is a description of the equipment and experimental techniques used to measure aqueous solubility, the characterization of the starting materials, and preliminary results so far achieved.

ACTIVITIES IN FISCAL YEAR 1978

Equipment

The heart of the system is a 1-liter autoclave manufactured by Autoclave Engineers, Inc.,

which can be operated to pressures of 7,500 psi, at temperatures up to 400°C. It is fabricated out of Hastelloy-C 276, an alloy that is highly resistant to corrosion by hot brines. The autoclave is equipped with an air-driven stirring system with a magnetically coupled sealed shaft, thereby eliminating contamination from the bearing packing. The sampling system allows us to sample either the vapor phase at the top of the vessel or the liquid phase 2 in. from the bottom of the vessel.

A recharge system has been assembled so that the autoclave can be refilled while maintaining pressure and temperature within the vessel. The principal components of the system consist of a 1:150 air-driven Sprague pump, a 1/2-liter oil-water separator, and an adjustable (5,000 to 10,000 psi) relief valve. The pump and relief valve work against each other to balance the pressure in the autoclave when it is refilled. Auxiliary plumbing permits refilling of the oil-water separator. Figure 1 is a schematic diagram of the system.

Heat is provided by an external resistance furnace. A Leeds & Northrup recorder with D.A.T. controller is used to operate the furnace and provide a record of the temperature in the autoclave. The temperature-sensing element is a chromel-alumel thermocouple, which is located in a thermocouple well that is the same length as the liquid-phase sampling tube.

Although the autoclave meets the ASME code for manned-area safe operations, a safety shield of 1/4-in. iron plate with 3/4-in. plywood lining has been erected around it. These specifications are recommended by Holloway (1971) for high-pressure systems. In addition to the rupture disk installed by the manufacturer on the autoclave, a second rupture disk assemby has been added to the high-pressure line from the separator. Both rupture disks are rated 10% over the maximum working pressure of the autoclave.

Characterization of Starting Material

The initial results of a search for a chemically pure albite have been described elsewhere (Apps and Neil, 1978). The reported analyses of a Franciscan vein albite from Oregon (Coleman, 1978, unpub. data) did not contain calcium at the level reported in the provisional analyses (1.1 wt %). Therefore, we decided to make point chemical analyses of the selected Cazadero albite with an electron microprobe to check the bulk chemical analyses and to identify and determine the chemical composition of coexisting phases.

The analyses were made with an ARL, eight channel, electron microprobe (Model SEMQ), using standards of similar composition to the unknowns. All results were corrected for background and machine drift, and the empirical matrix correction of Bence and Albee (1968), and of Albee and Ray (1970) were applied to all results. The albite analyses are listed in Table 1. The albite analyses have been normalized to 32 oxygens using the method of Deer et al. (1966) and are tabulated in Table 2. An Amelia Courthouse albite analysis from Deer et al. (1963) is included for comparison.

With the exception of two points on a traverse across a twinned albite where the calcium concentration attained 0.26 and 0.24 wt% (Ab-007C), the calcium analyses were 0.06 wt % or less. The normalized analyses give the molecular percentage of albite in the range of 98.8 to 99.8, which indicates that the material being used for the study is almost pure albite.

The accessory minerals observed include lawsonite, omphacite, quartz, and an unidentified phyllosilicate. Lawsonite is the probably source of calcium contamination in the bulk analysis. In the future, heavy liquid separations will be used to remove traces of this phase from the albite.

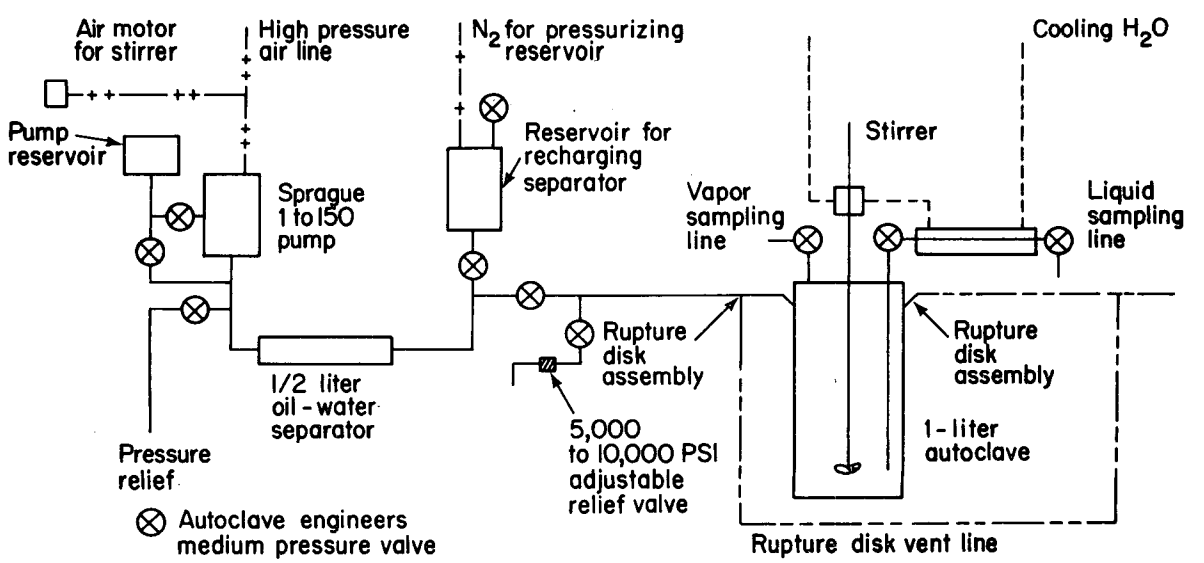

Figure 1. Schematic diagram of the 1-liter autoclave and its support system.

Table 1. Analyses of albite samples from Cazadero, California, in wt% ± s.*

	Ab-007A†	Ab-007B‡		Ab-007C§			Ab-007D**	
	1	1	2	1	2	3	1	2
	Number of Point Analyses							
	16	13	9	5	13	9	5	10
Na_2O	11.8 ± 0.10	12.0 ± 0.01	12.2 ± 0.02	12.0 ± 0.03	11.9 ± 0.03	12.1 ± 0.05	11.6 ± 0.02	11.8 ± 0.05
TiO_2	-0.00 ± 0.005	-0.00 ± 0.005	-0.00 ± 0.002	-0.01 ± 0.002	0.00 ± 0.003	-0.00 ± 0.004	-0.00 ± 0.006	-0.00 ± 0.001
K_2O	0.04 ± 0.039	0.03 ± 0.005	0.01 ± 0.001	0.01 ± 0.002	0.03 ± 0.003	0.02 ± 0.002	0.05 ± 0.011	0.04 ± 0.001
MgO	-0.01 ± 0.0002	-0.01 ± 0.003	-0.01 ± 0.002	-0.01 ± 0.004	-0.01 ± 0.001	-0.01 ± 0.001	-0.01 ± 0.010	-0.01 ± 0.002
SiO_2	67.2 ± 0.31	67.8 ± 0.04	68.1 ± 0.002	67.6 ± 0.40	67.1 ± 0.19	67.8 ± 0.06	67.7 ± 0.28	67.9 ± 0.13
FeO	0.00 ± 0.005	0.01 ± 0.001	0.00 ± 0.0001	0.01 ± 0.018	0.00 ± 0.005	0.01 ± 0.001	0.00 ± 0.001	0.01 ± 0.006
CaO	0.04 ± 0.014	0.01 ± 0.001	0.00 ± 0.002	0.11 ± 0.024††	0.06 ± 0.026	0.03 ± 0.008	0.03 ± 0.001	0.05 ± 0.001
Al_2O_3	19.9 ± 0.09	20.1 ± 0.01	19.9 ± 0.10	20.1 ± 0.02	20.0 ± 0.07	19.8 ± 0.02	19.8 ± 0.03	19.9 ± 0.07
Total	99.0 ± 0.24	99.9 ± 0.01	100.3 ± 0.04	99.9 ± 0.03	99.0 ± 0.02	99.8 ± 0.001	99.1 ± 0.10	99.7 ± 0.19

$$*s = \sqrt{\frac{\Sigma (x_i - x)^2}{n - 1}}$$

†Ab-007A: 1, traverse.
‡Ab-007B: 1, adjacent to an omphacite crystal; 2, traverse
§Ab-007C: 1, traverse across twinned albite; 2, crystal with good cleavage; 3, traverse
**Ab-007D: 1, albite with mottled extinction; 2, traverse
††Includes values of 0.26 and 0.24 wt%.

Table 2. Cazadero, California, albite analyses calculated on the basis of 32 oxygen atoms $X_4Z_{16}O_{32}(Na,K,Ca)$ $[Al_4Si_{12}O_{32}]$.

	Ab-007A	Ab-007B		Ab-007C				Ab-007D		Amelia Courthouse Sample
Sample	1	1	2	1	1A*	2	3	1	2	
Na	4.043	4.073	4.131	4.144	4.106	4.075	4.116	3.962	4.012	3.897
Ti	---	---	---	---	---	---	---	---	---	---
K	0.008	0.006	0.002	0.002	0.002	0.006	0.002	0.011	0.008	0.034
Mg	---	---	---	---	---	---	---	---	---	---
Si	11.875	11.869	11.895	11.876	11.762	11.851	11.896	11.922	11.905	11.905
Fe II†	0.000	0.001	0.000	0.001	0.001	0.000	0.001	0.000	0.001	---
Fe III	---	---	---	---	---	---	---	---	---	0.005
Ca	0.007	0.002	---	0.021	0.048	0.012	0.005	0.005	0.010	0.028
Al	4.145	4.147	4.096	4.120	4.249	4.164	4.095	4.110	4.112	4.125
Z	16.02	16.02	15.99	16.00	16.01	15.99	15.99	16.03	16.02	16.03
X	4.058	4.082	4.133	4.168	4.157	4.093	4.124	3.978	4.031	3.96
Or (mol%)	0.2	0.15	0.05	0.05	0.05	0.15	0.05	0.20	0.20	0.8
Ab (mol%)	99.6	99.8	99.95	99.4	98.8	99.6	99.8	99.6	99.5	98.5
An (mol%)	0.2	0.07	0.00	0.5	1.2	0.29	0.15	0.13	0.27	0.7

*Average of two analyses from Ab-007C-1 containing 0.26 and 0.24 wt% CaO.
†Total iron reported as Fe II.

Ion-beam-thinned sections of the Cazadero albite were also examined by transmission electron microscopy at magnifications up to 100,000 in order to determine whether or not the albite is homogeneous (consists of one phase only). Phase homogeneity was confirmed. However, the albite has a very large number of dislocations ($10^8/cm^2$ of exposed surface) and bent twins, which is indicative of a high stress and is unusual for albite. Currently, samples of albite growing into vugs from the same location are being prepared for analysis of dislocations and single crystal diffraction studies are being conducted to confirm the degree of Al-Si order in the sample.

Experimental Procedure

So far, five preliminary solubility experiments have been successfully completed on the saturation curve of the aqueous phase at temperatures of 125° and 250°C. They were run to verify the experimental plan, to identify problems, and to develop and verify analytical procedures on typical solution samples. It is particularly important to determine the appropriate rates of reaction since this information allows us to estimate the time needed to achieve equilibrium between the albite and the aqueous phase.

The generalized procedure of a run is to load 25 grams of -65 + 100 mesh albite into the autoclave, and add the appropriate volume of 0.1 N NaCl solution to it (usually 700 ml). Once the closure is secured, the autoclave takes approximately 45 min. to reach the operating temperature, and approximately 2 additional hours for the temperature to stabilize. The controller functions as a critically damped oscillator once it has reached the temperature of the run.

After the temperature has stabilized, a sample is taken and the stirring is started. Initially, samples were taken every 2^n min. When n = 12, the time between samples became excessive and subsequent samples were taken approximately every 1 1/2 days. After evaluating the results of this strategy, we decided to sample at 5-hr or 10-hr intervals in order to clarify fluctuations in component concentrations during the latter part of any run.

A run is completed when sufficient samples have been taken for the purposes of the test or when the water level drops below the end of the liquid-phase sampling tube. After the autoclave has cooled to room temperature, the water and albite are removed. The aqueous phase is pressure-filtered, and filtrate is divided into three aliquots for verification of the analytical procedures. The filter cake and residual albite is retained for scanning electron microscopy to identify any secondary phases that may have formed and to observe the amount of corrosion of the starting material.

Solution samples were initially analyzed by atomic absorption spectroscopy for Si, Al, Na, and Ca concentrations. Additional confirmatory analyses for aluminum and silica have been made using respectively an aluminon method (Packham, 1958), and the molybdosilicate method (American Public Health Ass., 1975). These colorimetric techniques have proven satisfactory and will be employed henceforth for aluminum and silica analyses of the solutions.

The pH of the solution samples are measured with a Vanlab standard combination glass pH electrode as soon as they cool to room temperature. The electrode is standardized immediately before the sample pH is determined. The pH of samples have been observed to change during the pH determination and probably reflect the disequilibirum state of the solution at the time of the measurement or uptake of atmospheric carbon dioxide. Further studies are under way to clarify pH measurements.

Because of some concern regarding corrosion of the autoclave due to the presence of residual oxygen, the autoclave atmosphere is purged of oxygen with nitrogen. During one run, the autoclave was flushed with nitrogen for 5 min., and 0.5 ml of hydrazine was added. However, the hydrazine raised the pH. In succeeding runs, the autoclave was flushed with nitrogen only.

As a result of the preliminary runs, the sampling procedure has been modified to include the following steps:

1. The agitator of the autoclave is stopped for one minute before sampling.

2. The sample is taken after rejection of the initial 5 ml of solution.

3. The sample is centrifuged for 5 min., and the 20 ml of clear solution is drawn off and mixed with 5 ml of 0.01 N KOH solution.

4. The remainder of the solution is used to measure pH.

In this way we hope to avoid some current uncertainties regarding the stability of the solutions between sampling and analysis.

Preliminary Results

Figure 2 illustrates the results of one run at 240°C showing analyses for silica and aluminum. The ratio of silica to aluminum that has entered solution exceeds the stoichiometric ratio in albite, which indicates that dissolution is incongruent.

Five hours after agitation commenced, it appears that aluminum saturated the solution, although silica continued to increase in concentration for another 25 hours. Thereafter, both aluminum and silica concentrations declined, suggesting precipitation of a secondary phase. Further study is required to determine if and when albite reaches saturation in the 0.1-N NaCl solution.

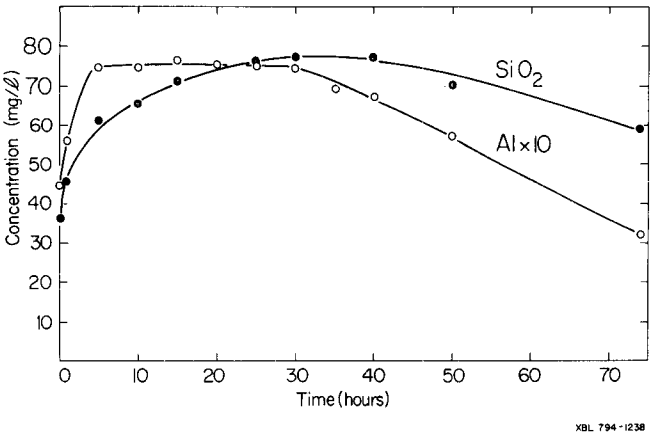

Figure 2. The dissolution of 25 g of -65 + 100 mesh Cazadero albite in 0.1 N NaCl at 250°C.

A comparison of scanning electron microscope images of the albite charge, both before and after the dissolution study, indicates that the albite cleavage fragments suffered minor corrosion or erosion through rounding of the edges, and scalloping and pitting of the faces. There is no evidence of epitaxial growth of secondary phases, or any indication that the finer fractions of the particulate material is other than dust originally adhering to the charge.

FUTURE WORK

The immediate need will be to continue solubility measurements of albite along the saturation curve of water between 125° and 300°C in 0.1 N NaCl solutions. After sufficient experience has been gained in sampling and analyzing the solutions, an extended study will be made of solutions of varying NaCl concentration between 0.001 N and 1.0 N, and of NaOH between 0.001 N and 0.1 N. All solubility measurements will be made along the saturation curve of water. At this point the pressurized system operated at 500 bars will be tested, and further solubility measurements made up to 400°C at that pressure.

Data reduction and evaluation will continue. A refined model to describe activity coefficients of the species in solution at elevated temperatures will be investigated, and improved thermodynamic data for alteration products and aqueous species will be calculated from recent calorimetric data described in the published literature.

The equilibration studies currently under way and projected will provide much valuable semiquantitative information on reaction rates between albite and the aqueous phase. Such information will be evaluated with the objectives of identifying the mechanisms of albite dissolution and precipitation, and of predicting rates of albite growth under a wide range of environmental conditions.

ACKNOWLEDGEMENT

The authors are indebted to Professor H. R. Wenk, University of California, Berkeley, for making the TEM study of albite.

REFERENCES CITED

Albee, A. L., and Ray, L., 1970. Correction factors for electron probe microanalysis of silicates, oxides, phosphates, and sulfates, Analytical Chem., v. 42, pp. 1408-1414.

American Public Health Association, 1975. Standard methods for the examination of water and wastewater, 14th ed. Amer. Pub. Health Assoc. pp. 486-490.

Apps, J. A., and Neil, J. M., 1978. Selected albites as candidates for hydrothermal solubility measurements. Berkeley, Lawrence Berkeley Laboratory, LBL-7058, pp. 10-13.

Bence, A. E., and Albee, A. L., 1968. Empirical correction factors for electron microanalysis of silicates and oxides. Jour. Geology, v. 76, pp. 382-403.

Deer, W. A., Howie, R. A., and Zussman, J., 1963. Rock-forming minerals in framework silicates. London, Longmans, Green and Co., Ltd., v. 4, p. 110.

_____, 1966. An introduction to the rock-forming minerals. New York, John Wiley, pp. 515-517.

Holloway, J. R., 1971. Internally heated pressure vessels, in Ulmer, G. C., ed., Research techniques for high pressure and high temperature. New York, Springer-Verlag, pp. 247-249.

Packham, R. F., 1958. The absorptrometric determination of aluminum in water, in Proc. Soc. Water Treat. Exam. 1. pp. 226-734.

THERMODYNAMIC PROPERTIES OF SILICATE MATERIALS

I. S. E. Carmichael, M. S. Ghiorso, L. Moret, and S. A. Nelson

INTRODUCTION

The liquid state is the essence of igneous activity and therefore a significant part of the way the earth works. A great deal is now known of the composition of natural liquids, but the physical and thermodynamic properties of silicate liquids are hardly known at all. This project was designed to rectify this situation, and also to contribute to the more extensive knowledge of the solid phases which initially saturate a cooling silicate liquid either on or below the surface.

ACTIVITIES IN FISCAL YEAR 1978

In siliceous liquids, one of the earliest phases to precipitate is quartz (SiO_2). If this phase is accompanied by others, it is possible to calculate the pressure at which the crystal assemblage equilibrated. This pressure, equivalent to depth, places a limiting value on the source region of a particular siliceous magma. Thus quartz crystals occurring as early crystallizing phases (phenocrysts) in a wide variety of lavas were examined to determine the extent of solid solution, the variation in the temperature of the α-β transition (~848 K), the enthalpy associated with this transition, and the heat capacity of both α and β-quartz.

We found that the α-β inversion temperature, $T_{\alpha-\beta}$, is strongly influenced by the Al content of quartz, which ranged between 17 and 380 ppm. The enthalpy associated with the α-β transition, $\Delta H_{\alpha-\beta}$, was measured over a range of 9.0°C by differential scanning calorimetry (DSC), but there is no measurable compositional effect on $\Delta H_{\alpha-\beta}$. However, the finer the samples are crushed, the smaller the value of $\Delta H_{\alpha-\beta}$. The observed decrease in $\Delta H_{\alpha-\beta}$ as a function of grain size could be attributed to a surface energy of 682 ergs/cm^2. A single piece of quartz requires 107.7 ± 1.4 cal/mole for the temperature interval of 842 to 851 K, which includes the enthalpy associated with the α-β inversion.

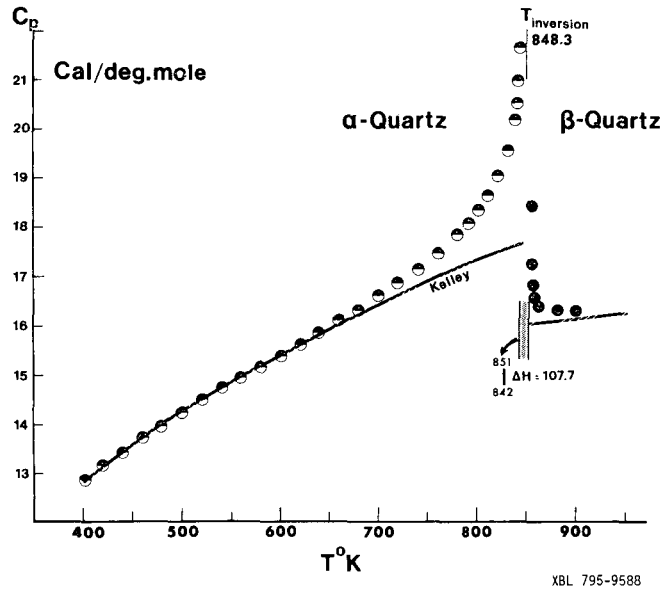

Figure 1. Heat capacity of quartz, Cp, as a function of temperature obtained by DSC. Half-circles are values for α-quartz and filled circles for β-quartz. The shaded area represents the temperature range 842 to 851 K, for which ΔH is 107.7 cal/mole (Table 2). The variation of Cp with temperature taken from Kelley (1960) is also shown.

The heat capacity of two samples of quartz were measured by heating on the DSC, and there is a marked premonitory effect, which starts about 200°C below $T_{\alpha-\beta}$ (Figure 1). Values of Cp at 10° intervals are given in Table 1, but at smaller interals as $T_{\alpha-\beta}$ is approached because Cp rises to very high values on both sides of the inversion interval.

Table 1. Molar heat capacity of α-quartz and β-quartz (Cp in cal/mole·deg.).

α-quartz						β-quartz	
T(°K)	Cp	T(°K)	Cp	T(°K)	Cp	T(°K)	Cp
400	12.9	610	15.5	820	19.0	851	18.3
410	13.0	620	15.6	822	19.1	852	17.2
420	13.2	630	15.8	824	19.2	854	16.7
430	13.3	640	15.9	826	19.3	856	16.5
440	13.4	650	16.0	828	19.4	858	16.5
450	13.6	660	16.1	830	19.6	860	16.4
460	13.7	670	16.2	832	19.7	870	16.3
470	13.8	680	16.4	834	19.8	880	16.2
480	14.0	690	16.5	836	20.0	890	16.2
490	14.1	700	16.6	838	20.3	900	16.4
500	14.2	710	16.7	840	21.0		
510	14.3	720	16.9	842	22.8		
520	14.4	730	17.0				
530	14.6	740	17.2				
540	14.7	750	17.3				
550	14.8	760	17.5				
560	14.9	770	17.7				
570	15.0	780	17.9				
580	15.2	790	18.1				
590	15.3	800	18.3				
600	15.4	810	18.6				

Table 2. Values of enthalpy of α-β transition and integrated (Cp from 400 to 900 K).

	$\Delta H_{\alpha-\beta}$ (cal/mole)	$H_{-} + \int_{400}^{900} CpdT$ (cal/mole)
This report:	107.7±1.4	7,891
Kelley (1960):	290	8,090
Robie et al. (1978):	114	7,930

Values of $H_{900}-H_{400}$ for quartz may be obtained by integrating the area under the Cp curve from 400 to 842, and from 851 to 900, then adding the measured value of $\Delta H_{\alpha-\beta}$ obtained over the range of 842 to 851 K. Our values are compared with published values in Table 2, and the agreement with the more modern data is excellent. This study on quartz, which includes the measurement of lattice parameters and cell volumes of 52 specimens of quartz phenocrysts (which grew in the β-quartz stability field) is presently in press (Ghiorso et al., 1979).

The density, or specific volume, of 12 silicate liquids of widely varying composition have been measured over the temperature range of 1,100° to 1,550°C. The preparation of starting glassy material free of gas bubbles, which would strongly affect the measured density, involves care and considerable time at high temperature in the furnace. The density was measured by weight loss of a Pt bob of known volume that was suspended just above the silicate liquid, and then immersed a known distance into it. Surface tension corrections for the suspension wire were avoided by using two Pt bobs of different volumes, but with suspension wires of similar radius. All liquids, quenched to glasses at room temperature, were then analyzed by wet chemical techniques, and in all cases considerable amounts (200 ppm) of dissolved Pt were found. At the high temperatures of these experiments, the tips of the Pt bobs were prone to recrystallize to a few large crystals. This effectively prevented the bob entering the silicate liquid, for it was immediately drawn to the side of the crucible on touching the liquid, where it became welded to the walls of the Pt crucible. This effect could only be eliminated by machining new Pt bobs every two of three months.

The 12 liquids whose densities have been measured are composed of the following oxide components: SiO_2, TiO_2, Al_2O_3, MgO, CaO, Na_2O, and K_2O. Preliminary values of the partial molar volumes of these oxide components are plotted in Figure 2, together with error bars representing plus or minus twice the standard error. Included in these data are published measurements, and all data were regressed

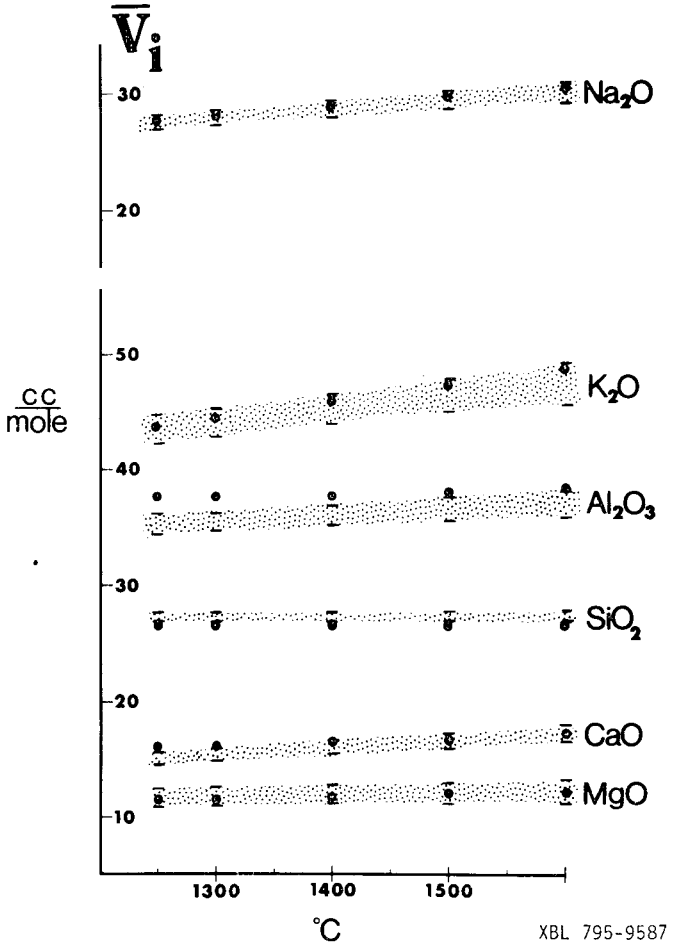

Figure 2. Partial molar volumes of oxide components (labeled) in silicate liquids obtained from 91 compositions. The width of the shaded areas represents ±2 standard errors about the mean. Published values of these quantities (Bottinga and Weill, 1970) are represented by solid circles.

by the multiple regression program in the SPSS package version 7.0. Figure 2 shows that published values (Bottinga and Weill, 1970) of the partial molar volumes may lie outside the 95% confidence limits, particularly for Al_2O_3. Least squares analysis of the partial molar volumes with temperature leads to the value given in Table 3.

Particular molar volumes for TiO_2 have not been given, as these are notably composition-dependent, and at 1,400°C may vary between 22.5 and 28.8 cm^3/mole. In Al_2O_3-free silicate liquids, $d\bar{V}_{TiO_2}/dt$ has a positive slope, but in the presence of Al_2O_3 this becomes negative. The interactions of TiO_2 with other components in silicate liquids are presently being investigated.

PLANNED ACTIVITIES FOR FISCAL YEAR 1979

The density of silicate liquids with FeO and TiO_2 as additional components will be measured

Table 3. Preliminary values of partial molar volumes of oxide components in silicate liquids without FeO or TiO_2. Applicable range is 1,523 to 1,873 K, and data are in cm^3/mole.

$$\bar{V}_{SiO_2} = 27.138 + 9.939 \times 10^{-5}\ T$$

$$\bar{V}_{Al_2O_3} = 27.500 + 5.095 \times 10^{-3}\ T$$

$$\bar{V}_{MgO} = 9.608 + 1.406 \times 10^{-3}\ T$$

$$\bar{V}_{CaO} = 5.811 + 6.115 \times 10^{-3}\ T$$

$$\bar{V}_{Na_2O} = 17.831 + 6.340 \times 10^{-3}\ T$$

$$\bar{V}_{K_2O} = 26.982 + 10.839 \times 10^{-3}\ T$$

over a range of temperatures, and thus the partial molar volumes of these two components will be derived. The heat capacity of densified glasses, made of Na_2O-Al_2O_3-SiO_2, will be measured in an attempt to identify any coordination change of Al from four-fold to six-fold as a function of pressure. The high-temperature heat content of compositions in the system $NaAlSi_3O_8$-$CaAl_2Si_2O_8$-$CaMgSi_2O_6$ will be measured in order to obtain heats of fusion of these three components. We anticipate that a study of the thermal expansion of silicate glasses of various compositions, as a function of termperature, will allow any compositional effect on the galss transformation temperature to be isolated.

REFERENCES CITED

Bottinga, Y., and Weill, O. F., 1970. Densities of liquid silicate systems calculated from partial molar volumes of oxide components. Amer. Jour. Sci., v. 269, p. 169.

Ghiorso, M. S., Carmichael, I. S. E., and Moret, L. K., 1979. Inverted high-temperature quartz: unit cell parameters and properties of the α-β inversion. Contrib. Mineral. Petrol. (in press).

Kelley, K. K., 1960. High temperature heat-content, heat capacity, and entropy data for the elements and inorganic compounds. U. S. Bureau of Mines Bull. 584, 232 p.

Robie, R. A., Hemingway, B. S., and Fisher, J. R., 1978. Thermodynamic properties of minerals and related substances at 298.15 K and 1 bar (10^5 pascals) pressure and at higher temperatures. U. S. Geol. Survey Bull. 1452, 456 p.

DEVELOPMENT OF A DATA BASE FOR AQUEOUS SOLUTIONS

R. J. Otto, H. Ozbek, and S. L. Phillips

INTRODUCTION

The research and development of geothermal energy depends on the availability of adequate transport and thermodynamic reference data. However, the necessary data are widely scattered, varying in quality and generally unevaluated. One objective of the National Geothermal Information Resource is to provide a single, comprehensive data base on the basic energy properties of aqueous solutions to elevated pressures and temperatures. To this end, a bibliographic data base containing references to over 1,000 articles and reports providing basic physiochemical data relevant to geothermal energy has been estbalished (Phillips et al., 1978; Fair and Phillips, 1976). The computerized bibliography is maintained by the Berkeley Database Management System (BDMS).

The primary objective of the aqueous solutions data base is to provide evaluated and correlated transport and thermodynamic data, compilation, and recommended interpolating equations for generating tables of smoothed values. The initial focus has been on properties of aqueous sodium chloride solutions in the temperature region between 0 and 350°C and having pressures between vapor saturation and 50 MPa. The compilation, evaluation, and correlation covering viscosity, thermal conductivity, solubility, density, enthalpy, and heat capacity is nearing completion and will constitute a data book of current information on NaCl for research, development, modeling, and construction for both electrical power and direct use of geothermal energy. In addition, the results of this work include identification of areas where data are either lacking or inadequate, and recommendations for research designed to provide the needed data.

The data base is compiled from the following principal sources of information: (a) experimental values and correlations in the published literature; (b) reports from U. S. Department of Energy contractors; (c) reports from other government agencies and their contractors, for example, U. S. Geological Survey; (d) data from the CODATA system; and (e) data synthesis and correlation from computer-assisted interpolation and extrapolation.

FISCAL YEAR 1978 ACCOMPLISHMENTS

The compilation of data for the enthalpy, density, viscosity, thermal conductivity, and solubility were completed and represent comprehensive surveys of the literature from 1929 to September 1978. The need for enthalpy and heat capacity data above 200°C at all NaCl concentrations is strikingly apparent. New results on the heat capacity and heat of solution up to 300°C have become available since the most recent and comprehensive thermodynamic compilation of Silvester and Pitzer (1977). These data have been refit, and a new revised set of values for the total enthalpy and heat capacity of solution has been generated in tabular form.

Information on solubility is comparatively complete for the entire temperature region between 0° and 800°C and has recently been reviewed by Potter et al. (1977). Published values for the thermal conductivity of aqueous NaCl solutions are sparse and only available up to 150°C. Between 100° and 150°C, only the six data points published by Korosi and Fabuss (1968) for water desalination studies are available. A Russian publication by Yusufova et al. (1975) contains figures that show over 50 points from 100 to 330°C, along with a correlation expression. We have selected this correlation as a preliminary interpolating equation for providing tables of smoothed values.

Over 1,000 experimental values for the density of NaCl solutions are available for evaluation and correlation. We have established two subsets: (a) data of geothermal interest up to 350°C and 50 MPa, and (b) data to 750°C and 200 MPa. A parametric correlation expression is being developed that will fit the data in all regions except near the critical region.

The previously published viscosity compilation and correlation (Ozbek et al., 1977) was revised mainly to include: a new correlation for temperatures up to 150°C; recent data up to 35 MPa pressure provided by Kestin and Khalifa (unpublished); and the extrapolating procedure developed by Potter (1978), which provides for values to 300°C.

FISCAL YEAR 1979 PLANS

In fiscal year 1979, we expect to complete our critical evaluation of the following properties of aqueous NaCl solutions: density, enthalpy, heat capacity, viscosity (revision), thermal conductivity, and solubility. The result of the evaluations are mathematical equations that reproduce the data, generally to 350°C, 50 MPa pressure, and to saturation concentrations. We expect to begin critical evaluation and correlation for the scale-causing substances: silicates and silica, calcite, and sulfides.

REFERENCES CITED

Fair, J. A., and Phillips, S. L., 1976. Establishment of a computer data base on geothermal properties of aqueous NaCl, KCl, $CaCl_2$ solutions, in selected papers relevant to energy. 5th International CODATA Conference, Boulder, June 28-July 1, 1976. CODATA Bull. 23.

Korosi, A., and Fabuss, B. M., 1968. Thermophysical properties of saline water. Monsanto Research & Development Corp., Office of Saline Water, Report No. 363.

Ozbek, H., Fair, J. A., and Phillips, S. L., 1977. Viscosity of aqueous sodium chloride solutions from 0-150°C. Berkeley, Lawrence Berkeley Laboratory, LBL-5931.

Phillips, S. L., Ozbek, H., and Otto, R. J., 1978. Basic energy properties of electrolyte solutions database. Sixth International CODATA Conference, Santa Flavia (Palermo), Italy, May 22-25, 1978, and Berkeley, Lawrence Berkeley Laboratory, LBL-7827.

Potter, R. W., 1978. Viscosity of Geothermal Brines. Trans., Geothermal Resources Council, v. 2, p. 543-544.

Potter, R. W., Babcock, R. S., and Brown, D. L., 1977. A new method for determining the solubility of salts in aqueous solutions at elevated temperatures. Jour. Res., U. S. Geol. Survey, v. 5, p. 389.

Silvester, L. F., and Pitzer, K. S., 1977. Thermodynamics of electrolytes: VIII, high temperature properties, including enthalpy and heat capacity, with application to sodium chloride. Jour. Phys. Chem., v. 81, p. 1822.

Yusufova, V. D., Pepinov, R. I., Nikolaev, V. A., and Guseinov, G. M., 1975. Thermal conductivity of aqueous NaCl solutions. Inj. Phiz. Journ. v. 29, no. 4, pp. 600-605.

KINETICS OF PRECIPITATION OF AMORPHOUS SILICA FROM AQUEOUS SOLUTION

O. Weres, A. Yee, and L. Tsao

INTRODUCTION

A large amount of high-quality experimental data has been generated on the kinetics of the conversion of dissolved silica in geothermal-brine-like aqueous solutions to solid amorphous silica (AS). Two processes have been separately studied: molecular deposition of dissolved silica onto preexisting amorphous silica surfaces (using commercially available colloidal silica of well-defined properties), and the formation of new colloidal silica particles through the process of homogeneous nucleation.

We found that, within the accuracy required for practical applications, the rate of molec-

ular deposition is fully determined by the concentration of dissolved silica, temperature, pH, and concentrations of univalent anions in solution. In geothermal practice, only chloride and fluoride need to be considered. Most of these data have already been reduced and the results are ready for use in preliminary form.

The rate of homogeneous nucleation depends upon the free energy of a colloidal silica particle of critical nucleus size, and the rate of molecular deposition. The nucleation-free energy is a function of the surface tension of the H_2O/SiO_2 interface, dissolved silica concentration, and temperature; the surface tension is itself a function temperature, salinity, and pH. Our approach to analyzing the homogeneous nucleation data is to model the process numerically, and adjust the value of the surface tension until the calculated curve of dissolved silica vs. time, under any given condition, matches the experimental curve. A sophisticated computer code has been developed for this purpose and data reduction has been completed. The code itself and its documentation will be publicly released.

ACCOMPLISHMENTS IN FISCAL YEAR 1978

Mechanisms of Silica Precipitation

It appears that under most conditions, silica precipitates as relatively pure amorphous silica. This conclusion is supported by geothermal field experience, laboratory research, and theoretical considerations. The scope of our study was restricted accordingly.

The process of amorphous silica precipitation from supersaturated bulk aqueous phase consists of the following steps:

1. Growth of polymeric silicic acid complexes to critical nucleus size

2. Nucleation of an amorphous silica (AS) phase in the form of colloidal particles

3. Growth of the supercritical AS particles by further molecular deposition of silicic acid on their surfaces

4. Coagulation or flocculation of colloidal particles to give a gel

5. Cementation of the particles in the gel by chemical bonding and further deposition of silica between the particles

6. Rarely, growth of a secondary phase in the interstices between the AS particles (Such secondary deposition of FeS and of calcite has been reported, but is uncommon.)

The above process occurs when the concentration of dissolved silica is high enough for homogeneous nucleation to occur at a significant rate. Very roughly, this requires a saturation ratio (concentration divided by the equilibrium solubility) of 2 or greater. If this condition is met, massive precipitation occurs. This is the case with the residual (flashed) brine at Niland, California, Cerro Prieto, Mexico, and Wairakei, New Zeland. Dealing with the consequences of precipitation presents the greatest technical problems encountered at these sites.

If the concentration of dissolved silica is too low for massive homogeneous nucleation to occur, relatively slow molecular deposition upon solid surfaces becomes the major precipitation mechanism. The product of this process (essentially step 3 of the above scheme alone) is a dense vitreous silica. This material has been observed to form in portions of the surface piping at Cerro Prieto at a rate of about 1 mm/yr. This is a very small rate, but the vitreous silica is almost impossible to remove once formed.

The goal of this study has been to generate sufficient experimental data and theoretical analysis concerning steps 1 to 3 to enable us quantitatively to predict and interpret their phenomenology and kinetics over most of the range of practical concern.

Homogeneous Nucleation of Colloidal AS

The voluminous gel-like deposits encountered at Niland, Cerro Prieto, and Wairakei consist of flocculated colloidal AS. The crumbly grey and white scales associated with the gel-like materials are cemented colloidal aggregates. This colloidal silica is produced by homogeneous nucleation in the liquid phase, that is, nucleation by growth of polymers to critical nucleus size without the participation of some preexisting solid particle.

With most substances, heterogeneous nucleation is dominent, and homogeneous nucleation is very slow, rare in nature, and difficult to study in the laboratory. The precipitation of AS is an apparent exception to this because of the very low surface tension of the silica-water interface--between 35 and 50 ergs cm^{-2} over the range of major practical interest. (By comparison, the surface tension of the water-air interface is about 70 to 80 ergs cm^{-2}.) This means that enormous numbers of particles can be produced by homogeneous nucleation (on the order 10^{17} to 10^{19} per liter), and this completely swamps the effects of heterogeneous nucleation.

A practical consequence of the dominance of homogeneous nucleation is that the precipitation of AS is experimentally reproducible and predictable. This is because the rate of homogenous nucleation is determined by basic thermodynamic and chemical variables (concentration, surface tension), and not by often unknown trace contaminants, as is the case with heterogeneous nucleation.

Figure 1 shows some typical experimental results, which depict the decline of dissolved

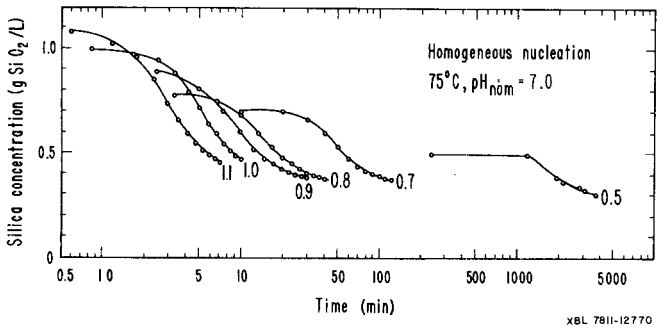

Figure 1. Decrease of dissolved silica concentration with time under conditions of homogeneous nucleation at 75°C, pH 7.0, and sodium activity = 0.069 M. Numbers indicate initial dissolved silica concentrations.

silica with time via the homogeneous nucleation mechanism. These experiments were performed at various pH's in a low-salinity buffered medium in which the sodium ion activity was approximately 0.069 M, and the time scales were shifted to convert all data to a nominal pH of 7.0. These conditions are approximately equivalent to an 0.088 M (= 5,200 ppm) NaCl solution at pH 7. Note that the time scale in Figure 1 is logarithmic. With an initial concentration of 1.1 g/l of SiO_2, the reaction runs most of the way to completion in less than 10 min. (Here and elsewhere in this paper, concentrations expressed in terms of grams or moles/liter refer to room temperature. Therefore, this solution would contain 1.1 g/l SiO_2 if cooled to room temperature, but not necessarily at 75°C).

With an initial concentration of 0.5 g/l, the reaction takes about 5,000 min. In other words, with a large initial saturation ratio, amorphous silica gels may form within the process equipment and associated piping. This is observed at Cerro Prieto and Niland. With small saturation ratios (0.5 g/l corresponds to S = 1.9 at this temperature), massive precipitation will not occur within the process equipment, but just as certainly will occur somewhere further downstream. Also note that 0.5 and 0.7 g/l curves show an induction period during which the concentration does not change noticeably.

We have generated a large quantity of such nucleation data from room temperature to 100°C, and have written a computer program that can numerically (and rigorously) model the homogeneous nucleation process. That is, it can reproduce the curves in Figure 1. We are now able to model and predict the process quantitatively, even under the experimentally inaccessible conditions characteristic of field practice. This program will be documented and made available to interested outside users.

Molecular Deposition on Solid Surfaces

Molecular deposition means the formation of compact, nonporous amorphous silica by chemical bonding of dissolved silica molecules directly onto solid surfaces.

Below about 100°C, homogeneous nucleation is usually the dominant precipitation mechanism. The major significance of molecular deposition here is that it is the molecular mechanism of the growth of colloidal particles and of the conversion of gel-like deposits to solid scale. However, at higher temperatures molecular deposition from solution may, by itself, produce scale at a significant rate. Although the deposition rate is very small (about 1 mm/yr in the flashed brine pipes close to the steam separators at Cerro Prieto), this scale is almost indestructible once formed.

We studied the molecular deposition process by adding known amounts of colloidal silica of known specific surface area to the solutions. Deposition rates at pH 7, $[Na^+]$ = 0.069 and various temperatures and dissolved silica concentrations were calculated (and extrapolated) from our experimental data and are presented in Figure 2. The dashed line represents the approximate concentration limit above which homogeneous nucleation supersedes deposition on

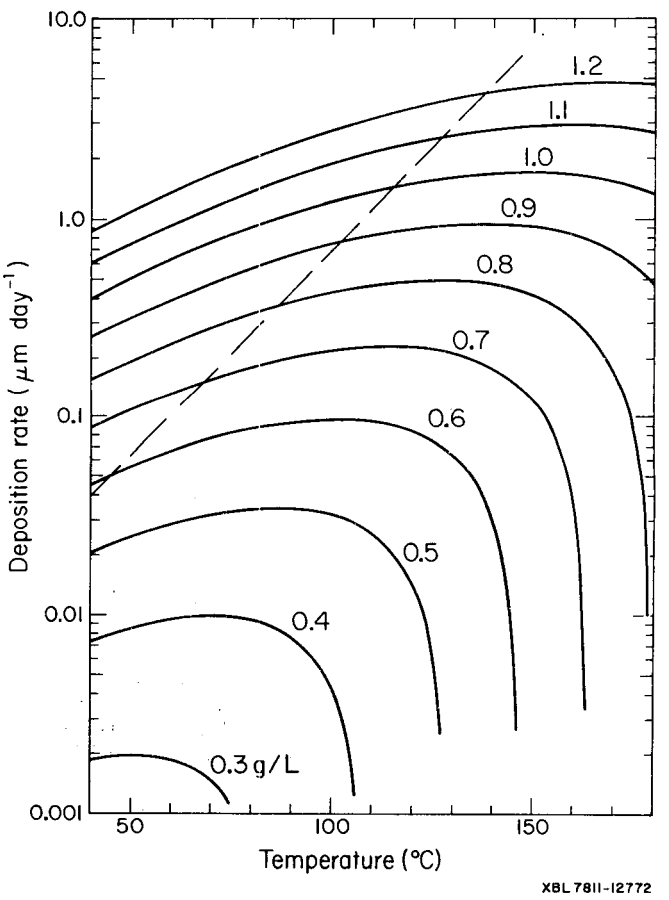

Figure 2. Rates of molecular deposition of silica on a flat surface at pH 7.0 and sodium activity = 0.069 M. Dissolved silica concentrations corresponding to each curve indicated in g/l refer to room temperature.

added particles as the dominant mechanism. Our data actually cover only the range between 50° and 100°C and below the dashed line. However, we believe the extrapolated values to be good enough for practical application.

At any given concentration, there is a temperature at which the deposition rate has a maximum value. Below this temperature, the rate of deposition increases with temperature in the usual way. Above this temperature, the rate of deposition decreases because the increasing solubility of silica causes the rate of the back-reaction (dissolution) to increase even more rapidly. At the saturation temperature for any given concentration, the deposition rate goes to zero. The practical consequence of this is that the molecular deposition rate is a weak function of temperature at lower than 15°C below the saturation temperature. However, the rate varies strongly with silica concentration. (Our data are best fitted by an apparent fourth-order rate law.)

Effects of pH and Salinity

It has long been believed that the rate of AS deposition is proportional to the surface density of ionized silanol groups on the silica surface. Our experiments on the pH dependence of the rate proved this hypothesis conclusively. We found that the rate as a function of pH calculated from our data matched surface charge vs. pH data in the literature to within experimental error.

The rate of molecular deposition as a function of pH for $[Na^+] = 0.069$ is presented in Figure 3. The function plotted in Figure 3 is the rate at any given pH relative to the rate at pH 7. Increasing the pH at constant salinity increases the rate by this factor.

We found that the reaction rate ceases to increase in proportion to surface change at about pH 8. This is due to the offsetting effect of the increase of silica solubility with increasing pH. Our data suggest that a constant pH correction factor of about 2.7 is adequate between about pH 8 and 9. The results presented here should not be used above pH 9.

Dissolved salts have two important effects upon these processes: (a) the salts decrease the solubility of amorphous silica and, thereby, increase the rate of homogeneous nucleation; and (b) increasing the salt concentration at constant pH increases the surface charge density and, thereby, the rate of molecular deposition.

The second effect increases the rates of molecular deposition and homogeneous nucleation by the same factor. The first effect increases only the rate of homogeneous nucleation.

Except at very low salinity, most of the dissociated silanols on the silica surface have cations bound to them--in our experiments, sodium. This means that sodium and hydrogen ion activity does not have independent effects upon

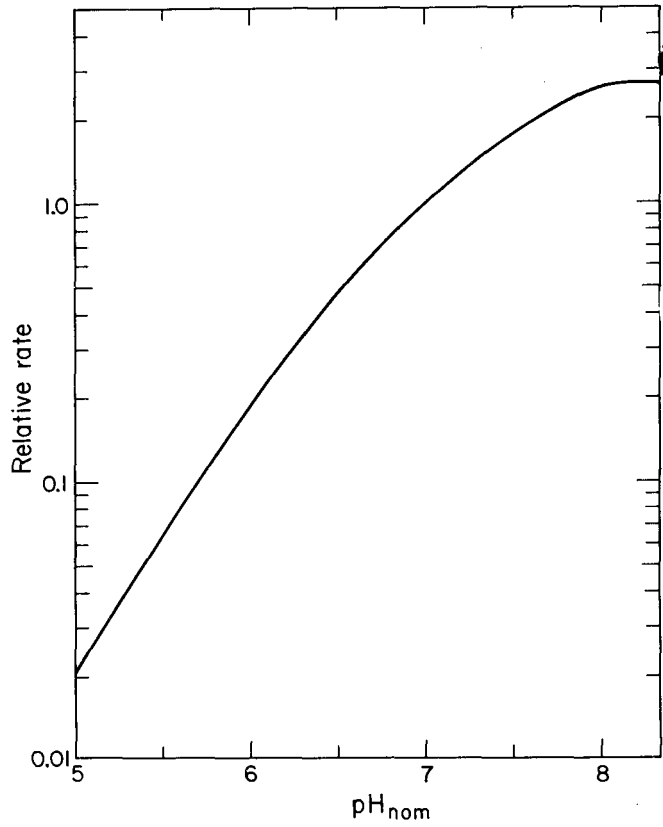

XBL 7811-12771

Figure 3. Variation of molecular deposition rate with pH_{nom}. Curve gives the rate as a function of pH_{nom} relative to the rate at $pH_{nom} = 7.0$. At pH_{nom} greater than 8, the value of the pH correction factor is 2.7. When sodium activity = 0.069 M, pH_{nom} = pH.

the rate. Rather, it is the ratio of sodium to hydrogen activity that is important. Therefore, Figure 3 may be used to calculate the effect of salinity upon the molecular deposition rate as well.

To do this, calculate a "nominal pH value" defined by

$$pH_{nom} = pH + \log \frac{[Na^+]}{0.069} , \qquad (1)$$

and then read off the pH correction factor from Figure 3 using the nominal pH value instead of the real one.

For example, to calculate the molecular deposition rate at 100°C, pH 6.5, $[Na^+] = 0.69$ M and 0.7 g/l dissolved silica, follow this procedure. First read the deposition rate at pH 7.0 and $[Na^+] = 0.069$ M from Figure 2. This value is 0.22 μm/day. Second, calculate pH_{nom} using equation (1). This is 7.5. Third, read the pH correction factor for pH 7.5 from Figure 3. This is 1.8. Finally, multiply the two numbers together to obtain the deposition rate, which is 0.40 μm/day.

Our data suggest that this procedure is adequate for solutions that contain up to at least 1 M NaCl and may be adequate at even higher salinities. However, we cannot recommend this procedure for use at salinities much below 5,200 ppm. At very low salinities, dissociation without ion pairing becomes important, and the basic assumption of the equivalent and opposite effects of hydrogen and sodium activity collapses.

The dissolved solids in real geothermal brines are usually predominantly sodium chloride, but other salts are also present. We have found that, in most cases, it is sufficient to use an "effective sodium ion activity" calculated as 0.77 times the (molar) concentration of chloride. If bicarbonate is present as a major ion, use the sum of the chloride and bicarbonate concentrations in place of chloride alone. The rationale for this procedure is that the various other major cations that may be present have essentially the same effects as sodium, and the activity-lowering effects of divalent anions approximately compensate for the concentration of the cations that accompany them.

Some Practical Examples

Case 1. Consider a hypothetical geothermal development at which the spent brine contains 5,200 ppm NaCl, 0.5 g/l dissolved SiO_2, and is delivered to the reinjection well at 75°C and pH 7. The brine delivered to the reinjection well is completely clear and goes right through a membrane filter. The decision is made to reinject. Reinjection commences at 400 t/hr into an aquifer of 200°C initial temperature, $\phi = 0.1$, h = 20 m, and volumetric solid-rock heat capacity = 2,460 kJ/m^3°C. After about 12 days, the thermal front is about 60 m into the formation, and the fluid travel time from wellbore to thermal front is about 50 hr (= 3,000 min.). Referring to Figure 1, we see that there is now ample time for homogeneous nucleation to occur before the fluid reaches the thermal front. The result is that the injectability of that horizon is damaged by silica precipitation. Furthermore, well treatments with caustic or HF are not effective because the damage is 30 to 60 m away from the wellbore.

Case 2. Can one reinject straight from the first-stage steam separators at Cerro Prieto? Assume the following typical brine conditions at the injection well: 160°C, 0.95 g/l dissolved SiO_2, effective $[Na^+] = 0.25$, and negligible suspended solids. The brine pH at injection temperature is not known, but is approximately 7.8 at room temperature. This gives a nominal pH of about 8.3 (which is within the range of weak pH dependence) and a pH factor of 2.7 (from Figure 3). The $pH_{nom} = 7.0$ deposition rate, from Figure 2, is about 1.3 μm/day. Correcting for pH, we obtain the actual deposition rate of 3.5 μm/day. Correcting for pH, we obtain the actual deposition rate of 3.5 μm/day (= 1.3 mm/yr). This is consistent with the observed rate of vitreous silica deposition near the separators at Cerro Prieto. Because pore permeability is dominant at Cerro Prieto, it is clear that injecting this brine would rapidly plug the injection well.

We hope that such mistakes will be avoided. However, we emphasize that both of these brine streams would be injectable under the criteria presently in vogue. They would be able to pass freely through a micron-sized membrane filter and would not cause visible fouling of metal surfaces during field tests of a few days duration. It is precisely the refinement of such criteria that we hope to have accomplished with the work summarized here.

ACTIVITIES PLANNED FOR FISCAL YEAR 1979

Our group is presently engaged in three areas of activity. First, we are completing the reduction of the experimental data generated during fiscal year 1978. Second, we are studying the chemistry of silica in the spent brines at the Cerro Prieto power plant by means of laboratory simulation. This work is oriented toward developing a prereinjection brine treatment for Cerro Prieto. It is supported by the Cerro Prieto project at LBL. Third, we are developing a computer model of a surface condenser in a geothermal power plant. The goal of this work is to enable the chemical operating characteristics of such a condenser to be interpreted and predicted. This model will first be applied to studying The Geysers Unit 15, which is the first geothermal power plant to be equipped with a surface condenser. This work is being funded by the Pacific Gas and Electric Company.

ENHANCED OIL RECOVERY WITH MOBILITY AND REACTIVE TENSION AGENTS

C. J. Radke and W. H. Somerton

INTRODUCTION

Use of alkaline solutions to recover selected acid crude oils has considerable economic advantage over commercial surfactant solutions. In spite of the longevity of the idea, however, a question remains as to its displacement effectiveness (Johnson, 1976). The objectives of the present study are: (a) to establish the conditions required for tertiary-mode displacement of acidic oils with high pH agents; and (2) to elucidate the dominant recovery mechanisms,

and hence permit development of an improved caustic flooding package. The overall project includes studies on core displacements from synthetic and natural systems, interfacial tensions, emulsion rheology and stability in porous media, and caustic loss.

CORE DISPLACEMENTS

Oil Field Studies

Caustic flooding tests have been run at reservoir temperature on a number of Ranger-zone cores using Ranger crude oil and simulated formation water. The test apparatus is similar to that used previously (Radke and Somerton, 1977) except that the core is mounted in a water bath maintained at a constant temperature of 125° ± 1°F. During saturation of the cores with Ranger-zone crude, the temperature of the system is increased to 180°F to ensure that all the asphaltenes are in solution in the crude, since these constituents may play an important role in the crude-oil behavior. This high temperature has led to failure of several types of plastic core holders, which have been used to minimize the corrosive effects of the caustic solutions. Currently, a thick-walled Teflon tube is used as the core holder with moderate success.

Frozen Ranger-zone cores are diamond-drilled using liquid nitrogen and then are quickly packed into the Teflon core holder under moderate pressure. The packed core is then mounted in the system and slowly brought to reservoir temperature. in the first series of tests, the native-state cores were first water-flooded with 1.43% NaCl brine. In all cases, the oil saturation was too low to recover oil (Table 1). The water flood was then followed by a caustic flood at a rate of 1.5 ft/day (0.1 wt% NaOH in softened Colorado River water followed by 0.1 wt% NaCl in the same water). Again the oil saturation was too slow to recover oil.

The native-state cores were extracted in situ using toluene followed by an acetone wash. (Because acetone was contributing to failure of the plastic tubes, the cleaning procedure was later changed to use Chevron 410H solvent followed by isopropyl alcohol.) After extracting and drying, the cores were saturated with brine and the brine was displaced with crude oil to irreducible water saturation. The water flooding and caustic flooding procedures were as given above, following THUMS planned procedure for field tests (City of Long Beach, 1977).

Table 1. Ranger-zone core floods.

Test	Condition	ϕ	K md	S_{wi}	S_{oi}	E_{rw}	E_{rc}
A-1	Native	0.35	-	0.24	0.25	0	0
A-2	Resat.	0.36	460	0.26	0.74	0.46	0.66
B-1	Native	0.39	-	0.40	0.24	0	0
B-2	Resat.	0.40	430	0.43	0.57	0.27	0.37
C-1	Resat.	0.27	65	0.43	0.57	0.51	0.82

Results of several of the tests are summarized in Table 1. The earlier test cores (A and B) had high porosities and permeabilities. By improved packing techniques in later cores (C), the porosity and permeability were greatly reduced. The resaturated core, A-2, recovered 46% of the oil in place by water flood and an additional 20% by caustic flood, for a total recovery efficiency of 66%. The second resaturated core gave much lower recovery efficiencies: 27% by water flood and an additional 10% by caustic. The large difference in the behavior of these two similar cores can probably be attributed to the lower initial oil saturation in the latter case.

Test core C-1 was prepared by a modified packing procedure giving much lower porosity and permeability. The core was extracted in situ, without running native state tests. The high recovery by both water flooding and caustic flooding (51% and 31%, respectively) was surprising for this low permeability core. Extraction of the core after the test confirmed the low residual oil saturation of 18%.

Figure 1 shows the recovery history of core C-1 plotted as a fraction of initial oil in place recovered as a function of pore volumes of water and caustic injected. It is interesting to note that no tertiary oil was recovered until nearly 2-1/2 pore volumes of caustic had been injected. The pH of the effluent remained low until after the first tertiary oil was recovered. This would indicate a very large consumption of caustic (probably most of it being adsorbed by the fine-grained, clayey reservoir rock) before any oil was produced. Thereafter, the pH and recovery curves tend to be parallel. The oil was produced in slugs with no sign of emulsification until the very last oil produc-

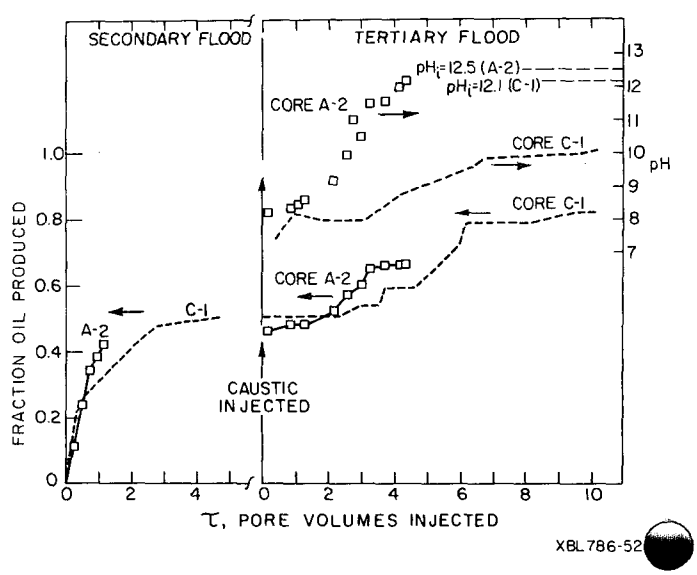

Figure 1. Production performance and pH history for core C-1. Tertiary flood is 0.2 PV of 1 wt% NaOH followed by 0.1 wt% NaCl with 1 wt% NaOH.

tion increment, which was in the form of a small oil slug followed by a very dilute oil in water emulsion.

In Figure 2, the production performance of core A-2 is compared with C-1. Recalling that the A-2 core was much more permeable than C-1, the much earlier recovery (from a pore-volume standpoint) might be expected for the A-2 core. The caustic consumption is also much lower in the case of the more permeable core, although the pH and oil-recovery curves are again parallel with oil production, ceasing as the effluent pH approaches the value for the injected fluid. A possible difference between these two cores is that A-2, the lower caustic consumer, was previously flooded with caustic in the native state, and all the adsorption may not have been reversed.

No sweeping conclusions can be reached from this limited number of tests on oil field cores. However, certain observations seem irrefutable. It is clear that with sufficient initial oil saturation, oil can be recovered in the tertiary mode by caustic injection, at least under laboratory conditions. Consumption of caustic by the fine-grained, clayey reservoir rock is high, especially for the low-permeability cores. The recovery mechanism with the oil field cores and fluids does not appear to involve emulsification. The vast majority of the oil produced was emulsion-free so if emulsions were formed in the core, they must have been of the unstable variety. No large changes in pressure gradients were noted and this would have occurred if emulsion entrapment were present.

The recovery of tertiary oil appears to be associated with caustic consumption. No oil is recovered until the effective caustic concentration in the core exceeds a critical level. At this point some oil is accumulated and produced in a mini-bank. This process continues in a step-like manner as the critical caustic saturation level is reached progressively down the tube. The recovery mechanism in this case may involve wettability reversal with sharp wettability gradients.

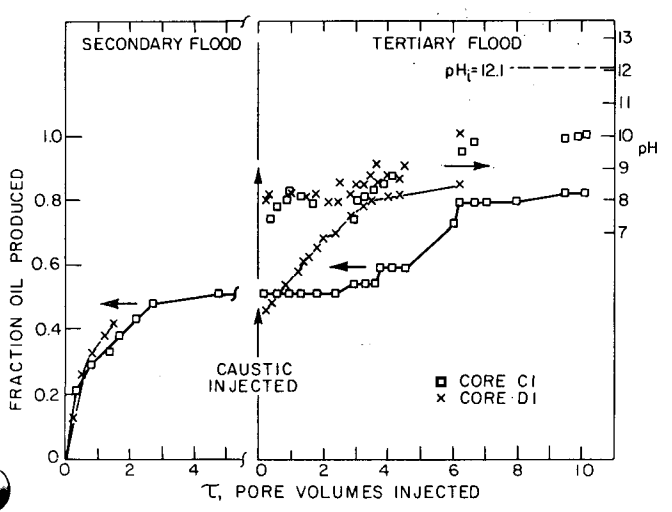

Figure 2. Production performance and pH history for A-2 compared with core C-1.

Synthetic System

To understand the complicated chemistry involved in alkali flooding, we are studying the displacement of oleic acid-doped mineral oil (1.5 cp and acid #2) from Ottawa sand packs (about 5 darcy) at a scaled rate (7 ft/day). Details of the experimental apparatus and procedures are available (Radke and Somerton, 1977).

Experimental results for the percentage recovery of oil remaining after water flooding to residual, as a function of pH at two NaCl salt contents, are shown in Figure 3. Without salt, no recovery of tertiary oil is found. As discussed previously (Radke and Somerton, 1977) nonsaline, high-pH (about 12) solutions lead to core plugging but not to tertiary oil recovery. However, high-saline solutions exhibit recovery, which is a strong function of pH. At pH values below about 11, the alkaline solutions are buffered to provide sufficient neutralizing capacity.

Interfacial tensions for the solutions in Figure 3 are all above 0.1 dyne/cm giving capillary numbers less than 10^{-3}. Hence recovery cannot be explained by the low-tension mechanism. Figure 4, however, provides considerable insight into the underlying surface chemistry. For salt solutions below 1 wt%, emulsions are of the oil-in-water type, whereas above 1% they invert to the water-in-oil type. Also above 1 wt% salt, the receding contact angles (measured

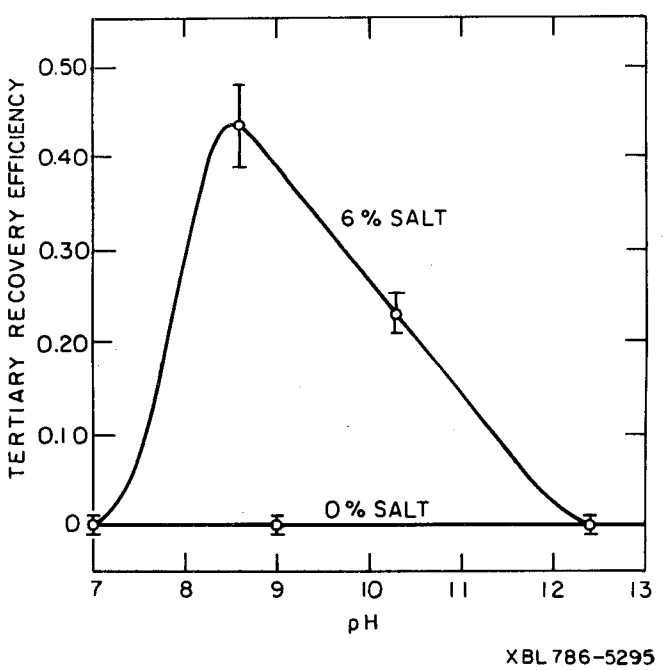

Figure 3. Tertiary recovery efficiency as a function of pH for two salt weight concentrations.

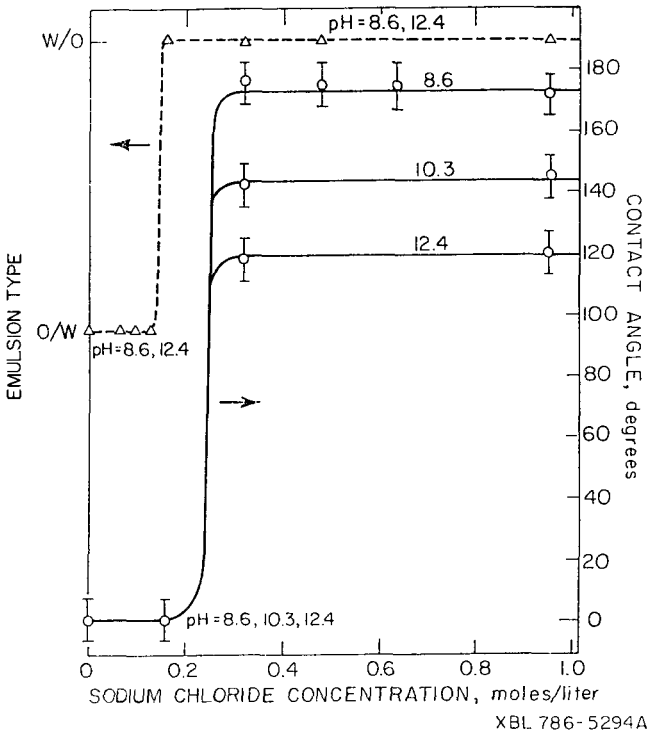

Figure 4. The effect of salt on emulsion type and contact angle.

through the water-phase against quartz) show a reversion to oil-wet. The degree of oil wetness is a function of solution pH. Note that the degree of oil wettability exactly parallels the recovery efficiencies in Figure 3. In this system, only solutions that form water-in-oil emulsions and that exhibit strong oil-wet conditions give tertiary oil production.

Displacement Modeling

The displacement of acidic crude oil from a porous medium by an alkaline solution is similar to an immiscible displacement process with chromatographic separation of the surfactant species among the oil, water, and rock phases. If the flow properties in an alkaline flood can be represented empirically by the relative permeability concept, then it is possible to extend the Buckley-Leverett water flood theory by allowing the relative permeability to be a function of saturation and concentration of the surfactant generated by the in-situ alkaline chemical reaction. Similar extensions of the Buckley-Leverett equation have been developed for enriched gas drives, detergent, polymer, alcohol, carbonated water, surfactant, and micellar flooding (Welge et al., 1961; Fayers and Perrine, 1959; Patton et al., 1971; Wachmann, 1964; Claridge and Bondor, 1974; Larson and Hirasaki, 1976; and Kremesec and Treiber, 1976, respectively).

INTERFACIAL TENSION

Crude Oil

Spinning drop (Cayias et al., 1975) interfacial tensions of Ranger-zone crude oil against different sodium hydroxide solutions are shown in Figure 5 at ambient temperature. As previously observed (Radke and Somerton, 1977; McCaffey, 1976), acid crude-oil tensions show a dynamic minimum. For the ultralow tensions, the return to high tension is not experimentally available. This is because the contracting drop succumbs to inevitable external disturbances and breaks into satellite drops.

Figure 5 also indicates the sensitivity of the minimum dynamic tension to small changes in hydroxyl ion concentration. This sensitivity to pH is further accenturated in Figure 6, which gives the minimum tension as a function of caustic pH. Here the narrow range of ultralow tensions typical of synthetic surfactants is evident.

The effect of aqueous salt content and pH on Ranger-zone crude oil minimum dynamic tension is portrayed in Figure 7. Addition of sodium chloride shifts the pH for dynamic minimum tensions less than (10^{-3}) dyne/cm to lower values. Also for the lower salt concentrations, the 10^{-3} dyne/cm isotension well broadens. Similar general conclusions can be drawn from

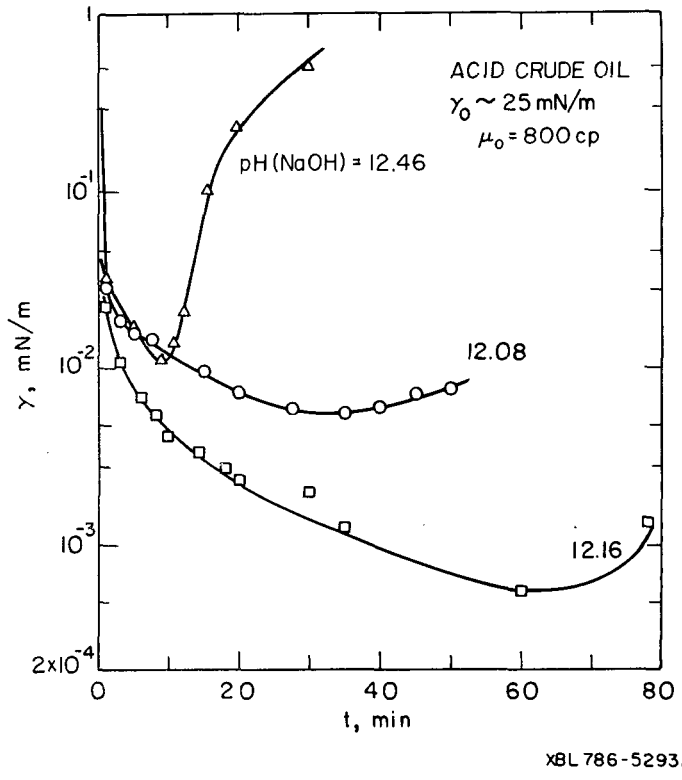

Figure 5. Dynamic tensions as functions of pH for Ranger-zone crude oil.

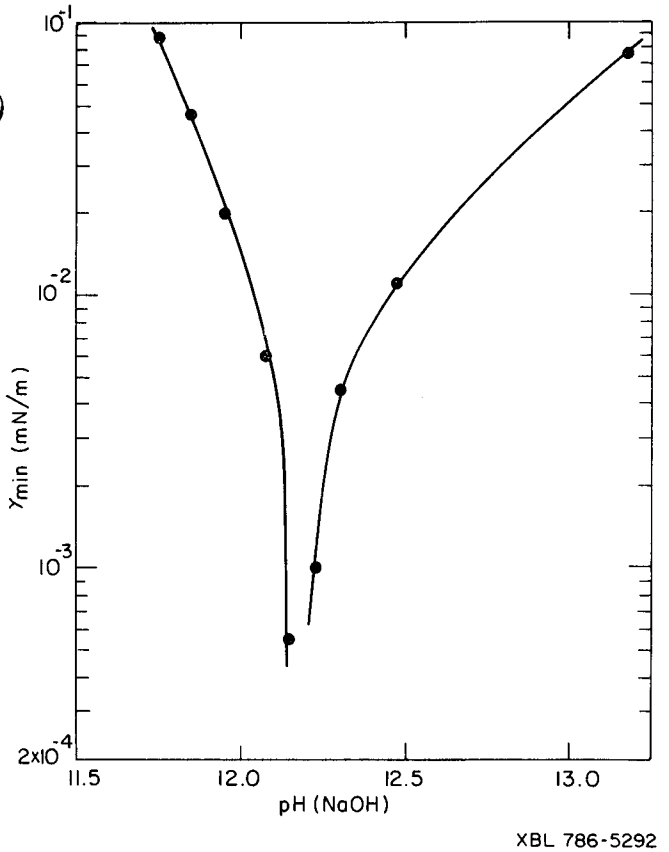

Figure 6. Minimum in dynamic tensions as a function of pH.

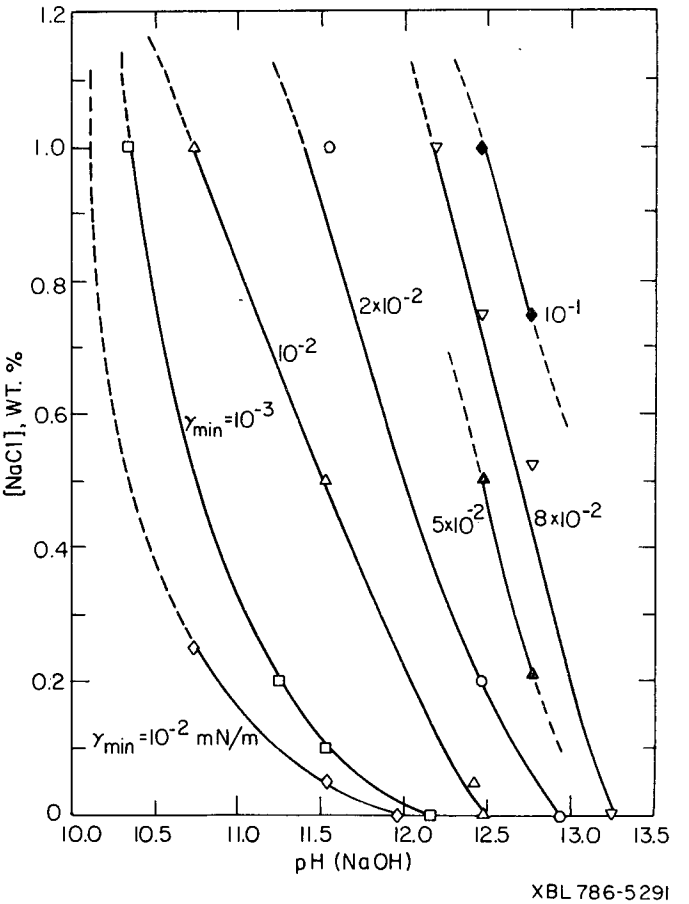

Figure 7. Constant dynamic minimum tensions for varying pH and salt contents.

the data of Jennings (1975). One important result from Figure 7 is that the original THUMS flood design does not appear to fall in the lower tension composition region (i.e., pH ~ 12.5 and [NaCl] = 1 wt%).

Dynamic Tensions

Previous reports (Radke and Somerton, 1977), as well as literature work show that dynamic tensions can exhibit a sharp minimum (McCaffery, 1976; Farmanion et al., 1978; Mansfield, 1952; England and Berg, 1971). This minimum is especially dramatic when an acidic California crude oil, or synthetic oils containing an oil-soluble hydrolyzable surfactant, are brought in contact with an aqueous alkaline solution (Figure 5). An appropriate explanation of this tension minimum is important not only in the proper interpretation of interfacial tension measurements, but in the potential exploitation of this phenomena for enhanced oil recovery.

A minimum in dynamic tension indicates a period when surfactant concentration at the interface reaches a maximum value (Radke and Somerton, 1977). During this period, emulsification into small oil droplets can occur with negligible shear energy input (e.g., spontaneous emulsification). If the duration of low interfacial tensions is long enough, emulsification may be possible with very low acid concentrations in the oil phase. However, if after the minimum, the tension rapidly rises back to a high value, propagation of the entrained droplets cannot take place except through the larger pores or by coalescence into an oil bank. A low-tension minimum followed by a rapid rise to a high-equilibrium tension seems well suited to the entrapment recovery mechanism.

EMULSION FLOW

Porous Media Flow

Two of the fundamental oil recovery mechanisms that have been suggested to alkali flooding involved emulsions (Johnson, 1976). These are emulsification and entrainment and emulsification and entrapment. The former was first discussed by Subkow (1942), who believed that the crude oil is emulsified in situ by lowering the interfacial tension, and then entrained as a continuous flowing alkaline water phase. This mechanism precluded any increase in recovery before caustic breakthrough, and the oil recovery is as an emulsion, flowing with the caustic front. The latter mechanism was proposed by McAuliffe (1973a,b), who noted that the size of the emulsion droplets generated in situ

is not small enough to penetrate through all small pore-throat constrictions. Instead, entrapment occurs between sand grains. This causes a reduction of water mobility and leads to an increase in sweep officiency and oil recovery in the low-permeability zones of the reservoir. The entrapment mechanism results in no significant reduction in ultimate residual oil saturation, but rather reduces the water-oil ratio required to reach this residual oil saturation. The oil recovered from this mechanism is as a separate phase.

The primary differences between these two mechanisms are the interfacial tension and the ratio of drop sizes to pore sizes. High interfacial tension and large drop-size to pore-size ratio will result in the entrapment mechanism. Low interfacial tension and small drop-size ratio will exhibit the entrainment mechanism. Thus, the purpose of this work is to study the effect of interfacial tension and drop-size to pore-size ratio on emulsion flow through porous media.

An experimental system has been constructed, as described previously (Radke and Somerton, 1977), to obtain the relation of pressure-drop to flow rate for dilute stable emulsion flow in consolidated and unconsolidated porous media. Further, a quantitative model, based on deep-bed filtration theory, has been developed to describe the bed permeability. The rudiments of this theory have been published (Radke and Somerton, 1977) and the details will be available in a forthcoming manuscript.

Caustic Loss

In this work, caustic consumption by reservoir rock is measured by frontal-analysis chromatography using a liquid chromatograph. This allows determination of both equilibrium consumption and band-broadening resistances in the same experiment. Equilibrium loss is obtained from the solute-residence time of an input concentration step-change and an overall solute material balance (Wang et al., 1978). Experimental determination of adsorption of sodium hydroxide on oil-free Ranger-zone sand at 20°C is shown in Figure 8. Because hydroxyl and hydrogen ion concentrations are never independent, the adsorption in Figure 8, Γ, is actually the difference between hydroxyl ion adsorption ($\Gamma_{OH^-} - \Gamma_{H^+}$), and not the hydroxyl ion adsorption alone. Further, $\Delta\Gamma$ is measured relative to water of pH 7, since hydroxyl ion concentration in water is always finite. Experimental data in Figure 8 include those obtained after reflushing the column to neutral pH, thus indicating reversible caustic adsorption at ambient temperature. The alkali adsorption loss given in Figure 8 falls in line with other reported reservoir data (Jennings et al., 1974). However, Figure 8 shows the strong influence of hydroxyl concentration.

The elution curve also gives information on adsorption kinetics. For simple external mass transfer and controlled adsorption in the linear

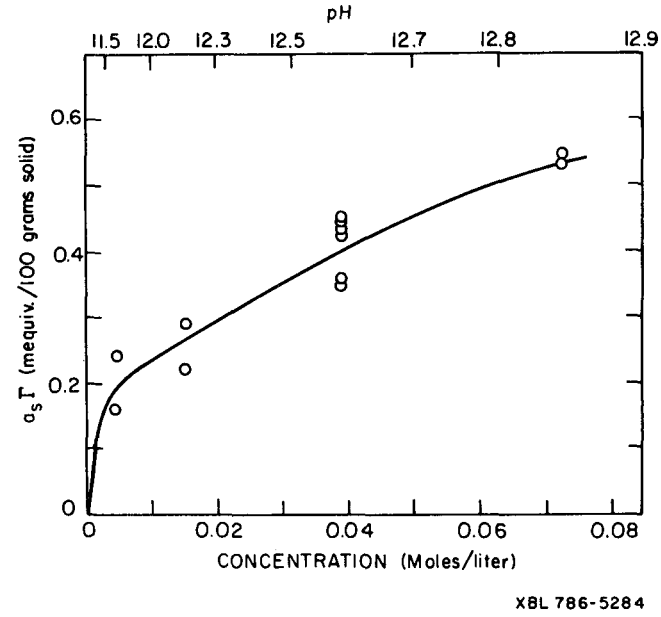

Figure 8. Equilibrium caustic adsorption as a function of hydroxyl concentration on Ranger-zone reservoir sand.

Henry law isotherm region, Thomas' analytical solution is applicable (Sherwood et al., 1975). Figure 9 compares the experimental caustic elution curve with the theoretical calculation, with the mass transfer coefficient estimated from the work of Newman and Tiedemann (1978). Clearly, external mass transfer (and/or axial dispersion) cannot explain the observed spread, and additional resistances must be considered. The most likely, but unexpected, candidate is an internal-particle mass-transfer resistance suggesting porous solids in the Ranger-zone sand. This possibility is strengthened by the high specific surface area of this sand (about 7 m^2g^{-1} by nitrogen BET) with particle sizes between 10 and 100 μm.

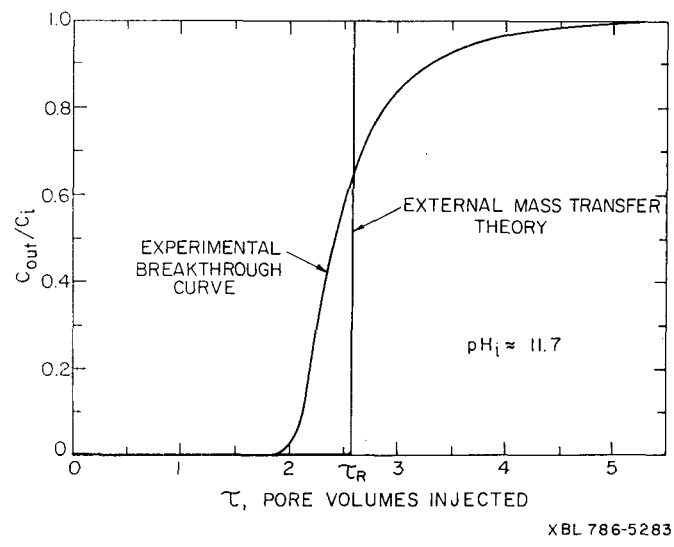

Figure 9. Experimental caustic elution curve compared to external mass transfer theory.

Considerable evidence indicates that caustic loss increases dramatically as a function of temperature (Robinson et al., 1977). This work is pursuing both the kinetic and equilibrium aspects of the temperature dependence of alkali loss using frontal-analysis chromatography.

PLANNED ACTIVITIES FOR FISCAL YEAR 1979

In fiscal year 1979, we will place more emphasis on alkaline tertiary flooding of Wilmington reservoir sands, including studies on the effects of pH and salt content, use of buffers, flooding rate, mobility control, and cheap surfactant additives. The present flooding apparatus will be altered to permit continuous operation and, after rebuilding a second mercury injection pump, another complete flooding apparatus will be constructed. These modifications will reduce the long times that are presently required to obtain a recovery result.

Studies on the caustic-loss problem will be expanded to include both batch and chromatographic tests in order to decide the importance of reservoir sand dissolution. We will also begin analysis of the clay content of the reservoir sand.

The emulsion studies of this coming year will be directed towards the use of dilute emulsions for mobility control. Secondary displacement tests of viscous oils in both homogeneous and heterogeneous cores will be used to ascertain the possible effectiveness of such emulsion mobility control.

REFERENCES CITED

Cayias, J. L., Schechter, R. S., and Wade, W. H., 1975. The measurement of low interfacial tension via the spinning drop technique in Adsorption at interfaces. A.C.S. Symposium Series 8.

Claridge, E. L., and Bondor, P. L., 1974. A graphical method for calculating linear displacement with mass transfer and continuously changing mobilities. Soc. Pet. Eng. Jour., v. 14, pp. 609-618.

City of Long Beach, Dept. Oil Properties, 1977. Improved secondary oil recovery by controlled water flooding pilot demonstration. Technical proposal for ERDA.

England, D. C., and Berg, J. C., 1971. Transfer of surface activity agents across a liquid-liquid interface. AIChE Jour., v. 17, no. 2, p. 313.

Farmanion, P. A., Davis, N., Kwan, K. T., Yen, T. F., and Weinbrandt, R. M., 1978. Isolation of native petroleum fractions for lowering interfacial tensions in aqueous-alkaline systems. Presented at Chemistry of Oil Recovery Symposium, American Chemical Society, Anaheim, California, March 1978.

Fayers, F. J., and Perrine, R. L., 1959. Mathematical description of detergent flooding in oil reservoirs. Trans. AIME, v. 216, pp. 276-283.

Jennings, H. Y., Jr., Johnson, C. E., Jr., and McAuliffe, C. D., 1974. Acaustic waterflooding process for heavy oils. Jour. Pet. Tech., v. 126, no. 12, pp. 1344-1352.

Jennings, H. Y., Jr., 1975. A study of caustic solution-crude oil interfacial tensions. Soc. Pet. Eng. Jour., v, 15, p. 197.

Johnson, C. E., Jr., 1976. Status of caustic and emulsion methods. Jour. Pet. Tech., v. 28, pp. 85-92.

Kremesec, V. J., and Treiber, L. J., 1976, Effect of system wettability on oil displacement by micellar flooding. Prepared for the 51st Annual Fall Technical Conference and Exhibition of the Soc. Pet. Eng. AIME, New Orleans, Oct. 3-6, 1976. Dallas, Soc. Pet. Eng. AIME, SPE 6001.

Larson, R. G., and Hirasaki, G., 1976. Analysis of the physical mechanisms in surfactant flooding. 51st Annual Fall Technical Conference and Exhibition, Soc. Pet. Eng. AIME, New Orleans, Oct. 3-6, 1976. Dallas, Soc. Pet. Eng. AIME, SPE 6003.

Mansfield, W. W., 1952. The spontaneous emulsification of mixtures of Oleic acid and paraffin oil in alkaline solutions. Australian Jour. Sci. Res. Sec. A, Physical Sciences, v. 5, pp. 331-338.

McAuliffe, C. D., 1973a. Crude-oil-in-water emulsion to improve fluid flow in an oil reservoir. Jour. Pet. Tech., v. 25, pp. 721-726.

_____, 1973b. Oil-in-water emulsions and their flow properties in porous media. Jour. Pet. Tech., v. 25, pp. 727-733.

McCaffery, F. G., 1976. Interfacial tensions and aging behavior of some crude oils against caustic solutions. Jour. Can. Pet. Tech., v. 15, pp. 1-4.

Newman, J., and Tiedemann, W., 1978. Flow-through process electrodes. Advances in Electrochemistry and Electrochemical Engineering, v. 11, pp. 353-438.

Patton, J. T., Coats, K. H., and Colegrove, G. T., 1971. Prediction of polymer flood performance. Soc. Pet. Eng. Jour., v. 11, pp. 72-84.

Radke, C. J., and Somerton, W. H., 1977. Enhanced recovery with mobility and reactive tension agents, Third ERDA Symposium on Enhanced Oil and Gas Recovery and Improved Drilling Methods, Tulsa. Washington, D. C., U. S. Energy Research and Development Administration. v. 1, p. B-5.

Robinson, R. J., Bursell, C. G., and Restine, J. L., 1977. Acaustic steamflood Pilot-Kern River field. Prepared for 47th Annual California Regional Meeting of the SPE and AIME, Bakersfield, California, April 13-15, 1977. Dallas, Soc. Pet. Eng. AIME, SPE-6523.

Sherwood, T. K., Pigford, R. L., and Wilke, C. R., 1975. Mass transfer. New York, McGraw-Hill, pp. 15-17.

Subkow, P., 1942. Process for the removal of bitumen from bituminous deposits. U. S. Patent No. 2288857 (July 7, 1942).

Wang, H. L., Duda, J. L., and Radke, C. J., 1978. Solution adsorption from liquid chromatography. Jour. Colloid Int. Sci., v. 66, pp. 153-165.

Wachmann, C., 1964. A mathematical theory for the displacement of oil and water by alcohol. Soc. Pet. Eng. Jour., v. 4, pp. 250-266.

Welge, H. J., Johnson, E. F., Ewing, S. P., Jr., and Brinkman, F. H., 1961. The linear displacement of oil from porous media by enriched gas. Jour. Pet. Tech., v. 13, pp. 787-796.

URANIUM IN ALKALINE ROCKS

B. Strisower, H. A. Wollenberg, M. Murphy, H. Bowman, S. Flexser, and I. S. E. Carmichael

INTRODUCTION

Uranium ores mined in the United States to date have come primarily from sedimentary deposits; crystalline rocks have yielded much of the uranium mined in the rest of the world. Among these crystalline rocks are the alkaline intrusive rocks, known to contain uranium as a result of exploration in Greenland and of mining in Brazil and Canada. A single alkaline intrusive occurrence in the United States, the Ross-Adams deposit in peralkaline granite at Bokan Mountain, Alaska, has been mined for uranium. Other alkaline intrusive occurrences in the United States might be expected to add to uranium resources. Within the category of alkaline igneous rocks are peralkaline nepheline syenites, alkaline-peralkaline granites, and carbonatites. Funded by Bendix Field Engineering Corp. for the U. S. Department of Energy, Lawrence Berkeley Laboratory completed a preliminary study of the potential for the occurrence of uranium in alkaline intrusive rocks. Results are detailed in a report by Murphy et al. (1978).

ACTIVITIES IN FISCAL YEAR 1978

The principal alkaline igneous occurrences of known uranium resource potential were characterized by on-site visits. On-site inspections were made of uraniferous nepheline syenites at Ilímaussaq, Greenland, and Poços de Caldas, Brazil. These alkaline intrusive occurrences, together with the uraniferous peralkaline granite at Bokan Mountain, Alaska, and the niobium-uranium occurrence in carbonatites of the Ottawa Graben of southeastern Canada, were used as type-localities.

Information gained from on-site visits and published reports dealing with the four type-localities was used to develop a set of criteria which were used for comparing other alkaline igneous occurrences in the United States.

The characteristics considered for comparison of alkaline intrusive areas included: petrology, mineralogy, tectonic setting, age of implacement, form of implacement, country rocks, late-stage hydrothermal activity, pathfinder elements, uranium mineralization, and radioactivity. Potential uranium resource areas in the alkaline rocks of the United States were identified by means of computer literature searches and review of relevant reports. These areas are identified in Table 1 and the accompanying map on page 183.

Of the 69 alkaline intrusive occurrences shown on the map, only 40 had enough reported data to be judged using the type-locality criteria. Based on these criteria, nine areas showed the most promise for exploration. There are:

1. Alkaline-carbonatitic occurrences at Magnet Cove and Potash Sulphur Springs, Arkansas
2. Carbonatite-pyroxenite nepheline syenitic Powderhorn intrusion near Gunnison, Colorado
3. Rocky Boy hydrothermally altered carbonatitic stock in the Bearpaw Mountains, Montana
4. Lujavritic stocks and sills of the Diablo Plateau, west Texas
5. Lujavritic-tinguaitic dike near Beemerville, New Jersey
6. Pegmatitic veins in riebeckite granite near Quincy, Massachusetts
7. Peralkaline pegmatites in the alkalic Quanah granite of the Wichita Mountains, Oklahoma
8. Hydrothermally altered shear zones at the contact between alkalic granite and Precambrian granite near Jamestown, Colorado
9. Sheared and altered granite and pegmatites of Mt. Rosa, Colorado

Because of the presence of secondary hydrothermal alteration combined with deep lateritic weathering, attributes of the Poços de Caldas uranium occurrence, the Magnet Cove/Potash Sulphur Springs area is considered the top-priority exploration target of the nine areas. More detailed descriptions of the areas are presented by Murphy et al. (1978).

A second line of investigation was a study of potential pathfinder elements--those occurring with uranium in the minerals contained in alkaline intrusive rocks. The question was: If no radioelement data existed in the literature on a given occurrence, could one use data on other elements to indicate the presence of appreciable uranium?

Trace-element and radioelement data from reports on the alkaline intrusive occurrences were collected for several elements--Zr, Nb, Be,

F, rare earths, Li, Zn, and Mo--as well as for U and Th in the same rocks. The compilation included data from (a) peralkaline granites of Bokan Mountain, Alaska; (b) peralkaline intrusives at Magnet Cove, Arkansas; Illímaussaq, Greenland; and Lovozero, Soviet Union; and (c) calc-alkalic intrusives of New England and the Sierra Nevada batholith. Concentrations of each element were plotted against uranium or uranium-plus-thorium contents, using available data from the literature.

In the country rock surrounding the mineralized occurrences, Zr had the strongest relationship to U + Th. The log-log plot (Figure 1) illustrates this correlation. After Zr, the next best correlation was La + Ce with U + Th as shown in Figure 2.

Relationships between other trace elements and radioelements were weaker, or data were too sparse to be useful. In many cases the analyses of trace elements reported in the literature were semiquantitative, which may account for the lack of strong correlations.

Quantitative analyses were done at LBL on samples of country rock from collections from Poços de Caldas, Brazil; Ilímaussaq, Greenland; Nemegos, Ontario; and Magnet Cove, Arkansas. Mean concentrations and ranges for major and trace elements are given for several alkaline intrusive rocks from these sites (Table 2). The 11 nepheline syenite samples were collected from Poços de Caldas, Brazil; Nemegos, Ontario; and Magnet Cove, Arkansas. For rock specimens collected from three different alkaline intrusives in widely separated geologic areas, the ranges are remarkably small.

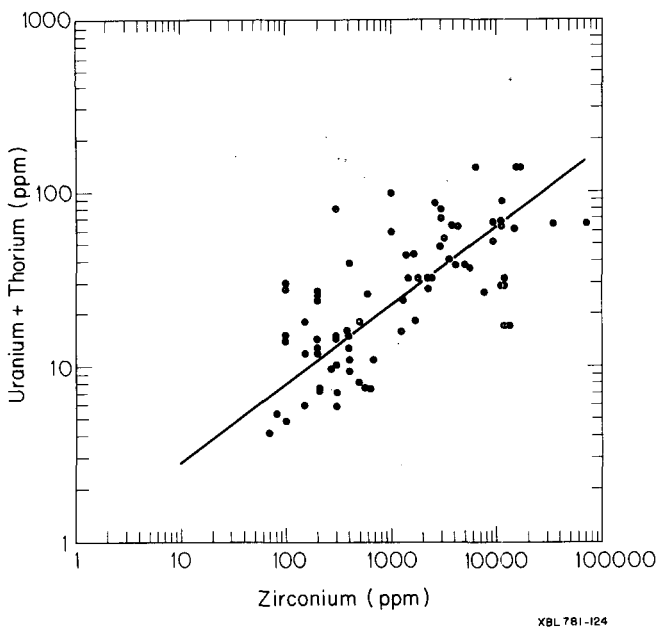

Figure 1. Zr vs. U + Th; data from the literature.

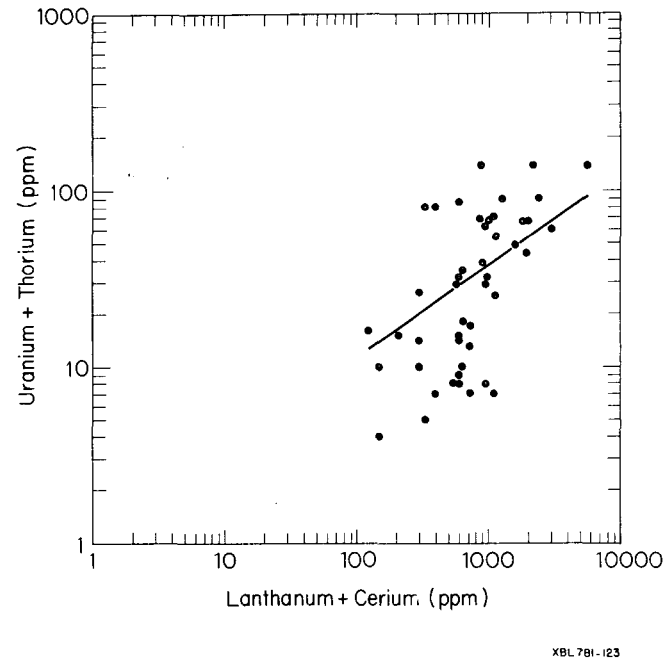

Figure 2. La + Ce vs. U + Th; data from the literature.

In these data, a good correlation is evident between the radioelements U + Th and the rare-earth elements La + Ce (Figure 3). Using the same data, there is essentially no correlation between U + Th and Zr. It is possible that in these rocks the minerals containing Zr are not necessarily those containing the radioand rare-earth elements.

These relationships suggest that Zr and rare-earth elements may be used as qualitative pathfinders for radioelements. The usefulness of these and other elements as pathfinders can be confirmed by more petrologic and chemical analytic work on a more controlled group of samples.

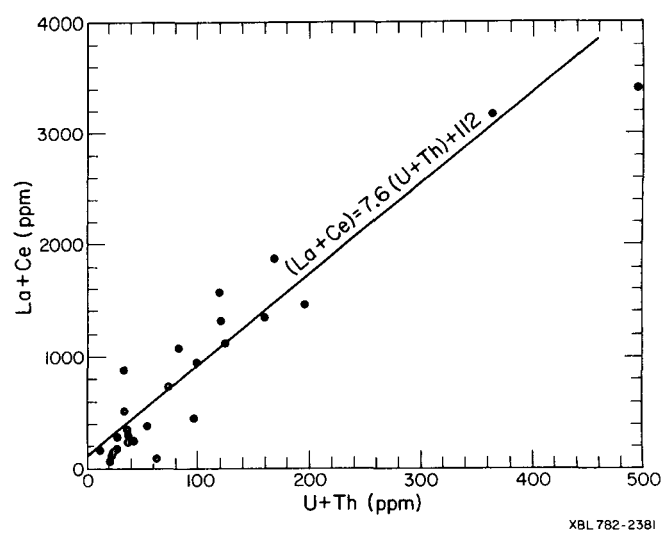

Figure 3. La + Ce vs. U + Th; data from LBL analyses.

TABLE 1

MASTER LIST OF U.S. ALKALINE OCCURRENCES

ALASKA

SELAWIK HILLS (1)

GRANITE MOUNTAIN (2)

DRY CANYON CREEK (3)

EKIEK CREEK (4)

CHICHAGOF ISLAND (5)

BOKAN MOUNTAIN (6)

ST. LAWRENCE ISLAND (67)

SALMON BAY (68)

WASHINGTON

SHASKET CREEK, FERRY COUNTY (7)

OREGON

NEWPORT, LINCOLN COUNTY (8)

CALIFORNIA

NEW IDRIA, SAN BENITO COUNTY (9)

COYOTE PEAK, HUMBOLT COUNTY (10)

TIN MOUNTAIN, INYO COUNTY (11)

MOUNTAIN PASS, SAN BERNARDINO COUNTY (12)

IDAHO

CARIBOU MOUNTAIN, BONNEVILLE COUNTY (13)

LEMHI PASS, LEHMI COUNTY (14)

HALL MOUNTAIN, BOUNDARY COUNTY (15)

MONTANA

LIBBY (Rainy Creek), LINCOLN COUNTY (16)

ROCKY BOY (Bearpaws), HILL COUNTY (17)

CRAZY MOUNTAINS, PARK COUNTY (18)

HIGHWOOD MOUNTAINS, CHOUTEAU COUNTY (19)

LITTLE BELT MOUNTAINS, MEAGHER COUNTY (20)

JUDITH MOUNTAINS, FERGUS COUNTY (21)

UTAH

LA SAL MOUNTAINS, SAN JUAN COUNTY (22)

COLORADO

POWDERHORN (Iron Hill), GUNNISON COUNTY (23)

JAMESTOWN, BOULDER COUNTY (24)

CRIPPLE CREEK, TELLER COUNTY (25)

MT. ROSA, TELLER/EL PASO COUNTY (26)

SOUTH PARK, PARK COUNTY (27)

McCLURE MT./GEM PARK (Wet Mountains), FREMONT COUNTY (28)

ARKANSAS RIVER (Wet Mountains), FREMONT COUNTY (29)

NEW MEXICO

PAJARITO MOUNTAIN, OTERO COUNTY (30)

TEXAS

DIABLO PLATEAU, HUDSPETH COUNTY (31)

BARRILLA MOUNTAINS, JEFF DAVIS COUNTY (32)

CHRISTMAS MOUNTAINS, BREWSTER COUNTY (33)

SOLITARIO, PRESIDIO/ BREWSTER COUNTY (34)

OKLAHOMA

WICHITA MOUNTAINS, COMANCHE COUNTY (35)

MISSISSIPPI

JACKSON DOME†, HINDS COUNTY (36)

C.B. BOX ESTATE†, HUMPHREYS COUNTY (37)

LOUISANA

MONROE FIELD†, OUACHITA COUNTY (38)

TENNESSEE

McGREGOR†, TIPTON COUNTY (39)

BATEMAN†, SHELBY COUNTY (40)

ARKANSAS

MAGNET COVE, HOT SPRINGS COUNTY (41)

WILSON SPRINGS (Potash Sulphur Springs), GARLAND COUNTY (42)

FOURCHE MOUNTAIN (Little Rock), PULASKI COUNTY (43)

BENTON, SALINE COUNTY (44)

NEBRASKA

ELK CREEK†, JOHNSON COUNTY (45)

WYOMING

DEVILS TOWER, CROOK COUNTY (46)

WISCONSIN

WAUSAU, MARATHON COUNTY (47)

MINNESOTA

SNOWBANK LAKE, LAKE COUNTY (48)

KEKEKABIC LAKE, LAKE COUNTY (49)

MICHIGAN

MARQUETTE, MARQUETTE COUNTY (50)

MAINE

LITCHFIELD, KENNEBEC COUNTY (51)

PLEASANT MOUNTAIN, CUMBERLAND/OXFORD COUNTY (52)

CASHES LEDGE, ATLANTIC OCEAN (53)

AGAMENTICUS, YORK COUNTY (54)

NEW HAMPSHIRE

RED HILL, CARROLL COUNTY (55)

WHITE MOUNTAINS, CARROLL/ COOS/GRAFTON COUNTY (56)

VERMONT

CUTTINGSVILLE, RUTLAND COUNTY (57)

BARBER HILL, CHITTENDEN COUNTY (58)

MT. ASCUTNEY, WINDSOR COUNTY (59)

MASSACHUSETTS

PEABODY/CAPE ANN, ESSEX COUNTY (60)

BLUE HILLS/QUINCY, NORFOLK COUNTY (61)

RATTLESNAKE HILL, NORFOLK COUNTY (62)

RHODE ISLAND

CUMBERLAND, PROVIDENCE COUNTY (63)

NEW JERSEY

BEEMERVILLE, SUSSEX COUNTY (64)

BROOKVILLE, HUNTERDON COUNTY (65)

VIRGINIA

STAUNTON, AUGUSTA COUNTY (66)

NORTH CAROLINA

MOUNT ROGERS, ASHE COUNTY (69)

† from drill core

XBL 7812-14096

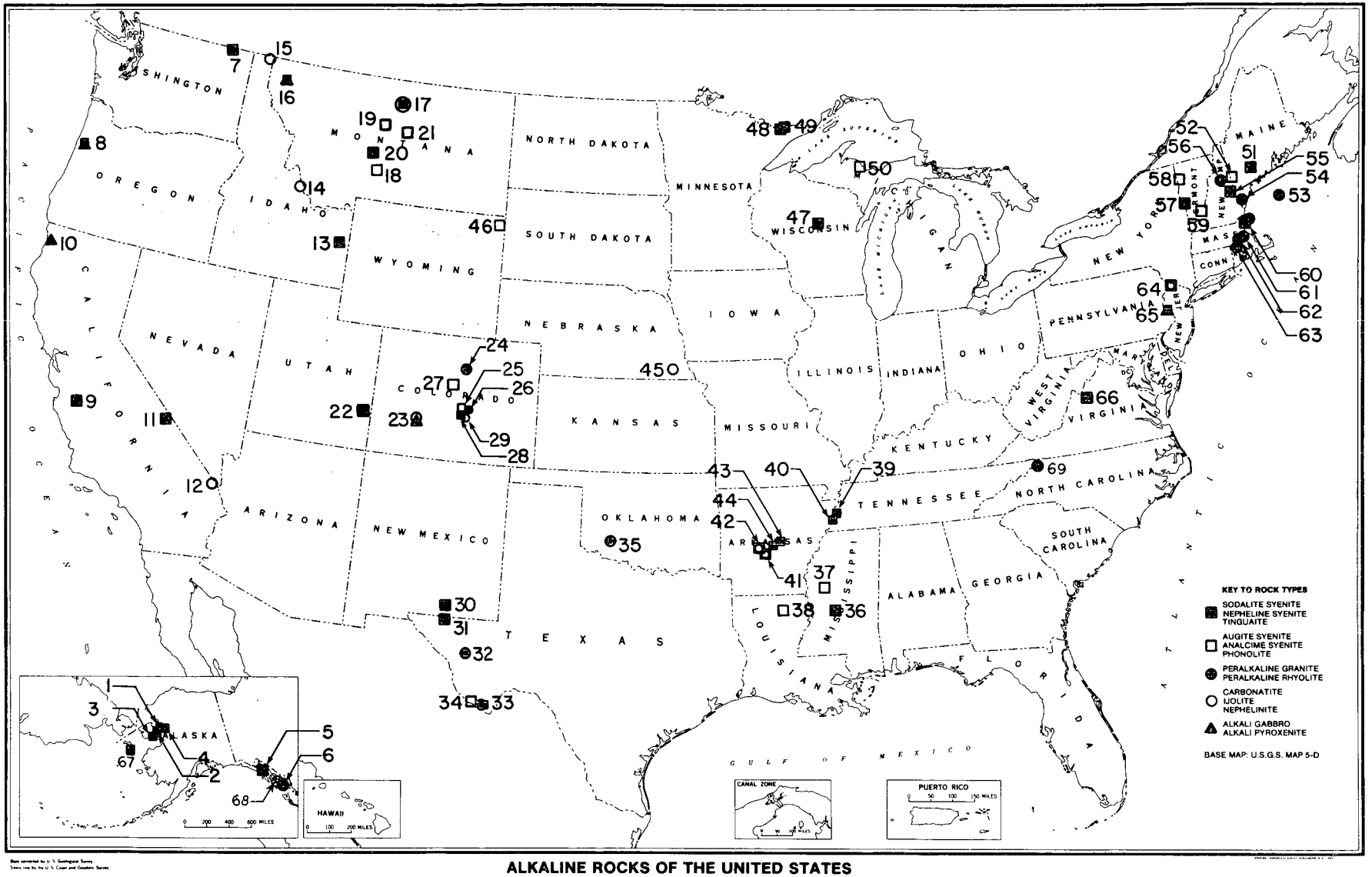

ALKALINE ROCKS OF THE UNITED STATES

XBL 782-7418

Table 2. Mean values and ranges of major and trace elements in rock types

PERCENT	NEPHELINE SYENITES		TINGUAITES		LUJAVRITES-GREENLAND		LUJAVRITES POCOS DE CALDAS		IJOLITES NEMEGOS	
	$\bar{X}$	Range	$\bar{X}$	Range	$\bar{X}$	Range	$\bar{X}$	Range	$\bar{X}$	Range
SiO_2	53.5	49.9-54.3	53.4	52.0-54.6	58.1	57.7-58.5	53.6	52.6-54.2	43.0	38.8-47.1
Al_2O_3	19.1	15.2-21.8	20.7	19.6-22.2	11.4	10.5-12.3	14.9	13.0-17.0	14.9	14.2-15.5
FeO	4.3	2.2-8.3	3.4	3.1-3.9	11.2	10.3-12.0	8.3	6.7-9.9	7.8	6.1-9.4
MgO	0.2	<0.1-0.9	0.1	<0.1-0.3	<0.1	<0.1	0.19	<0.1-0.4	2.3	1.2-3.4
CaO	2.3	1.2-5.8	2.8	1.9-4.0	0.4	0.3-0.4	2.5	2.4-2.5	7.4	4.3-10.5
Na_2O	7.5	5.2-10.0	7.9	6.5-8.9	9.3	8.1-10.4	7.9	7.9-8.0	6.3	5.3-7.2
K_2O	7.9	3.6-11.7	7.6	7.3-8.2	2.7	1.8-3.5	6.1	5.5-6.9	4.3	3.5-5.1
TiO_2	0.6	0.2-1.2	0.5	0.3-0.6	0.7	0.3-0.5	0.5	0.4-0.6	0.1	0.1
MnO	0.6	0.2-1.4	0.3	0.2-0.4	0.6	0.4-0.7	0.5	0.3-0.8	0.5	0.3-0.7
TOTAL	95.8		96.1		93.9		94.5		86.6	
Agpaitic Ratio*	1.07	0.97-1.23	1.00	0.81-1.13	1.56	1.35-1.77	1.29	1.18-1.44	0.97[5]	0.97-0.98
PPM										
U	16.5	5-26	7.3	5-9	430	420-440	13.3	11-18	5.7	4.1-7.3
Th	84.5	18-170	22.8	12-29	1510	1350-1670	54.0	17-82	25.5	20-31
Zr	2566.4	240-7100	722.5	390-1030	-	-	6766.7	3800-9200	615	610-620
Ta	8.8	4-18	2.6	1.5-5.4	5.3	4.5-6	12.1	8.3-17	6.5	5-8
Nb	362.1	135-761	128.8	63-189	-	-	458.3	314-616	127.0	107-147
Hf	46.7	8-131	10.9	5.7-20	11.5	10-13	137.3	72-190	7.0	7
La	397.6	60-870	111.3	30-210	5850	5400-6300	313.3	160-410	72.5	50-95
Ce	479.3	59-1010	154.5	40-310	7950	7300-8600	348.7	125-546	140.0	80-200
Nd	91.6	13-180	36.3	13-77	2100	1900-2300	58.3	20-100	65.0	30-100
Sm	10.8	1.1-21	4.9	1.6-10	245	240-250	6.6	2-12	13.0	7-19
Eu	2.6	0.3-4.8	1.1	0.4-2.5	14.5	14-15	1.6	0.5-3.0	3.5	1.9-5
Tb	1.3	0.2-2.4	0.4	0.2-0.9	26.5	26-27	2.9	0.2-1.5	1.0	0.6-1.4
Yb	6.5	0.9-15.5	1.7	0.8-3.3	50.5	50-51	6.8	4.5-9.8	5.2	4.2-6.2
Lu	1.1	0.2-2.0	0.4	0.3-0.4	19.5	19-20	1.2	0.9-1.8	1.1	1.0-1.1
Rb	293.5	70-630	201.3	180-240	485	340-630	216.7	210-225	175	100-250
Sr	1811.8	700-4500	1752.5	950-2400	-	-	2410	1570-3700	875	720-1030
Cs	4.4	1.0-8.5	4.2	1.9-6.8	2.5	1.5-3.4	10.5	1.5-25	1.4	0.7-2
Ba	765.0	100-3000	1625.0	500-3300	3500	1000-6000	250	200-300	1050	600-1500
Cr	8.6	<5-15	-	-	50	50	-	<10-26	-	-
Co	3.1	<1-12	2.0	1-4	<1.5	<1-<2	1.4	1.2-1.8	9.0	6.9-11
Ni	<20		-	-	-	-	<15	<10-<20	-	-
Mo	13.5	<5-30	18.3	<10-40	-	<20-400	<10	<10	<10	<10
Sc	2.1	<1-16	0.5	0.2-0.7	-	<1-3	<1.0	0.8-1.3	0.7	0.5-0.8
Zn	422.7	110-2000	162.5	130-200	2400	1900-2900	180	150-220	200	150-250
n =	11		4		2		3		2	

*Agpaitic Ratio calculated from (Na+K)/Al) where Na, K, and Al are molecular abundances of sodium, potassium, and aluminum.

PLANS FOR FISCAL YEAR 1979

The project was not funded in 1979.

REFERENCES

Murphy, M., Wollenberg, H., Strisower, B., Bowman, H., Flexser, S. and Carmichael, I. S. E., 1978. Uranium in alkaline rocks. Berkeley, Lawrence Berkeley Laboratory, LBL-7029.

GEODOSE PROJECT

H. A. Wollenberg and B. Strisower

INTRODUCTION

Under the auspices of EG&G, Inc., the geochemical literature was searched for data on the uranium, thorium, and potassium contents of the major rock types. The primary purpose of the project is to characterize rock and soil types by their natural gamma-ray exposure rates. This information helps us predict and interpret the gamma-ray exposure rates measured on radiological surveys by aircraft of the DOE/EG&G Aerial Measurements System.

ACTIVITIES IN FISCAL YEAR 1978

From radioelement contents, the computer program DOSECAL calculated gamma-ray exposure rates and radiogenic heat production. Exposure rates for an elevation of 1 m above the ground were calculated using the equations of Beck and de Planque (1968), relating the radiation field to distributed gamma-ray sources in the ground. Results of analyses of over 2,400 rocks are summarized in Table 1. Histograms of exposure rates comprise Figures 1, 2, and 3. Of the igneous rocks, the alkali feldspathoidal rocks

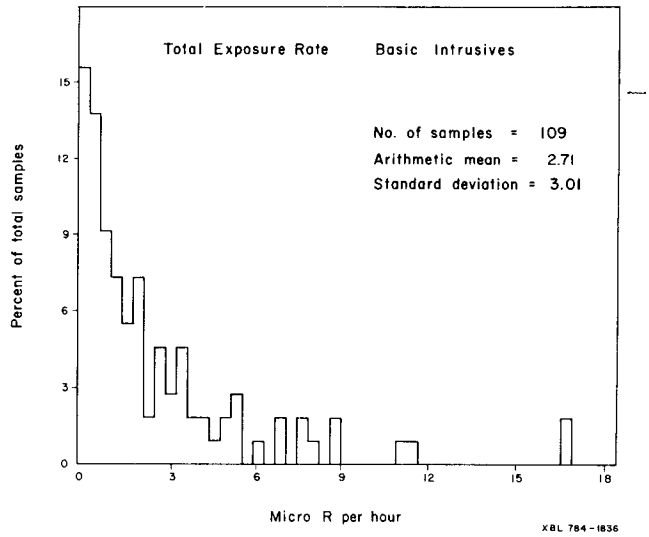

Figure 2. Histogram showing the total exposure rate for basic intrusive rocks.

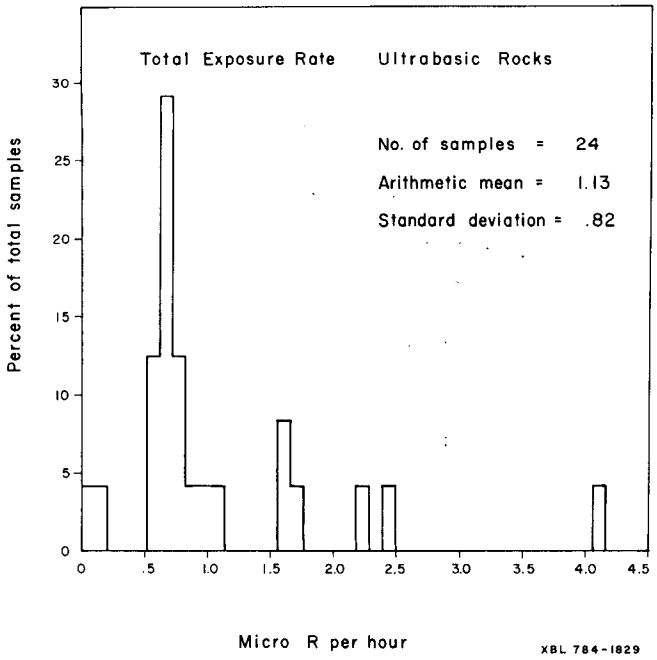

Figure 1. Histogram showing the total exposure rate for ultrabasic rocks.

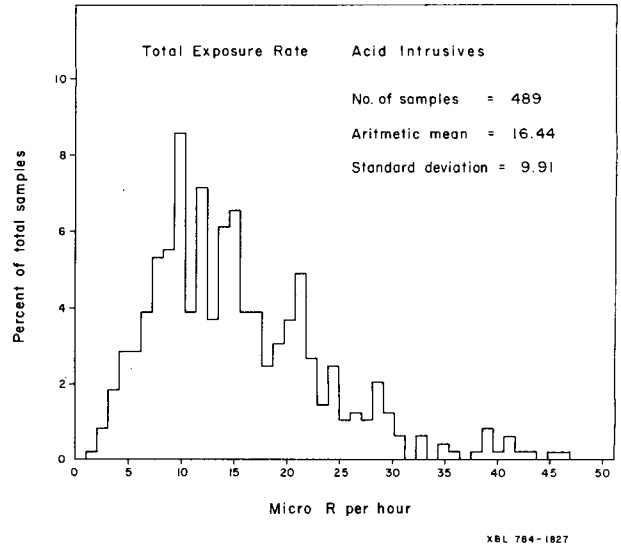

Figure 3. Histogram showing the total exposure rate for acid intrusive rocks. Note that the mean of total exposure rate for the acid intrusives is a factor of 10 higher than the mean for ultrabasic rocks. Basic intrusives have intermediate values.

Table 1. Summary of uranium, thorium, and potassium concentration, gamma-ray exposure rates, and radiogenic heat production for 16 major rock types.

										γ-RAY EXPOSURE RATES (μR/HOUR)															
	U (ppm)			Th (ppm)			K (%)			U			Th			K			TOTAL			RADIOGENIC HEAT PRODUCTION (cal cm^{-3} s^{-1} x 10^{-13})		
ROCK CLASS	MEAN	RANGE	n	MEAN	RANGE	n	MEAN	RANGE	n	MEAN	RANGE	n	MEAN	RANGE	n	MEAN	RANGE	n	MEAN	RANGE	n	MEAN	RANGE	n
Acid Extrusives	4.1	0.8-16.4	13	11.9	1.1-41.0	13	3.1	1.0-6.2	6	2.7	0.5-10.7	13	3.6	0.3-12.6	13	5.1	1.6-10.2	6	10.2	4.2-16.5	6	6.6	2.8-10.7	6
Acid Intrusives	4.5	0.1-30.0	489	25.7	0.1-253.1	493	3.4	0.1-7.6	493	2.9	0.1-19.6	489	7.9	0.03-77.7	493	5.6	0.2-12.5	493	16.4	2.7-98.3	489	10.5	1.7-58.7	489
Intermediate Extrusives	1.1	0.2-2.6	21	2.4	0.4-6.4	21	1.1	0.01-2.5	6	0.7	0.2-1.7	21	0.8	0.1-2.0	21	1.9	0.9-4.1	6	4.1	2.1-7.2	6	2.8	1.5-4.7	6
Intermediate Intrusives	3.2	0.1-23.4	271	12.2	0.4-106.0	273	2.1	0.1-6.2	273	2.1	0.05-15.3	271	3.7	0.1-32.5	273	3.5	0.2-10.2	273	9.4	0.3-41.2	271	6.2	0.2-27.6	271
Basic Extrusives	0.8	0.03-3.3	55	2.2	0.05-8.8	55	0.7	0.06-2.4	55	0.5	0.02-2.2	55	0.7	0.02-2.7	55	1.1	0.1-4.0	55	2.3	0.1-8.7	55	1.5	0.1-5.8	55
Basic Intrusives	0.8	0.01-5.7	119	2.3	0.03-15.0	110	0.8	0.01-2.67	129	0.5	0.01-3.7	119	0.7	0.01-4.6	110	1.3	0.1-10.3	12[illegible]	2.7	0.2-16.4	109	1.8	0.1-10.0	109
Ultrabasic	0.3	0-1.6	31	1.4	0-7.5	30	0.3	0-0.8	28	0.2	0-1.1	31	0.4	0-2.3	30	0.4	0-1.3	28	1.1	0.1-4.0	24	0.7	0.1-2.7	24
Alkali Feldspathoidal Intermediate Extrusives	29.7	1.9-62.0	138	133.9	9.5-265.0	139	6.5	2.0-9.0	36	19.4	1.2-40.1	138	41.1	2.9-81.4	139	10.7	3.4-14.9	36	71.5	16.8-117.1	35	48.4	11.1-80.7	35
Alkali Feldspathoidal Intermediate Intrusives	55.8	0.3-720.0	75	132.6	0.4-880.0	75	4.2	1.0-9.9	61	36.5	0.2-470.9	75	40.7	0.1-491.2	75	6.9	1.7-16.4	61	42.7	3.3-323.1	61	30.4	2.1-239.1	61
Alkali Feldspathoidal Basic Extrusives	2.4	0.5-12.0	20	8.2	2.1-60.0	20	1.9	0.2-6.9	20	1.5	0.3-7.9	20	2.5	0.6-18.4	20	3.2	0.3-11.4	20	7.2	2.8-36.7	20	4.8	2.0-23.9	20
Alkali Feldspathoidal Basic Intrusives	2.3	0.4-5.4	8	8.4	2.8-19.6	8	1.8	0.3-4.8	8	1.5	0.3-3.5	8	2.6	0.9-6.0	8	3.0	0.5-7.9	8	7.1	1.6-17.4	8	4.7	1.0-11.4	8
Chemical Sedimentary Rocks*	3.6	0.03-26.7	243	14.9	0.03-132.0	239	0.6	0.02-8.4	42	2.4	0.02-17.5	243	4.6	0.01-40.5	239	0.9	0.03-13.9	42	5.2	0.2-45.3	38	3.5	0.1-27.0	38
Carbonates	2.0	0.03-18.0	141	1.3	0-10.8	131	0.3	0.01-3.5	35	1.3	0.02-11.8	141	0.6	0-3.3	131	0.5	0.02-5.8	35	1.9	0.2-6.4	32	1.4	0.1-4.0	32
Detrital Sedimentary Rocks	4.8	0.1-80.0	412	12.4	0.2-362.0	411	1.5	0.01-9.7	298	3.1	0.05-52.3	412	3.8	0.1-111.1	411	2.5	0.02-16.1	298	8.9	0.4-146.6	298	6.2	0.2-95.1	298
Metamorphosed Igneous Rocks	4.0	0.1-148.5	128	14.8	0.1-104.2	128	2.5	0.1-6.1	128	2.6	0.1-97.1	128	4.6	0.02-32.0	128	4.2	0.2-10.0	128	11.3	0.8-124.6	128	7.5	0.6-108.7	128
Metamorphosed Sedimentary Rocks	3.0	0.1-53.4	207	12.0	0.1-91.4	208	2.1	0.01-5.3	208	2.0	0.05-34.9	207	3.7	0.2-28.1	208	3.4	0.02-8.7	208	9.1	0.4-50.5	207	6.0	0.2-42.3	207

* Includes carbonates

XBL 791-7832

(predominantly nepheline syenites) are highest in radioelement content, whereas basic to ultrabasic rocks (basalts, gabbro, periodotite) have exposure rates and heat production an order of magnitude lower.

Detrital sedimentary rocks (sandstone, shale, conglomerate) are relatively radioactive compared with chemical sedimentary rocks, especially the carbonates (limestone and dolomite). Within the metamorphic rocks, radioactivity depends primarily on the composition of their igneous or sedimentary predecessors, secondarily on the degree of metamorphism which the rocks have undergone.

PLANNED WORK IN FISCAL YEAR 1979

Additional data are being included as new results are published. Histograms and tabular summaries will be prepared and a final report written.

REFERENCE

Beck, H., and de Planque, G., 1968. The radiation field in air due to distributed gamma-ray sources in the ground. USAEC Health and Safety Lab. Rept. HASL-195.

THERMAL EFFECTS IN OVERLYING SEDIMENTARY ROCK FROM IN-SITU COMBUSTION OF A COAL SEAM

D. C. Mangold, H. A. Wollenberg, and C. F. Tsang

INTRODUCTION

The purpose of this investigation was to determine the times at which significant differences in temperature would occur, at varying depths in overlying sedimentary rock, in response to combustion of a coal seam. The results may be important for interpretation of airborne thermal infrared surveys, such as those flown by EG&G, Inc., over the U. S. Department of Energy's Hanna, Wyoming, in-situ coal gasification experimental facility. A more detailed description of the study is presented by Mangold et al. (1978).

The duration of the experimental "burns" (in excess of one-half year) associated with in-situ coal, oil-shale, or tar-sand combustion experiments raises the following questions. When might the surface temperature be affected due to the high temperatures at depth? Would surface-temperature effects be detectable by high-resolution aerial-survey equipment? The models in this preliminary investigation only considered thermal conduction as the heat-transfer mechanism. Heat transfer to the surface by convection within the overlying sedimentary rock or along fissures or cracks was not addressed.

NUMERICAL SIMULATION: MODEL AND RESULTS

The in-situ coal gasifcation was modeled by a thermal front, behind which the temperature was 1,200°C, progressing at the rate of 0.3 m/day along a horizontal coal seam 5 m thick at an average depth of 62.5 m.

The initial temperatures of the seam, rock, and surface were assumed to be 20°C, and the surface temperature was maintained at 20°C as a boundary condition for the calculations. The movement of the thermal front was simulated by assuming a flow through the seam of a fluid whose temperature is maintained at 1,200°C and whose density is the same as the seam itself. Heat transfer to the overlying rock was assumed to be by conduction only.

The numerical model CCC (Lippmann et al., 1977) was used to perform the calculations. Results were tabulated for the initial column of elements, whose nodal centers are all located 0.5 m horizontally from a line directly above the starting point of the coal-seam "burn." The heights of the nodal centers of the rock layers are 0.5, 2.5, 7, 22.5, and 47.5 m, respectively, above the top of the coal seam. The temperatures at the end of two-year intervals are shown in Figure 1. After eight years, the temperature in the layer, which is in contact with the surface would reach only 0.2°C above the initial temperature of 20°C and after 10 years, it would reach 20.4°C.

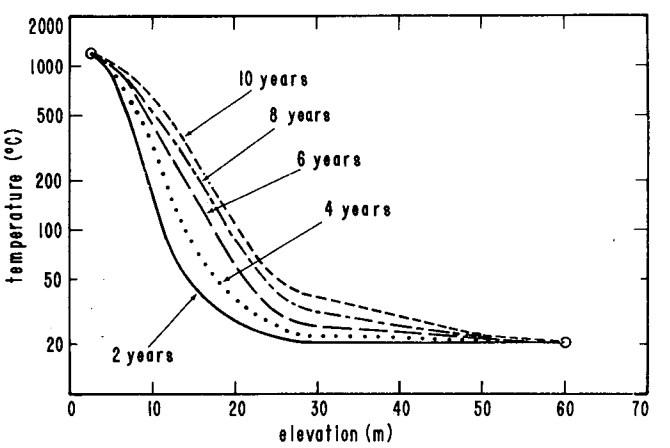

XBL 789-2056

Figure 1. Temperature distribution in overlying rock at various elevations above a progressively heated seam, obtained by numerical model CCC.

Therefore, in the model of a progressive front, if appreciable thermal effects were observed at the surface (60 m above the seam) less than eight years after combustion began, they would be due to leakage of heat along vents or cracks, or to convection within the overlying sedimentary rock.

Calculations were also made for the model with a closed boundary (no flow of heat) at the surface. The results were identical to the 20°C-boundary case in the 10-year period covered by both simulations.

ANALYTICAL MODELS AND RESULTS

To further check on the numerical calculations, an analytical model was used (Carslaw and Jaeger, 1959) assuming sudden, uniform heating of a rectangular slab of finite thickness, over an infinite length. Flow of heat is allowed at the upper boundary of the layered system. Under these conditions, of instantaneous uniform heating to 1,200°C and a boundary maintained at 20°C, the time of arrival of the 2°C thermal transient was calculated for various levels above the top of the seam. The results are presented in Figure 2. A further refinement incorporating a denser mesh in CCC yielded numerical results identical with those of the analytical calculations. (Discrepancies were on the order of 0.1% or less.)

In addition, another calculation was made using a model that assumes no flow of heat at the boundary and a variable overburden thickness (Carslaw and Jaeger, 1959, pp. 308-310). For a 60-m-thick slab, it takes approximately 5.5 years to achieve at 2°C temperature rise at 47.5 m above the seam, and approximately 8 years for a 2°C rise to reach the upper boundary (in contact with the surface). A similar model was used by Greene et al. (1969) to calculate thermal effects in strata overlying a coal-mine fire. They concluded that it may be two decades or more before the temperature increase at the surface could be observed for a 100°C temperature rise at 60 m below the surface.

CONCLUSION

This numerical and analytical investigation has shown that, even under the most favorable circumstances, it would be 5 to 8 years before an appreciable rise in temperature (i.e.,~2°C) would occur 60 m above a burning coal seam from effects due to conduction alone. If such a rise is detected earlier, it indicates that heat is being transferred along cracks and joints, and/or by convection in the overlying rock.

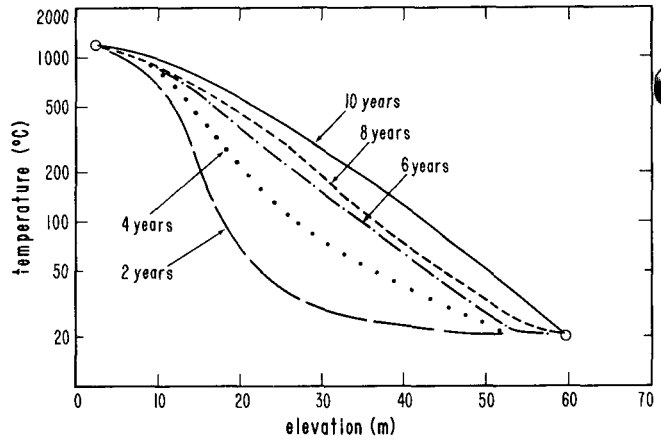

XBL 788-2052

Figure 2. Temperature distriburion in overlying rock at various elevations above a uniformly heated seam, obtained from analytical calculations.

PLANNED ACTIVITIES FOR FISCAL YEAR 1979

On the basis of these results, a further investigation is planned, to examine heat transfer by convection as well as by conduction. Further research may also be performed to study the effects of fissures and cracks in heat transfer in the overlying sedimentary rock.

REFERENCES

Carslaw, H. S., and Jaeger, H. S., 1959. Conduction of heat in solids, Oxford, Oxford University Press, 2nd ed.

Greene, G. W., Moxham, R. M., and Harvey, H. H., 1970. Aerial infrared surveys and borehole temperature measurements of coal mine fires in Pennsylvania, in Proc. Sixth Internat. Symp. on Remote Sensing of the Environment, Willow Run Laboratories, University of Michigan.

Lippmann, M. J., Tsang, C. F., and Witherspoon, P. A., 1977. Analysis of the response of geothermal reservoirs under injection and production procedures. Dallas, Soc. Pet. Eng. AIME, SPE-6537.

Mangold, D., Wollenberg, H., and Tsang, C. F., 1978. Thermal effects in overlying sedimentary rock from in-situ combustion of a coal seam. Berkeley, Lawrence Berkeley Laboratory, LBL-8172.

FOUR-CHANNEL SIMULTANEOUS COLLECTION SYSTEM FOR HIGH-PRECISION MASS SPECTROMETRY

M. C. Michel, D. F. Mosier, and W. R. Keyes

INTRODUCTION

Two years ago, we began a project to adapt our 5-ft-radius isotope separator to very high precision measurements of isotope ratios of interest to geochronology (for example, Sr and Nd). We felt that conventional techniques, involving sequential measurement of isotope beams, had been developed as much as possible and that exploiting the apparent advantages of collecting isotope beams simultaneously was a possible way of extending the precision. For practical reasons, this requires a relatively large-radius mass spectrometer.

Interest in higher precision has also developed among researchers in geochronological techniques as more sophisticated measurements are made with familiar systems such as Rb-Sr, and as the utility of new systems such as Sm-Nd becomes apparent (Carter et al., 1978).

A previous report (Michel, 1978) describes most of the preliminary work leading up to the first testing of the complete system during this year. As is often the case, the initial performance is somewhat below expectations, but it shows every evidence of responding to attempts at improvement. The present performance is quite similar to some of the best work by conventional techniques.

ACTIVITIES IN FISCAL YEAR 1978

The primary accomplishment of this year's work has been the actual construction, debugging, and use of the four-channel data readout system shown in Figure 1. (At present only three of the channels are in use, corresponding to the strontium isotopes of mass 86, 87, and 88.)

To summarize briefly, the ion beams corresponding to the three strontium isotopes above are incident on their respective Faraday cups, the collected current is amplified to a voltage proportional to the input current, periodically stored in corresponding channels of the sample and hold circuit, and then sequentially digitized by a single digitizing device.

Assuming that the Faraday cup currents are truly a measure of relative isotope abundances, we need only guarantee that the three amplifiers have the same (but not necessarily known) gain and are linear to the desired precision, in order to supply data to the sample and hold circuit (which is capable of giving the desired precision). If the sample and hold circuit does not introduce further discrimination, and if the digitizing device has the appropriate precision, the entire system should function as desired.

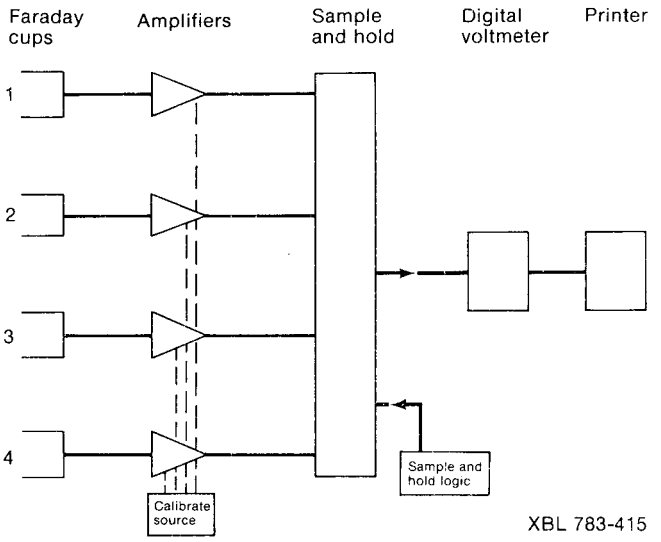

Figure 1. Block diagram of four-channel data system.

Calibration of the amplifier gains, made before each measurement, indicates stability of a few ppm for several days or longer, allowing one calibration per day to be sufficient. The limitation on calibration repeatability is the stability of the amplifier zero offset and averages about ±4 μV, almost independent of the calibration signal level. Table 1 shows the variation in the calibration of the three-amplifier system over a three-month period. As

Table 1. NBS strontium isotopic standard run on four different days.

Day	$^{87}Sr/^{86}Sr$*	
1	$0.71013_3 \pm 0.00003$	(2σ)
2	$0.71011_3 \pm 0.00003$	(2σ)
3	$0.71016_9 \pm 0.00003$	(2σ)
4	$0.71012_4 \pm 0.00003$	(2σ)
Average	$0.71013_5 \pm 0.0002_4$	(2σ)

Certified value = 0.71014

*Corrected for fractionation.

shown in the table, the calibration will not limit the precision except to levels of one part in 10^5 or less, and the use of higher calibration signals can improve this by at least a factor of three.

This three-amplifier system has been used to measure the National Bureau of Standards strontium isotopic standard to evaluate the system. Generally the results are satisfactory but much work can still be done to improve the results. The primary problems encountered during this work are discussed below.

Ion Source

As was generally recognized, thermal ion sources tend to emit ions nonuniformly, and bursts of ions of a few microseconds are common. This is one reason simultaneous collection looks so attractive. However, although the D.C. response of the amplifiers can be made identical, there is no guarantee that they can be matched in gain at all frequencies simultaneously, so that different transient responses may and in fact do occur. Much effort has gone into minimizing this effect electronically. We have been moderately successful, but only the performance with standard samples can prove the ultimate success of this work. The use of a silica gel matrix (see below) has also helped moderate this problem.

Ground Currents and Thermally Generated Voltages

As in any system where signal levels of μV are significant, careful attention must be paid to eliminating these effects, mostly by painstaking trial-and-error procedures. The last remaining problem of unknown size is a possible few-μV effect on the amplifier zero offset, produced by the permanent in-vacuum wiring in the mass spectrometer vacuum probe, on which the simultaneous collector is mounted. Redesign of this part of the instrument could easily eliminate this problem, but would be moderately expensive and may not be necessary.

Ion-Source Isotopic Fractionation

A persistent problem has been the extreme range of isotopic fractionation exhibited by our ion source over the useful life of a sample. The internal-discrimination correction, applied to all data based on the $^{86}Sr/^{88}Sr$ ratio, will remove this and all other errors linear in mass. However, we have serious doubts about the precision of data that have had a 1% to 3% correction of this type.

Ionization of strontium and several other elements from a silica-gel matrix tends to reduce the time variability of the ion beam. In trying this technique sharply decreased to reduce the effect of transients on amplifier response, we discovered that the technique sharply decreased the range of fractionation observed during a sample lifetime. There are plausible explanations for such behavior, but we do not really understand it in detail. Of course it is exciting to contemplate the reduction of fractionation to very low levels and the ability to make high-precision measurements on systems without an internal standard ratio.

Along with the reduction in fractionation, we observed a distinct improvement in the precision of the corrected isotopic ratios, indicating that as previously reported (Bentley et al., 1959) the fractionation may not be exactly linear in mass, and therefore not properly corrected by our linear internal standardization, unless the correction is kept quite small.

Beam Focusing and Positioning

Although our ion beams are very much narrower than the rectangular masks in front of the Faraday cups, we found a slight variation of isotope ratio with exact placement of the beam within the Faraday cup masks. This undoubtedly results from the long "tails" on the ion beams being intercepted partially and in different degrees for each isotope because of unavoidable mechanical dissimilarities of the masks. We anticipated this problem and found that a movable slit, much smaller than the mask (transmitting only 75% to 90% of the ion beam), allows quite reproducible focusing and positioning of the beam. In this way, only absolute differences in beam transmission (affecting absolute ratios but not precision) would be left. As might be expected, the effect of "tailing" is dependent on the effective ion-optical source in the mass spectrometer. For our system, this is the ion-source exit-hole diameter, nominally about 0.75 mm. Decreasing the size of this hole does improve the performance of the system, but since the sample has to be introduced to the ion source through this hole, there is a practical limit to reducing the hole size much further.

CONCLUSIONS

As an example of the present precision of the system, Table 2 shows the analysis of the NBS strontium standard over the life of a single loading, measured on four different days. Each day's average is the result of many individual determinations of the isotopic ratios corrected for linear discrimination effects as discussed above. It is clear that the precision within a day's run is quite reproducible at about four parts in 10^5, but that differences of this order do occur from day to day. This run was somewhat atypical in that no trend is visible with time--the usual effect being a slight decrease of ratio with time. This may be the result of nonlinear fractionation or some other unknown effect.

With real samples, a certain amount of rubidium impurity is often present, leading to erroneously high $^{87}Sr/^{86}Sr$ ratios early in the life of the sample. In principle, the fourth amplifier, reading the ^{85}Rb ion beam could be used to correct these data. However,

Table 2. Calibration with D.C. voltage standard of all three amplifiers in data readout system. Ratios of outputs of amplifiers 1 and 2 to amplifier 3 for identical input currents.

Day	Amp. 1/Amp. 3	Amp. 2/Amp. 3
1	0.999995	1.000011
2	0.999977	0.999998
3	0.999980	1.000003
4	0.999975	0.999976
5	0.999975	1.000011
6	0.999996	1.000020
7	0.999984	0.999974
8	1.000018	1.000054
9	1.000050	1.000009
10	1.000007	0.999991
11	1.000018	1.000028
12	1.000030	1.000008
13	1.000022	1.000027
Avg.	1.000002 ± 0.000013	1.000008 ± 0.000012

Note: all errors are 2σ.

because the ions result partly from diffusion from solid materials and are even more prone to sharp bursts, this is not very effective. In addition, the correct isotope ratio to be used for rubidium is unknown to at least 1% or 2%. This restricts the correction to very small amounts of rubidium indeed, and makes the rubidium content critical in determining the precision with which the ratios can be measured.

PLANNED WORK IN FISCAL YEAR 1979

The primary activity in fiscal year 1979 will be to determine the reliability and precision of the system with both standards and real samples. We will pay particular attention to eliminating the effects of rubidium contamination, beam tailing, and fractionation on the precision of the data. Work on further decreasing the total fractionation during a sample life will also receive emphasis, especially the use of dispersing agents other than silica gel to reduce fractionation and smooth the ion output.

We are confident that significant improvements in precision will result from increased experience with the system, as is the case with many new techniques.

REFERENCES CITED

Bentley, P. G., Bishop, J., Davidson, D. F., and Evans, P. B. F., 1959. Isotopic analysis of lithium by mass spectrometry. Jour. Sci. Inst., v. 36, pp. 32-34.

Carter, S. R., Evensen, N. M., Hamilton, P. J., and O'Nions, R. K., 1978. Neodymium strontium isotope evidence for crystal contamination of continental volcanics. Science, v. 202, pp. 743-747.

Michel, M. C., 1978. High-precision mass spectrometry, in Earth Sciences Division annual report 1977. Berkeley, Lawrence Berkeley Laboratory, LBL-7028, pp. 34-36.

DETERMINATION OF THE PROPERTIES OF SOILS BY IN-SITU MEASUREMENTS

W. C. B. Villet and J. K. Mitchell

INTRODUCTION

Accurate identification and characterization of subsurface conditions are essential for successful geotechnical design and construction. Reliable information on geologic conditions in general, and specific geotechnical parameters in particular, is required for the design of foundations on and in the ground, for the design of safe slopes, and for the analysis of problems related to the use of underground space. These problems include storage and extraction of energy, as well as groundwater pollution that may be caused by either injection or removal of fluids.

Site investigation to determine the required geotechnical parameters in a completely unknown area consists of a number of steps. The first step is developing a rough geologic model by mapping local geologic surface features as well as interpreting geologic maps (when available) and perhaps aerial photographs. Depending on the magnitude of the proposed project, it may be economically feasible to improve this initial model by preliminary drilling and/or indirect measurements such as seismic-refraction surveying. A detailed investigation program can then be planned, including the number, type, size, location, and approximate depth of boreholes, the kinds and location of samples, and the types and locations of tests. It is always imperative that such a final program remain flexible enough to be tailored to unexpected geologic conditions. Economic constraints normally limit the detail with which such investigations may be carried out.

Geotechical investigation of soils is complicated by the fact that sand and clay properties have traditionally been evaluated in rather different ways: sands, by means of the so-called standard penetration test, and clays by laboratory testing of "undisturbed" samples.

There exist severe limitations in both approaches. Standard penetration test results are very dependent on the exact equipment and testing procedures (which are not really "standard"). For clays, limitations are imposed by sample disturbance, changes in sample properties due to unloading and exposure, and the difficulties associated with retaining (or reestablishing) in the laboratory, the in-situ state of stress, temperature, and chemical and biological environments. Furthermore, if a soil layer of either type is drilled through, an additional borehole may be needed if tests are required in that layer. The above limitations have become particularly evident as the volume of offshore and underground construction has increased. The need for reliable techniques for the in-situ determination of the engineering properties of soils has, therefore, emerged as one of the most important geotechnical problems of the present time.

This research project, initiated in spring 1976, is concerned with the identification, development, and implementation of new and promising approaches for in-situ measurement of soil properties. A closely related objective has been the evaluation of presently available techniques.

ACCOMPLISHMENTS IN FISCAL YEAR 1978

Emphasis in the research project to date has been on evaluating existing techniques, and developing a new testing approach based on the analysis of acoustic emissions generated during the penetration of a soil layer by a rigid object.

Planned activities for 1978 were: (a) to publish a state-of-the-art report on in-situ measurement of soil properties by means of direct tests; (b) to study and evaluate the suitability and potential of remote sensing and geophysical techniques to provide data from which quantitative assessments of the mechanical properties of soils may be made; and (c) to study acoustical measurements during quasi-static cone penetration tests as a basis for determining soil types and properties. This latter study was separated from the LBL activity on March 1, 1978, when a substantial grant was received from the National Science Foundation for intensive research on the subject.

During fiscal year 1978, Mitchell et al. (1978) published a report entitled "The Measurement of Soil Properties In-Situ." This report presents: (a) a description of existing in-situ testing techniques and equipment; (b) their associated evaluation theories and correlations for obtaining geotechnical parameters; (c) an assessment of the current suitability of each method for determining specific geotechnical parameters; and (d) their potential for future development. The report is concerned with the following testing techniques:

1. Permeability tests by pump-in or -out methods, and by piezometer methods, employing both steady-state and transient techniques
2. The standard penetration test
3. Cone penetration tests of various kinds
4. The vane shear test
5. The Iowa borehole shear test
6. The pressure meter test
7. Plate bearing tests
8. Screw plate tests
9. Hydraulic fracturing tests
10. Down-hole and cross-hole seismic tests

The suitability of each test type is discussed in chapters dealing with permeability, shear strength, in-situ state of stress, and deformation constants. Extensive references are listed. The report should serve as a definitive starting point for anyone interested in the subject.

Several less direct techniques for determining soil properties and characterizing sites are still being studied. These predominantly involve geophysical techniques, and include: seismic methods, including refraction, reflection, down-hole and cross-hole surveys; resistivity surveys, including focused probes; gravimetric, magnetic, nuclear, radar, electromagnetic, spontaneous potential, and thermometric methods; and remote-sensing techniques such as GEOSAT.

As a result of these studies, a report is being prepared that will present the theory of each technique briefly, describe testing methods and evaluation theory, assess the current suitability of each technique for determining geotechnical properties quantitatively, and assess their potential for future development. This report will serve as a guide to what is currently available and feasible, and should be a stimulus for future research.

The research project progressed much as planned for fiscal year 1978, except that the report dealing with remote-measuring techniques has not yet been completed. This delay is the result of the immense wealth of information that must be reviewed and evaluated. The report should, however, be completed in the coming year.

PLANNED ACTIVITIES FOR FISCAL YEAR 1979

Additional support for this project will not be available for fiscal year 1979.

REFERENCE

Mitchell, J. K., Guzikowski, F. J., and Villet, W. C. B., 1978. The measurement of soil properties in-situ, present methods - their applicability and potential. Berkeley, Lawrence Berkeley Laboratory, LBL-6363.

STATISTICAL ANALYSIS OF THE CORRELATION OF EARTHQUAKES WITH RADON CONCENTRATION IN WATER FROM SHALLOW WELLS NEAR OROVILLE, CALIFORNIA

B. Berlin

INTRODUCTION

This report is an account of work performed from June 20 to September 25, 1978, funded by Lawrence Berkeley Laboratory Director's Development funds. This work is part of an investigation to determine whether a statistical relationship exists between varying radon concentration in well waters and the occurrence of nearby earthquakes. If such a dependence is verified, then certain patterns of changing radon activity may be useful for predicting earthquakes.

Radon concentration in two water wells near Oroville, California, the Prosise and the Gilley wells, were compared with periodic aftershocks of the August 1, 1975, Oroville earthquake for a period of about 600 days. The data are consistent with data being generated from a distribution of: (a) all noise, or; (b) long-term seismic fluctuations correlated with changes in the Prosise well, or short-term seismic fluctuations with changes in the Gilley well, or both. In both cases, the dependence must be expressed with different equations in different directions from the wells. Also the data are inconsistent with data being generated from a distribution where the dependence between seismic activity and radon activity is very strong in all directions.

DATA COLLECTION

The collection of radon data started a few days after the August 1, 1975, Oroville (California) earthquake of magnitude 6 on the Richter scale, and so coincides with the series of aftershocks. Sampling consisted of filling a pair of 500-ml-capacity polyethylene bottles at the wellhead, sealing them immediately against gas loss, transporting them to LBL within a few days of collection time, and making direct measurement of the radon content of the water by low-level gamma-ray spectrometry at the LBL Low Background Counting Facility.

One sample per day was collected from each of six wells in the region of aftershock occurrence, including wells drilled into poorly consolidated sediments and into bedrock formations. The location of these wells is given in Figure 1. Subsequent experience showed that only bedrock wells showed a significant radon variation. Sampling at other wells was then curtailed, and our efforts were concentrated on acquiring detailed data from three bedrock wells. The shallowest of these (the Norman well, 65-ft deep) is believed to have suffered occasional invasion of irrigation water applied to nearby pasture land. Data from this well are therefore of questionable value. Data from the two remaining bedrock wells (the Gilley and Prosise wells, each about 200-ft deep and dedicated to domestic use only) cover the time from August 12, 1975, to April 6, 1977--a stretch of 604 days. For each of these wells, there are fewer than 10 days of missing observations. Values were simulated for the missing days by linear or cubic interpolation from neighboring values. Typical data obtained from the Gilley and Prosise wells are illustrated in Figure 2.

The seismic data include earthquake time (to the second), epicenter coordinates, depth, and Richter magnitude. This information was obtained from lists compiled by the California State Department of Water Resources (SWR), Sacramento, California, and the United States Geological Survey National Center for Earthquake Research (USGS), Menlo Park, California.

STATISTICAL ANALYSIS

The objective is to measure the extent to which variations in the earthquake process (time, magnitude, distance from wells) are correlated with changes in radon activity. The technique used is described in detail by Brillinger (1975). A more elementary introduction to this topic is given by Kendall (1973).

NOTATION AND MODEL

Time is discretized in days. That is, both radon sampling times and earthquake event times are truncated to the nearest day. The days are numbered: $t = 1, 2, 3, \ldots, N = 600$. The number of days studied, 600, was chosen because computations involved in the analysis are much less time-consuming when N can be factored in many small primes ($600 = 2^3.3.5^2$).

Earthquake data are thought of as the dependent variable where: $Y_1(t) = 1$ if an earthquake occurs on day t, and where $Y_1(t) = 0$, if not. It would have been very desirable to deal simultaneously with the epicenter-well distance, thus: $Y_2(t) =$ 1/distance, if the earthquake occurs on day t,

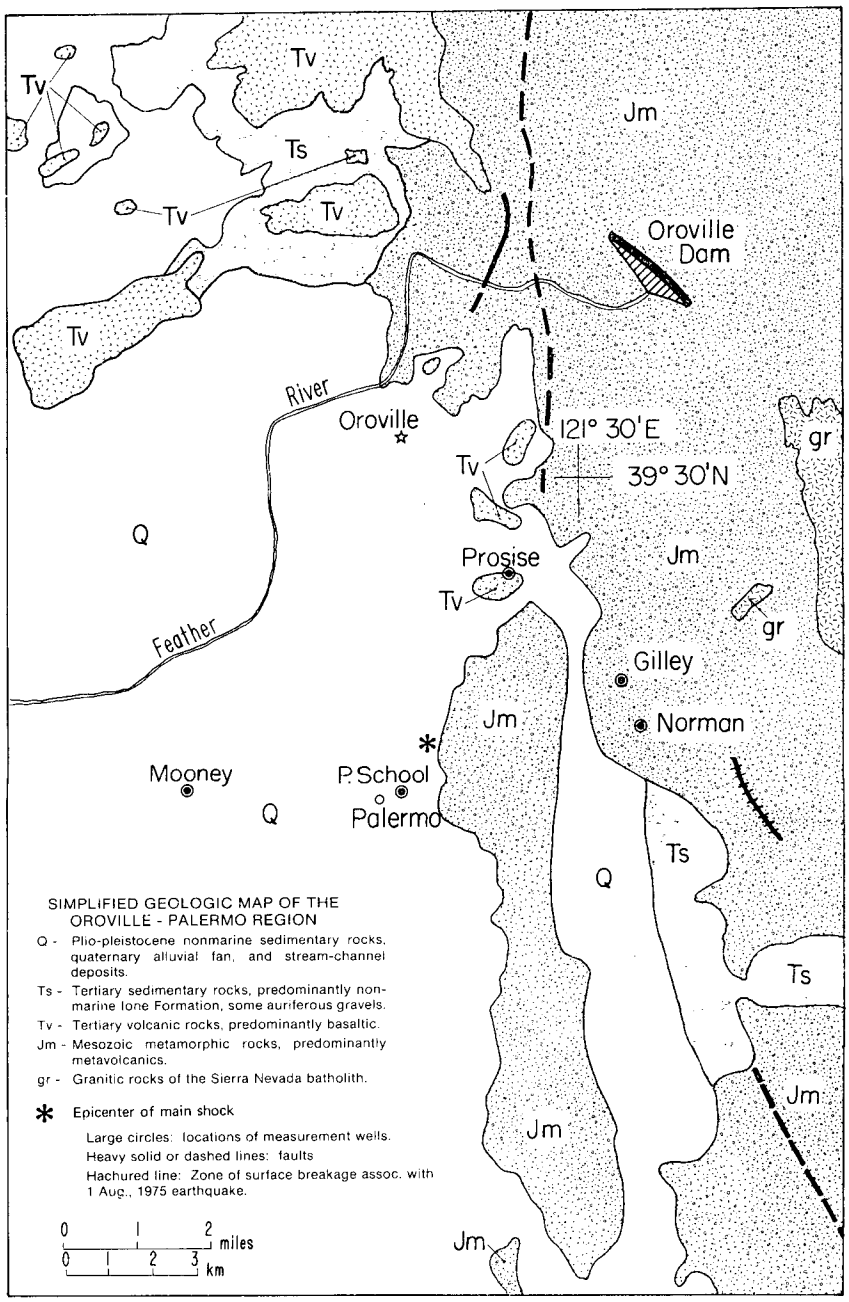

XBL 775-956

Figure 1. Simplified map of the Oroville, California, area, showing surface geology and the locations of sampled wells in relation to the August 1, 1975, earthquake.

and $Y_2(t) = 0$, if not. However, a problem arises here because $Y_2 = 0$ usually means that there was no earthquake. In the assumed model, $Y_2 = 0$ is confused with having a very distant earthquake; therefore, Y_2 is not used.

The appropriate model for simultaneous analysis of occurrence, location, and magnitude is a marked-point process in which the distribution of the location and magnitude is defined only when an earthquake occurs.

Well data are the independent variable where:

$X_1(t)$ = radon activity in Prosise on day t;

$X_2(t)$ = radon activity in Gilley on day t;

Many subsets of earthquakes have been fitted to models of the following type:

$Y(t) = Y_1(t)$, and $\underline{X}(t) = [X_1(t), X_2(t)]$.

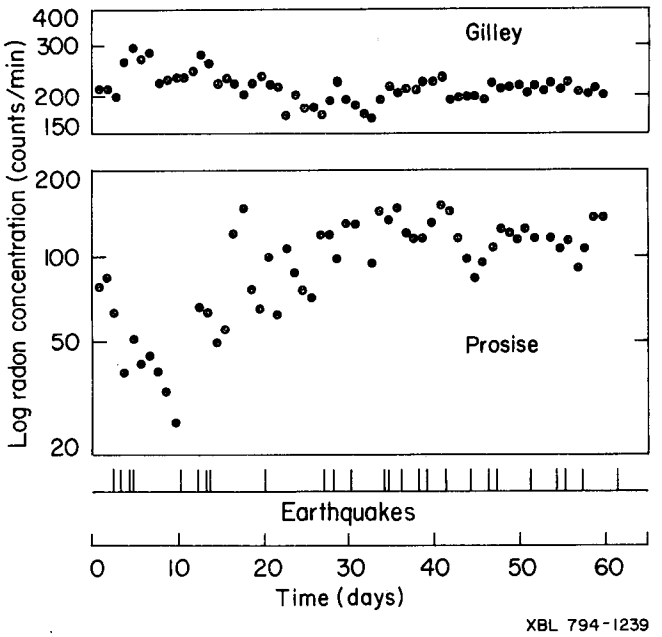

Figure 2. Typical data from the Gilley and Prosise wells for the period October to November 1975, showing daily radon activity and the occurrence times for all earthquakes with magnitudes greater than ~2 on the Richter scale.

These are assumed to be stationary time series. Therefore, we can conclude the following.

The expected values of Y(t) and $\underline{X}(t)$ remain constant in time, so that fluctuations are observed to occur about a fixed mean level. This is, strictly speaking, false. Both the seismic activity and the radon measurements in the two wells show trends. Linear components of all trends have been removed as a first step to treat the data. Although the rate of seismic events decreases, as during the time interval studied, radon activity in the Prosise well shows a positive trend and for the Gilley well it is negative. The change in average radon level is considerable. The Prosise radon level is 40% higher toward the end of the 600-day period compared with the beginning; for the Gilley well the decrease is also 40% over the same time period. The removal of such a trend is a concession that only changes can be analyzed, for which several cycles are observed in the 600 days available.

Any dependence within and between processes relates only to the length of time between the two points considered, rather than to their absolute location on the time scale. Thus, February and April of 1976 are assumed to be as strongly related as September and November of 1977 (two months apart in both cases).

These assumptions are expressed in terms of the covariances:

$$\mathrm{Cov}[X_i(t), X_j(t+u)] = c_{X_i,X_j}(u) \quad \text{for all } t,\ i,\ j = 1,\ 2$$

$$\mathrm{Cov}[Y(t), Y(t+u)] = C_{YY}(u) \quad \text{for all } t,\ i,\ j = 1,\ 2 \ .$$

$$\mathrm{Cov}[Y(t), X_j(t+u)] = c_{X_jY}(u) \quad \text{for all } t,\ i,\ j = 1,\ 2 \ .$$

The model commonly used to relate Y and $\underline{X}$ is linear:

$$Y(t) = \mu + \sum_{\mu=-\infty}^{+\infty} \underline{a}(u)\ \underline{X}(t-u) + \varepsilon(t) \quad , \quad (1)$$

meaning that the probability of an earthquake on day t, given a particular pattern of $\underline{X}$ around t, is:

$$\mu + \sum_{\mu=-\infty}^{+\infty} \underline{a}(u)\ \underline{X}(t-u) \quad .$$

Here, μ is the long-term probability of an earthquake, and $\underline{a}(u)$ is a function of the time lag u. For each u = 0, ±1, ±2, . . . , a(u) is a vector with two elements of unknown constants and $\varepsilon(t)$ is the error series, which also is stationary. If the variations in Y are well accounted for by equation (1) for some values of μ and $\underline{a}(u)$, then the variation in $\varepsilon(t)$ will be considerably less than in Y(t). Note that when u is allowed to assume values smaller than zero, the future of $\underline{X}$ (beyond t) is involved, so a good fit for equation (1) does not necessarily imply that a prediction based on past $\underline{X}$ only will be successful.

Equation (1) is reminiscent of multiple linear regression, but here observations are correlated even when they are made at different times. This complicates the analysis quite a bit; statisticians prefer to work with Fourier transforms of the series and their covariance functions because it is much easier to derive criteria to check if any patterns in the data are statistically significant, that is, if they are unlikely to have arisen only from random noise. In the covariance functions given above, dependence is described for observations u days apart. The Fourier transforms of these functions tell the same message, but the argument is a frequency λ, rather than the time lag u. In Fourier analysis, the time series is decomposed in a linear combination of many trigonometric functions (sines and cosines) of varying amplitudes. The different components have frequencies varying between 0 and π, where the highest frequency corresponds to u = 1, or cycles of 1 day. Here u and λ correspond to the same wave and are inversely proportional.

DISCUSSION OF RESULTS

Spectra for radon data alone reveal two things. First, the long-term variations (periods greater than 15 days) have much larger amplitude than components with periods of a few days. This phenomenon appears despite the fact that a linear trend has been removed. Second,

the correlation between the two wells is negligible. This suggests that any effect that increased stress has on radon activity is very local. The wells are 3.7 km apart.

It is more difficult to find a consistent pattern in the earthquake spectra. Whereas each attempt to fit the data involves the complete set of well observations, the set of selected earthquakes changes. This is done by including all earthquakes within some distance of the well considered.

Also, only earthquakes with a magnitude greater than 1.5 are included. For some selections, there is a tendency for the events to occur in cycles; in other cases the estimated dependence is weak, more like a Poisson process. This is a matter to which little attention has been given during this search for a relation between earthquakes and radon data. It is worth further investigation.

Finally, we considered the dependence between seismic events and radon activity. The extent to which the data fit the model (equation 1) is measured by the coherence $R^2_{YX}(\lambda)$, a generalization of the usual correlation coefficient used in simple linear regression. For a particular λ, it measures the dependence of the trigonometric wave in earthquake occurrence (frequency) on the linear expression of radon data, as in equation (1).

Looking first at the vicinity of the Prosise well, all earthquakes were picked within radii of 2, 3, and 4 km. In each case, the estimated coherence was low enough to be consistent with no dependence at all. Thereafter, semicircles and quadrants were tried with 3-km radii, or a total of eight different tests. In two cases the coherence assumed significant values. These are presented in Figure 3.

Geographical region for earthquake selection	max $R^2_{XY}(\lambda)$	Approximate period with largest coherence; days
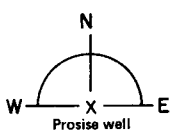	0.18	100
S 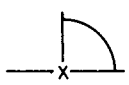	0.17	20

XBL 794 - 1240

Figure 3. Geographical selections of seismic events within a 3-km radius of the Prosise well showing the correlation between seismicity and radon activity.

Of course, the criteria for a significance are calculated for one particular run. Where many statistical tests are tried, the significance statements lose their power for drawing conclusions. Rather, attention is drawn here to the subsets of earthquakes with the highest correlation, without stating that it will hold up in the long run.

Likewise for the Gilley well, the earthquakes within circles show faint dependence with the radon data. The same is true for semicircles.

Quadrants look better, as shown in Figure 4. Note that $R^2_{xy}(\lambda) = 0.16$ is the 5% rejection limit. Why do all four quadrants show some dependence, but none of the semicircles? The reason is that the best fitting constants [$\underline{a}(u)$ in equation (1)] are quite different for the four quadrants, and compromise values necessary for semicircles fail to explain the variation in seismic activity.

Figure 5 is a plot of $\underline{a}(u)$ vs. u for the four quadrant zones around the Gilley well that showed some promise with respect to coherence. The horizontal u-axis has been reversed, putting negative u's to the right. The advantage is that the positive u's (corresponding to preceding days) will be to the left of the origin. The plots of $\underline{a}(u)$ all show strong oscillations from high to low values. What does this mean? A first idea would be to reconstruct what pattern of radon changes makes the right-hand

Geographical region for earthquake selection	max $R^2_{XY}(\lambda)$	Approximate period with largest coherence; days
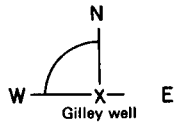	0.23	1 1/4
S 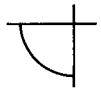	0.27	1 1/4
	0.33	1 2/3 to 2
	0.27	1 1/2

XBL 794 - 1241

Figure 4. Geographical selections of seismic events within a 3-km radius of the Gilley well showing the correlation between seismicity and radon activity.

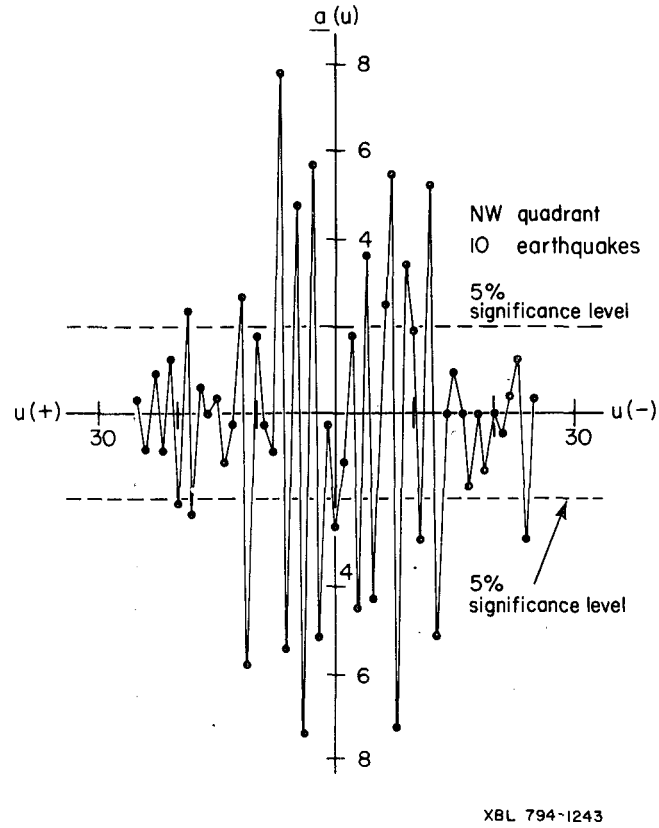

Figure 5. Profile of values for the constant a(u) in equation (1), computed for the 3-km-radius quadrant northwest of the Gilley well. Previous days are plotted to the left of the origin; future days, to the right. The ordinate scale is in terms of the estimated standard deviation on a(u) values.

side of equation (1) large for the given estimated a(u). That is, what makes the chance for an earthquake large? Also, what pattern makes the chance small?

Obviously, a day with a large positive a(u) calls for a positive radon count to contribute to a large probability. If a(u) has a large negative value, the radon count should be unusually small. Therefore, a strongly oscillating radon pattern would serve as a precursor. Further, an oscillating pattern out of phase with the former type would be an "antiprecursor" and make the chance small.

However, this idea is a dead end because the radon record simply does not have any such rapid oscillations. As mentioned earlier, the variation in radon activity is dominated by slow oscillations.

A more believable interpretation of the rapid fluctuations of a(u) is that the predictive effect of radon changes is very short term, about 1 to 2 days.

From the point of view of earthquake prediction, the long-term variations with large amplitude are noise that must be filtered away by the coefficients a(u). This is actually achieved with high and low a(u) following each other.

An object for further investigation is to study the quickly varying radon signal that remains after filtering, which actually serves as a precursor.

The combined predictive ability for the two wells was also tried by selecting earthquakes within ellipses that had the wells as foci, as illustrated in Figure 6(a).

As expected from the weak dependence of the two radon series, it turned out that for these subsets, the Prosise well had negligible dependence with the earthquakes, while the largest coherence observed so far occurred between the

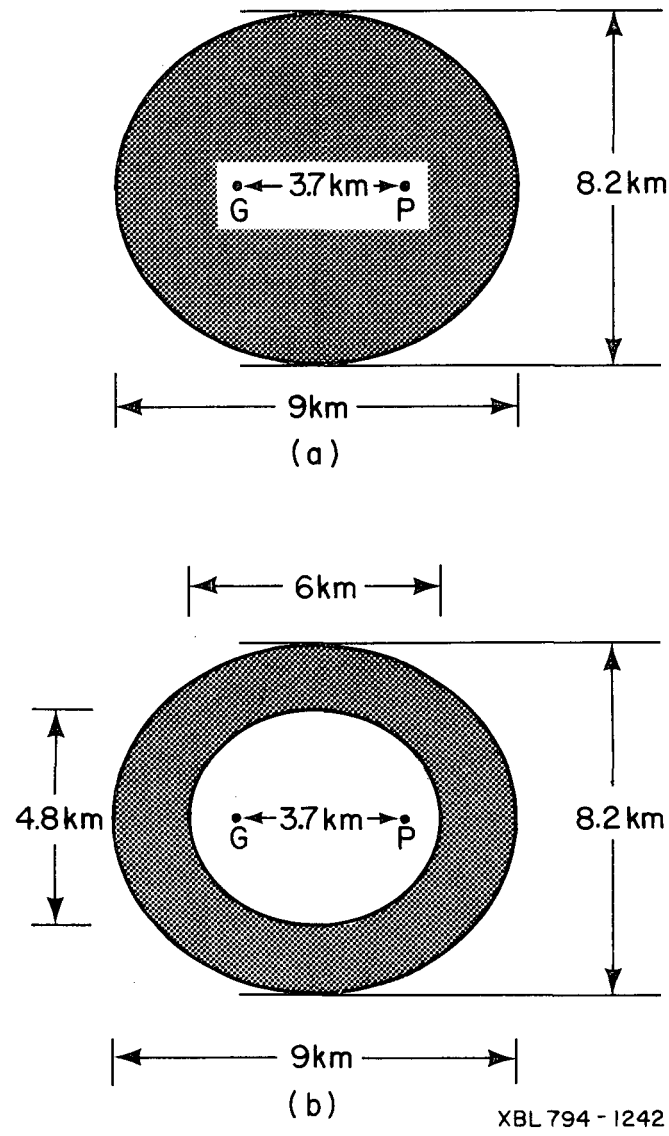

Figure 6. Configurations to test the combined predictive ability for Prosise and Gilley wells (shaded areas indicate regions in which earthquakes occurred).

Gilley well and the earthquakes. Ellipses of different sizes were tried and the fit improves further if an inner ellipse is excluded, as shown in Figure 6(b).

Further work should be done to identify a more reasonable looking zone where the Gilley well is sensitive. The substantial coherence appeared at a frequency corresponding to a period of 2-1/2 days.

RECOMMENDATIONS

To put the above inconclusive findings to a test, we recommend the following.

More data are needed, particularly from the Gilley well, which appears most promising. In the present data, the radon samples are not exactly 24 hours apart; they were taken at different times in the afternoon. To check the one- to four-day fluctuations, it would be useful to have radon activity recorded at exact 12-hr intervals.

With the statistical methods used here (continuous time series) there is no satisfactory way to take epicenter-to-well distance and magnitude into account simultaneously, as pointed out earlier with regard to the variable Y_2. A statistical method relating a marked-point process to a continuous time series should be developed.

It is useful to test the radon data against a model in which two types of earthquake precursors are postulated:

1. Signals whose appearance in prior-time are related to the magnitude of an impending earthquake--signals that may encompass the time domain of days to years

2. Signals whose appearance in prior-time are unrelated to the magnitude of an impending earthquake--signals that may encompass the time domain of hours to a few days (foreshocks)

The statistical method employed here should be well suited for identifying precursors of the second kind--those that occur at a (relatively) fixed time before an earthquake. However, in its present form, the method is not well suited for identifying precursors of the first kind--those that may occur over a few days to a few 10s of days for the aftershock magnitudes encountered during the Oroville study. Hence, adapting the present method or adopting some other approach, is important in order to include time/magnitude/distance parameters for individual earthquakes in the analysis procedure.

REFERENCES CITED

Brillinger, D. R., 1975. Time series, data analysis, and theory. New York, Holt, Rinehart and Winston.

Kendall, M. G., 1973. Time series. New York, Griffin.

UNDERGROUND NUCLEAR WASTE MANAGEMENT

Crystalline and argillaceous rocks are now being evaluated, both in the United States and elsewhere, as potential repository host rocks for nuclear waste. Properties such as mechanical response to thermal loading, fluid flow through fractures, and chemical sorptivity have not been systematically investigated for fractured rocks, yet they and their interactions must be understood or their magnitude ascertained before confidence can be given to predictions about disposing of wastes in repositories in fractured media. Thus fundamental investigations on most aspects of fractured media have been expanded in the Division and have assumed even greater practical importance. Activities reported in this section have been supported by the U.S. Department of Energy's Waste Isolation Management Program.

The Swedish-American cooperative program, begun in July 1977, is a first-of-its-kind experiment for fractured rocks. The fundamental questions about how to characterize materials and properties and how to measure them are being approached both experimentally and theoretically. Preliminary results from some experiments in the Stripa mine have already been obtained, and the correspondences and differences with predictions promise to lead to better predictions and to shape the next generation of experiments, which will improve our understanding of the physical and chemical phenomena that will control waste migration.

LBL is participating in several tasks in a planned waste isolation experiment at the Hanford Reservation in eastern Washington state. Building on experience at Stripa, LBL aided in designing the heater experiments planned for Hanford's near-surface test facility. A study of the hydrology of the region around the reservation was initiated, and field, laboratory, and modeling studies were performed. Also in conjunction with the planned Hanford experiment is an LBL examination of the minerals that line fractures in Pasco Basin basalts; and building on these data, make models of mass transport in the fractures to predict the fate of radionuclides released into this system. LBL also actively participates in the Waste Isolation Safety Assessment Program by obtaining the fundamental sorption and transport data and developing and testing transport models that use these data.

Because of the great important of the geochemistry, hydrology, and mechancial properties of fractured rock systems, LBL hosted a symposium in July 1978 to assess the state-of-the-art and to define needed research and instrumentation development. Simultaneously, LBL was asked by DOE to assess, as part of a generic environmental impact statement on nuclear waste disposal, the possibility of disposing of high-level waste in very deep holes. Reports on both of these activities have been published.

By its many yet interrelated activities, the Earth Sciences Division is actively involved in developing the science and technology that will be necessary to isolate wastes. Details of these activities are given in the following section.

SWEDISH-AMERICAN COOPERATIVE PROGRAM ON RADIOACTIVE WASTE STORAGE IN MINED CAVERNS IN CRYSTALLINE ROCK

P. A. Witherspoon, N. G. W. Cook, and J. E. Gale

INTRODUCTION

Underground storage of nuclear waste in crystalline rock requires long-term isolation of potential contaminants from the biosphere. Whether or not this requirement can be met depends on the interractions of heat flow, fluid flow, and rock mass properties. To determine how well we can predict the in-situ response of a real rock mass to high thermal loading, Lawrence Berkeley Laboratory, in conjunction with the Swedish Nuclear Fuel Supply Board (KBS), is conducting heater tests, hydrologic tests, and fracture system characterization studies in granite adjacent to an iron-ore mine at Stripa, Sweden.

This cooperative project officially began in July 1977. Much of the design and construction phases were started in fiscal year 1977 and completed in fiscal year 1978 (see Witherspoon et al., 1978). This report describes the work effort and results of fiscal year 1978. This year's activities included installing, calibrating, testing, and starting heater experiments; mapping and collecting data for the hydrology task; and thermomechanical modeling of Stripa granite. Preliminary results are based on the first several months of data from heater experiments, fracture characterization, and borehole measurements for geophysical and hydrologic characteristics. As more of the data are gathered and analyzed, a comprehensive report on the results will be prepared.

Under the direction of KBS, the Swedish portion of the cooperative study began by extending the mine excavations for the large-scale

experiment and drilling some 3,500 m of boreholes. Other KBS responsibilities include characterizing the Stripa granite, performing rock and thermal stress measurements, and assessing pressure and temperature effects on rock permeability. The information generated from these tasks has been useful to Lawrence Berkeley Laboratory in the design and analysis of their tasks in the cooperative study.

The United States' portion of this cooperative work program consists of three main research efforts supported by a program of measurement. The principal investigations at Stripa are in-situ heater experiments, both full-scale and time-scaled, and fracture hydrology assessment. The support activities include geophysical measurement, laboratory material properties, and in-situ stress measurements. Layout of the experiments is given in Figure 1. Each of these activities will be discussed in the following sections and results and analyses will be outlined for fiscal year 1978. A brief statement on the projected activities of fiscal year 1979 will conclude the report.

IN-SITU HEATER EXPERIMENTS

In-situ heater experiments are being conducted at Stripa to measure the effects of thermal loading in rock. These experiments will produce quantitative data that will aid in the safe design of underground nuclear waste repositories.

The temperature in a two-dimensional repository reaches a maximum value about 25 years after emplacement of reprocessed high-level waste (40 years after emplacement of spent fuel), assuming it is emplaced 10 years after removal from the reactor (Figure 2). The value of this peak temperature is directly proportional to the initial loading density of the repository. This peak temperature should be reached experimentally within a short period of time to allow us to verify our prediction of the thermal pulse before waste need be sealed in a repository.

Two full-scale experiments have been designed to (a) assess the near-field, thermomechanical response of the rock close to canisters in the short-term; and (b) make the same assessment under simulated long-term rock temperature. The full-scale tests use electrical heaters, with a maximum power output of 20 kW, in simulated high-level radioactive waste canisters 0.3 m in diameter with a heater length of 2.5 m. These heaters have been installed 22 m apart, in vertical boreholes 0.4 m in diameter by 5.5 m deep, drilled into the floor of the full-scale test drift.

The first heater is operating at a power output of 5 kW, corresponding to that from a canister of reprocessed high-level waste 3-1/2 years after removal of the fuel from a nuclear reactor (OWI, 1976). To simulate the effects of thermal interaction, the full-scale heater is surrounded by eight peripheral heaters on a radius of 0.9 m, each with a length of 4.3 m and

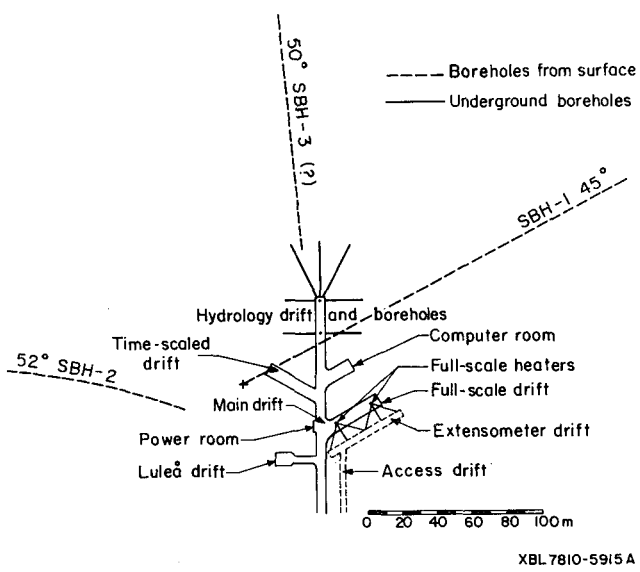

Figure 1. A plan of the test site at Stripa showing the time-scale and full-scale drifts, the extensometer drift for the full scale experiment, which is located at a lower elevation, and other drifts and boreholes.

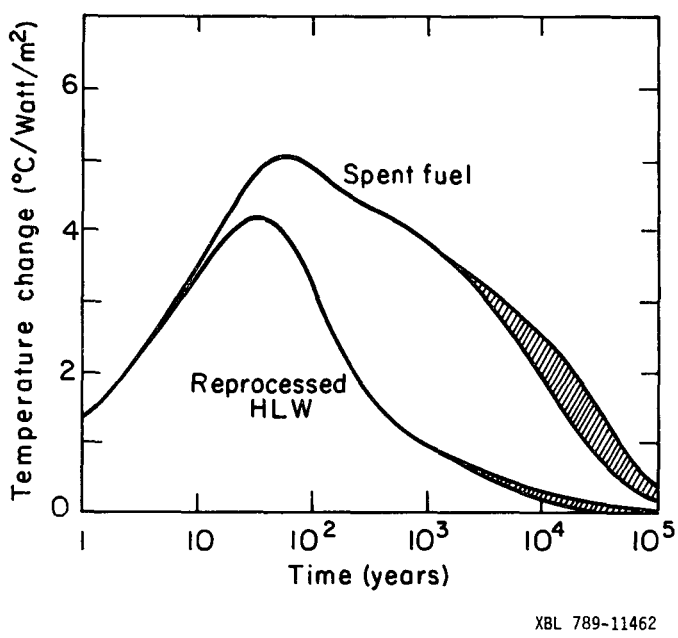

Figure 2. Curves showing how the average temperature of a planar repository for spent fuel and reprocessed high-level waste are expected to change with time. The hatched tail of each curve represents the range of temperature differences caused by different depths of the repository below surface.

a power output of approximately 2.2 kW. The second full-scale heater is operating at a power level of 3.6 kW, corresponding on the thermal output of a canister of reprocessed high-level waste five years after removal of the fuel from a nuclear reactor (OWI, 1976).

In order to study the interaction of adjacent heaters and measure the response of a larger volume of rock than can be done in full-scale experiments, a time-scaled experiment is being conducted in a separate drift. The linear scale of the time-scaled heaters has been reduced so that time is accelerated by a factor of 10:2. The power output has been reduced by the same amount as the linear scale to maintain similitude of temperature. The time-scaled experiment uses eight heaters, 0.8 mm long, placed in vertical boreholes on centers of 7 x 3 m, and drilled 11-m deep below the floor of the drift.

To assess the in-situ response of the rock to the heater experiments, three sets of measurements are being made. First, the temperature fields provide the coefficients of thermal diffusivity (from short-term data), and conductivity (from long-term data). Thermal anisotropy and departures from conductive heat flow will be detected. Second, measurements of thermally induced displacements provide the coefficient of thermal expansion of the rock mass when we make reasonable assumptions about values for Poisson's ratio. Finally, measurements of thermally induced stress provide the in-situ value of Young's modulus for the rock mass, although stress is inferred from displacements on a small scale rather than measured directly.

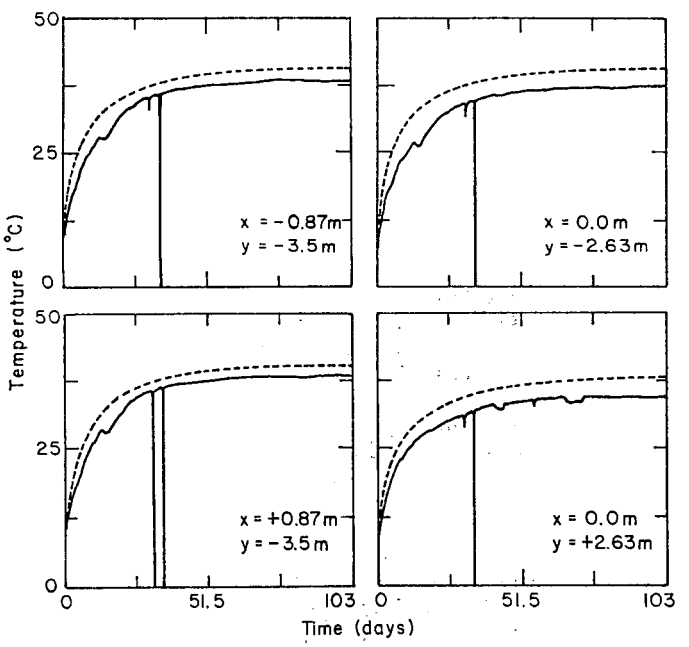

Figure 3. Curves showing the predicted (dashed) and measured (solid) temperatures as a function of time at a radius of 0.87 m from the midpoints of the two innermost heaters on the Y axis as shown in Figure 5, from which the hole locations can also be found. The near-vertical excursions of the measured values reflect malfunction in the data collection system.

Preliminary Results

Predicted and measured temperature in the mid-plane of the time-scaled heaters along different directions are shown in Figure 3, from the time the heaters were switched on to 103 days. Measured temperatures are slightly lower than predicted, partly as a result of water in the heater holes. Predicted isotherms are plotted in Figure 4, together with measured temperatures 90 days after heating started. Again, the comparison between measured and predicted values is close, although the effects of heat transfer up the hole by evaporation and condensation can be seen in the higher values of measured temperatures above the heaters.

Plots of rock movements between anchor points in the time-scaled drift are illustrated in Figure 5. Important features of this figure include: absence of initial measured displacements; large disparities between the measured and the predicted values; and the discontinuous nature of these displacements. Checks of the differential movements between anchor points above the below the heater mid-plane have shown that similar disparities exist between measured and predicted displacements and the ratio be-

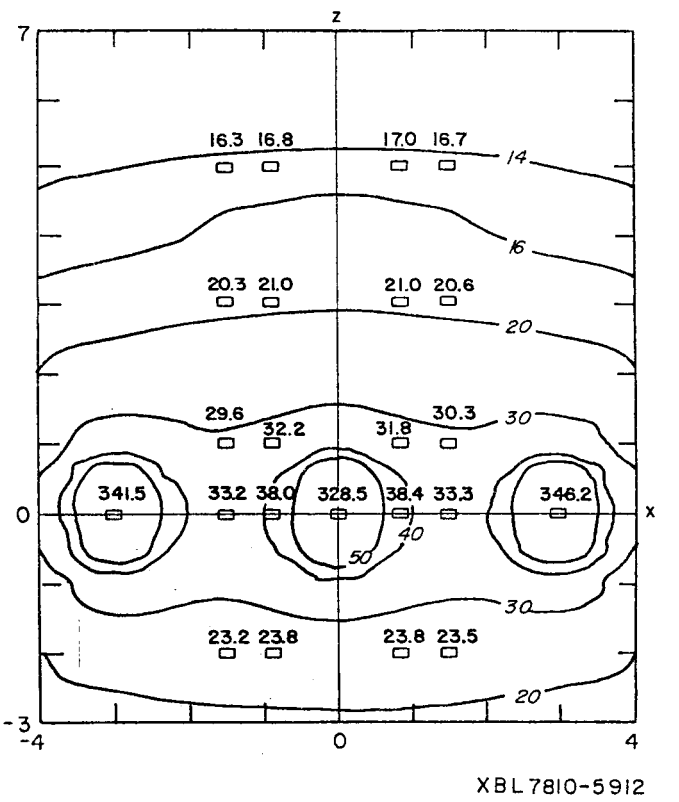

Figure 4. Predicted isotherms and measured temperatures in a vertical plane (y = -3.5) containing three of the time-scale heaters, 90 days after heating began. (Scale for both X and Z axes is given in meters.)

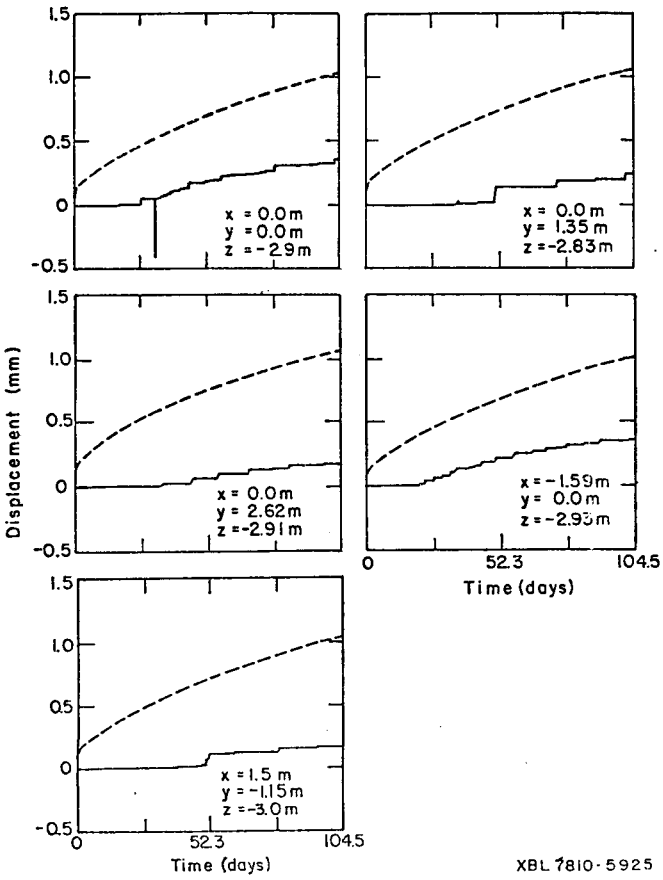

Figure 5. Predicted (dashed) and measured (solid) relative displacements between anchor points 3 m below the heater midplane and the hole collars in the floor of the time-scale drift, plotted as a function of time.

tween them varies between 1/4 and 1/2. The discontinuous displacements often occur within a short time period, at different anchor positions of the same extensometer and at different extensometers, suggesting that the rock is behaving as a mass of coupled blocks.

The maximum measured displacements around the 5-kW full-scale heater are significantly less than the predicted values but the shapes of the predicted and measured curves are remarkably similar.

In both full-scale experiments, one horizontal extensometer is anchored on opposite sides of a diameter below the bottom of the heater. The relative displacement between these two anchor points is the least ambiguous of all the displacement measurements because they are least affected by the presence of the drifts. Predicted and measured values for these displacements for the 5-kW full-scale heater were plotted and again, measured values of displacement are significantly less than predicted.

Analyses of data collected in fiscal year 1978 were not complete, but some tentative conclusions can be drawn. The temperature measurements made in fiscal year 1978 suggest that a flow in the rock mass is predominantly by conduction and that theoretical calculations, which use laboratory values of thermal coefficients, can be used to predict rock temperatures reasonably well.

Displacement measurements have yielded puzzling results. Measured values of displacement are all from 1/2 to 1/4 of predicted values, even though both change with time. Predicted and measured values have been checked for consistent error, which would explain this disparity; both appear to be accurate. Thermal expansion of the rock mass into open joints would explain the disparity and would cause displacements to differ from those predicted by theory in several days. Initially, displacements may be very small, as the thermal expansion of the rock is taken up by spaces between joint surfaces. Thereafter, as stressed are generated across joint surfaces, the displacements would become increasingly linear. The relative disparities between measured and predicted displacements may be expected to vary with the direction in which they are made because of the anisotropy of jointing. Displacements may tend to be discontinuous because of stick-slip caused by friction across joints (Jaeger and Cook, 1976). Although evidence for each of these deviations can be found, there are exceptions. If displacement into spaces between joints were as important as the disparity between predicted and measured values suggests, the value of Young's modulus would be much less than that of laboratory specimens. From this, it would follow that the magnitudes of the thermally induced stress would be correspondingly smaller. Although we have experienced difficulties in making stress measurements, many of the measured indicate that thermally induced stresses are closer to the predicted values than stress measurements based on displacements.

DATA ACQUISITION SYSTEM

The Stripa heater experiments acquire data from approximately 800 sensors, which requires high reliability in data acquisition, storage, and display. To quickly detect and correct faulty operation, periodic and detailed monitoring of each sensor's output is required.

Hardware for a powerful and flexible computer-based data aquisition system was specified, purchased, integrated, and installed in the Stripa mine to support the heater experiments. A graphics software system was designed, implemented, and installed to enable even noncomputer-oriented scientists to rapidly request graphical displays of predicted and actual experimental results in real time.

Graphical data displays have helped us to quickly detect and correct problems associated with water in the boreholes, relay failures, electrical grounding, occasional U. S. Bureau of Mines gauge malfunctions, and corrosion that caused failure of numerous stainless-steel-clad thermocouples. The ability to graphically overlay data from selected extensometers helped us interpret displacement, especially the stick-slip type of displacement.

THERMOMECHANICAL MODELING OF HEATER EXPERIMENTS

Analytical and numerical modeling studies were conducted to: guide the design and operation of the experiments; provide predicted temperatures, displacements, and stresses to be sorted in an on-site computer for instant graphic comparison with field data; and develop a predictive model for long-term thermomechanical and associated hydrological responses of nuclear waste repositories in hard rocks.

Temperature calculations for the full-scale experiments performed in fiscal year 1978 differ from those made in fiscal year 1977 in two respects. In 1978, we used thermal properties measured in small laboratory specimens of Stripa granite and we assumed that peripheral heaters were switched on 180 days later than the central 5-kW heater and were operated at a power of 0.72 kW each. Detailed temperature calculations were carried out for the time-scaled experiment using decaying heat sources to simulate reprocessed pressurized water reactor (PWR) high-level waste.

The finite-element thermomechanical models were compared with the analytic solution for an infinite hollow cylinder. The effects of the heater drift and extensometer drift are included in the finite-element thermomechanical models for the full-scale experiments.

Thermally induced displacements and stresses were calculated for the time-scaled experiment using a three-dimensional finite element model. The predicted thermal stresses and displacements were converted to quantities measured by the extensometers, USBM gauges, and IRAD gauges. Temperatures, displacement, and stresses were written onto magnetic tapes in a readily readable file structure so that they can be used as input files for the graphics system in the MODCOMP computer at Stripa for real-time graphic display together with field data.

A computer graphics package was developed for plotting time histories, temperature and stress contours, and displacement vector maps for use on the CDC-7600 computer at LBL. Predicted temperatures, displacements, and stresses were plotted against time for nearly all instrument locations.

A least-squares method, utilizing the finite-line source solution in the Marquadt algorithm, was developed and applied to extract the in-situ thermal conductivity and thermal diffusivity for Stripa granite from the 5-kW full-scale experiment temperature data.

FRACTURE SYSTEM CHARACTERIZATION

The mechanical behavior of a rock mass is controlled primarily by the deformation of the fractures within the mass. To assess and predict the influence of discontinuities, we must determine their spatial orientation, frequency, size, and mechanical properties to a practicable degree. Therefore, considerable effort has been directed toward defining the fracture system in the graphite surrounding the heaters.

Two approaches were used to define the fracture system. First, major features mapped on the floor of the drift were correlated with borehole interceptions, as determined by detailed core description. Second, a statistical approach using stereographic evaluation showed distinct joint sets. The distribution of fractures within these sets is located so that approximate three-dimensional "blocks" of intact rock can be defined. These statistical blocks, along with the discrete continuous fractures, constitute a model by which rock deformation data can be interpreted. The analysis of the fracture system is complemented by geophysical and mechanical borehole logging techniques. Data from these studies will help indicate which fractures or sets of fractures are significant. Fracture system characterization was undertaken for the full-scale and time-scale drifts separately.

In the full-scale drift, the main continuous features are the pegmatite dikes and a subparallel fault system that also cuts the pegmatite at several places. The area is heavily faulted with some fracture closed by secondary mineralization. Most of the fractures are filled with epidote, chlorite, or calcite and are helpful in correlation.

In the time-scale drift, the fractures strike roughly perpendicular to the drift center line and are continuous throughout the drift. They are typically 1- to 15-cm wide, filled with chlorite or epidote, and are frequently slickensided. Because of their prominence, these features could be projected downward from their mapped locations and correlated to fractures identified in the core samples. Projections were computed analytically, and the resulting subsurface correlations were checked visually on a three-dimensional physical model. The factors considered, other than borehole position, include similarity of orientation and infilling characteristics.

Although definitive results are not yet available, it is worthwhile to review current findings. Four major fracture systems illustrated in the core sections (Figure 6) become important because of their proximity to the heaters. Compressive stresses are generated in the rock surrounding a heater. For any point in this field, shear and normal stress components may be resolved for planes not parallel to the principal stresses. For fracture planes near the heaters, the induced shear stress may exceed the available shear strength of the surface, and thus cause displacement. Because blocks of rock bounded by discontinuous fractures tend to interlock and thus provide shear resistance, we expect that most shear deformation will take place along the major continuous surfaces. However, since the induced shear stresses are not uniform and the surfaces are not fully planar, the shear displacement should not be uniform. In other words, the <u>entire</u> surface of the fracture need not shear in order to release

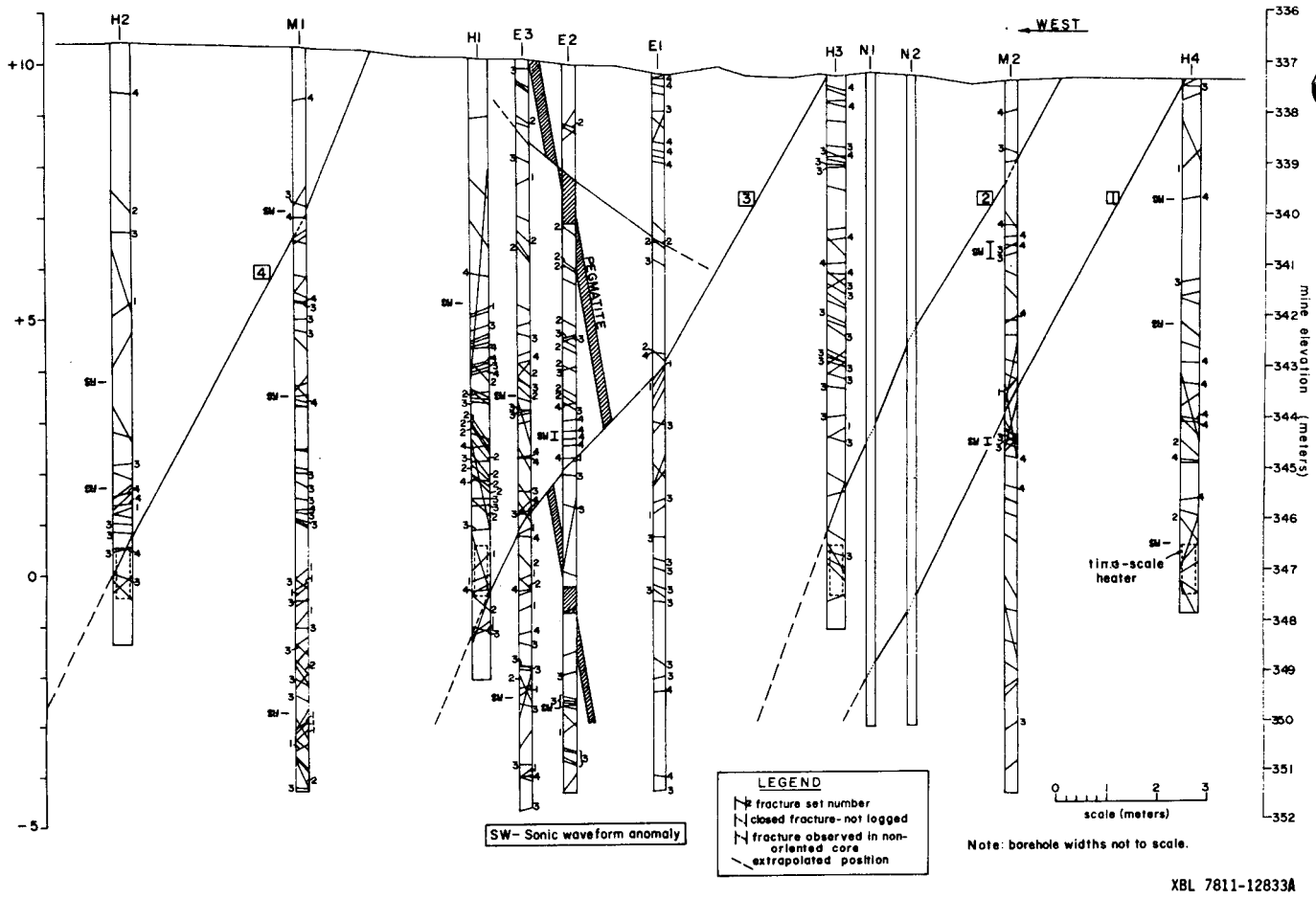

Figure 6. Major fractures in profile along the center line through time-scale experiments; major fractures and joint sets shown.

the strain energy around the area of failure. Indeed, this much strain energy is probably dissipated through deformation of the surrounding discontinuous fractures.

FRACTURE HYDROLOGY

The primary objective of the fracture hydrology task is to determine (a) the magnitude and velocities of groundwater movement through the fractured granite rock mass at Stripa; and (b) how these parameters vary as a function of time and temperature. Secondary objectives are to: (a) develop and test borehole tools for measuring groundwater pressures and flow rates, and (b) sample groundwaters to determine their age and degree of chemical equilibrium with surrounding rock with very low permeabilities.

To accomplish these objectives, it is necessary to: define the geometrical properties of the fracture systems, determine the distribution of fluid pressures and permeabilities associated with these systems, collect and analyze samples of groundwater from several locations within the rock mass; and analyze these data to provide a coherent description of the groundwater flow in the vicinity of the underground openings.

The drilling program can be divided into its surface and subsurface components. The surface studies are centered around two oriented diamond-cored 76-mm-diam boreholes, SBH-1 and SBH-2. The subsurface efforts include drilling three groups of 76-mm-diam boreholes.

Injection tests have been performed in about 100 m of SBH-1 using a 1.8-m packer spacing. The low hydraulic heads encountered will require modification of existing equipment to provide greater control of injection pressure when testing in low permeability rocks. Hydraulic tests in subsurface boreholes completed in fiscal year 1978 include: in-situ pressure measurements and withdrawal tests in S-1 and S-2; and in-situ pressure measurements, withdrawal and injection tests in R8, R9, R19, HG3, and HB4.

Pump tests were conducted from four surface wells drilled on a pattern dictated by the dominant fracture orientation. Two wells were designed as observation wells and were positioned along the strike of the major joint set orientation relative to the pumping well (WT-7). An additional well (WT-5) was positioned perpendicular to the strike of the dominant joint set. The function of this layout was to determine hydraulic anisotropy of the

rock mass due to the dominant set. Differences in drawdown between wells would then be interpreted in terms of the length of the fractures.

Data from well WT-7 fit horizontal fracture-type curves (Figure 7) by applying the methods of Gringarten and Bertrand (1977). Preliminary transmissibility calculations of 1.5×10^{-5} cm^2/sec from the type curve are in good agreement with the value of 1.3×10^{-5} cm^2/sec obtained from the semilog straight-line method.

There was no response in the observation wells to the pumping in WT-7; the absence of a response may have been due to either a lack of hydraulic continuity between the wells or very low permeability of the rock around the wells. To test these hypotheses, a pump test was attempted (Test 2, WT-6). Pumping at a rate of approximately 20 m^3/day, the well did not yield water except from wellbore storage. That is, there was no appreciable flow from the formation. An estimate of the transmissivity of this well using slug test techniques (Cooper et al., 1967) suggests a permeability of 1×10^{-8} cm/sec, three orders of magnitude less than for well WT-7.

Geochemical Studies

A large number of water samples collected from surface and subsurface boreholes have been analyzed for major ions, dissolved gases, deuterium, ^{18}O, ^{14}C, ^{13}C, and uranium isotopes. They key sampling points and the preliminary isotope results are given in Figure 8. The ^{14}C results suggest groundwater dating ages of about 20,000 years B. P. A detailed discussion of the geochemical results is given in the report by Fritz et al. (1979). Geochemical studies related to the time-scaled experiment have been delayed due to funding limitations but will proceed in fiscal year 1979. These studies will attempt to monitor changes in water chemistry, water pressure, and permeability at a number of points within and near the time-scaled heater experiment. An attempt will be made to correlate changes in water chemistry with the fracture mineralogy determined from samples of the fracture planes obtained from the monitor boreholes.

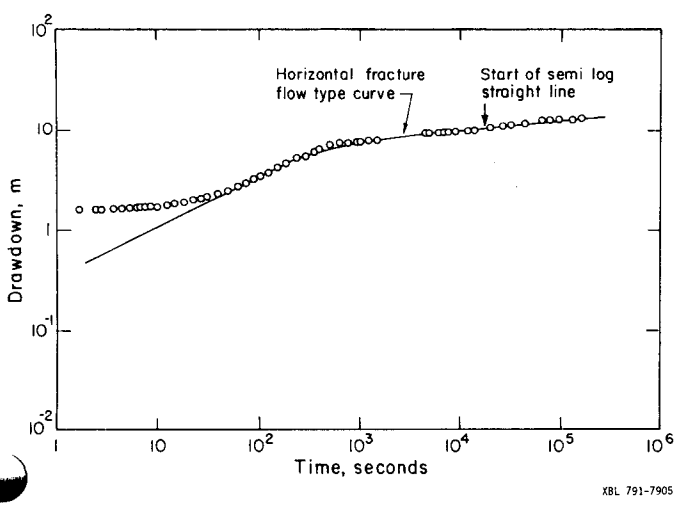

Figure 7. Drawdown data versus time, well WT-7, August 21-22, 1978.

Water-Pressure Monitoring Systems

The extent of an hydraulic potential field is a major factor in influencing groundwater flow and these data are necessary input for repository siting. The potential field must be known, not only before repository construction but during the operational and post-operational phases, to determine what effect the excavation and increased temperatures have on water flow.

In low-permeability rocks, reliable fluid-potential data are difficult to obtain due to the transient effects associated with drilling boreholes and cross flow between zones within boreholes. Therefore, a long-term water-pressure monitoring program is essential for repository site characterization. Testing the monitoring systems for boreholes is an important part of the Stripa hydrology program. One of the basic requirements for pressure-monitoring systems, or piezometers, is that a large number of measurement points must be available within a single hole. We feel this is essential since many boreholes may comprise the containment potential of the rocks.

Considerable efforts were made in fiscal year 1978 to develop field equipment to measure accurately low flow rates (~1 ml in 30 to 60 min) at high pressures during injection tests in the boreholes at Stripa. A multiple-point piezometer and fluid-pressure monitoring system (Figure 9) was installed; its operational char-

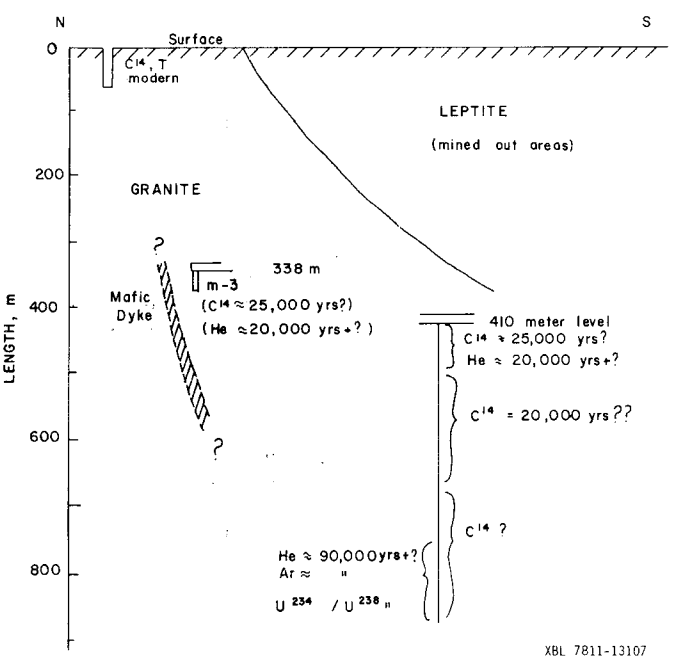

Figure 8. Preliminary isotope results.

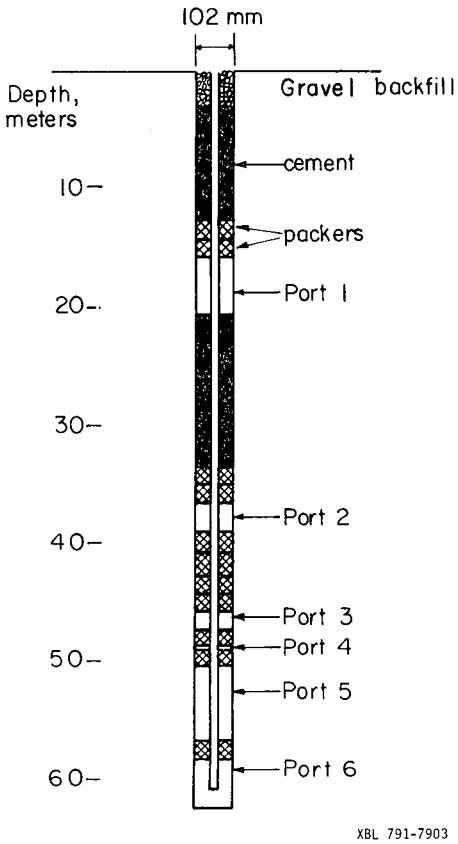

Figure 9. Configuration of LBL piezometer test hole.

acteristics are currently being monitored. Additional laboratory work is planned to determine the adequacy of the packer system used in the piezometer before the installation in SBH-1 and SBH-2.

An assessment of equipment needed to prepare boreholes for long-term hydrologic monitoring indicates a need for a packer that could be emplaced hydraulically but locked in place mechanically. The initial design and fabrication work on a hydraulic-mechanical packer was completed in fiscal year 1978.

ROCK MECHANICS INSTRUMENTATION

The rock mechanics instrumentation activities have been carried out by Terra Tek and have focused on (a) laboratory testing of Stripa granite, (b) laboratory evaluation of borehole instrumentation, (c) field installation and calibration of borehole instrumentation, and (d) in-situ modulus measurements.

Laboratory testing in fiscal year 1978 was directed at measuring the mechanical and thermal properties of the Stripa granite, selecting suitable materials for instrument construction, evaluating the thermal behavior of the instrumentation, and determining field installation, calibration, and data reduction requirements for the borehole instrumentation. Properties of the granite are summarized in Table 1.

Borehole instrumentation layout for the heater tests was designed and the instrumenta-

Table 1. Properties of granite from Stripa mine.*

Property	Quantity
Physical	
Bulk density (dry)	2.608 g/cm^3
Grain density	2.653 g/cm^3
Porosity	1.7%
Permeability	<1.7 x 10^{-5} md
Thermal	
Thermal expansion	11.1 x 10^{-6} cm/cm°C
Thermal conductivity	3.6 - 0.3745 x 10^{-2} T W/m°C
Specific heat	0.2 cal/g°C
Mechanical	
Compressive strength	210 MPa (31,500 psi)
Tensile strength	13.27 MPa (1,925 psi)
Young's modulus	51.3 GPa (7.7 x 10^{-6} psi)
Poisson's ratio	0.23
Compressional wave velocity	5.60 km/sec (18.370 fps)
Shear wave velocity	3.44 km/sec (11,289 fps)

*The samples used to obtain the properties were cored from large blocks of granite taken from the general area of the heater experiments.

tion was purchased, evaluated, installed, and calibrated in fiscal year 1978. In-situ measurements of deformation modulus in boreholes were conducted. Design, fabrication, and emplacement of both an acoustic velocity crosshole system and the Terra Tak stress-monitoring system were also completed.

Field work performed at Stripa by Terra Tek involved installation of the following instrumentation: 35 four-point extensometers; 30 three-component USBM gauges; 30 Creare vibrating wire stressmeters; and 330 thermocouples. On-site calibration of all instrumentation except the Creare stressmeters was performed. In addition, dewatering capabilities were provided for all full-scale, 38-mm vertical holes. No major difficulty was encountered with any of the instrumentation installations.

Geophysical Measurements

During fiscal year 1978, four separate systems of geophysical and rock mechanics instrumentation were used to measure the physical properties of the rock mass to obtain information for site selection and to observe temperature-induced change during heater tests.

The four instrumentation sets are as follows.

1. A portable borehole logging unit, supplied by LBL, with natural gamma, neutron/thermal-neutron, gamma-gamma (density), temperature, spinner, (flowmeter), caliper, and electrical resistivity tools. This set of instruments was used to log surface borehole SBH-1, most of the vertical boreholes in the time-scale and full-scale drifts, some of the boreholes in the ventilation (macro-permeability) drift, and to perform ongoing neutron-monitoring measurements.

2. The CSM cell and the Goodman Jack. These were used to measure Young's modulus in-situ.

3. Borehole equipment operated by the Swedish Geological Survey (SGU). This set was used to obtain electrical resistivity and differential resistance measurements.

4. Two sets of ultrasonic borehole equipment, supplied by the University of Saskatchewan and by Terra Tek.

In addition to the borehole measurements at Stripa, laboratory experiments continued in the Engineering Geoscience Department, University of California at Berkeley, to develop the design and fabrication of a reflection profiling system operating at ultrasonic frequencies to detect fractures and discontinuities within the rock mass (Waters et al., 1979).

The suite of logs obtained in borehole SBH-1 covers the interval from 250 to 340 m. Figure 10 displays seven borehole logs, fractures, and other geological features identified

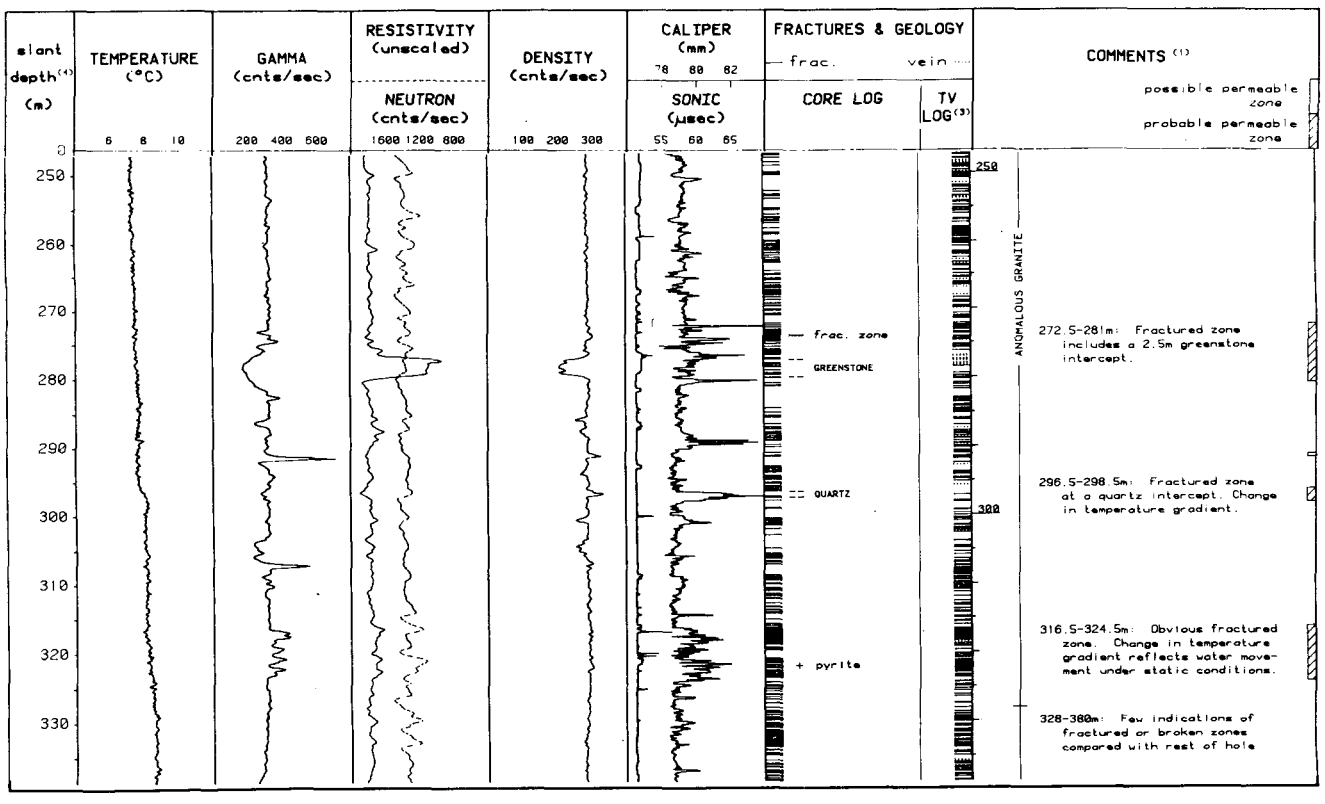

Figure 10. Logs from borehole SBH-1, showing the fracture logs from core examination and television commentary based upon the logs. The column at left gives the slant depth in meters below the surface.

in the core and television logs. Also indicated are zones that are likely to be more permeable than the average interval.

In-situ modulus measurements were performed by Terra Tek in the time-scale and full-scale boreholes with both the CSM cell and the Goodman Jack. The CSM cell was capable of operating in the 38-mm holes and testing was conducted in all vertical holes for a total of 385 measurements, including 30 repeat measurements. Figure 11 shows the modulus measurements. The deformation modulus averaged 35-40 GPa, whereas the Young's modulus from the laboratory tests was 53 GPa. The Goodman Jack was used for measurements in nine vertical 76-mm boreholes in the full-scale test area, and the data are being evaluated.

Neutron Monitoring Measurements

A neutron/thermal-neutron probe has been used at Stripa to log the variations in the water content of the rock. This is accomplished by detecting the number of thermalized (low-energy) neutrons reaching a detector a fixed distance from a high-energy neutron source. The probe was used to log the surface hole SBH-1 and the underground holes. In addition, periodic borehole measurements are carried out during the heater tests to detect any change in the water content of the rock as its temperature rises. After several months of heating in the time-scale room (4 months), at H10 (3 months) and H9 (1 month), no changes in the water content in the adjacent rock were detected at the sensitivity of the instrument, which is about 0.1% (volumetric).

Ultrasonic Measurements

Cross-hole measurements between boreholes have been performed before and during the operation of heater H9 using ultrasonic P- and S-wave transducers. Preliminary analysis of the arrival times picked from the osciloscope face, indicates a reduction of velocities in the zone where the core also shows an increase in the frequency of fine fractures. A second result is that the P- and S-wave velocities increased by a few percent during the first month of H9 operation. This increase is attributed to the expansion of the rock and the closing of the fractures. The ultrasonic measurements are recorded on magnetic tape and can be examined in greater detail to substantiate the preliminary findings. These measurements are discussed further by Nelson et al. (1979).

Ultrasonic Reflection Experiments

Before designing an ultrasonic reflection profiling system, laboratory experiments were performed on granitic test blocks with ultrasonic transducers in the Engineering Geoscience Department, University of California. Experiments provided experience in examining shear-wave reflection from open cracks, a water-filled crack, and a partially filled crack simulated by a lead block pressed against the bottom surface of a granite block. Enhancement of the signal-to-noise ratio has been possible with the use of spatial filtering using linear arrays, and by using slots near the source to reduce interference from surface waves. In addition, deconvolution using a state-of-the-art signal processor has shown that additional progress is possible.

ACTIVITIES PLANNED FOR FISCAL YEAR 1979

Fiscal year 1979 activities at Stripa will continue to focus on the effect of elevated temperatures on the geomechanical behavior of granite and the fracture hydrology of the rock mass.

Collection and analysis of data from all heater experiments will continue. In addition,

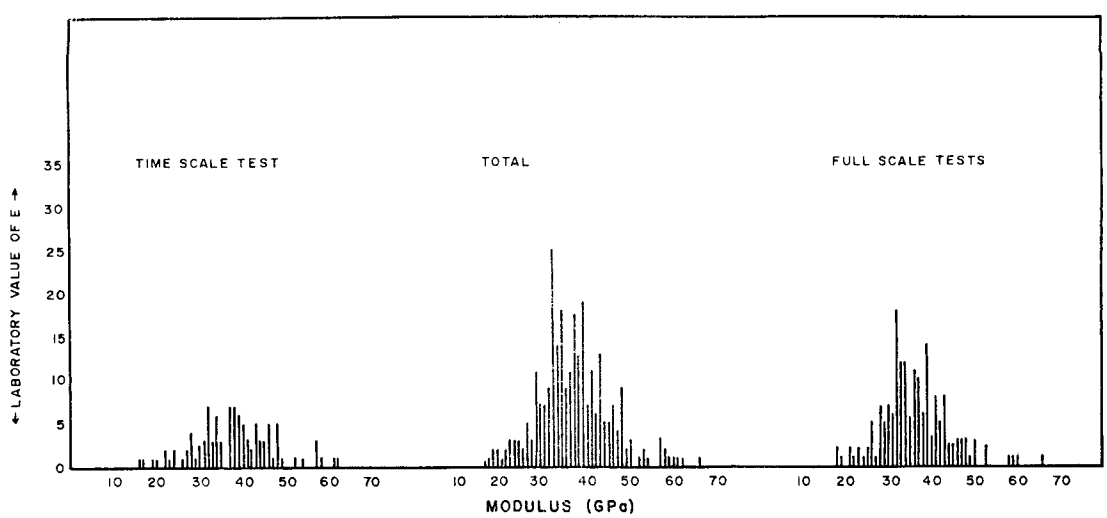

XBL 794-9283

Figure 11. Distribution diagram of Young's moduli measured with the CSM cell in the full-scale and time-scale boreholes.

the peripheral heater experiments will begin after the 5-kW heater load has provided a sufficiently stable temperature field to proceed. The interaction of thermal fields, simulated by peripheral heater turn on, will then be investigated. Due to the additional heat load produced from the peripheral heaters, we expect gross decrepitation of the 406-mm, 5-kW heater borehole wall to occur. These effects will be carefully studied.

The time-scaled experiment analysis will continue. As heat loads are decreased, simulating the decay in energy output with time, steady state condition should be reached. Since a much larger mass of rock has been subjected to elevated temperatures in the time-scale experiments, the role of rock mass discontinuities in determining rock mass response will be investigated.

Rock mass expansion has taken place during the heating periods of the respective experiments and its effects analyzed. Toward the end of the fiscal year, the heating phase of the experiments will end and a study of cooldown effects will follow. Cooldown investigations are expected to continue into fiscal year 1980.

Fracture hydrology assessment will proceed with the completion of fluid pressure and fracture permeability testing of surface boreholes SBH-1, SBH-2, and SBH-3, which is scheduled to be drilled early in the field season.

An additional hydrological experiment will be initiated to determine the gross seepage rate in the granitic rocks underground and to correlate this rate with the surrounding hydraulic pressure field. A global permeability can then be calculated and compared with results obtained from surface borehole hydrology studies. This underground experiment will be conducted in a 30-m sealed-off drift adjacent to the heater experiments. Measuring devices will be installed to monitor air flow, temperature, humidity, and barometric pressures of the rock. Pressure gradient in the rock will be measured using boreholes that penetrate 30 m into the rock matrix.

All field work at Stripa should be completed by the middle of fiscal year 1980. However, analysis of the various experiments is expected to continue through the year and possibly into fiscal year 1981.

REFERENCES CITED

Cooper, H. H., Boedehoeft, J. D., and Papadopoulos, I. S., 1967. Response of a finite diameter well to an instantaneous change of water. Water Resources Res., v. 3, pp. 263-269.

Fritz, P., Barker, J. F., and Gale, J. E., 1979. Geochemistry and isotope hydrology of groundwater in the Stripa granite: results and preliminary interpretations. Berkeley, Lawrence Berkeley Laboratory, LBL-8285, SAC-12.

Gringarten, A. C., and Bertrand, L., 1977. Determination des characteristiques hydrauliques des aquiferes fissures pour pompages d'essai en regime transistoire--application aux Nappe de la Craie. Orleans, France, Bureau de Recherches Geologiques et Minieres.

Jaeger, J. C., and Cook, N. G. W., 1976. Fundamentals of rock mechanics. New York, John Wiley and Sons.

Nelson, P., Paulsson, B., Rachiele, R., Andersson, L., Schrauf, T., Hustrulid, W., Duran, O., and Magnusson, K. A., 1979. Preliminary report on geophysical and mechanical borehole measurements at Stripa. Berkeley, Lawrence Berkeley Laboratory, LBL-8280, SAC-16.

Office of Waste Isolation, Union Carbide Corp., Nuclear Div., 1976. National waste terminal storage program--progress report. Oak Ridge, National Technical Information Service., Report Y/OWI/8.

Waters, K. H., Palmer, S. P., and Farrell, W. E., 1979. Fracture detection in crystalline rock using ultrasonic shear waves. Berkeley, Lawrence Berkeley Laboratory, LBL-7051 (in press).

Witherspoon, P. A., Cook, N. G. W., Gale, J. E., Brown, C. A., Kurfurst, P., McEvoy, M., Amick, C. H., Tsang, C. F., Hood, M., Nelson, P. H., Doe, T., and Mirk, K., 1978. Cooperative work program with Swedish Nuclear Fuel Supply Company on radioactive waste storage in mined caverns, in Earth Sciences Division annual report 1977. Berkeley, Lawrence Berkeley Laboratory, LBL-7028, pp. 143-149.

REGIONAL THERMO-HYDROLOGICAL EFFECTS OF A RADIOACTIVE WASTE REPOSITORY IN HARD ROCK

J. S. Y. Wang, C. F. Tsang, N. G. W. Cook, and P. A. Witherspoon

INTRODUCTION

Hazardous radioactive wastes from nuclear reactor operations must be isolated to prevent dangerous spreading in the biosphere. One possible long-term solution to this critical problem is to place the wastes in a deep underground repository. A largely unknown aspect in the use of underground nuclear waste repositories is the impact of the heat generated by the radioactive decays of the wastes on the surrounding rock formation. The thermal loading may affect the regional effectiveness of the rock formation as a waste barrier to the ground surface. The state of knowledge for predicting long-term, regional thermal effects of a waste repository is very limited at the present time.

For buried radioactive waste, the only important mechanism for potential transfer of radionuclides from a repository to the biosphere is through groundwater transport. The groundwater movement depends on the hydrological properties of the formation, the boundary condition of the basin, and the three-dimensional potential field that provides the driving force in the region. In normal groundwater systems, gravity is the dominant driving force. When the density of the groundwater is not uniform, some movements caused by the gravity forces may occur and tend to reduce the discrepancies in the density field. With the emplacement of the wastes, the induced temperature field around the repository will lower the density of water. The viscosity of water also decreases as the temperature increases. These changes favor the development of upward buoyancy flow.

This study is on the thermohydrological effects of a repository in fractured hard-rock formations. The objectives of this project are to:

1. Calculate the temperature field change around a repository induced by the waste heating
2. Study the dependence of the local and regional temperature field on different waste types, repository dimensions, and rock formations
3. Calculate the flow field change in the formation induced by the density and viscosity changes of water
4. Study the dependence of the buoyancy flow on the temperature field and the hydrological conditions of the groundwater basin.

This project started in April 1978 as a technical development project. An LBL report is being prepared (Wang et al., 1979).

ACCOMPLISHMENTS FOR FISCAL YEAR 1978

Because the driving mechanism of the buoyancy flow is the induced temperature change around the repository, the time-dependent temperature distribution by waste heating is first calculated. For the study of long-term and regional effects, and idealized disk-shaped repository, loaded uniformly with wastes, is considered. The temperature field is calculated by integrating the instantaneous disk source (Carslaw and Jaeger, 1959) over the thermal power density function.

The data for the power densities (Kisner et al., 1978) of the wastes from pressurized water reactors are plotted in Figure 1. The nuclear wastes contain fission products and actinides. The fission products generate most of the heat at early life of the wastes but decay very rapidly, with an approximate half-life of 30 years. The actinides and their daughters are

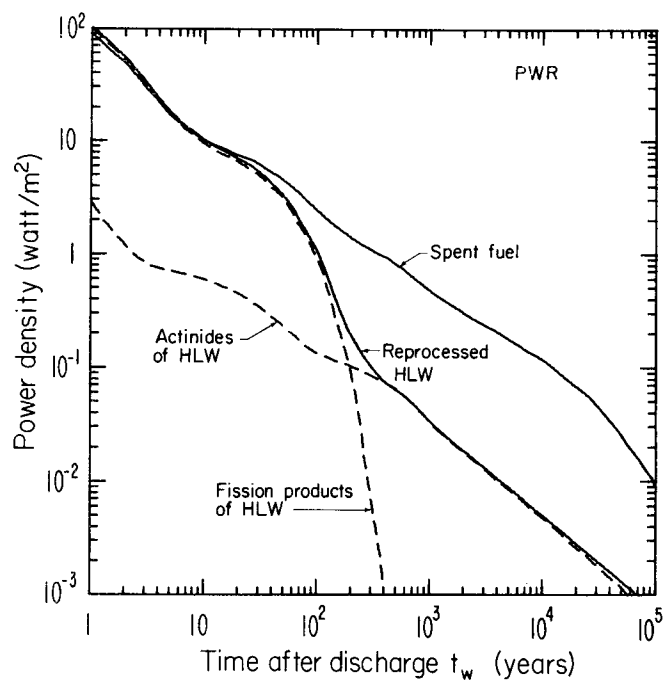

XBL 7810-11962

Figure 1. Areal power densities of spent fuel and reprocessed high level waste versus time after discharge from a pressurized water reactor. The power densities are normalized to 10 W/m^2 at 10 years after discharge when the wates are assumed to be stored in a respository. The wastes contain the short-lived fission products and the long-lived actinides. In the reprocessed waste, 99.5% of the actinides U and Pu are removed.

the main heat source at long storage times. If the wastes are reprocessed to remove most of the uranium and plutonium, the power density of reprocessed high-level waste is much smaller than unreprocessed spent fuel after a long time. In Figure 1, the power densities are normalized to 10 W/m^2 at 10 years after discharge from the reactor. The 10-year-old wastes are assumed to be stored in the repository.

An example of the temperature changes and isotherms for a repository containing spent fuel or reprocessed waste 1,000 years after burial in the repository is illustrated in Figure 2. It is important to note how much greater the magnitudes of these changes are for spent fuel than for reprocessed waste at 1,000 years. To represent the local effects of thermal loading by the wastes, the time dependence of the temperature rise at the center of the repository is plotted in Figure 3. The temperature rise at the repository increases rapidly at early times, reaches the maximum before 100 years, and then decreases slowly back to zero. To represent the far-field effects, and in particular the effects at the ground surface, the time-dependence of the surface temperature gradient at the epicenter above the repository is plotted in Figure 4. The heat flux from the repository will reach the surface in a few hundred years and approaches its maximum values within a period of a few thousand years for a depth D = 500 m in granite. The effects of the long-term difference between the power densities of spent fuel and reprocessed high-level waste on the temperature field are very pronounced. Especially in the surface temperature gradient, the maximum values of the two wastes differ by more than three times with the same power densities at loading.

We have studied in detail the effects of storing the wastes on the surface before emplacement for different times and the effects of different fuel cycles of reactor operation and reprocessing treatment. These factors change the amounts of fission products or actinides in the wastes. The temperature field is very

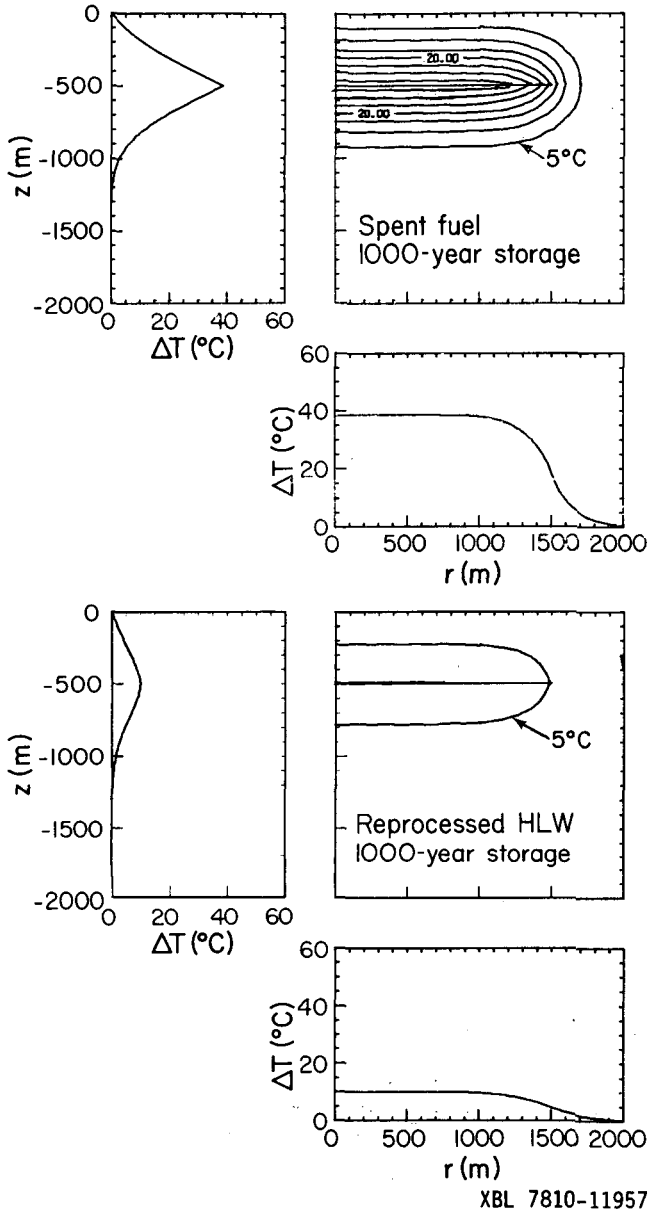

Figure 2. Temperature rise contours around repository after 1000 years of waste storage and the corresponding temperature profiles along the vertical axis through the center of the repository and along the radial axis in the plane of the repository. The repository, in granite with 500 m in depth and 1500 m in radius, is stored with either spent fuel or reprocessed waste at initial loading density of 10 W/m^2 at 10 years after discharge from PWR.

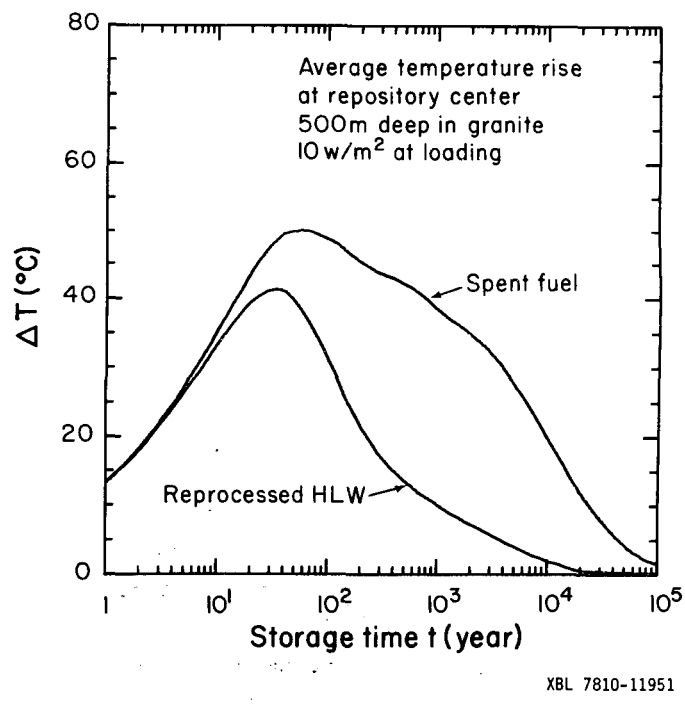

Figure 3. Temperature rise ΔT at the center of repository versus storage time. The repository, in granite with 500 m in depth and 1500 m in radius, in stored with either spent fuel or reprocessed waste at initial loading density of 10 W/m^2 at 10 years after discharge from PWR.

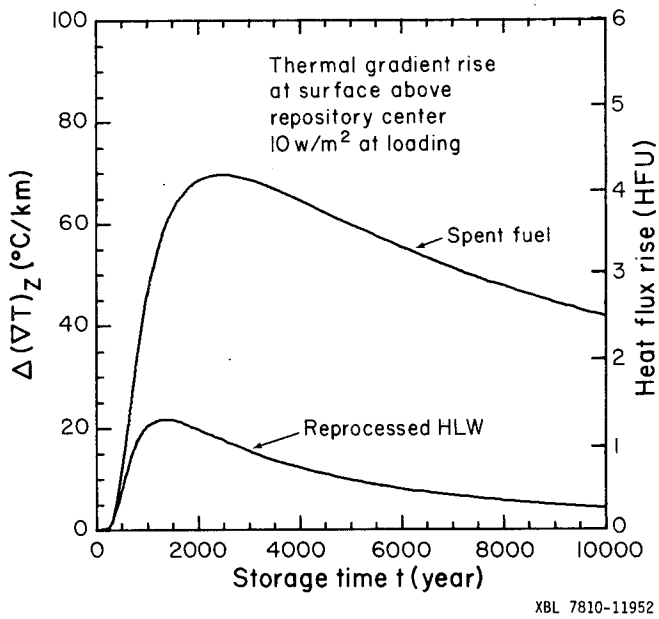

Figure 4. Ground surface temperature gradient rise $\Delta(\nabla T)_z$ and heat flux rise $\Delta(K(\nabla T)_z)$ (in HFU = $\mu cal/cm^2/sec$) at the epicenter above the repository. The repository, in granite with 500 m in depth and 1500 m in radius, is stored with either spent fuel or reprocessed waste at initial loading density of 10 W/m^2 at 10 years after discharge from PWR.

sensitive to these variations. We have also calculated temperature fields for different repository depths and radii in different rock formations.

With the temperature increases around the repository, the buoyancy force on the low-density hot water will induce an upward flow.

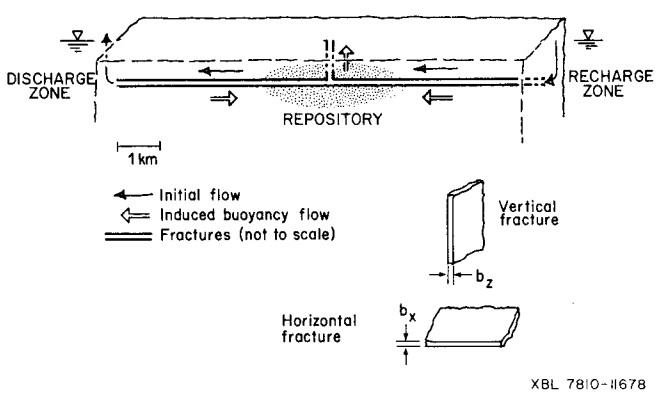

Figure 5. Two fracture model for simulating groundwater movement through a repository located between the recharge and discharge zone. The thermal loading at the repository induces the buoyant flow along the vertical fracture to the ground surface. The horizontal fracture (with aperture b_x; and length 2L if the repository is located midway between the recharge and discharge zone) recharges the vertical fracture (with aperture b_z; and length D) to maintain the buoyant flow.

In this study, a simple model with one vertical and one horizontal fracture passing the center of the repository (Figure 5) is used to study the buoyancy flow.

The water level, initially at the repository bottom, will move upward as the temperature field changes. In Figure 6, the water displacements along the vertical fracture are plotted. The buoyancy flow from spent-fuel waste heating is much larger than the buoyancy flow from reprocessed high-level waste heating. The buoyancy flow is determined by the whole temperature field in the groundwater basin and is more sensitive to the regional, long-term temperature distribution than the local, short-term temperature rise near the repository. The amount of actinides in the wastes is an important factor in determining the buoyancy flow.

The buoyancy flow depends not only on the driving temperature field but also on the hydrological conditions of the formation. For the development of upward flow along the vertical fracture, the moving water must be replaced by recharge from an ambient cold-water region. The connecting flow path from the repository to the cold zone is represented by the horizontal fracture. The density contrast between the hot water around the repository and the cold water at the recharge and discharge zone must be maintained to sustain the buoyancy driving force.

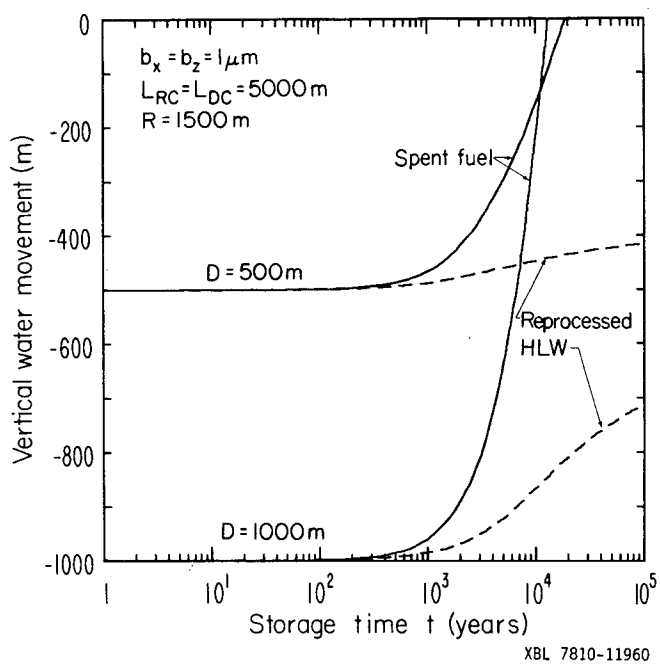

Figure 6. Water movement along vertical fracture from the repository versus storage time. The repository depth is either 500 m or 1000 m. The stored waste is either spent fuel or reprocessed waste at initial loading density of 10 W/m^2 at 10 years after discharge from PWR. The repository is in granite with radius of 1500 m and distance to the recharge and discharge zone of 5000 m. Both horizontal and vertical fractures have 1 μm aperture.

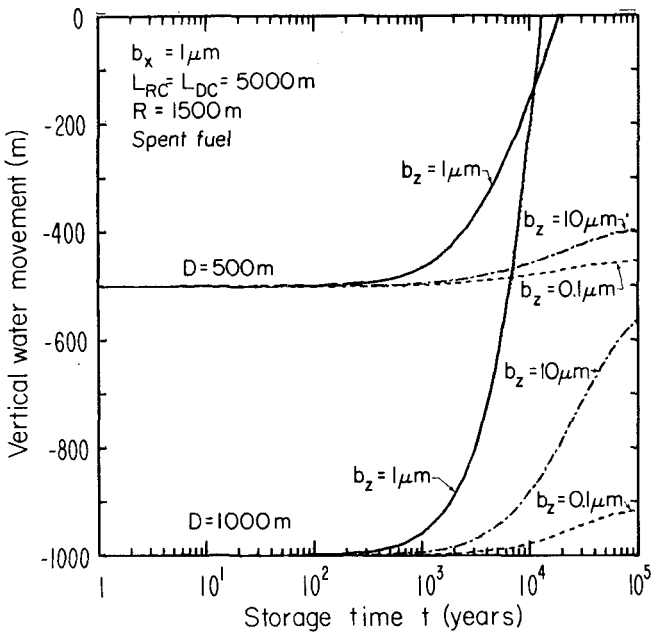

XBL 7810-11961

Figure 7. Effects of different vertical fracture apertures b_z on the water movement along the vertical fracture from the repository versus storage time. The horizontal fracture aperture b_x is constant at 1 μm. The repository depth is either 500 m or 1000 m. The stored waste is spent fuel at initial loading density of 10 W/m^2 at 10 years after discharge from PWR. The repository is in granite with radius of 1500 m and distance to the recharge and discharge zone of 500 m. The water movement is significantly slower both for the case of $b_z = 10\ b_x$ and $b_z = 0.1\ b_x$ than with $b_z = b_x$.

To have a physically reasonable representation of a repository in a low-permeable hard-rock formation, the connecting path (horizontal fracture) must have a nonzero distance, L, and a finite aperture, b_x.

In the two-fracture model, the buoyancy flow is approximately proportional to

$$b_z^2/(1 + 0.5(b_z/b_x)^3 L/D)$$

For a finite recharge capacity, with the distance from the repository to the ambient cold region $L \neq 0$ and the aperture $b_x \neq \infty$, the buoyancy flow does not become infinite as the vertical aperture b_z increases. On the contrary, the flow approaches zero as b_z corresponds to ∞, that is, a large vertical fracture with storage capacity reduces buoyant flow. The buoyant flow in the vertical fracture has an upper bound, which is determined by the permeability of the horizontal fracture rather than the permeability of the vertical fracture. In Figure 7 results with a constant aperture b_x = 1 μm, and with a range of apertures b_z = 10 μm, 1 μm and 0.1 μm, are illustrated. The movement of the water in the vertical fracture is significantly slower both for the case of $b_z = 10\ b_x$ and $b_z = 0.1\ b_x$ than with $b_z = b_x$. The finite recharge capacity through the horizontal fracture restricts the vertical buoyant flow. This simple model demonstrates the sensitive dependence of the buoyant flow on the hydrological conditions of a fractured hard rock formation.

PLANNED ACTIVITIES FOR FISCAL YEAR 1979

1. Thermal conduction calculations for studying the effects of sequential waste loading, multilayer repository, repository shape, and waste container distribution.

2. Coupled thermal-flow modeling for studying the convective motion with or without recharge.

3. Buoyancy flow calculations in multiple-fracture models and equivalent porous formation models.

4. Thermal-stress and stress-flow calculations for studying the regional thermal impact.

REFERENCES

Carslaw, H. S., and Jaeger, J. C., 1959. Conduction of heat in solids. London, Oxford at the Clarendon Press, 2nd ed., p. 260.

Kisner, R. A., Marshall, J. R., Turner, D. W., and Vath, J. E., 1978. Nuclear waste projections and source-term data for FY 1977. Oak Ridge, Office of Waste Isolation, Y/OWI/TM-34.

Wang, J. S. Y., Tsang, C. F., Cook, N. G. W., and Witherspoon, P. A., 1979. A study of regional temperature and thermohydrogeological effects of an underground repository for nuclear wastes in hard rock. Berkeley, Lawrence Berkeley Laboratory, LBL-8271.

THE VERY DEEP HOLE CONCEPT: EVALUATION OF AN ALTERNATIVE FOR NUCLEAR WASTE DISPOSAL

M. T. O'Brien, L. H. Cohen, T. N. Narasimhan, T. L. Simkin, H. A. Wollenberg, W. F. Brace,† S. Green,† and H. P. Pratt†

INTRODUCTION

The U. S. Department of Energy (DOE) is selecting an appropriate system for permanently isolating commercial radioactive wastes in a way that is safe, permanent, and economical. DOE requested that a generic environmental impact statement (GEIS) be prepared to provide a systematic assessment of environmental input for this decision. GEIS describes alternative treatment processes, emplacement media, and waste-management technologies for the disposal or storage of nuclear wastes generated in the commercial sector (for instance, in power plants, and medical and research facilities). Further, GEIS will provide environmental input into later decisions about appropriate emplacement media and disposal technology. The 10 alternatives reviewed in GEIS for managing nuclear wastes include conventional geologic disposal, chemical resynthesis, very deep holes, rock melting, island disposal, sub-seabed geologic disposal, icesheet disposal, reverse-well disposal, partitioning and transumutation, and space disposal. DOE asked Lawrence Berkeley Laboratory to review and assess the feasibility of one concept: the very deep hole (DOE, 1979, Section 3.3; O'Brien et al., 1979).

CONCEPT DESCRIPTION

The very deep hole concept provides one alternative for nuclear waste management, isolating high-level radioactive waste in very deep holes. The method would rely on surrounding rock to contain the wastes, and on great depths to delay the release and reentry of nuclear material to the water supply and the earth's surface. It is understood from the outset that disposal in very deep holes does not permit retrieval of wastes. Rather, it provides for disposal of radioactive wastes at the greatest depth below the surface and therefore, should represent the ultimate that can be achieved by geologic isolation. The very deep hole would also provide assurance that no climatic or surface change will affect safe and adequate disposal. The utility of the deep hole concept is affected by three factors, which depend upon the specific site characteristics and the size of the hole.

The first factor is the depth of the hole. How deep is deep enough for satisfactory isolation? In this context, very deep certainly means below depths where radioactive waste would be stored in existing underground mines or specially mined cavities. For example, at modest depths, say 1.5 km (5,000 ft), a mined storage cavity, with or without retrieval planned, would not be considered in contrast to irretrievable disposal in very deep holes. Whatever the depth, deep isolation requires that circulating groundwaters would not transport radioactive materials from the repository to the biosphere.

This consideration requires knowledge of the distribution of porosity (water content), permeability of rocks, and the occurrence of water with depth. In a general sense, the very deep hole concept will require depths within the earth's crust at which effective rock porosities and, therefore, water contents, are extremely small (a fraction of a percent), and rock permeabilities are exceedlingly low, probably in the ten to hundred nanodarcy range (10^{-12} cm/sec). In addition, the concept may also require depths at which temperatures, pressures, and hydraulic gradients, which tend to drive groundwaters towards the biosphere, are relatively weak. Available data from the literature--primarily from the oil and gas industry--suggest that rocks are porous and permeable to great depths, in excess of 9 km (30,000 ft), at least in sedimentary formations. Investigations of crystalline rock formations, although very limited, suggest that at much shallower depths, some formations have relatively low porosities and permeabilities. Hence, "very deep" for these crystalline rocks may mean one to a few kilometers instead of greater than 9 km as for the sedimentary formations.

In order to design a satisfactory isolation repository, the depth for a given site must be defined. This requires determining limits on the transport of radioactive materials to the biosphere using the rock properties of the proposed site and the heat-source configuration (waste packing) for the system. Once the depth has been determined, then our ability to make the hole to the required depth to accept the heat-source configuration for the system becomes the limiting factor. It is clear that the design parameters--making the hole and properties of the seal--must all be considered together. That is, the depth and heat-source configuration dictate how the hole can be made, which dictates the seal plug design, both of which effect the transport of radioactive materials.

The second factor is the need to establish our capability to excavate a very deep hole. Presently it is possible to drill a narrow deep hole to 10 km (35,000 ft) or to sink a wide shaft to about 4 km (15,000 ft). Whether or not the hole would have to be cased depends on the rock strength and confining pressures.

---

*Extracted from O'Brien et al. (1979).

†Terra Tek, Salt Lake City, Utah.

The third factor is the uncertainty of our ability to adequately seal the deep hole. This must include sealing the rock around the hole, which may have been affected adversely by making the hole. Oil-field practice routinely seals drillholes at great depth to prevent gas leakage; however, this sealing may not be adequate for radioactive waste.

System Uncertainties

The feasibility of the very deep hole cannot be assessed because our information is inadequate. This is not to say that the concept is not feasible, but at present, we cannot confirm that radioactive waste can be isolated deep enough--with practical heat-source configurations (packings) to avoid transport of radioactive material to the biosphere. The main uncertainty is the lack of information about porosity, permeability, and water conditions at great depths.

To remove these uncertainties, one or more very deep holes need to be drilled and extensive geophysical measurements made. Depending on the depths required, advancements in technology might be needed to drill, seal, or plug these holes. Geochemical uncertainties, as they would affect the generation and transport of radioactive materials, may be less important than the above considerations. If the heat-source configuration allows melting of the waste and surrounding rock, the reactions are more complicated. However, in all cases, the "great depth" is intended to isolate the waste and it is likely that geochemical uncertainties will not be the limiting criteria.

SUMMARY

Any feasibility analysis of the very deep hole concept beyond this study should be site-specific. In practice, the variations of rock porosity, permeability, and occurrence of groundwater with depth are extremely site-specific in nature. The ability to make and seal very deep holes will also be site-specific. Such a feasibility study should include analysis of geotechnical data from drilled holes at the prospective site--and laboratory evaluation of cores taken at depth. With the drilling of one or more very deep holes at selected promising sites, the feasibility of the very deep hole concept could be established.

REFERENCES CITED

O'Brien, M., Narasimhan, T. N., Simkin, T. L., Wollenberg, H. A. Green, S., and Pratt, H., 1979. The very deep hole concept: evaluation of an alternative for nuclear waste disposal. Berkeley, Lawrence Berkeley Laboratory, LBL-7089.

U. S. Department of Energy, 1979. Draft environmental impact statement: management of commercially generated radioactive waste. Washington, D. C., U. S. Department of Energy, DOE/EIS-0046-D (2 volumes).

GEOTECHNICAL ASSESSMENT AND INSTRUMENTATION NEEDS FOR NUCLEAR WASTE ISOLATION IN CRYSTALLINE AND ARGILLACEOUS ROCKS

M. T. O'Brien

INTRODUCTION

The Geotechnical Assessment and Instrumentation Needs (GAIN) Symposium offered a forum for analysis of nuclear waste issues from a broad range of scientific and engineering perspectives. The symposium was held on July 16-20, 1978, and arranged by Lawrence Berkeley Laboratory at the request of the U. S. Department of Energy (DOE).

A systems approach was used to develop the GAIN Symposium in order to integrate the ideas and information from the technical and engineering disciplines with the constraints and characteristics of nuclear waste. Figure 1 illustrates the interdependency of these technical parameters over time with the phase development of a hypothetical waste isolation system.

In view of the extensive research in the United States associated with disposal in salt, it is appropriate to accelerate assessment of other rock types. In recent years, granitic rocks, basalt, and shale have been considered (Schneider and Platt, 1974; Yardley and Goldich, 1975). Several European governments have initiated studies in crystalline and argillaceous rocks (ERDA, 1976). The report to the American Physical Society on Nuclear Fuel Cycle and Waste Management (1978) emphasizes the need to evaluate both salt and nonsalt rocks for waste disposal. The report states, "We conclude that at least one demonstration facility should be developed in a medium other than salt, preferably granite, and thoroughly evaluated before the decision is made to develop a facility into a full repository" (APS, 1978, p. S108). The Interagency Review Group (1978) confirms the need to investigate more than one rock type. It states, "Detailed studies of specific, potential repository sites in different geologic environments should begin immediately"(IRG, 1978, p. 26).

The objectives of the GAIN Symposium were to:

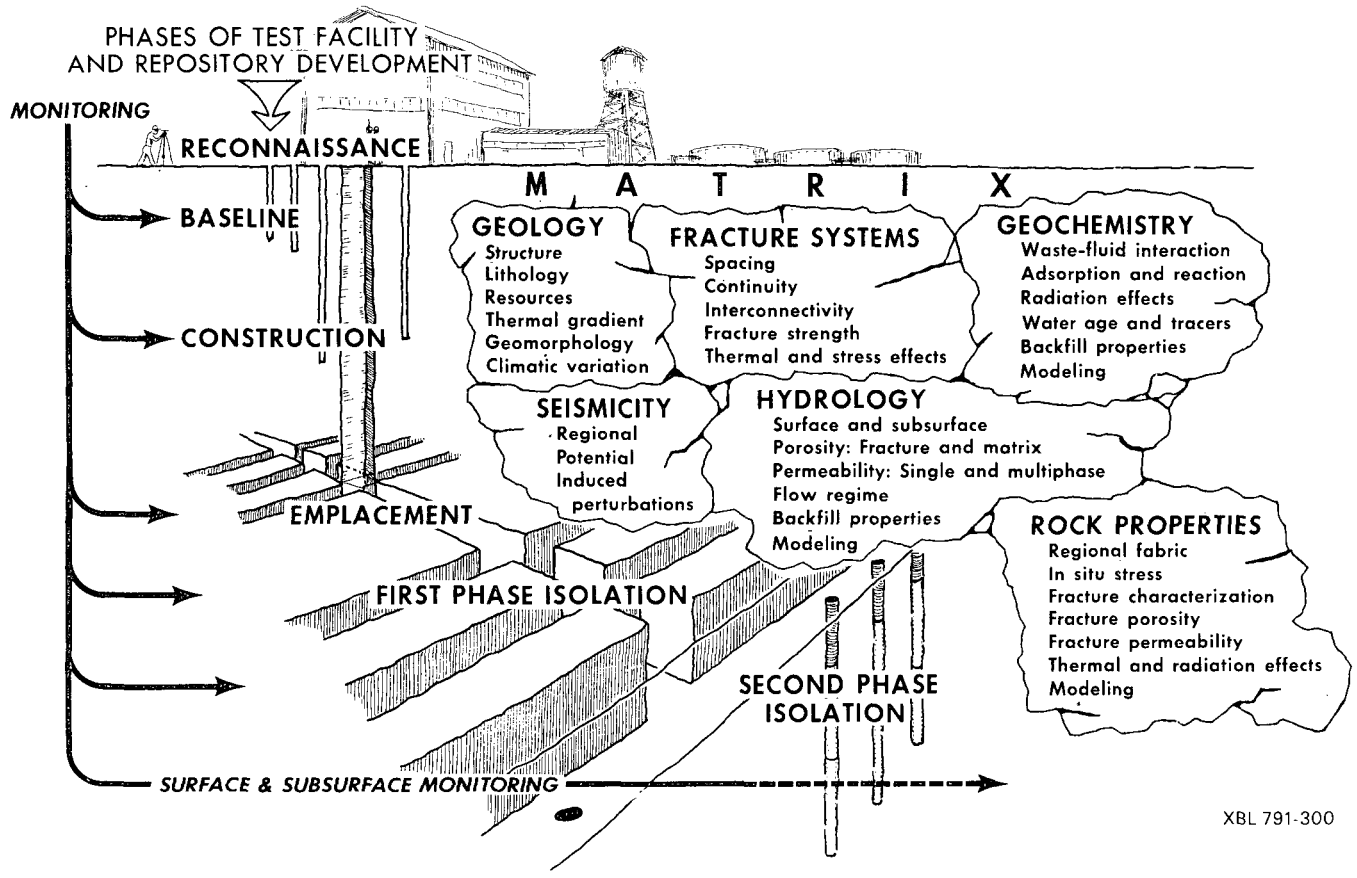

Figure 1. Geotechnical parameter matrix for full-scale nuclear waste disposal test facility and repository development.

- Establish the state of the art in nuclear waste isolation in crystalline and argillaceous rock
- Determine the factors to be considered in assessing waste/rock interactions
- Define the additional research needed before enough is known to evaluate each of these factors adequately
- Establish the particular research and development issues or projects that are of the highest priority
- Determine the instrumentation needs to measure the parameters used in site selection and development and establish priorities in developing the needed instrumentation

The philosophy of this symposium was that the host rock would be the primary container for wastes; however, some consideration was given to the "engineered barriers" such as backfill material, canister composition, and waste form. Determining the effectiveness of this "container system" for waste isolation depends upon knowing the properties of the host rock, the movement of interstitial water if it exists in fractures, the geochemistry of groundwater and, ultimately, interactions of waste with the surrounding rock. The symposium participants consequently formed panels in three interdependent areas: Rock Properties, Fracture Hydrology, and Geochemistry.

SYMPOSIUM RECOMMENDATIONS

All panels agreed that full-scale test facilities should be established in crystalline and argillaceous rocks in order to help engineers and geoscientists obtain experience with every aspect of disposal problems. Only within the past few years has attention been given to fluids in largely impermeable rocks; hence the body of knowledge and experience generated to date is relatively small.

Before we can have confidence in predictions regarding waste disposal in such rock masses, much more experience under field conditions is necessary. Test facilities should therefore be established as soon as possible in several rock types and geologic environments. Confirmatory testing will also be required at each actual repository. Several years of continuing site evaluation will probably be necessary, during which time the repository could be in operation before confidence in long-term containment is achieved. This requires that retrievability be

assured over along periods of time and not be limited by canister design, should predicted and actual rock-mass behavior diverge.

Rock Properties

The Rock Properties Panel recommended expanded research and development to maximize the ability to collect data from small-diameter (76-mm) boreholes. Some specific recommendations were: drilling techniques and fluids should be optimized to decrease disturbance and contamination; slim-hole tools should be developed to retain moisture and pore pressure in cores; surface tools should be evaluated and improved so borehole walls can be observed more accurately; and development of procedures for retrieving core should be continued so that joint apertures and other properties can be measured in the laboratory.

There is a need for a suite of slim-hole logging tools, particularly with regard to detecting fractures and evaluating their apertures, frequencies, and orientations. Almost all our experience in log interpretation is in the oil fields, in sedimentary rocks and with different types of fluids, and largely under different temperature regimes. Hence tools and methods to be used in crystalline rocks must be field-calibrated and tested in these and other rock types that may be considered for a repository.

The in-situ state of stress is of central importance to disposal siting because stress affects not only the mechanical stability of the repository, but the potential for deformation, seismic activity, and permeability changes along existing and new fractures. Overcoring and hydraulic fracturing are used to evaluate stress, the latter being the only technique presently used for significant depths in boreholes. Thus, research should be conducted on borehole stress measurements including methods of determining stress from a borehole that would represent a large mass of rock. Downhole tools that have stabilities on the order of a decade are needed for stress determinations at depths of 500 m or greater. The accuracy of the various methods of stress determination should be studied by working with large rock masses (e.g., 1-m cubes) under triaxial stress in the laboratory.

Both the Rock Properties and the Fracture Hydrology panels strongly recommended full-scale heating experiments in addition to the very few that have been and will be implemented. Full-scale experiments in a number of rock types are needed for fundamental data gathering, testing correlations and theories, and constructing and validating models. Full-scale experiments recommended by the Rock Properties panel would examine thermally induced deformation and changes in permeability, sonic velocity, thermal cracking, and electrical conductivity.

Modeling was discussed by all panels, and it was generally agreed that adequate techniques are available to construct models. However, the fundamental engineering and scientific knowledge to be incorporated into the models and to validate them under varied conditions is lacking. Individual models that are already available can handle fluid flow, heat transfer, mechanical behavior, and chemical reactions separately, but many of these have not been adequately validated. Higher-order models include effects of coupling between two or more of the above categories; several of these coupled models are available and are being constructed. Various experiments can be performed to test the accuracy of these models and verify whether or not adequate physics and chemistry have been incorporated to describe a given field situation. It was a consensus, however, that validation of models will remain in doubt until large-scale experiments have been conducted for at least five years and compared with simulation results. Until these are performed, it is uncertain how much additional work will be necessary to validate predictions of behavior in the far future.

Fracture Hydrology

The Fracture Hydrology Panel recommended a significant research effort to improve determination of fracture permeability in rock masses. Methods are needed for determining the hydraulic continuity of fractures and the effect of stresses (thermal, tectonic, and lithostatic) on aperture and permeability.

Only recently has consideration been given to the problem of in-situ measurements of fracture permeability in largely impermeable rocks. Laboratory and field tests are currently under way to determine fracture permeability by introducing a pressure transient in a borehole. One test is in progress to assay permeability in a mine opening by monitoring changes in the humidity of ventilation air. Determination of directional permeability is also in an initial stage of testing, and new techniques require further theoretical and instrument development. Determining the effect of stresses on fracture apertures and permeability is both a laboratory and field problem. It is also an area of research recommended by the Rock Properties Panel. Determining the hydraulic continuity of fractures is another problem that needs incisive, fundamental work.

Of particular importance in extrapolating laboratory data to field conditions is the assurance that the laboratory sample corresponds to a representative elementary volume of the rock mass. When examining fractured rocks, a representative elementary volume may be larger than current testing machines can handle, as suggested in a recent experiment. Both conceptual models and experimental investigations are therefore needed to allow confident extrapolation of laboratory data on fracture permeability to field occurrences.

Fracture volume, size distribution, and interconnection are important variables in estimating fluid velocity for travel-time computations and in estimating the void surface

area available for geochemical reactions. The panel concluded that no effective means now exist for directly measuring these properties, particularly in situ. Theoretical and experimental work should be encouraged, but the problem should also be approached by means of field tests employing tracers and radionuclides. Such field tests, which would be partially site-specific until enough was learned to generalize, were recommended by both the Fracture Hydrology and Geochemistry panels.

Geochemistry

Geochemistry is of importance in investigating the groundwater flow regime at potential depository sites; synthesizing the most refractory form of waste material; recommending the most effective plugging and backfill materials; and determining the results of chemical reactions between waste materials and the groundwater/rock system.

Much discussion in the Geochemistry Panel centered about the rock barrier--elucidation of the flow regime, sorption of waste products on fracture surfaces, and consideration of potential mechanisms such as colloid formation and organic complexing that might reduce or enhance the rock's effectiveness as a natural barrier. Geochemical reactions may slow radionuclide migration with respect to water flow and diffusion; if so, this extra safety factor should be known and incorporated into models.

Sorption of waste products by rock surfaces is only now being investigated. Continued intensive work is needed in this area, and it is very important that laboratory studies be designed so that their results will be useful in rigorous thermodynamic calculations. Kinetic factors in sorption experiments should also be carefully specified so that the data can be incorporated into models.

There is a general lack of information on the behavior of the actinide aqueous and solid species that are important in dissolution of waste forms and in groundwater transport processes; there is also a dearth of information on the potential for actinides to form colloids in groundwater. Recent work suggests that actinides may form complexes with organic materials that naturally occur in groundwater; this important topic also needs much further investigation.

Once this body of thermodynamic and kinetic data becomes available, it will be incorporated into models and results compared with field radionuclide and tracer tests to provide model validation.

Major instrumentation needs are techniques for measuring dissolved aluminum, better methods for contamination-free drilling and sampling, and stable and long-lived borehole electrochemical sensors. The panel also recommended that an additional groundwater dating technique be developed to confirm ^{14}C dating.

Three publications were prepared as a result of GAIN symposium. They are:

1. An Appraisal of Underground Radioactive Waste Disposal in Argillaceous and Crystalline Rocks: Some Geochemical, Geomechanical and Hydrological Questions, J. A. Apps, N. G. W. Cook, and P. A. Witherspoon (June 1978, LBL-7047).

2. Instrumentation/Measurement Techniques and Philosophies for Nuclear Waste Repositories, William Hustrulid (May 1978, Pub. 246).

3. Geotechnical Assessment and Instrumentation Needs for Nuclear Waste Isolation in Crystalline and Argillaceous Rocks: Symposium Proceedings, July 16-20, 1978 (LBL-7096).

REFERENCES CITED

American Physical Society, 1978. Report to the APS by the study group on nuclear fuel cycles and waste management. Reviews of Modern Physics, v. 50, no. 1, Part II, 186 p.

Interagency Review Group, 1978. Report to the president by the Interagency Review Group on nuclear waste management (draft). U. S. National Tech. Info. Serv., TID-28817.

Schneider, K. J., and Platt, A. M., eds, 1974. High-level radioactive waste management alternatives. Richland, Battelle Pacific Northwest Lab., BNWL-1900.

U. S. ERDA, 1976. International Symposium on the Management of Wastes from the LWR Fuel Cycle (1976), proceedings. U. S. Energy Research and Development Administration, CONF-76-0701.

Yardley, D. H., and Goldich, S. S., 1975. Preliminary review of Precambrian shield rocks for potential waste repository. Oak Ridge, Office of Waste Isolation, Y/OWI/SUB-4367/2.

GEOHYDROLOGICAL STUDIES FOR NUCLEAR WASTE ISOLATION AT THE HANFORD RESERVATION*

J. Apps, T. Doe, B. Doty, S. Doty, R. Galbraith, A. Kearns, B. Kohrt, J. Long, A. Monroe, T. N. Narasimhan, P. Nelson, C. R. Wilson, and P. A. Witherspoon

INTRODUCTION

A study of the Pasco Basin near Richland, Washington, was initiated by Lawrence Berkeley Laboratory for Rockwell Hanford Operations during fiscal year 1978. This work was part of a long-term study conducted by Rockwell's Basalt Waste Isolation Program for the National Waste Terminal Storage Program of the U. S. Department of Energy, on the feasibility of nuclear waste disposal in the Columbia River basalt underlying the Hanford Reservation.

The Hanford Reservation lies within the Pasco Basin near the center of the Columbia River flood basalt physiographic province, which spans parts of Washington, Oregon, and Idaho (Figure 1). The overall feasibility study has been directed to the concept of a mined repository at a depth of about 3,000 ft, possibly in the Umtanum Unit--a dense 200-ft-thick basalt flow. The feasibility of this concept largely depends on the degree of hydrologic isolation afforded by the basalts. Hydrologic isolation can be determined only by actual field testing and subsequent modeling.

In October 1977 a work plan was formulated which included three hydrologic subtasks: physical testing, geochemical sampling, and numerical modeling. Progress on these three subtasks through September 1978 is reported here. In addition to these subtasks, an analysis of existing geophysical data is summarized here. Hydrologic work by LBL ceased at the end of fiscal year 1978.

A physical testing program designed to provide hydrologic information for mathematical modeling of the deep basalts in the Pasco Basin was initiated in fiscal year 1978. LBL performed hydrologic testing on several deep drillholes on the reservation and obtained and analyzed water samples from drillholes and surface water. A technical approach was developed for obtaining and integrating the hydrological, geophysical, and geochemical data required for modeling. A field program oriented toward the collection of needed data was then initiated. A full testing program was planned for implementation over a period of several years. Included in this program were: pressure measurements to determine hydraulic potential gradients; tracer tests to determine flow direction and velocity; geochemical sampling of wells and surface waters; borehole fracture logging to quantify the geometric parameters of the fracture systems; hydraulic fracturing to determine in-situ stress conditions; a wide variety of permeability tests on both multiple and single fractures; and development of a multipoint piezometer for long-term pressure monitoring in wells.

FISCAL YEAR 1978 ACCOMPLISHMENTS

Hydrology Field Program

During fiscal year 1978, LBL designed downhole instrumentation and packer systems for pressure, temperature, and permeability testing. Pressure measurements at depths of less than 3,000 ft were made with a packer-mounted probe containing a single pressure and temperature sensor with no downhole packer release. A second tool was designed to operate at greater depths and do injection tests as well as pressure measurements. This tool included downhole solenoid valves to deflate packers and to bleed the test cavity of pressure pulses due to packer inflation, and an extra pressure transducer for monitoring packer pressure.

Pressure testing was performed in wells DC-2, DC-6, and DC-8 and permeabilities were estimated from artesian flow in DC-6. Figure 2 shows the location of these wells within the Hanford reservation.

Well-DC-2. Well DC-2 is a 3,300-ft-deep hole drilled about 40 ft from well DC-1, a 5,661-ft hole. Five standpipe piezometers were installed in DC-1 in 1972 and water levels have since been measured periodically.

Pressure measurements were made in 11 zones in DC-2 between depths of 2,269 and 3,273 ft. The LBL test data, shown on Figure 3, appear to indicate that the vertical component of hydraulic gradient is sharply downward over the interval tested. Comparison with open-hole data, however, showed that a close correlation exists between the falling water level in the well and the test zone measurements. This influence is thought to result from either vertical circulation of water through the formation or from residual effects of formation prepressurization, which occurred when the well was filled for cleaning before testing. The tests were continued until the effects of the packer inflation pulse were essentially dissipated. However, time constraints did not permit the longer-term testing periods that would have been required for complete dissipation of the overpressure induced by packer inflation and by well cleaning in the lower-permeability test zones. Increased testing times and sophistication of equipment will be required to determine the degree to which wellbore pressurization and the vertical permeability affect test results in well DC-2.

*Extracted from Apps et al., 1979, Executive Summary.

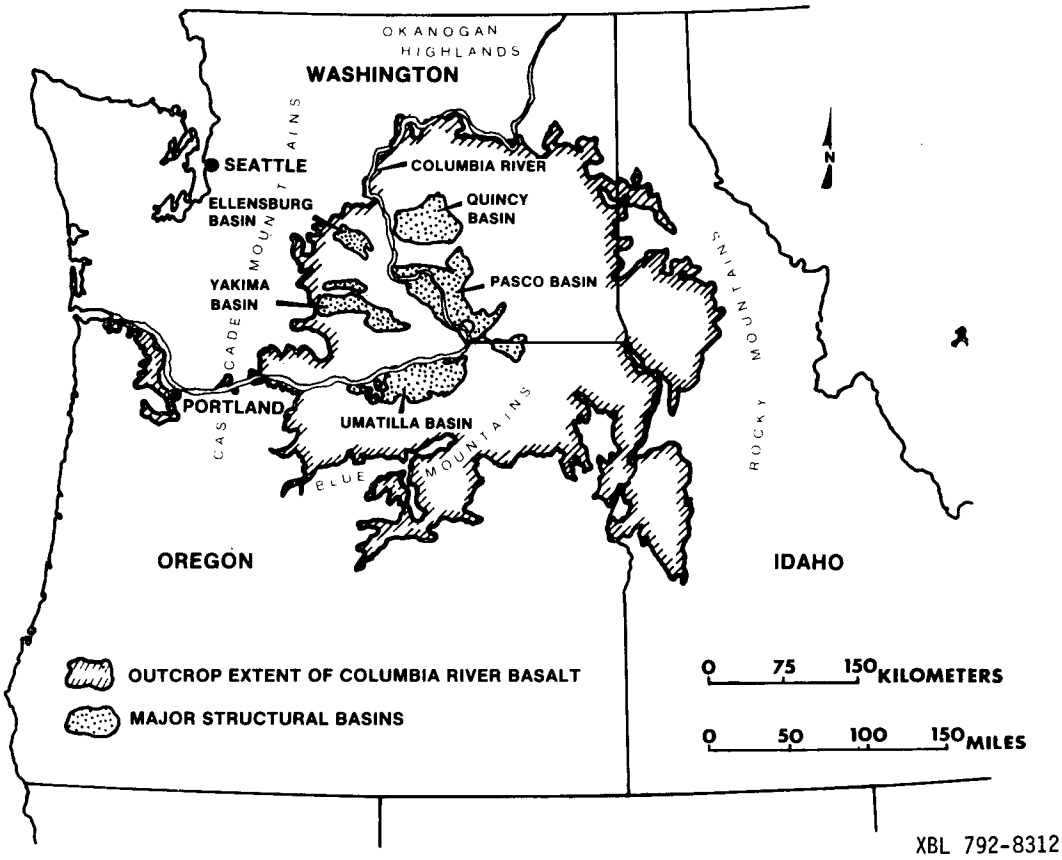

Figure 1. Location map of the Columbia River basalt (after Rockwell International, 1977).

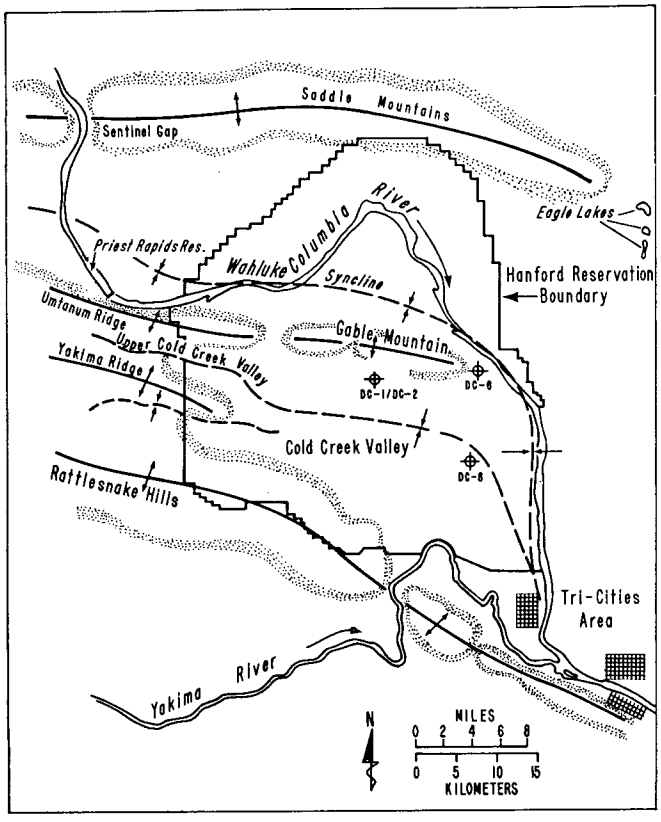

Figure 2. The Pasco Basin, Washington.

The open-hole water level in DC-2 fell throughout the test period and was at an elevation of about 360 ft when the tests were concluded. This indicates that the minimum natural formation head within the open part of DC-2 is equal to or less than 360 ft elevation. Figure 3 also shows pressure measurements made by LaSala and Doty (1971) in well DC-1 before the piezometers were installed, and piezometer levels in well DC-1 at the time of testing in DC-2. Based on these data and on observed dynamic changes in DC-1 due to swabbing in DC-2, we conclude as follows:

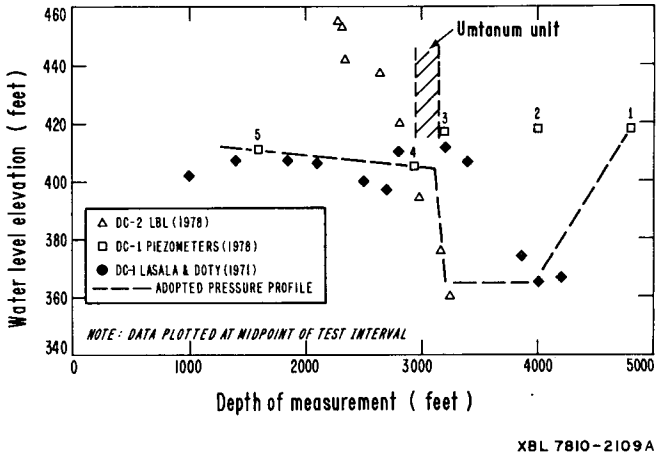

Figure 3. Pressure measurements in wells DC-1 and DC-2.

1. Piezometer 2 and 3 readings are erroneously high because of vertical flow through leaks in the cement seals in well DC-1 from a high-pressure zone deeper than piezometer 2.

2. The true formation pressure head elevation at the depth of piezometers 2 and 3 is on the order of 360 ft.

3. Piezometers 4 and 5 appear to be adequately isolated from the rest of the well.

4. A downward pressure gradient apparently exists from at least the depth of piezometer 5 (2,000 ft), passing through the Umtanum Unit.

5. An upward pressure gradient apparently exists from at least the depth of piezometer 1 (4,800 ft) to approximately the depth of piezometer 2 (4,000 ft).

6. The Umtanum Unit appears to be acting as a partial barrier to vertical flow.

Well DC-8. Pressure testing was performed in well DC-8 at nine zones between depths of 1,710 and 2,700 ft, with a constant packer interval of 30 ft. Open-hole measurements were made immediately before packer inflation and after packer deflation. Filling the wellbore during testing resulted in considerable variations in open-hole water level during the early part of the testing period. The lowest water elevation recorded during the test period was an open-hole head elevation of 413 ft. This measurement indicates that the formation pressure head within some part of the open portion of the well is at least as low as 413 ft. Data collected in well DC-8 are shown in Figure 5.

The tests generally appear to be less influenced by open-hole pressure than in DC-2, perhaps indicating a lower vertical permeability at well DC-8. A downward gradient was measured within the depth range of 1500 to 2100 ft. Based on extrapolation of this gradient, the minimum pressure head of 413 ft would occur at a depth of about 2,300 ft.

Well DC-6. Well DC-6 is artesian and was flowing at a rate of about 17 gpm at the time of testing. The first artesian zone was encountered during drilling in March 1978 between 2,300 and 2,710 ft, and additional artesian flows were encountered as the hole was deepened.

Water pressures were measured in 15 zones between 2,240 and 4,336 ft of depth. Artesian discharge from the well was measured in 12 zones between 2,483 and 4,336 ft, and permeabilities were computed for these zones. The groundwater pressure, flow, and permeability data are shown in Figure 4.

All pressure measurements indicate artesian heads above the elevation of the hole collar, hence all test zones are contributing to the flow from the hole. Between depths of 2,240 and 3,055 ft the pressure heads average about 450 ft. The scatter in the data does not allow reliable definition of either an upward or a downward gradient. Below 3,055 ft, heads decline reaching a local minimum elevation of approximately 430 ft in a water-producing zone about 3,700-ft deep. An increase in head below

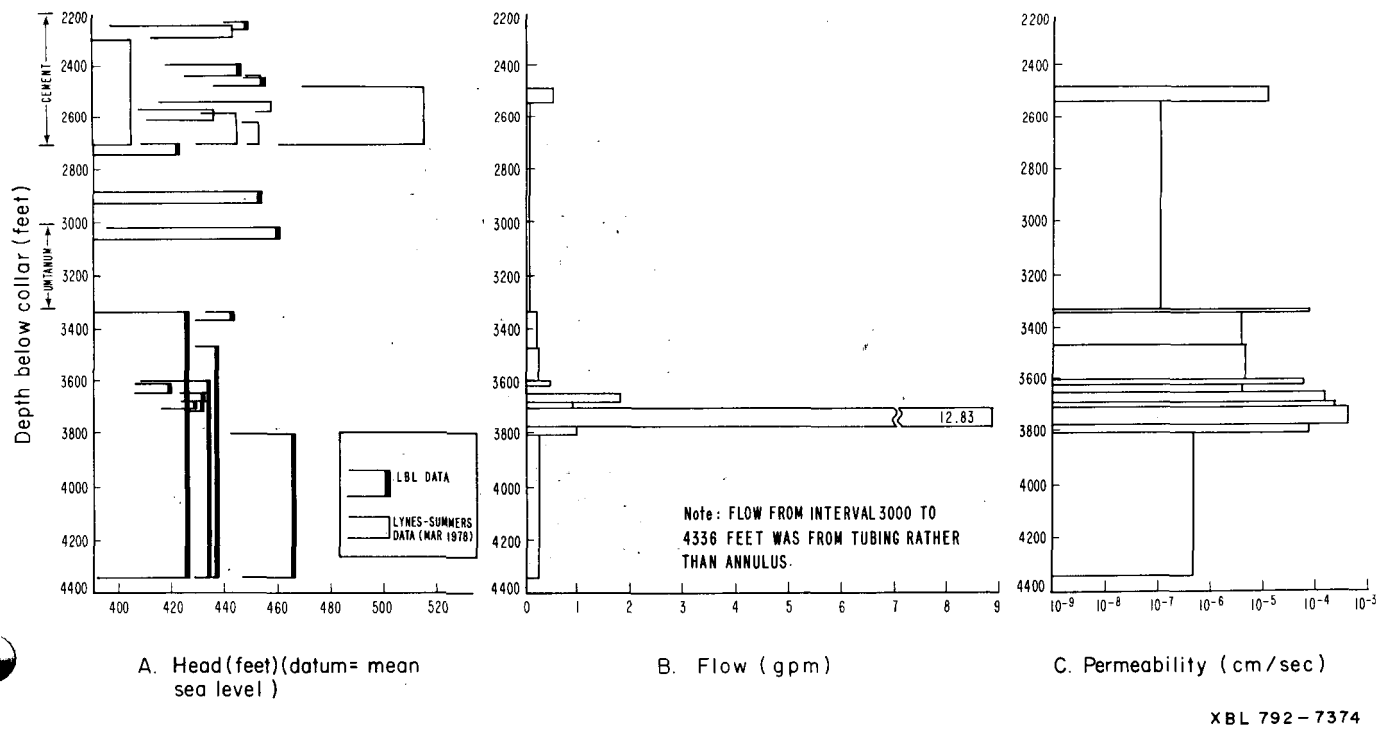

Figure 4. Water heads, flow rates, and permeabilities in well DC-6.

3,700 ft is shown by the head of 446 ft recorded for the zone between 3,802 and 4,336 ft. There is generally good agreement between the heads measured by Lynes and W. K. Summers Associates in March 1978 and the values determined by LBL (see Figure 4A).

The most prolific flowing zone yeilded about 70% of the total flow and occurs between depths of 3,692 and 3,769 ft, as shown on Figure 4B. This zone was logged as a highly altered flow breccia. Flows on the order of 1 gpm were also measured from similar breccia zones between 3,650 and 3,692 ft.

Permeabilities were estimated using the assumption of steady radial flow. The results are shown in Figure 4C and represent the average for the zone tested. The largest permeabilities were on the order of 10^{-4} cm/sec, measured in the zone between 3,650 and 3,800 ft. This zone is about 400 ft below the Umtanum Unit. The lowest average permeabilities were on the order of 10^{-7} cm/sec, measured in and above the Umtanum Unit.

Comparison of pressure results. The results of pressure measurements in wells DC-1/DC-2, DC-6, and DC-8 are shown in relation to stratigraphy on Figure 5. These data show a downward gradient between the Vantage interbed and the Umtanum Unit in DC-1/DC-2. The gradient is poorly defined, however, in the same zone in DC-6. DC-8 shows a downward gradient between the Mabton and the Vantage interbeds. Head elevations reach a local minimum in DC-1/DC-2 and DC-6 about 300 ft below the bottom of the Umtanum and there is evidence that gradients may be upward below that depth. The low-pressure zone encountered below the Umtanum would act as a drain for any vertical flow coverging upon it, thus the recharge and discharge areas of this zone are of great interest.

Pressure data for the zone immediately below the Umtanum are presently available only for wells DC-1/DC-2 and DC-6. Wells DC-1/DC-2 are in the northern flank of Cold Creek Valley syncline, formed between Gable Mountain anticline to the north and Rattlesnake Hills anticline to the southwest (see Figure 2). The water-level elevations measured in and below the Umtanum unit in DC-1/DC-2 range from 395 to 362 ft. The only part of the Pasco Basin with lower elevations that would serve as a discharge area is the Columbia River bed and adjacent lands from the Tri-Cities area to Wallula Gap. The most likely flow path from DC-1/DC-2 to this discharge area is through Cold Creek Valley.

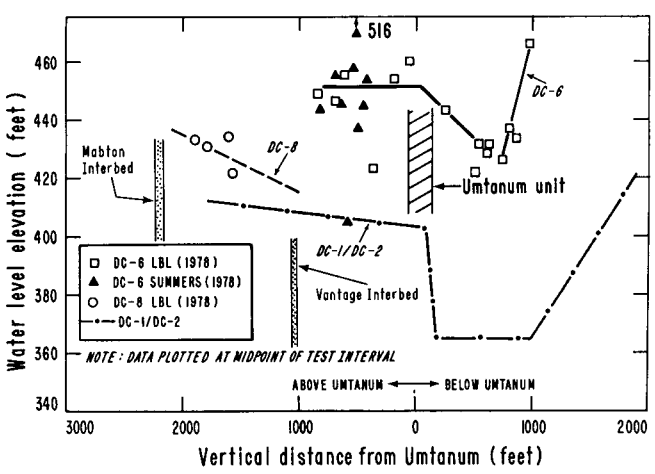

Figure 5. Summary of pressure measurements.

Pressure head elevations measured in well DC-6 in and below the Umtanum Unit range from 421 to 466 ft. The relatively low pressures measured in the deep basalts in Cold Creek Valley and the higher pressures measured in DC-6 suggest higher water tables to the north and east of DC-6. The most likely source of recharge for these high heads is the Columbia River from Sentinel Gap to Priest Rapids Reservoir. The basalt units beneath the Umtanum are at or near the ground surface in this area, and the river is a source of abundant volumes of water. The most likely flow path to well DC-6 from this potential recharge area would be along the Wahluke syncline, a structural and topographic valley between Gable Mountain/Umtanum Ridge anticline, and the Saddle Mountain anticline. Other potential rechange areas, such as the Saddle Mountains or the Eagle Lakes/ Scooteney Reservoir area to the northeast of DC-6, are either relatively dry or do not have outcrops of the Umtanum and underlying units. They are therefore less likely to be primary recharge areas.

The pressure data and recharge hypotheses for the deep basalts at DC-6 imply that water pressures throughout the Wahluke syncline are substantially higher than those measured in Cold Creek Valley at well DC-2. Such a difference would suggest the existence of a barrier to groundwater flow in the general vicinity of the Gable Mountain/Umtanum Ridge anticline. This hypothesis is supported by a lack of likely recharge areas for the Umtanum and underlying units in the vicinity of Cold Creek Valley. Gable Mountain on the north side of the valley is low and provides essentially no recharge. The Yakima Ridge area to the east of the valley and the Rattlesnake Hills to the south rise to elevations of several thousand feet, but like the Saddle Mountains, are relatively dry. Further, the Umtanum Unit is at least 1,000 ft deep in all of these areas. Some underflow in the deep basalts may be occurring through structural valleys paralleling Yakima Ridge, but as noted by Newcomb et al. (1972, p. 32), the high heads found in a number of deep artesian wells near the western boundary of the Hanford Reservation suggest the presence of a second flow barrier cutting across these structural valleys. The presence of relatively high heads at Juniper Springs and Rattlesnake Spring versus the relatively low heads measured in DC-1/DC-2 supports the assumption of an additional flow barrier. The possible existence of these flow barriers is of significant interest in repository siting and should be investigated further.

Comparison of flow data. Radioactive tracer and temperature logs in well DC-1 have indicated three zones of relatively high permeability at depths of 3,228 to 3,234 ft; 3,972 to 3,980 ft; and 4,824 to 4,854 ft. The average permeability of these zones is 9.4 x 10^{-4} cm/sec. The first two of these zones are 50 and 794 ft below the bottom of the Umtanum Unit.

In well DC-6 the major flowing zone has a permeability greater than 10^{-4} cm/sec and occurs between depths of 3,650 and 3,700 ft, which is 442 ft below the Umtanum. There are likely to be, in addition, other zones with permeabilities greater than 10^{-6} cm/sec between the bottom of the Umtanum and the high permeability zone at 3,650 ft, but the large spacing between packer settings in the LBL flow tests did not allow better definition of the exact location of these higher-permeability zones.

Comparing the data for the two wells, it is clear that the most permeable zones encountered are below the Umtanum, but these zones do not appear to occur at the same stratigraphic levels relative to the Umtanum Unit in the two wells. The similarity of geochemical stratigraphy for the two holes suggests that these permeable zones may be occurring at different basalt flow contacts. The extent to which these zones may be hydraulically interconnected through a continuous weathered horizon, through faults, or through primary fractures will be important to radionuclide migration from a repository and should be the subject of further studies.

Pasco Basin Modeling

The Pasco Basin hydrology modeling effort had three products: a literature survey, a recommendation for a well drilling and testing program; and a series of numerical solutions for use in designing hydrologic field tests such as pump tests and leaky aquifer tests, where wellbore storage is significant.

Literature survey. The literature survey was undertaken to help define such flow model inputs as boundary conditions, initial conditions, geometry as defined by structural geology, and material properties. The system boundaries are apparently complex and irregular. The groundwater flow system is further complicated by numerous folds and faults and basalt flows of variable continuity. Although primary porosity may be important locally, by and large the flow paths are governed by fractures of widely variable pattern (horizontal, columnar, etc.) and spacing. The system is probably characterized by time-dependent boundary conditions and a variable, three-dimensional distribution of fluid potentials.

Such input data will always be accompanied by uncertainty and hence the simulation results will also be uncertain. A limitation of the current LBL models is that they all are intrinsically deterministic. Because the flow system parameters cannot be known with certainty, confidence limits on the potential rage of system response must be provided for the decision-making process. The LBL models would therefore be improved by the accomodation of statistically expressed input and output parameters indicating the distribution of possible system responses. Further work on the development of such models is recommended to permit adequate risk assessment of repository safety.

Well drilling and testing program. Based on the results of the field work, the literature survey, and the input requirements, a well drilling and testing program was developed for further study of the Pasco Basin. In order to provide an overview of the regional flow system, six first-stage wells, DC-12 through DC-17, were proposed (Figure 6). These wells, when combined with existing wells, are designed to provide sufficient information to indicate the origin, flow paths, velocities, and disposition of groundwater within the basin on a gross scale.

Well DC-12 would be in the center of the basin. This well would provide data for determining gradients in several directions within the basin. Well DC-13 is in the "horn" of the Columbia River. This well would help to determine the hydrologic significance of the Saddle Mountains boundary and the influence of the Columbia River on the deep flow system. It would also provide an important data point in

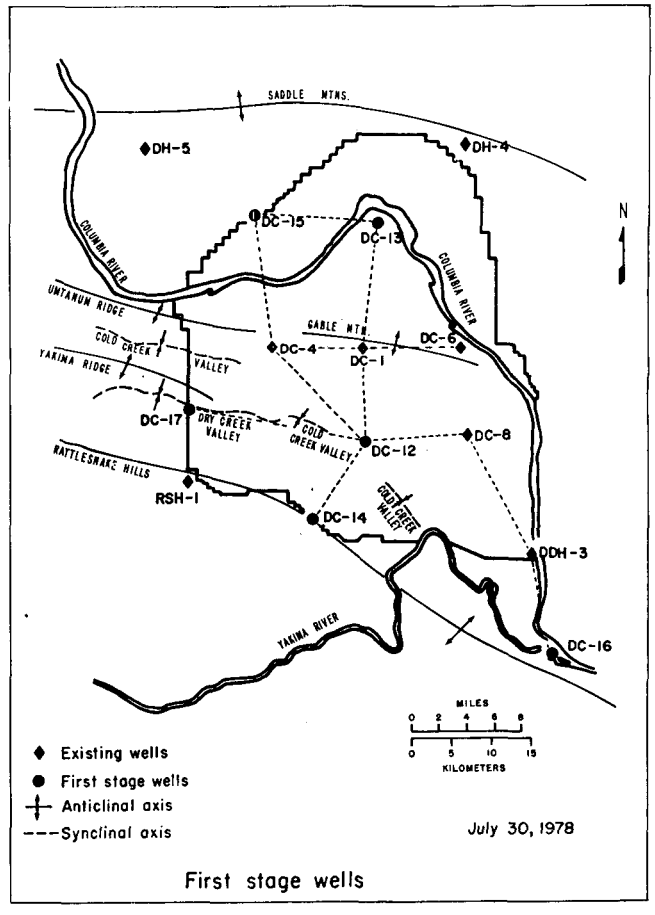

XBL 794-9411

Figure 6. Proposed first-stage wells.

the Wahluke syncline. The role of the Rattlesnake Hills as a recharge zone in the basin needs to be investigated. Well DC-14 would provide information on the extent of this recharge and the possible existence of perched waters. The southwestern boundary of the basin can also be examined.

Well DC-15 would be drilled to examine the extent of recharge from the Sentinel Gap area. The area is important because basalt flows, which lie deep under the center of the basin, crop out at Sentinel Gap. This well, in conjunction with DC-4, will also help determine the direction of deep groundwater flow between Cold Creek Valley and the Columbia River valley. In conjunction with DC-13, well DC-15 will enable an examination of deep flow systems along the Wahluke syncline.

If the rough analysis of groundwater flow patterns seems favorable for siting a repository, these wells will provide a basis for locating second-stage wells that may be necessary for a more detailed analysis of the flow system.

Wellbore storage effects. Pumping tests were planned for several wells on the reservation. Due to the low rock permeability, it was feared wellbore storage (Papadopoulos and Cooper, 1967) would affect the test results, hence numerical analyses were made of two antieipated wellbore storage problems. The first problem was to describe the response of an observation well in a pumping test where wellbore storage was significant. The second problem was to see how wellbore storage would affect the data collected in a leaky aquifer test. The LBL groundwater flow program TERZAGHI was used for both problems.

In the first analysis, dimensionless drawdown curves were obtained for values of dimensionless storage parameter, α, of 10^{-1}, 10^{-2}, 10^{-3}, 10^{-4}, and 10^{-5}. A sample is shown in Figure 7. The curves approach the Theis solution with decreases in radius of the well and increase in α. The time necessary to obtain a response in the observation well increases with an increase in wellbore storage effect.

For the problem of leaky aquifer response with wellbore storage, 15 cases were analyzed for times up to 100 days, comprising three different pumping well radii (0.05, 0.09 and 0.1125 m) and five values of α (10^{-1}, 10^{-2}, 10^{-3}, 10^{-4}, and 10^{-5}). A sample of results is plotted in Figure 8 showing the ratio of drawdown in the aquitard (s') to drawdown in the aquifer (s) as a function of wellbore radius. Completed drawdown with wellbore storage can be as little as half the drawdown predicted without wellbore storage.

Figure 9 shows the time it would take to get a drawdown, s', in an aquitard 9.0 m from a pumping well and 0.5 m from an aquifer. The parameters and geometry used are typical of what might be found in the Pasco Basin. At least 15 days of pumping would be required to get any measurable response in the aquitard for these conditions. This model could be used for well test analysis by developing a set of type curves for any specific well radius and distance to an observation well.

Groundwater Chemistry Program

The sampling and analysis of groundwaters for the Pasco Basin was initiated as part of the LBL Hanford Waste Isolation Project. Comprehensive chemical and isotopic analyses of 36 deep well samples, 20 spring samples, and 9 duplicate samples were planned. The chemical analyses were made to provide information that would permit determination of the source, history, and age of the waters of the Pasco Basin. This information, when used in conjunction with hydrologic data and regional hydrologic simula-

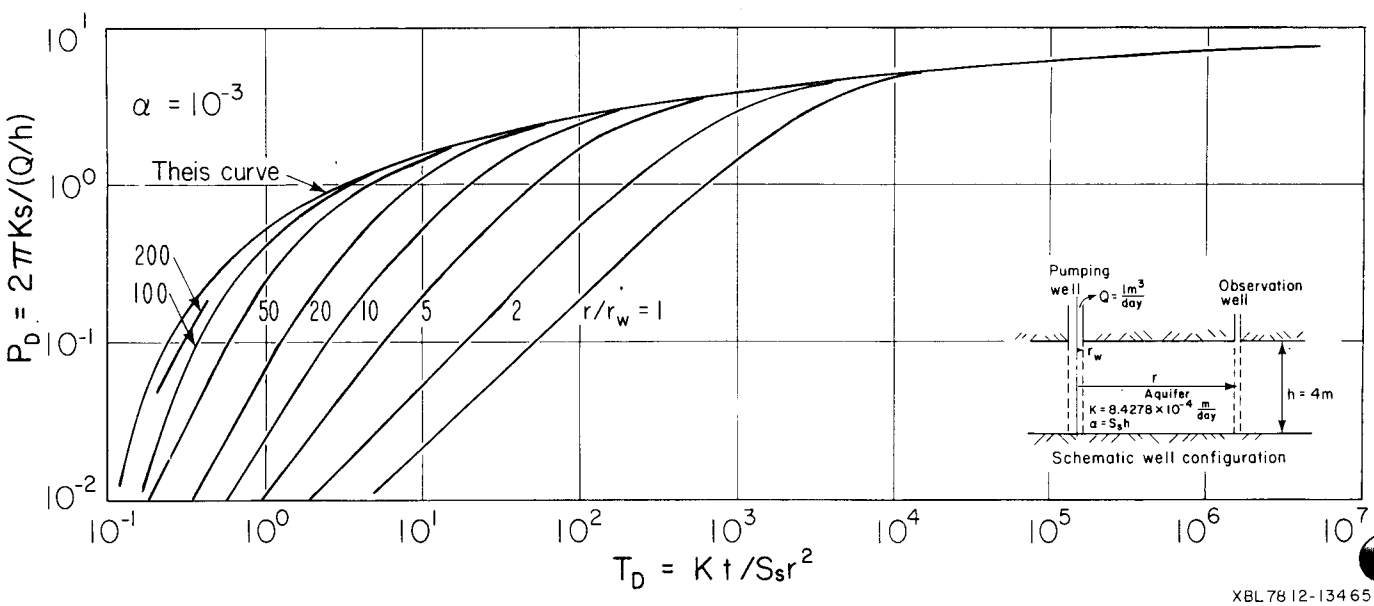

Figure 7. Drawdown in an observation well with wellbore storage in the pumping well, $\alpha = 10^{-3}$.

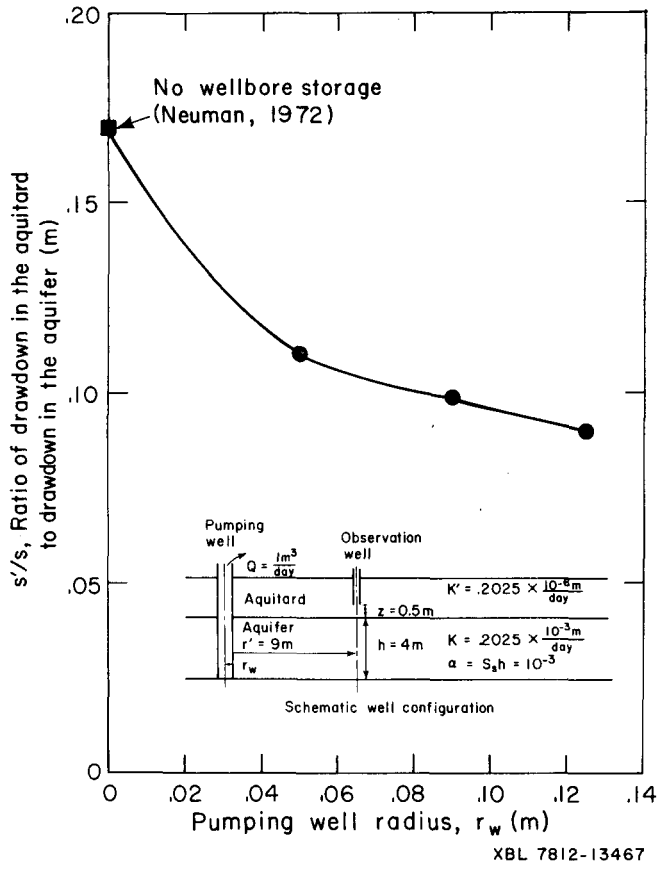

Figure 8. Ratio of drawdown in the aquitard to drawdown in the aquifer (s/s') at r = 9 m, as a function of pumping well radius at t = 100 days, $\alpha = 10^{-3}$.

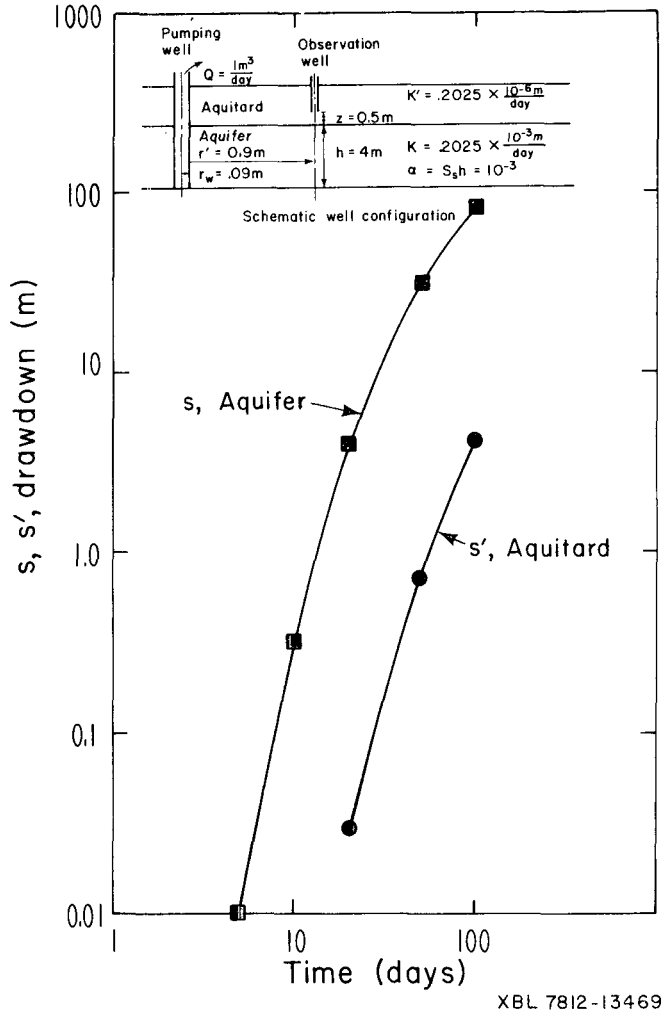

Figure 9. Drawdown as a function of time for $\alpha = 10^{-3}$, $r_w = 0.09$ m.

tions of groundwater movement, was expected to provide the basis for predicting the rate and type of chemical evolution of the groundwaters during flow. Such an evaluation is a necessary prerequisite for quantitative predictions of radionuclide migration in the same environment.

Previous studies of deep groundwater chemistry in the Pasco Basin are for the most part limited to those by La Sala and Doty (1972), who gave evidence that sampling deep well waters without contamination from extraneous sources would be both difficult and time consuming. Earlier drilling activities in the Pasco Basin by Fenix and Scisson Inc. also indicated a minimum of these zones between 2,888 and 3,392 ft, which appeared to justify further investigation of locations for mined caverns. Aquifers adjacent to these zones were considered the prime target for investigation.

The chemical analyses planned for the groundwater samples included all major cationic and anionic species as well as trace elements, gas analyses and on-site measurements of those species or properties that were likely to change during transport. The purpose of these analyses was to allow comparison with the compositions and thermodynamic stabilities of coexisting alteration products, to make internal checks on the validity of the analyses, and to permit estimation of the sources and the relative ages of the groundwaters. Trace elements were to be tested for their value as tracers for given aquifer waters or horizons.

A number of stable and radioisotopic analyses were also planned, including those for D/H, $^{18}O/^{16}O$, $^{13}C/^{12}C$, $^{34}S/^{32}S$, ^{3}H, ^{14}C, ^{36}Cl, ^{222}Rn, ^{226}Ra, and $^{238}U/^{234}U$. Each of these isotopic analyses contributes to an interpretation of the source, temperature, history, or age of the groundwater. Some of the isotopic measurements have been difficult either to measure or to interpret. Consequently, part of the study was directed toward elucidating the problem associated with the use of ^{36}Cl and $^{238}U/^{234}U$ as tools for dating groundwaters.

Because of the requirement for on-site analysis of fugitive components, separation procedures for isotopic analyses, and the filtration of samples, LBL staff recognized the need for adequate laboratory services readily acces-

sible from the sampling site. A mobile field laboratory was therefore designed and constructed to perform all necessary on-site analyses and sample preparation. An 8x20-ft box trailer was leased for this purpose and adequate facilities for two chemists were provided. The mobile laboratory proved to be very satisfactory from the functional standpoint, but some logistical problems were encountered in transportation.

The complex sampling requirements for each of the several analytical and isotopic techniques involved in the study necessitated standard operating procedures for quality assurance documentation. These procedures became the focal point of organizing and finding the latest and most desirable methods for sampling, treating, and packaging groundwater. Several meetings were held with leading isotope and chemical analysts in order to bridge the gap between analytical expertise and field sampling methodology. These meetings, combined with an exhaustive literature survey of groundwater sampling, resulted in a draft of Field Operating Procedures for the groundwater chemistry part of the Hanford Waste Isolation Project (Kearns, 1979). This document included procedures for both well and spring sampling. Improvements were incorporated as field experience was gained.

On January 30, 1978, a meeting was held among Rockwell Hanford Operations, LBL, and other interested parties to develop the field program. Between then and June 14, 1978 (when swabbing of DC-2 started), isotope and analytical chemists were committed to provide support for the project, a Quality Assurance Manual was prepared, and the mobile field laboratory was designed, constructed, and equipped. Sampling and refinement of field procedures continued with occasional interruptions until August 16, 1978, when field work was terminated.

Groundwater samples from deep wells were obtained by swabbing, because no other technique had been developed that would permit recovery of large samples from the depths specified in the narrow-diameter wells available for sampling. Only well DC-2 was sampled, from the zone between 3,243 and 3,273 ft. In the short time available for sampling, it was not possible to pump enough water to obtain a sample that was free of contamination by diesel oil.

Springs were identified from topographic maps, and chosen for sampling after a discussion with Rockwell geologists. Only those springs that issued directly from bedrock were sampled--a total of four. Access to the spring sites was difficult and required four-wheel-drive vehicles. Three artesians wells (DC-6, Ford, and McGee) and the Columbia River were also sampled using techniques similar to those developed for spring samples. Chemical and isotopic analyses were performed on the nine samples collected. The chemical analyses covered most of the elements and aqueous species originally specified. Analyses of some minor components were not performed, primarily because the project was terminated before the work could be completed. However, all major components were analyzed. In many cases different analytical methods were used to measure the same component, thus providing checks on the accuracy of the values obtained. Cation/anion balances were performed on major components ($\geq$1% TDS) of the solutions. In all cases except one, the discrepancy between total cation and anion equivalents was less than 5%.

The major components and some important minor components in solution were used as input to the distribution of species stage of the FASTPATH code, and checks were made on the internal consistency of pH, alkalinity, Eh, sulfide/sulfate, carbonate/bicarbonate, and $SiO(OH)_3^-/Si(OH)_4$. With minor exceptions, results were good. Isotopic analyses for D/H, $^{10}O/^{16}O$, and ^{3}H were also determined, However, $^{13}C/^{12}C$, $^{34}S/^{32}S$, and ^{14}C analyses were not performed because of problems with the procedure used to separate carbonate from solutions.

Analytical development of isotope measurement techniques using the 88-Inch Cyclotron at LBL demonstrated the feasibility of measuring ^{14}C in CO_2 evolved from one liter samples. The detection of ^{36}Cl was also attempted, and a limit of 10^{-12} for the $^{36}Cl/^{35}Cl$ mass ratio was achieved with possibilities of improvement using a new ion source. Measurement of the $^{234}U/^{238}U$ ratios on the water samples is continuing using a 5-ft-radius, high-precision mass spectrometer. A precision of about 2% is expected for the $^{234}U/^{238}U$ ratio.

The deep waters of the Pasco Basin (i.e., the waters from DC-2 and DC-6) are dilute chloride-bicarbonate waters of high pH (~10) containing significant quantities of fluoride (20 to 40 ppm) and silica (up to 150 ppm). Important minor components such as Mg, Ca, Fe, and Al are present in very low concentrations. Dissolved gases, particularly the rare gases, are also present in low concentrations. The compositions of the spring waters are typical of waters from basaltic terrains.

An evaluation of the chemical analyses in terms of their origin, history, and age is not possible because of the small number of samples taken, the incomplete isotopic analyses, and the diversity of regimes from which the samples were obtained. No spatial relations between samples can be worked out until more samples have been obtained and analyzed, over more horizons, and over a greater areal extent of the Pasco Basin. However, the work done to date leads to the following recommendations.

1. Because of the low concentration of many important components in the deep waters of the Pasco Basin, great care should be taken to avoid contamination both during and after sampling.

2. Development of improved isotopic techniques requiring smaller samples should continue; this applies particularly to ^{14}C, ^{36}Cl, ^{81}Kr, and $^{234}U/^{238}U$.

3. A more sensitive technique is needed for analyzing aluminum in solution particularly

in the presence of large amounts of fluorine ion.

4. More sensitive gas detection and analysis techniques should be developed.

5. Downhole sampling devices need to be designed and constructed that eliminate contamination from gas sources.

6. Drilling methods that minimize contamination of aquifers should be used.

7. On-site contamination monitoring should be developed using tracers incorporated in the drilling fluids.

Review of Geophysical Well Logs

The work performed in fiscal year 1978 consisted of a review of preexisting well log data and data obtained during the year by other Rockwell subcontractors. The well logs at Hanford can be used in several ways to aid the hydrology program: (a) to examine rock properties such as porosity, density, and fracture character on a continuous coverage basis; (b) to delineate zones of fluid flow; and (c) to correlate geologic units between wells.

Figure 10 demonstrates the response of four standard logs to the basalt in the 2,800- to 3,400-ft interval in well DC-1. As porosity increases, all quantities measured by the four sondes deflect to the left. For example, the large deflection from 2,950 to 3,000 ft is an interbed of much higher porosity than the dense basalt below, from 3,000 to 3,180 ft. Currently it is not possible to quantify the porosity accurately, because all the sondes are calibrated for sedimentary sequences. Further work with the available logs and core samples could soon overcome this problem.

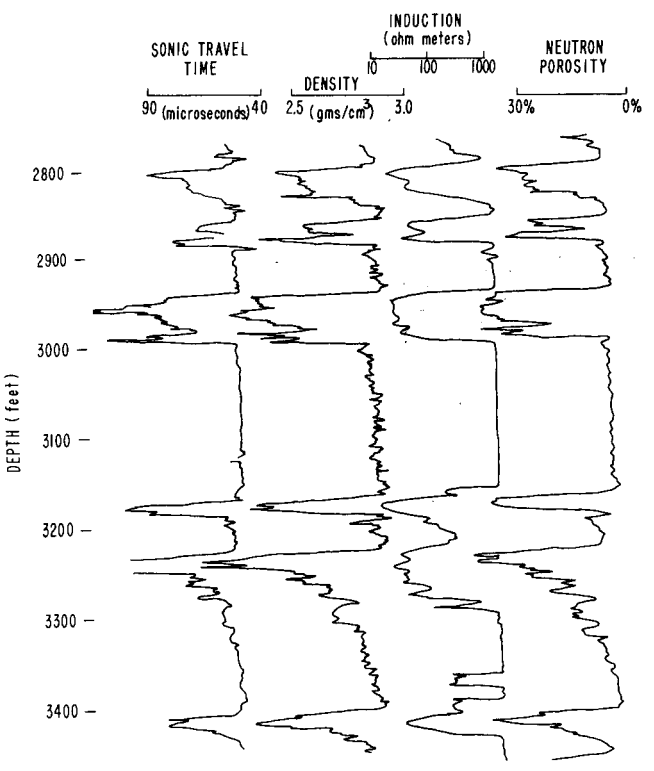

Figure 10. Four porosity-type logs in well DC-1.

Figure 11 shows temperature logs and flow profiles from the entire 5,000-ft length of well DC-1. Breaks in the temperature gradient occur where fluid has left the wellbore and entered the formation, thereby cooling the rock below the temperature dictated by the geothermal gradient. These temperature breaks are confirmed by the flow profiles, which were obtained with the radioactive tracer technique. With this method, the downward velocity of the borehole fluid is measured by injecting a tracer into the water column and detecting its transit time past detectors in the sonde. The abrupt drops in velocity occur where fluid leaves the wellbore and enters the formation. The obvious zones in Figure 11 were detected on several logs run at different times, confirming the validity of the methods.

In the course of the review, it became clear that the hydrology program would be assisted by

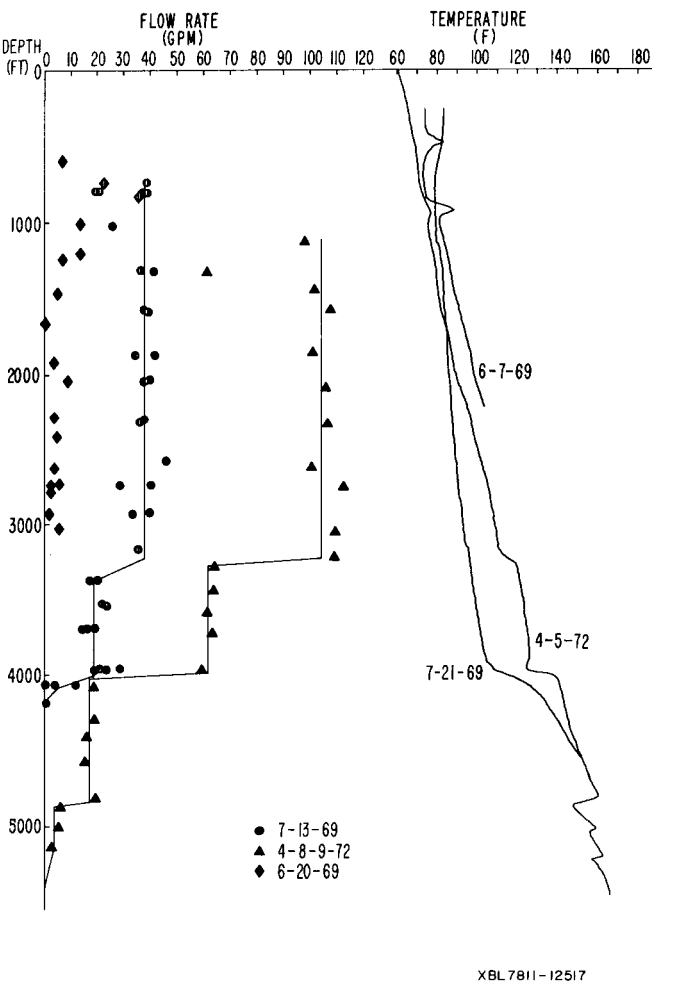

Figure 11. Summary figure of anomalous flow zones in well DC-1.

a greater effort in well log interpretation and a coordinated program in acquiring new logs. Among the recommendations are the following:

1. Routinely obtain flow profiles in all new holes, with the spinner tool the preferred method.

2. Establish a reliable method of quantifying the porosity in the basalt.

3. Correlate the existing well logs and auxiliary data onto base sheets.

4. Continue to pursue those logs, such as spectral gamma and magnetic susceptibility, that promise to yield correlative geological data among holes.

SUMMARY

Hydrological and geophysical data for basalt units between 2,000- and 5,000-ft deep have indicated the presence of a zone of lower hydraulic head and moderate hydraulic conductivity between depths of 3,000 to 4,000 ft. This zone is beneath the lower-conductivity Umtanum Unit and appears to act as a drain for flow converging upon it from both overlying and underlying strata. Water level elevations imply that the Gable Mountain/Umtanum Ridge anticline may be acting as a barrier to flow, and that the most likely discharge area for groundwater in the deeper basalts is the Columbia River bed between the Tri-Cities area and Wallula Gap. The greatest hydraulic conductivities were encountered in this zone of lower hydraulic head and are on the order of 10^{-4} cm/sec.

Groundwater samples were obtained from several wells and springs. Samples obtained from the deep basalts indicate a dilute chloride-bicarbonate water of high pH (~10) containing significant quantities of fluoride (20 to 40 ppm) and silica (up to 150 ppm). Evaluation of the chemical analyses in terms of their origin, history, and age was not possible because of the small number of samples taken within a relatively large and complex basin.

Recommendations for further work are presented in the form of a comprehensive well drilling and testing program, which is designed to provide the remaining information required to determine the hydrologic feasibility of constructing a waste repository in geologic media at the Hanford site (Long and Wilson, 1978). The recommendations include theoretical, field, and laboratory studies and procedural refinements in many areas--particularly in hydrologic testing and geochemical sampling in deep boreholes.

REFERENCES CITED

Apps, J., Doe, T., Doty, B., Doty, S., Galbraith, R., Kearns, A., Kohrt, B., Long, J., Monroe, A., Narasimhan, T. N., Nelson, P., Wilson, C. R., and Witherspoon, P. A., 1979. Geohydrological studies for nuclear waste isolation at the Hanford Reservation. Berkeley, Lawrence Berkeley Laboratory, LBL-8764.

Kearns, A., 1979. Field operation procedures; groundwater sampling, in Apps, J., Doe, T., Doty, B., Doty, S., Galbraith, R., Kearns, A., Kohrt, B., Long, J., Monroe, A., Narasimhan, T. N., Nelson, P., Wilson, C. R., and Witherspoon, P. A., 1979. Geohydrological studies for nuclear waste isolation at the Hanford Reservation. Berkeley, Lawrence Berkeley Laboratory, LBL-8764.

LaSala, A. M., Jr., and Doty, G. C., 1971. Preliminary evaluation of hydrologic factors related to radioactive waste storage in basaltic rocks at the Hanford Reservation. U. S. Geological Survey Open-file report.

Long, J. C. S., and Wilson, C. R., eds., 1978. Recommended well drilling and testing program, Pasco Basin hydrology program. Berkeley, Lawrence Berkeley Laboratory, Pub 5011.

Newcomb, R. C., Strand, J. R., and Frank, F. J., 1972. Geology and groundwater characteristics of the Hanford Reservation of the USAEC, Washington. U. S. Geological Survey Professional Paper 717.

Papadapoulos, I., and Cooper, H. H., Jr., 1967. Drawdown in a well of large diameter. Water Resources Res., v. 8, pp. 1284-1298.

Rockwell International, Department of Waste Isolation, 1977. Basalt waste isolation program annual report. Richland, Rockwell Hanford Operations, RHO-ST-9.

NATURE AND DISTRIBUTION OF SECONDARY MINERALS IN THE BASALTS OF THE PASCO BASIN, WASHINGTON, AND THEIR RELATION TO THE DISPOSAL OF NUCLEAR WASTES

L. V. Benson, C. L. Carnahan, J. A. Apps, D. J. Corrigan, C. J. Frisch, C. A. Mouton, and L. K. Teague

INTRODUCTION

The specific objectives of this study are to: (a) determine the nature of the minerals that coat vesicle and fracture surfaces in basalts of the Pasco Basin; (b) simulate the mass transfer, which led to their precipitation; and (c) predict the mass transfer associated with the dissolution of spend unreprocessed fuel rods.

ACTIVITIES IN FISCAL YEAR 1978

Considerable progress has been made in meeting these objectives. Scanning electron microscope, petrographic, x-ray diffraction, and electron microprobe analyses have been made on a series of samples taken from core hole DC-2. In addition, preliminary simulations of mass transfer associated with the dissolution of basalt have been accomplished. The mass-transfer code has been modified to facilitate data base changes including the incorporation of uranium and plutonium thermochemical data.

Mineral Studies

Scanning electron microscopy. Sixty samples of secondary mineral assemblages from 24 depths were examined. Fractures and breccia were found to contain clay (smectite) and silica with an occasional occurrence of pyrite. Vesicles were commonly lined with smectite, silica, and the zeolite clinoptilolite. In 40 of the 45 vesicles, smectite was the first-formed mineral. Clinoptilolite and silica alternated as the secondand third-formed phases. In many instances a smectite was the final mineral to form. Figures 1 to 5 depict the crystallization sequence found in a single vesicle (sample DC6 290853) at a depth of 886 m. The order of crystallization was smectite, silica, clinoptilolite, and smectite/potassium feldspar.

X-ray diffraction. These studies supplemented the morphological identification of solid phases by scanning electron microscopy. Additional phases identified by x-ray diffraction were illite, pyrite, mordenite, erionite, and analcime.

Electron microprobe. Electron microprobe analyses show the clay to be an Fe- and Mg-rich variety of smectite (nontronite), and the zeolite to contain approximately equal amounts of sodium and potassium in the exchange sites.

Mass Transfer Simulations

Preliminary computer simulations of mass transfer in the water-basalt system were made with and without the presence of carbon dioxide at 25°, 60°, 100°, 200°, 250°, and 300°C. Results of these simulations are reported by Apps (1978). Discussion is here limited to 60°C, a temperature that most nearly approximates that found at a depth of 3,000 m in the Pasco Basin.

An idealized chemical composition of the Pomona basalt was used in the simulations. Each mole of Pomona basalt was allowed to dissolve in almost pure water according to an equation relating the composition of the basalt with the chemical constituents in solution. Simulations with carbon dioxide also present as a reactant were made in order to define its effect on pH buffering. Most groundwaters from basaltic terrains contain significant concentrations of aqueous bicarbonate (HCO_3^-) that buffer the pH of the groundwater between 7 and 8, resulting in a different alteration sequence from that observed in carbonate-free systems.

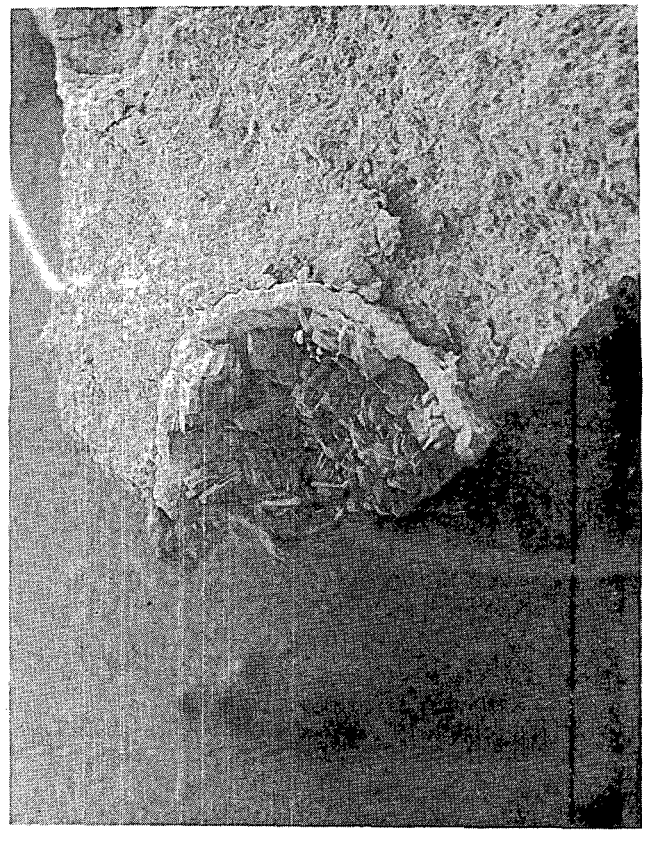

Figure 1. Vesicle (2.25-mm diam) coated with a series of mineral phases.

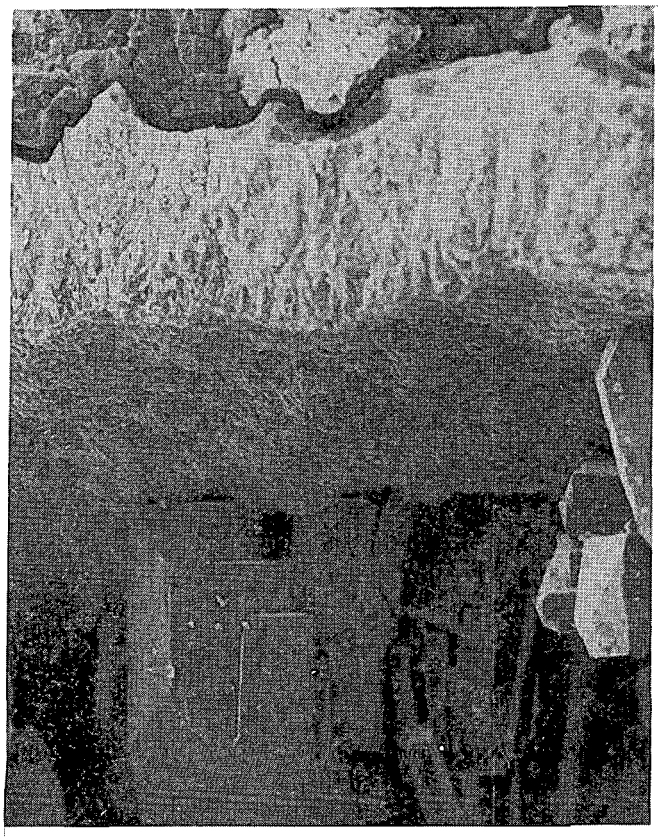

Figure 2. Enlargement of Figure 1. Gray material at top of picture is a smectite clay, white material is silica, and platy crystals are clinoptilolite. Note small particles of smectite on surfaces of the clinoptilolite. Silica layer is 150 μm thick.

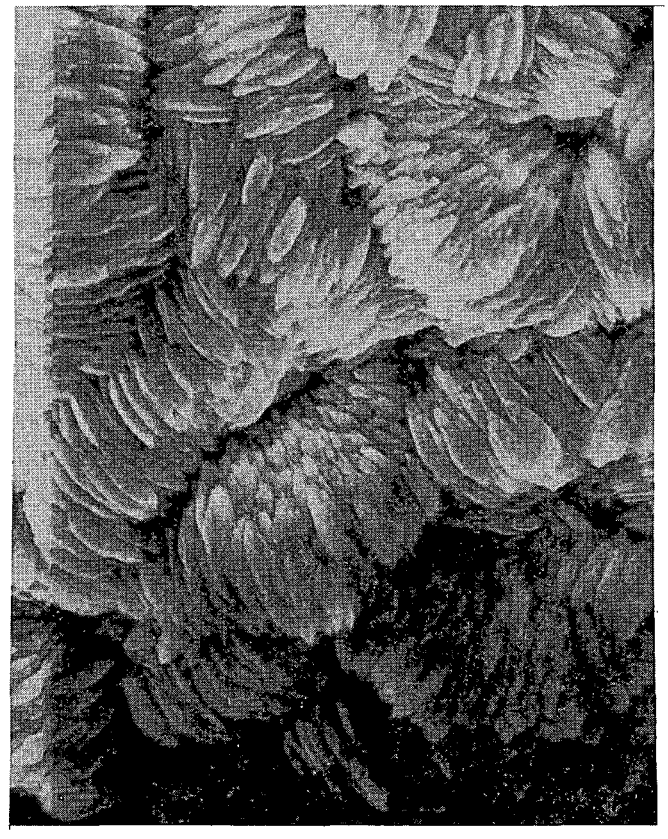

Figure 3. Enlargement of silica surface shown in Figure 2.

The simulation containing carbon dioxide produced not only the carbonate minerals calcite and siderite, but also four noncarbonate minerals (talc and the clay minerals kaolinite, calcium montmorillonite, and sodium montmorillonite). These noncarbonate minerals did not appear in the reaction system lacking carbon dioxide. Magnesium chlorite appeared in both systems at low values of reaction progress, but was consumed reversibly in the system containing carbon dioxide, where talc became the more stable magnesium-containing phase at higher values of reaction progress. Also, tremolite and prehnite were precipitated in the carbonate-free system, but did not reach saturation in the system containing carbonate. Four other product mineral phases common to both reaction systems were fayalite, laumontite, adularia, and low albite. Differences in concentrations of noncarbonate aqueous species and noncarbonate product mineral phases are attributable principally to the pH-buffering effect of the bicarbonate-carbonic acid equilibrium.

In the carbonate-free system, the pH gradually increases from its initial value of 7 and eventually stabilizes at a value slightly higher than 11. On the other hand, in the system containing carbon dioxide, the pH stabilizes at about 8.

Comparisons were made between results of the reaction progress simulation in the presence of carbon dioxide and chemical analyses of groundwater samples obtained from basalt horizons beneath the Pasco Basin. The analyses were used as input to the distribution-of-species mode of the two mass-transfer codes used in the study. In addition, one code was used to determine the optimum assemblage of mineral phases, which would remove all supersaturations from each groundwater sample.

The reductions of total elemental concentrations in the aqueous phases needed to remove supersaturation were minor for most elements. However, significant reductions of concentrations of aluminum and iron were required, amounting to about 4 and 12 orders of magnitude, respectively. These reductions probably result from incorrect chemical analyses.

The computer-generated solid-phase assemblages that removed supersaturation from the groundwater samples contained such minerals as muscovite, chalcedony, nontronite, kaolinite, celadonite, and microcline. Of these, muscovite and kaolinite have not been observed, and silica does not form as chalcedony. Potassium feldspar has been observed only once.

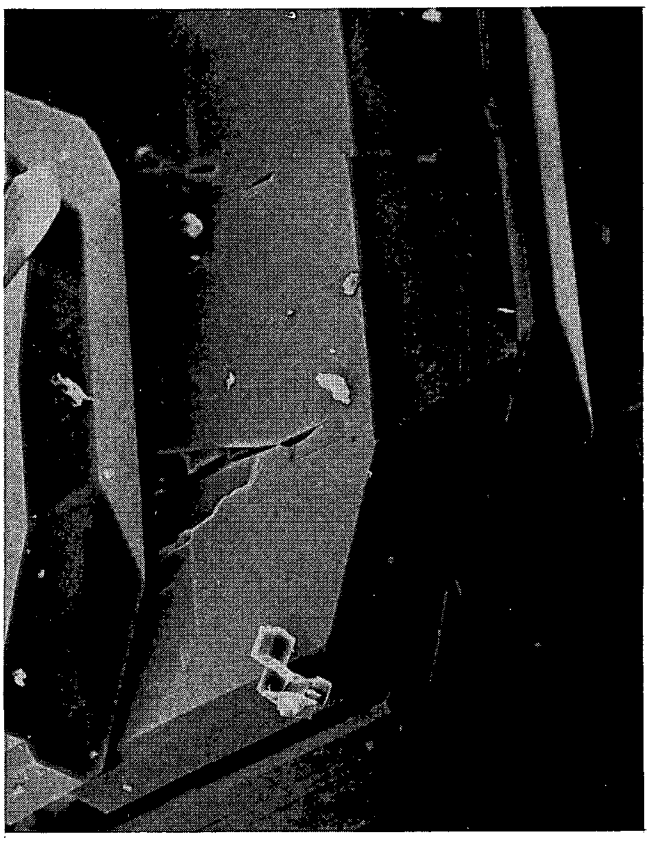

Figure 4. Enlargement of clinoptilolite crystals shown in Figure 2. Note irregularly shaped clay particles and grouping of several potassium fedspar crystals on lower outside edge of the clinoptilolite crystal in center of the figure.

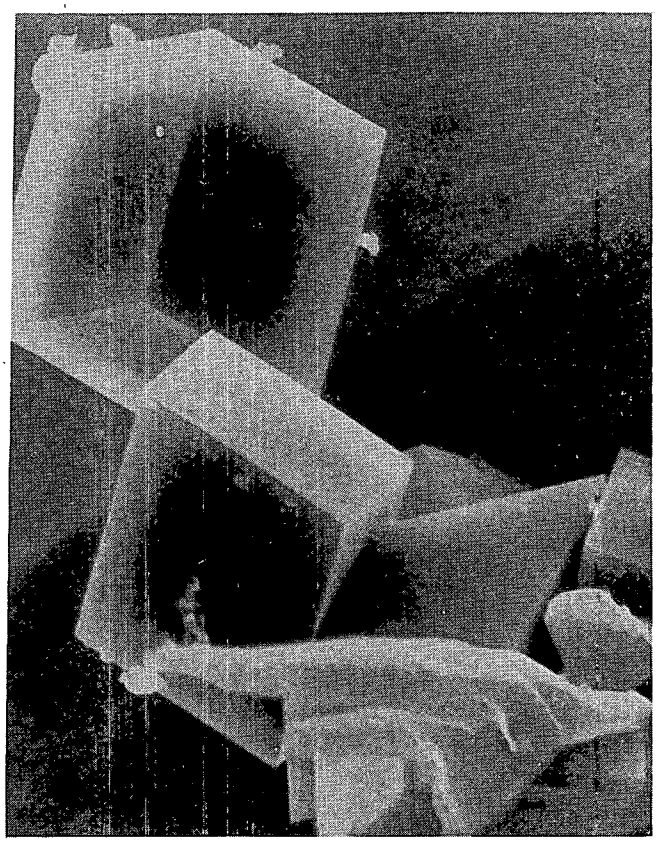

Figure 5. Enlargement of the potassium feldspar crystals shown in Figure 4. Crystals are 6 μm wide.

A comparison of the results of the simulations with the mineralogy of the altered basalts indicates that considerable refinement is still required, primarily through the aquisition of the presently lacking thermochemical data of observed mineral phases. Incorporation of such data would allow more realistic modeling of the alteration history than is now possible.

PLANNED ACTIVITIES IN FISCAL YEAR 1979

Continued characterization of cores DC-2, DC-6 and DH-5 will be accomplished, including a determination of the types, compositions, relative amounts, order of crystallization, and location of secondary phases. The compositions of the secondary phases will be used to approximate their standard free energies of formation, which will in turn be input to the database of the mass-transfer code. Simulations of basalt-water reactions in both open and closed systems will be made under conditions of high and low oxidation potential (Eh). This will provide baseline data to be compared with the results of nuclear waste basalt-water reaction simulations. The results of the simulations will also be compared with data on groundwater compositions in the Pasco Basin and the results of the mineral characterization studies.

REFERENCE

Apps, J. A., 1978. The simulation of reactions between basalt and ground water. Berkeley, Lawrence Berkeley Laboratory, UCID-8066.

HANFORD NEAR-SURFACE TEST FACILITY HEATER EXPERIMENTS*

A. DuBois

INTRODUCTION

An underground test facility is being constructed for the U. S. Department of Energy (DOE) by the Rockwell Hanford Operations (RHO) section of Rockwell International Energy Systems Group at Gable Mountain on the Hanford Reservation, Hanford, Washington. The near-surface test facility (NSTF) is the site for a group of experiments designed to evaluate the thermomechanical suitability of a deep basalt stratum as a permanent repository for nuclear waste. In January 1978, the Lawrence Berkeley Laboratory (LBL) Earth Sciences Division was authorized to assist RHO in designing suitable thermomechanical heater tests for the NSTF, based on LBL's background in the field of rock mechanics and experience in designing and executing a similar group of experiments at the Stripa iron mine in Sweden.

ACCOMPLISHMENTS IN FISCAL YEAR 1978

After consulting with LBL's Earth Sciences Division and Terra Tek Inc. (a subcontractor to LBL), RHO published the "Near Surface Test Facility (NSTF) Test Plan" in December 1977 (Board and Marron, 1977). As a result of continuing discussions, this preliminary plan has been modified.

LBL, with their subcontractor Terra Tek, generated a borehole and instrumentation array for the three proposed heater tests: Full-Scale Test #1 (lined borehole), Full-Scale Test #2 (unlined borehole), and Time-Scale Test.

LBL has performed thermomechanical modeling to help design the three instrumentation arrays and to predict the thermal environment of the heaters and instruments. Heaters, instrumentation, and data acquisition system designs and recommendations were based on the Swedish experience. Drawings and specifications were provided to guide the RHO Title I design of the NSTF drifts and services, and RHO designs and specifications were reviewed. A quality assurance plan was developed, and a program schedule, compatible with earlier assumptions regarding LBL conduct of the tests, was prepared. Component procurement and fabrication planning was initiated through LBL purchasing and shops, but no formal plan was completed. A year-end summary report was drafted describing the LBL effort and recommended designs.

Experiment Design and Procedures

LBL recommended the experimental objectives, procedures, and layout based upon experience gained at Stripa, Sweden, taking into consideration the constraints and geology of the Hanford site. The experimental activities at the NSTF are divided into two parts. The first set of activities--geological, geotechnical, and geophysical--are primarily carried out before the rock instrumentation is installed into the boreholes and the subsequent initiation of the heater experiments. These activities have a number of objectives, including: the definition of the three-dimensional fracture network in the vicinity of the heaters, the spatial distribution of permeability and porosity and their quantification insofar as possible; the mapping of changes in physical properties of the rock that may provide insight into its behavior during thermal loading; and, assessment of different techniques in delineating the fracture system in the basalt. Some of the activities planned for the NSTF are: core logging and core photography, television borehole logging, geophysical borehole logging, air injection permeability, and characterization of fracture discontinuities.

The second set of activities is the operation of the heater tests, including the installation, calibration, check-out, operation, maintenance, and acquisition of data. Among the objectives of the heater tests are:

1. To investigate canister retrievability
2. To measure borehole decrepitation as a function of power level
3. To observe temperature and displacement fields and compare the measured levels with predicted levels
4. To examine the effects of fractures and jointing on the thermomechanical properties
5. To assess the long-term response and interaction of an array of storage holes

The specific measurements planned for the NSTF are:

1. Thermal and mechanical measurements. Most of the instruments around the two full-scale and the time-scale heaters are thermocouples, linear extensometers, and borehole deformation gauges. The specifics of the design were altered for the NSTF at Hanford based on two considerations. First, the thermal conductivity is considerably lower in basalt, dramatically altering the predicted thermal field. Second, isotropy is not assumed in the Hanford basalts, and additional boreholes have been added to detail any departure from axial symmetry.

*Extracted from DuBois et al., 1979.

2. Geophysical and hydrological measurements. Such measurements are designed to assess changes in the rock mass during the heater tests so that in the future, reliable methods to monitor rock mass behavior in an operating repository will be available. The methods to be tested include air permeability, acoustic velocity, neutron detection of moisture fluctuations, acoustic emission, electrical resistivity, and radio frequency electromagnetic propagation.

Thermal and Thermomechanical Modeling

The work reported here includes thermal calculations for the full-scale and time-scaled experiments in the NSTF and thermomechanical calculations for the full-scale experiments. The purpose of these calculations is to provide predicted temperatures, displacements, and stresses to be used in the design and layout of the heaters and measuring devices as well as to help in choosing suitable power schedules for the heaters.* The heater experiments will, in turn, indicate the essential features that must be included in the models. Thus both the calculations summarized here and the experiments being modeled should be viewed as part of the iterative process aimed at solving the problem of storing radioactive wastes.

Detailed results, necessary for the design of the experiments, are given elsewhere (Chan and Remer, 1978a). Only selected results are highlighted here. Table 1 summarizes the type of calculations made and models studied during 1978.

Experiments modeled. The heater experiments consist of two full-scale experiments and a time-scaled experiment, essentially an adaptation of the concept used in the Stripa Heater Project (Cook and Witherspoon, 1978). Each full-scale experiment consists of a central heater surrounded by a ring of eight peripheral heaters. The central heater in each full-scale experiment represents a full-sized canister of spent fuel of a different age and will be used to study the short-term, local thermomechanical effects of a buried heat source. The peripheral heaters will be turned on some time after the start of the experiment (a one-year delay has been used in the calculations) in order to simulate the rise of ambient temperature caused by the canisters in a repository.

The time-scaled experiment consists of a planar rectangular array of nine scaled down (by a factor of 3.2) 1.125-kW heaters at 7 m or 3 m center-to-center spacing. In addition, there are four secondary heaters of the same size at interstitial positions, which will be turned on one year after the start of the experiment to simulate the effect of an additional loading of canisters. According to the laws of heat conduction (Cook and Witherspoon, 1978), one year of the time-scaled experiment represents 10.22 years of real time.

*The calculations summarized here do not reflect the latest design changes.

Temperature calculations. An analytical solution for the heat conduction problem for a finite-length line source has previously been derived using the Green's function method and has been coded into a computer program, FILINE (Chan et al., 1978). The advantage of using the analytical solution in this way is that temperature calculations may be made for just a few points rather than for the large number needed for a finite difference or finite element calculation. Excellent agreement between measured (Cook and Hood, 1978) and predicted temperatures (Chan et al., 1978) gives us confidence in using the same program to calculate the temperatures for the NSTF.

Detailed results as well as the development of equations for finite-length cylinder and disc sources with arbitrary time-dependent heat generation may be found in a paper by Chan and Remer (1978a).

The following assumptions have been made in the present model:

1. Conduction is the only mode of heat transfer.
2. The rock medium is homogeneous and isotropic.†
3. The heaters and surrounding rock are in perfect thermal contact and have the same constant (temperature-independent) thermal properties.

Three possible boundary conditions have been considered for the full-scale experiment. In the first, the rock mass is treated as an infinite medium. The second and third models treat the heater drift, which is 4.25 m above the heater mid-plane, as an isothermal or adiabatic boundary, respectively. Calculations for the latter two boundary conditions are accomplished by using image sources.

The different cases studied are listed in Table 1. In the calculations, we have included an overload test in the third year of each full-scale experiment. In this test, the power level of the central heater will be increased 1 kW every 60 days. The peripheral heaters will not be energized until the central heater has been on for one year. Their power level will be held constant at either 0.5 or 1 kW. Temperature profiles for the power schedule giving the largest (power of central heater = 5 kW, power of each peripheral heater = 1 kW) and the smallest (power of central heater = 1 kW, power of each peripheral heater = 0.5 kW) temperatures inside of the ring of peripheral heaters are shown in Figure 1.

The most important feature to note is the exceedingly high temperatures reached for power schedule 1A (power of central heater = 5 kW, power of each peripheral heater = 1 kW) even before the overload test begins. This is due in part to the low thermal conductivity of Pomona basalt (1.62 W/m°C at 200°C) based on

†Generalization to the case of an anisotropic medium is discussed by Chan and Remer, 1978a, in Appendix B.

Table 1. Summary of calculations made and models studied.

Power Schedule	Temperature calculations		Displacement calculations		Stress calculations	
	Infinite medium	Isothermal boundary	Mesh 1	Mesh 7	Mesh 1	Mesh 7
Full-scale experiments						
1A Power of central heater = 5 kW Power of each peripheral heater = 1 kW	X	X	X	X	X	X
1B Initial power of central heater = 2.5 kW, increased to 5 kW after 180 days Power of each peripheral heater = 1 kW	X					
1C Power of central heater = 2.5 kW Power of each peripheral heater = 0.5 kW	X					
2A Power of central heater = 2 kW Power of each peripheral heater = 1 kW	X	X	X	X	X	X
2B Initial power of central heater = 1 kW, increased to 2 kW after 180 days Power of each peripheral heater = 1 kW		X				
2C Power of central heater = 1 kW Power of each peripheral heater = 0.5 kW		X				
Interference between experiments with 1A and 2A			X		X	
Time-Scaled Experiment						
3 Power of each primary heater = 1.125 kW Power of each secondary heater = 1.125 kW	X					

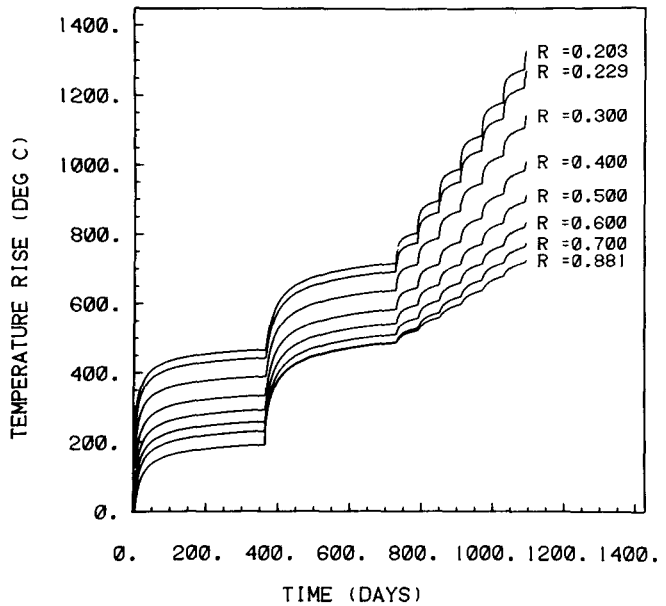

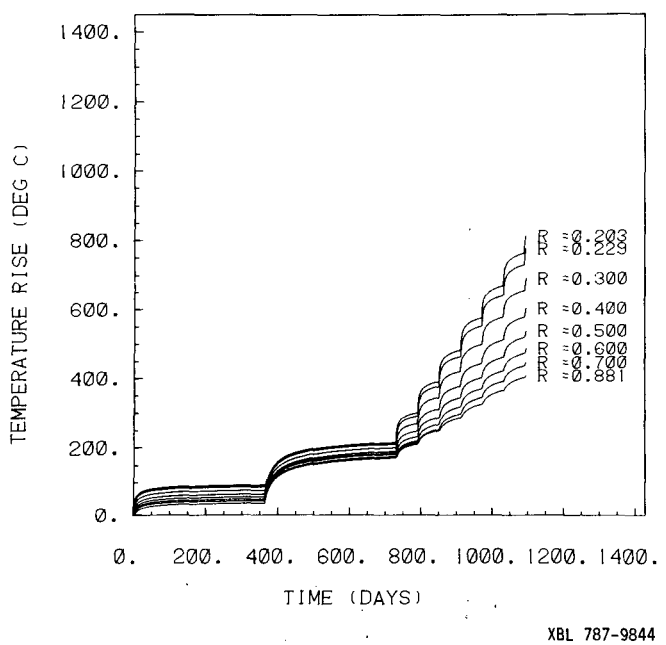

Figure 1. Temperature profiles for Hanford full-scale experiment; Z = 0.0 m, θ = 0.0 deg, R = 0.203 to 0.881 m. TOP, power schedule 1A; BOTTOM, power schedule 2C.

laboratory measurements by Martínez-Baez and Amick (1978).

Another important point is that the ring of 1-kW peripheral heaters increases the temperature within its circumference by 250°C. This represents a very extreme case of the ambient temperature field due to other waste canisters.

Because some of the predicted temperatures exceed the temperature ratings of the extensometers and U. S. Bureau of Mines and IRAD gauges (200 to 250°C) and the highest mock up test temperatures (500 to 600°C), instrument failure is likely to occur during the full-scale experiments. In addition, a number of drastic events are likely such as heater failure, thermal run-away resulting from borehole decrepitation, or even rock melting, which would invalidate the present calculations.

A consequence of the low thermal diffusivity of Pomona basalt is that the high temperature zone is localized. For example, the 100°C incremental isotherm has moved radially away from the 5-kW central heater by only 2 m during the first year and by an additional 1.5 m during the second year.

Example contour plots of incremental isotherms for the time-scaled experiment are shown in Figure 2. The effect of spacing is apparent; the two heaters at 3 m spacing interact sooner than those at 7 m spacing and at a higher temperature throughout the experiment. The secondary heaters, which start interacting with the primary heater one week after they are

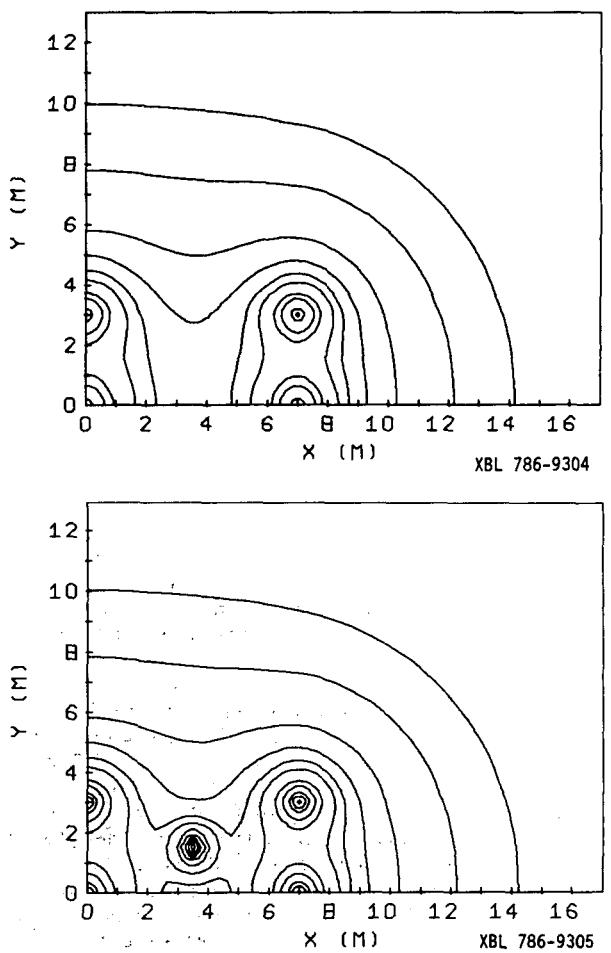

Figure 2. Isotherms in the horizontal plane for the Hanford time-scaled experiment: Z = 0.0 m, power of heaters = 1.125 kW, secondary heaters energized after 730 days. TOP, contours plotted for 375, 200, 100, 75, 50, 40, 30, 20, 10, and 5°C. BOTTOM, contours plotted for 150°C in addition to others.

turned on (Figure 2b), increase the temperatures near the primary heaters by about 30°C, from approximately 365 to 395°C in a year's time. At a radial distance of 0.5 m from any heater, the maximum temperature rise at any time is less than 200°C. As a result, instrument failure is unlikely at that radius.

In the calculations presented above for the time-scaled experiment, the power level of the heaters is assumed to remain constant throughout the experiment. If a decaying power source is used to simulate heat generation from radioactive waste, the temperature will reach a peak value and then start declining (Chan and Remer, 1978b). The maximum temperature of the rock at the edge of the heater hole will be about the same, but the maximum temperature farther away from the individual heaters will be lower.

Displacement and stress calculations. Thermally induced displacements and stresses have been calculated using the finite-element program SAPIV (Bathe et al., 1974). The program assumes linear thermoelasticity and in the present calculation the rock medium has been approximated as a homogeneous, isotropic continuum. This is necessary only because of the lack of data on in-situ rock mass properties. Actually the finite-element method is well suited for heterogeneities and the SAPIV program can handle orthotropic, temperature-dependent material properties.

In constructing the finite-element models for the full-scale experiments, two other approximations were introduced:

1. The system is axially symmetric about the axis of the central heater.

2. The mid-plane of the heater array is a plane of symmetry.

Two finite-element meshes have been used. The first (mesh 1) treats the rock medium, except for the central heater hole, as infinite. In the second mesh (mesh 7), the elements within the heater drift and extensometer drift have been removed. Zero normal-displacement boundary conditions were applied to the outer horizontal and vertical boundaries of the model block.

Maximum radial displacements in the heater mid-plane at the end of the first, second, and third years were found to be 0.8, 2, and 3 mm for power schedule 1A (power of central heater = 5 kW, power of each peripheral heater = 1 kW) and 0.35, 1.5, and 2.5 mm for power schedule 2A (power of central heater = 2 kW, power of each peripheral heater = 1 kW). The presence of the heater drift, the floor of which is 4.25 m above the heater mid-plane, and the extensometer drift, which is approximately 10 m away from the central heater, have little effect on the maximum values of the radial displacement, u_r, but have a remarkable effect on the radial distribution of u_r at longer times.

Maximum vertical displacements are about twice as large as the maximum radial displacement because of the elongated shape of the heated zone and the proximity of the heater drift to the heaters. The significance of the presence of the heater drift can be seen in Figure 3, where the lines designating mesh 1 represent the deformation of an imaginary boundary in an infinite rock medium. The lines designated mesh 7 represent the deformation of the periphery of the heater drift, which is tilted by the thermal loading.

Examples of the normal components of the thermal stress as a function of radial distance along the heater mid-plane are shown in Figure 4. Initially, over a short range of distances from the central heater, both the axial stress (σ_z) and the tangential stress (σ_θ) are tensile with a maximum magnitude of 1 MPa. This tensile portion rapidly spreads out and dimenishes in magnitude as time progresses. During the tests the highest tensile stresses occur immediately beneath the floor of the heater drift. The values of the tensile tangential stress (σ_θ) are extremely high, far exceeding the in-situ compressive stress. The net tensile stress may therefore exceed the tensile strength of intact Pomona basalt (Duvall et al.,

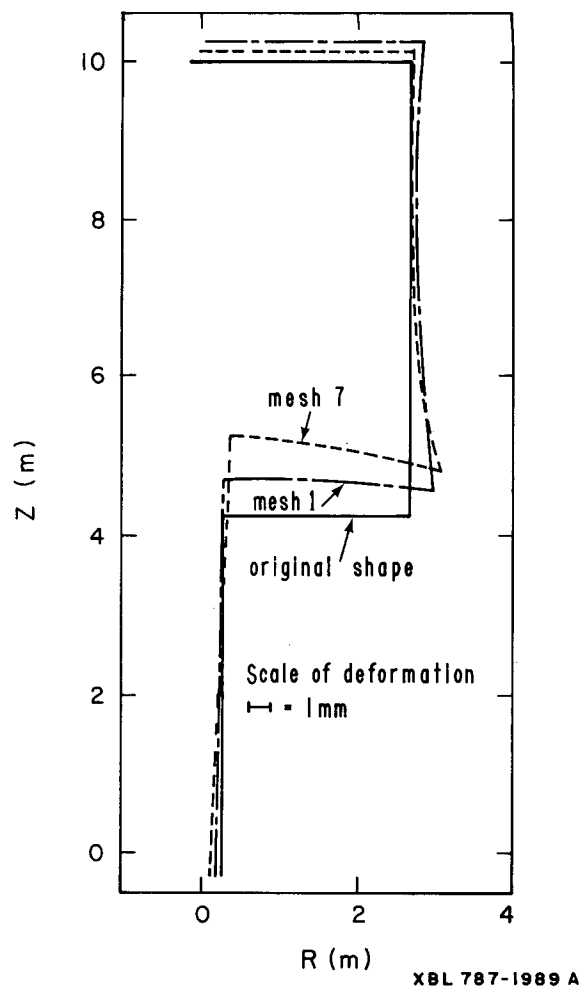

Figure 3. Power schedule 1A for full-scale experiment. Deformation of drift and borehole after 730 days.

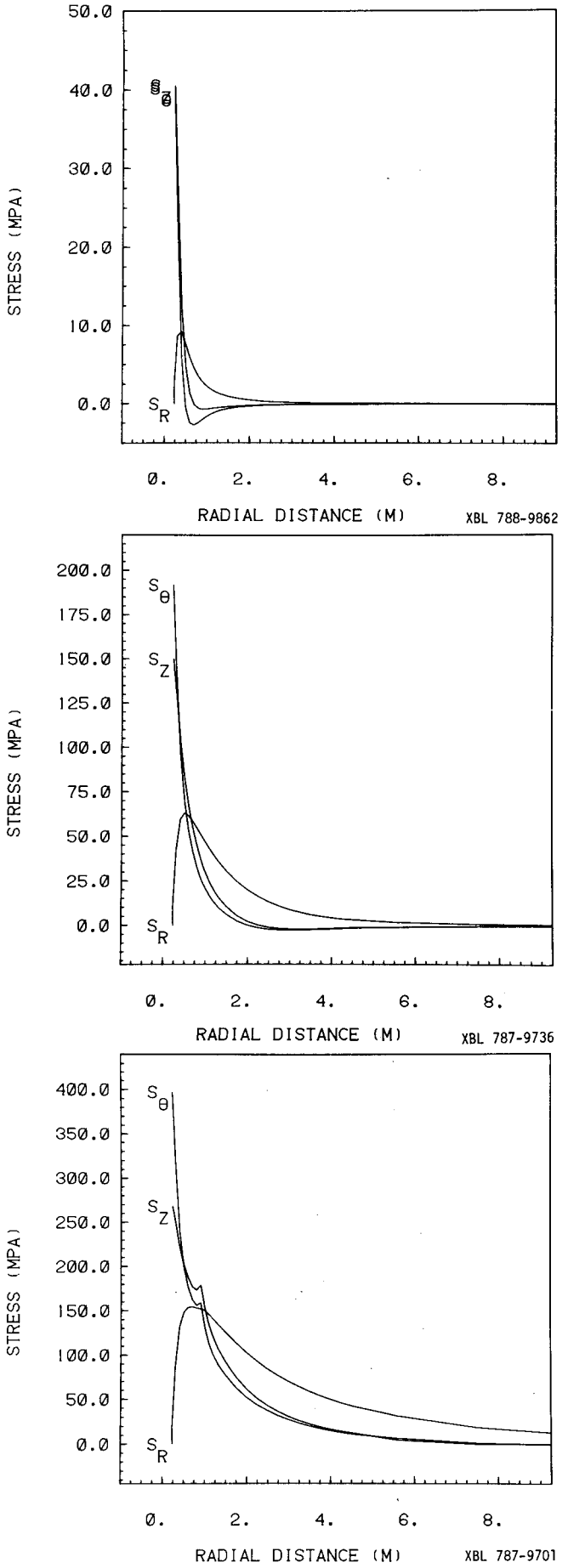

Figure 4. Stress profiles for mesh 1 for the full-scale experiment. Main heater = 5 kW, peripheral heater = 1 kW, Z = 0.0 m, θ = 0.0 deg. TOP, 1 day; MIDDLE, 30 days; and BOTTOM, 730 days.

1978) some time during the experiment causing the floor of the drift to crack.

At the edge of the central heater hole, both the axial stress (σ_z) and the tangential stress (σ_θ) are compressive and reach high values even at relatively short times. For example, 30 days after the turn-on (Figure 4b) of the 5-kW central heater, σ_z (150 MPa) and σ_θ (191 MPa) already fall within the range of values for the uniaxial compressive strength of Pomona basalt (75 to 378 MPa as measured by Duvall et al.) in small intact specimens. Consequently, thermal decrepitation may occur early in the experiment.

Interference between full-scale experiments. The two full-scale experiments separated by 21 m are practically thermally independent. With regard to the thermally induced displacement, however, the two experiments interact quite strongly. For example, see Figure 5. Interference of the radial stresses due to the two experiments is moderately serious.

In the interpretation of the field data, comparison should be made with the superposed predicted displacements and stresses. Otherwise, the experimental results may be misunderstood as being due to anisotropy of the rock mass.

Conclusions and recommendations. On the basis of these calculations, we made a number of conclusions and recommendations regarding the power schedules of experiments, additional measurements that are considered desirable, and further necessary calculations. The reader is referred to Chan and Remer (1978a) for details. The following two points may be of general interest. First in view of the low thermal conductivity of Pomona basalt, unless the results of the heater experiments indicate otherwise, it would be prudent to limit the initial power of any spent fuel canister placed undergound to 0.4 kW/m (corresponding to a 1-kW full-scale heater 2.5-m long) to ensure that the temperature of the fuel cladding does not exceed 200°C. Second, since the temperature fields in all these heater experiments are localized, it is necessary to carry out larger-scale heating experiments to investigate thermomechanical response on excavation and repository scales.

Heater and Rock Instrumentation Layout

A proposed arrangement for the 31 heater and 216 rock instrumentation boreholes specified for the three NSTF heater experiments was prepared. The borehole locations, dimensions, and specifications were presented in tabular form with

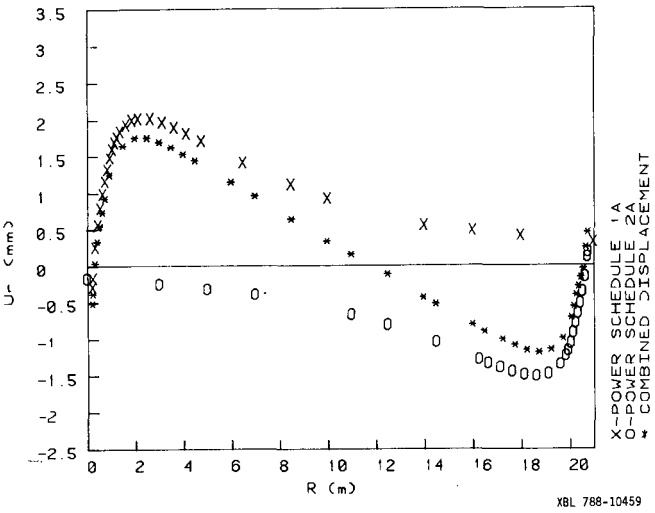

Figure 5. Interference between two full-scale experiments: displacement (U_r) profiles at Z = 0.0 m, θ = 0.0 deg. for mesh 1, 730 days.

supporting drawings showing the physical relationships between these boreholes and the NSTF drifts in which they were to be installed. The rock instrumentation proposed for mounting in these boreholes was described by Terra Tek, Inc. (1978).

Heaters and Controls

Several electrical heaters, with associated controllers and instrumentation are to be installed within the NSTF to simulate the discrete heat loads to be expected from canisters of nuclear waste. Heater controllers and instrumentation designs for the NSTF were adapted by LBL from similar equipment designed for the test program in granite at the Stripa, Sweden, iron mine. Recent changes being considered for the Rockwell test plan may require changes in the designs provided.

LBL adapted many details from the earlier Stripa designs and also generated new drawings and specifications. The electrical heaters are of three types: full scale, peripheral, and time scale.

The principal elements of each heater installation are:

1. A vertical borehole in the mine floor for receiving the heater assembly
2. A cylindrical enclosure (canister), which houses the electrical heater elements
3. The electrical heater elements
4. The electrical leads
5. An upper tube to support the canister and the lead
6. A thermal insulation plug to prevent heat loss up the borehole

The following are optional features recommended for use on certain heaters:

1. A borehole liner to ensure canister retrievability
2. Temperature monitoring equipment to track the heater, liner, and borehole temperature
3. A borescope and guide tubes for viewing the borehole wall for evidence of decrepitation
4. Dewatering apparatus to remove liquid and steam from the borehole

The full-scale heaters are designed to duplicate the geometry (12.75-in. diameter x 8.5-ft length) of one possible waste canister and to provide a heat load (5-kW maximum) that might be delivered by such a waste container. Two such heaters will be installed at separate locations within the excavation. One heater will operate at high power in a lined borehole. The second unit will operate at a lower power level and may be installed in an unlined borehole. Either or both of these units may operate within the thermal field of eight peripheral heaters.

Electrical heater controllers. LBL proposed a specific heater control and monitoring scheme similar to the Swedish system for use in the Hanford NSTF heater tests. LBL provided 120 detail controller-design drawings from the Swedish experiment, which were applicable for use at Hanford.

Electrical heater controllers are required for 2 full-scale heaters, 8 or 16 peripheral heaters, and 13 time-scaled heaters. Power for heater controllers will be derived from a 208/120 V three-phase, Y-connected power system. Heater elements have, therefore, been specified to operate at maximum power outputs with voltage settings of 208 V ac from the power controllers. Table 2 shows the various heater voltages settings to be provided by the controllers for designated heater power outputs.

Following the philosophy used in the Swedish experiment, each full-scale heater will have four heater elements each driven and monitored by its own power controller. Under normal operation, the power load will be shared by the four elements and associated controllers. Each element and controller is designed to handle the full heater power in the event of failure of up to three heater elements, controller channels, or both. Each controller is also a modular unit capable of replacement within a few minutes. Several other controller philosophies were discussed with RHO as possible alternatives to the direct autotransformer controller used in Sweden.

The peripheral heaters are single-element heaters. Each heater will be driven and moni-

Table 2. Heater element operating power and voltage.

	Full-scale #1	Full-scale #2	Peripheral	Time-scale
Heater assemblies per project	1	1	16	13
Heating elements per assembly	4	4	1	2
Maximum power per element (kW)	5	5	1.5	1.5
Maximum voltage setting (VAC)	208	208	208	208
Normal power (kW), all elements energized	1.25	0.5	1.0	0.5
Normal voltage (VAC), all elements energized	104	66	170	120
Normal power (kW), one element energized	5	2	1.0	1.0
Normal voltage (VAC), one element energized	208	132	170	170

tored by an individual power controller capable of providing 1.5 kW, and can be identical to the controllers used in the time-scale experiment.

The time-scaled heater canisters each contain two heater elements. Like the full-scale heater, each element is controlled and monitored by an independent controller. Under normal operation both elements and their associated controllers share the burden of supplying canister power. However, each element and controller can supply full heater power in the event of emergency. Each controller is also constructed as a modular chassis for ease of replacement.

The various controllers all follow the same basic design philosophy. Each unit contains an autotransformer as a voltage source for the heater elements. Electrical transducers and signal conditioners are provided to monitor heater power. Operational amplifiers are used as buffers between the transducer/signal conditioner outputs and lines driving analog panel meters, digitial panel meters, data logger inputs, and computer multiplexer inputs.

Racks containing the heater controller and instrumentation electronics will be housed in two buildings within the experiment drift. One structure is to be located at the time-scaled experiment and the other at the full-scale experiment. LBL drawings were given to RHO outlining the required building dimensions, door locations, and internal configurations. During review meetings held at Hanford, LBL provided RHO with recommendations regarding such subjects as ventilation, floor construction, fire control, and lighting.

Instrumentation and Data Acquisition

Specific instrumentation was proposed that would determine the mechanical and thermal response of basalt to the full and time-scaled heater tests. These instruments included thermocouples, stressmeters, and extensometers similar to those currently being used by LBL in Sweden.

Terra Tek compiled a rough instrumentation proposal in January 1978 that included an instrumentation count of 390 rock-temperature-monitoring thermocouples, 33 USBM gauges with three channels per gauge, 35 vibrating wire stressmeters, and 35 four-point extensometers. This instrumentation count was changed in April 1978 to 712 rock instrumentation thermocouples, 74 USBM gauges requiring 222 data channels, 148 vibrating wire stressmeters, 279 channels of three- and four-point extensometers, and other block motion transducers. To this count, LBL added 130 heater thermocouples and 190 current, voltage, and power-monitoring signals from the heater controllers.

With a total of more than 1,681 data acquisition channels required, LBL and Terra Tek developed a first iteration of block diagrams for the instrumentation Data Acquisition systems (DAS). The DAS for the two full-scale experiments and time-scaled experiment included ten 96-channel ice-point references for thermocouples, three general-purpose data loggers, strain-gauge signal conditioning circuits for 222 channels of USBM gauges, and custom data loggers for the vibrating wire stressmeters.

Terra Tek's revision of borehole instrumentation requirements in August 1978 lowered the

required number of DAS channels from 1,681 to 1,576. The initial basic DAS block diagrams are still generally valid; however, changes have been recommended as a result of recent experience in Sweden.

LBL defined a DAS for the NSTF including requirements for a spent fuel facility, estimated its cost including test equipment and spares, and recommended how to meet the early turn-on requirements. Acquired data are to be logged on magnetic tape, converted to engineering units, smoothed, checked for alarm conditions, and stored on a local disc file. The DAS also provides a means of calibrating the instruments on-site. Real-time graphic displays facilitate rapid examination of the acquired data and aid in detecting and diagnosing problems. Predicted temperature, displacement, and stress data will also be maintained on a local disc file. Displaying both predicted and actual results together accentuates unexpected results.

LBL, with Rockwell and Vitro Engineering, determined the requirements for normal, standby, uninterruptible, and emergency power. A power interlock system, local audible alarms, and an automatic telephone-dialer and warning system will be provided.

A Modular Computer Sytems ModComp IV/35B was proposed as the basis for the DAS. The proposed system configuration is detailed in a U. S. Department of Energy 1830 format and in "Functional Specifications of the Data Acquisition System" that LBL provided to Rockwell. The 1830 provided justification for the "Acquisition of Automatic Data Processing Equipment and Sole Source Procurement." This system was proposed to: utilize off-the-shelf remote analog I/O processors; maintain compatibility with the software developed for the Swedish system thus reducing software development costs; and provide memory expansion capability. A large data base, which includes the operating system, application software, collected and predicted data for processing and display, calibration data, and engineering conversions is maintained on discs. An uninterruptible power supply will be used to protect against short power outages. Redundant computer peripherals, raw-data log-tapes, a file checkpoint/restart feature, and back-up data loggers were proposed to minimize data loss caused by any single failure.

The computer system may be housed in a computer room that will be constructed underground near the heater experiments. Remote data acquisition units will be housed in instrumentation sheds that will be constructed adjacent to both the full-scale and the time-scaled heater experiments. LBL proposed a room layout, air conditioning, lighting, fire protection, floor and equipment arrangements, power layout, and emergency lighting for the enclosure for the computer and instrument electronics.

PLANNED ACTIVITIES FOR FISCAL YEAR 1979

The LBL effort for the hanford Near-Surface Test Facility for fiscal year 1979 will be limited to activities required for a smooth transition to RHO design and direction of the heater tests. These activities will include consulting in the design of the heater, instrumentation, and data acquisition systems; supporting geophysical site characterization, geologic mapping, and hydrologic studies; thermomechanical modeling of the heater tests; and final editing of the fiscal year 1978 Hanford project annual report (DuBois et al., 1979).

REFERENCES CITED

Bathe, K. J., Wilson, E. L., and Peterson, F. E., 1974. SAPIV, a structural analysis program for static and dynamic response of linear systems. Berkeley, University of California, College of Engineering, report EERC 73-11.

Board, M. P., and Marron, J. F., 1977. Near-surface test facility (NSTF) test plan. Richland, Rockwell Hanford Operations.

Chan, T., Cook, N. G. W., and Tsang, C. F., 1978. Theoretical temperature fields for the Stripa heater project. Berkeley, Lawrence Berkeley Laboratory, LBL-7082.

Chan, T., and Remer, J. S., 1978a. Preliminary thermal and thermomechanical modeling for near surface testing facility heater experiment at Hanford. Berkeley, Lawrence Berkeley Laboratory, LBL-7069, v. 1.

____, 1978b. Semi-analytic thermal calculations for arrays of nuclear waste canisters buried in rock. Trans. Am. Geophys. Union, v. 59, p. 1189, Abstract T-75.

Cook, N. G. W., and Hood, M., 1978. Full-scale and time-scale heating experiments at Stripa: preliminary results. Berkeley, Lawrence Berkeley Laboratory, LBL-7072, SAC-10.

Cook, N. G. W., and Witherspoon, P. A., 1978. Mechanical and thermal design considerations for radioactive waste repositories in hard rock. Berkeley, Lawrence Berkeley Laboratory, LBL-7073, SAC-11.

DuBois, A., Binnall, E., Chan, T., McEvoy, M., Nelson, P., and Remer, J., 1979. Heater test planning for near-surface test facility at the Hanford Reservation. Berkeley, Lawrence Berkeley Laboratory, LBL-8730, v. I.

Duvall, W. I., Miller, R. J., and Wang, F. D., 1978. Preliminary report on physical and thermal properties of basalt, drill hole DC-10, Pomona flow Gable Mountain. Golden, Colorado School of Mines, Earth Excavation Inst., report RHO-BWI-C-11.

Martínez-Báez, F., and Amick, C. H., 1978. Thermal properties of Gable Mountain basalt cores, Hanford Nuclear Reservation. Berkeley, Lawrence Berkeley Laboratory, LBL-7038.

Terra Tek, Inc., 1978. Borehole instrumentation layout for Hanford near-surface test

facility, in DuBois, A., Binnal, E., Chan, T., McEvoy, M., Nelson, P., and Remer, J., Heater test planning for near-surface test facility at the Hanford Reservation. Berkeley, Lawrence Berkeley Laboratory, LBL-8730, v. II.

U. S. Department of Energy, 1978. DOE 1830 appendix proposal for radioactive waste disposal research program computer system. Submitted to RHO by LBL in September 1978.

WASTE ISOLATION SAFETY ASSESSMENT PROGRAM

R. J. Silva, L. V. Benson, and J. A. Apps

INTRODUCTION

This project is part of the Waste Isolation Safety Assessment Program (WISAP), which is managed by Battelle Pacific Northwest Laboratories for the U. S. Department of Energy's Office of Waste Isolation. One of the most likely plans for high-level radioactive wastes is disposal in underground geologic media. The radiation and toxicity of high-level wastes necessitate isolation for nearly a million years before radioactive decay will reduce the material to safe levels. Satisfactory containment will depend on geologic stability, failure rate of storage containers, hydrologic properties of the storage media, and radionuclide-geologic media interactions. The overall objective of WISAP is to develop methods and models for a comprehensive evaluation of the safety of long-term waste disposal for selected sites.

The LBL project supports Task 4 of WISAP, "The Collection and Generation of Transport Data." The specific goal of Task 4 is the development of quantitative data and predictive methods for describing radionuclide-geologic media interactions that control the transport of the nuclides through geologic environment of the type anticipated for terminal waste storage facilities. This interaction is important since sorption of the radionuclides by the geologic material will have a retarding effect on nuclide migration.

The first year of this program, fiscal year 1977, was devoted to a review of the literature on the thermodynamic data for aqueous complexes and solid phases of Np, Pu, Am, and Cm likely to form in the natural environment, and on the transport mechanisms of radionuclides in water-saturated rocks. An assessment was made of factors influencing the radionuclide-rock interactions, quantitatively expressed as distribution coefficients for conditions expected in a terminal storage facility. Preliminary considerations were determined for an experimental method of measuring radionuclide transport in water-saturated rocks. This work was reported in detail (Apps et al., 1977).

ACTIVITIES IN FISCAL YEAR 1978

In order to begin to identify the parameters that should be incorporated in a predictive sorption model, a study of the interaction of U, Np, Pu, Am, and Cm with basalt, shale, and granite was initiated in fiscal year 1978.

The sorption/desorption processes were studied by a batch-type technique. Aqueous solutions were prepared by mixing rock powders with distilled deionized water. For the sorption experiments, portions of these aqueous solutions were loaded with tracer quantities of a single radioactive nuclide and contacted with wafers of a given rock type. For the desorption experiments, wafers from the sorption experiments were contacted with the remaining portions of the aqueous solutions.

The progress of the contact experiments was monitored by gamma-ray counting of solutions. Actinide tracer concentrations on the wafers and in the solutions were measured at the end of the contact period by alphaand gamma-ray counting. These data were used to calculate sorption and desorption coefficients. Autoradiography of the wafers is being performed to gather information on sorption specificity.

Fiscal Year 1978 Subtasks

Preparation of rock samples. Wafers 3.2-cm in diameter and 0.5-cm thick were cut from samples of: basalt from the Umtanum Unit in the Pasco Basin, Washington; quartz monzonite from the Climax Stock of the Nevada Test Site; and shale (metashale) from the Eleana Formation of the Nevada Test Site.

Purification and characterization of actinide tracers. Before the tracer solutions were used, it was necessary to insure elemental purity and freedom from other contaminants. In addition, one oxidation state was selected for each element as the starting point for the experiments. The 6+ oxidation state for U, 5+ for Np, 4+ for Pu, and 3+ for both Am and Cm were used. These selections were accomplished through the use of cation-exchange chromatography. The isotopes used were ^{233}U, ^{237}Np, $^{237,242}Pu$, ^{243}Am, and $^{243,248}Cm$.

Bulk characterization of rock samples. Measurements of porosity, permeability, specific surface area, and bulk chemical composition were made on the three rock-types.

Microscopic characterization of rock samples. Thin sections of the core material were prepared and used for petrographic, scanning electron microscopic, and x-ray diffraction studies. From these studies, the types of mineral phases and their compositions were determined, as were the location and extent of microfractures. When possible, the secondary phases that coated voids and fractures were characterized.

Rock dissolution experiments. In order to prepare an aqueous electrolyte solution for the sorption/desorption studies with a composition closely approximating the natural aqueous systems and in chemical equilibirum with the solid surface of the wafers, 120 g each of basalt, quartz monzonite, and shale were ground to powders less than 37 micron in diameter. Each of the samples was placed in 2 liters of distilled deionized water that had been pre-equilibrated with an atmosphere containing 10% CO_2, 90% Ar, and contaminated with ~10 ppm O_2. The experiment was carried out in an inert atmosphere box at room temperature (26 $\pm$ 2°C). Samples of the fluid (10 ml) were extracted at various times over a 35-day period and filtered (0.05 μm). Analyses for Na, K, Mg, Ca, Fe, Al, SiO_2 (aq), Eh, and pH were made on each sample. The experiment was terminated at the end of 846 hours and analyses for HCO_3, SO_4, and Cl were made on each of the fluids.

Rock/tracer sorption experiments. Two wafers of each rock type were placed in linear polyethylene containers holding 150 ml of the appropriate prepared water. The wafers were allowed to equilibrate with the water for three days and then 5 λ of tracer solution were added. The resultant solutions contained ~5 x 10^{-8} M of each element. A blank solution, not containing wafers, was prepared in a similar manner for each of the five actinides by mixing 50 ml of each of the three water types. The containers were sealed and gently agitated for six weeks. The concentrations of tracers in solution were determined periodically in situ by gamma-ray counting of the containers. At the end of the six weeks, the wafers were removed from the containers. One wafer was immediately placed in a new container with 50 ml of aqueous solution for the desorption study. The other wafer was rinsed lightly, allowed to dry, and counted. Aliquots of the solution were taken for alpha and gamma-ray counting. In addition, aliquots of the solutions were passed through 0.05-μm filters and samples taken for alpha counting. Both alpha and gamma count rates of the wafers were measured.

Rock/tracer desorption experiment. One of the rock wafers from each of the containers used in the sorption experiments was placed in a new polyethylene bottle containing 50 ml of the appropriate aqueous solution and gently agitated for six weeks. Tracer concentrations in solution were measured periodically, as described previously. At the end of six weeks, the experiments were terminated, the wafers removed from the containers, and the tracer concentrations of the components of the system determined in the same manner as in the adsorption experiments.

Autoradiography of rock samples. At the completion of the sorption and desorption experiments, the rock wafers were placed in contact with Kodak AR.10 nuclear emulsion films to obtain alpha-particle induced autoradiographs. Due to the low concentrations of tracers on many of the wafers, rather lengthy exposure times (up to three months) are needed to obtain autoradiographs that can be readily studied under low magnification (x5). The autoradiographs will be compared with the microstructure and mineral phases of the wafer surfaces and correlations made between sorption and these parameters. Individual mineral phases exhibiting selective uptake will be used as sorptive substrates in future experiments.

Results and Discussion

The final compositions of the waters resulting from the three dissolution experiments have been summarized and listed together with compositions of waters from natural systems in Table 1. Changes in the composition of the prepared water were quite small by the end of the 35-day period. The experimental and natural basalt waters have very similar compositions; however, the experimental quartz monzonite water has a higher-than-natural K content whereas the shale water has higher-than-natural K and Na contents. The HCO_3 content of each of the experimental waters is higher than the content of its natural counterpart, whereas the opposite is true for SO_4. The differences in compositions are probably due to the fact that phases containing these ions (illite, smectite, and so on) have sufficient time to form in natural systems but did not form in the experimental system. The high HCO_3 content of the experimental system is due to contact with an infinite reservoir of CO_2 having a partial pressure of 0.1 atmosphere.

Changes in concentrations of the actinides in solution in the blank containers are shown in Figure 1. A large fraction of Pu, Am, and Cm was removed from solution and only a small amount of the U and none of the Np was lost from solution. Since the starting concentration of Pu may have exceeded the solubility for the hydroxide (or hydrated oxide), the Pu could have precipitated (Lloyd and Haire, 1973); the behavior of Am and Cm cannot be explained by a similar mechanism. However, there is recent experimental evidence that indicates that the solubility products for Am and Cm carbonates may be on the order of 10^{-41} (Beall, 1978, private commun.). If this is the case, there was sufficient carbonate ion concentration in the solutions to cause precipitation of these compounds.

Figures 2, 3, and 4 show the results of the contact experiments for the basalt, shale, and quartz monzonite samples. The rate of sorption was rapid during the first two weeks and changed slowly thereafter. In these experiments Pu, Am, and Cm exhibited behavior similar to the results obtained in the blank experiments. Uranium showed moderate sorption (about 50%) on the basalt but only slight sorption (10 to 20%) on

Table 1. Comparison of prepared waters with waters from natural systems (mg/l).

	DC3-3600	(A)	U15E-7	(B)	(C)	UE-17E	(D)	(E)
Na	52	37	20	93	6.0	77	12	18
K	8.0	7.0	26	3.0	1.6	9.0	1.1	1.5
Mg	4.4	8.0	19	18	1.7	13	16	19
Ca	11	19	38	117	10	32	29	96
Fe	1.2	0.2	2.3	0.2	0.01	1.4	0.02	0
Al	0.12	-	0.01	0.2	0.02	0.02	0	0
SiO_2	63	55	42	33	25	33	16	15
pH	6.4	7.8	6.6	7.6	6.8	6.8	4.9	7.8
HCO_3	190	150	290	214	57	380	126	133
Cl	1.5	10	1.5	32	1.1	0.8	12	25
SO_4	2	20	2	337	2.4	3	22	208

A, average composition of groundwaters from Columbia River basalts (525 samples)
B, seepage waters from climax stock (quartz monzonite)
C, average composition of perennial springs in quartz monzonites and grandodiorites of the Sierra Nevadas (56 samples)
D, groundwater from the Brunswick Shale of New Jersey
E, groundwater from the Chicopee Shale of Massachusetts

the shale and quartz monzonite wafers. Neptunium showed strong sorption (70 to 80%) on the shale, and slight sorption (about 10%) on the basalt and quartz monzonite.

The calculated sorption coefficients (K) are presented in Table 2. K (alpha) refers to results from alpha-counting the wafers and solutions, whereas K (gamma) refers to results from gamma-counting. K (filter) refers to results from the alpha-counting of wafers and filtered solutions.

Measurement precision of the K values is ±5 to 10% for K (alpha) and K (filter). Precision of the K (gamma) measurements are ±5 to 10% for

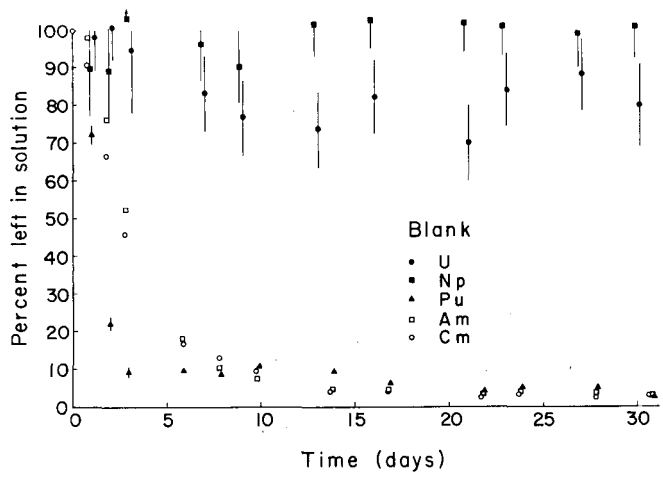

Figure 1. Percentage of initial concentrations of tracers left in solution as a function of time for the sorption experiments with the blank containers.

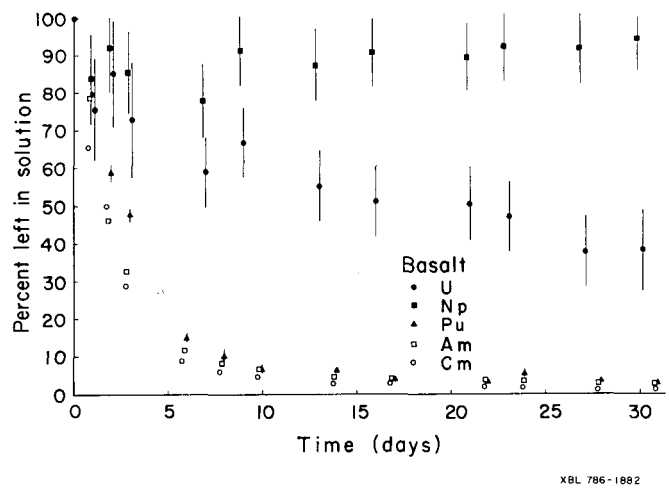

Figure 2. Percentage of initial concentrations of tracers left in solution as a function of time for the sorption experiments with the basalt samples.

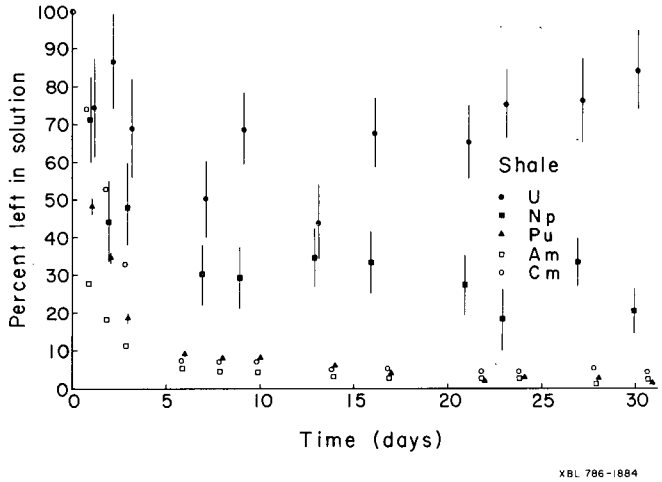

Figure 3. Percentage of initial concentrations of tracers left in solution as a function of time for the sorption experiments with the shale samples.

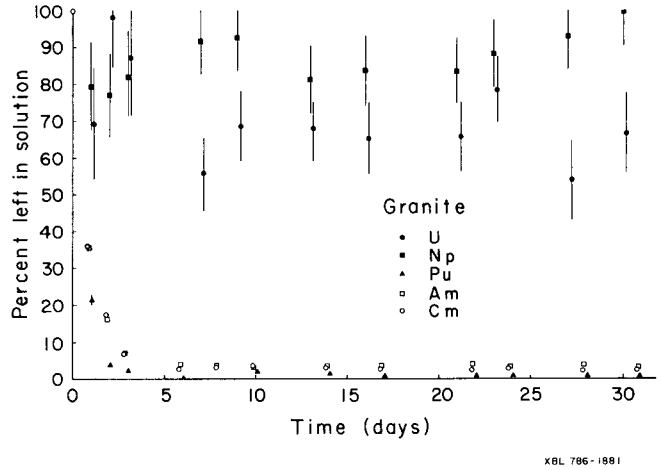

Figure 4. Precentage of initial concentrations of tracers left in solution as a function of time for the sorption experiments with the quartz monzonite samples.

Table 2. Adsorption coefficients, K = (d/m/gm)/(d/m/ml).

Sample*	Up/Down	K(alpha)	K(filter)	K(gamma)
I - U	1.51	1.87	2.01	2.80
II - U	7.78	0.761	0.797	6.65
III - U	2.33	0.316	0.343	0.287
I - Np	1.09	0.416	0.394	0.459
II - Np	0.797	1.53	1.29	48.7
III - Np	1.53	0.199	0.204	0.471
I - Pu	4.33	48.9	423	60.1
I - Pu - A	7.00	137		139
II - Pu	3.50	188	729	145
III - Pu	3.50	261	2973	225
III - Pu - A	11.0	113		143
I - Am	7.73	1,270	14,300	1,033
II - Am	3.02	97.8	394	962
III - Am	6.02	1,290	12,700	1,323
I - Cm	4.35	746	4,900	535
II - Cm	2.78	44.2	724	219
III - Cm	3.29	164	6,460	171

*I = Basalt, II = Shale, III = Quartz monzonite, A = Altered.

Am and Cm; ± 20% for Pu; and ± 30 to 35% for Np and U. These values represent only errors associated with the counting.

Except for Np, alpha counting showed that wafer surfaces facing upward consistently had higher counting rates than surfaces facing downward. The up/down ratios are also presented in Table 2. This behavior suggests that a process such as precipitation followed by settling may be involved.

Comparison of K (alpha) and K (gamma) show good agreement for each given rock type and element except for the shale samples. With the exception of Pu, K (gamma) values for the shale samples were considerably larger than K (alpha) values. Since alpha counting detects only material on the surface, while gamme counting detects both surface and bulk-sorbed material, sorption on the basalt and quartz monzonite samples represents a surface process, and the shale samples exhibit a diffusional effect in addition to surface sorption. Differential migration of the actinides into the samples was not expected since the measured permeabilities and porosities for the three rock types were nearly equivalent. However, the permeability and porosity data obtained on the samples may not be representative for the experimenta conditions.

Finally, a comparison of K (alpha) and K (filter) for each rock type and element shows that, although the values for U and Np agree quite well, the values differ substantially for Pu, Am, and Cm. Apparently, there were still considerable amounts of filterable or sorbable species left in solution after the six weeks contact time.

The data obtained from the gamma-ray spectra taken during the course of the desorption experiments were not useful for monitoring the rates of desorption. For the samples containing U and Np, only a small amount of activity appeared in solution, and therefore the counting errors precluded a meaningful analysis. Though the counting errors for samples containing Pu, Am, and Cm were small, large fluctuations in the measured values again made detailed analysis fruitless. However, there were some general trends that should be mentioned. Most of the material that appeared in solution did so in two to three days; in general, the basalt and quartz monzonite wafers desorbed three to five times more tracer than the shale wafers; and the Pu, Am, and Cm values fluctuated by a factor of 2 to 3 about the mean.

The calculated desorption coefficients are given in Table 3. The symbols are the same as used previously. For K (alpha), the counting precision is ±10% for the U, Am, and Cm samples, and ±20 to 30% for the Np and Pu samples. For K (filter), the counting precision is ±10% for U, ±10 to 20% for Np, Am, and Cm, and ±30 to 40% for the Pu samples. For K (gamma), the counting precision is ±10% for Am and Cm, and ±40 to 50% for U, Np, and Pu.

The up/down effect was also apparent in the data of the desorption experiment (Table 3). This probably results from the original deposition pattern. However, the desorption data for shale differ significantly from the sorption data, i.e., the up/down ratios are closer to unity in the desorption experiments. A comparison of K (alpha) and K (filter) show substantial differences for Am, Cm, and Pu (basalt) samples. Comparison of K (alpha) and K (gamma) show reasonably good agreement except for the U, Np, Am, and Cm shale samples.

The observed differences among the elements could presumably be attributed to differences in sorption properties of the chemical species present. Unfortunately, with the possible exception of Np, the lack of a complete set of thermodynamic data precludes a quantitative prediction of the concentrations of the various possible species in solution or of the conditions for the formation of solid phases. However, the data suggest that precipitation or colloid formation were the major reactions of Pu, Am, and Cm in the solutions.

The data obtained from the filtered solutions can be used to estimate an upper limit to the concentrations of soluble Pu, Am, and Cm under the conditions of the experiments. These concentrations were approximately 2×10^{-10} M for Pu, and 2×10^{-11} M for Am and Cm.

The hydroxide was expected to be the stable solid phase for Pu^{4+} under the conditions of the experiments. Reported and estimated solubility product constants range from 10^{-52} (Cleveland, 1970) to 10^{-62} (Baes, 1976), saturated solution concentration range = 10^{-6} to 10^{-16} M. The major hydrolysis product for Pu^{4+} was estimated to be $Pu(OH)_4^o$; $K[Pu^{4+} + 4OH^- = Pu(OH)_4^o] = 10^{46.5}$ (Baes and Mesmer, 1976). Using this hydrolysis constant, an apparent solubility product quotient of 10^{-56} was calculated from the data.

In general, the chemical behavior of Am and Cm in solution is quite similar, and similar to that of the trivalent lanthanides. The americium hydroxide and carbonate solubility product constants were estimated as $10^{-23.3}$ (Baes and Mesmer, 1976) and 10^{-33} (Smith and Martel, 1976), respectively, from published values on lanthanide compounds. The values for Cm would be expected to be nearly the same. The carbonate was calculated to be the stable solid phase; saturated solution concentration = 10^{-7} M. Since the starting concentration of Am was about 5×10^{-8} M, precipitation was not anticipated. However, as mentioned previously, the assumed carbonate solubility may be high by eight orders of magnitude. From the data, solubility product quotients for the possible compounds $Am_2(CO_3)_3$ and $AmOHCO_3$ were estimated as 10^{-41} and 10^{-25}, respectively. The values for Cm

Table 3. Desorption coefficients (d/m/gm)/(d/m/ml).

Sample*	Up/Down	K(alpha)	K(filter)	K(gamma)
I - U	3.65	2.36	3.21	4.63
II - U	3.83	1.06	1.12	7.06
III - U	2.52	1.91	1.54	2.76
I - Np	1.35	1.29	1.05	1.92
II - Np	1.20	1.20	0.877	83.4
III - Np	1.10	3.69	2.77	2.72
I - Pu	5.20	59.5	687	32.1
II - Pu - A	2.18	371		514
II - Pu	1.32	316	191	363
III - Pu	2.98	101	96.3	62.3
III - Pu - A	11.07	749		787
I - Am	4.33	246	4,790	277
II - Am	1.01	697	1,159	14,036
III - Am	4.71	176	1,581	209
I - Cm	5.57	774	11,115	699
II - Cm	1.75	239	1,426	2,889
III - Cm	4.08	533	2,542	591

*I = Basalt, II - Shale, III = Quartz monzonite, A = Altered.

should be similar. A detailed account of this work is given by Silva et al. (1978).

PLANNED ACTIVITIES FOR FISCAL YEAR 1979

In fiscal year 1979, theoretical and experimental efforts will be concentrated on developing and testing an advanced sorption model to predict sorption coefficients for radionuclides on rock substrates. It will involve bringing computer code MINEQL to full operational status at LBL, providing the necessary experimental data required by the model and preliminary testing of the model to predict sorption coefficients for ^{137}Cs on the substrates silica and montmorillonite.

REFERENCES CITED

Apps, J. A., Lucas, J., Mathur, A. K., and Tsao, L., 1977. Theoretical and experimental evaluation of waste transport in selected rocks: 1977 annual report of LBL contract no. 45901AK. Berkeley, Lawrence Berkeley Laboratory, LBL-7022, p. 8.

Baes, C. F., and Mesmer, R. E., 1976. The hydrolysis of cations. New York, Wiley-Interscience, p. 169.

Cleveland, J. M., 1970. The chemistry of plutonium. New York, Gordon and Breach Science Publications, p. 81.

Lloyd, M. H., and Haire, R. G., 1973. Studies on the chemical and colloidal nature of Pu (IV) polymer. XXIVth International Union of Pure and Applied Chemistry Congress, Hamburg, Germany, September 1973.

Silva, R. J., Benson, L. V., and Apps, J. A., 1978. WISAP 4: collection and generation of transport data, 1978 annual report for LBL contract no. 45901AK. Berkeley, Lawrence Berkeley Laboratory, LBL-8450.

Smith, R. M., and Martel, A. E., 1976. Critical stability constants, in Inorganic complexes. New York, Plenum Press, v. 4, p. 37.

APPENDIXES

APPENDIX A: PUBLICATIONS

Andersson, B., and Halen, P., 1978. Mining methods used in the underground tunels and test rooms at Stripa: Swedish-American cooperative program on radioactive waste storage in mined caverns in crystalline rock. LBL-7081, SAC-08, 22 p.

Apps, J. A., 1977. The definition of engineering development and research problems relating to the use of geothermal fluids for electric power generation and nonelectric heating. LBL-7025, 57 p.

Apps, J. A., Cook, N. G. W., and Witherspoon P. A., 1978. An appraisal of underground radioactive waste disposal in argillaceous and crystalline rocks: some geochemical, geomechanical, and hydrogeological questions. Background information for GAIN symposium, LBL-7047, 50 p.

Apps, J. A., Lucas, J., Mathur, A. K., and Tsao, L., 1977. Theoretical and experimental evaluation of waste transport in selected rocks: 1977 annual report of LBL contract no. 45901AK. LBL-7022, 139 p.

Barber-Nichols Engineering Company, 1978. Design definition of a 500-kW direct contact geothermal pilot plant. UCID-8009, 40 p.

Benson, L. V., Carnahan, C. L., Apps, J. A., Mouton, C. A., Corrigan, D. J., Frisch, C. J., and Shomura, L. K., 1978. Basalt alteration and basalt-waste interaction in the Pasco Basin of Washington State. LBL-8532, 85 p.

Carlsson, H., 1978a. Stress measurements in the Stripa granite: Swedish-American cooperative program on radioactive waste storage in mined caverns in crystalline rock. LBL-7078, SAC-04, 21 p.

_____, 1978b. A pilot heater test in the Stripa granite: Swedish-American cooperative program on radioactive waste storage in mined caverns in crystalline rock. LBL-7086, SAC-06, 158 p.

Chan, T., Cook, N. G. W., and Tsang, C. F., 1978. Theoretical temperature fields for the Stripa heater project. LBL-7082, SAC-09, 2 volumes, 293 p.

Churchman, C. W., Nelson, H. G., and Eacret, K., 1977. Value distribution assessment of geothermal development in Lake County, California. LBL-6875, 111 p.

Concus, P., and Proskurowski, W., 1977. Numerical solution of a nonlinear hyperbolic equation by the random choice method. LBL-6487, 29 p.

Cook, N. G. W., 1977. An appraisal of hard rock for potential underground repositories of radioactive wastes. LBL-7004, 15 p.

Cook, N. G. W., and Hood, M., 1978. Full-scale and time-scaled heating experiments at Stripa: preliminary results. Presented at the Seminar on in-situ heating experiments in geological formations, Stripa, Sweden, Sept. 12-15, 1978, LBL 7027 Abs., 5 p.

Cook, N. G. W., and Witherspoon, P. A., 1978. In-situ heating experiments in hard rock: their objectives and design, presented at the Ludvika-Stripa Seminar on In-Situ Heating Experiments in Geological Formations, Stripa, Sweden, Sept. 12-15, 1978. Organisation for Economic Co-operation and Development. LBL-7073 Abs. 6 p.

Corwin, R. F., Díaz C., S., and Rodríguez B., J., 1978. Self-potential survey at the Cerro Prieto geothermal field, Baja California, Mexico. Presented at the Geothermal Resources Council 1978 annual meeting, Hilo, Hawaii, July 25-28, 1978. LBL-7065, 7 p.

Corwin, R. F., and Hoover, D. B., 1978. The self-potential method in geothermal exploration. Geophysics, v. 44 (1979), pp. 226-245 and LBL-7075, 63 p.

Corwin, R. F., Morrison, H. F., Díaz C., S., and Rodriguez B., J., 1978. Self-potential studies at the Cerro Prieto geothermal field, in Abstracts, First Symposium on the Cerro Prieto Geothermal Field, Baja California, Mexico, Sept. 20-22, 1978. LBL-7098 Abs.

Cosner, S. R., and Apps, J. A., 1978. Compilation of data on fluids from geothermal resources in the United States. LBL-5936, 112 p.

Dey, A., and Morrison, H. F., 1977. Resistivity modeling for arbitrarily shaped three-dimensional structures. Geophysics, v. 44 (1979), pp. 753-780 and LBL-7010, 56 p.

Earth Sciences Division, 1977a. Geothermal reservoir engineering management program plan (GREMP Plan). LBL-7000, 136 p.

_____, 1977b. Proceedings, first invitational well-testing symposium. LBL-7027, 195 p.

_____, 1978a. Earth Sciences Division annual report 1977. LBL-7028, 169 p.

_____, 1978b. Proceedings, workshop on modeling of electrical and electromagnetic methods, 17-19 May 1978. LBL-7053, 203 p.

_____, 1978c. Fundamental geosciences program annual report 1977. LBL-7058, 44p.

_____, 1978d. Abstracts, First Symposium on the Cerro Prieto Geothermal Field, Baja California, Mexico, September 20-22, 1978, San Diego, California. LBL-7098 ABS., 32 p.

Fulton, R. L., 1978. Heat exchanger module test. Presented at the EPRI Second Geothermal Conference and Workshop, Taos, New Mexico, June 20-23, 1978, LBL-7077, 6 p.

Gadgil, A. J., Gibson, G., and Rosenfeld, A. H., 1978. Twozone: user's manual. LBL-6840, 118 p.

Gamble, T. D., 1978. Remote reference magnetotellurics with SQUIDs. Ph. D. thesis, University of California, Berkeley, LBL-8062.

Gamble, T. D., Goubau, W. M., and Clark, J., 1978a. Error analysis for remote reference magnetotellurics. Geophysics, v. 44 (1979), pp. 959-968 and LBL-7085, 40 p.

_____, 1978b. Magnetotellurics with a remote magnetic reference. Geophysics, v. 44 (1979), pp. 53-68 and LBL-7032, 45p.

Gamble, T. D., Goubau, W. M., Clarke, J., and Goldstein, N. E., 1978. Referenced

magnetotellurics at Cerro Prieto, in Abstracts, First Symposium on the Cerro Prieto Geothermal Field, Baja California, Mexico, Sept. 20-22, 1978. LBL-7098 Abs.

Goldstein, N. E., 1977. Northern Nevada geothermal exploration strategy analysis. LBL-7012, 55 p.

Goldstein, N. E., and Mozley, E., 1978. A telluric-magnetotelluric survey at Mt. Hood, Oregon, a preliminary study. LBL-7050, 93 p., 5 maps.

Goldstein, N. E., Norris, R. A., and Wilt, M. J., 1978. Assessment of surface geophysical methods in geothermal exploration and recommendations for future research. LBL-6815, 166 p.

Goldstein, N. E., and Paulsson, B., 1977. Interpretation of gravity surveys in Grass and Buena Vista Valleys, Nevada. Geothermics, v. 7 (1978), no. 1, pp. 29-50 and LBL-7013, 43 p.

Goranson, C., McEdwards, D., and Schroeder, R., 1978. Review of Desert Hot Springs well test. LBL-4028, 12 p.

Goranson, C., and Schroeder, R., 1978. Static downhole characteristics of well CGEH-1 at Coso Hot Springs, China Lake, California. LBL-7059, 34 p.

Grannell, R. B., Tarman, D. W., Clover, R., Goldstein, N. E., Chase, D. S., Eppink, J., and Leggewie, R., 1978. Precision gravity studies at Cerro Prieto, in Abstracts, First Symposium on the Cerro Prieto Geothermal Field, Baja California, Mexico, Sept. 20-22, 1978.

Green, M. A., Doyle, P. A., Pines, H. S., Pope, W. L., and Silvester, L. F., 1977. The optimization of alternative energy cycles using program GEOTHM. Presented at the Miami International Conference on Alternative Energy Sources, Miami, Dec. 5-7, 1977, LBL-6308, 18 p.

Howard, J. H., 1977. The ERDA-DGE/LBL geothermal reservoir engineering management program. Presented at the EPRI Geothermal Program Progress Report and Workshop, Geothermal Milestones 1977, Kah-nee-ta, Oregon, July 25-28, 1977, LBL-6826, 6 p.

_____, 1978. Overview of geothermal technology. Presented at the Geothermal Seminar-1978, Sacramento, CA, May 9, 1978. LBL-7048, 49 p.

Howard, J. H., Campbell, D. A., Hinrichs, T. C., Mathias, K. E., and Narasimhan, T. N., 1978. Geothermal resource investigations and development plans at East Mesa, California. LBL-9026, 30 p.

Hustrulid, W., 1978. Instrumentation/measurement techniques and philosophies for nuclear waste repositories: background information for GAIN Symposium. PUB-246, 64 p.

Jain, B. K., 1978. A low frequency electromagnetic prospecting system. Ph. D. thesis, University of California, Berkeley, LBL-7042, 128 p.

Jamison, D. B., and Cook, N. G. W., 1978. An analysis of the measured values for the state of stress in the earth's crust: Swedish-American cooperative program on radioactive waste storage in mined caverns in crystalline rock. LBL-7071, SAC-07, 19 p.

Jonsson, V., 1978. Similation of the Krafla geothermal field. LBL-7076, 61 p.

Kurfurst, P. J., Hugo-Persson, T., and Rudolph, G., 1978. Borehole drilling and related activities at the Stripa mine: Swedish-American cooperative program on radioactive waste storage in mined caverns in crystalline rock: LBL-7080, SAC-05, 56p.

Lee, K. H., 1978. Electromagnetic scattering by a two-dimensional inhomogeneity due to an oscillating magnetic dipole. LBL-8275, 81 p.

Lee, K. H., Labson, V., Wilt, M., and Goldstein, N., 1978. Catalogue of magnetotelluric apparent resistivity pseudosections over two-dimensional models. LBL-7057, 68 p.

Liaw, A. L., 1977. Microseisms in geothermal exploration studies in Grass Valley, Nevada. Ph. D. thesis, University of California, Berkeley, LBL-7002, 181 p.

Lippmann, M. J., Narasimhan, T. N., and Witherspoon, P. A., 1977. Modeling subsidence due to geothermal fluid production. Prepared for the ASCE Fall Convention and Exhibit, San Francisco, October 17-21, 1977. LBL-7007, 25 p.

Lippmann, M. J., and Tsang, C. F., 1978. Three-dimensional numerical simulation of single-phase, non-isothermal fluid flow in porous reservoirs. Presented at the Meeting of the Society of Petroleum Engineers of AIME, Denver, CO, Jan/Feb 1979. LBL-7056.

Lippmann, M. J., Tsang, C. F., and Witherspoon, P. A., 1978. A study of groundwater temperature changes during aquifer uses related to power production. Submitted for the Meeting of the American Geophysical Union, Miami Beach, Florida, April 17-21, 1978, LBL-7031 Abs., 1 p.

Long, J., and Wilson, C., eds., 1978. Recommended well drilling and testing program, Pasco Basin, Hanford Reservation. Pub-5011.

Lundstrom, L., and Stille, H., 1978. Large scale permeability test of the granite in the Stripa mine and thermal conductivity test: Swedish-American cooperative program on radioactive waste storage in mined caverns in crystalline rock. LBL-7052, SAC-02, 42 p.

Majer, E. L., 1978. Seismological investigations in geothermal regions. Ph. D. Thesis, University of California, Berkeley, LBL-7054, 225 p.

Majer, E. L., and McEvilly, T. V., 1977. Seismological investigations at The Geysers geothermal field. Geophysics, v. 44 (1979), pp. 246-269 and LBL-7023, 78 p.

Mangold, D., Wollenberg, H. A., and Tsang, C. F., 1978. Thermal effects in overlying sedimentary rock from in-situ combustion of a coal seam. LBL-8172, 9 p.

Mañon, A., Mazor, E., Jiménez, M., Sánchez, A., Fausto, J., and Zenizo, C., 1977. Extensive geochemical studies in the geothermal field of Cerro Prieto, Mexico. LBL-7019, 113 p.

Martínez-Baez, L. F., and Amick, H., 1978. Thermal properties of Gable Mountain basalt cores, Hanford Nuclear Reservation. LBL-7038, 8 p.

McEvilly, T. V., and Schechter, B., 1977. East Mesa seismic study, report no. 2. UCID-4029, 10 p.

McEvilly, T. V., and Schechter, B., 1978. East Mesa seismic study, report no. 3. UCID-4030.

Mitchell, J. K., Guzikowski, F., and Villet, W. C. B., 1978. The measurement of soil properties in situ, present methods--their applicability and potential. LBL-6363, 67 p.

Morrison, H. F., Goldstein, N. E., Hoversten, G. M., Oppliger, G., and Riveros, C., 1978. Description, field test, and data analysis of a controlled-source EM system (EM-60). LBL-7088, 150 p.

Murphy, M., Wollenberg, H., Strisower, B., Bowman, H., Flexser, S., and Carmichael, I., 1978. Uranium in alkaline rocks. LBL-7029, 185 p.

Narasimhan, T. N., 1978. The significance of the storage parameter in saturated-unsaturated groundwater flow. Submitted to Water Resources Res., LBL-7041, 33 p.

Narasimhan, T. N., Schroeder, R. C., Goranson, C. B., McEdwards, D. G., Campbell, D. A., and Barkman, J. H., 1977. Recent results from tests on the Republic geothermal wells, East Mesa, California. Presented at the 3rd Geothermal Workshop, Stanford University, Stanford, CA, Dec. 14-16, 1977, LBL-7017, 7 p.

Narasimhan, T. N., and Witherspoon, P. A., 1978a. Numerical model for saturated-unsaturated flow in deformable porous media: 2, the algorithm. Water Resources Res., v. 14, no. 2., pp. 255-261, LBL-5932.

_____, 1978b. Numerical model for saturated-unsaturated flow in deformable porous media: applications. Water Resources Res., v. 14, no. 6, p. 1017-1034, and LBL-7037, 66 p.

Nelson, P. H., 1978. Geophysical program at experimental waste storage site at Stripa, Sweden. Submitted for the meeting of the European Association for Exploration Geophysicists, Dublin, Ireland, June 27-30, 1978, LBL-7035 Abs., 1 p.

Noble, J. E., Mañon M., A., Lippmann, M. J., and Witherspoon, P. A., 1977. A study of the structural control of fluid flow within the Cerro Prieto geothermal field, Baja California, Mexico, 52nd Annual Fall Technical Conference and Exhibition of the Soc. Pet. Eng. AIME, SPE-6763 and LBL-7003.

Phillips, S. L., 1978. National geothermal information resource annual report. LBL-7803, 68 p.

Pines, H. S., Green, M. A., Pope, W. L., and Doyle, P. A., 1978. Floating dry cooling, a competitive alternative to evaporative cooling in a binary cycle geothermal power plant. Presented at the 1978 Annual Winter Meeting of the ASME, San Francisco, Dec. 10-15, 1978, LBL-7087, 10 p.

Pines, H. S., Pope, W. L., Green, M. A., Doyle, P. A., Silvester, L. F., and Fulton, R. L., 1978. The thermodynamic and cost benefits of a floating cooling geothermal binary cycle power plant at Heber, California. Presented at the Geothermal Resources Council 1978 Annual Meeting, Hilo, Hawaii, July 25-28, 1978, LBL-7040, 6 p.

Pitzer, K. S., Peterson, J. R., and Silvester, L. F., 1977. Thermodynamics of electrolytes: IX, rare earth chlorides, nitrates, and perchlorates. Submitted to Jour. Solution Chem., LBL-6399, 25 p.

Pitzer, K. S., and Silvester, L. F., 1977. Thermodynamics of electrolytes: XI, properties of 3-2, 4-2, and other high-valence types. Submitted to Jour. Phys. Chem., LBL-7021, 15 p.

Pope, W. L., Pines, H. S., Silvester, L. F., Doyle, P. A., Fulton, R. L., and Green, M. A., 1978. Optimizations of geothermal cycle shell and tube exchangers of various configurations with variable fluid properties and site specific fouling. Presented at the Geothermal Resources Council 1978 Annual Meeting, Hilo, Hawaii, July 25-28, 1978, LBL-7039, 4 p.

Pruess, K., Schroeder, R., Zerzan, J., and Witherspoon, P. A., 1978. SHAFT78, a three-dimensional two-phase computer program for geothermal reservoir simulation (abstract). LBL-8264, 1 p.

Razo M., A., Arellano G., F., and Fonseca L., H., 1978. CFE resistivity studies at Cerro Prieto, in Abstracts, First Symposium on the Cerro Prieto Geothermal Field, Baja California, Mexico, Sept. 20-22, 1978. LBL-7098 Abs.

Schwartz, S. R., 1978. Geothermal emissions data base, Wairakei geothermal field. UCID-4035, 402 p.

Silva, R. J., Benson, L. V., and Apps, J. A., 1978. Studies of actinide sorption on selected geologic materials. LBL-8904, 33 p.

Silvester, L. F., and Pitzer, K. S., 1977. Thermodynamics of electrolytes: X, enthalpy and the effect of temperature on the activity coefficients. Submitted to Jour. Solution Chem., LBL-7009, 20 p.

Simkin, T. L., and Noble, J. E., eds., 1978. Geothermal subsidence research program, project summaries. UCID-8035, 46 p.

Swan, G., 1978. The mechanical properties of Stripa granite: Swedish-American cooperative program on radioactive waste storage in mined caverns in crystalline rock. LBL-7074, SAC-03, 32 p.

Tsang, C. F., 1978a. A summary of current studies in aquifer thermal energy storage. Presented at the Second International Helioscience Institute Conference on Alternative Energy, Palm Springs, California, April 8-11, 1978, LBL-7066, 16 p.

_____, 1978b. Aquifer thermal energy storage. Presented at the Institute of Gas Technology symposium on advanced technologies for storing energy, Chicago, Illinois, July 10-13, 1978, LBL-7070, 32 p.

_____, 1978c. Numerical modeling studies in well test analysis. LBL-8363, abstract.

Tsang, C. F., Bodvarsson, G., Lippmann, M. J., and Rivera, J. R., 1978. A study of alternative reinjection schemes for the Cerro Prieto geothermal field, Baja California, Mexico. Presented at the Geothermal Resources Council 1978 annual meeting, Hilo, Hawaii, July 25-28, 1978, LBL-7064, 17 p.

Urbanek, M. W. (DSS Engineers, Inc.), 1978. Development of direct contact heat exchangers for geothermal brines: final

report, October 4, 1977 - June 30, 1978. LBL-8558, 132 p.

Wang, J. S. Y., Narasimhan, T. N., Tsang, C. F., and Witherspoon, P. A., 1977. Transient flow in tight fractures, in Proceedings, Invitational Well-Testing Symposium, October 19-21, 1977, Berkeley, California. LBL-7027, pp. 103-116.

Weres, O., and Schroeder, R. C., 1978. Documentation for program OGRE. LBL-7060, 64 p.

Weres, O., Yee. A., and Tsao, L., 1978a. Empirical equations and type curves for predicting the precitation of silica from geothermal brines. Presented at the 1979 SPE International Symposium on Oilfield and Geothermal Chemistry, Houston, Texas, Jan. 22-24, 1979, SPE-7888. LBL-7090 Abs., 6 p.

_____, 1978b. Predicting the precipitation of amorphous silica from geothermal brines. Presented at the Fourth Annual Stanford Geothermal Program Workshop, Stanford University, Stanford, December 13-15, 1978.

Wilt, M., Goldstein, N., and Razo M., A., 1978. LBL resistivity studies at the Cerro Prieto geothermal field, in Abstracts, First Symposium on the Cerro Prieto Geothermal Field, Baja California, Mexico, Sept. 20-22, 1978, LBL-7098 Abs.

Witherspoon, P. A., 1978. An approach to the fracture hydrology at Stripa: preliminary results. Ludvika-Stripa Seminar on In Situ Heating Experiments in Geological Formations, September 13-15, 1978.

Witherspoon, P. A., Alonso E., H., Lippmann, M. J., Mañon M., A., and Wollenberg, H. A., 1978. Mexican-American cooperative program at the Cerro Prieto geothermal field. LBL-7095, Cerro Prieto-001, 43 p.

Witherspoon, P. A., Cook, N. G. W., and Gale, J. E., 1978. Radioactive waste storage in argillaceous and crystalline rock masses, in Bergman, M., ed., Rockstore 77: Proceedings of the First International Symposium on Storage in Excavated Caverns, Stockholm, Sweden, September 5-8, 1977. Oxford, Pergamon Press, v. 3.

Witherspoon, P. A., and Degerman, O., 1978. Swedish-American cooperative program on radioactive waste storage in mined caverns, program summary: Swedish-American cooperative program on radioactive waste storage in mined caverns in crystalline rock. LBL-7049, SAC-01, 26 p.

Witherspoon, P. A., and Gale, J. E., 1978. Flow in fractured rock systems--implications for radioactive waste storage (abstract). Third International Congress of Engineering Geology, International Association of Engineering Geology, Madrid, Spain, September 4-8, 1978.

APPENDIX B: EARTH SCIENCES DIVISION STAFF

PAUL A. WITHERSPOON*
Associate Director, Lawrence Berkeley Laboratory
Division Head, Earth Sciences Division

DIVISION ADMINISTRATION

Kenneth F. Mirk, Deputy Division Head
Karl Olson, Assistant Division Head
Monique Adam, Division Office Administrator

STAFF FOR FISCAL YEAR 1978

Jack Angevine
John A. Apps
Lois Armetta
Vinod Agrawal
Mohammed Ayatollahi

George Badger
Lawrence O. Beaulaurier
Larry V. Benson
Sally M. Benson
Eugene Binnall
Gudmundur Bodvarsson*
Milford Bookman
Harry R. Bowman
Daniel J. Bradley
Choate Brown
Wendy Brubaker
Marc S. Bukowinski*

Annette L. Bunge
Thomas Buscheck
Timonthy Buscheck
Patricia A. Butler

Hans Carlsson
Ian S. E. Carmichael*
Chalon L. Carnahan
Joseph Chan
Tin Chan
Eric Cheney
Jerry Chin
Clement K. Chou
Jeri Chu
John Clarke*
Lewis Cohen*
Neville G. W. Cook*
Donald J. Corrigan

Alain R. Curneir

James V. Davey
Robert Davis
E. F. De Zabala
Thomas Doe
Benjamin Doty
Sandra Doty
Christine Doughty
Padraic Doyle
Allan Dubin
Andrew DuBois

Laurel Egenberger
Paul Elias
Janice Elliot
Eugene Eno
James W. Evans

*Faculty member, University of California, Berkeley.

Steve Flexser
Douglas Frink
Conny J. Frisch
Mauro Foglia
Philip Fong
Ted Fujita
Robert Fulton

Robert Galbraith
John E. Gale*
Thomas Gamble
Anoushiravan Ghaffari
Orah Goldman
Norman E. Goldstein
Colin B. Goranson
Sudhanshu Goshal
Wolfgang Goubau
Keshav Goyal
Alexander N. Graf
Joyce Graves
Thomas Green
Roy F. S. Greenwald

Joseph Haney
Leif Hansen
Niamh Harty
Ramsey John Haught
Mary Hege
Harold Helgeson*
Kunio Higashi*
Deborah Hopkins
John H. Howard
Michael Hood*
Richard Hsu
Charles Hyde

Jeffrey Irvine

Dennis Jamison
Julie Jeffrey
Randall Jones
Sirisak Juprasert
Valdimar Jonsson

Marlene Kam
Brian Kanehiro
Allen J. Kearns
William R. Keyes
Tjiep Kho
Stanley M. Klainer
Steven Kramer
Brent Kohrt
James S. Kuo
Pavel Kurfurst

Raymond T. Lee
I. Wayne Lee
Donald Lippert
Marcelo J. Lippmann
Nicholas Littlestone
Jane A. Long
Steve Lundgren

Ernest Majer
Donald Mangold
Donald McCarthy

Donald G. McEdwards
Thomas McEvilly*
Maurice B. McEvoy
Ellen McKeon
Janet McQuillan
Maynard C. Michel
Constance Miller
Susan L. Miller
James K. Mitchell
Sofia Mitina
Milton Moebus
Alison Monroe
Leuren V. Moret
H. Frank Morrison*
Catharine Mouton

T. N. Narasimhan
John M. Neil
Philip H. Nelson
S. A. Nelson
Narry Ng
Helen Nicholas
John E. Noble
Duane Norgren

Maura T. O'Brien

Walter S. Palen
Bjorn Paulsson
Susan Payne
Christopher J. Peiper
Louise Pellerin
Scott Peterson
Ronald C. Philips
S. L. Phillips
Thomas Pigford*
Howard Pines
Kenneth S. Pitzer*
William Pope
Karsten Pruess

Clayton G. Radke*
William Ralph
Pascal Rapier
Ruthie Redic
Janet Remer
Carlos Riveros
Morris D. Roach
Gene Rochlin
Pamela Z. Rogers
Donald J. Rondeau
M. Theresa Ruiz
Jacqueline Runnels

Sharad Sarvate
Marie Schauer
Bruce Schechter
Rolly Schilling
Ronald C. Schroeder
Werner J. Schwarz
Lisa K. Shomura
Robert J. Silva
Lenard F. Silvester
Terrance L. Simkin
Ray Solbau
Wilbur H. Somerton*

Harold Sonenklar
Hwaili Soo
Barbara Srulovitz
Mitchell Stark
Andrew Stromdahl
Rebecca Sterbentz
Robert Stolzman
Beverly Strisower
Ho-Jeen Su

Nina Taylor
Jerome Thomas
Richard K. Thorpe
Marc Trujillo
Chin Fu Tsang
Leon Tsao
Badawi W. Tleimat

William C. B. Villet
Stephen Vonder Haar

David Watkins
Cherie Walker
Oliver Wan
Joseph Wang
Christopher S. Weaver
Virginia Weaver
Oleh Weres
Jerry West
Richard E. Whiteman
Charles Wilson
Michael J. Wilt
Harold A. Wollenberg, Jr.
Frank Wong
Lester C. Wong
William Wong

Andrew Yee

John M. Zerzan

---

*Faculty member, University of California, Berkeley.

GPO 693-244/32

This report was done with support from the Department of Energy. Any conclusions or opinions expressed in this report represent solely those of the author(s) and not necessarily those of The Regents of the University of California, the Lawrence Berkeley Laboratory or the Department of Energy.

Reference to a company or product name does not imply approval or recommendation of the product by the University of California or the U.S. Department of Energy to the exclusion of others that may be suitable.

TECHNICAL INFORMATION DIVISION
LAWRENCE BERKELEY LABORATORY
UNIVERSITY OF CALIFORNIA
BERKELEY, CALIFORNIA 94720